



Edited by
M. Sánchez Sorondo and A. Zichichi

SUBNUCLEAR PHYSICS: PAST, PRESENT AND FUTURE



The Proceedings of the International Symposium • 30 October -2 November 2011

VATICAN CITY 2014

Subnuclear Physics: Past, Present and Future

Pontificiae Academiae Scientiarum Scripta Varia 119

*The Proceedings
of the International Symposium on*

Subnuclear Physics: Past, Present and Future

30 October -2 November 2011

Edited by

Marcelo Sánchez Sorondo
Antonino Zichichi



EX AEDIBVS ACADEMICIS
IN CIVITATE VATICANA • MMXIV

The Pontifical Academy of Sciences
Casina Pio IV, 00120 Vatican City
Tel: +39 0669883195 • Fax: +39 0669885218
Email: pas@pas.va • Website: www.pas.va

The opinions expressed with absolute freedom during the presentation of the papers of this meeting, although published by the Academy, represent only the points of view of the participants and not those of the Academy.

ISBN 978-88-7761-107-9

© Copyright 2014

All rights reserved. No part of this publication may be reproduced, stored in a retrieval system, or transmitted in any form, or by any means, electronic, mechanical, recording, photocopying or otherwise without the expressed written permission of the publisher.

PONTIFICIA ACADEMIA SCIENTIARVM • VATICAN CITY



H.H. Benedict XVI in the garden of the Basilica di Santa Maria degli Angeli e dei Martiri with the statue of "Galilei Divine Man" donated to the Basilica by CCAST of Beijing.

The great Galileo said that God wrote the book of nature in the form of the language of mathematics. He was convinced that God has given us two books: the book of Sacred Scripture and the book of nature. And the language of nature – this was his conviction – is mathematics, so it is a language of God, a language of the Creator.

Encounter of His Holiness Benedict XVI with the Youth, St Peter's Square, Thursday, 6 April 2006.

In the last century, man certainly made more progress – if not always in his knowledge of himself and of God, then certainly in his knowledge of the macro- and microcosms – than in the entire previous history of humanity. ... Scientists do not create the world; they learn about it and attempt to imitate it, following the laws and intelligibility that nature manifests to us. The scientist's experience as a human being is therefore that of perceiving a constant, a law, a *logos* that he has not created but that he has instead observed: in fact, it leads us to admit the existence of an all-powerful Reason, which is other than that of man, and which sustains the world. This is the meeting point between the natural sciences and religion. As a result, science becomes a place of dialogue, a meeting between man and nature and, potentially, even between man and his Creator.

Address of His Holiness Benedict XVI to Participants in the Plenary Session of the Pontifical Academy of Sciences, Clementine Hall, Thursday, 28 October 2010.







Contents

Introduction

Antonino Zichichi	12
-------------------------	----

Programme	13
-----------------	----

List of Participants	17
----------------------------	----

Scientific Papers

The Reasons for This Symposium on Past, Present and Future of Subnuclear Physics

Antonino Zichichi	21
-------------------------	----

The Early History of String Theory and Supersymmetry

John H. Schwarz	69
-----------------------	----

Achievements in Subnuclear Physics at Fermilab

Pier Oddone	82
-------------------	----

The Origin of LEP and LHC

Robert Aymar	97
--------------------	----

The ISR Legacy

Pierre Darriulat	109
------------------------	-----

From Nonlinear Statistical Mechanics to Nonlinear Quantum Mechanics – Concepts and Applications

Constantino Tsallis	120
---------------------------	-----

The Cosmological Constant Problem, Dark Energy, and the Landscape of String Theory

Raphael Bousso	129
----------------------	-----

The High Energy Frontier. Past, Present and Future

Rolf-Dieter Heuer	152
-------------------------	-----

Highlights from RHIC Plus some earlier BNL Highlights in Subnuclear Physics

Michael J. Tannenbaum	164
-----------------------------	-----

The Birth and Development of the First Hadron Collider The CERN Intersecting Storage Rings (ISR)

K. Hubner and T.M. Taylor	180
---------------------------------	-----

The INFN Contribution to Subnuclear Physics in Europe

Enzo Iarocci	193
--------------------	-----

From d-bars to Antimatter- & Hyperclusters from the Stars to FAIR in Europe

J. Steinheimer, H. Stoecker, Zhangbu Xu	203
---	-----

The Mystery of Neutrino Mixing	
Guido Altarelli	218
Novel Perspectives for Hadron Physics	
Stanley J. Brodsky	229
Black Holes in the Superworld	
Laura Andrianopoli, Riccardo D’Auria, Sergio Ferrara	246
Highlights from Atlas	
Peter Jenni	260
Quarks: as Constituents and in QCD	
Frank Close	274
Composite Weak Bosons, Leptons and Quarks	
Harald Fritzsch	280
HERA – From an Idea to Results	
Albrecht Wagner	291
New Physics without New Energy Scale	
Mikhail Shaposhnikov	301
Results from the XENON100 Dark Matter Search Experiment	
Laura Baudis	315
Origin and Status of the Gran Sasso INFN Laboratory	
Lucia Votano	328
The Proton Beam for the Neutrino Velocity Measurement with Opera	
Lyndon Evans	337
Can the Neutrino Speed Anomaly Be Defended?	
Jürgen Knobloch	343
The Origin and Status of the Third Neutrino	
Alessandro Bettini	347
Status and Results of the Lvd Experiment	
Paolo Giusti	360
Origin and Status of LUNA at Gran Sasso	
Carlo Broggini	370
The Origin and Status of Spontaneous Symmetry Breaking	
François Englert	379
Study of Low Energy Neutrinos from Sun and Earth with Borexino	
Gianpaolo Bellini	394

The Little Bang in the Laboratory: Heavy Ions @ LHC with ALICE	
Paolo Giubellino	416
An Interesting Result in pp collisions at 7 TeV	
A. Agostinelli, A. Alici, P. Antonioli, S. Arcelli, R. Baldini Ferroli, F. Bellini, G. Cara Romeo, L. Cifarelli, M. Colocci, A. De Caro, D. De Gruttola, S. De Pasquale, M. Fusco Girard, B. Guerzoni, D. Hatzifotiadou, A. Margotti, R. Nania, F. Noferini, P. Pagano, A. Pesci, R. Preghenella, E. Scapparone, G. Scioli, M.C.S. Williams, C. Zampolli, A. Zichichi	429
Perturbative Quantum Gravity from Gauge Theory	
Zvi Bern	438
High Energy Physics: Science and Technology Benefiting Humanity	
Harvey B. Newman	451
Blueprints of the No-Scale Multiverse at the LHC	
Tianjun Li, James A. Maxin, Dimitri V. Nanopoulos, Joel W. Walker	472
Black Holes and Qubits	
Michael J. Duff	488
Testing Strings at the LHC?	
Ignatios Antoniadis	497
The LAA Project and the Consequences on LHC	
Horst Wenninger	503
Lattice Fields in the LHC Era	
Richard Kenway	510
The Large Hadron Collider of CERN and the Roadmap Toward Higher Performance	
Lucio Rossi	517
Latest Results from MRPC Time Resolution	
Crispin Williams	531
Highlights From CMS	
Tejinder S. Virdee	539
The Alpha Magnetic Spectrometer (AMS) Experiment	
Samuel Ting	553

Introduction

The purpose of the Symposium is to discuss the origin, the status and the future of the new frontier of Physics, the Subnuclear World, whose first two hints were discovered in the middle of the last century: the so-called “Strange Particles” and the “Resonance $^{++}$ ”. It took more than two decades to understand the real meaning of these two great discoveries: the existence of the Subnuclear World with regularities, spontaneously plus directly broken Symmetries, and totally unexpected phenomena including the existence of a new fundamental force of Nature, called Quantum ChromoDynamics.

In order to reach this new frontier of our knowledge, new Laboratories were established all over the world, in Europe, in USA and in the former Soviet Union, with thousands of physicists, engineers and specialists in the most advanced technologies, engaged in the implementation of new experiments of ever increasing complexity. At present the most advanced Laboratory in the world is CERN where experiments are being performed with the Large Hadron Collider (LHC), the most powerful collider in the world, which is able to reach the highest energies possible in this satellite of the Sun, called Earth. To understand the laws governing the Space-Time intervals in the range of 10^{-17} cm and 10^{-23} sec will allow our form of living matter endowed with Reason to open new horizons in our knowledge.

■ ANTONINO ZICHICHI

Programme

SUNDAY, 30 OCTOBER 2011

9:00 Arrivals

13:30 Lunch at the Casina Pio IV

SESSION N. 1

15:00 *Welcome*

W. Arber, President of the Pontifical Academy of Sciences

M. Sánchez Sorondo, Chancellor of the Pontifical Academy of Sciences

15:10 Opening Lecture: *The Reasons for this Symposium on Past, Present and Future of Subnuclear Physics*

A. Zichichi

15:40 *Remarks on the History of String Theory and Supersymmetry*

J.H. Schwarz

16:10 *Achievements in Subnuclear Physics at Fermi-Lab*

P.J. Oddone

SESSION N. 2

16:40 *The Origin of LEP and LHC*

R. Aymar

17:10 *The Results Obtained with the First (pp) Collider ISR*

P. Darriulat

17:40 *From Nonlinear Statistical Mechanics to Nonlinear Quantum Mechanics – Concepts and Applications*

C. Tsallis

18:10 *The Cosmological Constant Problem and the Landscape of String Theory*

R. Bousso

18:40 End of Session n. 2

Cultural Event (19:30–22:30)

20:00 • **Visit to Michelangelo's Italian State Basilica Santa Maria degli Angeli e dei Martiri (*)**

• **Visit to the Galilei Divine Man Exhibit (**)**

21:00 Dinner at the State Basilica Santa Maria degli Angeli e dei Martiri

21:45 Concert of the *Organ* at the State Basilica

(*) The Basilica of St Mary of the Angels and Martyrs contains the following works of art by major contemporary artists: *Altar with Deposition* by Umberto Mastroianni (author of the Erice Monument), *The Angel of Light* by Ernesto Lamagna (author of the doors of the Papal Basilica of San Vito dei Normanni which enshrine the words of HH John Paul II: “*Voluntary Science is one of the noblest expressions of love for one's fellow men*”), *Skylight* by Narcissus Quagliata (engraved with the sentence by HH John Paul II: “*Science has its roots in the Immanent but leads man towards the Transcendent*”), *Angels' Gates* by Igor Mitoraj (dedicated to HH John Paul II), *Altar Pieces of Mary Magdalene* by Piero Guccione (illustrator of Galileo Galilei's book “*Discourses and Mathematical Demonstrations Relating to Two New Sciences*” with a foreword by HH John Paul II), *Ambo* by Giuseppe Gallo (author of the pendulum placed in the nave of the Basilica for the exhibition “*Galilei divine man*”).

(**) You can admire the bronze statue of *Galileo Galilei Divine Man* designed by the most famous Chinese physicist Tsung Dao Lee (former pupil of Enrico Fermi), Nobel laureate and Director of the prestigious CCAST (Chinese Center of Advanced Science and Technology). The statue is a gift by the CCAST scientists to the Italian State Basilica.

MONDAY, 31 OCTOBER 2011**SESSION N. 3**

- 9:00 *The High Energy Frontier: Past, Present and Future*
R.-D. Heuer
- 9:30 *Highlights from RHIC*
M.J. Tannenbaum
- 10:00 *The Birth of the First (pp) Collider*
K. Hubner
- 10:30 *The INFN Contribution to Subnuclear Physics in Europe*
E. Iarocci
- 11:00 *From Antideuterons to Antimatter-Clusters and Hyperclusters*
H. Stoecker

SESSION N. 4

- 11:30 *The Mystery of Neutrino Mixings*
G. Altarelli
- 12:00 *Hot Topics in QCD*
S. Brodsky
- 12:30 *Subnuclear Technology to Study Climate Problems*
J. Kirkby
- 13:00 *Black Holes in the Superworld*
S. Ferrara

13:30 Lunch at the Casina Pio IV

SESSION N. 5

- 15:00 *Highlights from ATLAS*
P. Jenni
- 15:30 *The Quark Model and QCD*
F. Close
- 16:00 *Composite Weak Bosons at the LHC*
H. Fritzsch
- 16:30 *Highlights from CMS*
T. Virdee

SESSION N. 6

- 17:00 *New Physics without New Energy Scale*
M. Shaposhnikov
- 17:30 *Results From The Xenon100 Dark Matter Search Experiment*
L. Baudis
- 18:00 Cultural Event
• **Visit to the world-famous Vatican Museums**
- 21:30 Dinner at the Casina Pio IV

TUESDAY, 1 NOVEMBER 2011**SESSION N. 7**

- 9:00 *Origin and Status of the Gran Sasso Lab*
L. Votano
- 9:30 *Neutrino Beam to Gran Sasso*
L. Evans
- 10:00 *OPERA Results on Neutrinos from CERN*
Y. Déclais
- 10:30 *Is there a Neutrino Speed Anomaly?*
J. Knobloch

11:00 Coffee Break

SESSION N. 8

- 11:30 *The Origin and Status of the Third Neutrino*
A. Bettini
- 12:00 *Status and Results of the LVD Experiment*
P. Giusti
- 12:30 *Origin and Status of Luna at Gran Sasso*
C. Brogini
- 13:00 *The Origin and Status of SBS (Spontaneously Broken Symmetries)*
F. Englert

13:30 Lunch at the Casina Pio IV

SESSION N. 9

- 15:00 *Study of the Low Energy Neutrinos from Sun and Earth with Borexino*
G. Bellini
- 15:30 *The Little Bang in the Laboratory*
P. Giubellino
- 16:00 *An Interesting Result at 7 TeV*
L. Cifarelli
- 16:30 *Perturbative Quantum Gravity from Gauge Theory*
Z. Bern

17:00 Coffee Break

SESSION N. 10

- 17:30 *Subnuclear Physics – Technology to Benefit Humanity*
H. Newman
- 18:00 *Blueprints of the No-Scale Multiverse at the LHC*
D.V. Nanopoulos
- 18:30 *Black Holes and Qubits*
M.J. Duff
- 19:00 *Mass Hierarchies in String Theory and Experimental Predictions*
I. Antoniadis
- 20:30 Dinner at the Casina Pio IV

WEDNESDAY, 2 NOVEMBER 2011

SESSION N. 11

- 9:00 *The LAA Project and the Consequences on LHC*
H. Wenninger
- 9:30 *The Lattice Fields in the LHC Era*
R.D. Kenway
- 10:00 *The Large Hadron Collider of CERN and the Roadmap Toward Higher Performance*
L. Rossi
- 10:30 *Latest Results from MRPC Time Resolution*
C. Williams

11:00 Coffee Break

SESSION N. 12

- 11:30 *The Origin and the Results Obtained at HERA*
A. Wagner
- 12:00 *Search for Nuclear Antimatter in Space*
S.C.C. Ting
- 12:30 General Discussion
- 13:00 *Conclusions*
A. Zichichi

13:30 Lunch at the Casina Pio IV

14:30 Departure

List of Participants

Prof. Werner Arber

President of the Pontifical Academy of Sciences; Biozentrum, Department of Microbiology, University of Basel
Basel (Switzerland)

H.E. Msgr. Marcelo Sánchez Sorondo

Chancellor
The Pontifical Academy of Sciences
(Vatican City)

Prof. Guido Altarelli

Physics Department
University of Roma Tre
Rome (Italy)

Prof. Ignatios Antoniadis

Centre de Physique Théorique
École Polytechnique
Palaiseau (France)

Prof. Robert Aymar

CERN
Geneva (Switzerland)

Prof. Rinaldo Baldini Ferroli

Enrico Fermi Centre
Rome (Italy)

Prof. Laura Baudis

University of Zürich
Zürich (Switzerland)

Prof. Gianpaolo Bellini

Physics Department
Milan University
Milan (Italy)

Prof. Zvi Bern

University of California at Los Angeles – UCLA
Los Angeles, CA (USA)

Prof. Sergio Bertolucci

CERN – Research Director
Geneva (Switzerland)

Prof. Alessandro Bettini

INFN and University of Padua (Italy) *and*
Canfranc Underground Laboratory,
Canfranc (Spain)

Prof. Raphael Bousso

Center for Theoretical Physics and
Department
of Physics
University of California
Berkeley, CA (USA)

Prof. Stanley J. Brodsky

SLAC National Accelerator Laboratory
Stanford University, CA (USA)
and Southern Denmark University
Odense (Denmark)

Prof. Carlo Brogini

University of Padua and INFN
Padua (Italy)

Prof. Luisa Cifarelli

University of Bologna and INFN
Bologna (Italy)

Prof. Frank Close

Rudolf Peierls Centre for Theoretical Physics
University of Oxford
Oxford (UK)

Prof. Eugenio Coccia

INFN and Department of Physics
Tor Vergata University
Rome (Italy)

Prof. Michael J. Creutz

Brookhaven National Laboratory (BNL)
Upton, NY (USA)

Prof. Pierre Darriulat

Vietnam Auger Training Laboratory
Institute for Nuclear Science & Technology
Hanoi (Vietnam)

Prof. Yves Déclais

IPNL/IN2P3/CNRS/Lyon University
Domaine Scientifique de la Doua
Villeurbanne Cedex (France)

Prof. Dmitri Denisov

Fermilab
Batavia, IL (USA)

Prof. Michael James Duff

Imperial College London
London (UK)

Prof. François Englert

Université Libre de Bruxelles
Brussels (Belgium)

Prof. Lyn Evans

CERN
Geneva (Switzerland)

Prof. Sergio Ferrara

CERN
Geneva (Switzerland) *and*
LNF-INFN
Frascati (Italy)

Prof. Harald Fritzsch

Ludwig-Maximilians-Universität
Munich (Germany)

Prof. Piero Galeotti

Department of Physics
University of Torino
Turin (Italy)

Prof. Paolo Giubellino

Università degli Studi di Torino
Turin (Italy)

Prof. Paolo Giusti

University of Bologna and INFN
Bologna (Italy)

Prof. Rolf-Dieter Heuer

DG CERN
Geneva (Switzerland)

Prof. Kurt Hübner

CERN
Geneva (Switzerland)

Prof. Enzo Iarocci

La Sapienza University
Rome (Italy)

Prof. Adam Włodzimierz Jacholkowski

CERN
Geneva (Switzerland)

Prof. Peter Jenni

CERN, PH Department
Geneva (Switzerland)

Prof. Richard D. Kenway

University of Edinburgh
Edinburgh, Scotland (UK)

Prof. Jasper Kirkby

CERN, PH Department
Geneva (Switzerland)

Prof. Juergen Knobloch

CERN, PH Department
Geneva (Switzerland)

Prof. Antonio Masiero

Direttore INFN Sezione di Padova
Padua (Italy)

Prof. Dimitri V. Nanopoulos

Texas A&M University
College Station, TX (USA)

Prof. Harvey Newman

California Institute of Technology (Caltech)
Pasadena, CA (USA)

Prof. Piermaria J. Oddone

Director Fermi National Accelerator Lab
Batavia, IL (USA)

Prof. Lucio Rossi

CERN
Geneva (Switzerland)

Prof. John Henry Schwarz

C.C. Laritsen Lab of High Energy Physics
CALTECH
Pasadena, CA (USA)

Prof. Michael Shaposhnikov

Ecole Polytechnique Federale de Lausanne
(EPFL); Institute of Theoretical Physics
Laboratory for Particle Physics and
Cosmology
Lausanne (Switzerland)

Prof. Graham M. Shore

University of Wales
Swansea (UK)

Prof. Horst Stöcker

GSI
Darmstadt (Germany)

Prof. Michael J. Tannenbaum

Brookhaven National Laboratory
Upton, NY (USA)

Prof. Thomas Taylor

CERN
Geneva (Switzerland)

Prof. Samuel C.C. Ting

Thomas Dudley Cabot Professor of Physics
Massachusetts Institute of Technology
Cambridge, MA (USA)

Prof. Constantino Tsallis

Head, Department of Theoretical Physics
Centro Brasileiro de Pesquisas Fisicas *and*
Head, National Inst. of Science and Technology
for Complex Systems, Rio de Janeiro (Brazil)

Prof. Tejinder Virdee

Department of Physics
Imperial College, London, UK *and*
CERN
Geneva (Switzerland)

Prof. Lucia Votano

Director LNGS
L'Aquila (Italy)

Prof. Albrecht Wagner

DESY
Hamburg (Germany)

Prof. Horst Wenninger

CERN
Geneva (Switzerland)

Dr. Crispin Williams

CERN
Geneva (Switzerland)

Prof. Antonino Zichichi

CERN, Geneva (Switzerland) *and*
INFN and University of Bologna (Italy) *and*
President Enrico Fermi Centre, Rome (Italy)

Scientific Papers

THE REASONS FOR THIS SYMPOSIUM ON PAST, PRESENT AND FUTURE OF SUBNUCLEAR PHYSICS

■ ANTONINO ZICHICHI

*Pontifical Academy of Sciences, Vatican City
INFN and University of Bologna, Italy
CERN, Geneva, Switzerland
World Federation of Scientists, Beijing, Geneva, Moscow, New York*

This is the first time that the Pontifical Academy of Sciences places the field of Subnuclear Physics at the centre of its attention. On behalf of all my colleagues engaged in this frontier of Modern Science I would like to express to our President, H.E. Professor Werner Arber and to our Chancellor H.E. Monsignor Marcelo Sánchez Sorondo, our deep gratitude.

This Seminar has two purposes: one is *Pure Physics*, the other is *Scientific Culture*.

Our field of activity competes in terms of number of people and of financial support with gigantic projects such as the one aimed at having the man going to the satellite of the Sun called Mars. This is why we cannot ignore the “tax payers”, i.e. the Culture of our Time, called Modern Culture.

As you know H.H. Benedict XVI has focused the attention of Modern Culture to the complex property of our form of living matter called Reason.

The greatest achievement of Reason in the Immanentistic Sphere of our existence is the Rigorous Experimental Logic, called Science.

- Science is the latest achievement of Reason;
- it came 3 thousands years after the discovery of the Rigorous Theoretical Logic, called Mathematics;

- and 10 thousands years (probably even 50.000) after the discovery of Permanent Collective Memory (better known as Written Language).

The future of Subnuclear Physics needs our engagement in order to have the Culture of our Time supporting Subnuclear Physics. For this to happen depends on our engagement for Scientific Culture. Let me give you an example.

When people see my friend David Scott, Commander of Apollo XV, performing the famous Galilei experiment at the Moon and saying “*Galilei was Right*” we need to explain that if this could be done it is because in our Labs we have been able to continue the Galileian search in trying to understand the Logic of Nature: i.e. first level Science.

Tonight you will see the NASA film at the Michelangelo’s Italian State Basilica “*Santa Maria degli Angeli e dei Martiri*”.

It is first level Science that has given all instruments we use in every day-life and the life-expectations of over 80 years to our form of living matter.

We need to let “tax payers” know that the effective motor for progress in the immanent part of our world is scientific discovery, which is a direct consequence of Reason.

Thanks to H.H. Benedict XVI, Reason is finally going to be a strong part of Modern Culture.

Our field is the most recent achievement of Reason in the search to understand the Logic of Nature.

It was borned slightly more that a (1/2) century ago, in 1947 with three discoveries:

- 1) the Lamb-shift;
- 2) the so much wanted but never found before “nuclear glue”, i.e. the π -meson and
- 3) the “Strange-particles”.

Let me show few pictures of years 1929, 1947, 1947 and 1963.

– 1929 –



Figure 1: Lord Patrick Maynard Stuart Blackett, Pyotr L. Kapitza, Paul Langevin, Lord Ernest Rutherford, Charles Thomson Rees Wilson outside Cavendish Laboratory (1929).

– 1947 –

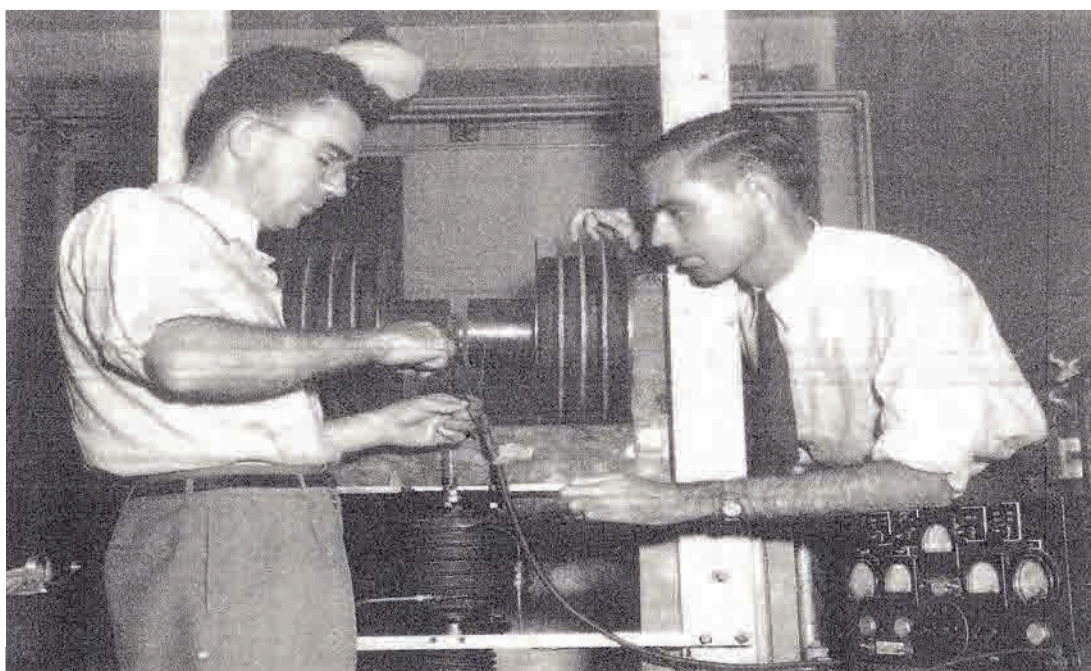


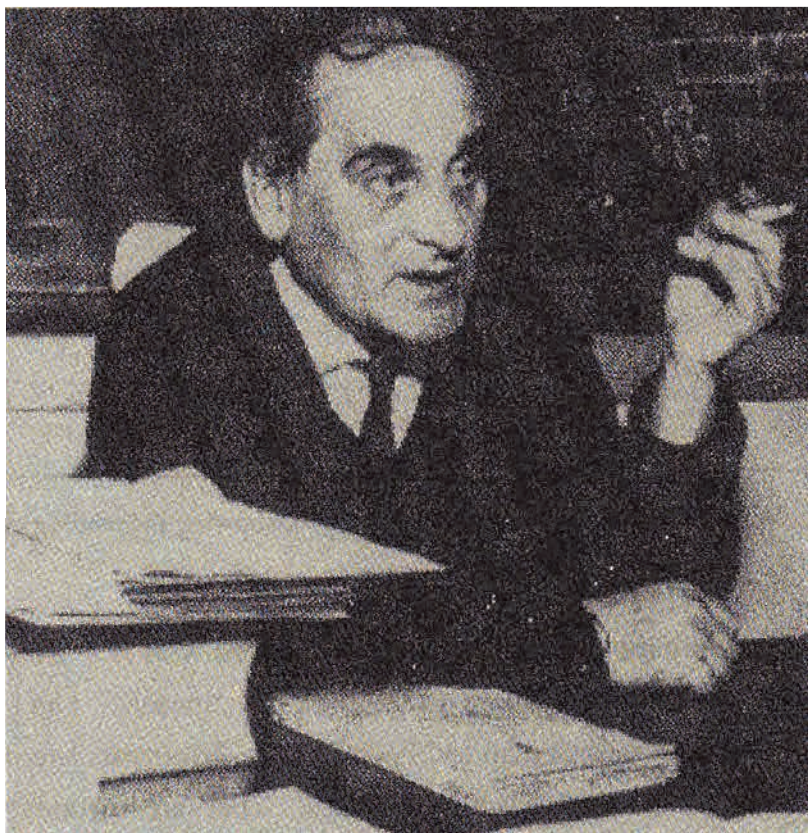
Figure 2: This picture was taken in September 1947 and shows W.E. Lamb and R. Retherford working on the Lamb-shift experiment.

– 1947 –

π –meson



Giuseppe Occhialini and Cecil Frank Powell

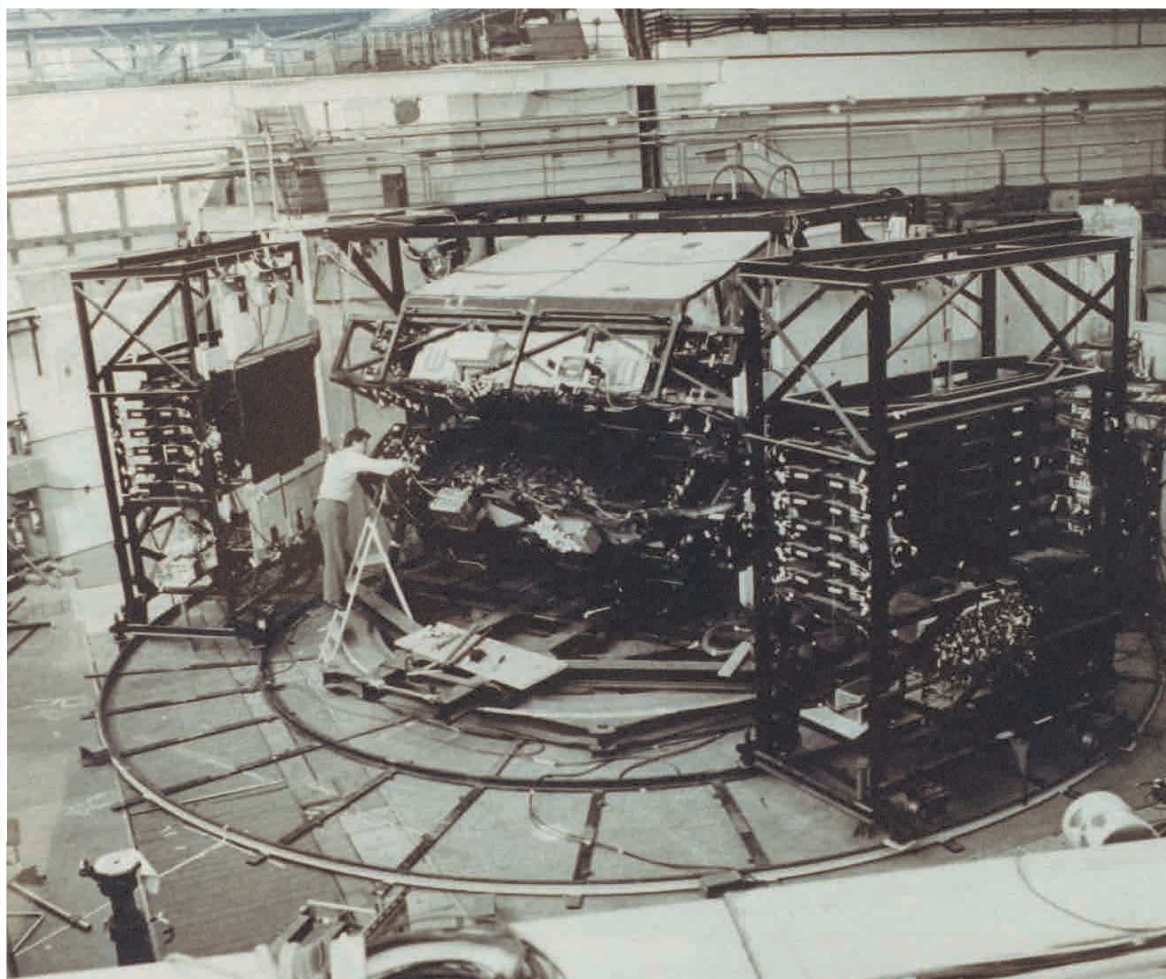


Giuseppe Occhialini

Figure 3

– 1963 –

This is the first example of what is now "standard" in experimental subnuclear physics: very large acceptance detectors.



On the rails the “neutron missing mass spectrometer”.

PAPLEP
Proton AntiProton into Lepton Pairs
first search for the 3rd lepton
and
 $\theta_{PS} \neq \theta_V$.

Figure 4

The “pre-shower” technology implemented in the CERN experimental set-up for the study of the rare decay modes of the pseudoscalar and vector mesons.

SUBNUCLEAR PHYSICS: PAST, PRESENT AND FUTURE

Why Past?

Enrico Fermi: *Neither Science Nor Civilization Could Exist Without Memory.*

On the occasion of the twenty-fifth anniversary of the Ettore Majorana Foundation and Centre for Scientific Culture (EMFCSC), in order to promote the values of scientific culture worldwide and following a proposal by the World Federation of Scientists (WFS), a special law was voted unanimously by the Sicilian Parliament to establish the

“Ettore Majorana Prize – Erice – Science for Peace”.

The Prize is to be awarded to men of Culture and Science, who played a leading role in promoting and implementing the goals outlined in the “Erice Statement”.

P.A.M. Dirac, P.L. Kapitza, A.D. Sakharov, E. Teller, V.F. Weisskopf, J.B.G. Dausset, S.D. Drell, M. Gell-Mann, H.W. Kendall, L.C. Pauling, A. Salam, C. Villi, R. Doll, J.C. Eccles, T.D. Lee, L. Montagnier, Qian Jaidong, J.S. Schwinger, U. Veronesi, G.M.C. Duby, R.L. Garwin, S.L. Glashow, D.C. Hodgkin, R.Z. Sagdeev, K.M.B. Siegbahn, Y.P. Velikhov, J. Karle, J.M.P. Lehn, A. Magnéli, N.F. Ramsey, H. Rieben, J.J. van Rood, C.S. Wu, R.L. Mössbauer, A. Müller, H. Kohl, M.S. Gorbachev, H.H. John Paul II, R. Clark, M. Cosandey, A. Peterman, R. Wilson, J. Alderdice, J.J. Friedman, M. Koshiha, S. Coleman, A.N. Chilingarov, P.C.W. Chu, L. Esaki, W.N. Lipscomb Jr., J. Szysko, M.-K. Wu, H.A. Hauptman, D.H. Hubel, R. Huber, B.I. Samuelsson, H. Sun, A.E. Yonath, G. 't Hooft, Y.T. Lee, W. Arber, S.C.C. Ting.

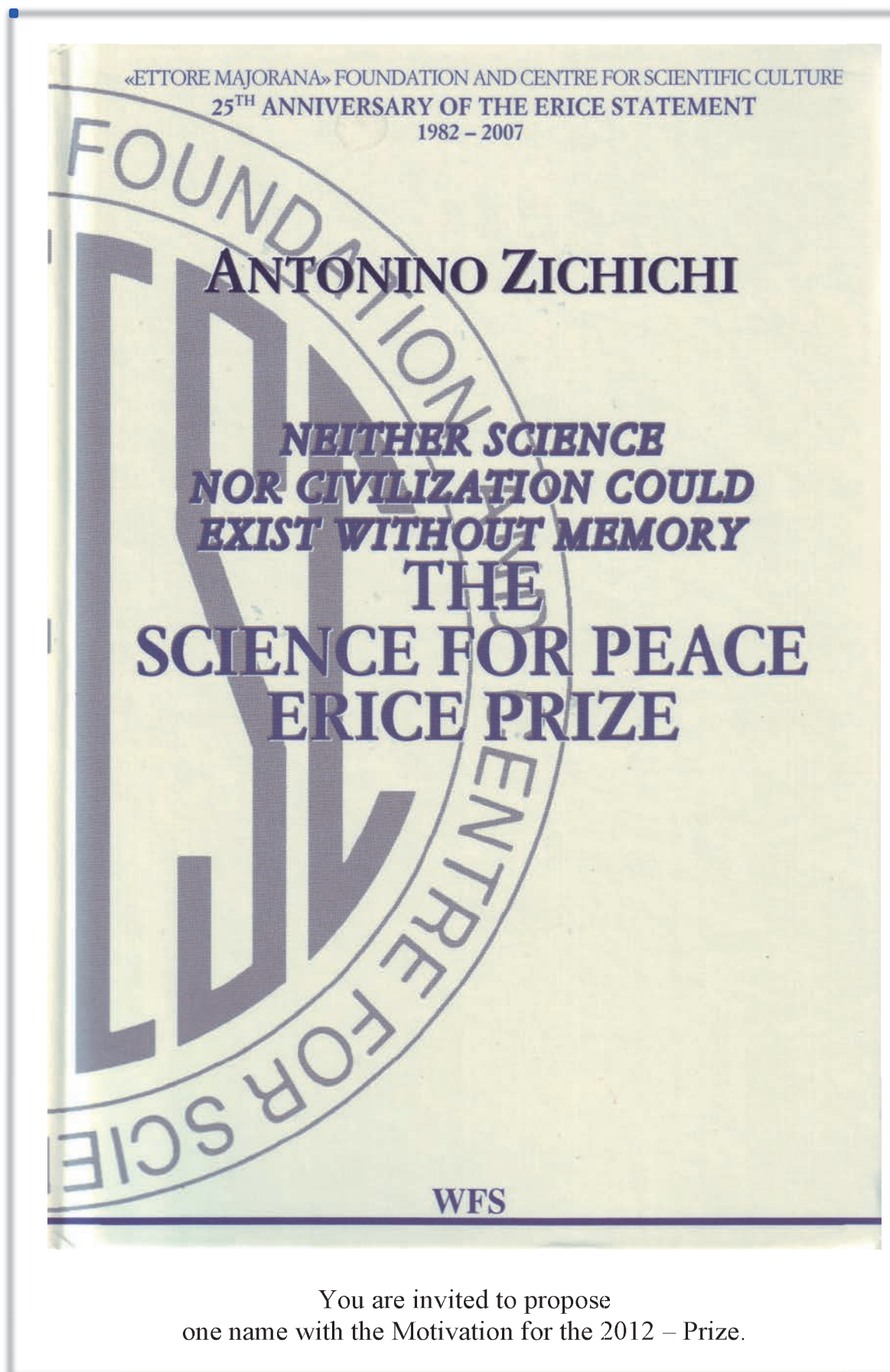


Figure 5

Present and Future need no explanation

1947 SUBNUCLEAR PHYSICS is born
 Lamb-shift
 π -meson
 Strange particles

These three great discoveries are now understood as being:

- 1) the first example of “virtual” physics;
- 2) the first example of a bound system made of a quark-antiquark ($q\bar{q}$) pair;
- 3) the first example of a new flavour beyond the first family.

Without “Virtual Physics” we could never have reached the dream of Gauge Unification and the great competition with Historian who have invented “Virtual History”.

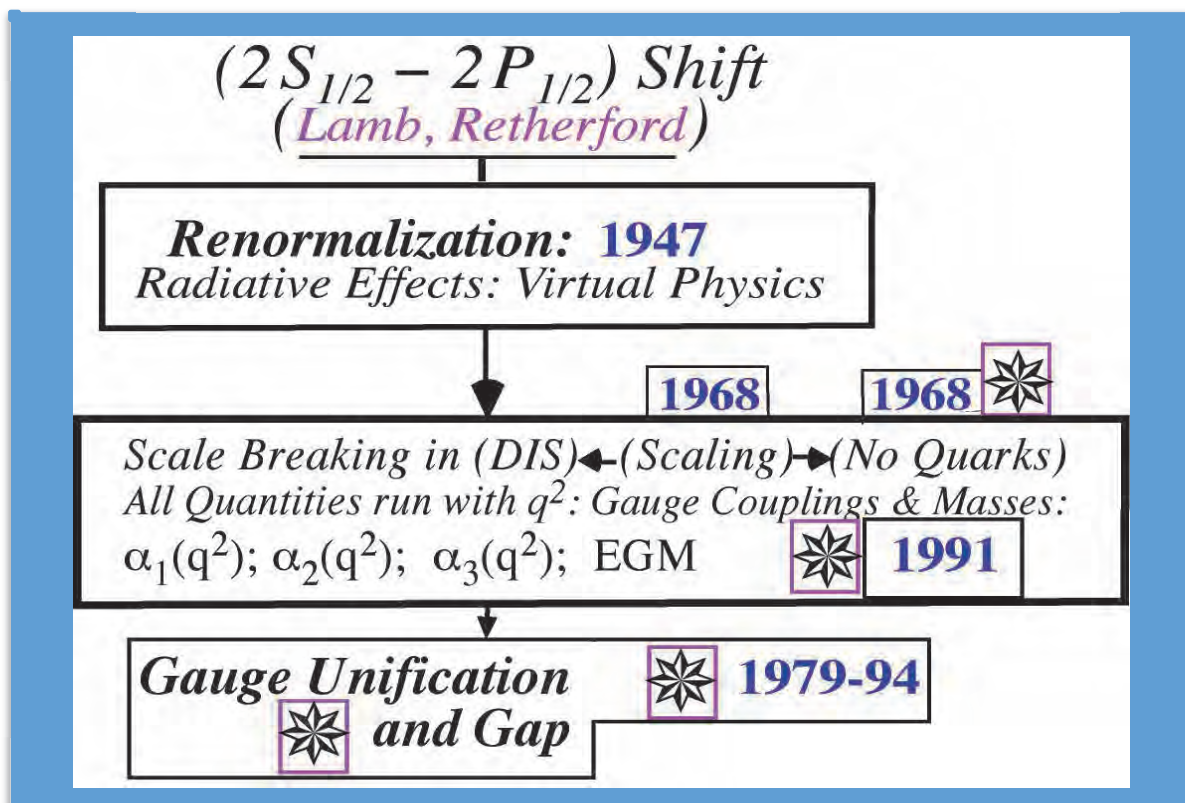


Figure 6

GUT (Grand Unified Theory): the Mathematics

THE UNIFICATION OF ALL FUNDAMENTAL FORCES

The lines in Figure 8 result from calculations executed with a supercomputer using the following system of equations:

$$\mu \frac{d\alpha_i}{d\mu} = \frac{b_i}{2\pi} \alpha_i^2 + \sum_j \frac{b_{ij}}{8\pi^2} \alpha_i \alpha_j$$

This is a system of coupled non-linear differential equations where the existence of the Superworld is taken for granted. This system describes how the gauge couplings $(\alpha_1, \alpha_2, \alpha_3)$ vary with “ μ ”, the basic parameter which depends on the energy of the elementary process, from the maximum level of Energy (Planck Scale) to the energy level of our world.

Figure 7

During more than ten years (from 1979 to 1991), no one had realized that the energy threshold for the existence of the Superworld was strongly dependent on the “running” of the masses.

This is now called: the EGM effect (from the initials of Evolution of Gaugino Masses).

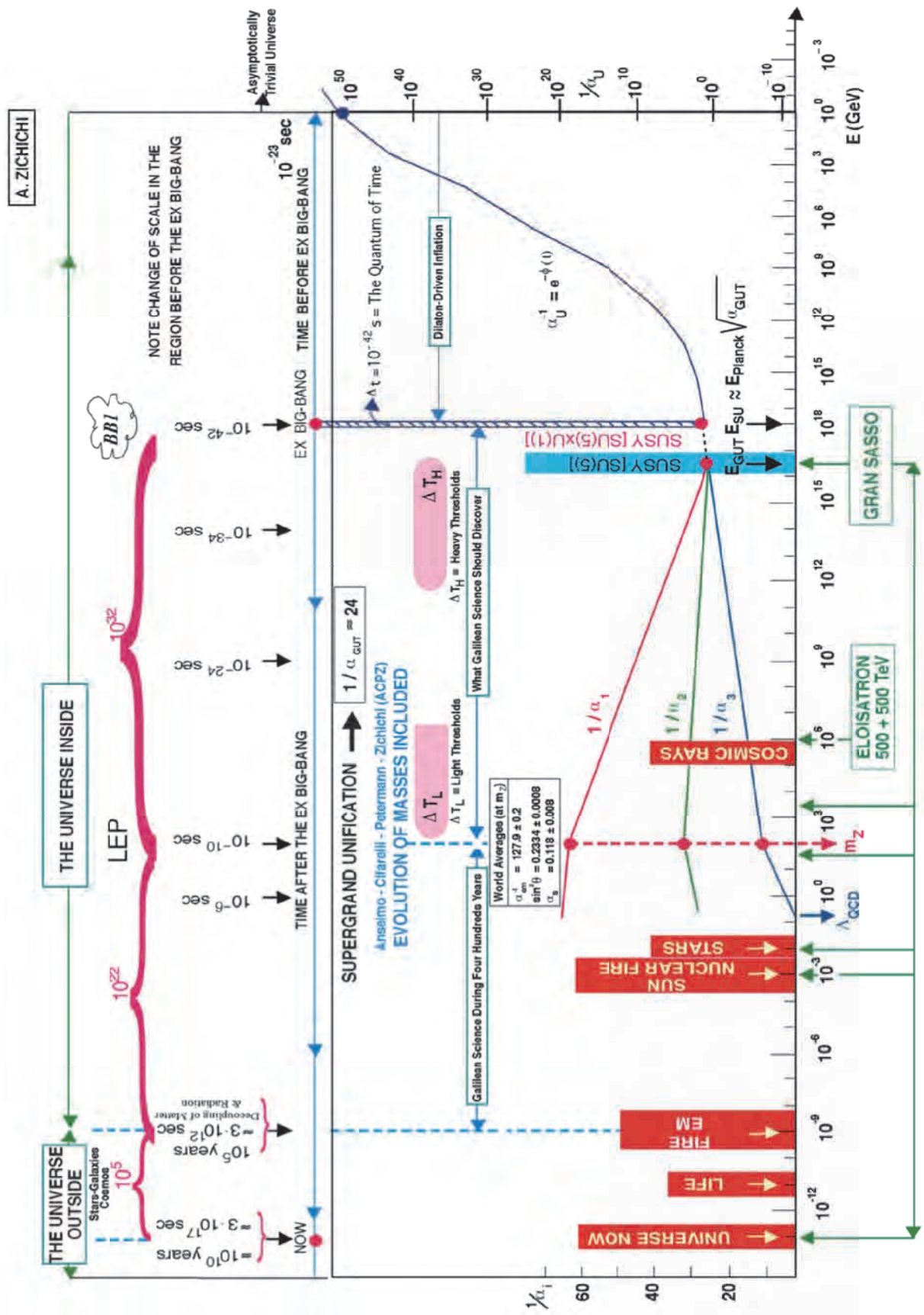


Figure 8

To compute the energy threshold using only the “running” of the gauge couplings ($\alpha_1, \alpha_2, \alpha_3$) corresponds to neglecting nearly three orders of magnitude in the energy threshold for the discovery of the first particle (the lightest) of the Superworld [1], as illustrated in Figure 9.

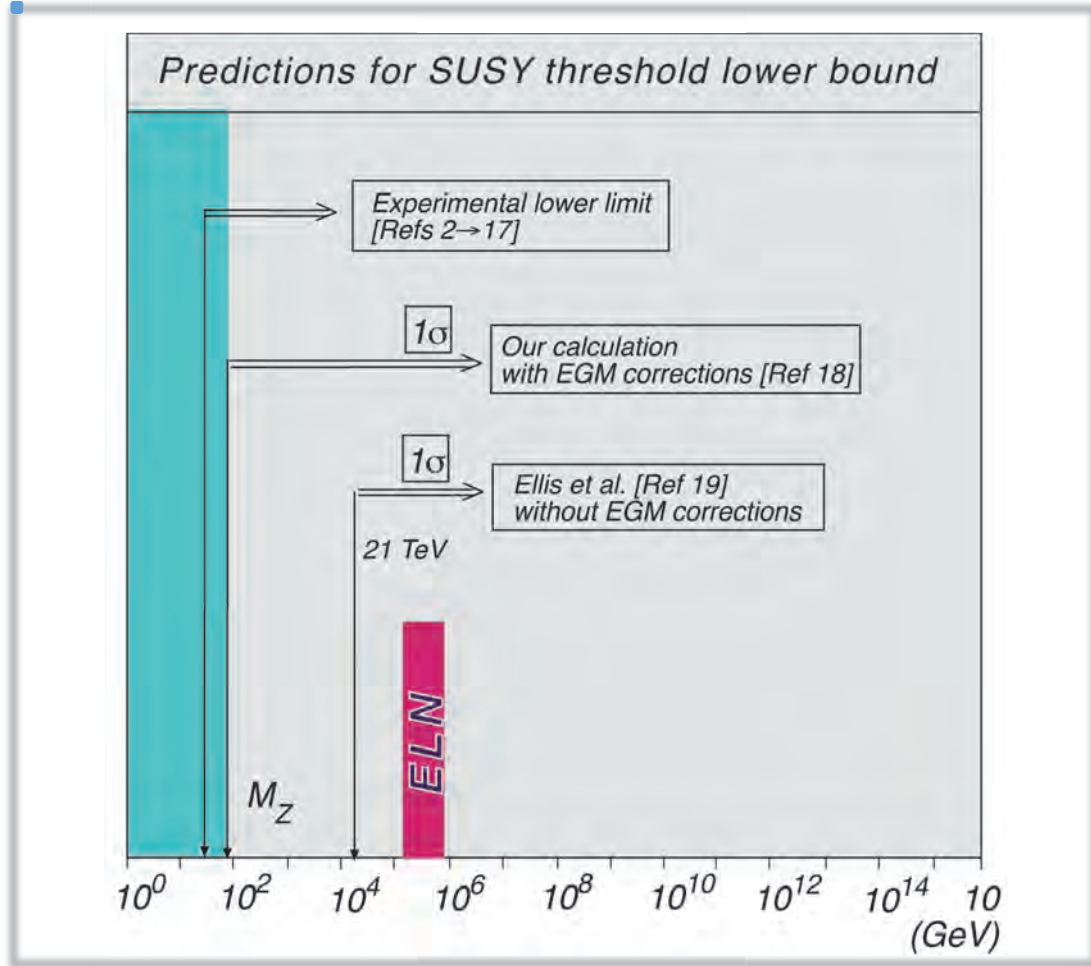


Figure 9

Figure 9 illustrates the EGM effect which lowers by a factor 700 the threshold for the production of the lightest superparticle.

The mathematical formalism used to obtain the results shown in Figures 8 and 9 is a system of three differential non-linear equations (shown in Figure 7) describing how the gauge couplings

$$\alpha_i, \alpha_j \text{ (with } i = 1, 2, 3; \text{ and } J = 1, 2, 3 \text{ but } i \neq j),$$

vary with “ μ ”, the basic parameter which depends on the energy of a given elementary process.

DETAILS

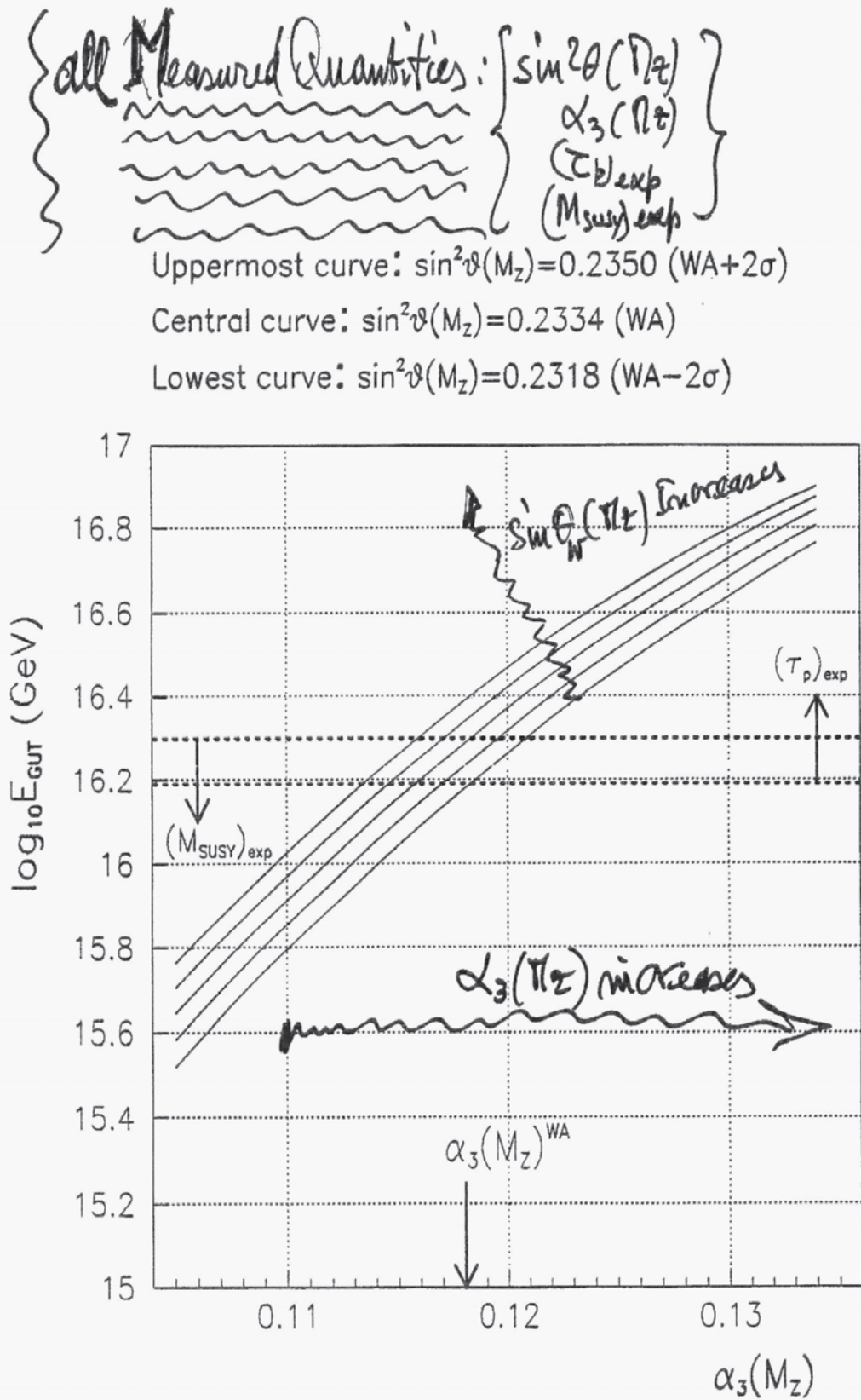


Figure 10

The GAP between E_{GUT} and E_{Planck}

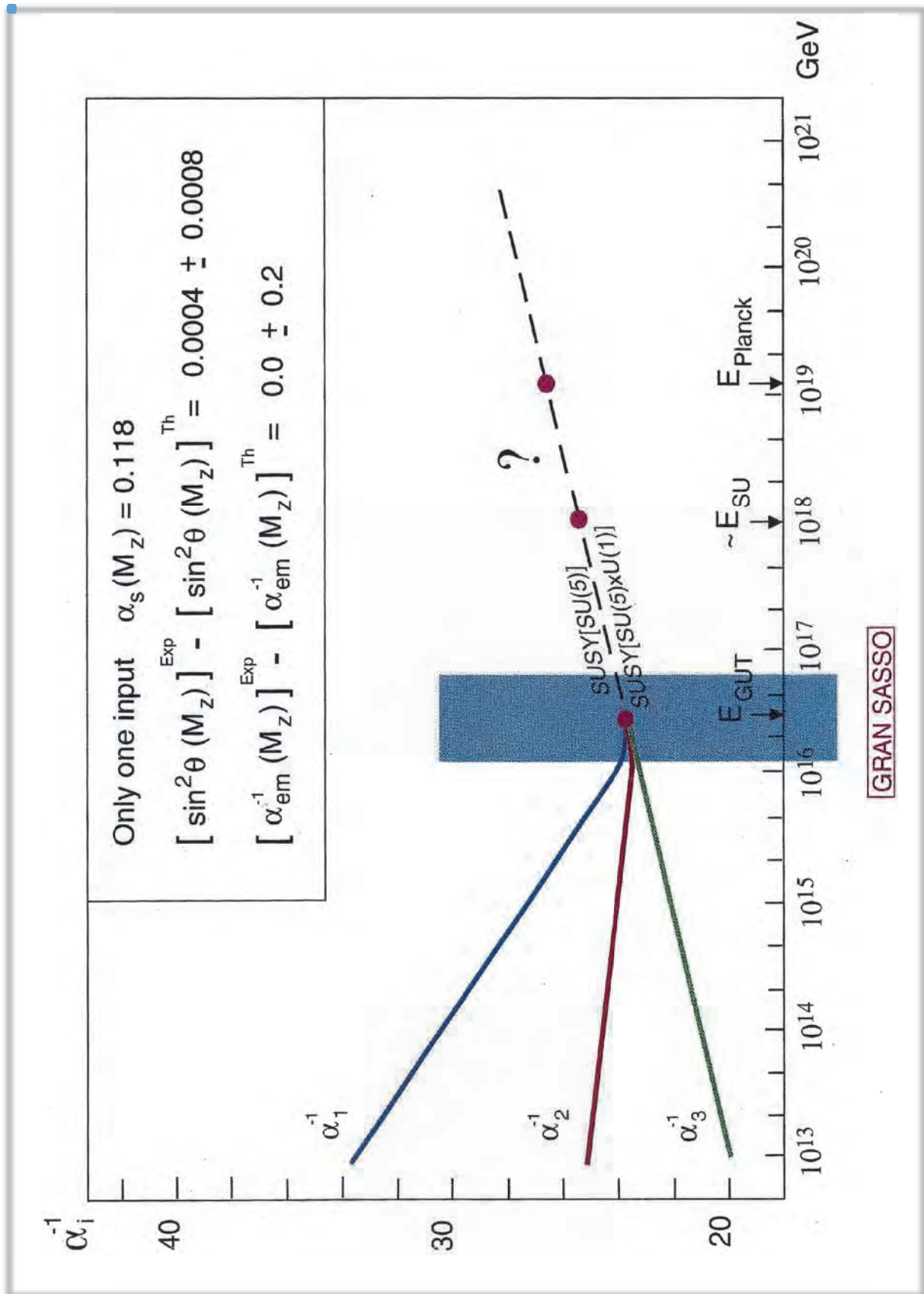


Figure 11

A different way to describe how the gauge couplings α_1 , α_2 , α_3 vary with energy is reported in Figure 12. The simplest way to get GUT (the point where all fundamental forces are together: Grand Unification Theory) would be the straight line. But the real world does not follow this “platonic” straight line.

The sequence of points (the big red points), in steps of 100 GeV, is very different from the Platonic line (dotted blue points). The way nature goes is reported by the sequence of the big red points which are the result of the mathematics reported in Figure 12.

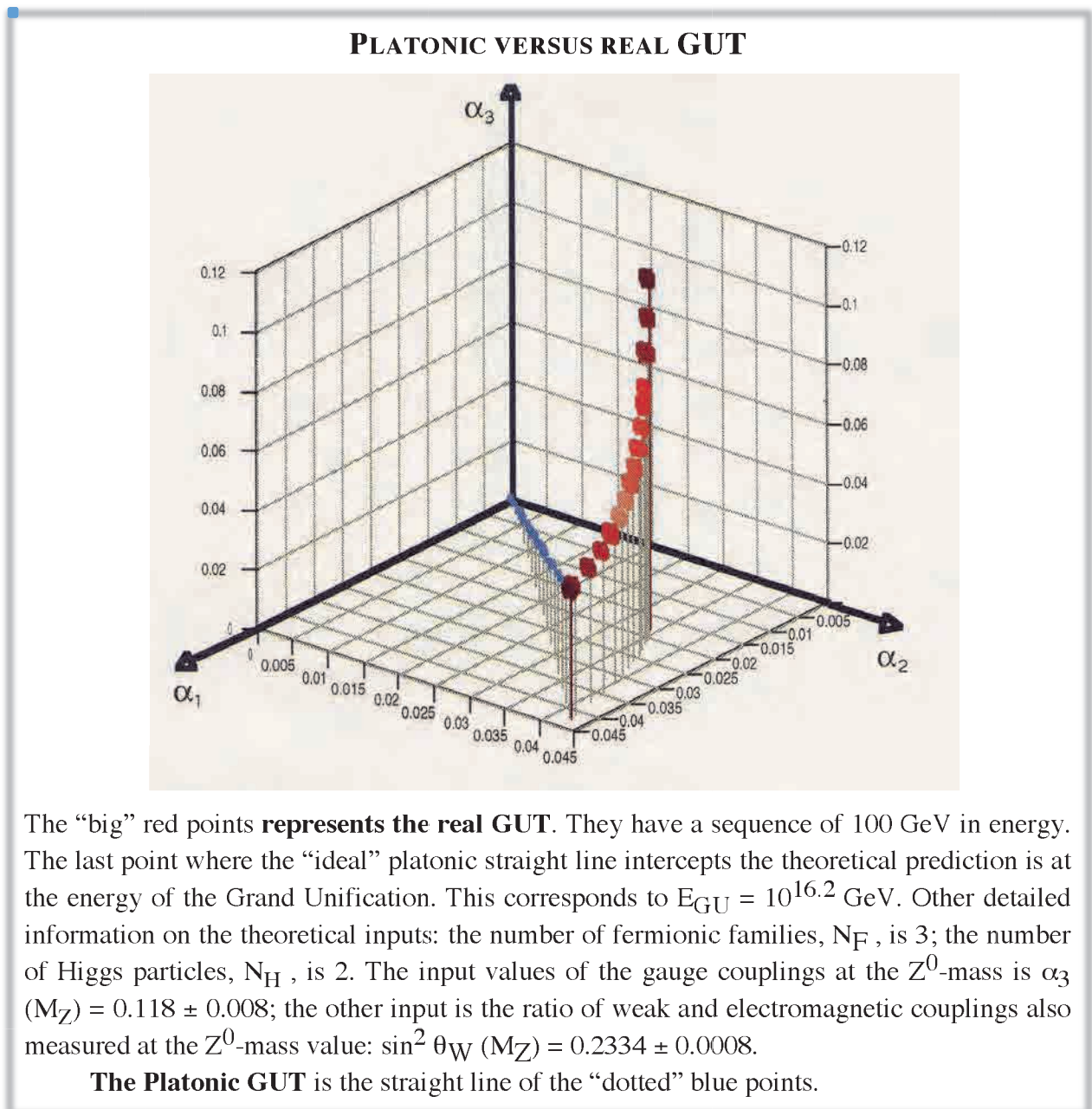


Figure 12

All problems mentioned so far are based on computations using the existence of Virtual Phenomena which have to obey the Fundamental Logic of Nature, i.e. Virtual Physics which is the most exact limit we are able to compute towards the perfect knowledge of the Logic of Nature started by Galileo Galilei.

Virtual Physics has given rise to the existence of Virtual History.

From Virtual Physics to Virtual History

What is Virtual History? If we compare Virtual History and Virtual Physics, the conclusion is that only if destiny was there Virtual History could obey the same Logic as Virtual Physics does.

VIRTUAL HISTORY

‘WHAT IF?’			
	In History = EWRL		In Science = EBUS
I	What if Julius Caesar had been assassinated many years before?	I	What if Galileo Galilei had not discovered that $F = mg$?
II	What if Napoleon had not been born?	II	What if Newton had not discovered that $F = G \frac{m_1 \cdot m_2}{R_{12}^2} ?$
III	What if America had been discovered a few centuries later?	III	What if Maxwell had not discovered the unification of electricity, magnetism and optical phenomena, which allowed him to conclude that light is a vibration of the EM field?
IV	What if Louis XVI had been able to win against the ‘Storming of the Bastille’?	IV	What if Planck had not discovered that $h \neq 0 ?$
V	What if the 1908 Tunguska Comet had fallen somewhere in Europe instead of Tunguska in Siberia?	V	What if Lorentz had not discovered that space and time cannot both be real?
VI	What if the killer of the Austrian Archduke Francisco Ferdinand had been arrested the day before the Sarajevo event?	VI	What if Einstein had not discovered the existence of time-like and space-like real worlds? Only in the time-like world, simultaneity does not change, with changing observer.
VII	What if Lenin had been killed during his travelling through Germany?	VII	What if Rutherford had not discovered the nucleus?
VIII	What if Hitler had not been appointed Chancellor by the President of the Republic of Weimar Paul von Hindenburg?	VIII	What if Hess had not discovered cosmic rays?
IX	What if the first nuclear weapon had been built either by Japan before Pearl Harbour (1941) or by Hitler in 1942 or by Stalin in 1943?	IX	What if Dirac had not discovered his equation, which opens new horizons, including the existence of the antiworld?
X	What if Nazi Germany had defeated the Soviet Union?	X	What if Fermi had not discovered weak forces?
XI	What if Karol Wojtyla had not been elected Pope, thus becoming John Paul II?	XI	What if Fermi and Dirac had not discovered the Fermi–Dirac statistics?
XII	What if the USSR had not collapsed?	XII	What if the ‘strange particles’ had not been discovered in the Blackett Lab?

Table 1

1947

SUBNUCLEAR PHYSICS

is born

Lamb-shift

OK

π -meson

NOW

Strange particles

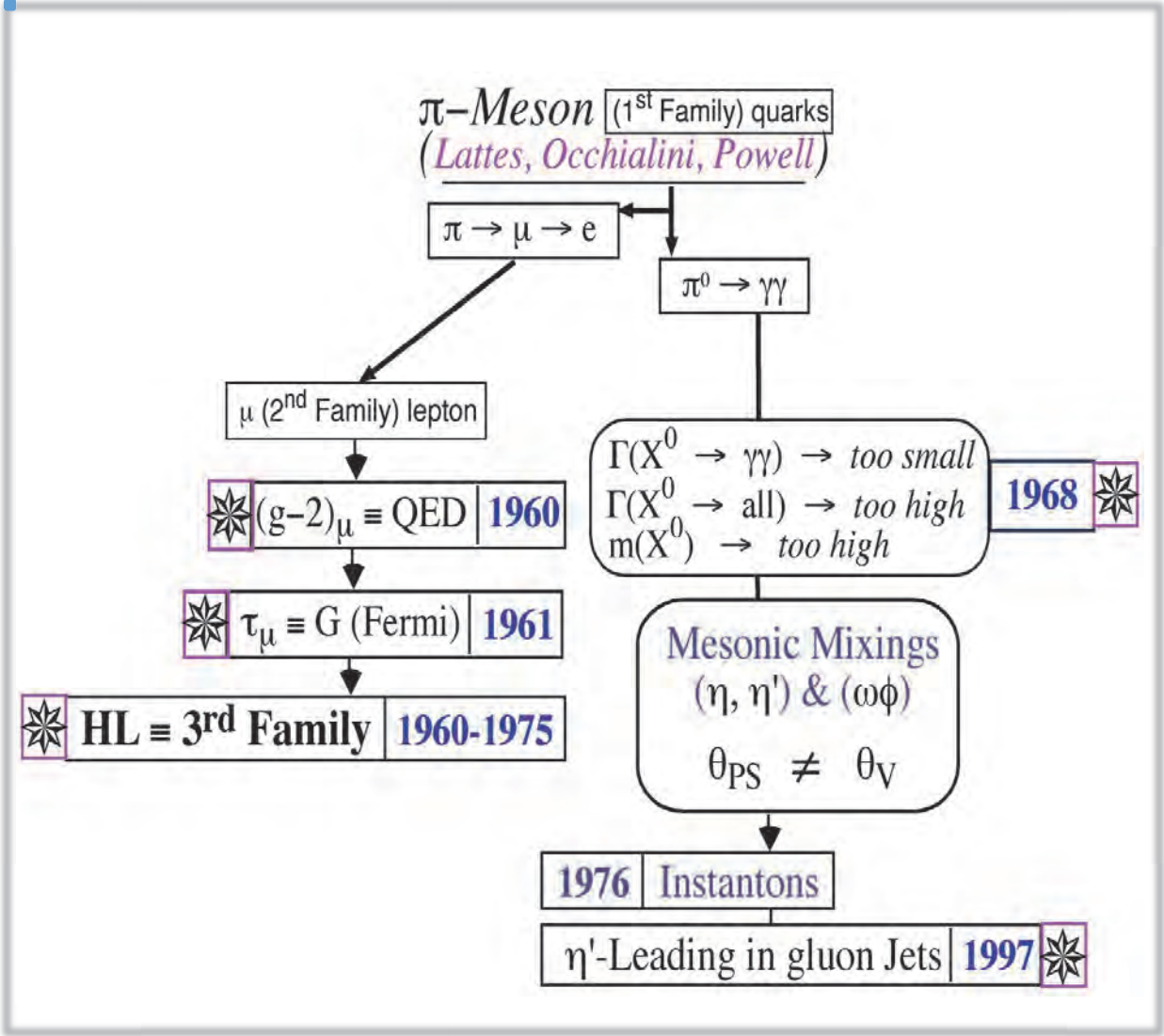


Figure 13

From the π -meson to the Third Family of Leptons

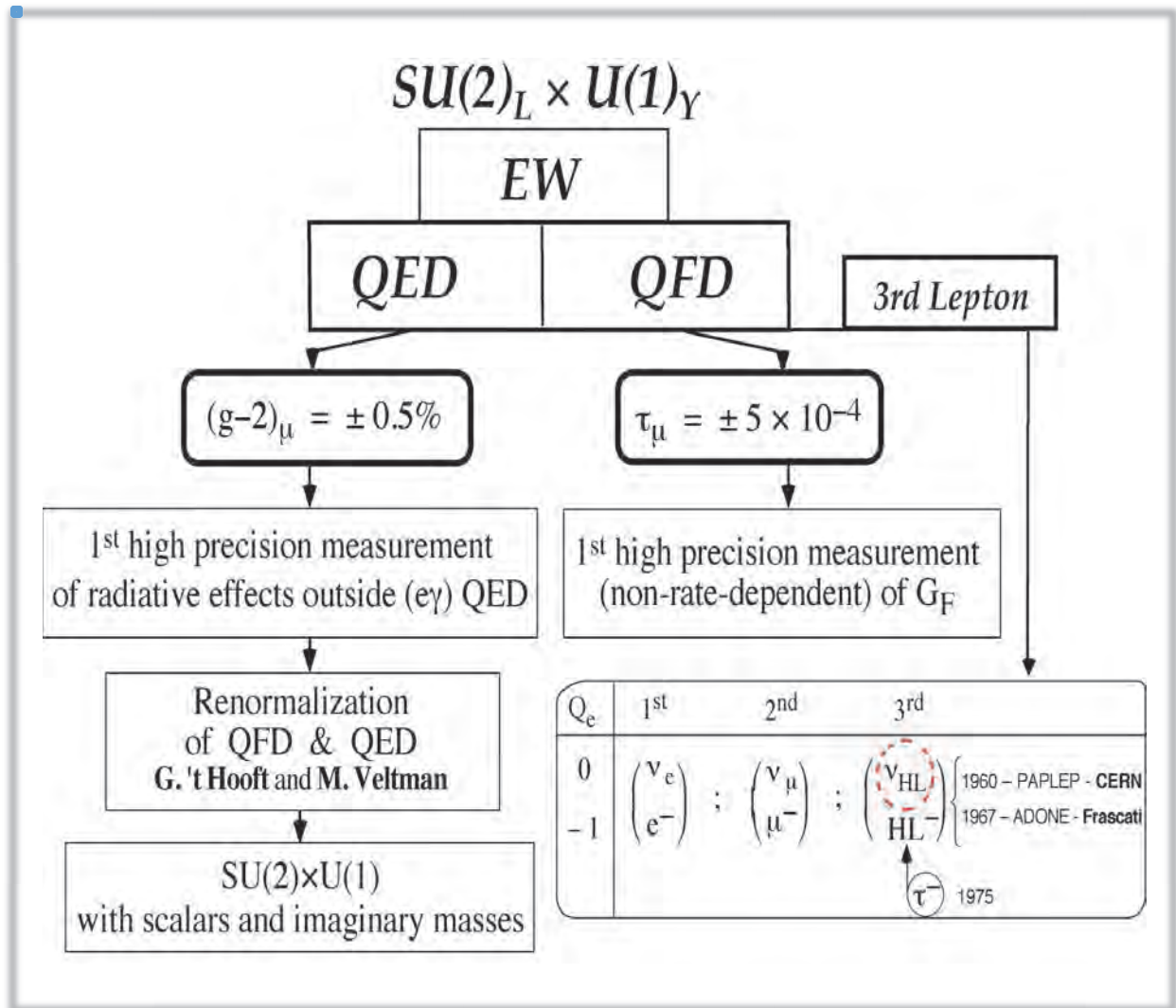


Figure 14

$$* \quad (g-2)_\mu \equiv (\pm) 0,5\%$$

This experiment required the construction of the largest and highest precision "flat" magnet of the world, whose schematic drawing is reported in Figure 15.

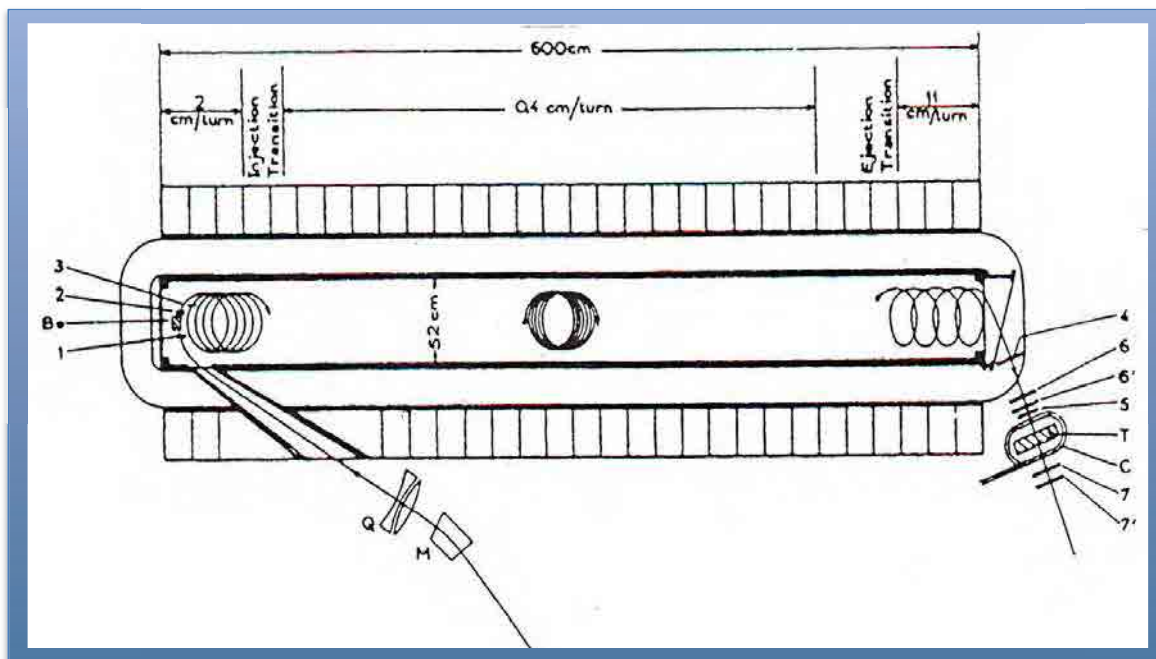


Figure 15: (Figure from [20]). General plan of the 6-metre magnet. M : bending magnet; Q : pair of quadrupoles; 1, Be, 2, 3: injection assembly consisting of Be-moderator and counters 1, 2, 3; T : methylene-iodide target; counters 66', 77': "backward" and "forward" electron telescopes. A stored and ejected muon is registered as a coincidence 4, 5, 66' $\bar{7}$, gated by a 1, 2, 3 and by either a forward or backward electron signal.

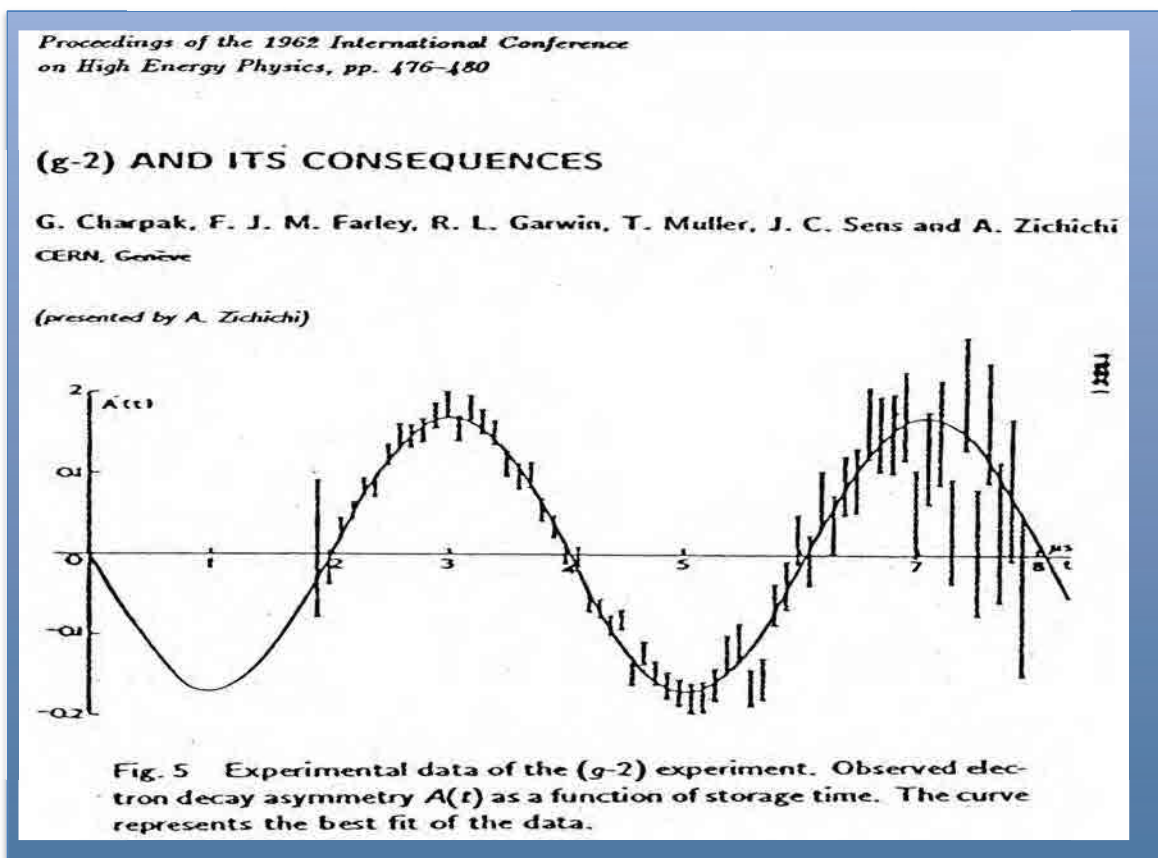


Figure 16

Fig. 5 Experimental data of the (g-2) experiment. Observed electron decay asymmetry $A(t)$ as a function of storage time. The curve represents the best fit of the data.

RESULTS OF G - 2 EXPERIMENT	
Experimental	Theoretical
	$\frac{g-2}{2} = \frac{\alpha}{2\pi} + 0.75 \left(\frac{\alpha}{\pi}\right)^2$
$\frac{g-2}{2} = 0.001162 \pm 0.000005$	$= 0.001161 + 0.000004$
	$= 0.001165$
Muon mass	$= (206.768 \pm 0.003) m_e$
Charge of muon	$= (1.00000 \pm 0.00005) e$
Charge of ν_μ	$= (0.00000 \pm 0.00005) e$

18 December 1961.

Figure 17

The first high precision measurement of QED radiative effects outside the (electron and photon) world [21] are in Figures 16 and 17.

Conclusion: the μ is a heavy electron to within $\pm 0.5\%$.

$$\tau_\mu = GF \equiv \pm 5 \times 10^{-4}$$

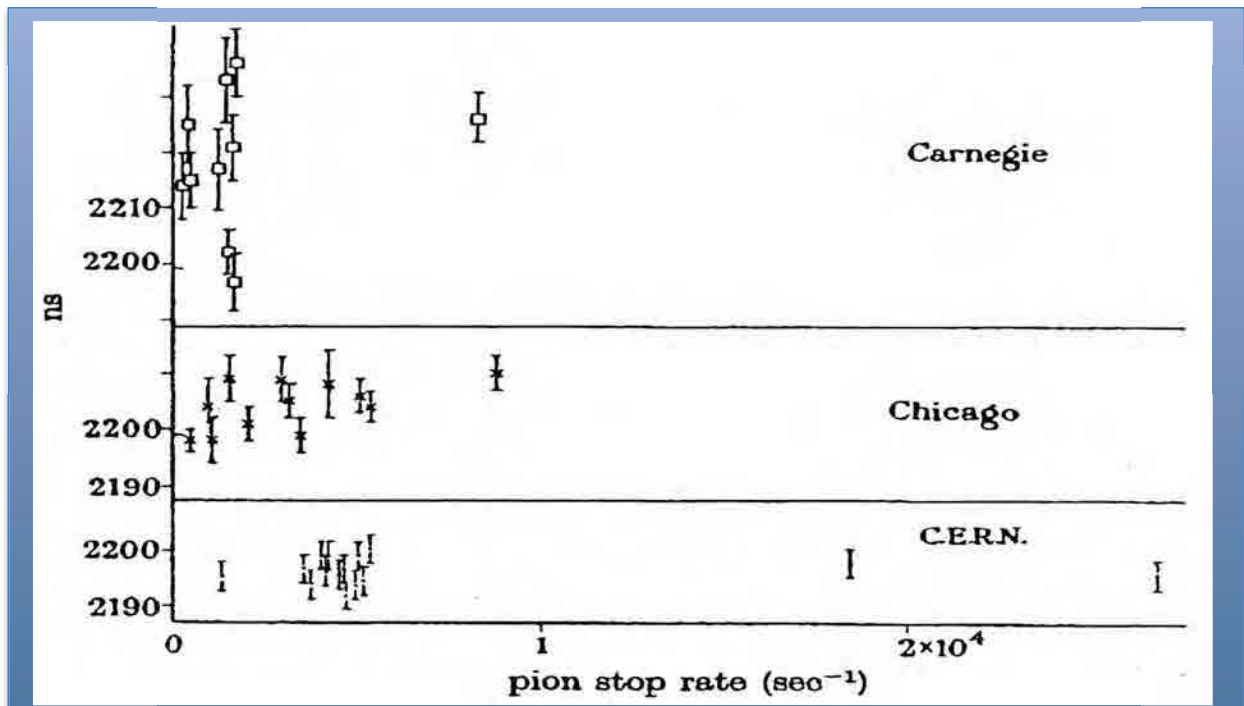


Figure 18: (Figure from [22]) The diagram above shows that the experimental results on τ_μ obtained in Chicago and Carnegie were affected by a rate dependent systematic effect which invalidates the data. The CERN result is the first without this trouble.

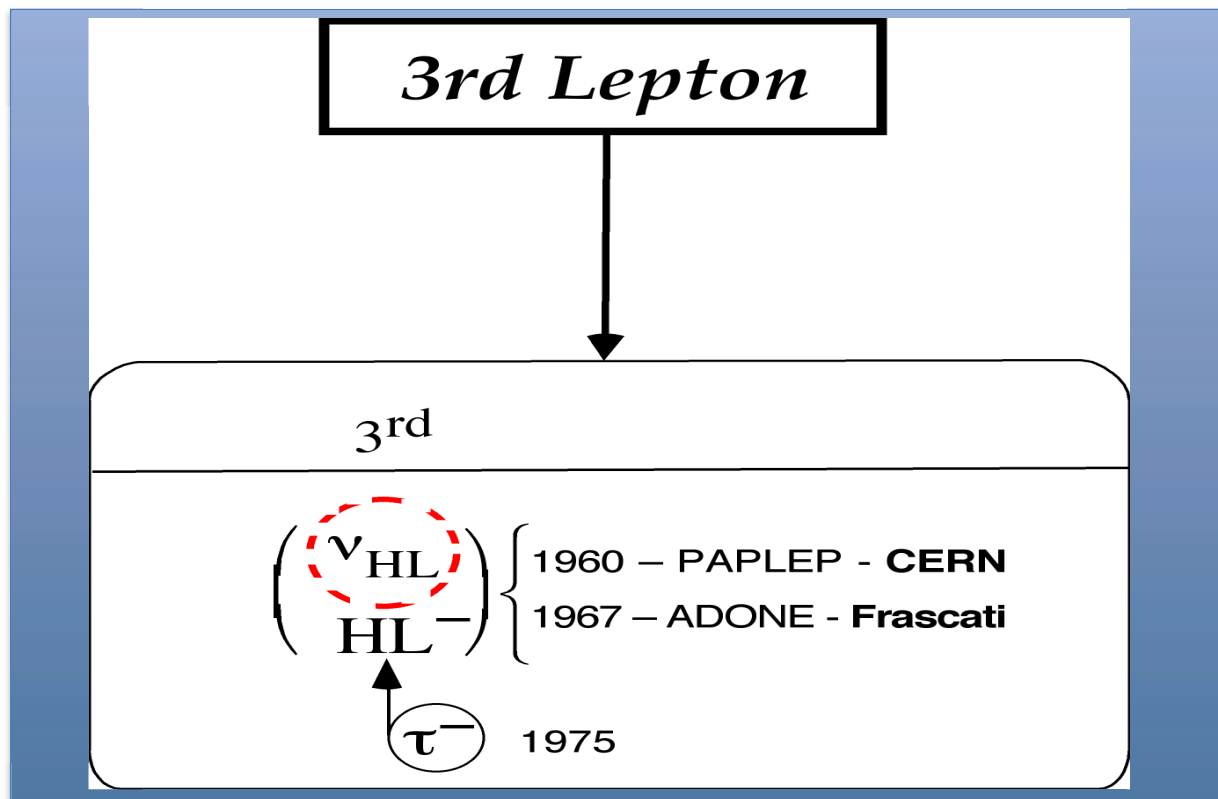


Figure 19

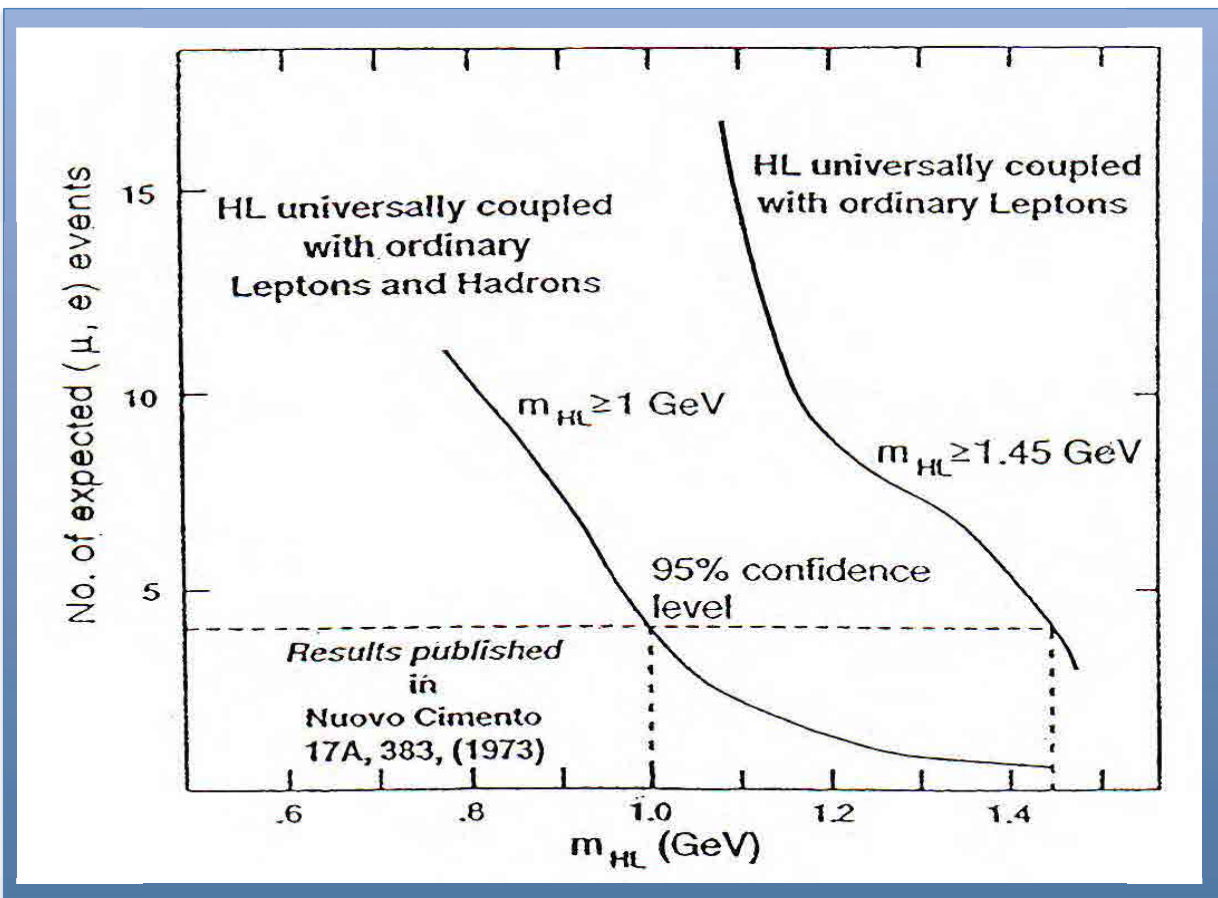


Figure 20: (Figure from [23]) The expected number of ($e^\pm \mu^\mp$) pairs vs. m_{HL} , i.e. the heavy lepton mass, for two types of universal weak couplings of the heavy lepton.

THE THREE COLUMNS		
$\begin{pmatrix} \nu_e \\ e^- \end{pmatrix}$	$\begin{pmatrix} \nu_\mu \\ \mu^- \end{pmatrix}$	$\begin{pmatrix} \nu_{HL} \\ HL^- \end{pmatrix} \Rightarrow \begin{pmatrix} \nu_\tau \\ \tau^- \end{pmatrix}$
$\begin{pmatrix} u \\ d \end{pmatrix}$	$\begin{pmatrix} c \\ s \end{pmatrix}$	$\begin{pmatrix} t \\ b \end{pmatrix}$
I	II	III

Figure 21

From the π -meson to the Instantons we need the experimental discovery of $\theta_{PS} \neq \theta_V$

THE STANDARD MODEL AND BEYOND
<p>① RGEs (α_i ($i = 1, 2, 3$); m_j ($j = q, l, G, H$)): $f(k^2)$.</p> <ul style="list-style-type: none"> • GUT ($\alpha_{GUT} \approx 1/24$) & GAP ($10^{16} - 10^{18}$) GeV. • SUSY (to stabilize $m_F/m_P \approx 10^{-17}$). • RQST (to quantize Gravity). <p>② Gauge Principle (hidden and expanded dimensions).</p> <ul style="list-style-type: none"> — How a Fundamental Force is generated: $SU(3)$; $SU(2) \times U(1)$ and Gravity. <p>③ The Physics of Imaginary Masses: SSB.</p> <ul style="list-style-type: none"> — The Imaginary Mass in $SU(2) \times U(1)$ produces masses (m_{W^\pm}; m_{Z^0}; m_q; m_l), including $m_\gamma = 0$. — The Imaginary Mass in $SU(5) \Rightarrow SU(3) \times SU(2) \times U(1)$ or in any higher Symmetry Group (not containing $U(1)$) $\Rightarrow SU(3) \times SU(2) \times U(1)$ produces Monopoles. — The Imaginary Mass in $SU(3)_c$ generates Confinement. <p>④ Flavour Mixings & CP, P, CP, T.</p> <ul style="list-style-type: none"> — No need for it but it is there. <p>⑤ Anomalies & Instantons.</p> <ul style="list-style-type: none"> — Basic Features of all non-Abelian Forces.

Figure 22

1947	SUBNUCLEAR PHYSICS	is born
	Lamb-shift	<i>OK</i>
	π -meson	<i>OK</i>
	Strange particles	<i>NOW</i>

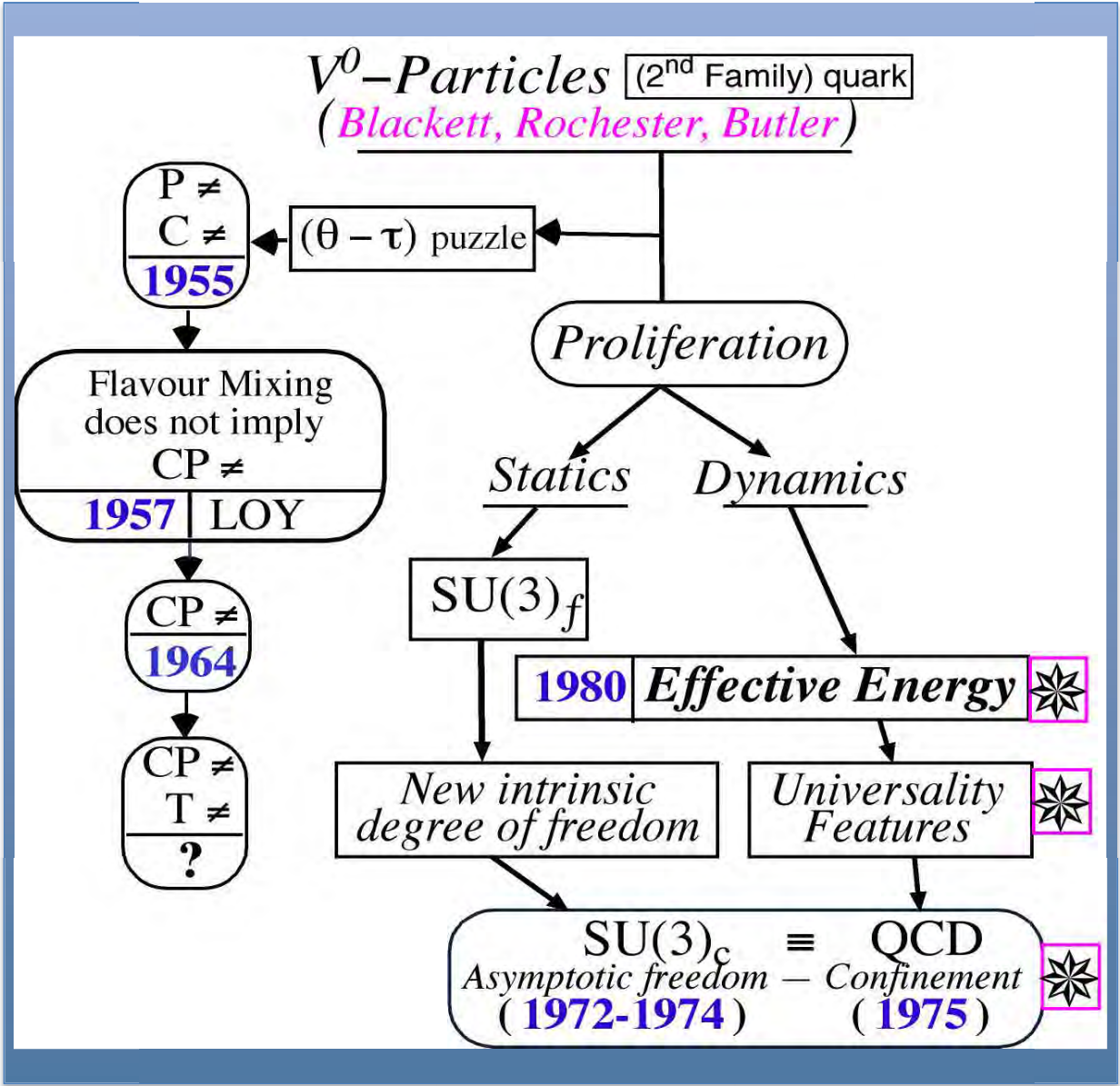


Figure 23

THE EFFECTIVE ENERGY

Introduction of the “Effective Energy”

EVIDENCE OF THE SAME MULTIPARTICLE PRODUCTION MECHANISM IN p - p COLLISIONS AS IN e^+e^- ANNIHILATION

M. Basile, G. Cara Romeo, L. Cifarelli, A. Contin, G. D'Alì, P. Di Cesare,
B. Esposito, P. Giusti, T. Massam, F. Palmonari, G. Sartorelli, G. Valenti and
A. Zichichi.

Physics Letters 92B, 367 (1980).

*“The agreement between the momentum distributions
obtained in e^+e^- annihilation and in p - p collisions
suggests that the mechanism for transforming energy
into particles in these two processes, so far considered
very different, must be the same”.*

Figure 24: The first paper where the effective energy was introduced
in the study of high energy (pp) interactions at ISR.

The proliferation in the "dynamic" sector was the multitude of final states produced by pairs of interacting particles, in strong, electromagnetic and weak processes:

Strong	EM	Weak
$\left\{ \begin{array}{l} \pi p \\ K p \\ p p \\ p n \\ \bar{p} p \end{array} \right.$	$\left\{ \begin{array}{l} \gamma p \\ e p \\ \mu p \\ e^+e^- \end{array} \right.$	νp

It is the introduction of the effective energy which allowed one to put all the different final states on the same basis.

This basis is the quantities measured in the multihadronic final states:

- i) the average charged multiplicity; $\langle n_{ch} \rangle$;
- ii) the fractional energy distribution; $d\sigma / dx_i$;
- iii) the transverse momentum distribution $d\sigma / dp_{t_i}$; etc.

THE END OF A MYTH: HIGH- P_T PHYSICS

M. Basile, J. Berbiers, G. Cara Romeo, L. Cifarelli, A. Contin, G. D'Alì, C. Del Papa, P. Giusti, T. Massam, R. Nania, F. Palmonari, G. Sartorelli, M. Spinetti, G. Susinno, L. Votano and A. Zichichi.

Opening Lecture in Proceedings of the XXII Course of the
"Ettore Majorana" International School of Subnuclear Physics, Erice, Italy,
5-15 August 1984: "Quarks, Leptons, and their Constituents"
(Plenum Press, New York-London, 1988), 1.

"So far, the main picture of hadronic physics has been based on a distinction between high- $-p_T$ and low- $-p_T$ phenomena.

In the framework of parton model, high- $-p_T$ processes were the only candidates to establish a link between

- purely hadronic processes
- (e^+e^-) annihilations
- (DIS) processes.

The advent of QCD has emphasized in a dramatic way the privileged role of high- $-p_T$ physics due to the fact that, thanks to asymptotic freedom, QCD calculations via perturbative methods can be attempted at high- $-p_T$ and results successfully compared with experimental data [1]. The conclusion was: we can forget about everything else and limit ourselves to high- $-p_T$ physics.

Being theoretically off limits, low- $-p_T$ phenomena, which represent the overwhelming majority of hadronic processes (more than 99% of physics is here), have been up to now neglected. By subtracting the leading proton effects in order to derive the effective energy available for particle production and by using the correct variables, the BCF collaboration has performed a systematic study of the final states produced in low- $-p_T$ (pp) interactions at the ISR and has compared the results with those obtained in the processes listed below:

<u>Process</u>	<u>Data Sources</u>
(e^+e^-)	SLAC, DORIS, PETRA
(DIS)	SPS/EMC
(pp)	[ISR (AFS) SPS Collider (UAI) PETRA/TASSO (leading subtraction)
$(\bar{p}p)$] Transverse physics	
(e^+e^-)	

The results of this study [2-18] show that, once a common basis for comparison is found by the use of the correct variables, remarkable analogies are observed in processes so far considered basically different like

- low- $-p_T$ (pp) interactions
- (e^+e^-) annihilations
- (DIS) processes
- high- $-p_T$ (pp) and $(\bar{p}p)$ interactions

This is how universality features emerge, and this is the basis to proceed for a meaningful comparison, i.e.:

*first identify the correct variables to establish a common basis,
then proceed to a detailed comparison*."*

* The root of this new approach to the study of hadronic interactions goes back a long time to a proposal by the CERN-Bologna group: "Study of deep inelastic high momentum transfer hadronic collisions" PMI/com-69/35, 8 July 1969."

Figure 25: Reproduction of the conclusions of a review paper [24].

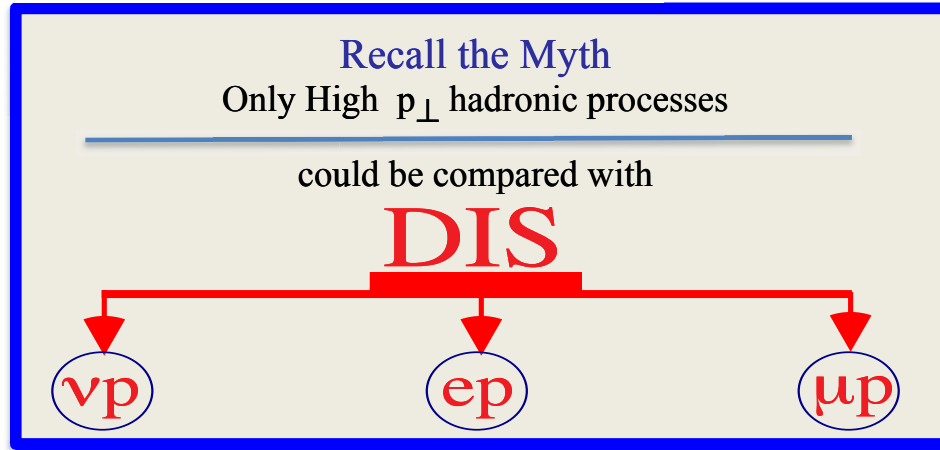


Figure 26: A synthesis of the high transverse momentum myth.

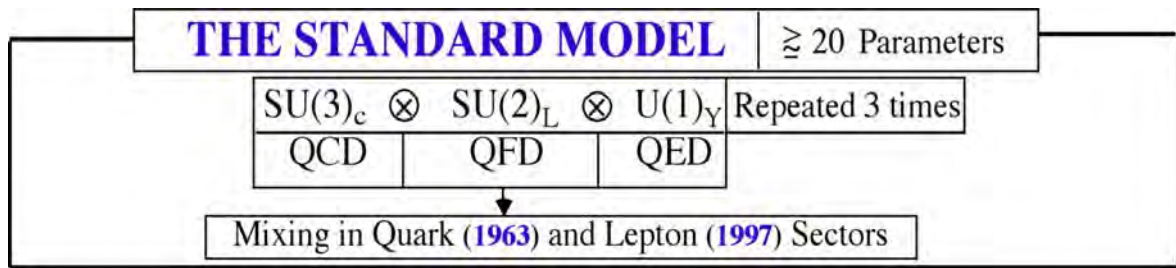


Figure 27

SM&B

THE STANDARD MODEL AND BEYOND

- ① **RGEs** (α_i ($i = 1, 2, 3$); m_j ($j = q, l, G, H$)): $f(k^2)$.
 - GUT ($\alpha_{\text{GUT}} \approx 1/24$) & GAP ($10^{16} - 10^{18}$) GeV.
 - SUSY (to stabilize $m_F/m_P \approx 10^{-17}$).
 - RQST (to quantize Gravity).
- ② **Gauge Principle (hidden and expanded dimensions)**.
 - How a Fundamental Force is generated: $SU(3)$; $SU(2)$; $U(1)$ and Gravity.
- ③ **The Physics of Imaginary Masses: SSB**.
 - The Imaginary Mass in $SU(2) \times U(1)$ produces masses (m_{W^\pm} ; m_{Z^0} ; m_q ; m_l), including $m_\gamma = 0$.
 - The Imaginary Mass in $SU(5) \Rightarrow SU(3) \times SU(2) \times U(1)$ or in any higher (not containing $U(1)$) Symmetry Group $\Rightarrow SU(3) \times SU(2) \times U(1)$ produces Monopoles.
 - The Imaginary Mass in $SU(3)_c$ generates Confinement.
- ④ **Flavour Mixings & $CP \neq$, $T \neq$** (direct \neq , not via SSB).
 - No need for it but it is there.
- ⑤ **Anomalies & Instantons**.
 - Basic Features of all Non-Abelian Forces.

Figure 28

NOTE

q = quark and squark;	m_F = Fermi mass scale;
l = lepton and slepton;	m_P = Planck mass scale;
G = Gauge boson and Gaugino;	k = quadrimomentum;
H = Higgs and Shiggs;	C = Charge Conjugation;
RGEs = Renormalization Group Equations;	P = Parity;
GUT = Grand Unified Theory;	T = Time Reversal;
SUSY = Supersymmetry;	\neq = Breakdown of Symmetry Operators.
RQST = Relativistic Quantum String Theory;	
SSB = Spontaneous Symmetry Breaking.	

Figure 29

The five basic steps in our understanding the Logic of Nature

- ① The renormalization group equations (RGEs) imply that the gauge couplings (α_i) and the masses (m_j) all run with k^2 . It is this running which allows GUT, suggests SUSY and produces the need for a non point-like description (RQST) of physics processes, thus opening the way to quantize gravity.
- ② All forces originate in the same way: the gauge principle.
- ③ Imaginary masses play a central role in describing nature: SSB & Confinement.
- ④ The mass-eigenstates are mixed when the Fermi forces come in: the matrix describing the mixing is the product of two fundamental matrices. Why the mixing is there?
- ⑤ The Abelian force QED has lost its role of being the guide for all fundamental forces. The non-Abelian gauge forces dominate and have features which are not present in QED.

THE STANDARD MODEL AND BEYOND

- ① **RGEs** (α_i ($i \equiv 1, 2, 3$); m_j ($j \equiv q, l, G, H$)) : $f(k^2)$.
 - GUT ($\alpha_{\text{GUT}} \equiv 1/24$) & GAP ($10^{16} - 10^{18}$) GeV.
 - SUSY (to stabilize $m_F/m_P \equiv 10^{-17}$).
 - RQST (to quantize Gravity).
- ② **Gauge Principle (hidden and expanded dimensions).**
 - How a Fundamental Force is generated: $SU(3)$; $SU(2) \times U(1)$ and Gravity.
- ③ **The Physics of Imaginary Masses: SSB.**
 - The Imaginary Mass in $SU(2) \times U(1)$ produces masses (m_{W^\pm} ; m_{Z^0} ; m_q ; m_l), including $m_\gamma = 0$.
 - The Imaginary Mass in $SU(5) \Rightarrow SU(3) \times SU(2) \times U(1)$ or in any higher Symmetry Group (not containing $U(1)$) $\Rightarrow SU(3) \times SU(2) \times U(1)$ produces Monopoles.
 - The Imaginary Mass in $SU(3)_c$ generates Confinement.
- ④ **Flavour Mixings, $S \neq C$, $P \neq$, $CP \neq$, $T \neq$.**
 - No need for it but it is there.
- ⑤ **Anomalies & Instantons.**
 - Basic Features of all non-Abelian Forces.

Figure 22

Instantons

The Instanton [25, 26] is a solution of the classical field equations in Euclidean space-time. It is originated by the properties of the vacuum which is strongly coupled to the field quanta of a given gauge force. In a quantized world the Instanton corresponds to tunnelling effects in Minkowski space-time. These tunnelling effects are recognized in practice by the fact that they violate a global symmetry-law. There are two kinds of Instantons, one for QCD and one for the QFD, the electro-weak forces.

In both cases, $SU(3)_c$ and $SU(2)_L$, i.e. QCD and QFD, the effects produced by the Instantons can be understood in terms of the properties of the Dirac sea. In fact, the vacuum, made of fermions, has fermionic properties.

In QCD, these properties determine the "non-spontaneous", i.e. direct, breakdown of "chirality" invariance. This has allowed to understand the behaviour of the η and the η' mesons [27, 28, 29, 30].

In $SU(2)_L$ the effect of Instantons is linked to the fact that the non-Abelian gauge force, QCD, acts only on left-handed states and Instantons generate baryon number non-conservation, which is another $U(1)$ breaking.

Instantons typically have the effect of explicitly breaking $U(1)$ symmetries.

Why we need the Instantons? In order to explain $\theta_{PS} \neq \theta_V$.

SU(3) States

Note that the $SU(3)$ states are (in terms of the quark composition):

$$\eta_8 = \frac{u\bar{u} + d\bar{d} - 2s\bar{s}}{\sqrt{6}}$$

(8^{th} multiplet of $SU(3)$ octet)

$$\eta_1 = \frac{u\bar{u} + d\bar{d} + s\bar{s}}{\sqrt{3}}$$

($SU(3)$ singlet).

In the real world we have the physical states

$$J^{PC} = 0^{-+} \begin{cases} \eta(m \approx 500 \text{ MeV}) = \frac{u\bar{u} + d\bar{d} - \sqrt{2}s\bar{s}}{\sqrt{4}} \\ \eta'(m \approx 950 \text{ MeV}) = \frac{u\bar{u} + d\bar{d} + \sqrt{2}s\bar{s}}{\sqrt{4}} \end{cases}$$

$$J^{PC} = 1^{--} \begin{cases} \omega(m \approx 750 \text{ MeV}) = \frac{u\bar{u} + d\bar{d}}{\sqrt{2}} \\ \phi(m \approx 1020 \text{ MeV}) = s\bar{s} \end{cases}$$

with $\theta_{PS} \approx 10^\circ$

$$\begin{cases} \eta = \eta_8 \cos \theta_{PS} - \eta_1 \sin \theta_{PS} \\ \eta' = \eta_8 \sin \theta_{PS} + \eta_1 \cos \theta_{PS} \end{cases}$$

and $\theta_V \approx 45^\circ$

$$\begin{cases} \omega = \omega_8 \cos \theta_V - \omega_1 \sin \theta_V \\ \phi = \omega_8 \sin \theta_V + \omega_1 \cos \theta_V \end{cases}.$$

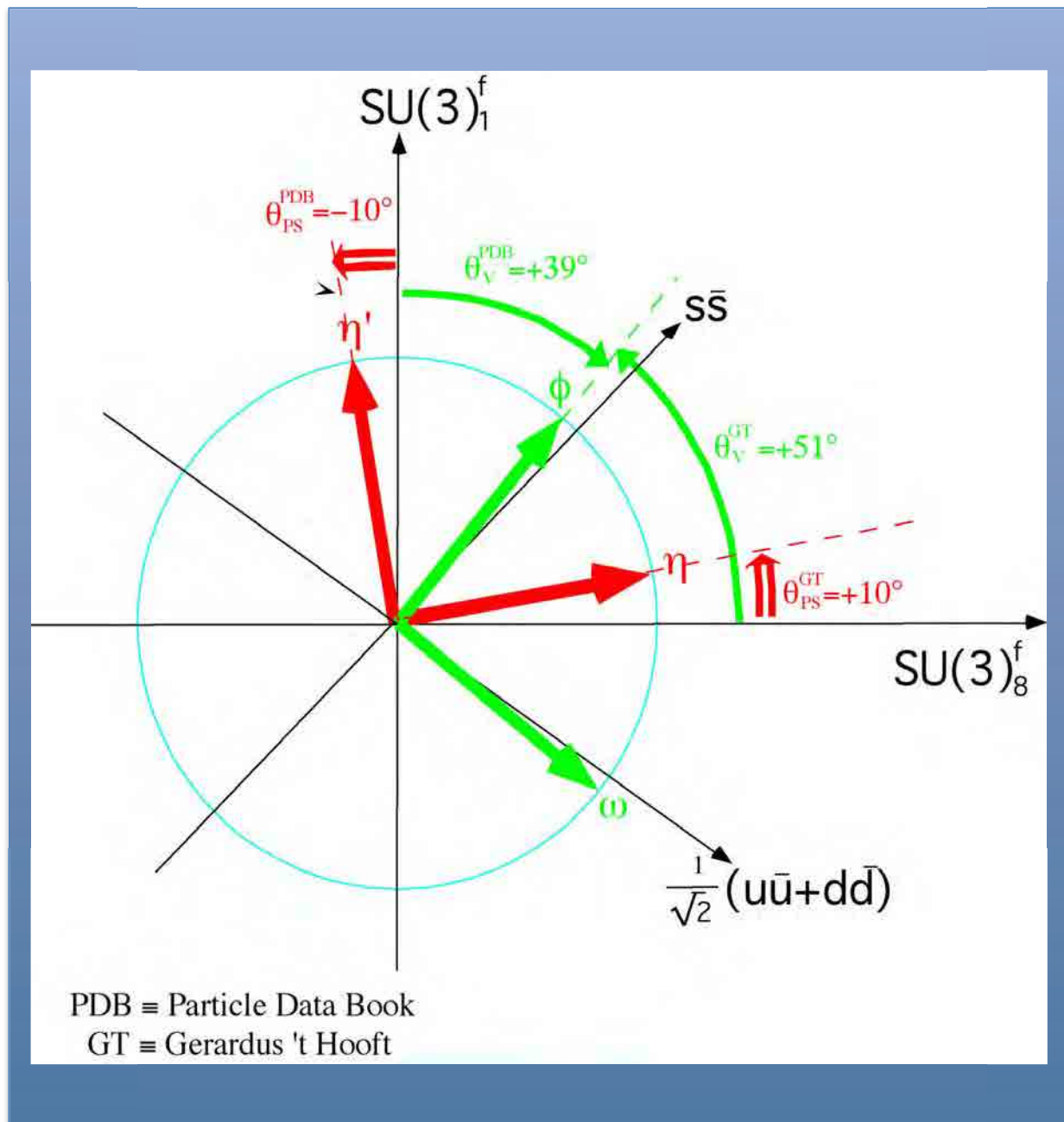
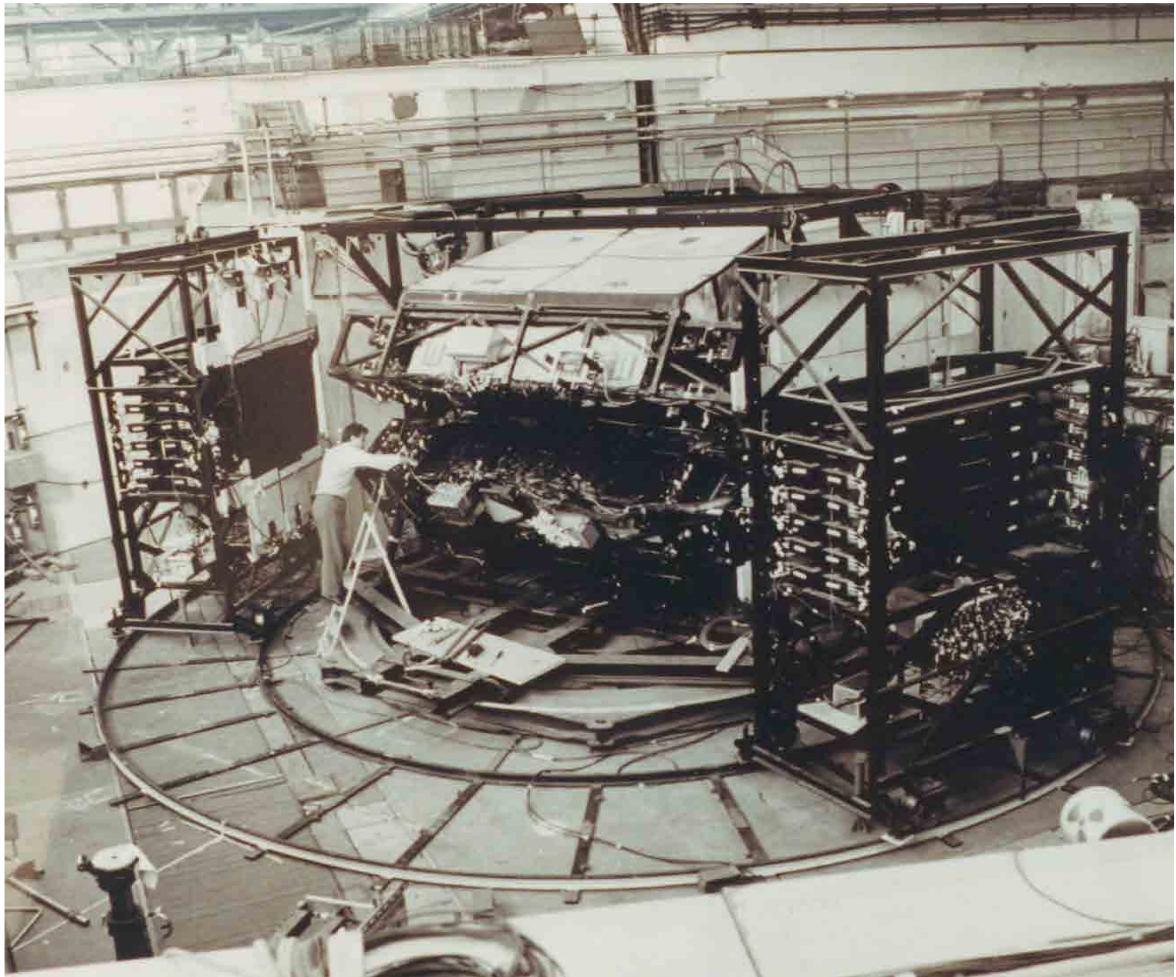


Figure 30

– 1963 –

This is the first example of what is now "standard" in experimental subnuclear physics: very large acceptance detectors.



On the rails the “neutron missing mass spectrometer”.

PAPLEP
Proton AntiProton into Lepton Pairs
first search for the 3rd lepton
and
 $\theta_{PS} \neq \theta_V$.

Figure 4

THE STANDARD MODEL AND BEYOND

- ① **RGEs** ($\alpha_i (i = 1, 2, 3); m_j (j = q, l, G, H) : f(k^2)$.
 - GUT ($\alpha_{\text{GUT}} \cong 1/24$) & GAP ($10^{16} - 10^{18}$) GeV.
 - SUSY (to stabilize $m_F/m_P \cong 10^{-17}$).
 - RQST (to quantize Gravity).
- ② **Gauge Principle (hidden and expanded dimensions).**
 - How a Fundamental Force is generated: SU(3); SU(2) \times U(1) and Gravity.
- ③ **The Physics of Imaginary Masses: SSB.**
 - The Imaginary Mass in SU(2) \times U(1) produces masses ($m_{W^\pm}; m_{Z^0}; m_q; m_l$), including $m_\gamma = 0$.
 - The Imaginary Mass in SU(5) \Rightarrow SU(3) \times SU(2) \times U(1) or in any higher Symmetry Group (not containing U(1)) \Rightarrow SU(3) \times SU(2) \times U(1) produces Monopoles.
 - The Imaginary Mass in SU(3)_c generates Confinement.
- ④ **Flavor Mixings & C \neq , P \neq , CP \neq , T \neq .**
 - No need for it but it is there.
- ⑤ **Anomalies & Instantons.**
 - Basic Features of all non-Abelian Forces.

Figure 22

Anomalies

The anomalies correspond to quantum effects [31, 32].

The term "anomaly" is not so well-chosen since it refers to several different features in elementary particle theory. The term originated in QED where radiative effects were first discovered. It was introduced in order to describe quantum effects in Abelian QFT such as the "anomalous" magnetic moment of the muon.

- **Non-Abelian QFT have chiral anomalies** which must be cancelled, thus imposing severe conditions on the basic structures of the matter fields (example: the top quark needed in the third family).
- **Anomalies exist also in Abelian theories**, such as those needed to describe $\pi^0 \rightarrow \gamma\gamma$ [33, 34, 35]. They can thus be used to predict physical processes.

Relativistic Quantum String Theory (RQST)

The Standard Model deals with only two of the three known forces.

However quantum mechanics is contagious and gravity cannot avoid quantization.

Much of our hope has become focused on string theory.

Unfortunately **RQST** has not yet descended to low energy, and goes on making predictions at inaccessible energies.

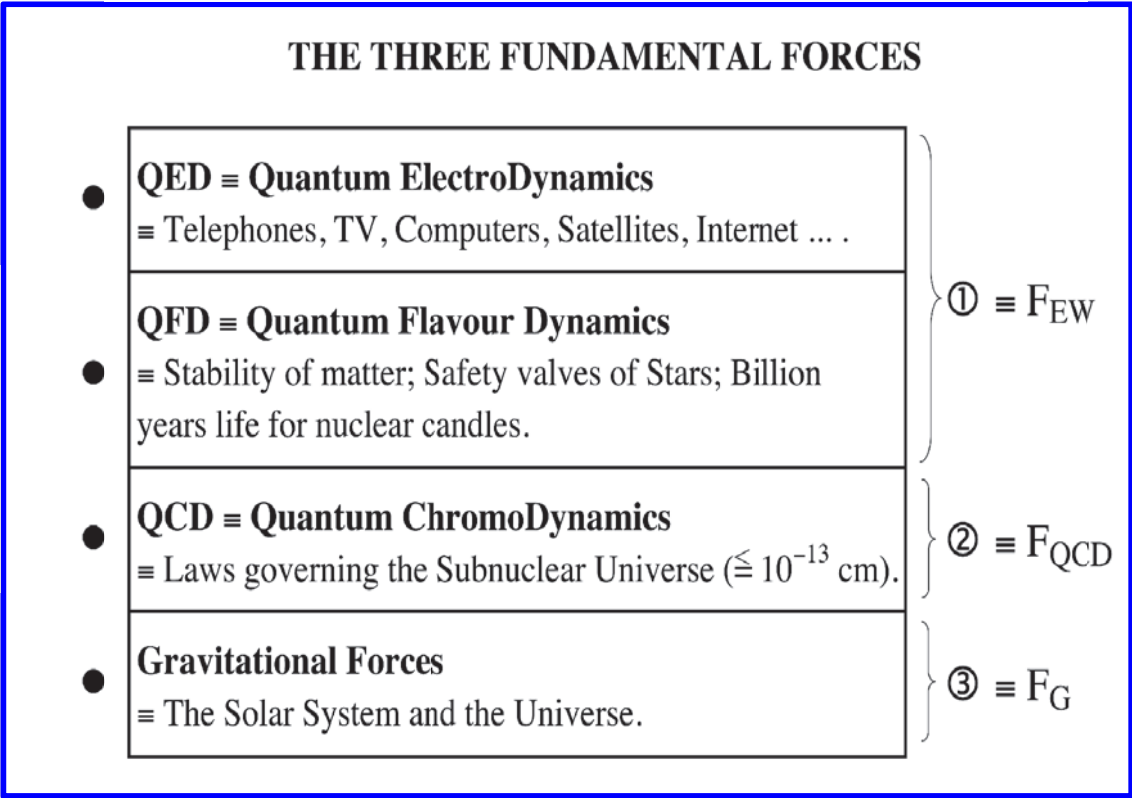


Figure 31

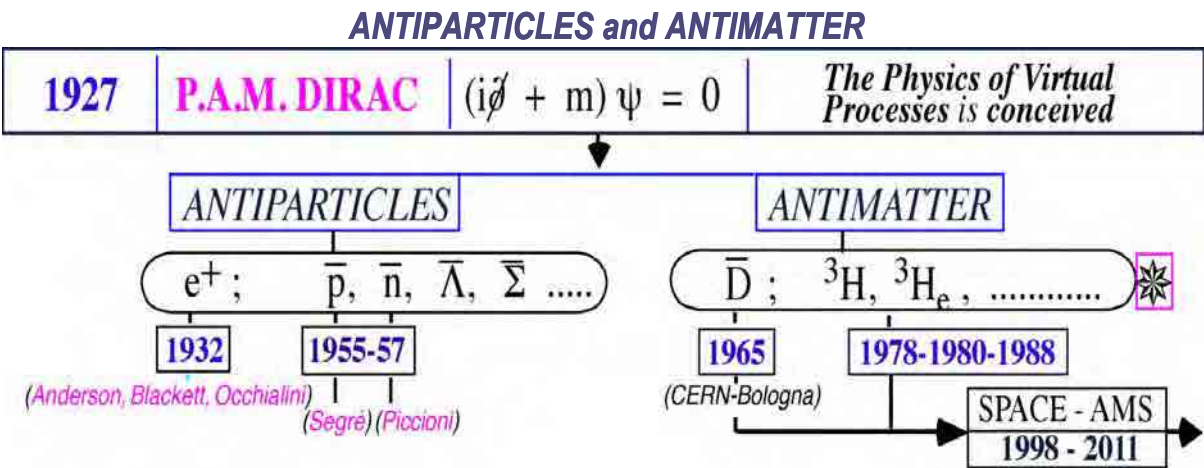


Figure 32

The problem of understanding the difference between mass and matter is illustrated in Figure 33. The incredible series of events which originated with the problem of understanding the stability of matter is shown in Figure 34, together with the unexpected violation of the Symmetry Operators (C, P, T, CP) and the discovery of Matter-Antimatter Symmetry.

When (1905) Einstein discovered that

$$mc^2 = E$$

he could not sleep at night.
(Peter G. Bergmann testimony)

Mass \neq Matter

$$|m_i\rangle \equiv \text{Mass} \equiv \text{Antimass} \equiv |\bar{m}_i\rangle$$

$i \equiv 1$ (Intrinsic); $i \equiv 2$ (Confinement); $i \equiv 3$ (Binding)

$$C |m_i\rangle = |m_i\rangle \quad \boxed{***}$$

$i \equiv 1, 2, 3$

$$|m_i Q_j\rangle \equiv \text{Matter} \neq \text{Antimatter} \equiv |m_i \bar{Q}_j\rangle$$

$Q_j \equiv$ Flavour Charges

$$J \equiv (u \quad d \quad c \quad s \quad t \quad b) \equiv (1, 2, 3, 4, 5, 6)$$

$$(\nu_e \quad e^- \quad \nu_\mu \quad \mu^- \quad \nu_{HL} \quad HL^-) \equiv (7, 8, 9, 10, 11, 12)$$

\downarrow
 τ^-

$$C |m_i Q_j\rangle = |m_i \bar{Q}_j\rangle \quad \boxed{***}$$

$i \equiv 1, 2, 3 ; J \equiv 1, 2, 3, 4, 5, 6, 7, 8, 9, 10, 11, 12$

Figure 33

Figure 34 shows seven decades of developments, started from the antielectron and C-invariance and brought us to the discovery of nuclear antimatter and to the unification of all gauge forces.

THE INCREDIBLE STORY
TO UNDERSTAND THE ORIGIN OF THE STABILITY OF MATTER
SEVEN DECADES FROM THE ANTIELECTRON TO ANTIMATTER
AND THE UNIFICATION OF ALL GAUGE FORCES

• **The validity of C invariance from 1927 to 1957.**

After the discovery by Thomson in 1897 of the first example of an elementary particle, the Electron, it took the genius of Dirac to theoretically discover the Antielectron thirty years after Thomson.

1927 → Dirac equation [36]; the existence of the antielectron is, soon after, theoretically predicted. Only a few years were needed, after Dirac's theoretical discovery, to experimentally confirm (Anderson, Blackett and Occhialini [37]) the existence of the Dirac antielectron.

1930-1957 → **Discovery of the C operator** [(charge conjugation) H. Weyl and P.A.M. Dirac [38]]; discovery of the P Symmetry Operator [E.P. Wigner, G.C. Wick and A.S. Wightman [39, 40]]; discovery of the T operator (time reversal) [E.P. Wigner, J. Schwinger and J.S. Bell [41, 42, 43, 44]]; discovery of the CPT Symmetry Operator from RQFT (1955-57) [45].

1927-1957 → Validity of C invariance: e^+ [37]; \bar{p} [46]; \bar{n} [47]; $K_S^0 \rightarrow 3\pi$ [48] but see LOY [49].

• **The new era starts: C ≠ ; P ≠ ; CP ≠ (*) .**

1956 → Lee & Yang P ≠ ; C ≠ [50].

1957 → Before the experimental discovery of P ≠ & C ≠, Lee, Oehme, Yang (LOY) [49] point out that the existence of the second neutral K-meson, $K_S^0 \rightarrow 3\pi$, is proof neither of C invariance nor of CP invariance. Flavour antiflavour mixing does not imply CP invariance.

1957 → C.S. Wu et al. P ≠ ; C ≠ [51]; CP ok [52].

1964 → $K_S^0 \rightarrow 2\pi \equiv K_L$: CP ≠ [53].

1947-1967 → QED divergences & Landau poles.

1950-1970 → The crisis of RQFT & the triumph of S-matrix theory (i.e. the negation of RQFT).

1965 → Nuclear antimatter is (experimentally) discovered [54]. See also [55].

1968 → The discovery [56] at SLAC of Scaling (free quarks inside a nucleon at very high q^2) but in violent (pp) collisions no free quarks at the ISR are experimentally found [57]. Theorists consider Scaling as being evidence for RQFT not to be able to describe the Physics of Strong Interactions. The only exception is G. 't Hooft who discovered in 1971 that the β -function has negative sign for non-Abelian theories [58].

1971-1973 → $\beta = -$; 't Hooft; Politzer; Gross & Wilczek. The discovery of **non-Abelian** gauge theories. Asymptotic freedom in the interaction between quarks and gluons [58].

1974 → All gauge couplings $\alpha_1 \alpha_2 \alpha_3$ run with q^2 but they do not converge towards a unique point.

1979 → A.P. & A.Z. point out that the new degree of freedom due to SUSY allows the three couplings $\alpha_1 \alpha_2 \alpha_3$, **to converge towards a unique point** [59].

1980 → QCD has a "hidden" side: the multitude of final states for each pair of interacting particles: (e^+e^- ; $p\bar{p}$; πp ; Kp ; vp ; pp ; etc.)
 The introduction of the Effective Energy allows to discover the Universality properties [60] in the multihadronic final states.

1992 → All gauge couplings converge towards a unique point at the gauge unification energy: $E_{GU} \approx 10^{16}$ GeV with $\alpha_{GU} \approx 1/24$ [61, 1].

1994 → The Gap [62] between E_{GU} & the String Unification Energy: $E_{SU} \approx E_{Planck}$.

1995 → **CPT loses its foundations at the Planck scale (T.D. Lee)** [63].

1995-1999 → **No CPT theorem from M-theory (B. Greene)** [64].

1995-2000 → A.Z. points out the need for new experiments to establish if matter-antimatter symmetry or asymmetry are at work.

(*) The symbol ≠ stands for "Symmetry Breakdown".

50th ANNIVERSARY OF THE KARLSRUHE NUCLIDE CHART**ANTIPARTICLES AND ANTIMATTER:
THE BASIC DIFFERENCE****Antonino Zichichi***CERN, Geneva, Switzerland**Enrico Fermi Centre, Rome, Italy**INFN and University of Bologna, Italy*

«Those who say that antihydrogen is antimatter should realize that we are not made of hydrogen and we drink water, not liquid hydrogen». These are Dirac's own words to a group of physicists (Figure 35) gathered around him, who, with a single equation [36, 65], opened new horizons to human knowledge.



Figure 35: Dirac surrounded by young physicists in Erice, after a lecture when he explained the difference between antiparticles and antimatter. It is on this occasion that he made the statement previously quoted.

Professor Antonino ZICHICHI
University of Bologna and
Bologna Academy of Science
Via Zamboni 31
40126 BOLOGNA, Italy

Tallahassee, 16 December 1995

Dear Nino,

on the occasion of the International Symposium in your honour, to celebrate the 30th Anniversary of the Discovery of Nuclear Antimatter, let me recall the joy that I saw in Paul's eyes when he received the phone call from his friend Abdus Salam, telling him that the first example of nuclear antimatter had been discovered at CERN by Nino Zichichi.

This is how we got to know each other : I still remember your first visit to us. I had prepared a typical hungarian cake. Do you remember how much did you eat of it and enjoyed it because it was like the pastry of your native country, Sicily?

That was a great evening for Paul and me because it was the beginning of an unforgettable friendship that brought to many interesting results, like the Erice Seminars on Nuclear Wars. Paul was very proud of his activity in Erice for Peace and Freedom when the world was separated by the iron curtain.

I wish I could be in Bologna but I remind you that you have promised me to be here in Tallahassee soon.

With lots of love to you and Maria Ludovica.

Yours,

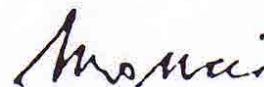
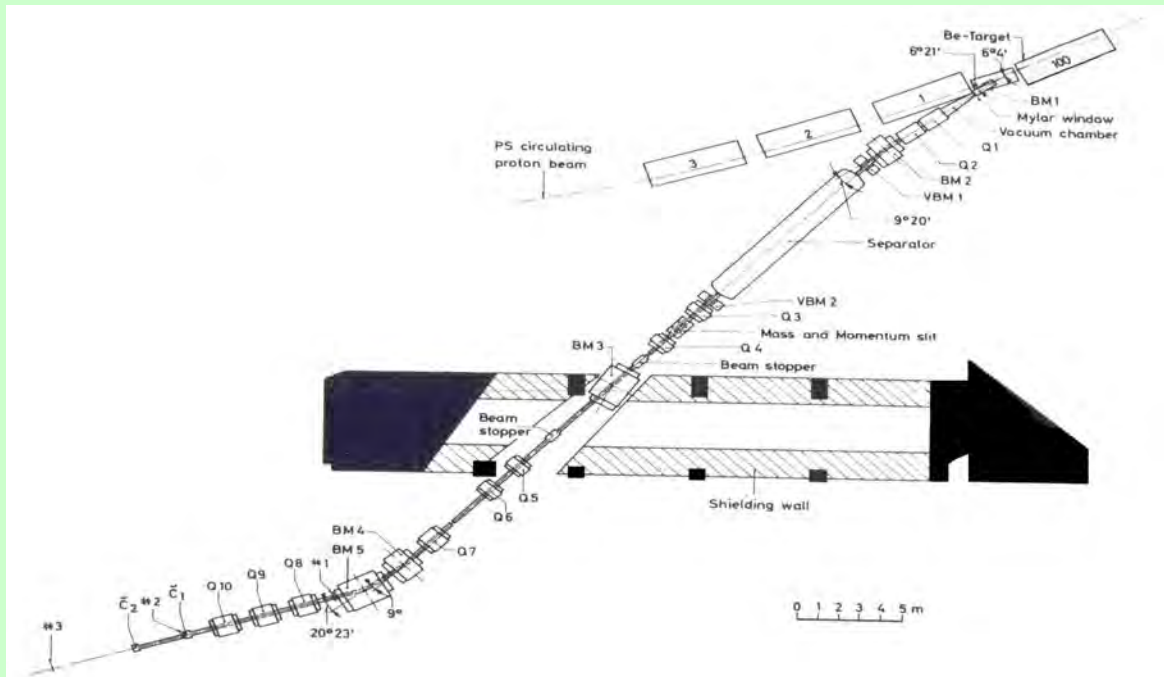


Figure 36: Letter by Mrs Mancy Dirac.

$$\text{TOF} \equiv \pm 75 \text{ psec}$$



$$\begin{array}{ccc} 10^{-7} & \rightarrow & 10^{-8} \quad \bar{D}/\pi^- \\ \uparrow & & \uparrow \\ \text{No Signal} & \rightarrow & \text{signal} \end{array}$$

Figure 37: Schematic layout of the experimental set-up that allowed the discovery of antimatter. The combined system of bending magnets (BM) coupled with magnetic quadrupoles (Q) and the Separator allowed to have the most intensive negative beam ever built (authors of the beam-project: M. Morpurgo, G. Petrucci and A. Zichichi). The scintillation counters, #1, #2, #3, are for the time of flight (TOF) measurements. The precision achieved was 75 psec. \check{C}_1 and \check{C}_2 are Cerenkov detectors for particles identification.

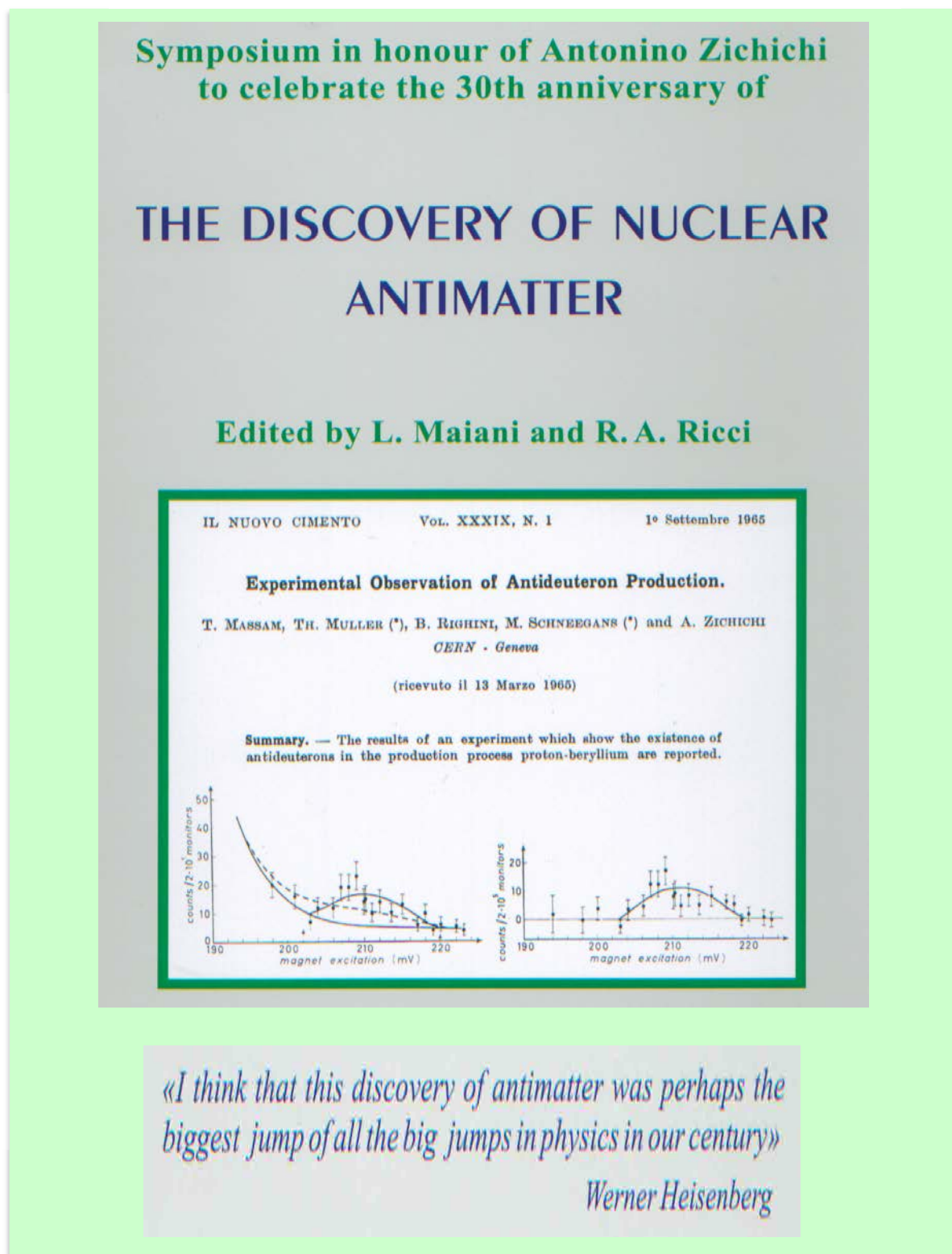


Figure 38: Front cover of the book celebrating the 30th anniversary of the antideuteron discovery.

Note – 1

To obtain water, hydrogen is not sufficient by itself. You also need oxygen whose nucleus is made of 8 protons and 8 neutrons. Hydrogen is the only element in Mendeleev's Table to be constituted of two charged particles, the electron and the proton, without any role being played by the Nuclear Forces.

The first element on which Nuclear Forces come into play is the heavy hydrogen, whose nucleus, called deuteron, is made with one proton and one neutron. For these two particles to remain together the “nuclear glue” is needed. Starting from the heavy hydrogen, all the elements of the Table, to exist, must have their nuclei made with protons, neutrons and the nuclear glue.

If these last two ingredients, the neutron and the nuclear glue, were not available, nothing but the “light” hydrogen could exist. Farewell water and farewell all material which we are familiar with.

Note – 2

In Dirac's famous statement, 70 years of theoretical and experimental discoveries are taken into consideration, with the conclusion that the existence of antimatter is supported exclusively on an experimental basis.

In fact – as evidenced by T.D. Lee [63], – the CPT theorem is invalidated at the Planck Scale ($\cong 10^{19}$ GeV) where all Nature's Fundamental Forces converge. Since the Grand Unification is the source of everything, if CPT collapses at the energy level of the Grand Unification we can then bid farewell to all that derives from CPT.



Figure 39 : Eugene P. Wigner, A. Zichichi and Paul Dirac (Erice, 1982).

Conclusions

This Seminar is devoted to review the main steps as seen from the reference frame, each one of us has chosen and cannot therefore be unbiased.

Let me cite Rabi:

*«Physics is Intellectual Freedom.
Our interest is to understand nature.
It is to our liking to choose the best way.
Every physicist has his own interests
and his own likes and dislikes».*

This Seminar should review the development of Subnuclear Physics associated with a concrete concern about the future of our field.

It is this concern at the origin of our activity devoted towards the implementation of new projects.

The experimental results acquired so far in Subnuclear Physics tell us that the Standard Model cannot be the definitive theory, in spite of the fact that it is the most powerful synthesis of all known and rigorously measured phenomena.

Looking back at the last 64 years, the amount of new knowledge acquired is really overwhelming.

Richard P. Feynman – 1964, Erice – Global & Local Conservation Laws from *Discussions* at the International School of Subnuclear Physics.

«If a cat were to disappear in Pasadena and at the same time appear in Erice, that would be an example of global conservation of cats. This is not the way cats are conserved. Cats or charge or baryons are conserved in a much more continuous way. If any of these quantities begin to disappear in a region, then they begin to appear in a neighbouring region. Consequently, we can identify a flow of charge out of a region with the disappearance of charge inside the region. This identification of the divergence of a flux with the time rate of change of a charge density is called a local conservation law. A local conservation law implies that the total charge is conserved globally, but the reverse does not hold. However, relativistically it is clear that non-local global conservation laws cannot exist, since to a moving observer the cat will appear in Erice before it disappears in Pasadena.»

We could relax and enjoy the Standard Model, but we already know that this superb synthesis is just the starting point of a new horizon.

For this new horizon to be investigated, a project for a new collider able to work at extreme energy and luminosity is needed.

This is ELN (**E**uroasiatic **L**Ong **I**ntersecting **S**torage **A**ccelerator), a (pp) collider with the highest energy and luminosity which could be built with simple extrapolation of the presently known technologies.

The ELN project is very ambitious but we should be encouraged by our previous experiences.

In fact, the path leading to the ELN has already gone through the Gran Sasso project (now the largest and most powerful underground laboratory in the world), the LEP-white-book which allowed this great European venture to overcome the many difficulties that had blocked its implementation during many years, the HERA collider (now successfully completed), and the roots of LHC, as for example the 5-metres diameter (not 3 metres) for the 27 Km (not 13 Km) LEP tunnel, and the LAA-R&D project, implemented to find the detector technologies needed for **LHC**.

These past achievements in project realization are mentioned in order to corroborate my optimism and enthusiasm in encouraging new actions and new ideas for the future of Subnuclear Physics in Europe and in the world, all having as focus CERN, the greatest Subnuclear Physics Lab in the world.

REFERENCES

- [1] *The Simultaneous Evolution of Masses and Couplings: Consequences on Supersymmetry Spectra and Thresholds*
F. Anselmo, L. Cifarelli, A. Petermann and A. Zichichi, *Nuovo Cimento* **105A**, 1179 (1992).
- [2] *Search for Supersymmetric Particles using Acoplanar Charged Particle Pairs from Z^0 decays*
ALEPH Collab., D. Decamp et al., *Phys. Lett.* **B236**, 86 (1990).
- [3] *Search for Neutral Higgs Bosons from Supersymmetry in Z decays*
ALEPH Collab., D. Decamp et al., *Phys. Lett.* **B237**, 291 (1990).
- [4] *Search for Neutralino Production in Z decays*
ALEPH Collab., D. Decamp et al., *Phys. Lett.* **B244**, 541 (1990).
- [5] *Search for the Neutral Higgs Bosons of the MSSM and other two Doublet Models*
ALEPH Collab., D. Decamp et al., *Phys. Lett.* **B265**, 475 (1991).
- [6] *Search for Heavy Charged Scalars in Z^0 decays*
DELPHI Collab., P. Abreu et al., *Phys. Lett.* **B241**, 449 (1990).
- [7] *Search for Pair Production of Neutral Higgs Bosons in Z^0 decays*
DELPHI Collab., P. Abreu et al., *Phys. Lett.* **B245**, 276 (1990).
- [8] *Search for Scalar Quarks in Z^0 decays*
DELPHI Collab., P. Abreu et al., *Phys. Lett.* **B247**, 148 (1990).
- [9] *A Search for Sleptons and Gauginos in Z^0 Decays*
DELPHI Collab., P. Abreu et al., *Phys. Lett.* **B247**, 157 (1990).
- [10] *Mass Limits for Scalar Muons, Scalar Electrons and Winos from e^+e^- Collisions near $S^{**}(1/2) = 91\text{--}GeV$*
L3 Collab., B. Adeva et al., *Phys. Lett.* **B233**, 530 (1989).
- [11] *Search for the Neutral Higgs Bosons of the Minimal Supersymmetric Standard Model from Z^0 Decays*
L3 Collab., B. Adeva et al., *Phys. Lett.* **B251**, 311 (1990).
- [12] *Search for the Charged Higgs Boson in Z^0 decay*
L3 Collab., B. Adeva et al., *Phys. Lett.* **B252**, 511 (1990).
- [13] *A Search for Acoplanar Pairs of Leptons or Jets in Z^0 decays: Mass Limits on Supersymmetric Particles*
OPAL Collab., M.Z. Akrawy et al., *Phys. Lett.* **B240**, 261 (1990).
- [14] *A Search for Technipions and Charged Higgs Bosons at LEP*
OPAL Collab., M.Z. Akrawy et al., *Phys. Lett.* **B242**, 299 (1990).
- [15] *A Direct Search for Neutralino Production at LEP*
OPAL Collab., M.Z. Akrawy et al., *Phys. Lett.* **B248**, 211 (1990); P.D. Acton et al., preprint CERN-PPE/91-115, 22 July 1991.
- [16] *Searches for Supersymmetric Particles Produced in Z Boson decay*
MARK II Collab., T. Barklow et al., *Phys. Rev. Lett.* **64**, 2984 (1990).

- [17] *Searches for New Particles at LEP*
M. Davier, LP-HEP 91 Conference, Geneva, CH, Preprint LAL 91-48, December 1991.
- [18] *The Evolution of Gaugino Masses and the SUSY Threshold*
F. Anselmo, L. Cifarelli, A. Peterman and A. Zichichi, *Nuovo Cimento* 105A, 581 (1992).
- [19] *A Detailed Comparison of LEP Data with the Predictions of the Minimal Supersymmetric SU(5) GUT*
J.R. Ellis, S. Kelley, D.V. Nanopoulos, preprint CERN-TH/6140-91, *Nucl. Phys.* B373, 55 (1992).
- [20] *Measurement of the Anomalous Magnetic Moment of the Muon*
G. Charpak, F.J. Farley, R.L. Garwin, T. Muller, J.C. Sens, V.L. Telegdi and A. Zichichi, *Phys. Rev. Lett.* 6, 128 (1961).
- [21] *(g-2) and Its Consequences*
G. Charpak, F.J. Farley, R.L. Garwin, T. Muller, J.C. Sens and A. Zichichi
Proceedings of the International Conference on *High-Energy Physics*, Geneva, Switzerland, 4-11 July 1962, 476 (CERN, Geneva, 1962).
- [22] *A Measurement of the μ^+ Lifetime*
F.J. Farley, T. Massam, T. Muller and A. Zichichi
Proceedings of the International Conference on *High-Energy Physics*, Geneva, Switzerland, 4-11 July 1962, 415 (CERN, Geneva, 1962); and
CERN Work on Weak Interactions
A. Zichichi, in the February 1964 Meeting of the Royal Society. *Proc. Roy. Soc.* A285, 175 (1965).
- [23] *A Proposal to Search for Leptonic Quarks and Heavy Leptons Produced by ADONE*
M. Bernardini, D. Bollini, E. Fiorentino, F. Mainardi, T. Massam, L. Monari, F. Palmonari and A. Zichichi, *INFN/AE-67/3*, 20 March 1967; see also
Limits on the Electromagnetic Production of Heavy Leptons
V. Alles-Borelli, M. Bernardini, D. Bollini, P.L. Brunini, T. Massam, L. Monari, F. Palmonari and A. Zichichi, *Lettere al Nuovo Cimento* 4, 1156 (1970);
Limits on the Mass of Heavy Leptons
M. Bernardini, D. Bollini, P.L. Brunini, E. Fiorentino, T. Massam, L. Monari, F. Palmonari, F. Rimondi and A. Zichichi, *Nuovo Cimento* 17A, 383 (1973); and
The Origin of the Third Family
C.S. Wu, T.D. Lee, N. Cabibbo, V.F. Weisskopf, S.C.C. Ting, C. Villi, M. Conversi, A. Petermann, B.H. Wiik and G. Wolf; O. Barnabei, L. Maiani, R.A. Ricci and F. Roversi Monaco (eds), Rome (1997); and World Scientific (1998).
- [24] For a complete set of references concerning this topic see "*The Creation of Quantum ChromoDynamics and the Effective Energy*" V.N. Gribov, G. 't Hooft, G. Veneziano and V.F. Weisskopf; N.L. Lipatov (ed), Academy of Sciences and University of Bologna, INFN, SIF, published by World Scientific, 1998.
- [25] *Pseudoparticle Solutions of the Yang-Mills Equations*
A.A. Belavin, A.M. Polyakov, A.S. Schwartz and Yu.S. Tyupkin, *Phys. Lett.* 59B, 85 (1975).
- [26] *Computation of the Quantum Effects due to a four-Dimensional Pseudoparticle*
G. 't Hooft, *Phys. Rev.* D14, 3432 (1976); and *err. Phys. Rev.* D18, 2199 (1978).

- [27] *Vacuum Periodicity in a Yang-Mills Quantum Theory*
R. Jackiw and C. Rebbi, *Phys. Rev. Lett.* 37, 172 (1976); for a clear Lecture on the subject see [29].
- [28] *The Structure of the Gauge Theory Vacuum*
C.G. Callan, R.F. Dashen and D.J. Gross, *Phys. Lett.* 63B, 334 (1976).
- [29] *The uses of Instantons*
S. Coleman, in "The Whys of Subnuclear Physics", Erice 1977, A. Zichichi (ed), Plenum Press, New York and London, 805 (1979).
- [30] *How Instantons Solve the U(1) Problem*
G. 't Hooft, *Phys. Rept.* 142, 357 (1986).
- [31] *Speakable and Unspeakable in Quantum Mechanics*
J.S. Bell, Cambridge University Press, London (1987).
- [32] *Current Algebra and Anomalies*
S.B. Treiman, R. Jackiw, B. Zumino and E. Witten (eds), pages 81 and 211, World Scientific.
- [33] *A PCAC Puzzle: $\pi^0 \rightarrow \gamma\gamma$ in the σ -Model*
J.S. Bell and R. Jackiw, *Nuovo Cimento* A60, 47 (1969).
- [34] *Axial-Vector Vertex in Spinor Electrodynamics*
S.L. Adler, *Phys. Rev.* 177, 2426 (1969).
- [35] *Absence of Higher-Order Corrections in the Anomalous Axial-Vector Divergence Equation*
S.L. Adler and W.A. Bardeen, *Phys. Rev.* 182, 1517 (1969).
- [36] *The Quantum Theory of the Electron*
P.A.M. Dirac, *Proc. Roy. Soc. (London)* A117, 610 (1928); and
The Quantum Theory of the Electron, Part II
P.A.M. Dirac, *Proc. Roy. Soc. (London)* A118, 351 (1928).
- [37] *The Positive Electron*
C.D. Anderson, *Phys. Rev.* 43, 491 (1933); and
Some Photographs of the Tracks of Penetrating Radiation
P.M.S. Blackett and G.P.S. Occhialini, *Proc. Roy. Soc.* A139, 699 (1933).
- [38] *Gruppentheorie und Quantenmechanik*
H. Weyl, 2nd ed., 234 (1931).
- [39] *Unitary Representations of the Inhomogeneous Lorentz Group*
E.P. Wigner, *Ann. Math.*, 40, 149 (1939).
- [40] *Intrinsic Parity of Elementary Particles*
G.C. Wick, E.P. Wigner, and A.S. Wightman, *Phys. Rev.* 88, 101 (1952).
- [41] *Über die Operation der Zeitumkehr in der Quanten-mechanik*
E.P. Wigner, *Gött. Nach.* 546-559 (1931). Here for the first time an anti-unitary symmetry appears.
- [42] E.P. Wigner, *Ann. Math.* 40, 149 (1939).

- [43] J. Schwinger, *Phys. Rev.* 82, 914 (1951).
- [44] *Time Reversal in Field Theory*
J.S. Bell, *Proc. Roy. Soc. (London)* A231, 479-495 (1955).
- [45] To the best of my knowledge, the CPT theorem was first proved by W. Pauli in his article “*Exclusion Principle, Lorentz Group and Reflection of Space-Time and Charge*”, in “*Niels Bohr and the Development of Physics*” [Pergamon Press, London, page 30 (1955)], which in turn is an extension of the work of J. Schwinger [*Phys. Rev.* 82, 914 (1951); “*The Theory of Quantized Fields. II.*”, *Phys. Rev.* 91, 713 (1953); “*The Theory of Quantized Fields. III.*”, *Phys. Rev.* 91, 728 (1953); “*The Theory of Quantized Fields. VI.*”, *Phys. Rev.* 94, 1362 (1954)] and G. Lüders, “*On the Equivalence of Invariance under Time Reversal and under Particle-Anti-particle Conjugation for Relativistic Field Theories*” [*Dansk. Mat. Fys. Medd.* 28, 5 (1954)], which referred to an unpublished remark by B. Zumino. The final contribution to the CPT theorem was given by R. Jost, in “*Eine Bemerkung zum CPT Theorem*” [*Helv. Phys. Acta* 30, 409 (1957)], who showed that a weaker condition, called “weak local commutativity” was sufficient for the validity of the CPT theorem.
- [46] *Observation of Antiprotons*
O. Chamberlain, E. Segrè, C. Wiegand, and T. Ypsilantis, *Physical Review* 100, 947 (1955).
- [47] *Anti-Neutrons Produced from Anti-Protons in Charge Exchange Collisions*
B. Cork, G.R. Lambertson, O. Piccioni, W.A. Wenzel, *Physical Review* 104, 1193 (1957).
- [48] *Observation of Long-Lived Neutral V Particles*
K. Lande, E.T. Booth, J. Impeduglia, L.M. Lederman, and W. Chinowski, *Physical Review* 103, 1901 (1956).
- [49] *Remarks on Possible Noninvariance under Time Reversal and Charge Conjugation*
T.D. Lee, R. Oehme, and C.N. Yang, *Physical Review* 106, 340 (1957).
- [50] *Question of Parity Conservation in Weak Interactions*
T.D. Lee and C.N. Yang, *Phys. Rev.* 104, 254 (1956).
- [51] *Experimental Test of Parity Conservation in Beta Decay*
C.S. Wu, E. Ambler, R.W. Hayward, D.D. Hoppes, *Phys. Rev.* 105, 1413 (1957);
Observation of the Failure of Conservation of Parity and Charge Conjugation in Meson Decays: The Magnetic Moment of the Free Muon
R. Garwin, L. Lederman, and M. Weinrich, *Phys. Rev.* 105, 1415 (1957);
Nuclear Emulsion Evidence for Parity Non-Conservation in the Decay Chain $\pi^+\mu^+e^+$
J.J. Friedman and V.L. Telegdi, *Phys. Rev.* 105, 1681 (1957).
- [52] *On the Conservation Laws for Weak Interactions*
L.D. Landau, *Zh. Éksp. Teor. Fiz.* 32, 405 (1957).
- [53] *Evidence for the 2π Decay of the K_2^0 Meson*
J. Christenson, J.W. Cronin, V.L. Fitch, and R. Turlay, *Physical Review Letters* 113, 138 (1964).
- [54] *Experimental Observation of Antideuteron Production*
T. Massam, Th. Muller, B. Righini, M. Schneegans, and A. Zichichi, *Nuovo Cimento* 39, 10 (1965).

- [55] *The Discovery of Nuclear Antimatter*
L. Maiani and R.A. Ricci (eds), Conference Proceedings 53, Italian Physical Society, Bologna, Italy (1995); see also A. Zichichi in “*Subnuclear Physics - The first fifty years*”, O. Barnabei, P. Pupillo and F. Roversi Monaco (eds), a joint publication by University and Academy of Sciences of Bologna, Italy (1998); World Scientific Series in 20th Century Physics, Vol. 24 (2000); see also
Why antihydrogen and antimatter are different
A. Zichichi, CERN Courier Vol. 49, n. 4, pp 15-17, May (2009).
- [56] The first report on “scaling” was presented by J.I. Friedman at the 14th International Conference on *High Energy Physics* in Vienna, 28 August-5 September 1968. The report was presented as paper n. 563 but not published in the Conference Proceedings. It was published as a SLAC preprint. The SLAC data on scaling were included in the Panofsky general report to the Conference where he says «... the apparent success of the parametrization of the cross-sections in the variable v / q^2 in addition to the large cross-section itself is at least indicative that point-like interactions are becoming involved». “*Low q^2 Electrodynamics, Elastic and Inelastic Electron (and Muon) Scattering*”, W.K.H. Panofsky in Proceedings of 14th International Conference on *High Energy Physics* in Vienna 1968, J. Prentki and J. Steinberger (eds), page 23, published by CERN (1968). The following physicists participated in the inelastic electron scattering experiments: W.B. Atwood, E. Bloom, A. Bodek, M. Breidenbach, G. Buschhorn, R. Cottrell, D. Coward, H. DeStaebler, R. Ditzler, J. Drees, J. Elias, G. Hartmann, C. Jordan, M. Mestayer, G. Miller, L. Mo, H. Piel, J. Poucher, C. Prescott, M. Riordan, L. Rochester, D. Sherden, M. Sogard, S. Stein, D. Trines, and R. Verdier. For additional acknowledgements see J.I. Friedman, H.W. Kendall and R.E. Taylor, “*Deep Inelastic Scattering: Acknowledgements*”, *Les Prix Nobel 1990*, (Almqvist and Wiksell, Stockholm/Uppsala 1991), also *Rev. Mod. Phys.* 63, 629 (1991). For a detailed reconstruction of the events see J.I. Friedman “*Deep Inelastic Scattering Evidence for the Reality of Quarks*” in “*History of Original Ideas and Basic Discoveries in Particle Physics*”, H.B. Newman and T. Ypsilantis (eds), Plenum Press, New York and London, 725 (1994).
- [57] *Quark Search at the ISR*
T. Massam and A. Zichichi, *CERN preprint*, June 1968;
Search for Fractionally Charged Particles Produced in Proton-Proton Collisions at the Highest ISR Energy
M. Basile, G. Cara Romeo, L. Cifarelli, P. Giusti, T. Massam, F. Palmonari, G. Valenti and A. Zichichi, *Nuovo Cimento* 40A, 41 (1977); and
A Search for quarks in the CERN SPS Neutrino Beam
M. Basile, G. Cara Romeo, L. Cifarelli, A. Contin, G. D'Alì, P. Giusti, T. Massam, F. Palmonari, G. Sartorelli, G. Valenti and A. Zichichi, *Nuovo Cimento* 45A, 281 (1978).
- [58] A. Zichichi in “*Subnuclear Physics - The first fifty years*”
O. Barnabei, P. Pupillo and F. Roversi Monaco (eds), a joint publication by University and Academy of Sciences of Bologna, Italy (1998); World Scientific Series in 20th Century Physics, Vol. 24 (2000).
- [59] *New Developments in Elementary Particle Physics*
A. Zichichi, *Rivista del Nuovo Cimento* 2, n. 14, 1 (1979). The statement on page 2 of this paper, «*Unification of all forces needs first a Supersymmetry. This can be broken later, thus generating the sequence of the various forces of nature as we observe them*», was based on a work by A. Petermann and A. Zichichi in which the renormalization group running of the couplings using supersymmetry was studied with the result that the convergence of the three couplings improved. This work was not published, but perhaps known to a few. The statement quoted is the first instance in

which it was pointed out that supersymmetry might play an important role in the convergence of the gauge couplings. In fact, the convergence of three straight lines ($\alpha_1^{-1}\alpha_2^{-1}\alpha_3^{-1}$) with a change in slope is guaranteed by the Euclidean geometry, as long as the point where the slope changes is tuned appropriately. What is incorrect about the convergence of the couplings is that, with the initial conditions given by the LEP results, the change in slope needs to be at $M_{\text{SUSY}} \sim 1 \text{ TeV}$ as claimed by some authors not aware in 1991 of what was known in 1979 to A. Petermann and A. Zichichi.

- [60] V.N. Gribov, G. 't Hooft, G. Veneziano and V.F. Weisskopf “*The Creation of Quantum ChromoDynamics and the Effective Energy*”, L.N. Lipatov (ed), a joint publication by the University and the Academy of Sciences of Bologna, Italy (1998); World Scientific Series in 20th Century Physics, Vol. 25 (2000).
- [61] *The Effective Experimental Constraints on M_{SUSY} and M_{GUT}*
F. Anselmo, L. Cifarelli, A. Petermann and A. Zichichi, *Nuovo Cimento* 104A, 1817 (1991).
- [62] *A Study of the Various Approaches to M_{GUT} and α_{GUT}*
F. Anselmo, L. Cifarelli and A. Zichichi, *Nuovo Cimento* 105A, 1335 (1992).
- [63] *Are Matter and Antimatter Symmetric?*
T.D. Lee, in Proceedings of the “*Symposium to celebrate the 30th anniversary of the Discovery of Nuclear Antimatter*”, L. Maiani and R.A. Ricci (eds), Conference Proceedings 53, page 1, Italian Physical Society, Bologna, Italy (1995).
- [64] *String Theory: the Basic Ideas*
B. Greene, Erice Lectures - Discussion 1999 in “*Basics and Highlights in Fundamental Physics*”, A. Zichichi (ed), World Scientific (2001).
- [65] *Quantised Singularities in the Electromagnetic Field*
P.A.M. Dirac, *Proc. Roy. Soc.* A133, 60 (1931);

The Principles of Quantum Mechanics
P.A.M. Dirac, (4th edn), Clarendon Press, Oxford (1958).

THE EARLY HISTORY OF STRING THEORY AND SUPERSYMMETRY

■ JOHN H. SCHWARZ

*California Institute of Technology
Pasadena, CA 91125, USA*

Abstract

This lecture presents a brief overview of the early history of string theory and supersymmetry. It describes how the S-matrix theory program for understanding the strong nuclear force evolved into superstring theory, which is a promising framework for constructing a unified quantum theory of all forces including gravity. The period covered begins with S-matrix theory in the mid 1960s and ends with the widespread acceptance of superstring theory in the mid 1980s. Further details and additional references can be found in Schwarz (2007).

1 S-Matrix Theory

In UC Berkeley, where I was a graduate student in the mid 1960s, Geoffrey Chew (my thesis advisor), Stanley Mandelstam, and others focussed their efforts on constructing a theory of the strong nuclear force, *i.e.*, a theory of hadrons. Chew's approach to understanding the strong nuclear force was based on *S-matrix theory*. He argued that quantum field theory, which was so successful in describing QED, was inappropriate for describing a strongly interacting theory, where a weak-coupling perturbation expansion would not be useful. One reason for holding this view was that none of the hadrons seemed more fundamental than any of the others. Therefore a field theory that singled out some subset of the hadrons did not seem sensible. Also, it seemed impossible to formulate a quantum field theory with a fundamental field for every hadron. Chew spoke of *nuclear democracy* and the *bootstrap principle* to describe this situation. Chew advocated focussing attention on physical quantities, especially the S Matrix, which describes on-mass-shell scattering amplitudes. The goal was to develop a theory that would determine the hadron spectrum and hadronic S matrix.

The quark concept also arose during this period, but the prevailing opinion in the mid 1960s was that quarks are mathematical constructs, rather than physical entities, whose main use is as a mathematical technique for understanding symmetries and quantum numbers. The SLAC deep inelastic scattering experiments in the late 1960s made it clear that quarks and gluons are physical (confined) particles. It was then natural to try to base a quantum field theory on them, and QCD was developed a few years later with the discovery of asymptotic freedom. Thus, with the wisdom of hindsight, it is clear that Chew *et al.* were wrong to reject quantum field theory. Nonetheless, their insights were very influential, perhaps even

crucial, for the discovery of string theory, which can be regarded as the ultimate realization of the S-matrix theory program.

Some of the ingredients that went into the S-matrix theory program, such as unitarity and maximal analyticity of the S matrix, were properties (deduced from quantum field theory) that encode the requirements of causality and nonnegative probabilities. Another important ingredient was analyticity in angular momentum. The idea is that partial wave amplitudes $a_l(s)$, which are defined in the first instance for angular momenta $l = 0, 1, \dots$, can be extended to an analytic function of l , $a(l, s)$. The uniqueness of this extension results from imposing suitable asymptotic behavior in l . The Mandelstam invariant s is the square of the center-of-mass energy of the scattering reaction. The analytic function $a(l, s)$ can have isolated poles called *Regge poles*. (Branch points are also possible, but they are usually ignored.) The position of a Regge pole is given by a *Regge trajectory* $l = \alpha(s)$. A value of s for which $l = \alpha(s)$ takes a physical value corresponds to a physical hadron of spin l .

Theoretical work in this period was strongly influenced by experimental results. Many new hadrons were discovered in experiments at the Bevatron in Berkeley, the AGS in Brookhaven, and the PS at CERN. Plotting masses squared versus angular momentum (for fixed values of other quantum numbers), it was noticed that the Regge trajectories are approximately linear with a common slope

$$\alpha(s) = \alpha(0) + \alpha' s \quad \alpha' \sim 1.0 (\text{GeV})^{-2}.$$

Using the crossing-symmetry properties of analytically continued scattering amplitudes, one argued that exchange of Regge poles (in the t channel) controlled the high-energy, fixed momentum transfer, asymptotic behavior of physical amplitudes:

$$A(s, t) \sim \beta(t)(s/s_0)^{\alpha(t)} \quad s \rightarrow \infty, t < 0.$$

In this way one deduced from data that the intercept of the ρ trajectory, for example, was $\alpha_\rho(0) \sim .5$. This is consistent with the measured mass $m_\rho = .76 \text{ GeV}$ and the Regge slope $\alpha' \sim 1.0 (\text{GeV})^{-2}$.

The approximation of linear Regge trajectories describes long-lived resonances, whose widths are negligible compared to their masses. This approximation is called the *narrow resonance approximation*. In this approximation branch cuts in scattering amplitudes, whose branch points correspond to multiparticle thresholds, are approximated by a sequence of resonance poles. This is what one would expect in the tree approximation to a quantum field theory in which all the resonances appear as fundamental fields. However, there was also another discovery, called *duality*, which clashed with the usual notions of quantum field theory. In this context duality means that a scattering amplitude can be expanded in an infinite series of s -channel poles, and this gives the same result as its expansion in an infinite series of t -channel poles. To include both sets of poles, as usual Feynman diagram techniques might suggest, would amount to double counting.

2 The Discovery of String Theory

Veneziano (1968) discovered a simple analytic formula that exhibits duality with linear Regge trajectories. It is given by a sum of ratios of Euler gamma functions:

$$T = A(s, t) + A(s, u) + A(t, u), \quad \text{where} \quad A(s, t) = g^2 \frac{\Gamma(-\alpha(s))\Gamma(-\alpha(t))}{\Gamma(-\alpha(s) - \alpha(t))},$$

g is a coupling constant, and α is a linear Regge trajectory

$$\alpha(s) = \alpha(0) + \alpha' s.$$

The Veneziano formula gives an explicit realization of duality and Regge behavior in the narrow resonance approximation. The function $A(s, t)$ can be expanded as an infinite series of s -channel poles or of t -channel poles. The motivation for writing down this formula was largely phenomenological, but it turned out that formulas of this type describe scattering amplitudes in the tree approximation to a consistent quantum theory!

A generalization to incorporate adjoint $SU(N)$ quantum numbers was formulated by Paton and Chan (1969). Chan–Paton symmetry was initially envisaged to be a global (flavor) symmetry, but it was shown later to be a local gauge symmetry.

Very soon after the appearance of the Veneziano amplitude, Virasoro (1969) proposed an alternative formula

$$T = g^2 \frac{\Gamma(-\frac{1}{2}\alpha(s))\Gamma(-\frac{1}{2}\alpha(t))\Gamma(-\frac{1}{2}\alpha(u))}{\Gamma(-\frac{1}{2}\alpha(t) - \frac{1}{2}\alpha(u))\Gamma(-\frac{1}{2}\alpha(s) - \frac{1}{2}\alpha(u))\Gamma(-\frac{1}{2}\alpha(s) - \frac{1}{2}\alpha(t))},$$

which has similar virtues. Since this formula has total stu symmetry, it describes particles that are singlets of the Chan–Paton symmetry group.

Over the course of the next year or so, *dual models*, as the subject was then called, underwent a sudden surge of popularity, marked by several remarkable discoveries. One was the discovery (by several different groups) of an N -particle generalization of the Veneziano formula

$$A_N(k_1, k_2, \dots, k_N) = g_{\text{open}}^{N-2} \int d\mu_N(y) \prod_{i < j} (y_i - y_j)^{\alpha' k_i \cdot k_j},$$

where y_1, y_2, \dots, y_N are real coordinates. I will omit the description of the measure $d\mu_N(y)$, which can be found in Schwarz (2007). This formula has cyclic symmetry in the N external lines. Soon thereafter Shapiro (1970) formulated an N -particle generalization of the Virasoro formula:

$$A_N(k_1, k_2, \dots, k_N) = g_{\text{closed}}^{N-2} \int d\mu_N(z) \prod_{i < j} |z_i - z_j|^{\alpha' k_i \cdot k_j},$$

where z_1, z_2, \dots, z_N are complex coordinates. This amplitude has total symmetry in the N external lines.

Both of these formulas for multiparticle amplitudes were shown to have poles whose residues factorize in a consistent manner on an infinite spectrum of single-particle states.

This spectrum is described by a Fock space associated to an infinite number of harmonic oscillators

$$\{a_m^\mu\} \quad \mu = 0, 1, \dots, d-1 \quad m = 1, 2, \dots$$

where d is the dimension of Minkowski spacetime, which was initially assumed to be four. There is one set of such oscillators in the Veneziano case and two sets in the Shapiro–Virasoro case. These spectra were interpreted as describing the normal modes of a relativistic string: an open string (with ends) in the first case and a closed string (loop) in the second case. Amazingly, the formulas were discovered before this interpretation was proposed. In the above formulas, the y coordinates parametrize points on the boundary of a string world sheet, where particles that are open-string states are emitted or absorbed, whereas the z coordinates parametrize points on the interior of a string world sheet, where particles that are closed-string states are emitted or absorbed. (It is also possible to construct amplitudes in which both types of particles participate.)

Having found the factorization, it became possible to compute radiative corrections (loop amplitudes). Gross, Neveu, Scherk, and Schwarz (1970) discovered unanticipated singularities in a particular one-loop diagram for which the world sheet is a cylinder with two external particles attached to each of the two boundaries. The computations showed that this diagram gives branch points that violate unitarity. This was a very disturbing conclusion, since it seemed to imply that the classical theory does not have a consistent quantum extension. However, soon thereafter it was pointed out by Lovelace (1971) that these branch points become poles provided that

$$\alpha(0) = 1 \quad \text{and} \quad d = 26.$$

Prior to this discovery, everyone assumed that the spacetime dimension should be $d = 4$. We had no physical reason to consider extra dimensions. It was the mathematics that forced us in that direction. Later, these poles were interpreted as closed-string states in a one-loop open-string amplitude. Nowadays this is referred to as *open-string/closed-string duality*. This is closely related to *gauge/gravity duality*, which was discovered 27 years later.

The analysis also required there to be an infinite number of decoupling conditions, which turned out to coincide with the constraints proposed by Virasoro (1970) and further elaborated upon by Fubini and Veneziano (1971). Since the string has an infinite spectrum of higher-spin states, there are corresponding gauge invariances that eliminate unphysical degrees of freedom. The operators that describe the constraints that arise for a particular covariant gauge choice satisfy the Virasoro algebra

$$[L_m, L_n] = (m - n)L_{m+n} + \frac{c}{12}(m^3 - m)\delta_{m,-n},$$

where m, n are arbitrary integers. These operators can also be interpreted as generators of conformal symmetry for the two-dimensional string world sheet. The central charge (or conformal anomaly) c is equal to the spacetime dimension d . This anomaly cancels for $d = 26$ when the contribution of Faddeev–Popov ghosts is included.

3 The RNS Model and the Discovery of Supersymmetry

In a very inspired and important development, Ramond (1971) constructed a stringy analog of the Dirac equation, which describes a fermionic string. Just as the string momentum p^μ is the zero mode of a density $P^\mu(\sigma)$, where the coordinate σ parametrizes the string, he proposed that the Dirac matrices γ^μ should be the zero modes of densities $\Gamma^\mu(\sigma)$. Then he considered the Fourier modes of the dot product:

$$F_n = \int_0^{2\pi} e^{-in\sigma} \Gamma(\sigma) \cdot P(\sigma) d\sigma \quad n \in \mathbb{Z}.$$

In particular,

$$F_0 = \gamma \cdot p + \text{additional terms.}$$

He proposed that physical states of a fermionic string should satisfy the following analog of the Dirac equation

$$(F_0 + M)|\psi\rangle = 0.$$

He also observed that in the case of the fermionic string the Virasoro algebra generalizes to a super-Virasoro algebra

$$\{F_m, F_n\} = 2L_{m+n} + \frac{c}{3}m^2\delta_{m,-n}$$

$$[L_m, F_n] = \left(\frac{m}{2} - n\right)F_{m+n}$$

$$[L_m, L_n] = (m - n)L_{m+n} + \frac{c}{12}m^3\delta_{m,-n}.$$

Ramond's paper does not include the central extension, which turns out to be $c = 3d/2$, where d is the spacetime dimension. A little later, it was realized that consistency requires $d = 10$ and $M = 0$. These conditions are the analogs of $d = 26$ and $\alpha(0) = 1$ for the bosonic Veneziano string theory.

A couple of months later Neveu and Schwarz (1971a) constructed a new interacting bosonic string theory, which was called the *dual pion model*. It has a similar structure to the fermionic string, but the periodic density $\Gamma^\mu(\sigma)$ is replaced by an antiperiodic one $H^\mu(\sigma + 2\pi) = -H^\mu(\sigma)$. Then the Fourier modes, which differ from an integer by $1/2$,

$$G_r = \int_0^{2\pi} e^{-ir\sigma} H \cdot P d\sigma \quad r \in \mathbb{Z} + 1/2$$

satisfy a similar super-Virasoro algebra. Neveu and Schwarz (1971a) refers to this algebra as a *supergauge algebra*, a terminology that was sensible in the context at hand. The Neveu–Schwarz bosons and Ramond fermions were combined in a unified interacting theory of bosons and fermions by Neveu and Schwarz (1971b) and by Thorn (1971). This theory (the RNS model) was an early version of superstring theory. As will be explained shortly, a few crucial issues were not yet understood.

After a few more months, Gervais and Sakita (1971) showed that the the RNS model is described by the string world-sheet action

$$S = T \int d\sigma d\tau \left(\partial_\alpha X^\mu \partial^\alpha X_\mu - i \bar{\psi}^\mu \gamma^\alpha \partial_\alpha \psi_\mu \right),$$

where the coefficient T is the string tension. They also explained that it has *two-dimensional supersymmetry*, though that terminology was not used yet, by showing that it is invariant under the transformations

$$\delta X^\mu = \bar{\varepsilon} \psi^\mu, \quad \delta \psi^\mu = -i \gamma^\alpha \varepsilon \partial_\alpha X^\mu,$$

where ε is an infinitesimal constant spinor. To the best of my knowledge, this is the first supersymmetric theory identified in the literature! There are two possibilities for the world-sheet fermi fields ψ^μ . When it is antiperiodic $\psi^\mu = H^\mu$, which gives the boson spectrum (Neveu–Schwarz sector), and when it is periodic $\psi^\mu = \Gamma^\mu$, which gives the fermion spectrum (Ramond sector).

Five years later, Brink, Di Vecchia, and Howe (1976) and Deser and Zumino (1976) constructed a more fundamental world-sheet action with local supersymmetry. This formulation of the world-sheet theory has the additional virtue of also accounting for the super-Virasoro constraints. From this point of view, the significance of the super-Virasoro algebra is that the world-sheet theory, when properly gauge fixed and quantized, has *superconformal symmetry*. Again, the anomaly cancels for $d = 10$ when the Faddeev–Popov ghosts are included.

At about the same time as Ramond’s paper, the four-dimensional super-Poincaré algebra was introduced in a paper by Golfand and Likhtman (1971), who proposed constructing 4d field theories with this symmetry. This paper went unnoticed in the West for several more years. In fact, the celebrated paper of Wess and Zumino (1974), which formulated a class of 4d supersymmetric theories, was motivated by the search for 4d analogs of the 2d Gervais–Sakita world-sheet action. The Wess-Zumino paper launched the study of supersymmetric field theories, which proceeded in parallel with the development of supersymmetric string theory. Wess and Zumino (1974) used the expression *supergauge*, following the terminology of Neveu and Schwarz (1971), but in their subsequent papers they switched to *supersymmetry*, which was more appropriate for what they were doing.

4 The Temporary Demise of String Theory

String theory is formulated as an on-shell S-matrix theory in keeping with its origins discussed earlier. However, the SLAC deep inelastic scattering experiments in the late 1960s made it clear that the hadronic component of the electromagnetic current is a physical off-shell quantity, and that its asymptotic properties imply that hadrons have hard pointlike constituents. Moreover, all indications (at that time) were that strings are too soft to describe hadrons with their pointlike constituents.

By 1973–74 there were many good reasons to stop working on string theory: a successful and convincing theory of hadrons (QCD) was discovered, and string theory had severe problems as a theory of hadrons. These included an unrealistic spacetime dimension ($d = 10$ or $d = 26$), an unrealistic spectrum (including a tachyon and massless particles), and the absence of pointlike constituents. A few years of attempts to do better had been unsuccessful. Moreover, convincing theoretical and experimental evidence for the Standard Model was rapidly falling into place. That was where the action was. Even for those seeking to pursue speculative theoretical ideas there were options other than string theory that most people found more appealing, such as grand unification and supersymmetric field theory. Understandably, string theory fell out of favor. What had been a booming enterprise involving several hundred theorists rapidly came to a grinding halt. Only a few diehards continued to pursue it.

5 Gravity and Unification

Among the problems of the known string theories, as a theory of hadrons, was the fact that the spectrum of open strings contains massless spin 1 particles, and the spectrum of closed strings contains a massless spin 2 particle (as well as other massless particles), but there are no massless hadrons. In 1974, Joël Scherk and I decided to take string theory seriously as it stood, rather than forcing it to conform to our preconceptions. This meant abandoning the original program of describing hadron physics and interpreting the massless spin 2 state in the closed-string spectrum as a graviton. Also, the massless spin 1 states in the open-string spectrum could be interpreted as particles associated to Yang–Mills gauge fields. Specifically, Scherk and Schwarz (1974) proposed trying to interpret string theory as a unified quantum theory of all forces including gravity. Neveu and Scherk (1972) had shown that string theory incorporates the correct gauge invariances to ensure agreement at low energies (compared to the scale given by the string tension) with Yang–Mills theory. Yoneya (1973,1974) and Scherk and Schwarz (1974) showed that it also contains gauge invariances that ensure agreement at low energies with general relativity.

To account for Newton’s constant, the most natural choice for the fundamental string length scale was $l_s \sim 10^{-33}$ cm (the Planck length) instead of $l_s \sim 10^{-13}$ cm (the typical size of a hadron). Thus the strings suddenly shrank by 20 orders of magnitude, but the mathematics was essentially unchanged. The string tension is proportional to l_s^{-2} , so it increased by 40 orders of magnitude.

The proposed new interpretation had several advantages:

- Gravity and Yang–Mills forces are required by string theory.
- String theory has no UV divergences.
- Extra spatial dimensions could be a good thing.

Let me say a few words about the last point. In a nongravitational theory, the spacetime geometry is a rigid background on which the dynamics takes place. In that setup, the fact

that we observe four-dimensional Minkowski spacetime is a compelling argument to formulate the theory in that background geometry. As you know very well, this is part of the story of the Standard Model. However, in a gravitational theory that abides by the general principles laid out by Einstein, the spacetime geometry is determined by the dynamical equations. In such a setup extra dimensions can make sense provided that the equations of the theory have a solution for which the geometry is the product of four-dimensional Minkowski spacetime and a compact manifold that is sufficiently small to have eluded detection. It turns out that there are many such solutions. Moreover, the details of the compact manifold play a crucial role in determining the symmetries and particle content of the effective low-energy theory in four dimensions, even when the compact dimensions are much too small to observe directly.

6 Supersymmetry, Supergravity, and Superstrings

In the second half of the 1970s the study of supersymmetric field theories became a major endeavor. A few important supersymmetric theories that were formulated in that era included

- $\mathcal{N} = 1$, $d = 4$ supergravity, discovered by Freedman, Van Nieuwenhuizen, and Ferrara (1976) and Deser and Zumino (1976).
- $\mathcal{N} = 1$, $d = 10$ and $\mathcal{N} = 4$, $d = 4$ supersymmetric Yang–Mills theory discovered by Brink, Scherk, and Schwarz (1977) and Gliozzi, Scherk, and Olive (1977).
- $\mathcal{N} = 1$, $d = 11$ supergravity discovered by Cremmer, Julia and Scherk (1978).

Gliozzi, Scherk, and Olive (1976, 1977) proposed a truncation of the RNS string theory spectrum – *the GSO Projection* – that removes half of the fermion states and the “odd G-parity” bosons. In particular, the latter projection eliminates the tachyon. They showed that after the projection the number of physical bosonic degrees of freedom is equal to the number of physical fermionic degrees of freedom at every mass level. This was compelling evidence for *ten-dimensional spacetime supersymmetry* of the GSO-projected theory. Prior to this, we knew about the supersymmetry of the two-dimensional string world-sheet theory, but we had not considered the possibility of spacetime supersymmetry. In fact, the GSO projection is not just an option; it is required for consistency.

In 1979 Michael Green and I began a collaboration, which had the initial goal of understanding and proving the ten-dimensional spacetime supersymmetry of the GSO-projected version of the RNS theory. The highlights of our work included Green and Schwarz (1981, 1984a), which developed a new formalism in which the spacetime supersymmetry of the GSO-projected RNS string is manifest, and Green and Schwarz (1982), which classified the consistent ten-dimensional superstring theories and giving them the names Type I, Type IIA, and Type IIB. We were excited about these (and other) developments, but they did not arouse much interest in the theory community. String theory was still in the doldrums.

In the early 1980s there was growing interest in supersymmetry and extra dimensions. In particular, a small community became intrigued by Kaluza–Klein reduction of 11-dimensional

supergravity. Only the string ingredient was missing from their considerations. That changed following our next discovery.

7 Anomalies

If a unified theory is to make contact with the Standard Model, and have a chance of being realistic, parity violation is an essential ingredient. However, parity-violating classical theories generically have *gauge anomalies*, which means that they cannot be used to define quantum theories. The gauge symmetry is broken by one-loop quantum corrections, rendering the would-be quantum theory inconsistent. In the case of the Standard Model, if one were to change the theory by removing all of the leptons or all of the quarks, the theory would become inconsistent. When both the quarks and the leptons are included all gauge anomalies beautifully cancel, and so the Standard Model is a well-defined quantum theory. These considerations raise the question whether the potential gauge anomalies in chiral superstring theories also cancel, so that they give consistent quantum theories.

We knew that Type I superstring theory is a well-defined ten-dimensional theory at tree level for any $SO(n)$ or $Sp(n)$ gauge group, and that for every such group it is chiral (*i.e.*, parity violating). However, evaluation of a one-loop hexagon diagram in ten-dimensional super Yang–Mills theory, which describes the massless open-string states, exhibits explicit nonconservation of gauge currents, signalling a gauge anomaly. The only hope for consistency is that inclusion of the closed-string (gravitational) sector cancels this gauge anomaly without introducing new ones.

Type IIB superstring theory, which only has a closed-string gravitational sector, is also chiral and therefore potentially anomalous. It was not known how to analyze such anomalies until Alvarez-Gaumé and Witten (1984) derived general formulas for gauge, gravitational, and mixed anomalies in an arbitrary spacetime dimension. Using their results, they discovered that the gravitational anomalies, which would imply nonconservation of the stress tensor, cancel in Type IIB superstring theory. In their calculation this cancellation appears quite miraculous, though the UV finiteness of the Type IIB loop amplitudes implies that it had to work. Thus, Type IIB is a consistent chiral superstring theory. On the other hand, it did not look promising for describing the real world, since it does not contain any Yang–Mills gauge fields. (Many years later, nonperturbative Type IIB solutions that do contain Yang–Mills fields were discovered.) At that time, the last hope for constructing a realistic model seemed to reside with the Type I superstring theories, which are chiral and do contain Yang–Mills fields.

After a couple years of failed attempts, Green and I finally managed to compute the one-loop hexagon diagrams in Type I superstring theory. We found that both the cylinder and the Möbius-strip world-sheet diagrams contribute to the gauge anomaly and realized that there might be a gauge group for which the two contributions cancel. Green and Schwarz (1985) showed that $SO(32)$ is the unique choice for which the cancellation occurs. Since this

computation only demonstrated the cancellation of the pure gauge part of the anomaly, we decided to explore the low-energy effective field theory to see whether the gravitational and mixed anomalies also cancel. Using the results of Alvarez-Gaumé and Witten (1984), Green and Schwarz (1984b) verified that all gauge, gravitational, and mixed anomalies do in fact cancel for the gauge group $SO(32)$.

The effective field theory analysis showed that $E_8 \times E_8$ is a second (and the only other) gauge group for which the anomalies could cancel for a theory with $\mathcal{N} = 1$ supersymmetry in ten dimensions. In both cases, it is crucial for the result that the coupling to supergravity is included. The $SO(32)$ case could be accommodated by Type I superstring theory, but we didn't know a superstring theory with gauge group $E_8 \times E_8$. We were aware of the article by Goddard and Olive (1983) that pointed out (among other things) that there are exactly two even self-dual Euclidean lattices in 16 dimensions, and these are associated with precisely these two gauge groups. However, we did not figure out how to exploit this fact before the problem was solved by Gross, Harvey, Martinec, and Rohm (1985).

8 Epilogue

Following these discoveries there was a sudden surge of interest in superstring theory. After more than a decade, string theory had emerged from the doldrums. In my view, some of the new converts made a phase transition from being too pessimistic about string theory to being too optimistic about the near-term prospects for finding a realistic model. However, after a few years, almost all practitioners had a much more sober assessment of the challenges that remain. Superstring theory (including M-theory, which is part of the same theoretical framework) has remained a very active subject ever since 1984. Even though the construction of a complete and realistic model of elementary particles still appears to be a distant dream, the study of string theory has been enormously productive. For example, insights derived from these studies have had a profound impact on fundamental mathematics and are beginning to inspire new approaches to understanding topics in other areas of physics.

For many years string theory was considered to be a radical alternative to quantum field theory. However, in recent times – long after the period covered by this lecture – dualities relating string theory and quantum field theory were discovered. In view of these dualities, my current opinion is that string theory is best regarded as the logical completion of quantum field theory, and therefore it is not radical at all. There is still much that remains to be understood, but I am convinced that we are on the right track and making very good progress.

This work was supported in part by the U.S. Dept. of Energy under Grant No. DE-FG03-92-ER40701.

References

- Alvarez-Gaumé, L. & Witten, E. (1984). Gravitational anomalies. *Nuclear Physics B*, 234, 269-330.
- Brink, L., Di Vecchia, P., & Howe, P. (1976). A locally supersymmetric and reparametrization invariant action for the spinning string. *Physics Letters B*, 65, 471-474.
- Brink, L., Schwarz, J. H., & Scherk, J. (1977). Supersymmetric Yang-Mills theories. *Nuclear Physics B*, 121, 77-92.
- Cremmer, E., Julia, B., & Scherk, J. (1978). Supergravity theory in eleven-dimensions. *Physics Letters B*, 76, 409-412.
- Deser, S., & Zumino, B. (1976a). Consistent supergravity. *Physics Letters B*, 62, 335-337.
- Deser, S., & Zumino, B. (1976b). A complete action for the spinning string. *Physics Letters B*, 65, 369-373.
- Freedman, D. Z., Van Nieuwenhuizen, P., & Ferrara, S. (1976). Progress toward a theory of supergravity. *Physical Review D*, 13, 3214-3218.
- Fubini, S., & Veneziano, G. (1971). Algebraic treatment of subsidiary conditions in dual resonance models. *Annals of Physics*, 63, 12-27.
- Gervais, J. L., & Sakita, B. (1971). Field theory interpretation of supergauge in dual models. *Nuclear Physics B*, 34, 632-639.
- Gliozzi, F., Scherk, J., & Olive, D. (1976). Supergravity and the spinor dual model. *Physics Letters B*, 65, 282-286.
- Gliozzi, F., Scherk, J., & Olive, D. (1977). Supersymmetry, supergravity theories and the dual spinor model. *Nuclear Physics B*, 122, 253-290.
- Goddard, P., & Olive, D. (1983). Algebras, lattices and strings. DAMTP-83/22. Reprinted in Goddard, P. (Ed.), & Olive, D. (Ed.): *Kac-Moody and Virasoro Algebras* (pp. 210-255). World Scientific 1988.
- Golfand, Yu. A., & Likhtman, E. P. (1971). Extension of the algebra of Poincaré group

- generators and violation of P invariance. *JETP Lett.*, *13*, 323-326.
- Green, M. B., & Schwarz, J. H. (1981). Supersymmetrical dual string theory. *Nuclear Physics B*, *181*, 502-530.
- Green, M. B., & Schwarz, J. H. (1982). Supersymmetrical string theories. *Physics Letters B*, *109*, 444-448.
- Green, M. B., & Schwarz, J. H. (1984a). Covariant description of superstrings. *Physics Letters B*, *136*, 367-370.
- Green, M. B., & Schwarz, J. H. (1984b). Anomaly cancellation in supersymmetric $D = 10$ gauge theory and superstring theory. *Physics Letters B*, *149*, 117-122.
- Green, M. B., & Schwarz, J. H. (1985). The hexagon gauge anomaly in Type I superstring theory. *Nuclear Physics B*, *255*, 93-114.
- Gross, D. J., Neveu, A., Scherk, J., & Schwarz, J. H. (1970). Renormalization and unitarity in the dual resonance model. *Physical Review D*, *2*, 697-710.
- Gross, D. J., Harvey, J. A., Martinec, E. J., & Rohm, R. (1985). The heterotic string. *Physical Review Letters*, *54*, 502-505.
- Lovelace, C. (1971). Pomeron form factors and dual Regge cuts. *Physics Letters B*, *34*, 500-506.
- Neveu, A., & Schwarz, J. H. (1971a). Factorizable dual model of pions. *Nuclear Physics B*, *31*, 86-112.
- Neveu, A., & Schwarz, J. H. (1971b). Quark model of dual pions *Physical Review D*, *4*, 1109-1111.
- Neveu, A., Schwarz, J. H., & Thorn, C. B. (1971). Reformulation of the dual pion model. *Physics Letters B*, *35*, 529-533.
- Neveu, A., & Scherk, J. (1972). Connection between Yang-Mills fields and dual models. *Nuclear Physics B*, *36*, 155-161.
- Paton, J. E., & Chan, H. (1969). Generalized Veneziano model with isospin. *Nuclear Physics B*, *10*, 516-520.

- Ramond, P. (1971). Dual theory for free fermions. *Physical Review D*, 3, 2415-2418.
- Scherk, J., & Schwarz, J. H. (1974). Dual models for non-hadrons. *Nuclear Physics B*, 81, 118-144.
- Schwarz, J. H. (2007). The early years of string theory: a personal perspective. arXiv:0708.1917 [hep-th].
- Shapiro, J. A. (1970). Electrostatic analog for the Virasoro model. *Physics Letters B*, 33, 361-362.
- Thorn, C. B. (1971). Embryonic dual model for pions and fermions. *Physical Review D*, 4, 1112-1116.
- Veneziano, G. (1968). Construction of a crossing-symmetric Regge-behaved amplitude for linearly rising Regge trajectories. *Nuovo Cimento A*, 57, 190-197.
- Virasoro, M. (1969). Alternative constructions of crossing-symmetric amplitudes with Regge behavior. *Physical Review*, 177, 2309-2311.
- Virasoro, M. (1970). Subsidiary conditions and ghosts in dual resonance models. *Physical Review D*, 1, 2933-2936.
- Wess, J., & Zumino, B. (1974). Supergauge transformations in four dimensions. *Nuclear Physics B*, 70, 39-50.
- Yoneya, T. (1973). Quantum gravity and the zero slope limit of the generalized Virasoro model. *Nuovo Cimento Letters*, 8, 951-955.
- Yoneya, T. (1974). Connection of dual models to electrodynamics and gravodynamics. *Progress in Theoretical Physics*, 51, 1907-1920.

ACHIEVEMENTS IN SUBNUCLEAR PHYSICS AT FERMILAB

■ PIER ODDONE

Fermilab

Outline

- 1) Introduction
- 2) The early fixed-target era: discovery of the bottom quark
- 3) Fixed target experiments with the *Tevatron*: first observation of the tau neutrino
- 4) The *Tevatron Collider* era: discovery of the top quark
- 5) The current neutrino program and future extensions
- 6) The future muon campus: *g-2* and *Mu2e*
- 7) *Project X* and its scientific reach
- 8) Connection to the cosmic frontier
- 9) The follow-up to the *LHC* at the energy frontier

1. Introduction

In such a short presentation, I will be very selective in describing the physics achievements at Fermilab. Of the thousands of papers and results over the four decades of Fermilab's life I will be able to highlight only a few major achievements. I will also project into the future and highlight the plans for Fermilab at the three frontiers of particle physics: the energy frontier, the intensity frontier and the cosmic frontier.

Fermilab is a relatively young laboratory. It was created in 1965 when the University Research Association, a corporation that included a large number of research universities, signed a contract with the Atomic Energy Commission for the creation of Fermilab. Previous AEC laboratories had been mostly regional, dominated by the institutions that managed them, often single universities. Fermilab was to be different: a true national laboratory. The National Accelerator Laboratory (NAL), the first name for Fermilab, would be the home of the highest energy machine in the world by a large margin, more than a factor of 10 higher than the existing machines at the time, the Proton Synchrotron at CERN and the Alternating Gradient Synchrotron (AGS) at Brookhaven National Laboratory.

The original proposal to build a large accelerator had been developed by the Lawrence Berkeley Laboratory. It was for a 200 GeV machine, conservatively designed, based on combined function magnets. The founding director of Fermilab, Robert Wilson scrapped the Berkeley design and led a new design. This design was based on a lattice of separated-function magnets, of smaller aperture, capable of reaching 500 GeV and at the same time more economical than the Berkeley design.

Robert R. Wilson's own recollection of the early years of the laboratory, written in the 1987 URA Annual Report, has been published as a Fermilab "Golden Book"¹. Robert R. Wilson's imprint on the laboratory was huge: the ambitious design of the accelerator, the establishment of a Fermilab culture to serve the

university community, his promotion of international collaborations, the nature of its scientific program, the esthetics of the site, the stewardship of the natural environment, the novel architecture and his own ubiquitous sculptures that are an extraordinary melding of art and science.

The laboratory was built quickly at the current Fermilab site. The land was acquired by the Atomic Energy Commission (AEC) from 56 farming families in what at the time was a rural area in the proximity of Chicago. The aggregation of this farm land yielded a site of 6800 acres, appropriate to be the home of very large accelerators.

Ground-breaking for the Linear Accelerator, the front end of all machines at Fermilab, was in December 1st, 1968, and groundbreaking for the *Main Ring* was on October 3rd 1969; the first 200 GeV beam was achieved on March 1, 1972. A few months later, in December, Fermilab achieved the first 400 GeV beam. Robert Wilson's ultimate goal of 500 GeV was reached on May 14th, 1976. The National Accelerator Laboratory was dedicated to Enrico Fermi on May 14th, 1974 and became the Fermi National Accelerator Laboratory (FNAL) or Fermilab.

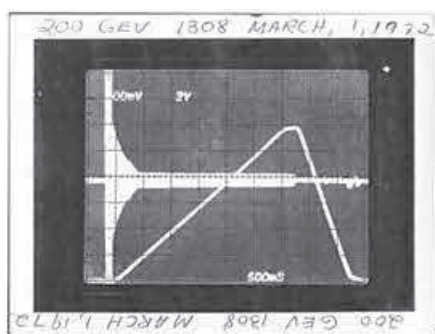


Figure 1: Screen shot and celebration on achieving 200 GeV; March 1, 1972



2. The early fixed target era: discovery of the bottom quark

During the initial phases of Fermilab, the entire program was based on fix target experiments that spanned a broad range of particle beams: primary proton beams, selected hadron and photon beams and neutrino beams. The program was characterized by a multiplicity of experiments using quite varied techniques: bubble chambers, multi-wire proportional chambers, Cerenkov counters and a variety of scintillation counters. The results of these experiments contributed to the gradual completion of the Standard Model of particle physics.

The most important experiment of this era was the discovery of the bottom quark by Leon Lederman and his team² in 1977. The original proposal had been submitted in 1970 to study single and double leptons from proton interactions. With the discovery of the J/Ψ at Brookhaven and SLAC in 1974, it became clear that the di-muon channel would be a powerful tool to discover “onium” states beyond charmonium. Ironically, Lederman’s early experiment at Brookhaven had detected a shoulder in the di-muon distribution that at the time was left unresolved. It was at the mass where San Ting and his team later discovered the J . In 1977 the experiment produced unmistakable evidence for the Upsilon at 9.5 GeV, making it a re-play of the charm discovery three years earlier.

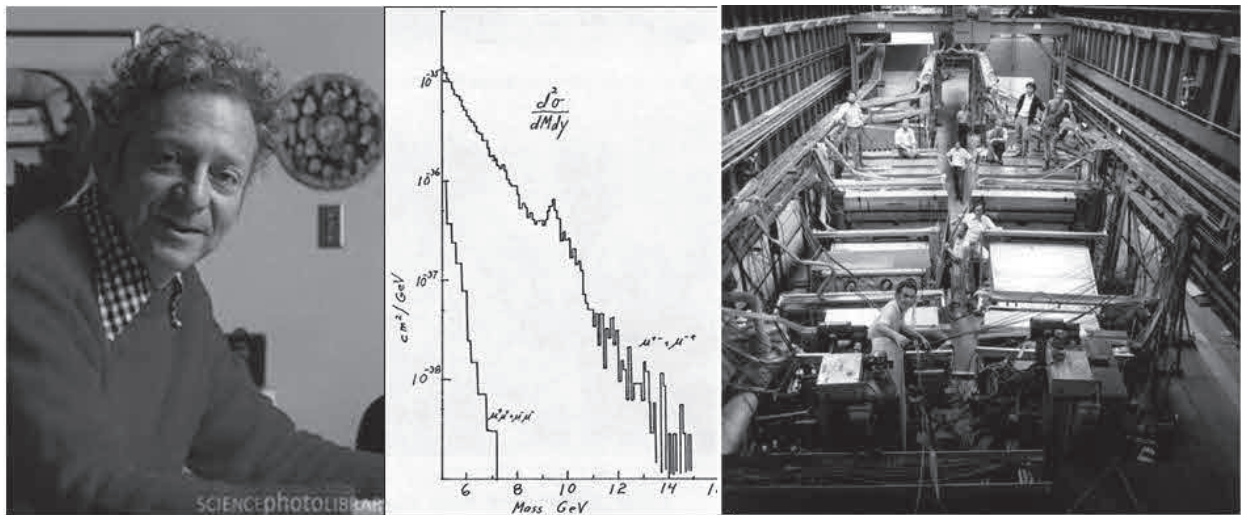


Figure 2: Discovery of the bottom quark: Lederman, data and detector

Another important set of experiments concerned the confirmation of the discovery by Gargamelle of neutral currents, one of the early back-and-forth between experiments at CERN and Fermilab.

3. Fixed target experiments with the *Tevatron*: first observation of the *tau* neutrino

Already during the construction of the *Main Ring*, there was considerable interest in the development of higher energy machines. The key was the development of superconducting magnets. The project initially called the *Energy Doubler/Saver* would double the energy of the main ring and save half the power. The second Director of Fermilab, Leon Lederman, decided to proceed with completing the superconducting ring instead of pursuing a race for the W and Z bosons by trying for a collider program with the existing *Main Ring*³.

With the advent of the *Energy Saver/Doubler* (dubbed the *Tevatron*), with its high energy and with both short and long spills, a set of powerful experiments ensued. The results of over 40 experiments were reviewed at a symposium in the year 2000⁴. The fixed target program was quite vast and important

covering QCD; the structure of protons, neutrons and mesons; charm and beauty mesons and their properties; hyperons; neutrinos and symmetry tests. For any given topic there was often a sequence of experiments that one could call a program of ever increasing capabilities. These programs led to five Panofsky prizes awarded for work either done entirely in the fixed target program at Fermilab or substantially done there⁵:

1990: Witherell (Charm)
 1994: Devlin & Pondrom (Hyperons)
 1995: Sciulli (Neutrinos)
 2004: Bodek (Neutrinos).
 2007: Winstein (Kaons, CP violation)

One of the examples was the series of experiments started with *E691*, in the study of charm. This experiment exploited the advent of silicon detectors to identify vertices and identify charm events. The experiment exploited the very large rates of charm production in a tagged photon beam compared to electron-positron colliders. The experiment produced more than 100 million events while keeping backgrounds under control⁶.

A second series of beautiful experiments was the study of direct matter-antimatter symmetry violation (CP violation) in neutral kaon decays, culminating with the *KTeV* experiment⁷. The results of *E731* and *KTeV* at Fermilab and the results of *NA31* and *NA48* at CERN alternated with progressively smaller systematic and statistical errors, ultimately establishing direct CP violation at greater than 5 sigma level. The competition between the two groups was fierce for a number of years and the progression of their results on the measurement of direct CP violation, the primary aim of the experiments, is shown below.

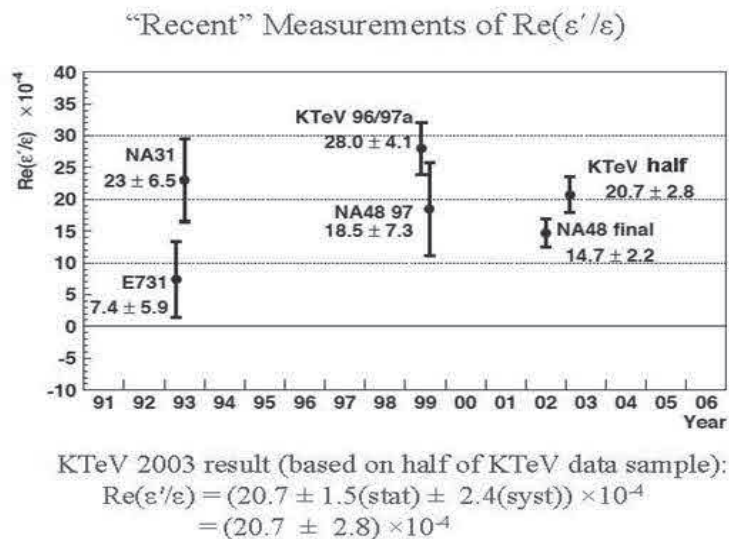
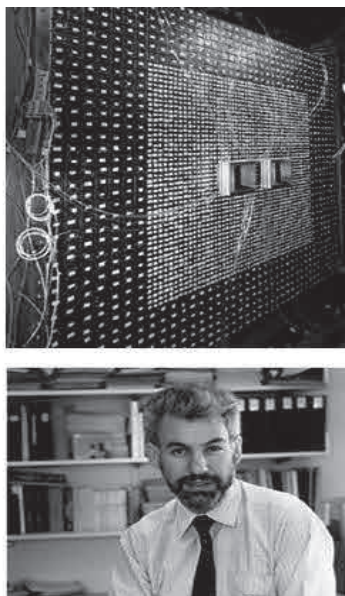


Figure 3: KTeV CsI Calorimeter, Bruce Weinstein and 2003 results

A beautiful example of the high-energy fixed target operation of the *Tevatron* was the first observation of the tau neutrino⁸. The existence of the third generation of quark and leptons was first established at SPEAR with the discovery of the charged tau-lepton. Using the high energy of the *Tevatron*, a high energy beam of neutrinos was used to produce quasi-elastic charged current events in which an outgoing charged tau lepton signaled the presence of an incoming tau neutrino.

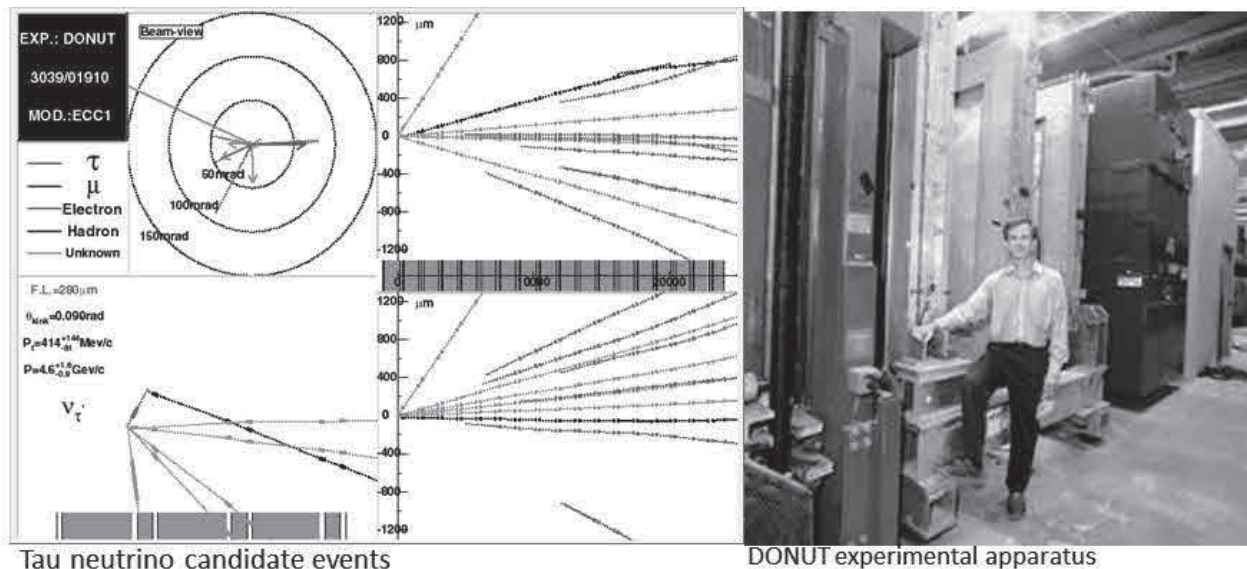


Figure 4: the DONUT experiment observes tau neutrino

4. The *Tevatron* Collider era: discovery of the top quark

With the advent of the *Tevatron* in its collider mode, Fermilab became the leader at the energy frontier, a position it maintained from 1985 through the advent of the *Large Hadron Collider* at CERN in 2010. Two very large detectors, the *Collider Detector Facility (CDF)*⁹ and the *DZero Detector*¹⁰, each manned by very large international collaborations, defined the scientific program. During the two and a half decades as the forefront facility at the energy frontier the *Tevatron* produced major discoveries and hundreds of publications and Ph.D. thesis.

During the collider era we can distinguish two main periods. The first period takes us from the first collisions in 1985 through the discovery of the top quark in 1995 and is characterized by relatively low luminosities. From the first collisions through the discovery of the top quark the *Tevatron* integrated less than 0.2 inverse femtobarns. In the second period, with the new injector (the *Main Injector*), various improvements to the cryogenic system to reach 2 TeV CM energy and finally the implementation of electron cooling of antiprotons, the *Tevatron* reached a peak luminosity of $4 \cdot 10^{32} \text{ cm}^{-2} \text{ sec}^{-1}$ and a total integrated luminosity of 12 inverse femtobarns.

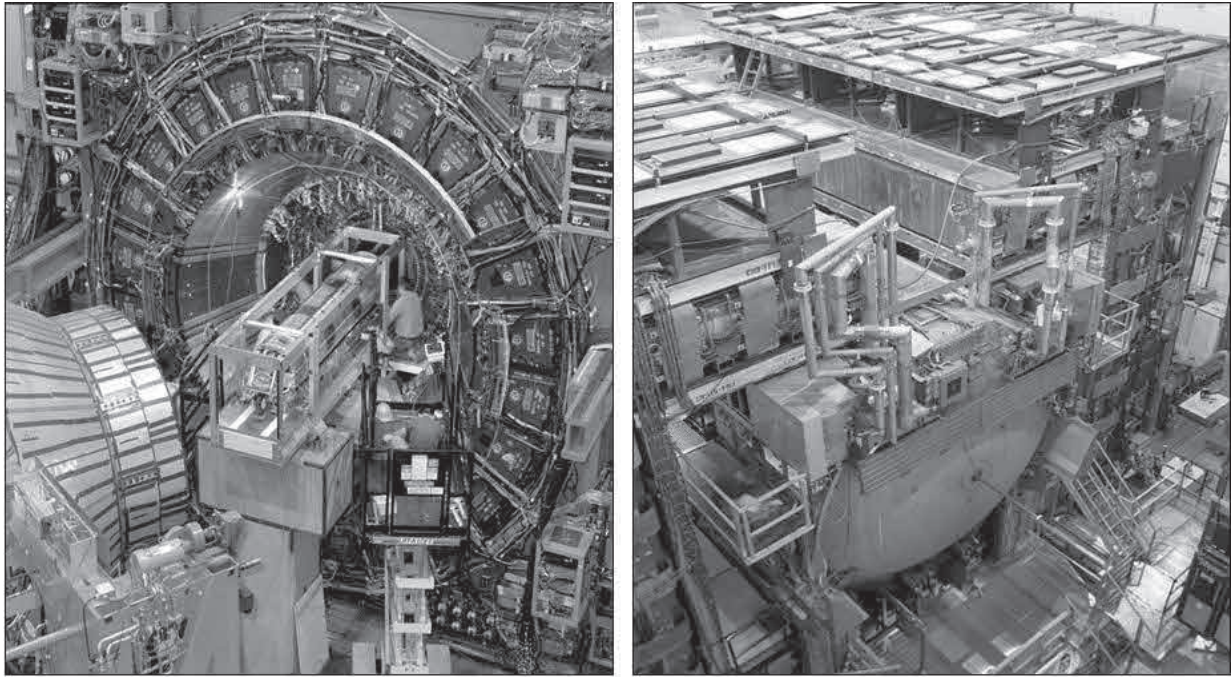


Figure 5: $\sim 10 \text{ fb}^{-1}$ recorded to tapes by each CDF and DZero

The discovery of the top quark culminated a world-wide saga where after accelerators fell short of the necessary energy to produce the top quark. In a series of measurements in the early 90s, *CDF* and *DZero* gradually raised the lower limit on the mass of the top. Finally in 1995 both experiments announced the discovery of the top quark¹¹. Subsequent to the discovery and for the next 16 years, the *Tevatron* was the only facility capable of producing the top quark and studying its properties. Many measurements confirmed the expectations of the top quark in the Standard Model: QCD predictions for production rate and transverse momentum distributions; its invariant mass; $2/3$ charge; and the study of properties of the $t\bar{b}W$ vertex. At the *Tevatron* the mass of the top, was measured to better to about 0.5% (Figure 6) and is an important ingredient in determining the region of mass where the Standard Model Higgs should be. With the increased data samples, studies of t - $t\bar{b}$ correlations became possible and the two collaborations, *CDF* and *DZero* observed an asymmetry in t - $t\bar{b}$ production larger than predicted by the standard model, a result that remains unexplained at this date.

The *Tevatron* collaboration explored electroweak physics to an unprecedented level. Precision measurements of the W boson mass to four parts in ten thousand were achieved, with millions of events per leptonic channel in each experiment. This together with the top quark measurement limits the mass region for the Standard Model Higgs. All di-boson production WW , ZZ , WZ Wg Zg agrees with QCD predictions and their production rates are shown in Figure 7.

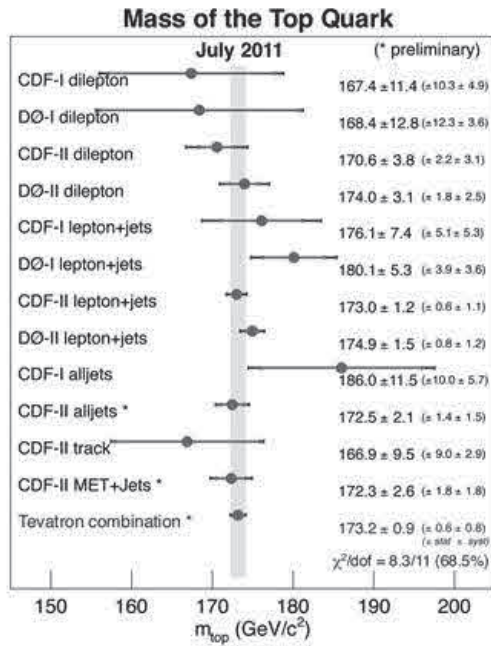


Figure 6: evolution of top-quark mass measurements

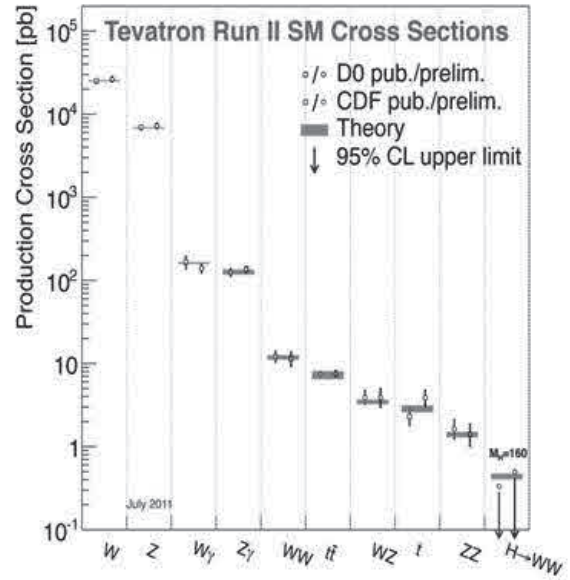


Figure 7: di-boson production

Remarkably enough the *Tevatron* had an impact on the spectroscopy of heavy mesons and baryons, a subject normally associated with electron-positron colliders. All the knowledge about the top quark comes from the *Tevatron*. The discovery of the B_c meson and the measurement of its properties were first done at the *Tevatron*. The *Tevatron* has contributed to the measurement of masses and lifetimes and observed B mesons and baryons. With the baryons discovered at the *Tevatron* we have a complete picture all the $\frac{1}{2}$ spin baryons containing a b quark as shown in Figure 8.

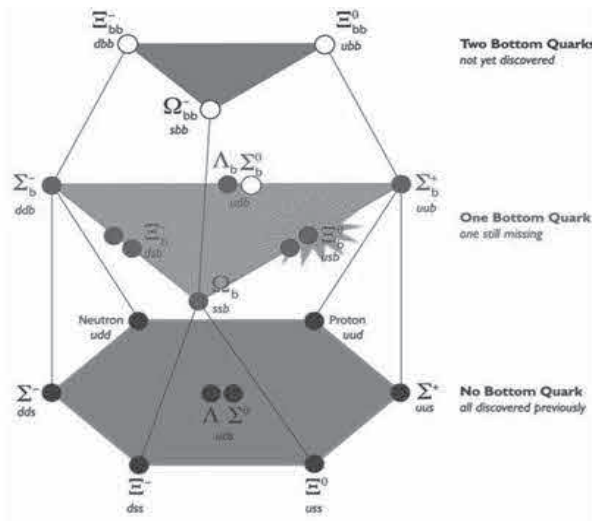


Figure 8: b-baryon spectroscopy

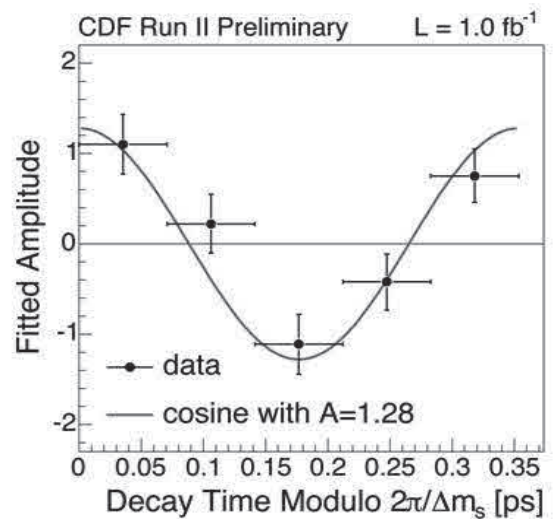


Figure 9: B_s oscillations

One of the most remarkable measurements was the very fast oscillations of the B_s system. After limits first published by *DZero*, *CDF* determined the oscillation frequency of 17.77 ± 0.13 ns shown in Figure 9.

The *Tevatron* pushed the kinematic limits over which the strong interaction was tested. QCD was tested over a broad set of transverse momenta. The transverse momentum distributions over many orders of magnitude are shown in Figure 10. Single jet and multijet distributions validate perturbative QCD and have served to tune parameters for the planning of detectors for *LHC*.

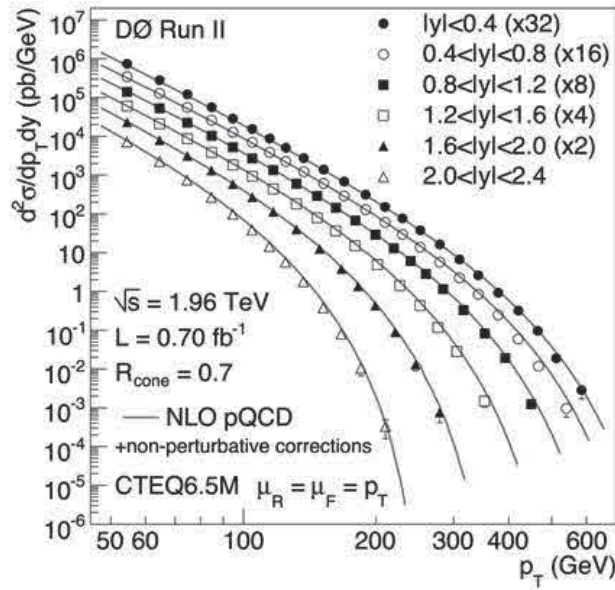


Figure 10: Data and NLO calculations

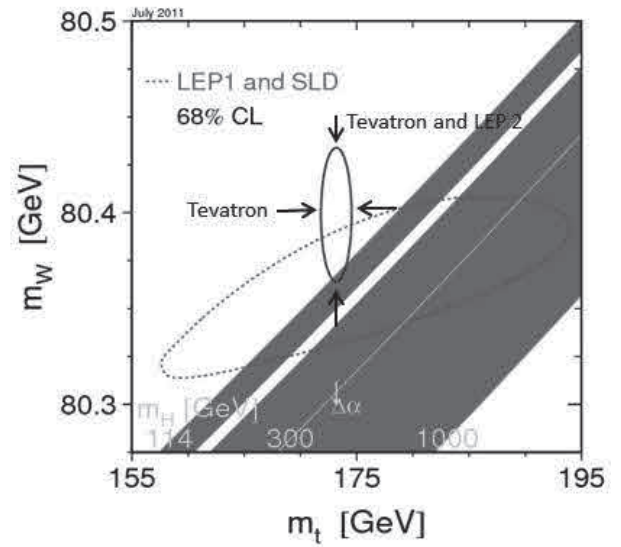


Figure 11: indirect Higgs mass

A large enterprise at the *Tevatron* was the search for phenomena beyond the Standard Model. Searches for extra spatial dimensions, supersymmetry, technicolor, monopoles, new forces of nature and many more yielded no observations. A few results at the 3 standard deviation remain puzzling and will have to be elucidated either with the remaining analysis at the *Tevatron* and more likely with the much more abundant data at the *LHC*.

The search for the *Higgs* has been a principal endeavor of the *Tevatron*. The *Tevatron* excluded new regions of the mass range for the first time since the *LEP* collider. If the *Higgs* is not there, the *Tevatron* has the potential to exclude the *Higgs* at the 95% confidence level from the *LEP* limit of 115 GeV to about 185 GeV. At this point, the regions where the *Tevatron* has enough sensitivity to discover the *Higgs* have been excluded as shown in Figure 12.

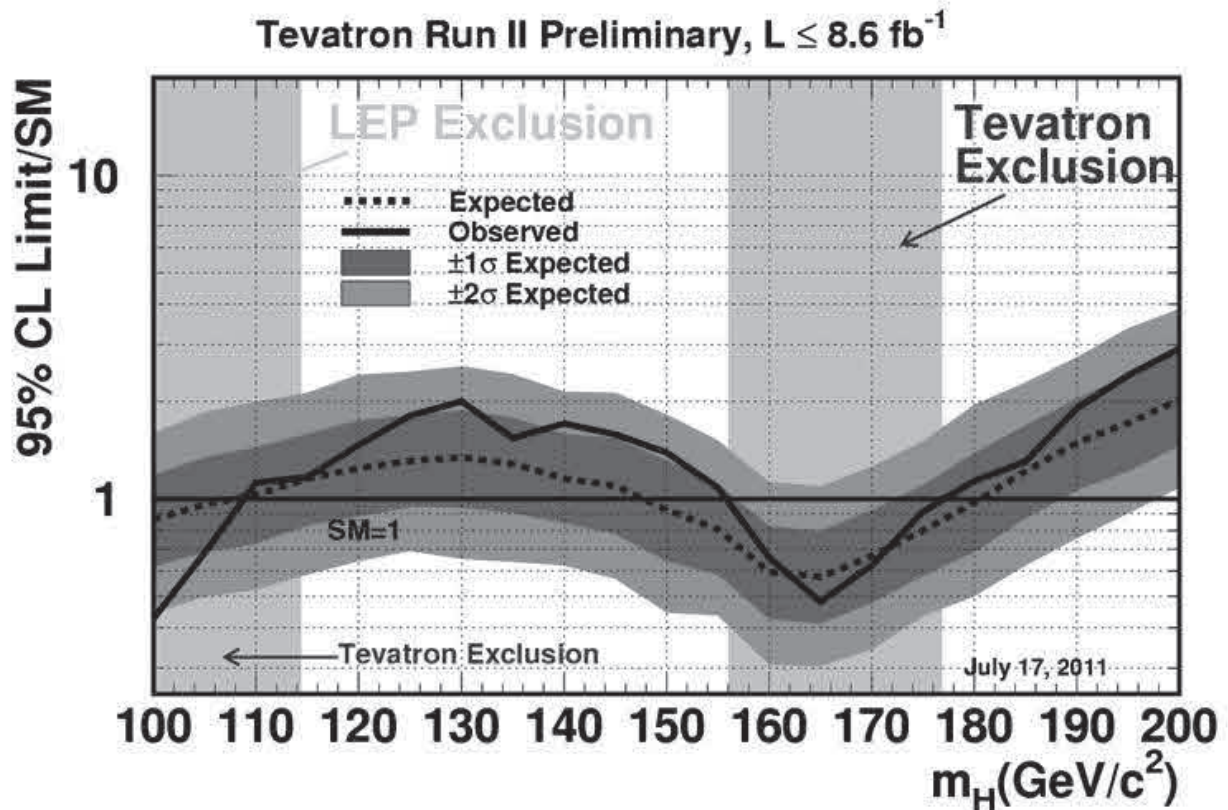


Figure 12: Higgs limits combined CDF and DZero

5. The current neutrino program and future extensions

To achieve the high luminosity of the *Tevatron*, the front end accelerators were developed to achieve high intensity. The 8 GeV booster is a rapid cycling accelerator running at 7 Hertz (with an ultimate capability of 15 Hz) and the *Main Injector* produces 120 GeV beam every 2.3 seconds, relatively rapidly for such a large synchrotron. Using these machines Fermilab developed both a long and a short baseline neutrino programs.

Our understanding of neutrinos lags our understanding of all other known particles. Today we believe in a picture with three generation of neutrinos. Even in this picture many parameters remain to be measured. While we know that neutrinos have a very small mass, we do not know the absolute value of the masses, only the mass differences between pairs of neutrinos. The mass eigenstates of neutrinos are combinations of the different flavor of neutrinos, but in some instances we do not know what those combinations are. Finally we do not know whether neutrinos and anti-neutrinos respect matter-antimatter symmetry. So even if the overall picture we have of neutrinos is correct, there is much to be done in understanding them. Furthermore, we may not have the totally correct picture; additional interactions could exist that affect the neutrino world. In particular, there may be sterile neutrinos that mix with regular neutrinos and would indicate a totally different kind of particle with no standard interactions. The neutrino program at Fermilab aims to study all these different possibilities.

Today the Fermilab short baseline program has two experiments: *MiniBooNE*¹², and *MINERvA*¹³. The *MINERvA* experiment studies neutrino-nucleus interactions and started taking data in 2010. The *MiniBooNE* detector has operated for several years and has investigated the possibility of neutrino oscillations claimed by the *LSND* experiment that do not fit the standard picture. Using a neutrino beam, *MiniBooNE* disproved the oscillations observed by *LSND*. The results of *MiniBooNE* with anti-neutrinos is more ambiguous: they could be consistent with *LSND* but suffer from small statistics. More interestingly *MiniBooNE* has observed a statistically significant excess of events at low energies that may indicate new phenomena. *MiniBooNE* which is based on Cerenkov detector cannot resolve this issue.

To resolve the *MiniBooNE* excess we are building *MicroBooNE*¹⁴, a fine grain detector. Placed in the Fermilab booster beam, the *MicroBooNE* detector will be an approximately 150-ton, liquid Argon Time Projection Chamber (LArTPC). The experiment will measure low energy neutrino cross sections, and investigate the low energy excess events observed by the *MiniBooNE* experiment. The detector serves as the necessary next step in a phased program towards the construction of massive, kiloton range, LArTPC detectors. It will be operational in 2014.



Figure 13: MINERvA Detector

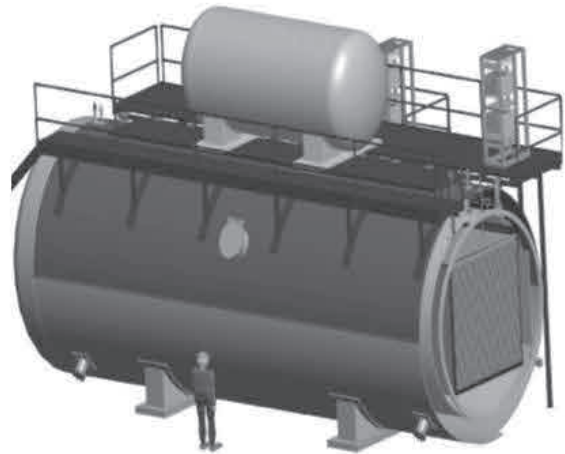


Figure 14: MicroBooNE Detector

The long base line neutrino oscillation experiments used a high energy beam from the *Main Injector* to the Soudan mine in Minnesota. The first of these experiments is the *MINOS*¹⁵ experiment which has produced the most accurate measurement of the mass difference and improved the measurement of the mixing angle in the region of atmospheric neutrinos. The *MINOS* experiment has measured the oscillation parameters of neutrinos and antineutrinos and found them equal within statistics. It has ruled out some models for sterile neutrinos and is in the process to measure the speed of neutrinos to verify the *OPERA* results. It also has set limits on electron appearance.

The *NOvA*¹⁶ detector is under construction and is aimed at studying electron appearance. It is a 15 kton totally active detector. It will measure electron appearance accurately and the mixing angle θ_{13} . It will have some sensitivity to the mass hierarchy and to CP violation. The *NOvA* detector is the next step in understanding the neutrino mixing matrix and verifying the current understanding of neutrinos with three generations of neutrinos.

To fully measure the mass hierarchy and CP violation one needs a longer baseline experiment. This is currently planned for the Homestake mine in South Dakota. The experiment, *LBNE*¹⁷, would be a massive 33 kton liquid argon TPC one mile underground that would not only permit the study of all the oscillation parameters, but also the study of proton decay, atmospheric neutrinos and supernova bursts. The reach in oscillations for the three generation of experiments MINOS → NOvA → LBNE is shown in Figure 15.

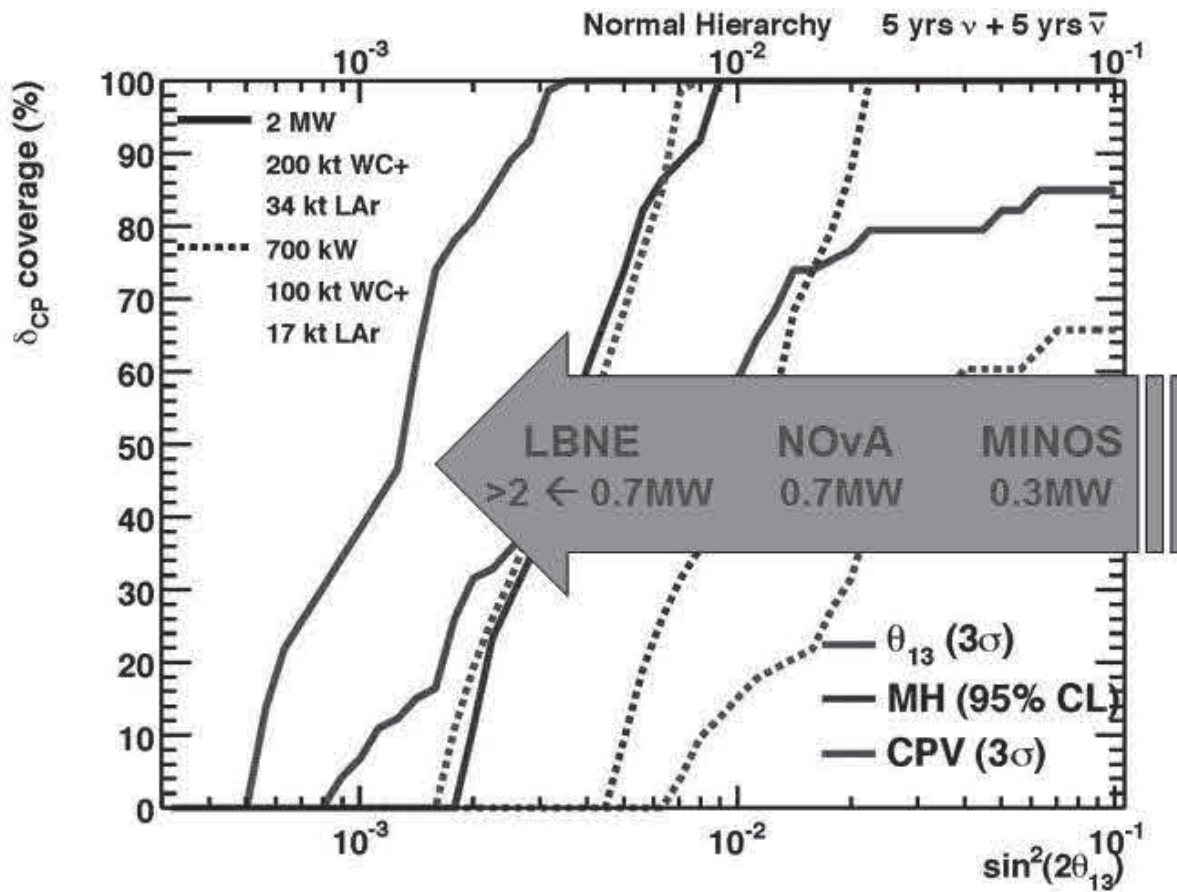


Figure 15: Evolution of sensitivities

6. The future muon campus: *g-2* and *Mu2e*

The measurement of the anomalous magnetic moment of the muon, $g-2$ ¹⁸, is a classic experiment that has become the “gateway” experiment through which every model of physics beyond the Standard Model has to pass. The Fermilab experiment will have 20 times the previous statistics and reduce the error of the previous Brookhaven National Laboratory experiment by a factor of four to 0.14ppm. The experiment will be based on the storage ring built at BNL for the previous measurement of $g-2$. This storage ring will be moved to Fermilab and housed in the muon campus. The experiment will start operations in the 2016-2017 time frame.

The $Mu2e^{19}$ experiment will study the conversion of a muon to an electron in the field of the nucleus. This conversion cannot occur in the Standard Model except through neutrino mixing which would be at an infinitesimal rate. Any measured rate is an indication of new physics beyond the Standard Model. Depending on the couplings, indirect sensitivities to masses of 1000 TeV and more can be achieved. If a finite rate is measured, variations in the nuclear target can give information on the nature of the new physics. The experiment is quite complex and involves producing an intense muon beam impinging on a target and a detector to measure the mono-energetic electron produced by this process. The picture of the experiment is shown in Figure 16.

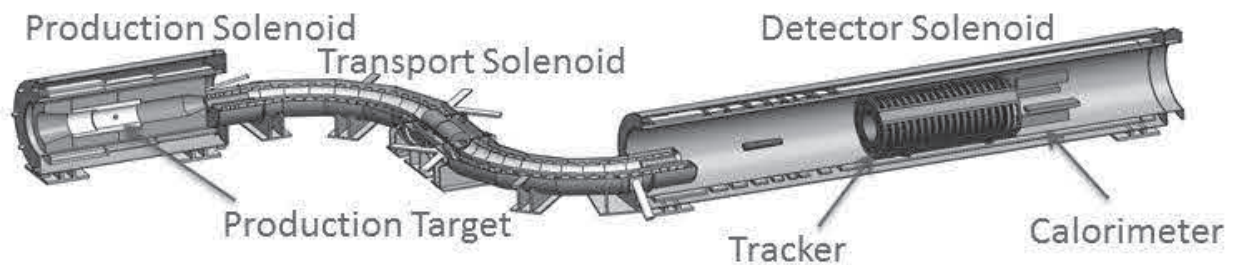


Figure 16: Mu2e experiment

7. *Project X*²⁰ and its scientific reach

To have a broad program at the intensity frontier, Fermilab has proposed to build a continuous wave (CW) superconducting linac with an energy above kaon threshold. This 3 GeV, 3 MWatt linac would fuel a powerful program of rare muon and kaon decays. It would provide megawatt beams with precisely tailored timing characteristics that would enable experiments of high precision that have not been possible before. In addition megawatt class beams could be delivered to nuclear targets for EDM measurements and also for a specialized station for materials studies and spallation targets.

The 3 GeV CW linac would provide a fraction of the beam to a pulsed superconducting linac for acceleration to 8 GeV, with several hundred kilowatts of power delivered at that energy. Finally acceleration of a fraction of the beam from 8 GeV to 60-120 GeV would provide 2.3 MWatts to the Long Baseline Neutrino Experiment. *Project X* is being planned in such a way that it would serve as the front end for a neutrino factory or a muon collider. A schematic of *Project X* is shown in Figure 17.

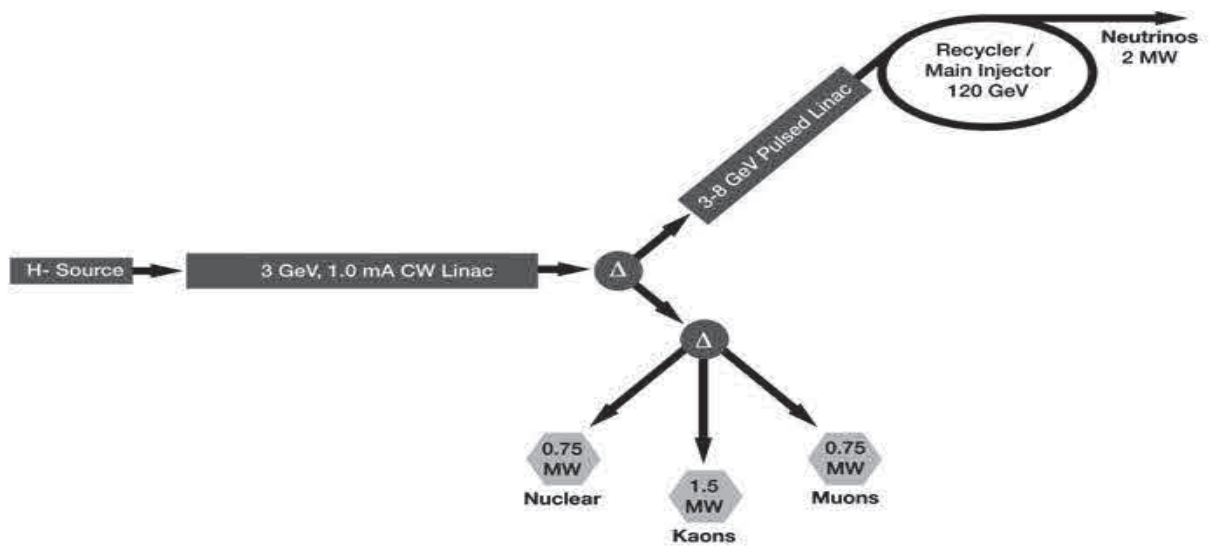


Figure 17: Schematic of Project X

8. Connection to the cosmic frontier

Particle physics is intimately related to cosmology. Fermilab played a leading role in the theoretical underpinnings of this connection with the establishment of one of the earliest groups of theoretical particle astrophysics. It established an experimental program with the *Sloan Digital Sky Survey (SDSS)*, which has an enormous impact on the determination of cosmological parameters. Today Fermilab is carrying out a leading program on the study of dark matter with the *Cold Dark Matter Search (CDMS)* experiment in the Soudan mine, and the development of other techniques to reach background free condition including the *COUPP* detector now being tested at *SNO*.

SDSS observed baryon acoustic oscillations, a powerful component of studying dark energy. Fermilab is following *SDSS* with the *Dark Energy Survey (DES)* employing a 0.5 gigapixel camera mounted on the 4m Blanco telescope in CerroTololo, Chile. This experiment should give the first indications on whether the acceleration parameter has been constant or is changing through the expansion of the Universe.

Fermilab has played a leading role in the development of the Pierre Auger Observatory studying the highest energy particles in nature.

9. The follow-up to the LHC at the energy front

At the time of this writing the *LHC* is working extremely well and we are at the threshold of discovering if the Standard Model Higgs provides the mechanism of symmetry breaking. The biggest issue in the field today is what should follow the *LHC*.

Fermilab is participating in a major way in the worldwide *ILC* R&D. If the phenomena discovered at the *LHC* are below 1 TeV, then it is likely that there will be an *ILC* somewhere in the world. If on the other hand the phenomena extend well beyond 1 TeV, then different technology will be necessary to explore these phenomena. At Fermilab we are concentrating on demonstrating the feasibility of a muon collider while at CERN there is development of the warm RF *CLIC* linac with high electric field gradients and using a two-beam accelerator.

The muon collider feasibility study requires solving many challenges in the production, capturing and acceleration of muons. The new technologies developed in this enterprise include very high field (40T) magnets, rapid acceleration to TeV energies, high power targets and muon ionization cooling.

The overall future program for Fermilab is shown in Figure 18 in the Appendix.

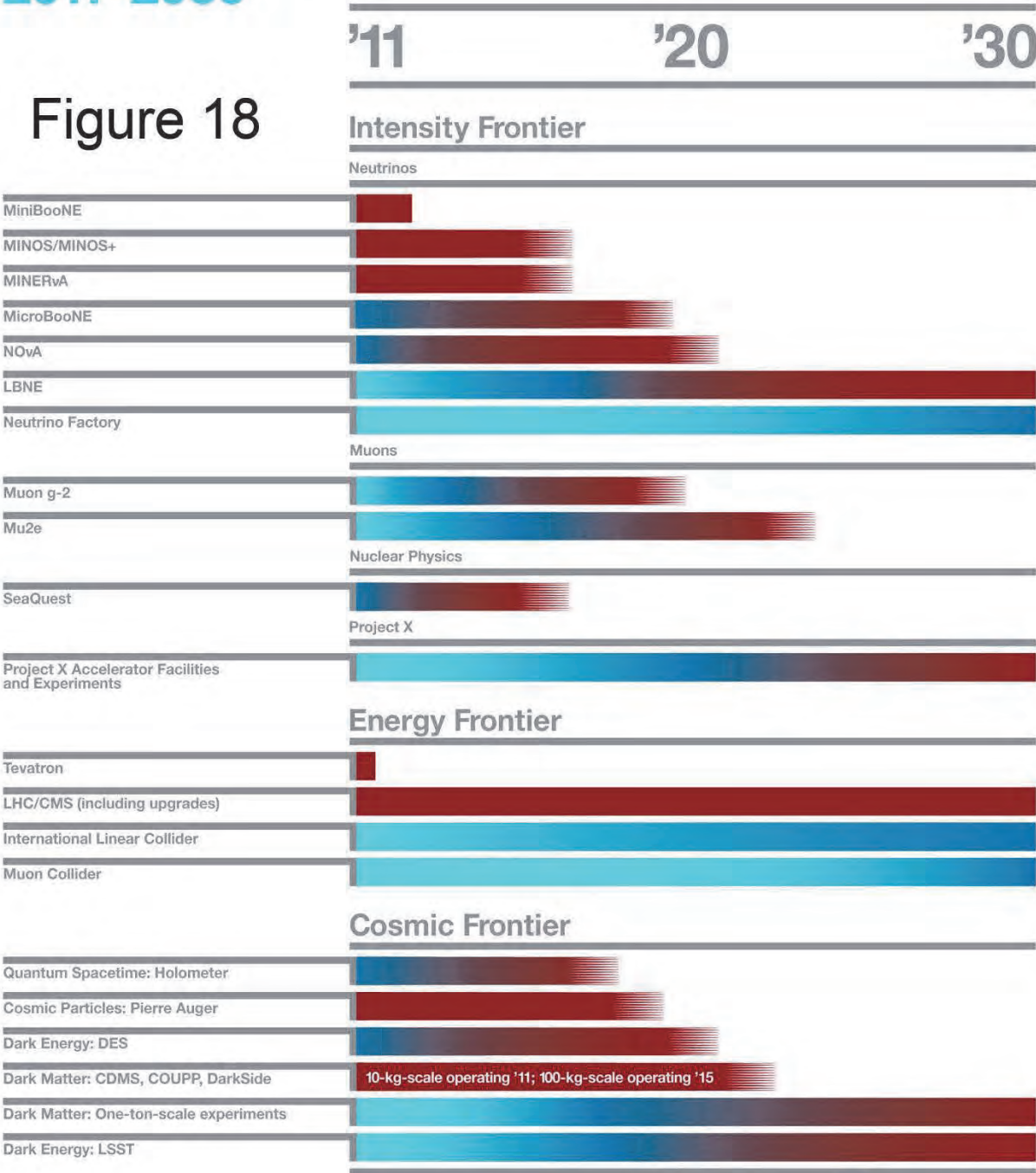
References

1. Fermilab Golden Book: http://history.fnal.gov/GoldenBooks/gb_wilson2.html
2. S.W. Herb, et. al., Phys. Rev. Lett. **35**, 333 (1977)
3. “*Fermilab, the Frontier and Magascience*”, Lillian Hoddeson, Adrienne Kolb and Catherine Westfall, University of Chicago Press, 2008
4. Fermilab Fixed Target Symposium 2000: (<http://conferences.fnal.gov/tevft/book/>)
5. APS Panofsky Prize: <http://www.aps.org/programs/honors/prizes/panofsky.cfm>
6. Experiment E691: <http://conferences.fnal.gov/tevft/book/SECTION5.htm#e691>
7. KTeV Experiment: <http://ktev.fnal.gov/public/ktev.html>
8. DONUT Experiment: <http://www-donut.fnal.gov/>
9. CDF: <http://www-cdf.fnal.gov/>
10. DZero: <http://www-d0.fnal.gov/>
11. CDF Collaboration, F. Abe et. al., Phys. Rev. Lett., **74**, 2626 (1995); DZero Collaboration, Abachi et. al., Phys. Rev. Lett. **74**, 2632 (1995)
12. MiniBooNE: <http://www-boone.fnal.gov/>
13. MINERvA: <http://minerva.fnal.gov/>
14. MicroBooNE: <http://www-microboone.fnal.gov/>
15. MINOS: <http://www-numi.fnal.gov/>
16. NOvA: <http://www-nova.fnal.gov/>
17. LBNE: <http://lbne.fnal.gov/>
18. g-2: <http://gm2.fnal.gov/>
19. Mu2e: <http://mu2e.fnal.gov/>
20. Project X: <http://projectx.fnal.gov/>

Opportunities for Discovery 2011–2030

Legend
R&D
Construction
Operation

Figure 18



The timeline on this page shows experiments and major accelerators currently in the R&D, construction or operation phases. All experiments currently in the R&D phase

require additional levels of approval from the Department of Energy before construction can begin. Construction of a Neutrino Factory or a lepton collider, at Fermilab or at any other

worldwide site, would proceed only if discoveries at the LHC or elsewhere point to a need for such a machine.

THE ORIGIN OF LEP AND LHC

■ ROBERT AYMAR

The Origin of LEP and LHC

1- Introduction

1.1 Innovations in theory

In Subnuclear Physics, the decade 1965-1975 has seen an impressive number of innovations in theory, which brought the modelling of fundamental forces and relationships between particles in term of a single theory framework, a unified quantum field theory.

Without being exhaustive, a few essential new concepts should be quoted:

- The introduction of the concept of quarks/antiquarks to build hadrons (Gell-Mann and Zweig in 1964); the quark distribution in the nucleus was observed in 1969 ("partons" distribution). The new concept brought order into the complex zoology of hadrons then available;
- The introduction of the concept of supersymmetry in 1971-1974, of QCD and "asymptotic freedom" in the strong interaction domain, etc...;
- The application of gauge theory to interactions (local symmetry);
- The mechanism of spontaneously broken symmetry, when the symmetries of the interaction Lagrangian are not symmetries of the vacuum.

1.2 The electro-weak interaction

A unified quantum field theory for electromagnetic and weak interactions was established in the lepton sector (Glashow, Salam, Weinberg in 1967-1968) and later in the hadron sector (Weinberg in 1972), after the charm quark was introduced.

The very short range of the weak force, described from Fermi until then through the "contact model" of four fermions, questioned the possibility of quantum fields to model properly the case. It was potentially answered by Higgs in 1963, when he noted that vector fields become massive from interaction with scalar fields, a property to justify later the fermions masses.

This unification of two forces into one unique electroweak interaction was a very brilliant achievement, from application of the $SU(2) \times U(1)$ gauge group and of the spontaneous symmetry breaking resulting from the introduction of a scalar (higgs) field.

The corresponding gauge bosons are the three W bosons of weak isospin from $SU(2)$ (W^+ , W^- , W^0) and the B^0 boson of weak hypercharge from $U(1)$.

The symmetry breaking provides mass to the bosons and causes the W^0 and B^0 to mix into two different bosons one massive neutral Z^0 and one massless the photon γ ; the mixing is parameterized by the angle θ_w .

The masses and interactions of the vector bosons are predicted in term of the single angle θ_w ; the mass of the scalar Higgs boson was unknown and free, but its couplings with the fermions are also predicted to provide their masses.

1.3 Experimental discoveries

At the same time, an irresistible move occurred to show that the concepts introduced by theory were not only mathematical entities, but real particles or interactions: experiments were designed to verify the theoretical results. A few important examples are:

- The lepton τ was discovered at SLAC (SPEAR), making 3 lepton families;
- Identification of quarks: an experiment at SLAC, under Friedman, Kendall, and Taylor in 1968, found that electrons were sometimes scattered from nucleons at large angles, showing the existence of point-like “partons”;
- Different types of quarks were identified: up, down, strange, bottom;
- After the theoretical prediction of the necessary existence of the charm quark by Glashow, Iliopoulos and Maiani in 1970, the charmonium was discovered by Richter-Ting in 1974, followed by the naked charm quark at SLAC (1976); only the top quark was missing to build also 3 quark families; the essential question at that time was if more families were to come;
- In matter of e-weak interactions, the discovery of neutral currents at CERN in neutrino scattering in “Gargamelle” in 1973 was an essential step to confirm the theory and to justify the preparation of experiments to verify the other quantitative predictions: $M_Z = 90$ GeV and $M_W = 80$ GeV from the theoretical relations:

$$M_W = M_Z \cdot \cos \theta_w \quad \text{and} \quad \sin^2 \theta = 0.23-0.25; \quad \text{and} \quad G_F \cdot 4\sqrt{2} \cdot (M_W \cdot \sin \theta)^2 = e^2.$$

1.4 The Standard Model

The success in the electroweak interactions from the introduction of gauge theory pushed to apply it also to strong interactions, which will become the description of Quantum Chromo Dynamics. The $SU(3)$ symmetry group in the three color space with no spontaneous breakdown led to massless mediators, 8 Gluons, as carriers of the strong force.

Therefore around 1975, a theoretical model was available for all particles and their interactions known at that time, using the symmetries of the non-Abelian group $SU(3) \times SU(2) \times U(1)$ introducing 12 vectors gauge fields with

self-interaction. This model, called now **the Standard Model of Particles and their Interactions**, was confirmed by all discoveries to come later.

2- The Origin of the Large Electron- Positron Collider: LEP

2.1 The preliminary studies

In early 1976, when the SPS construction was coming to its end, John Adams organized a Group at CERN (chaired by Darriulat) to study the possibility of a e^+e^- collider to be built at CERN in order to verify the electro-weak (e-w) model predictions.

The Group envisaged the concept of a storage ring where beams of 100 GeV collide with a luminosity of $10^{32} \text{ cm}^{-2}\text{s}^{-1}$; it was supported by ECFA in its meetings of 1976 and 1977, which created its own ECFA Working Group (chaired by Zichichi) to bring the majority of physicists behind the study of all aspects of the e^+e^- collider concept, as the most sensible to pursue for establishing the next experimental programme for Europe in High Energy Physics.

An international Review at “Les Houches” in 1978, presented with the “Blue Book” (100 GeV per beam in a ring of 22 km length) showed the common confidence in the predictions of the e-w theory on which to base all experimental expectations.

The wish to reach the highest energy in order to increase the probability to discover new massive particles (other quarks and fermions??; supersymmetric particles ??) led ECFA in November 1979 to recommend another design (130 GeV in 30 km long ring) described in the “Pink Book” and to show the general consensus to see the project, called LEP (Large Electron Positron collider) to be built at CERN.

2.2 A short cut to the W, Z Discovery

In 1976, even among people working on LEP studies, impatience was high, having to wait for more than a decade to identify W, Z and H in LEP. A proton collider was probably the fastest complementary solution; the ISR (Intersecting Storage Rings : the very first collider) had not enough energy (30 GeV/beam); none was available in the world in the range 100-200 GeV. A proposal was made by Carlo Rubbia in 1976: to use the SPS after its start of operation, but with only one single ring it should become a $p\text{-}\bar{p}$ collider.

The difficulties to build a source of anti-protons to provide a beam as intense as the proton beam led people to be skeptical. Only Carlo Rubbia’s vision, competences and determination have assured the final success.

The p-pbar collider in the SPS was accepted as an experiment in 1978 (not as a Project in order to avoid any political damage to the LEP project). In 3 years, Carlo achieved the "tour de force" to realize the appropriate anti-proton source, after building an Accumulator/ Collector (AA/AC), testing the cooling methods (proposed by van der Meer) in ICE, and promoting the realization of two large detectors UA1 and UA2.

Collisions began in 1981 and Z and W were identified in 1983, for a Nobel Price in 1984, never before granted so rapidly after a discovery.

2.3 The decision to build LEP

In 1979, John Adams proposed a policy to get approval of LEP construction by CERN Council, even if no new specific resources would be granted. LEP could be built inside the current CERN budget under certain constraints:

- closing the programmes of SC (**Synchro-Cyclotron**) and ISR in early 80ies,
- starting LEP investment only when the ppbar experiment is ready for operation in 1982,
- assuming the LEP construction achieved in 7 years for 150 MCHF/year,
- sharing some tasks and exchanging staff with National Labs.

As the investment in LEP (mainly civil work and RF costs) varies as E^2 , the square of the beam energy, its design should look for economic choices inside the above constraints and the inevitable limits of the electrical power drawn by CERN from the mains to a value around 200 MW. **Finally the ECFA-LEP Working Group, chaired by A. Zichichi, recommended to construct a 27 km accelerator ring-tunnel adjacent to CERN between the French Jura and Geneva airport.** Accordingly the main LEP design parameters were decided:

- Tunnel length: 26.6 km, with 8 arcs of 3.1 km radius and 8 straight sections, and 4 caverns excavated at P 2, 4, 6, 8, for experiments, (tunnel cross-section large enough to add a possible proton collider)
- Beam energy: 60 GeV each with Cu cavities, and a possible extension to 100 GeV when the R&D on superconducting cavities (SC), launched immediately, will have led to interesting results.

The positive decision to build LEP was taken in CERN Council in December 1979, assuming 3 years of preparation before a start of construction in 1982 and of operation in 1989. Four general purposes detectors will be installed in four caverns around the ring: L 3, ALEPH, OPAL, and DELPHI.

A few years after the start of LEP construction, a decision was reached in the US to also build a e^+e^- collider, the SLC, at SLAC reusing the available 50 GeV Linear Accelerator which thus allowed the SLC to start operation at the same time as LEP. The two colliders had similar research programmes during LEP Phase I; it was a period of “collaborative competition”. Because of its more limited beam energy the SLC could not compete with the following LEP Phases.

3- The LEP Design, Construction and Operation

3.1 The different Phases

The physics objectives of LEP pushed to consider two Phases in Operation with respectively a minimum beam energy of 60 GeV to create single Z, and 85 GeV to produce W^+W^- pairs using Cu cavities.

Phase I was authorized for investment in 1979 (Phase II for planning only) including besides the civil work:

- 128 Cu cavities to be installed in 272 m of active length (1.5 MV/m) fed by 16 MW of RF power from Klystrons at 350 MHz with a total dissipation of 75 MW,
- Beam Injection at 20 GeV through a chain including an e^+e^- accumulator at 600 MeV, the PS at 3.5 GeV and SPS at 20 GeV (compatible with interlacing proton acceleration to 450 GeV for other experiments),
- Operation at 45-60 GeV with a luminosity $> 10^{31} \text{cm}^{-2} \text{s}^{-1}$ (at 55 GeV) with four bunches/beam.

Phase II was started with the goal to reach 85 GeV with 192 SC, added to the previous 128 Cu cavities, and built with a film of Nb sputtered on Cu after a successful development.

Phase III was approved in 1993 to replace 64 Cu cavities by 32 SC cavities and to operate with 8 bunches/beam. Phase IV was approved in 1995 adding 48 SC cavities. Thus the circumference Voltage has been increased through the Phases from an initial 400 MV to >3500 MV and the RF power from 16 MW to 48 MW; this has allowed to reach >96 GeV per beam and a peak luminosity of $1.4 \cdot 10^{32} \text{cm}^{-2}\text{s}^{-1}$. LEP operation was put to an end by December 2000 to give free access to the tunnel for removing components and start LHC construction.

3.2 Main Physics Results of LEP

3.2.1- During LEP Phase I, $18 \cdot 10^6$ Z were observed.

The analysis of the Z-line shape (Fig.1) in the cross-section from e^+e^- collisions leading to hadrons, of the decay branching ratios and of the asymmetries led to values of high precision : $M_Z = 91, 187.5 \pm 2.1$ MeV; $\Gamma_Z = 2495.2 \pm 2.3$ MeV and $\sin^2\theta = 0.23138 \pm 0.00014$ mass around 170 GeV (this mass was too large for the top to be directly produced).

3.2.2. There are only three families of leptons and of quarks.

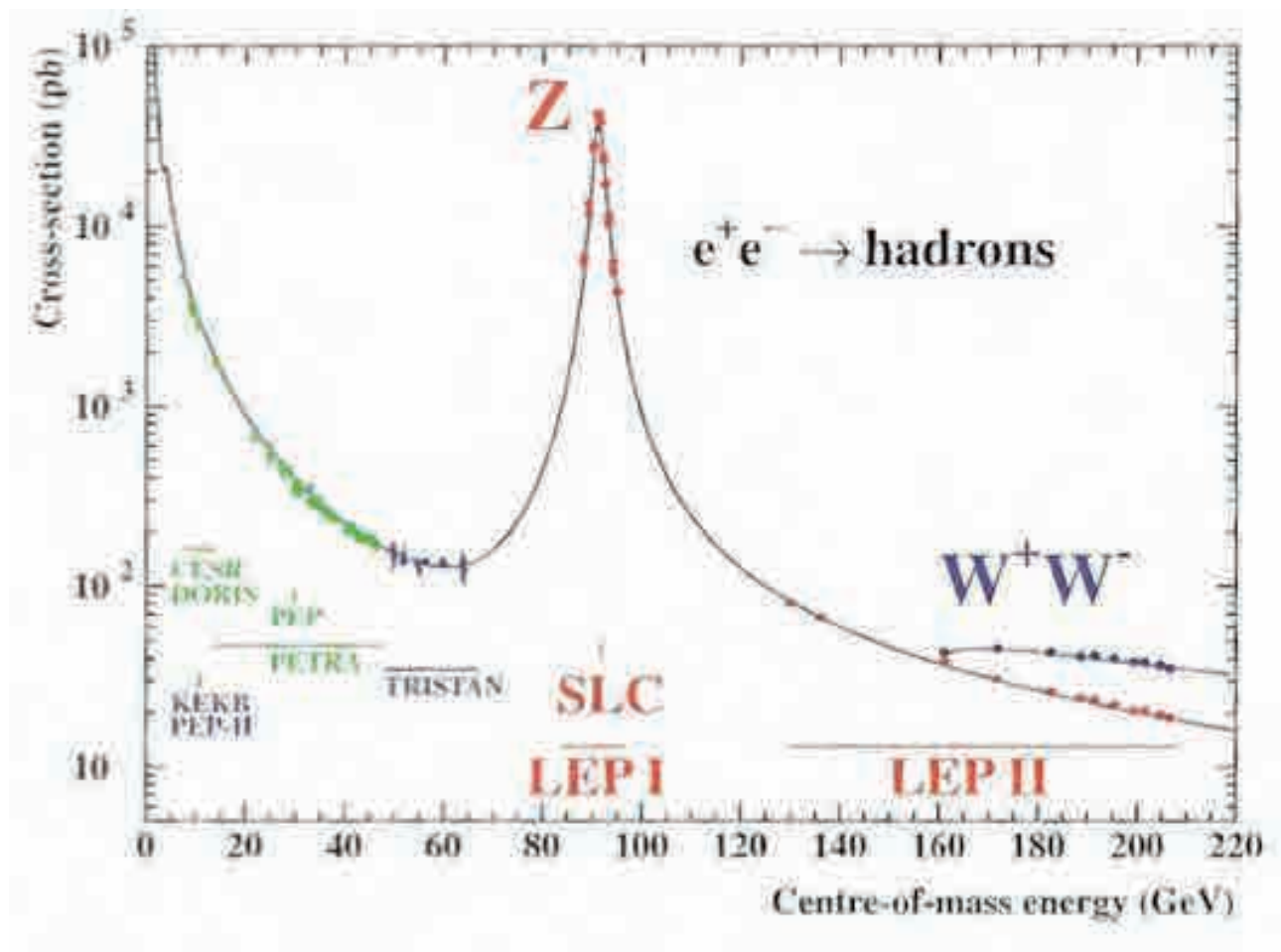


Fig. 1. The e^+e^- annihilation cross-section to hadrons from low energies to the range of energies accessible in the Phases of LEP operation (from lepewwg)

3.2.3. In Phase II, $80 \cdot 10^3$ W were observed and the direct measure of W mass and decay width was: $M_W = 80.4$ GeV and $\Gamma_W = 2.15$ GeV. The charged

$W+W$ -pairs are produced in $e+e^-$ collisions by three different mechanisms (photon, neutrino, Z -boson exchanges; if any of them is isolated from the others, suppressing their interference, it leads to a cross-section indefinitely rising instead of decreasing with energy as shown in Fig.2.

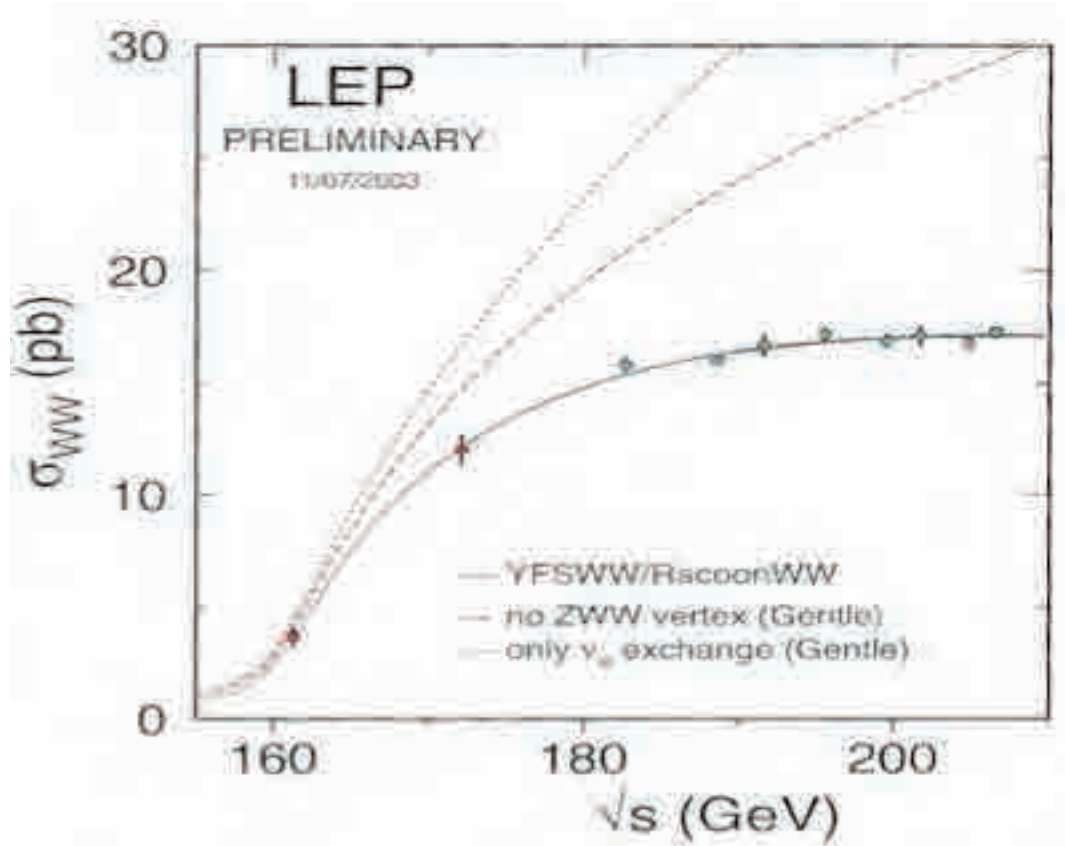


Fig. 2. The total cross-section of W -pairs production in $e+e^-$ collisions at LEP (from *lepewwg*)

3.2.4. The QCD coupling dependence with energy was confirmed leading to the “asymptotic freedom”, a feature of the non-Abelian gauge theories.

3.2.5. No evidence of Higgs or supersymmetric particles below 114 GeV.

In conclusion, LEP did not reveal anything new, but provided precise verification of every thing expected, confirming the Standard Model of Matter and Forces but missing the experimental proof of the process giving fermions their masses.

4- The Origin of the Large Hadron Collider: LHC

4.1. Preliminary studies

In 1984, in the middle of LEP construction and following the discovery of W-Z in UA 1 and UA 2, an ECFA Workshop was held just before an ICFA meeting, where US Physicists will describe the SSC proposal. The prepared answer from EU Physicists was that they were considering a proton-proton collider of 10-20 TeV in the center of mass, to be installed in the LEP tunnel, giving also access to e-p and heavy-ions collisions.

Another ECFA meeting at La Thuile in 1987 considered the relative discovery merits of p-p, e-p, e+e- colliders 10 T magnets, 7.7 TeV/beam, luminosity of $1.6 \cdot 10^{34} \text{cm}^{-2}\text{s}^{-1}$, 4725 bunches of 10^{11} p, spaced by 15 ns, reaching the extremely large value of energy in the beams 583 MJ /beam.

This preliminary design was quite ambitious, but already showing some attractive design features of the final LHC: “two in one” and HeII cryogeny; a strong R&D effort was proposed on superconducting magnets and on performing detectors (the most difficult task in the case of hadron collider) .

4.2. Key questions of Particle Physics

The LHC programme objectives was considered the natural long-term extension of the LEP programme , with remaining key questions:

- How is the electro-weak symmetry broken and what is the origin of mass?
- Is the Higgs mechanism responsible? only one Higgs particle or more?
- The 17 orders of magnitude gap from W, Z to Planck masses cannot be understood without new physics entering around one TeV.
- Is Supersymmetry a contender for this new physics, a key to the unification of the forces? Is it justifying the dark matter in the Universe?
- What could explain the replication of quark and lepton families?
- Are these particles not elementary, but composite?
- Is the left-right asymmetry of weak interaction only a low-energy effect?
- What is the origin of flavors and of CP violation?
- Might extra-dimensions scenarios change the above issues?

Accordingly, the LHC should be designed to provide p-p high collision rates at the highest energy technically feasible to answer some of these questions and to discover new physics, in addition to relativistic heavy-ion collisions to study quark-gluon plasmas.

4.3. Progress toward the decision to build the LHC

In May 1991, a review of the available design and the physics programme pushed the LHC project ahead in the conclusions of a CERN "Long Range Planning Committee", chaired by Carlo Rubbia:

- Ten prototypes of superconducting dipoles were ordered in Industry,
- Discussions among physicists went on to build international Teams around concepts of detectors, in particular ATLAS and CMS,
- An assumed positive decision of construction, optimistically expected in 1992, was thought, even more optimistically, to lead to a start of operation in 1998 after only 5.5 years of construction.

In 1992-93, an External Review Committee recommended the CERN Council to go ahead with the project, but to launch immediately a larger effort in R&D.

After a new design version in 1993 (the White Book), the Council approved the LHC project in December 1994, on the basis of a machine built in two stages, the first one using a missing magnet scheme.

The decision to go back to one stage project was taken in December 1996 after the non-European Countries agreed to join the project and to contribute.

4.4. Progress in the LHC Design

In October 1995, the machine design was frozen after many modifications, but keeping the main technical choices: "two in one", meaning two beams in a single cryostat, and Helium II cryogeny, meaning that the magnet windings at high field will benefit from cooling by a static bath of helium at 1.9 K and atmospheric pressure. The main changes from the initial design are the following:

- Removing LEP from the tunnel,
- Keeping 4 crossing points instead of 8 in LEP,
- Excavating two large caverns in addition to the LEP caverns,
- Center of mass energy: 2×7 TeV, luminosity: $10^{34} \text{cm}^{-2} \text{s}^{-1}$ in protons collisions, and $1,148, 2 \times 10^{27}$ respectively in heavy ions collisions,
- Bunch spacing increased to 25 ns – 7.5m and smaller number of bunches per beam 2835, leading to 335 MJ of stored energy per beam in protons collisions, and 125 ns, 608 bunches, only 4.8 MJ in ions collisions,
- Magnetic field: 8.4 T in longer dipoles of 15 m,
- Cryogenic piping in a separate line, not in the main cryostat,
- A long (150m) magnet Test String was built with the prototype magnets in order to gain operational experience for all components to use.

4.5. The Detectors Challenges

Two very large, general purpose detectors, ATLAS and CMS, were built according to different designs and new technologies, and installed in the two new dedicated caverns; they are facing the same challenges:

- Rapidity: 30 events/bunch crossing every 25 ns, identified by 10^{11} tracks/s,
- Hermiticity and fine granulometry to provide the required accuracy in a huge volume,
- Radiation hardness of sensors and electronics (required level of hardness obtained thanks to the new 0.25 μm Silicon wafer technology),
- Huge number of cables (10^8) and, after reduction on-line from 40 GHz to 100 Hz, 0.1-1 Gbytes/s of measures to be transferred to a large memory (10 Peta-Bytes) and processed by 100.000 high-end processors distributed across the entire world in a "Computing Grid",
- Extraction (with the help of many Monte-Carlo analysis) from the large background of the signature, for example of a specific Higgs particle-decay which depends of the unknown H-mass; therefore a large range of possible Higgs mass must be explored.

Two other detectors were built for specific purposes and installed in LEP caverns; they require less luminosity to operate:

- ALICE observes collisions between Pb ions beams with an energy of 2.75 TeV/nucleon, producing a plasma of quarks and gluons when they are no more confined in the nucleus ,
- LHCb exploits the LHC as a b-factory to study rare b-decays and CP violation, to link with the ratio matter-antimatter.

5- Conclusion

The LHC will be the first accelerator to explore directly the TeV scale and reveal new physics. Providing answers to some essential questions about the universe is justified, in spite of its costs; these questions , without the LHC will remain unanswered for long.

Paraphrasing Glashow at Les Houches in 1978 about the LEP, it can be concluded that: **“The LHC is exciting, essential and expensive”**.

Efforts which were required for the LHC realization and next for its exploitation will be more than rewarded by **THE FUTURE DISCOVERIES**.

Limited List of References

- J. I. Friedman , and H.W, Kendall (1972) . Deep Inelastic Electron Scattering. *Annual Review of Nuclear Sciences*, **22**, 203-254.
- M. Gell-Mann (1964). A schematic Model of Baryons and Mesons. *Physics Letter*, **8**, 214.
- S. L. Glashow, J. Illiopoulos, and L. Maiani (1970). Weak Interactions with Lepton- Hadron Symmetry. *Physical Review D*, **2**, 1285-1292.
- F. J. Hasert and Collaboration Gargamelle (1973). Observation of Neutrino-Like Interactions without Muon or Electron in the Gargamelle Neutrino Experiment. *Physics Letter*, **46**, 138.
- P. W. Higgs (1964). Broken Symmetries and the Masses of Gauge Bosons. *Physical Review Letter*, **13**, 508.
- C. Rubbia, S. van der Meer (1984) Nobel Lectures.
- S. Weinberg (1967). A Model of Leptons. *Physical Review Letter*, **19**, 1264.
- A. Zichichi Chairman, ECFA – LEP Working Group Progress Report (1979)
ECFA European Committee for Future Accelerators, ECFA /79/39.

THE ISR LEGACY

■ PIERRE DARRIULAT

VATLY Astrophysics Laboratory, Hanoi, Vietnam

1. Introduction

It so happens that the life time of the CERN Intersecting Storage Rings (ISR), roughly speaking the seventies, coincides with a giant leap in our understanding of particle physics: the genesis of the Standard Model. Those of us who have worked at the ISR remember these times with the conviction that we were not merely spectators of the ongoing progress, but also – admittedly modest – actors. While the ISR contribution to the electroweak sector is indeed negligible, its contribution to the strong sector is essential and too often unjustly forgotten in the accounts that are commonly given of the progress of particle physics during that period. In the present article, I shall use three topics to illustrate how important it has been: the production of hadrons, large transverse momentum final states and the rising total cross-section.

When Vicky Weisskopf, in December 1965, in his last Council session as Director-General, obtained approval for the construction of the ISR, there was no specific physics issue at stake, which the machine was supposed to address; its only justification was to explore the *terra incognita* of higher centre of mass energy collisions (to my knowledge, since then, all new machines have been proposed and approved with a specific physics question in mind, which they were supposed to answer). The strong interaction was perceived as a complete mystery. The eightfold way, today understood as the approximate $SU(3)$ flavour symmetry associated with interchanges of u , d and s quarks, was not believed to have significant consequences in the dynamics of the strong interaction. The fact that no free quark had been found in spite of intensive searches, and that states such as Δ^{++} , with spin-parity $3/2^+$, could not be made of three identical spin $1/2$ u quarks without violating Fermi statistics, were discouraging such interpretations.

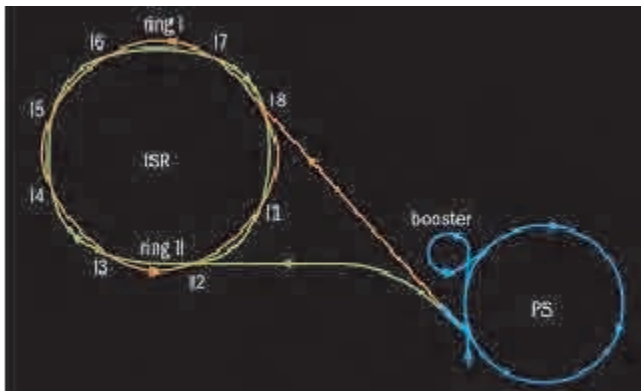


Figure 1. Schematic drawing of the ISR.

The ISR were the first hadron collider in the world (Figure 1). They consisted of two rings intersecting in 8 equidistant points at an angle of 15° . The circumference, 943 m, was chosen to be three halves of that of the CERN Proton Synchrotron (PS) that was used as an injector. Six of the intersections were used for physics, one for measuring the luminosity and one for dumping the beams. First protons were stored at 15 GeV on January 27th 1971. By May, the

energy had reached 26.5 GeV and finally reached 31.4 GeV where most of the physics data were collected. Beam intensities increased from ~ 10 A in May 1971 to up to 57 A and the luminosity from $3 \cdot 10^{29} \text{cm}^2 \text{s}^{-1}$ to $1.4 \cdot 10^{32} \text{cm}^2 \text{s}^{-1}$ with *low β* insertions. Coasting times for physics reached 50 h. In addition to protons, deuterons, alpha particles and

antiprotons had also been stored. The operation of the ISR turned out to be a remarkable success from the accelerator physics and technology point of view. Clearing electrodes and bake-outs (350°) of the stainless steel vacuum chamber made it possible to reach pressures as low as 10^{-11} Torr, which was essential to high luminosities. The machine has been an unprecedented laboratory for the study of proton beam dynamics, including that of transverse Schottky noise, which paved the way to Van der Meers's stochastic cooling.

Most ISR experiments had been designed with the idea that all particles would be forward produced. It took a long time for detectors equipped with large angle calorimeters and magnetic fields, as required for the study of short distance (large transverse momentum, p_T) interactions, to be available. The Split Field Magnet (SFM) was a general facility on which much of the physics results have been obtained; the magnetic field was concentrated forward and negligible at large angles (Figure 2).

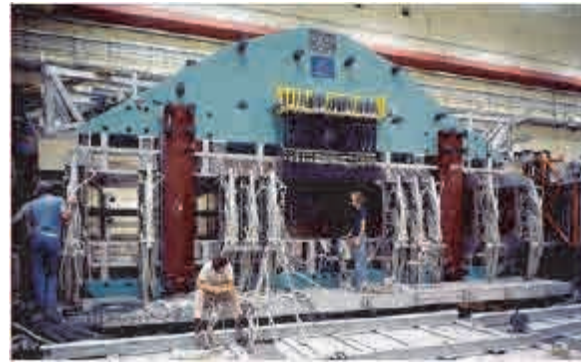


Figure 2. The Split Field Magnet.

2. The main milestones

Let us start with a brief reminder of the main events that marked the progress of our understanding of the strong interaction in the seventies. It started in 1968-1969 at SLAC [1] with the discovery of an important continuum in the deep inelastic region of electron-proton scattering. The 2-mile linear accelerator had started operation the preceding year and the experimental programme, using large spectrometers, extended over several years. From the very beginning, experimenters and theorists were in close contact, feeding each other with new data and new ideas, starting with Bjorken's ideas on scaling [2] and Feynman's ideas on partons [3], both early advocates of a proton structure consisting of point-like constituents. However, one had to wait until 1972 for the case for a quark model to become strong: by then, scaling had been established; the measurement of a small R value (the ratio of the absorption cross sections of transverse and longitudinal virtual photons) had eliminated competitors such as the then popular Vector Dominance Model; deuterium data had been collected allowing for a comparison between the proton and neutron structure functions; a number of sum rules had been tested; evidence for the quarks to carry but a part of the proton longitudinal momentum had been obtained; the first neutrino deep-inelastic data from Gargamelle had become available [4]. By the end of 1972, the way was paved for Gross, Wilczek and Politzer [5] to conceive the idea of asymptotic freedom and its corollary, infrared slavery, explaining why one could not see free quarks. By the end of 1973, the connection with non-abelian gauge theories had been established and the "advantages of the colour-octet gluon picture", including the solution of the Fermi statistics puzzle, had been presented by Fritzsche, Gell-Mann and Leutwyler [6]. QCD was born and, by 1974, was starting to be accepted by the whole community as *the* theory of the strong interaction. It took another three to four years for it to come of age.

By mid 1972, SPEAR, the Stanford electron-positron collider, had begun operation. In November 1974, it shook the physics community with what has since been referred to as a Revolution: the discovery of the Ψ going hand in hand with the simultaneous discovery of the J at Brookhaven. It immediately exploited its ability to produce pure quark-antiquark final states to measure the number of colours. However, there were so many things happening in the newly available energy domain (opening of the naked charm channels, crowded charmonium spectroscopy, production of the τ lepton) that it took some time to disentangle their effects and to understand what was going on. By the end of the decade, scaling violations had been studied both in neutrino interactions and in electron-proton annihilations (DORIS had started operation in Hamburg two years after SPEAR). QCD had reached maturity and the only puzzling questions that remained unanswered, the absence of a CP violating phase and our inability to handle the theory at large distances, are still with us today.

3. Hadron production: universality of the main features

Out of the many early pictures of the dynamics of strong interactions, two passed successfully the ISR test: Van Hove's Longitudinal Phase Space [7] and Feynman's Partons [3].

Longitudinal Phase Space (LPS) states that at high energies hadrons are produced with limited transverse momenta (with a distribution that is essentially the Fourier transform of the proton disk, $\hbar/1\text{ fm} \sim 220\text{ MeV}$) and a uniform rapidity distribution (Figure 3). Partons suggest a field theory basis for such a picture, strong interactions proceeding via bremsstrahlung-like radiation of "wee" partons with no privileged frame of reference in the limit of infinite momenta. The nature of such partons was left unspecified in the original picture, but QCD would identify them with gluons later on.

Remember that a Lorentz transformation of velocity β along Oz is a rotation by an angle $i\text{Argth}\beta$ in the (z, it) plane, simply shifting the rapidity (azimuth equivalent) by a constant: frame independence means uniform rapidity distribution and leads to Feynman's scaling in the infinite momentum frame.

While the role of QCD basic vertices (qqg , ggg and $gggg$) is explicit in perturbative expansions (short distances, large p_T), it is hidden in the low p_T regime that prevails in hadron production: so-called "QCD inspired" models that have bloomed in the late seventies and early eighties have given a sound basis to the above picture but have not added much significant new information to it. Kinematics play an important role, dominated by the slow (*lns*) increase of the width of the rapidity plateau with energy (the bulk of the low p_T physics is often nicknamed "*logs physics*" for this reason). Also, to a good approximation, the dependence of the production cross-section on the mass (m) of

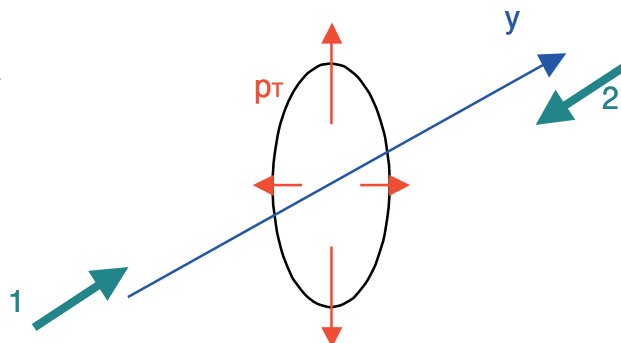


Figure 3. LPS implies limited transverse momentum (p_T) and uniform rapidity (y) distribution.

the produced hadrons is simply described as a function of the transverse mass, $m_T = \sqrt{(p_{T2} + m)^2}$.

Such general features of the hadronization mechanism are observed to be universal (understood as essentially resulting from the radiation of gluons) with a flat rapidity plateau, limited p_T , short range correlations (Figure 4) and $\ln s$ energy dependence. Such universality was demonstrated with clarity [8] by making explicit use of two essential concepts: effective energy and leading effect (Figure 5). The leading effect states that flavour (quark) quantum numbers are not radiated away and stay with the largest momentum hadron (the leader), a meson remaining a meson, and a baryon remaining a baryon. The effective energy is the energy available for hadronization after subtraction of that carried by the leader.

In the early eighties, when the CERN proton-antiproton collider started operation, the validity of the above picture [10a] could be made evident in its whole beauty [10b] and studied in details

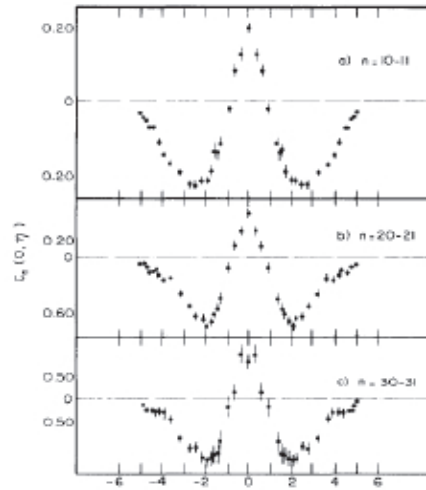


Figure 4. Short range rapidity correlations measured at the ISR [9] are displayed for different multiplicity bins. A simple cluster model gives a good description of the data

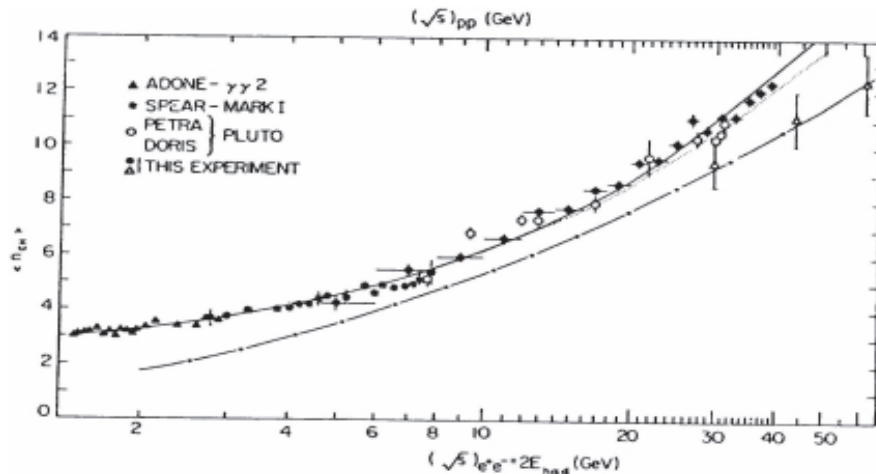


Figure 5. While charged multiplicities measured at the ISR and electron-positron colliders display a universal dependence on effective energy, they differ from each other when the leading energy is not subtracted (lower line).

4. Large transverse momentum production

By 1972, the basic parton ideas had found their expression in the picture [11] of large transverse momentum production being factorized in three steps (Figure 6): singling out a parton in each proton (structure functions), making them interact (how? was not clear) in a binary collision and letting the final state partons fragment into hadrons (fragmentation functions). In 1972-1973, three ISR teams (Figure 7) announced the

observation [12] of a copious pion yield at large p_T , orders of magnitude above the (traditionally called naïve) extrapolation of the exponential distribution observed at lower

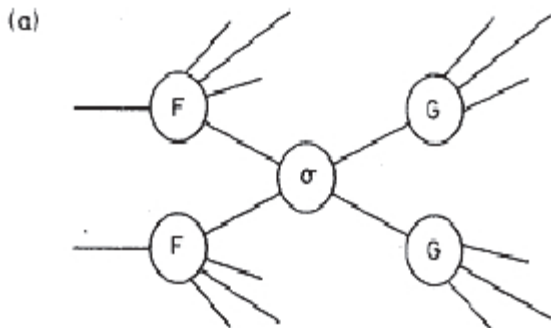


Figure 6. Parton model picture of high p_T hadron interactions. One parton of each of the incident hadrons (structure function F) experiences a binary collision (σ) and the outgoing partons fragment into hadrons

energies, $\sim \exp(-6p_T)$. This first discovery opened the ISR to high p_T studies providing a new short distance probe. But many experiments had been designed under the assumption that most hadrons would be forward produced and were not matched to such studies: those having detectors at large angles were not covering a large enough solid angle; moreover, the background that had been anticipated in the search for new particles had been strongly underestimated and such searches were now becoming much more difficult than had been hoped for.

Bjorken scaling was soon found to apply, in support of the parton picture, but the index of the p_T power law was twice as high as the value expected from point-like constituents, 8 rather than 4. Precisely, the π^0 inclusive invariant cross-section was of the

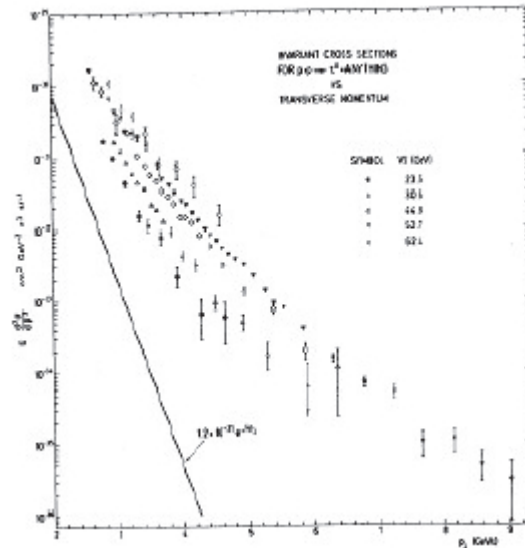


Figure 7. Early inclusive π^0 cross-section [12] giving evidence for copious production at high p_T well above the exponential extrapolation of lower energy data.

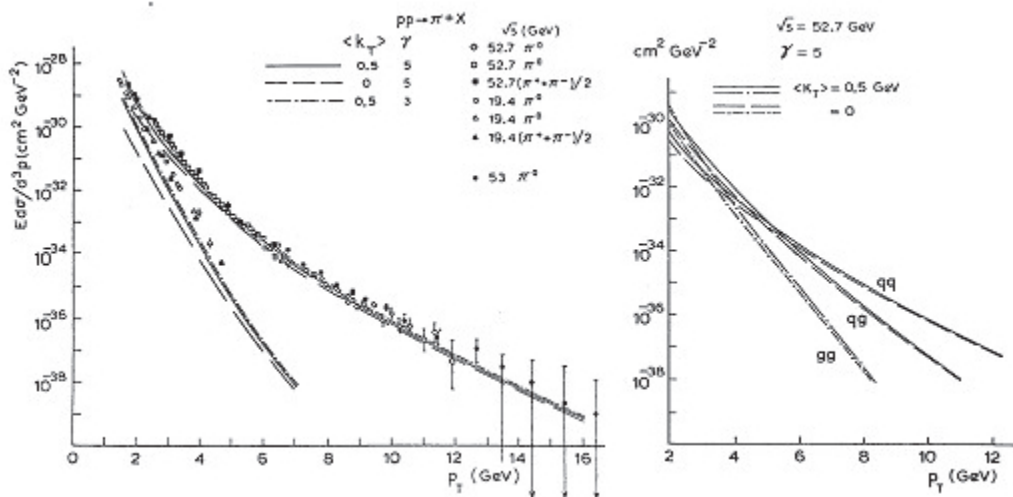


Figure 8. A typical QCD fit [14] to inclusive pion data (left) and the relative contributions of quark-quark, quark-gluon and gluon-gluon diagrams (right).

form $p_T \sim \exp(-kx_T)$ where $x_T = 2p_T/\sqrt{s}$, $n = 8.24 \pm 0.05$ and $k = 26.1 \pm 0.5$. The impact of this result was quite strong and brought into fashion the so-called constituent interchange model [13] that included mesons in addition to quarks among the parton constituents of protons. The model correctly predicted the power 8 measured at the ISR and had many successes but did not stand the competition with early QCD models that were starting to be developed. Such an example is illustrated in Figure 8, giving evidence for important quark-gluon and gluon-gluon contributions [14] beside the quark-quark term. It was soon understood that the p_T power law was indeed evolving to p_T^{-4} at high values of x_T , which, however, were only accessible, in practice, to larger centre of mass energy collisions. The successes of the constituent interchange models were then relegated to the rank of “higher twist corrections” to the leading order perturbative regime.

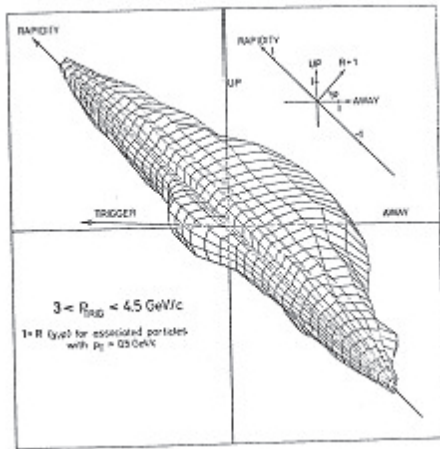


Figure 9. Longitudinal phase space density (relative to minimum bias events) associated with a single particle trigger at 90° (see text).

The early evidence in favour of the parton picture encouraged studies of the global event structure and, in particular, experiments aiming at the detection of the hadron jets into which the hard scattered partons were supposed to fragment. As none of the existing ISR experiments was matched to the task, some ISR collaborations decided to upgrade their detectors and, between 1973 and 1978, several of these studied the event structure: the evidence for hard jets in the final state, already clear in 1976, became very strong [15]. Diffraction was seen to be suppressed at large rapidities, a “same-side” jet is present alongside the trigger and “away-side jets”, at opposite azimuth to the trigger, cover a broad rapidity range (Figure 9). The presence of an “underlying event” implies a p_T threshold,

~ 1 GeV, below which a particle cannot be unambiguously identified as a fragment of a hard scattered parton. Single particle triggers distort the “same-side” jet fragmentation (trigger bias): an ideal experiment should trigger on the total transverse energy E_T using calorimeters.

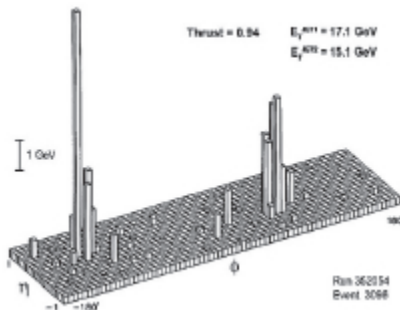


Figure 10. A lego plot from the AFS experiment showing two-jet dominance at larger E_T .

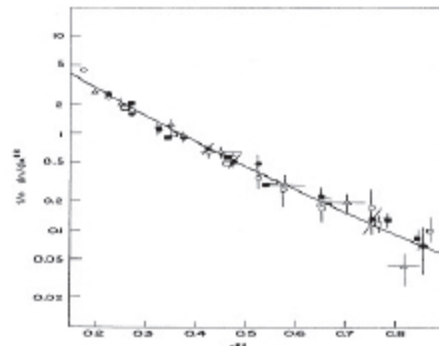


Figure 11. Jet fragmentation functions measured in different processes (DIS \circ , triangles; ISR, circles; e^+e^- , solid line).

However, one had to wait until the eighties, with the Axial Field Spectrometer in I8 and the Superconducting Solenoid in I1 to see detectors having large calorimeter coverage. When the ISR closed down in 1984, a rich set of important results had been obtained by these two groups [16], with two-jet events dominating the scene (Figure 10) for transverse energies in excess of 35 GeV [17] but the CERN proton-antiproton collider, which had published its first jets in 1982, had already taken the limelight away from the ISR.

Away-jets were compared with quark jets observed in deep inelastic scattering and e^+e^- annihilations (Figure 11). The dominant feature is the universality of the hadronization process when expressed in terms of effective energy. However, ISR jets being mostly gluon jets, one could have expected them to have a higher multiplicity than quark jets of the same effective energy, as a result of their higher colour charge. But the difference is small and the p_T range accessible to the ISR was too low: one had to wait for LEP and the proton-antiproton colliders to see it.

Table 1. Leading order processes involving quarks or gluons.

We use the symbol $><$ for s channel and $||$ for t channel exchanges. Leading order contributions are shown as bold. Diagram involving the ggg or $gggg$ vertices are shown in italic. Next to leading order contributions (scaling violations) involve only the qqg vertex and are shown in normal font.

e^+e^- annihilations	$e^+e^- \rightarrow \gamma^* q^+ q^-$	$e^+e^- \rightarrow \gamma^* q^+ q^- g$
<i>DIS (electron)</i>	$eq \gamma eq$	$eq \gamma eqg$
<i>DIS (neutrino, NC)</i>	$\nu q Z \nu q$	$\nu q Z \nu qg$
<i>DIS (neutrino, CC)</i>	$\nu q W lq$	$\nu q W lqg$
<i>pp Drell Yan</i>	$q^+ q^- \rightarrow \gamma^* l^+ l^-$	
<i>pp Direct photons</i>	$q^+ q^- q \gamma g$	$qg q \gamma q$
<i>pp Large p_T hadrons</i>	$qq g qq$	$qq q gg$
	$q^+ q^- \rightarrow g^* gg$	$q^+ q^- \rightarrow g^* q^+ q^-$
	$qg q qg$	$qg g qg$
	$qg>q qg$	$gg>g^* q^+ q^-$
	$gg>g^* gg$	$gg g gg$
	$gg q q^+ q^-$	$gg>^* gg$

It is important to recognize the role, in the large transverse momentum sector, played by the ISR as an exclusive gluon collider. In this sector, where perturbative QCD applies, gluons contribute to leading order (Table 1). In e^+e^- annihilations and deep inelastic scattering, they contribute to next to leading order only, in the form of radiative corrections associated with a bremsstrahlung gluon radiated from a quark. This does not mean that such gluon contributions are unimportant: the scaling violations which they induce have been one of the most powerful tool in the development of our understanding of QCD. But, at the ISR, gluons dominate the scene: in this low x_T regime, collisions involving gluons, either g - g or q - g , account for most of the high p_T cross-section. Gluon

interactions being the privileged domain of the ISR, and gluons having been the last component of the theory to be understood and digested, the ISR have played a major role in probing this essential QCD sector. In particular the ISR had exclusive access to the three and four gluon vertices, which are a specific expression of QCD as a non abelian gauge theory.

Finally, by the end of the seventies, the J/Ψ and the Y had been detected and their production cross-sections had been measured. Clear evidence for D production had been obtained – for the first time in hadron interactions [18]. Dilepton masses up to 20 GeV have been ultimately studied, giving evidence for strong next to leading order corrections to the Drell-Yan leading order diagram. The ISR were a privileged laboratory for the study of direct photon production [19], which proceeds mainly by Compton interaction between a quark and a gluon producing a quark and a photon.

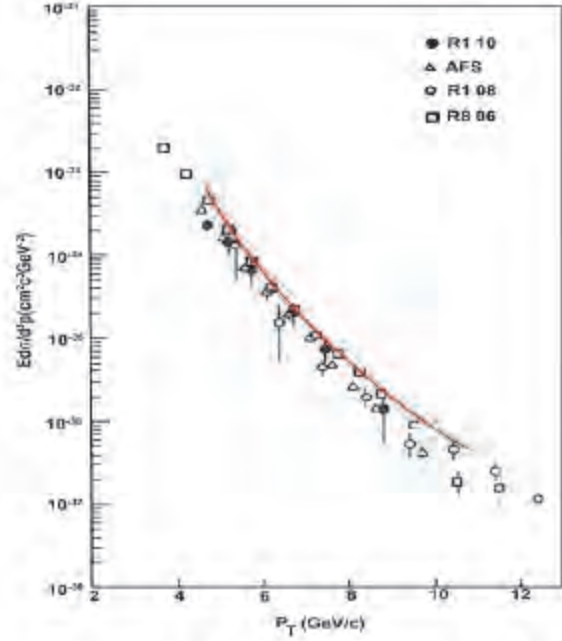


Figure 12. Direct photons at the ISR.

5. Total cross-section and elastic scattering

The rise of the total cross-section with energy was measured early at the ISR and came to many as a surprise [20]: it was generally believed that it should reach asymptotia. Seen as a diffraction process, elastic scattering gives the shape of the absorbing area globally associated with the total cross-section. Both σ_{tot} and $d\sigma/dt|_{t=0}$ (Coulomb interference region) were measured to obtain the scattering amplitude $F(s,t)$ near $t=0$. The following relations apply:

$$\sigma_{tot} = 16\pi s^2 d\sigma/dt|_{t=0} / (1 + \rho^2) \quad \text{where} \quad \rho(s) = \text{Re}(F(s,0)) / \text{Im}(F(s,0)).$$

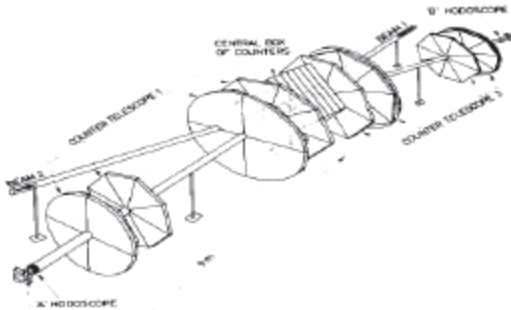


Figure 13. Total cross-section schematic layout (left) and a “Roman pot” (right) used for the measurement of the elastic cross section in the Coulomb interference region.

The measurement of the elastic cross-section in the interference region required detectors approaching the beam far closer than allowed by a standard vacuum chamber. This was achieved by inserting them in remote-controlled bellows, the so-called “Roman pots”, named after the CERN-Rome group who invented them. The trends measured at the ISR (Figure 14) were later on found to continue in the proton-antiproton and LHC energy ranges, confirming the inadequacy of a naïve diffractive picture implying a total cross-section independent of energy.

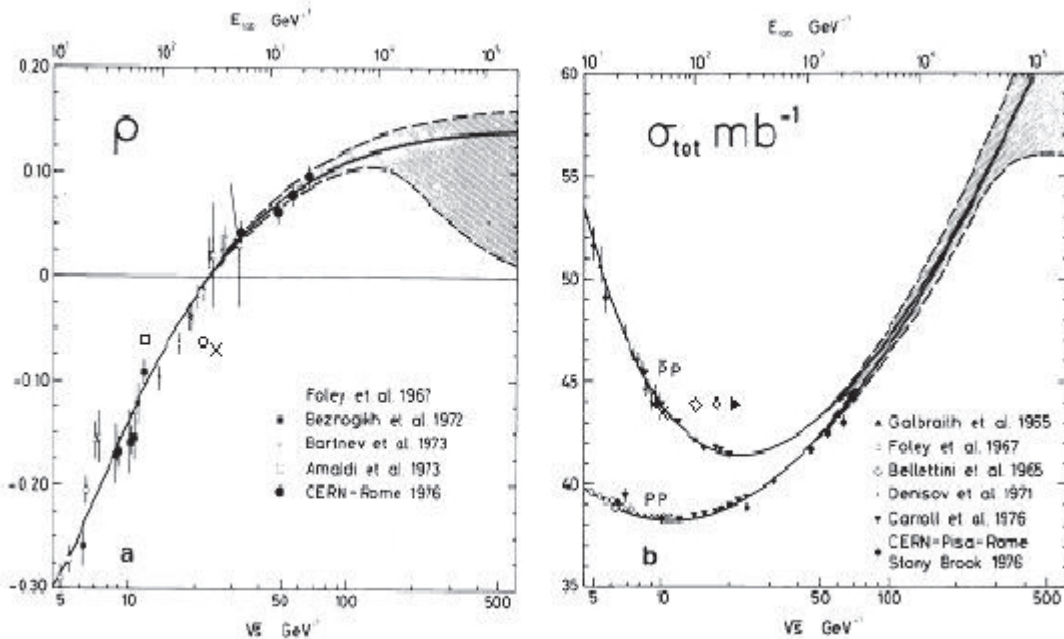


Figure 14. Energy dependence of the total cross-section (right) and of the ρ parameter (left).

Most of the ideas we have today of the strong interaction date from ISR times.

6. Conclusions

The dominant features of the strong interaction revealed at the ISR are still with us today, comforted but not deeply affected by QCD. The proton-antiproton and LEP colliders have made them evident and exposed them in full beauty.

They include at large distances: $\ln s$ dependence on energy, limited p_T , uniform rapidity plateau, short range rapidity correlations, transverse mass unification, and at short distances: jet production, factorization of the structure and fragmentation functions as well as of the underlying event. Their universality is made explicit by using the concept of effective energy that takes in due account the leading particle effect.

At the ISR, the complexity of the physics processes at stake, much larger than at e^+e^- colliders, made it difficult to devise decisive QCD tests independent from what had been learned at other accelerators. But ISR data have explored elementary processes which were not accessible to other accelerators and were found to nicely fit in a coherent QCD picture embedding deep inelastic scattering as well as e^+e^- annihilation results. This was clearly an independent and essential contribution but the fact that they always validated QCD predictions made the superficial observer underestimate their importance. This lack of recognition was also caused by the lack, for many years, of detectors optimized for the study of hard processes, the absence of the weak sector from the ISR

landscape and the fact that hard hadron collisions imply complex processes which may seem “dirty” to whom does not make the effort to study them in detail.

We, who worked at the ISR, tend not to attach much importance to this relative lack of recognition: for us, their main legacy has been to have taught us how to make optimal use of the proton-antiproton colliders, which were soon to come up. They had given us a vision of the new physics and of the methods to be used for its study which turned out to be extremely profitable. They had played a seminal role in the conception of the proton-antiproton colliders experiments, they were the first hadron collider ever built in the world and they were the machine where a generation of engineers and physicists learned how to design colliders and collider experiments. We see ISR and proton-antiproton colliders as a lineage, father and sons, the success of the latter being inseparable from the achievements of the former.

We were young then, we remember these times with emotion... With the LHC, the lineage has now extended to a third generation and we look at the future with the eyes of grand parents, full of tenderness and admiration for their grand son, whom we wish fame and glory.

Acknowledgements

It is a pleasure to thank Professor Antonino Zichichi and the organizers of the Colloquium for having invited me to give this brief recollection. I am deeply grateful to Luigi Di Lella for pertinent comments on the manuscript.

References

General reviews, such as those listed below, are an important source of references:

Giorgio M. Giacomelli and Maurice Jacob, *Physics at the CERN-ISR*, Phys. Rep. 55 (1979) 1.

Leon van Hove and Maurice Jacob, *Highlights of 25 Years of Physics at CERN*, Phys. Rep. 62 (1980) 1.

Maurice Jacob, in : *A review of Accelerator and Particle Physics at the CERN Intersecting Storage Rings*, CERN 64-13 (1984) 21-81.

U. Amaldi, P. Bryant, P. Darriulat, K. Hübner, Colloquium on the 40th Anniversary of the First Proton-Proton Collisions in the ISR, forthcoming CERN Report.

1. Jerome I. Friedman, *Deep Inelastic Scattering Evidence for the Reality of Quarks*, History of Original Ideas and Basic Discoveries in Particle Physics, H. B. Newman and T. Ypsilantis editors, NATO ASI series, B352 (1994) 725 and references therein.
2. James D. Bjorken, private communication to the MIT-SLAC group, 1968, and Phys. Rev. 179 (1969) 1547.
3. Richard P. Feynman, Phys. Rev. Lett. 23 (1969) 1415; *Proceedings of the IIIrd International Conference on High Energy Collisions*, Gordon and Breach, new York, 1969.
4. Donald H. Perkins, in *Proceedings of the XVIth International Conference on High Energy Physics, Chicago and NAL*, vol. 4 (1972) 189.
5. David J. Gross and Frank Wilczek, Phys. Rev. Lett. 30 (1973) 1343; Phys. Rev. D8 (1973) 3633 and Phys. Rev. D9 (1974) 980.

6. H. Fritzsch, Murray Gell-Mann and H. Leutwyler, Phys. Lett. 47B (1973) 368.
10. Alvaro De Rujula, *QCD in "her" Maiden Years*, History of Original Ideas and Basic Discoveries in Particle Physics, H. B. Newman and T. Ypsilantis editors, NATO ASI series, B352 (1994)123.
7. Leon Van Hove, Nucl. Phys. B9 (1969) 331.
8. V.N. Gribov, G. 't Hooft, G. Veneziano and V.F. Weisskopf, *The Creation of Quantum Chromodynamics and the Effective Energy*, World Scientific Series in 20th Century Physics, Vol. 25, edited by L.N. Lipatov.
- The complete set of results at the ISR from the Bologna-CERN-Frascati (BCF) - Collaboration can be found in the book, published on the occasion of the Galvani Bicentenary celebration in honour of A. Zichichi.
9. Lorenzo Foa, Phys. Rep. 22 (1975) 1 and references therein.
- 10a. M. Basile, G. Cara Romeo, L. Cifarelli, A. Contin, G. D'Ali, C. Del Papa, P. Giusti, T. Massam, R. Nania, F. Palmonari, G. Sartorelli, M. Spinetti, G. Susinno, L. Votano and A. Zichi *The Leading Effect explains the Charged Particle Multiplicity Distribution observed at the CERN pp Collider*, Lettere al Nuovo Cimento 41, 298 (1984).
- 10b. G.J. Alner *et al.* (UA5 Collaboration), Phys. Rep. 154/5-6 (1987) 247.
11. M. Berman and M. Jacob, Phys. Rev. Lett. 25 (1970) 1683; J.D. Bjorken and E.A. Paschos, Phys. Rev. 185 (1968) 1975; S.D. Drell, D.J. Levy and T.M. Yan, Phys. Rev. 187 (1969) 2159; S.M. Berman, J.D. Bjorken and J. Kogut, Phys. Rev. D4 (1971) 3388; J. Kuti and V.F. Weisskopf, Phys. Rev. D4 (1971) 3418; S.D. Drell and T.M. Yan, Phys. Rev. Lett. 25 (1970) 316.
12. B. Alper *et al.*, Phys. Lett. B44 (1973) 521 ; M. Banner *et al.*, Phys. Lett. B44 (1973); 537; F.W. Büsler *et al.*, Phys. Lett. B46 (1973) 471 and Proc. 16th Int. Conf. on High Energy Phys. (Chicago and NAL, 1972).
13. D. Sivers, R. Blankenbecler and S.J. Brodsky, Phys. Rep. C23 (1976)1 and references therein.
14. A.P. Contogouris, R. Gaskell and S. Papadopoulos, Phys. Rev. D17 (1978) 2314.
15. Pierre Darriulat, Proc. XVIIIth Int. Conf. on High En. Phys., Tbilisi, USSR, 1976, N.N. Bogolioubov *et al.* editors, JINR Dubna, 1977; *Large Transverse Momentum Hadronic Processes*, Ann. Rev. Nucl. Part. Sci. 30 (1980) 159 and references therein..
16. T. Åkesson *et al.*, Phys. Lett. B118 (1982) 185 and 193; Phys. Lett. B123 (1983) 133; Phys. Lett. B128 (1983) 354; Z. Phys. C25 (1984)13; Z. Phys. C30 (1986) 27; Z. Phys. C32 (1986) 317; Z. Phys. C34 (1987) 163; A.L.S. Angelis *et al.*, Phys. Lett. B126 (1983) 132; Nucl. Phys. B244 (1984) 1; Nucl. Phys. B303 (1988) 569. 21.
17. ChristianW. Fabjan and Norman McCubbin, *Physics at the CERN Intersecting Storage Rings (ISR) 1978-1983*, Phys. Rep. 403-404 (2004) 165-175.
18. Daniel Drijard *et al.*, Phys. Lett. B81 (1979) 250 and B85 (1979) 452.
19. M. Diakonou *et al.*, Phys. Lett. B87 (1979) 292 ; A.L.S. Angelis *et al.*, Phys. Lett. B94 (1980) 106; T. Ferbel and W.M. Molzon, Rev. Mod. Phys. 56 (1984) 181; L.F. Owens, Rev. Mod. Phys. 59 (1987) 485; P. Aurenche *et al.*, Nucl. Phys. B297 (1988) 661 and Eur. Phys. C9 (1999) 107.
20. Ugo Amaldi *et al.*, Phys. Lett. B 44 (1973) 112, Phys. Lett. B 62 (1976) 460, Phys. Lett. B 66 (1976) 390 and Nucl. Phys. B145 (1978) 367.
- S.R. Amendolia *et al.*, Phys. Lett. B44 (1973) 119.

FROM NONLINEAR STATISTICAL MECHANICS TO NONLINEAR QUANTUM MECHANICS – CONCEPTS AND APPLICATIONS*

■ CONSTANTINO TSALLIS

Centro Brasileiro de Pesquisas Físicas and
National Institute of Science and Technology for Complex Systems, Rua Xavier Sigaud 150, 22290-180 Rio de Janeiro-RJ, Brazil
and
Santa Fe Institute, 1399 Hyde Park Road, Santa Fe, NM 87501, USA

We briefly review a perspective along which the Boltzmann-Gibbs statistical mechanics, the strongly chaotic dynamical systems, and the Schroedinger, Klein-Gordon and Dirac partial differential equations are seen as *linear* physics, and are characterized by an index $q = 1$. We exhibit in what sense $q \neq 1$ yields *nonlinear* physics, which turn out to be quite rich and directly related to what is nowadays referred to as *complexity*, or *complex systems*. We first discuss a few central points like the distinction between additivity and extensivity, and the Central Limit Theorem as well as the large-deviation theory. Then we comment the case of gravitation (which within the present context corresponds to $q \neq 1$, and to similar nonlinear approaches), with special focus onto the entropy of black holes. Finally we briefly focus on recent nonlinear generalizations of the Schroedinger, Klein-Gordon and Dirac equations, and mention various illustrative predictions, verifications and applications within physics (in both low- and high-energy regimes) as well as out of it.

1 Introduction

The expression *nonlinear physics*, and even *nonlinear science*, has gradually entered in the specialized literature since already a few decades. In particular, it is quite frequently used in connection with complexity in natural, artificial and social sciences. The specific meaning of *linearity* (and concomitantly that of *nonlinearity*) is quite clear when we think of say Maxwell equations or Schroedinger equation, since they are linear in their respective fields. It is however less clear when we think of say statistical mechanics and its dynamical foundations. Here let us start by adopting a very simple and specific sense for the word *linear*, which will nevertheless prove to be, in fact, amazingly powerful. Consider the following (ordinary) differential equation:

$$(1) \quad \frac{dx}{dy} = ay^q \quad (q \in \mathcal{R}; y(0) = 1).$$

This differential equation is *linear* if $q = 1$, and *nonlinear* otherwise. Its solution is given by

$$(2) \quad y(x) = [1 + (1 - q)ax]^{\frac{1}{1-q}} \equiv e_q^{ax} \quad (e_1^{ax} = e^{ax}).$$

The function e_q^x will from now on be referred to as the *q-exponential* function; its inverse is given by the *q-logarithm* function

* Invited paper for the Proceedings of the International Symposium on *Subnuclear Physics: Past, Present and Future*, held at the Pontifical Academy of Sciences (Vatican, 30 October to 2 November 2011).

$$(3) \quad \ln_q z \equiv \frac{z^{1-q} - 1}{1 - q} (\ln_1 z = \ln z).$$

If we identify (x, y, a) with (t, ξ, λ_q) where t is time, ξ is the sensitivity to the initial conditions (defined as $\xi = \lim_{\Delta(0) \rightarrow 0} \frac{\Delta x(t)}{\Delta x(0)}$, $\Delta x(t)$ being the discrepancy of initially close trajectories in a one-dimensional nonlinear dynamical system), and λ_q is the generalized Lyapunov coefficient (λ_1 being the standard Lyapunov exponent), we obtain $\xi = e^{\lambda_q t}$. For $q = 1$, this expression yields the standard exponential divergence behavior corresponding to strongly chaotic systems (hence $\lambda_1 > 0$); for $q < 1$ we obtain the power-law behavior $\xi(t) \sim t^{1/(1-q)}$, which is typical of a wide class of weakly chaotic systems (with $\lambda_1 = 0$ and $\lambda_q > 0$).

If instead we identify (x, y, a) with $(E_i, p_i Z, -\beta_q)$, where E_i is the energy of the i -th state of a N -body Hamiltonian system, p_i is the probability of such state to occur in a stationary state at inverse (effective) temperature $\beta_q \equiv 1/k_B T$, and Z is the partition function, we obtain $p_i Z = e_q^{-\beta_q E_i}$. For $q = 1$, this expression recovers the celebrated Boltzmann-Gibbs (BG) weight for systems at thermal equilibrium; for $q \neq 1$ we obtain the distribution corresponding to stationary or quasi-stationary nonequilibrium states described by nonextensive statistical mechanics [1, 2, 3], i.e., for a wide class of systems whose geometrical-dynamical properties yield pathologies such as lack of ergodicity.

Finally, if we identify (x, y, a) with $(t, \Omega, -1/\tau_q)$, where Ω is some relaxing relevant quantity defined through

$$(4) \quad \Omega(t) \equiv \frac{O(t) - O(\infty)}{O(0) - O(\infty)},$$

O being some dynamical observable essentially related to the evolution of the system in phase space (e.g., the time evolution of entropy while the system approaches a stationary state), and τ_q is a characteristic relaxation time, we obtain $\Omega(t) = e_q^{-t/\tau_q}$. For $q = 1$ we recover the ubiquitous relaxation exponential behavior; for $q > 1$ we recover the power-law $\Omega(t) \sim t^{-1/(q-1)}$ which very many complex systems exhibit.

Let us stress at this point that the above q -indices, respectively associated with the sensitivity to the initial conditions ($q_{\text{sensitivity}}$), with the energy distribution at the stationary state ($q_{\text{stationary state}}$), and with the relaxation ($q_{\text{relaxation}}$), typically do *not* coincide among them (typically they satisfy $q_{\text{sensitivity}} \leq 1 \leq q_{\text{stationary state}} \leq q_{\text{relaxation}}$). But they simultaneously become $q_{\text{sensitivity}} = q_{\text{stationary state}} = q_{\text{relaxation}} = 1$ for the linear limit. Arguments exist (see, for instance, [3,4]) which suggest that, for a typical universality class of complex (nonlinear) systems, an infinite number of different q -indices are to be associated with various types of physical properties (low- and high-order space-time correlations of various micro-, meso- and macroscopic variables). However, only one or few of them are expected to be independent, all the others being (simple or nontrivial) functions of those few independent, which are dictated by the specific class of systems. In the linear limit, all those indices are frequently expected to merge onto the value $q = 1$, thus recovering the exponential behaviors that are standard for various relevant physical variables. The three q -indices mentioned here are frequently referred in the literature as the q -triplet, and have been exhibited in the solar wind, the ozone layer around the Earth, the edge of chaos of one-dimensional dissipative maps, and elsewhere [3].

In Section II we focus on the difference between additivity and extensivity for quantities such as the entropy. In Section III we briefly review the q -generalizations of the Central Limit Theorem (CLT) and of the theory of large deviations. In Section IV we analyze the case of the black-hole entropy with regard to the (frequently mentioned in the literature) bizarre violation of thermodynamical extensivity. In Section V, we flash some predictions, verifications and applications of the present ideas in natural, artificial and social systems, very specifically in recent high-energy experiments at LHC-CERN and RHIC-Brookhaven.

2 Additivity versus Extensivity

Following Penrose [5], we will say that an entropic functional $S(\{p_i\})$ is *additive* if, for two probabilistically independent arbitrary systems A and B , it satisfies

$$(5) \quad S(A + B) = S(A) + S(B).$$

We shall focus here on the entropy [1]

$$(6) \quad S_q = k_B \sum_{i=1}^W p_i \ln_q \frac{1}{p_i} = k_B \frac{1 - \sum_{i=1}^W p_i^q}{q - 1} \quad \left(\sum_{i=1}^W p_i = 1 \right),$$

where W is the total number of possible configurations of the system. S_q is the basis of a generalization of the BG statistical mechanics, currently referred (for reasons that will soon become clear) in the literature as *nonextensive statistical mechanics* [1, 6, 7].

The hypothesis $p_{i,j}^{A+B} = p_i^A p_j^B$ straightforwardly implies that

$$(7) \quad \frac{S_q(A + B)}{k_B} = \frac{S_q(A)}{k_B} + \frac{S_q(B)}{k_B} + (1 - q) \frac{S_q(A)}{k_B} \frac{S_q(B)}{k_B}.$$

Therefore S_q is additive for $q = 1$ (i.e., for $S_1 = S_{BG} \equiv -k_B \sum_{i=1}^W p_i \ln p_i$), and nonadditive for $q \neq 1$.

The definition of extensivity is quite different, namely the entropy of a given system is *extensive* if, in the $N \rightarrow \infty$ limit, $S(N) \propto N$, where N is the number of elements of the system. Consequently, the additivity only depends on the functional relation between the entropy and the probabilities, whereas extensivity depends not only on that, but also on the nature of the correlations between the elements of the system. Hence, checking the entropic additivity is quite trivial, whereas checking its extensivity for a specific system can be quite hard.

To simply illustrate these features let us consider two deeply different equal-probability situations. If the system is such that, for $N \rightarrow \infty$, $W(N) \propto \mu^N$ with $\mu > 1$, we have that the additive BG entropy $S_{BG}(N) = k_B \ln W(N) \propto N$, hence it also is extensive. But if $W(N) \propto N^\rho$ with $\rho > 0$, we have that $S_{BG}(N) \propto \ln N$, i.e., it is nonextensive, whereas the (nonadditive) entropy $S_q(N) = k_B \ln_q W(N) \propto N$ for $q = 1 - 1/\rho$, i.e., it is extensive. Another example with strong correlations between the N elements of the system can be seen in [4]. In this example, once again the *nonadditive* entropy S_q is *extensive* for a special value of $q < 1$, whereas the *additive* entropy S_{BG} is *nonextensive*. Nontrivial physical such examples (more precisely, strongly quantum-entangled magnetic systems) can be found in [8, 9]. Summarizing, to satisfy thermodynamic extensivity of the entropy we must use the BG entropy for systems whose elements are independent or closely so, and we must generically use nonadditive entropies (S_q for specific values of q , or even other entropies [12,13]; see also [14]) if the elements are strongly correlated.

3 Central Limit Theorems and Large-deviation Theory

If we sum many (N with $N \rightarrow \infty$) random variables characterized by the same probability distribution, we obtain (after appropriate centering and scaling) an attractor in the probability space if the variables are (strictly or nearly) independent. This attractor is a Gaussian if the variance (as well as higher-order moments) of the distribution is *finite*, and is a Lévy distribution (also referred to as α -stable distribution) if the variance *diverges* (and the distribution asymptotically decays as a power-law).

These two well known theorems of theory of probabilities have been recently q -generalized. More precisely, if the random variables that are being summed are strongly correlated in a specific manner (named q -independence), then the attractor is a q -Gaussian (see hereafter for its definition) if a certain q -generalized variance is finite [10], and it is a so called (q, α) -stable distribution if that same q -generalized variance diverges

[11]. The definition of q -independence is based on a q -generalization of the Fourier transform, which turns out to be a nonlinear integral transform. The q -generalization of the inverse Fourier transform exhibits in fact properties that are both delicate and interesting [15, 16, 17, 18].

The q -Gaussian distributions straightforwardly emerge from the extremization of the entropy S_q in its continuous form, and are defined as follows:

$$(8) \quad p_q(x) = \frac{e_q^{-\beta x^2}}{\int dy e_q^{-\beta y^2}} \propto \frac{1}{[1 + (q-1)\beta x^2]^{1/(q-1)}} \quad (\beta > 0; q < 3).$$

q -Gaussians recover Gaussians for $q = 1$, have a finite support for $q < 1$, and an infinite support for $q \geq 1$; they are normalizable for $q < 3$, have a finite variance for $q < 5/3$ and a diverging one for $5/3 \leq q < 3$. For $q = 2$ they recover the celebrated Cauchy-Lorentz distribution.

Since q -Gaussians are attractors in the presence of strong correlations (q -independence; see also [19, 20]), they are expected to emerge very frequently in nature. We shall present in Section V several such examples.

Another mathematical pillar of BG statistical mechanics is the theory of large deviations [21]. It consists in the fact that the probability of deviations around the mean value exponentially depends on the number N of independent (or nearly so) realizations ($N \rightarrow \infty$), the so called *rate function* of the exponent being related to the BG entropy. An illustration has been recently advanced [22] which suggests that in the presence of strongly correlated realizations (of the q -independence type), that same probability behaves q -exponentially instead of exponentially, the rate function possibly being related to S_q (see also [23]).

4 Reconciling The Black Hole Entropy With Thermodynamics

To be self-contained, let us reproduce here parts of the discussion presented in [24]. In his 1902 book *Elementary Principles in Statistical Mechanics* [25], Gibbs emphatically points that systems involving long-range interactions are intractable within the Boltzmann-Gibbs (BG) theory, due to the divergence of the partition function. As an illustration of his remark he refers specifically to the case of gravitation. This serious difficulty emerges in fact for any d -dimensional classical system including two-body interactions whose potential energy asymptotically decays with distance like $1/r^\alpha$ ($r \rightarrow \infty$), with $0 \leq \alpha/d \leq 1$. Indeed, under such conditions the potential is not integrable, i.e., the integral $\int_{\text{constant}}^{\infty} dr r^{d-1} r^{-\alpha}$ diverges. From the microscopic (classical) dynamical point of view, this is directly related to the fact that the entire Lyapunov spectrum vanishes in the $N \rightarrow \infty$ limit, which typically impeaches ergodicity (see [26, 27, 28] and references therein). This type of difficulty is also present, sometimes in an even more subtle manner, in various quantum systems (the *free* hydrogen atom constitutes, among many others, an elementary such example; indeed its BG partition function diverges due to the accumulation of electronic energy levels just below the ionization energy).

Along closely related lines, since the pioneering works of Bekenstein [29] and Hawking [30, 31], it has become frequent in the literature the (either explicit or tacit) acceptance that the black-hole entropy is anomalous in the sense that it violates thermodynamical extensivity. Indeed we read all the time claims that the entropy (*assumed to be the BG one*) of the black hole is proportional to the area of its boundary instead of being proportional to its volume [32, 33, 34, 35, 36, 37, 38, 39, 40]. Similarly we have the so called *area law* [41], which states that the entropy (*once again assumed to be the BG one, or occasionally the Renyi one*) of a class of quantum-entangled d -dimensional systems (with $d > 1$) is proportional to the d -dimensional area $A_d \equiv L^{d-1} \propto N^{(d-1)/d}$ instead of being proportional to its d -dimensional volume $V_d \equiv L^d \propto N$, i.e., where N is the number of elements of the system and L is a characteristic length ($d = 3$ precisely coincides with the case of the black hole).

Strangely enough, Gibbs's crucial remark and the dramatic theoretical features to which it is related are often overlooked in textbooks. Similarly, the thermodynamical violation related to the area law frequently is, somehow, not taken that seriously. Indeed, the inclination of some authors is to consider that, for such complex systems, the entropy is not expected to satisfy thermodynamics. Physically speaking, we consider such

standpoint a quite bizarre one. It is shown in [24] how this difficulty can be overcome. We simply argue that the fact (repeatedly illustrated in various manners for strongly quantum-entangled systems, black holes and, generically speaking, for systems satisfying the above mentioned area law) that the Boltzmann-Gibbs-von Neumann entropy is *not* proportional to N precisely shows that, for such strongly correlated systems, *the entropy is not the BG one (or the Renyi one, which, like the BG one, is additive) but a substantially different (nonadditive) one*.

It is clear that, for $N \gg 1$, N^ρ becomes increasingly smaller than μ^N . A similar situation occurs for

$$(9) \quad W(N) \propto C v^{N^\gamma} \quad (C > 0; v > 1; 0 < \gamma < 1),$$

which also becomes increasingly smaller than μ^N (though increasingly larger than N^ρ). The entropy associated with $\gamma \rightarrow 1$ is of course S_{BG} . What about $0 < \gamma < 1$? The answer is in fact already available in the literature (footnote of page 69 in [3], and also in [24]), namely,

$$(10) \quad S_\delta = k_B \sum_{i=1}^W p_i \left(\ln \frac{1}{p_i} \right)^\delta \quad (\delta > 0).$$

The case $\delta = 1$ recovers S_{BG} . This entropy is, like S_q for $q > 0$, concave for $0 < \delta \leq (1 + \ln W)$. And, also like S_q for $q \neq 1$, it is nonadditive for $\delta \neq 1$. Indeed, for probabilistically independent systems A and B , we verify $S_\delta(A+B) \neq S_\delta(A) + S_\delta(B)$ ($\delta \neq 1$).

For equal probabilities we have

$$(11) \quad S_\delta = k_B \ln^\delta W,$$

hence, for $\delta > 0$,

$$(12) \quad \frac{S_\delta(A+B)}{k_B} = \left\{ \left[\frac{S_\delta(A)}{k_B} \right]^{1/\delta} + \left[\frac{S_\delta(B)}{k_B} \right]^{1/\delta} \right\}^\delta.$$

It is easily verified that, if $W(N)$ satisfies (9), $S_\delta(N)$ is extensive for $\delta = 1/\gamma$. This is in fact true even if

$$(13) \quad W(N) \sim \varphi(N) v^{N^\gamma} \quad (v > 1; 0 < \gamma < 1),$$

$\varphi(N)$ being any function satisfying $\lim_{N \rightarrow \infty} \ln \varphi(N)/N^\gamma = 0$. We can unify S_q (Eq. (6)) and S_δ (Eq. (10)) as follows [24]:

$$(14) \quad S_{q,\delta} = k_B \sum_{i=1}^W p_i \left(\ln_q \frac{1}{p_i} \right)^\delta \quad \left(q \in \mathcal{R}; \delta > 0; \sum_{i=1}^W p_i = 1 \right)$$

$S_{q,1}$ and $S_{1,\delta}$ respectively recover S_q and S_δ ; $S_{1,1}$ recovers S_{BG} . Obviously this entropy is nonadditive unless $(q, \delta) = (1, 1)$, and it is expansible, $\forall (q, \delta)$. It is concave for all $q > 0$ and $0 < \delta \leq (qW^{q-1} - 1)/(q - 1)$. In the limit $W \rightarrow \infty$, this condition becomes $0 < \delta \leq 1/(1 - q)$, $\forall q \in (0, 1)$, and any $\delta > 0$ for $q \geq 1$.

We can address now the area law. It has been verified for those anomalous d -dimensional systems (with $d > 1$) that essentially $\ln W(N) \propto L^{d-1} \propto N^{(d-1)/d}$, which implies that $W(N)$ is of the type indicated in (13) with $\gamma = (d - 1)/d$. Therefore, $S_\delta = S_{1,\delta}$ for $\delta = d/(d - 1)$ is extensive, thus satisfying thermodynamics. At the present state of knowledge we cannot exclude the possibility of extensivity of $S_{q,\delta}$ for other special values of (q, δ) , particularly in the limit $\delta \rightarrow \infty$. Indeed, assume for instance that we have $\varphi(N) \propto N^\rho$ in

(13), and take the limit $\gamma \rightarrow 0$, hence $\delta \rightarrow \infty$. The condition $\lim_{N \rightarrow \infty} \ln \varphi(N)/N^\gamma = 0$ is satisfied for any $\gamma > 0$, but it is violated for $\gamma = 0$, which opens the door for S_q , or some other nonadditive entropic functional, being the thermodynamically appropriate entropy.

For example, for the $d = 1$ gapless fermionic system in [8], we have analytically proved the extensivity of S_q for a specific value of $q < 1$ which depends on the central charge of the universality class that we are focusing on. For the $d = 2$ gapless bosonic system in [8], we have numerically found that, once again, it is S_q with a value of $q < 1$ the entropy which is extensive and consequently satisfies thermodynamics. This kind of scenario might be present in many d -dimensional physical systems for which $\ln W(L) \propto \ln_{2-d} L$ (i.e., $\propto \ln L$ for $d = 1$, and $\propto L^{d-1}$ for $d > 1$)¹.

Summarizing, the thermostatics of systems or subsystems whose elements are strongly correlated (for instance, through long-range interactions, or through strong quantum entanglement, or both, like possibly in quantum gravitational dense systems or subsystems) should be based on nonadditive entropies such as $S_{q,\delta}$ (Eq. (14)), and typically not on the usual Boltzmann-Gibbs-von Neumann one. An illustration of the type of back-and-forth arguments that are plethorically present in the literature can be seen in [31]. We read in its Abstract (see Fig. 1): *A black hole of a given mass, angular momentum, and charge can have a large number of different unobservable internal configurations which reflect the possible different initial configurations of the matter which collapsed to produce the hole. The logarithm of this number can be regarded as the entropy of the black hole [...], and also This means that the standard statistical-mechanical canonical ensemble cannot be applied when gravitational interactions are important.* In the last of these sentences, Hawking refers to something which is undoubtedly true, and already known by Gibbs himself [25], i.e., that the BG exponential distribution cannot be used. Nevertheless, in the few lines just above, the formula that is adopted for the entropy precisely is the famous BG one, disregarding the crucial fact that that formula is but the equal-probability particular case of the BG entropic functional from which the BG distribution is (straightforwardly) derived!

5 illustrative Predictions, Verifications and Applications, Including q -generalized Schroedinger, Klein-Gordon and Dirac Equations

Following Eq. (2), the plane wave can be q -generalized as follows [43, 44]: $e_q^{i(kx-\omega t)}$. By using this class of functions (normalizable for $1 < q < 3$, in contrast with the well known non-normalizability of standard plane waves) it is possible to generalize into nonlinear forms: (i) The integral representation of the Dirac delta [45, 46, 47, 48], (ii) The Schroedinger equation [49, 50], and its classical field theory [51]; and (iii) The Klein-Gordon and the Dirac equations [49].

Predictions, verifications and applications have been performed in high-energy physics (in the CMS, ALICE and ATLAS Collaborations at the LHC/CERN, the PHENIX Collaboration at RHIC/Brookhaven, AUGER Project, among various others) [52, 53, 54, 55, 56, 57, 58, 59, 60, 61, 62, 63, 64], spin-glasses [65], cold atoms in optical lattices [66], trapped ions [67], anomalous diffusion [68], dusty plasmas [69], solar physics [70, 71, 72, 73, 74, 75, 76], conservative and dissipative many-body systems [26, 27, 28, 77, 78, 79], finance [80], to mention but a few.

6 Final remarks

The size of a geometric object such as a line, a plane, a body, a fractal, is efficiently determined (through a number which is *neither zero nor infinity*) by respectively asking the length, the area, the volume, or the measure in its Hausdorff dimension. In other words, it is the geometric nature of the object which determines the useful question to be asked in order to know its size. In complete analogy, the entropic functional to be efficiently used for a class of probabilistic/thermostatical system is not universal, but it is determined by the

¹ Logarithmic corrections to these asymptotic behaviors are also possible. For example, for a class of (connected bipartitions of) free-fermion gases it has been recently found $\ln W(L) \propto L^{d-1} \ln L$ [42]. We verify that this expression and $\ln_{2-d} L$ coincide for $d = 1$ but involve a logarithmic discrepancy for $d > 1$. For this class of systems we have $W(N) \propto C v^{N^\gamma \ln N}$ ($C > 0; v > 1; 0 < \gamma < 1$) (or even $W(N) \propto C(N) v^{N^\gamma \ln N}$, $C(N)$ being a slowly-varying pre-factor) instead of (9).

nature of the correlations between its elements (in particular, if this correlation is weak or inexistent, we must use the Boltzmann-Gibbs entropy). The basic criterion for choosing the appropriate functional form is to impose that, for that class of systems, it satisfies thermodynamics, i.e., the extensivity of the entropy. All other physical (dynamical, geometric) properties are believed (as exhibited in some particular instances) to consistently follow from this basic choice. We have shown in this brief review how this philosophy can be applied in sensibly different systems, and in particular in black holes. The (practical and epistemological) correctness of this approach is supported (analytically, numerically, experimentally and observationally) by a wide amount of predictions, verifications and applications in natural, artificial and social systems, some of which have been mentioned here. It is clear that such a physical structure must rely on some basic mathematical foundations, such as central limit theorems and related properties. Although quite succinctly, this has also been addressed here. For further information and a regularly updated bibliography the reader is invited to check [81].

PHYSICAL REVIEW D

VOLUME 13, NUMBER 2

15 JANUARY 1976

Black holes and thermodynamics*

S. W. Hawking[†]

California Institute of Technology, Pasadena, California 91125

and Department of Applied Mathematics and Theoretical Physics, University of Cambridge, Cambridge, England

(Received 30 June 1975)

A black hole of given mass, angular momentum, and charge can have a large number of different unobservable internal configurations which reflect the possible different initial configurations of the matter which collapsed to produce the hole. The logarithm of this number can be regarded as the entropy of the black hole and is a measure of the amount of information about the initial state which was lost in the formation of the black hole. If one makes the hypothesis that the entropy is finite, one can deduce that the black holes must emit thermal radiation at some nonzero temperature. Conversely, the recently derived quantum-mechanical result that black holes do emit thermal radiation at temperature $\kappa\hbar/2\pi kc$, where κ is the surface gravity, enables one to prove that the entropy is finite and is equal to $c^3 A/4G\hbar$, where A is the surface area of the event horizon or boundary of the black hole. Because black holes have negative specific heat, they cannot be in stable thermal equilibrium except when the additional energy available is less than $1/4$ the mass of the black hole. This means that the standard statistical-mechanical canonical ensemble cannot be applied when gravitational interactions are important. Black holes behave in a completely random and time-symmetric way and are indistinguishable, for an external observer, from white holes. The irreversibility that appears in the classical limit is merely a statistical effect.

Figure 1 Abstract of [31].

Acknowledgments

I acknowledge particularly fruitful conversations with M.J. Duff, which, during the event at the Vatican, motivated me to explore in more detail the black-hole entropy case. Partial financial support from CNPq, FAPERJ and CAPES (Brazilian agencies) is acknowledged as well.

References

- [1] C. Tsallis, J. Stat. Phys. **52**, 479 (1988).
- [2] M. Gell-Mann and C. Tsallis, eds., *Nonextensive Entropy - Interdisciplinary Applications* (Oxford University Press, New York, 2004).
- [3] C. Tsallis, *Introduction to Nonextensive Statistical Mechanics - Approaching a Complex World* (Springer, New York, 2009).
- [4] C. Tsallis, M. Gell-Mann and Y. Sato, Proc. Natl. Acad. Sc. USA **102**, 15377 (2005).
- [5] O. Penrose, *Foundations of Statistical Mechanics: A Deductive Treatment* (Pergamon, Oxford, 1970), p. 167.
- [6] E.M.F. Curado and C. Tsallis, J. Phys. A **24**, L69 (1991); Corrigenda: **24**, 3187 (1991) and **25**, 1019 (1992).
- [7] C. Tsallis, R.S. Mendes and A.R. Plastino, Physica A **261**, 534 (1998).

- [8] F. Caruso and C. Tsallis, Phys. Rev. E **78**, 021102 (2008).
- [9] A. Saguia and M.S. Sarandy, Phys. Lett. A **374**, 3384 (2010).
- [10] S. Umarov, C. Tsallis and S. Steinberg, Milan J. Math. **76**, 307 (2008).
- [11] S. Umarov, C. Tsallis, M. Gell-Mann and S. Steinberg, J. Math. Phys. **51**, 033502 (2010).
- [12] R. Hanel and S. Thurner, Europhys. Lett. **93**, 20006 (2011).
- [13] R. Hanel and S. Thurner, EPL **96**, 50003 (2011).
- [14] P. Tempesta, Phys. Rev. E **84**, 021121 (2011) (10 pages).
- [15] H.J. Hilhorst, J. Stat. Mech., P10023 (2010).
- [16] M. Jauregui and C. Tsallis, Phys. Lett. A **375**, 2085 (2011).
- [17] M. Jauregui, C. Tsallis and E.M.F. Curado, J. Stat. Mech. P10016 (2011).
- [18] A. Plastino and M. C. Rocca, 1112.1985 [math-ph].
- [19] C. Vignat and A. Plastino, J. Phys. A **40**, F969 (2007).
- [20] M.G. Hahn, X.X. Jiang and S. Umarov, J. Phys. A **43** (16), 165208 (2010).
- [21] H. Touchette, Phys. Rep. **478**, 1 (2009).
- [22] G. Ruiz and C. Tsallis, 1110.6303 [cond-mat.stat-mech].
- [23] M. Przystalski, Phys. Lett. A **374**, 123 (2009).
- [24] C. Tsallis and L.J.L. Cirto, *Reconciling the black hole entropy with classical thermodynamics*, (2011), to be published.
- [25] J.W. Gibbs, *Elementary Principles in Statistical Mechanics – Developed with Especial Reference to the Rational Foundation of Thermodynamics* (C. Scribner's Sons, New York, 1902; Yale University Press, New Haven, 1948; OX Bow Press, Woodbridge, Connecticut, 1981).
- [26] C. Anteneodo and C. Tsallis, Phys. Rev. Lett. **80**, 5313 (1998).
- [27] A. Campa, A. Giansanti, D. Moroni and C. Tsallis, Phys. Lett. A **286**, 251 (2001).
- [28] B.J.C. Cabral and C. Tsallis, Phys. Rev. E **66**, 065101(R) (2002).
- [29] J.D. Bekenstein, Phys. Rev. D **7**, 2333 (1973), and Phys. Rev. D **9**, 3292 (1974).
- [30] S.W. Hawking, Nature **248**, 30 (1974).
- [31] S.W. Hawking, Phys. Rev. D **13**, 191 (1976).
- [32] G. 't Hooft, Nucl. Phys. B **355**, 138 (1990), and references therein.
- [33] L. Susskind, Phys. Rev. Lett. **71**, 2367 (1993).
- [34] J. Maddox, Nature **365**, 103 (1993).
- [35] M. Srednicki, Phys. Rev. Lett. **71**, 666 (1993).
- [36] A. Strominger and C. Vafa, Phys. Lett. B **379**, 99 (1996).
- [37] A. Strominger, J. High Energy Phys. **2**, 009 (1998).
- [38] J. Maldacena and A. Strominger, J. High Energy Phys. **2**, 014 (1998).
- [39] T. Padmanabhan, *A dialogue on the nature of gravity*, 0910.0839v2 [gr-qc].
- [40] C. Corda, J. High Energy Phys. **08**, 101 (2011).
- [41] J. Eisert, M. Cramer and M.B. Plenio, Rev. Mod. Phys. **82**, 277 (2010).
- [42] P. Calabrese, M. Vintchev and E. Vicari, EPL **97**, 20009 (2012).
- [43] E.P. Borges, J. Phys. A **31**, 5281 (1998).
- [44] E.P. Borges, C. Tsallis, J.G.V. Miranda and R.F.S. Andrade, J. Phys. A **37**, 9125 (2004).
- [45] M. Jauregui and C. Tsallis, J. Math. Phys. **51**, 063304 (2010).
- [46] A. Chevreuil, A. Plastino and C. Vignat, J. Math. Phys. **51**, 093502 (2010).
- [47] M. Mamode, J. Math. Phys. **51**, 123509 (2010).
- [48] A. Plastino and M.C. Rocca, J. Math. Phys. **52**, 103503 (2011).
- [49] F.D. Nobre, M.A. Rego-Monteiro and C. Tsallis, Phys. Rev. Lett. **106**, 140601 (2011).
- [50] R.N. Costa Filho, M.P. Almeida, G.A. Farias and J.S. Andrade, Phys. Rev. A **84**, 050102(R) (2011).
- [51] F.D. Nobre, M.A. Rego-Monteiro and C. Tsallis, EPL **97**, 41001 (2012).
- [52] CMS Collaboration, Phys. Rev. Lett. **105**, 022002 (2010).
- [53] CMS Collaboration, J. High Energy Phys. **09**, 091 (2010).
- [54] CMS Collaboration, J. High Energy Phys. **05**, 064 (2011).
- [55] ALICE Collaboration, Phys. Lett. B **693**, 53 (2010).

- [56] ALICE Collaboration, Eur. Phys. J. C **71**, 1594 (2011).
- [57] ALICE Collaboration, Eur. Phys. J. C **71**, 1655 (2011).
- [58] A. Tawfik, Nuclear Phys. A **859**, 63 (2011).
- [59] ATLAS Collaboration, New J. Physics **13**, 053033 (2011).
- [60] PHENIX Collaboration, Phys. Rev. D **83**, 052004 (2011).
- [61] PHENIX Collaboration, Phys. Rev. C **83**, 024909 (2011).
- [62] PHENIX Collaboration, Phys. Rev. C **83**, 064903 (2011).
- [63] M. Shao, L. Yi, Z.B. Tang, H.F. Chen, C. Li and Z.B. Xu, J. Phys. G **37**, 085104 (2010).
- [64] C. Tsallis, J.C. Anjos and E.P. Borges, Phys. Lett. A **310**, 372 (2003).
- [65] R.M. Pickup, R. Cywinski, C. Pappas, B. Farago and P. Fouquet, Phys. Rev. Lett. **102**, 097202 (2009).
- [66] P. Douglas, S. Bergamini and F. Renzoni, Phys. Rev. Lett. **96**, 110601 (2006).
- [67] R.G. DeVoe, Phys. Rev. Lett. **102**, 063001 (2009).
- [68] J. S. Andrade Jr., G.F.T. da Silva, A.A. Moreira, F.D. Nobre and E.M.F. Curado, Phys. Rev. Lett. **105**, 260601 (2010); Y. Levin and R. Pakter, Phys. Rev. Lett. **107**, 088901 (2011); J. S. Andrade Jr., G.F.T. da Silva, A.A. Moreira, F.D. Nobre and E.M.F. Curado, Phys. Rev. Lett. **107**, 088902 (2011).
- [69] B. Liu and J. Goree, Phys. Rev. Lett. **100**, 055003 (2008).
- [70] L.F. Burlaga, A.F. Vinas, N.F. Ness and M.H. Acuna, Astrophys. J. **644**, L83 (2006).
- [71] L.F. Burlaga and N.F. Ness, Astrophys. J. **703**, 311 (2009).
- [72] L.F. Burlaga, N.F. Ness and M.H. Acuna, Astrophys. J. **691**, L82 (2009).
- [73] L.F. Burlaga and N.F. Ness, Astrophys. J. **725**, 1306 (2010); Astrophys. J. **737**, 35 (2011).
- [74] L.F. Burlaga and N.F. Ness, Astrophys. J. **737**, 35 (2011).
- [75] J. Cho and A. Lazarian, Astrophys. J. **701**, 236 (2009).
- [76] A. Esquivel and A. Lazarian, Astrophys. J. **710**, 125 (2010).
- [77] A. Pluchino, A. Rapisarda and C. Tsallis, Europhys. Lett. **80**, 26002 (2007); A. Pluchino, A. Rapisarda and C. Tsallis, Physica A **387** (2008); A. Figueiredo, T.M. Rocha Filho and M.A. Amato, Europhys. Lett. **83**, 30011 (2008); A. Pluchino, A. Rapisarda and C. Tsallis, Europhys. Lett. **85**, 60006 (2009); A. Figueiredo, T.M. Rocha Filho and M.A. Amato, Europhys. Lett. **85**, 60007 (2009).
- [78] G. Miritello, A. Pluchino and A. Rapisarda, Physica A **388**, 4818 (2009).
- [79] M. Leo, R.A. Leo and P. Tempesta, J. Stat. Mech. P04021 (2010).
- [80] J. Ludescher, C. Tsallis and A. Bunde, Europhys. Lett. **95**, 68002 (2011).
- [81] <http://tsallis.cat.cbpf.br/biblio.htm>

THE COSMOLOGICAL CONSTANT PROBLEM, DARK ENERGY, AND THE LANDSCAPE OF STRING THEORY

■ RAPHAEL BOUSSO^{a,b}

^a*Center for Theoretical Physics and Department of Physics,
University of California, Berkeley, CA 94720, U.S.A.*

^b*Lawrence Berkeley National Laboratory, Berkeley, CA 94720, U.S.A.*

ABSTRACT: In this colloquium-level account, I describe the cosmological constant problem: why is the energy of empty space at least 60 orders of magnitude smaller than several known contributions to it from the Standard Model of particle physics? I explain why the “dark energy” responsible for the accelerated expansion of the universe is almost certainly vacuum energy. The second half of the paper explores a more speculative subject. The vacuum landscape of string theory leads to a multiverse in which many different three-dimensional vacua coexist, albeit in widely separated regions. This can explain both the smallness of the observed vacuum energy and the coincidence that its magnitude is comparable to the present matter density.

Contents

1	The Cosmological Constant Problem	1
1.1	A Classical Ambiguity	1
1.2	Quantum Contributions to Λ	3
2	The Cosmological Constant	5
2.1	Observed Value of Λ	5
2.2	Why Dark Energy is Vacuum Energy	5
2.3	The Coincidence Problem	7
3	The Landscape of String Theory and the Multiverse	8
3.1	The Landscape of String Theory	8
3.2	The Spectrum of Λ	10
3.3	de Sitter Expansion and Vacuum Decay	11
3.4	Eternal Inflation	12
3.5	The Multiverse	13
3.6	Why Observers are Located in Regions With $ \Lambda \ll 1$	14
3.7	Predicted Value of Λ	15
3.8	Connecting with Standard Cosmology	17

1 The Cosmological Constant Problem

1.1 A Classical Ambiguity

In the field equation for General Relativity,

$$R_{\mu\nu} - \frac{1}{2}Rg_{\mu\nu} + \Lambda g_{\mu\nu} = 8\pi GT_{\mu\nu} , \quad (1.1)$$

there is an ambiguity: the cosmological constant, Λ , is not fixed by the structure of the theory.¹ There is no formal reason to set it to zero, and in fact, Einstein famously tuned it to yield an (unstable) static cosmological solution—his “greatest blunder”.

¹This paper aims at a level that would be accessible to a graduate student. It is based on colloquia given at Caltech, MIT, and the University of Michigan, Ann Arbor, and on a lecture presented at *Subnuclear Physics: Past, Present and Future*, Pontifical Academy of Sciences, Vatican (October 2011, to appear in the proceedings). In parts, I closely follow Refs. [1, 2].

After Hubble's discovery that the universe is expanding, the cosmological term was widely abandoned. But setting $\Lambda = 0$ was never particularly satisfying, even from a classical perspective. The situation is similar to a famous shortcoming of Newtonian gravity: nothing prevents us from equating the gravitational charge with inertial mass, but nothing forces us to do so, either.

A nonzero value of Λ introduces a length scale and time scale

$$r_\Lambda = ct_\Lambda = \sqrt{3/|\Lambda|} \quad (1.2)$$

into General Relativity. An independent length scale arises from the constants of Nature: the Planck length²

$$l_P = \sqrt{\frac{G\hbar}{c^3}} \approx 1.616 \times 10^{-33} \text{ cm} . \quad (1.3)$$

It has long been known empirically that Λ is very small in Planck units (i.e., that r_Λ is large in these natural units). This can be deduced just from the fact that the universe is large compared to the Planck length, and old compared to the Planck time.

First, consider the case of positive Λ . If no matter is present ($T_{\mu\nu} = 0$), then the only isotropic solution to Einstein's equation is de Sitter space, which exhibits a cosmological horizon of radius r_Λ [3]. A cosmological horizon is the largest observable distance scale, and the presence of matter will only decrease the horizon radius [4, 5]. But we observe scales that are large in Planck units ($r \gg 1$). Since r_Λ must be even larger, Eq. (1.2) implies that the cosmological constant is small.

Negative Λ causes the universe to recollapse independently of spatial curvature, on a timescale t_Λ [6]. Thus, the large age of the universe (in Planck units) implies that $(-\Lambda)$ is small. Summarizing the above arguments, one finds

$$-3t^{-2} \lesssim \Lambda \lesssim 3r^{-2} , \quad (1.4)$$

where t and r are any time scale and any distance scale that have been observed. We can see out to distances of billions of light years, so $r > 10^{60}$; and stars are billions of years old, so $t > 10^{60}$. With these data, known for many decades, Eq. (1.4) implies roughly that

$$|\Lambda| \lesssim 3 \times 10^{-120} . \quad (1.5)$$

Thus, in Planck units, Λ is very small indeed.

This result makes it tempting to set $\Lambda = 0$ in the Einstein equation; and at the level of the classical gravity theory, we are free to do so. However, in Eq. (1.1), the Λ -term is not the only term proportional to the metric. Another, much more problematic contribution enters through the stress tensor on the right hand side.

²Here G denotes Newton's constant and c is the speed of light. In this paper Planck units are used unless other units are given explicitly. For example, $t_P = l_P/c \approx .539 \times 10^{-43} \text{ s}$ and $M_P = 2.177 \times 10^{-5} \text{ g}$.

1.2 Quantum Contributions to Λ

In quantum field theory, the vacuum is highly nontrivial.³ In the Standard Model, the vacuum is responsible for physical phenomena such as confinement and the Higgs mechanism. Like any physical object, the vacuum will have an energy density. Lorentz invariance requires that the corresponding energy-momentum-stress tensor be proportional to the metric,

$$\langle T_{\mu\nu} \rangle = -\rho_{\text{vacuum}} g_{\mu\nu} . \quad (1.6)$$

This is confirmed by direct calculation. (See any introductory textbook on quantum field theory, such as Ref. [9].) The form of the stress tensor ensures that the vacuum looks the same to all observers independently of orientation or velocity. This property (and not, for example, vanishing energy density) is what distinguishes the vacuum from other objects such as a table.

Though it appears on the right hand side of Einstein's equation, vacuum energy has the form of a cosmological constant, and one might as well absorb it and redefine Λ via

$$\Lambda = \Lambda_{\text{Einstein}} + 8\pi\rho_{\text{vacuum}} . \quad (1.7)$$

Equivalently, one may absorb the “bare” cosmological constant appearing in Einstein's equation, $\Lambda_{\text{Einstein}}$, into the energy density of the vacuum, defining

$$\rho_{\Lambda} \equiv \rho_{\text{vacuum}} + \frac{\Lambda_{\text{Einstein}}}{8\pi} . \quad (1.8)$$

Eqs. (1.2), (1.4), and (1.5) apply to the total cosmological constant, and can be restated as an empirical bound on the total energy density of the vacuum:

$$|\rho_{\Lambda}| \lesssim 10^{-121} . \quad (1.9)$$

But in the Standard Model, the energy of the vacuum receives many contributions much larger than this bound. Their value depends on the energy scale up to which we trust the theory. It is enormous even with a conservative cutoff.

This would be true already in free field theory. Like a harmonic oscillator in the ground state, every mode of every free field contributes a zero-point energy to the energy density of the vacuum. In a path integral description, this energy arises from virtual particle-antiparticle pairs, or “loops” (Fig. 1a). For example, consider the electron, which is well understood at least up to energies of order $M = 100$ GeV [8].

³Further details can be found in Weinberg's classic review [7]. Among more recent reviews, I recommend Polchinski's concise discussion of the cosmological constant problem [8], which I follow in parts of this subsection.

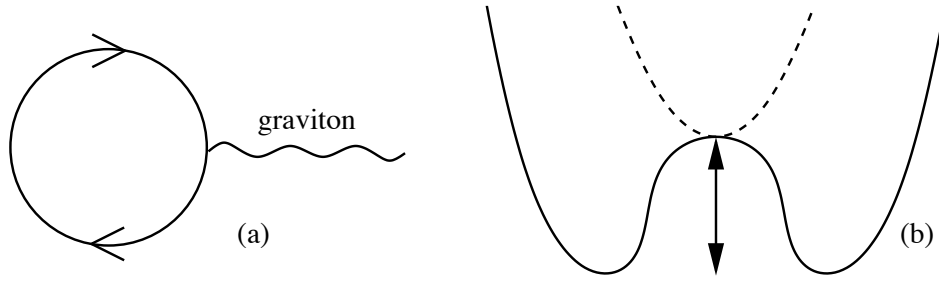


Figure 1. Perturbative and nonperturbative contributions to vacuum energy. (a) Virtual particle-antiparticle pairs, the zero-point fluctuations of the quantum fields (b) Effective scalar field potentials, such as the potential for the Higgs field shown here schematically. Before electroweak symmetry breaking in the early universe the vacuum energy was about 56 orders of magnitude greater than today's value (dashed line).

Dimensional analysis implies that electron loops up to this cutoff contribute of order $(100 \text{ GeV})^4$ to the vacuum energy, or 10^{-68} in Planck units.

Similar contributions are expected from other fields and from interactions. The real cutoff is probably of order the supersymmetry breaking scale, giving at least $(1 \text{ TeV})^4 \approx 10^{-64}$. It may be as high as the Planck scale, which would yield $|\rho_\Lambda|$ of order unity.⁴ Thus, quantum field theory predicts multiple perturbative contributions to $|\rho_\Lambda|$. Each contribution is some 60 to 120 orders of magnitude larger than the experimental bound, Eq. (1.5).

Additional contributions come from the effective potentials of scalar fields, such as the potential giving rise to symmetry breaking in the electroweak theory (Fig. 1b). The vacuum energy of the symmetric and the broken phase differ by approximately $(200 \text{ GeV})^4 \approx 10^{-67}$. Other symmetry breaking mechanisms at higher or lower energy, such as chiral symmetry breaking of QCD with $(300 \text{ MeV})^4 \approx 10^{-79}$, will also contribute. There is no reason why the total vacuum energy should be small in the symmetric phase, and even less so in the broken phase that the universe is in now.

I have exhibited various known contributions to the vacuum energy. They are uncorrelated with one another and with the (unknown) bare cosmological constant appearing in Einstein's equation, $\Lambda_{\text{Einstein}}$. Each contribution is dozens of orders of magnitude larger than the empirical bound today, Eq. (1.5). In particular, the radiative correction terms from quantum fields are expected to be at least of order 10^{-64} . They come with different signs, but it would seem overwhelmingly unlikely for such large terms to cancel to better than a part in 10^{120} , in the present era.

⁴Recall that Planck units are used throughout. $\rho_\Lambda = 1$ would correspond to a density of 10^{94} g/cm^3 .

This is the cosmological constant problem: *Why is the vacuum energy today so small?* It represents a serious crisis in physics: a discrepancy between theory and experiment, of 60 to 120 orders of magnitude. What makes this problem hard is that it arises from two otherwise extremely successful theories—the Standard Model and General Relativity—in a regime where both theories have been reliably and precisely tested and hence cannot be dramatically modified.

2 The Cosmological Constant

In exhibiting the cosmological constant problem, I made use only of a rather crude, and old, upper bound on the magnitude of the cosmological constant. The precise value of Λ is irrelevant as far as the cosmological constant *problem* is concerned: we have known for several decades that Λ is certainly much smaller than typical contributions to the vacuum energy that can be estimated from the Standard Model of particle physics. In this section, I will discuss the observed value and its implications.

2.1 Observed Value of Λ

The actual value of Λ was first determined in 1998 from the apparent luminosity of distant supernovae [10, 11]. Their dimness indicates that the expansion of the universe has recently begun to accelerate, consistent with a positive cosmological constant

$$\rho_\Lambda = (1.35 \pm 0.15) \times 10^{-123} , \quad (2.1)$$

and inconsistent with $\rho_\Lambda = 0$. The quoted value and error bars are recent (WMAP7 + BAO + H_0 [12]) and thus significantly improved relative to the original discovery.

Cross-checks have corroborated this conclusion. For example, the above value of ρ_Λ also explains the observed spatial flatness of the universe [12], which cannot be accounted for by baryonic and dark matter alone. And surveys of the history of structure formation in the universe [13] reveal a recent disruption of hierarchical clustering consistent with accelerated expansion driven by the cosmological constant of Eq. (2.1).

2.2 Why Dark Energy is Vacuum Energy

The observed vacuum energy, Eq. (2.1), is sometimes referred to as “dark energy”. This choice of words is meant to be inclusive of other possible interpretations of the data, in which $\Lambda = 0$. Dark energy might be a form of scalar matter (quintessence) which mimics a fixed cosmological constant closely enough to be compatible with observation, but retains some time-dependence that could in principle be discovered if it lurks

just beyond current limits. Another frequently considered possibility is that General Relativity is modified at distances comparable to the size of the visible universe, so as to mimic a positive cosmological constant even though $\Lambda = 0$. In both cases, model parameters can be adjusted to lead to predictions for future experiments that differ from those of a fixed cosmological constant.

Consideration of these theoretical possibilities, however, is at best premature. It conflicts with a basic tenet of science: adopt the simplest interpretation of the data, and complicate your model only if forced to by further observation.

Scenarios like quintessence or modified gravity are uncalled for by data and solve no theoretical problem.⁵ In particular, they do not address the cosmological constant problem. But such models contain adjustable parameters in addition to Λ . Therefore, they are less predictive than the standard Λ CDM model. Worse, in phenomenologically viable models, these additional parameters must be chosen small and fine-tuned in order to evade existing constraints.⁶ Again, such tunings are strictly *in addition* to the tuning of the the cosmological constant, which must be set to an unnaturally small or zero value in any case.

Therefore, dynamical dark energy should not be considered on the same footing with a pure cosmological constant. The discovery of any deviation from a cosmological constant in future experiments is highly unlikely, as is the discovery of a modification to General Relativity on large scales.

A frequent misconception that appears to underlie the consideration of “alternatives” to Λ is the notion that vacuum energy is somehow optional. The idea is that the cosmological constant problem only arises if we “assume” that vacuum energy exists in the first place. (This flawed argument is found in surprisingly prominent places [17].) It would be wonderful indeed if we could solve the cosmological constant problem with a single stroke, by declaring that vacuum energy just does not exist and setting Λ to zero.

But in fact, we know that vacuum energy exists in Nature. We can manipulate the amount of vacuum energy in bounded regions, in Casimir-type experiments. And if Λ had turned out to be unobservably small today, we would still know that it was large

⁵Some models have been claimed to address the coincidence problem described in Sec. 2.3 below. Aside from unsolved technical problems [14], what would be the point of addressing the (relatively vague) coincidence problem with a model that ignores the logically prior and far more severe cosmological constant problem (Sec. 1.2)?

⁶For example, quintessence models require exceedingly flat scalar field potentials which must be fine-tuned against radiative corrections, and their interaction with other matter must be tuned small in order to be compatible with observational limits on a long-range fifth force [14, 15]. More natural models [16] have become difficult to reconcile with observational constraints.

and positive in the early universe before electroweak symmetry breaking, according to the Standard Model of particle physics.⁷ More generally, the notion that the vacuum has energy is inseparable from the experimental success of the Standard Model as a local quantum field theory [8].

Contributions to Λ from Standard Model fields are large, so the most straightforward theoretical estimate of its magnitude fails. But just because Λ should be much larger than the observed value does not imply that it must be zero. In fact, no known extension or modification of the Standard Model predicts that $\Lambda = 0$ without violently conflicting with other observations (such as the facts that the universe is not empty, and that supersymmetry, if it exists, is broken).

Thus, the cosmological constant problem is present either way, whether we imagine that Λ is small (which is consistent with data) or that $\Lambda = 0$ (which is not, unless further considerable complications are introduced). Dark energy is experimentally indistinguishable from vacuum energy, and definitely distinct from any other previously observed form of matter. The only reasonable conclusion is that dark energy is vacuum energy, and that its density is given by Eq. (2.1).

2.3 The Coincidence Problem

The observed value of Λ does raise an interesting question, usually referred to as the coincidence problem or “why now” problem. Vacuum energy, or anything behaving like it (which includes all options still allowed by current data) does not redshift like matter. In the past, vacuum energy was negligible, and in the far future, matter will be very dilute and vacuum energy will dominate completely. The two can be comparable only in a particular epoch. It is intriguing that this is the same epoch in which we are making the observation.

Note that this apparent coincidence involves us, the observers, in its very definition. This constrains possible explanations (other than those involving an actual coincidence). In the following section, I will outline a framework which can solve both the coincidence problem and the (far more severe) cosmological constant problem of Sec. 1.2.

⁷The theory of electroweak symmetry breaking is supported by overwhelming experimental evidence (chiefly, the W and Z bosons, and soon perhaps the Higgs). It allows us to compute that $\Lambda \sim (200 \text{ GeV})^4$ at sufficiently high temperatures, when electroweak symmetry is unbroken [8]. Aside from the early universe, small regions with unbroken symmetry could be created in the laboratory, at least in principle.

3 The Landscape of String Theory and the Multiverse

The string landscape is the only theoretical framework I am aware of that can explain why Λ is small without conflicting with other data.⁸ (It is worth stressing, however, that the ideas I am about to discuss are still speculative, unlike those of the previous two sections.) The way in which string theory addresses the cosmological constant problem can be summarized as follows:

- Fundamentally, space is nine-dimensional. There are many distinct ways (perhaps 10^{500}) of turning nine-dimensional space into three-dimensional space by compactifying six dimensions.⁹
- Distinct compactifications correspond to different three-dimensional metastable vacua with different amounts of vacuum energy. In a small fraction of vacua, the cosmological constant will be accidentally small.
- All vacua are dynamically produced as large, widely separated regions in space-time
- Regions with $\Lambda \sim 1$ contain at most a few bits of information and thus no complex structures of any kind. Therefore, observers find themselves in regions with $\Lambda \ll 1$.

3.1 The Landscape of String Theory

String theory is naturally formulated in nine or ten spatial dimensions [19, 20]. This does not contradict observation but implies that all but three of these dimensions are (effectively) compact and small, so that they would not have been observed in high-energy experiments. I will discuss the case of six compact extra dimensions for definiteness.

Simple examples of six-dimensional compact manifolds include the six-sphere and the six-dimensional torus. A much larger class of manifolds are the Calabi-Yau spaces, which have a number of useful properties and have been extensively studied. They are topologically complex, with hundreds of distinct cycles of various dimensions. Cycles are higher-dimensional analogues of the handles of a torus. A rubber band that wraps a handle cannot be removed, or wrapped around a different handle, without ripping it apart. A more pertinent example are electrical field lines, which can wrap a one-cycle (such as one of the cycles on a two-dimensional torus).

⁸For alternative classes of approaches to the cosmological constant problem, and the obstructions they face, see Refs. [2, 8].

⁹Amazingly, this idea was anticipated by Sakharov [18] before string theory became widely known.

String theory contains a certain set of nonperturbative objects known as D -branes, which act as sources of $D + 2$ flux. For example, a zero-brane is a pointlike object and sources a Maxwell field, much like an electron would. Higher-dimensional objects such as membranes act as sources of higher-dimensional analogues of the Maxwell field. Unlike in the Standard Model, however, the values of D for which D -branes exist, their energy density, and their charge are all determined by consistency requirements. They are set by the string scale and are not adjustable parameters.

D -branes and their associated fluxes can wrap topological cycles the same way that rubber bands and electric field lines can wrap the handles of a torus. In string theory, the shape and size of the compact extra dimensions is determined by (among other things) the fluxes that wrap around the various topological cycles. The geometry of spacetime is dynamical and governed by equations that limit to Einstein's equations in the appropriate limit. The presence of matter will deform the compact manifold correspondingly; in particular, one expects that each cycle can at most support a few units of flux before gravitational backreaction causes it to pinch off (changing the topology of the compact manifold) or grow to infinite size ("decompactify").

Based on these arguments, we may suppose that there are on the order of 500 cycles, and that each can support between 0 and 9 units of flux. Then there are 10^{500} different, distinct choices for the matter content, shape, and size of the extra dimensions. This argument is a vast oversimplification, but it helps clarify how numbers like 10^{500} arise: by exponentiation of the number of topological cycles in a typical six-dimensional compact manifold.¹⁰

A useful way of picturing the set of three-dimensional vacua of string theory is as a potential function in a 500-dimensional discrete parameter space. (Of course, as far as actual pictures go, two parameters will have to suffice, as in a real landscape.) Each metastable configuration of fluxes corresponds to a local minimum in the landscape. In any one-dimensional cross-section of the parameter space, there will only be a handful of minima, but overall the number of minima can be of order 10^{500} .

¹⁰For a more detailed nontechnical version of this argument, see Ref. [21]. Despite early results that the number of compactifications could be large [22], the significance of this possibility was obscured by the unsolved problem of moduli stabilization and supersymmetry breaking [23]; see, however, Ref. [24]. The argument that string theory contains sufficiently many metastable vacua to solve the cosmological constant problem, and that vacua with $\Lambda \sim 10^{-123}$ are cosmologically produced and reheated was presented in Ref. [25]. An explicit construction of a large class of nonsupersymmetric flux vacua was first proposed in Ref. [26]. (Constructions in noncritical string theory were proposed earlier [27, 28].) More advanced counting methods [29] bear out the quantitative estimates of Ref. [25] for the number of flux vacua. See Ref. [23] for a review of flux vacua and further references.

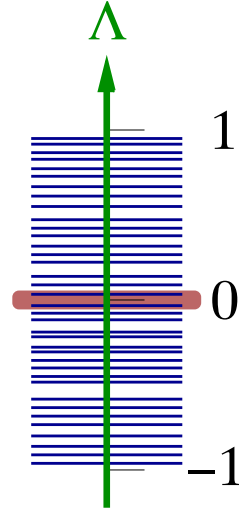


Figure 2. The spectrum of the cosmological constant (vacuum energy, dark energy) in the string landscape (schematic). Each blue line represents one three-dimensional vacuum. With 10^{500} vacua, the spectrum will be very dense, and many vacua will have values of Λ compatible with observation (red/shaded region).

3.2 The Spectrum of Λ

Each vacuum has distinct matter and field content at low energies, determined by the matter content of the extra dimensions. (Pictorially, the field spectrum corresponds to the details of each valley's shape near the minimum.) In particular, the energy of each vacuum is essentially a random variable that receives positive and negative contributions from all particle species. If we select one vacuum completely at random, the arguments of Sec. 1.2 tell us that its cosmological constant will probably be large, presumably of order unity in Planck units (Fig. 2)—as if we had thrown a dart at the interval $(-1, 1)$, with an accuracy not much better than ± 1 .

But this is true for every vacuum, so the overall spectrum of Λ will be quite dense, with an average spacing of order 10^{-500} . This means that there will be a small fraction (10^{-123}) but a large number (10^{377} , in this example) of vacua with cosmological constant $|\Lambda| \lesssim 10^{-123}$. Given enough darts, even a poor player will eventually hit the bullseye.

This is progress: at least, the theory contains vacua whose cosmological constant is compatible with observation. But why is the universe in such a special, rare vacuum? Did the universe start out in this particular valley of the landscape at the big bang, and if so, why? In fact, there is no need to assume that initial conditions selected for a vacuum with small cosmological constant. As we shall now see, such vacua are dynamically produced during cosmological evolution.

3.3 de Sitter Expansion and Vacuum Decay

Suppose that the universe began in some vacuum with $\Lambda > 0$. Since about half of all vacua have positive energy, this is not a strong restriction. We will not assume that the initial vacuum energy is particularly small; it may be of order one in Planck units.

The universe evolves as de Sitter space, with metric

$$ds^2 = -dt^2 + e^{2Ht}(dr^2 + r^2 d\Omega_2^2), \quad (3.1)$$

where the Hubble constant H is given by $(\Lambda/3)^{1/2}$, and $d\Omega_2^2$ denotes the metric on the unit two-sphere. This is an exponentially expanding homogeneous and isotropic cosmology. In the following, it is not important that the universe looks globally like Eq. (3.1). It suffices to have a finite initial region larger than one horizon volume, of proper radius $e^{Ht_0}r > H^{-1}$.

Classically, this evolution would continue eternally, and no other vacua would ever come into existence anywhere in the universe. This is because the vacuum itself is set by topological configurations of fluxes in the extra dimensions, which cannot change by classical evolution. Quantum mechanically, however, it is possible for fluxes to change by discrete amounts. This happens by a process completely analogous to the Schwinger process.

The Schwinger process is the spontaneous pair production of electrons and positrons in a strong electric field between two capacitor plates. It can be treated as a tunneling process in the semi-classical approximation. The two particles appear at a distance at which the part of the field that their charges cancel out compensates for their total rest mass, so that energy is conserved. Then the particles move apart with constant acceleration, driven by the remaining electric field, until they hit the plates (or in the case where the field lines wrap a topological circle, until they hit each other). The final result is that the electric flux has been lowered by a discrete amount, corresponding to removing one unit of electric charge from each capacitor plate.

Similarly, the amount of flux in the six extra dimensions can change as a result of Schwinger-like processes, whereby branes of appropriate dimension are spontaneously nucleated. (The Schwinger process itself is recovered in the case of zero-branes, i.e., charged point particles.) Again, this is a nonperturbative tunneling effect. Its rate is suppressed by the exponential of the brane action and is generically exponentially small.

Let us now give a description of this process from the 3+1 dimensional viewpoint. The effect of the six extra dimensions is to provide an effective potential landscape. Each minimum corresponds to a metastable vacuum with three large spatial dimensions. (Recall that the hundreds of dimensions of the landscape itself correspond to the topological cycles of the extra dimensions, not to actual spatial directions.)

The decay of a unit of flux, in this picture, corresponds to a transition from a higher to a lower-energy minimum in the potential landscape of string theory.¹¹ This transition does not happen simultaneously everywhere in three-dimensional space, because that process would have infinite action. Rather, a bubble of the new vacuum appears spontaneously, as in a first-order phase transition. Like in the Schwinger process, the initial size of the bubble is controlled by energy conservation. The bubble wall is a domain wall that interpolates between two vacua in the effective potential. The gradient and potential energy in the domain wall are compensated by the vacuum energy difference in the enclosed volume.

The bubble expands at constant acceleration. As it moves outward, it converts the old, higher energy parent vacuum into a new, lower-energy vacuum. The vacuum energy difference pays not only for the ever-expanding domain wall but can also lead to the production of matter and radiation inside the new vacuum.

The symmetries of a first-order phase transition in a relativistic theory dictate that the region inside the bubble is an open (i.e., negatively curved) Friedmann-Robertson-Walker universe. In particular, time slices of constant density are infinitely large, even though the bubble starts out at finite size. (This is possible because the choice of time variable in which we see the bubble expand is different from, and indeed inconsistent with, a choice in which constant time corresponds to hypersurfaces of constant density within the bubble.) For this reason, the interior of the bubble is sometimes referred to as a “universe”, “pocket universe”, or “bubble universe”, even though it does not constitute all of the global spacetime.

3.4 Eternal Inflation

We now turn to a crucial aspect of the decay of a metastable vacuum with positive energy: despite the decay and the expansion of the daughter bubble, the parent vacuum persists indefinitely. This effect is known as eternal inflation [33, 34].

The volume occupied by the parent vacuum expands exponentially at a rate set by its own Hubble scale $3H = 3(3/\Lambda)^{1/2}$. Some volume is lost to decay, at a rate Γ per unit Hubble volume. As long as $\Gamma \ll 3H$ (which is generic due to the exponentially suppressed nature of vacuum decay), the exponential expansion wins out, and the parent vacuum region grows on average.

The fact that the new vacuum expands after it first appears does not affect this result, since different regions in de Sitter space are shielded from one another by cosmological event horizons. A straightforward analysis of light propagation in the metric

¹¹The following description of vacuum decay is a straightforward application of seminal results of Coleman for a one-dimensional potential with two vacua [30, 31]. More complicated decay channels can arise in multidimensional potentials [32]; they do not affect the conclusions presented here.

of Eq. (3.1) shows that any observer (represented by a timelike geodesic) is surrounded by a horizon of radius H^{-1} . The observer cannot receive any signals from any point p beyond this horizon, by causality, no matter how long they wait. A bubble of a new vacuum that forms at p cannot expand faster than the speed of light (though it does expand practically at that speed). Therefore it can never reach an observer who is initially more than a distance H^{-1} from p at the time of bubble nucleation.

Because the parent vacuum continues to grow in volume, it will decay not once but infinitely many times. Infinitely many bubble universes will be spawned; yet, the overall volume of parent vacuum will continue to increase at a rate set by $3H - \Gamma \approx 3H$. If the parent vacuum has multiple decay channels, then each decay type will be realized infinitely many times. For example, in the string landscape we expect that a de Sitter vacuum can decay to any one of its hundreds of immediate neighbor vacua in the high-dimensional potential landscape. All of these vacua will actually be produced as bubble universes, in exponentially distant regions, over and over.

3.5 The Multiverse

Let us now turn our attention to one of the daughter universes. It is useful to distinguish three cases, according to the sign of its cosmological constant. First, suppose that its vacuum energy is positive and that the vacuum is sufficiently long-lived (greater than about t_Λ). In this case, the daughter universe will enter a phase of exponential de Sitter expansion, beginning at a time of order t_Λ after its nucleation. It will give rise to eternal inflation in its own right, decaying in infinitely many places and producing daughter universes, while persisting globally.

Thus, the entire landscape of string theory can in principle be populated. All vacua are produced dynamically, in widely separated regions of spacetime, and each is produced infinitely many times. This can be illustrated in a conformal diagram (or “Penrose diagram”), which rescales the spacetime metric to render it finite but preserves causal relations (Fig. 3). By convention, light-rays propagate at 45 degrees. Bubbles look like future light-cones because they expand nearly at the speed of light. Bubble universes that form at late times are shown small due to the rescaling, even though their physical properties are independent of the time of their production. As a result of eternal inflation, the future boundary of the diagram has a fractal structure.

Vacua with nonpositive cosmological constant are “terminal”. They do not give rise to eternal inflation. If $\Lambda < 0$, then the bubble universe begins to contract and collapses in a big crunch on a timescale of order t_Λ [31]. The spacelike singularity does not reach outside the bubble universe with $\Lambda < 0$; it does not affect global eternal inflation.

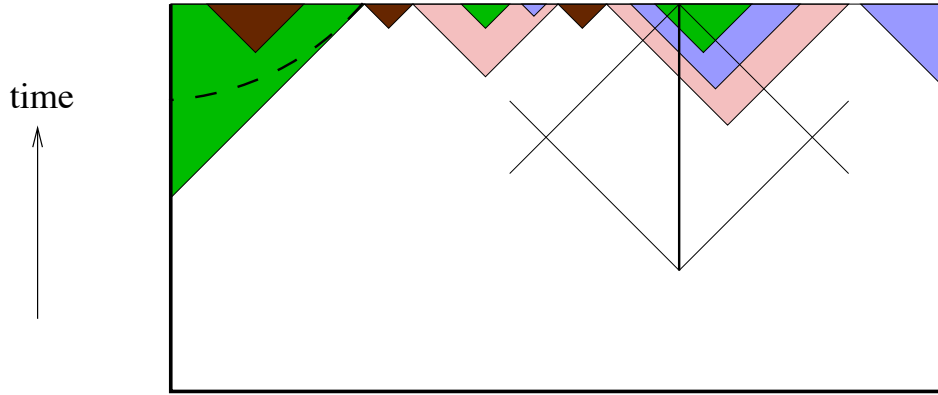


Figure 3. Conformal diagram of an eternally expanding multiverse (schematic). Light travels at 45 degrees. Different colors/shades represent different vacua in the string landscape. Bubble universes have a triangular shape in this diagram. They are bounded by domain walls whose expansion is so rapid that they look like future light-cones. Event horizons shield different regions from one another: a hypothetical observer who survives multiple vacuum decays (black vertical line) would still only be able to probe a finite region in the infinite multiverse (black diamond).

One expects that the case $\Lambda = 0$ arises only in vacua with unbroken supersymmetry. They are completely stable and do not end in a crunch. In the conformal diagram, they correspond to the “hat regions” near the future boundary (not shown in Fig. 3).

3.6 Why Observers are Located in Regions With $|\Lambda| \ll 1$

I have argued that the string landscape contains vacua with very small cosmological constant, such as ours. Moreover, such vacua will be dynamically produced by inflation, starting from generic initial conditions. But the bubble universes with $|\Lambda| \ll 1$, such as ours, are surely very atypical regions in the large multiverse. Typical regions (by almost any conceivable definition of “typical”) would have cosmological constant of order one in Planck units, since almost all vacua have this property. Why, then, do we find ourselves in one of the rare locations with $\Lambda \ll 1$?

Before addressing this question, it is worth noting that the same question could not be asked in a theory that failed to contain vacua with $\Lambda \ll 1$, or that failed to produce such vacua as spacetime regions. But in a theory that dynamically produces highly variable environments in different locations, it is important to understand correlations between environmental properties and the location of observers. What is typically observed depends on where one is observing, so these correlations will affect the predictions of the theory.

In Sec. 1, I discussed that the cosmological constant sets a largest observable length or time scale, of order $|\Lambda^{-1/2}|$. A more precise result can be stated in terms of the maximum area on the past light-cone of an arbitrary point (event) p in a universe with nonzero cosmological constant [35]. If $\Lambda > 0$, the past light-cone of any point p has maximum area of order Λ^{-1} ; if $\Lambda < 0$, it has maximum area of order $|\Lambda|^{-1}$ (if the universe is spatially flat), or Λ^{-2} (if the universe is open).

The maximum area on the past light-cone of p , in units of the Planck length squared, is an upper bound on the entropy in the causal past of p :

$$S \lesssim A \quad (3.2)$$

This follows from the covariant entropy bound [36, 37]. It implies that regions with $\Lambda \sim 1$ do not contain more than a few bits of information in any causally connected region. Whatever observers are made of, they presumably require more than one or two particles.

This means that observers can only be located in regions with $|\Lambda| \ll 1$. Because of cosmological horizons, they will not typically be able to see other regions. Though typical regions have $\Lambda = 1$, observations are made in regions with $|\Lambda| \ll 1$.

3.7 Predicted Value of Λ

The argument shows only that $|\Lambda| \ll 1$ is a prediction of the string landscape; it does not explain why we see the particular value $\Lambda \sim 10^{-123}$. In order to make this, or any other quantitative prediction, we would need to begin by regulating the infinities of eternal inflation. This is known as the “measure problem”, and it has little to do with the string landscape.

The measure problem arises in any theory that gives rise to eternal inflation. For this, one long-lived metastable de Sitter vacuum is enough. We appear to live in such a vacuum, so the measure problem needs attention independently of the number of other vacua in the theory. A discussion of this problem and of current approaches to its solution would go beyond the scope of the present paper. The reader is referred to Ref. [38] and references therein; here we quote only the main result of this paper (see also Ref. [39, 40]).

Consider a class of observers that live at the time t_{obs} after the nucleation of their bubble universe. Restricting attention to positive values of Λ , the causal patch measure [41] predicts that such observers will find a cosmological constant

$$\Lambda \sim t_{\text{obs}}^{-2} . \quad (3.3)$$

Using the observed value for the age of the universe, $t_{\text{obs}} \approx 13.7$ Gyr, this result is in excellent agreement with observed value for the cosmological constant (see Fig. 4).

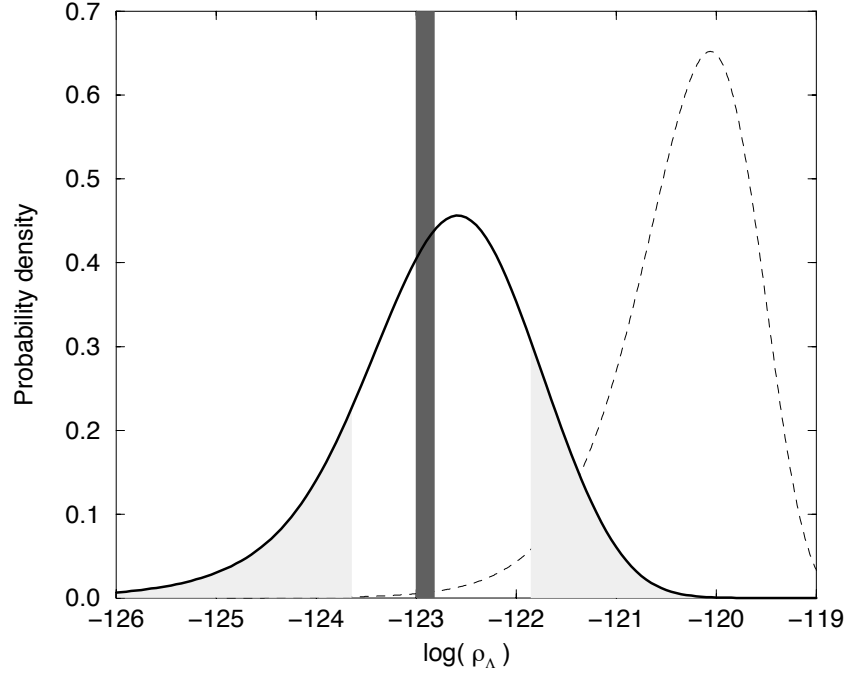


Figure 4. The vertical bar indicates the observed amount of vacuum energy (“dark energy”). The solid line shows the prediction from the causal patch measure applied to the landscape of string theory, with the central 1σ region indicated. This plot is from Ref. [39]. The agreement remains good independently of any assumptions about the nature of the observers. The only relevant input parameter is the time when the observers emerge, $t_{\text{obs}} \approx 13.7$ Gyr.

The successful prediction (or postdiction, in this case) of Λ obtains independently of the nature of the observers. For example, it applies to observers that do not require galaxies and even in vacua with very different low-energy physics. In addition to the cosmological constant problem, it also addresses the coincidence problem discussed in Sec. 2.3, since it predicts that observers should find themselves at the onset of vacuum domination, $t_{\Lambda} \sim t_{\text{obs}}$. Thus the prediction is more robust, and quantitatively more successful, than the seminal arguments of Weinberg [42] and other early arguments requiring specific assumptions about observers [43–46]. (The dashed line in Fig. 4 shows the prediction from the assumption that observers require galaxies, with an earlier measure developed in Ref. [47].

There are currently no fully satisfactory measures for regions with nonpositive cosmological constant [48]. This remains a major outstanding challenge. More broadly,

it will be important to establish a solid theoretical basis for understanding both the landscape of string theory and the measure problem of eternal inflation.

3.8 Connecting with Standard Cosmology

How is the picture of a multiverse compatible with the one universe we see? The multiverse is quite irregular, with different vacua in different places. This appears to conflict with the observed homogeneity and isotropy of the visible universe. We have not detected any other pocket universes. As far as we can see, the vacuum seems to be the same, with the same particles, forces, and coupling constants. Another concern is the claimed metastability of vacua. If vacua can decay, how come our own vacuum is still around after billions of years?

In fact, all of these observations are generic predictions of the model, and all arise from the fact that vacuum decay is an exponentially suppressed tunneling effect. This has three important consequences:

- Individual pocket universes, including ours, can have very long lifetimes easily exceeding 10 Gyr [25].
- When a bubble of new vacuum does form, it will be highly symmetric [30]. The symmetry of the decay process translates into the prediction that each pocket universe is a negatively curved, spatially homogeneous and isotropic universe [31]. (The spatial curvature radius can be made unobservably large, as usual, by a period of slow-roll inflation at early times in our own pocket universe.)
- Our parent vacuum need not produce many bubbles that collide with ours. For such collisions to be visible, they would have to occur in our past light-cone, and the expected number of collisions can be $\ll 1$ for natural parameters.

Thus, the fact that we observe only one vacuum is not in contradiction with the string landscape.

However, this does not mean that other vacua will never be observed. We would have to be somewhat lucky to observe a smoking gun signal of bubble collisions in the sky [49–52]; for a review, see Ref. [53]. But it is a possibility, so the computation of its signature in the CMB for future searches such as PLANCK is of great interest [54–57].

Slow-roll inflation tends to wipe out signals from any era preceding it by stretching them to superhorizon scales. If slow-roll inflation occurred after the formation of our bubble (as seems plausible), and if it lasted significantly longer than the 60 e-foldings necessary for explaining the observed flatness, then any imprints of bubble collisions or of our parent vacuum will have been stretched to superhorizon scales.

The decay of our own parent vacuum plays the role of what we used to call the big bang. The vacuum energy of the parent vacuum is converted in part to the energy of the expanding domain wall bubble that separates our pocket universe from the parent vacuum. But some of this energy can be dissipated later, inside our pocket universe. It can drive a period of slow-roll inflation followed by the production of radiation and matter.

The decay of our parent vacuum will have taken place in an empty de Sitter environment, so all matter and radiation in our vacuum must come from the vacuum energy released in the decay. In order to connect with standard cosmology, the energy density of radiation produced must be at least sufficient for nucleosynthesis. This constrains the vacuum energy of our parent vacuum:

$$\Lambda_{\text{parent}} \gg 10^{-88} . \quad (3.4)$$

This constraint is very powerful. Historically, it has ruled out one-dimensional potential landscapes such as the Abbott [58] or Brown-Teitelboim [59, 60] models, which were explicitly invented for the purpose of solving the cosmological constant problem. In such models, neighboring vacua have nearly identical vacuum energy, $\Delta\Lambda < 10^{-123}$. Each decay lowers Λ by an amount less than the observed value, so a very dense spectrum of Λ is scanned over time. This eventually produces a universe with Λ as small as the observed value. But because Eq. (3.4) is not satisfied, the universe is predicted to be empty, in conflict with observation. One could invent one-dimensional landscapes in which the vacuum energy is random, but in natural models decay paths would end in terminal vacua with $\Lambda < 0$ before reaching one of the rare vacua with $\Lambda \ll 1$.

In the string landscape, neighboring vacua typically have vastly different vacuum energy, with Λ differing by as much as $O(1)$ in Planck units (Sec. 3.2). Thus, matter and radiation can be produced in the decay of our parent vacuum. Because the landscape is high-dimensional, there are many decay paths around terminal vacua. Thus, all de Sitter vacua in the landscape can be cosmologically produced by eternal inflation from generic initial conditions.

It is interesting that string theory, which was not invented for the purpose of solving the cosmological constant problem, thus evades a longstanding obstruction.

References

- [1] R. Bousso, “Precision cosmology and the landscape,” [hep-th/0610211](#).
- [2] R. Bousso, “TASI Lectures on the Cosmological Constant,” [arXiv:0708.4231](#) [[hep-th](#)].

- [3] S. W. Hawking and G. F. R. Ellis, *The large scale structure of space-time*. Cambridge University Press, Cambridge, England, 1973.
- [4] G. W. Gibbons and S. W. Hawking, “Cosmological Event Horizons, Thermodynamics, and Particle Creation,” *Phys. Rev. D* **15** (1977) 2738–2751.
- [5] R. Bousso, “Positive vacuum energy and the N-bound,” *JHEP* **11** (2000) 038, [hep-th/0010252](#).
- [6] D. Edwards, “Exact expressions for the properties of the zero-pressure Friedmann models,” *M.N.R.A.S.* **159** (1972) 51–66.
- [7] S. Weinberg, “The Cosmological Constant Problem,” *Rev. Mod. Phys.* **61** (1989) 1–23.
- [8] J. Polchinski, “The cosmological constant and the string landscape,” [hep-th/0603249](#).
- [9] A. Zee, “Quantum field theory in a nutshell,”. ISBN-9780691140346.
- [10] **Supernova Search Team** Collaboration, A. G. Riess *et al.*, “Observational Evidence from Supernovae for an Accelerating Universe and a Cosmological Constant,” *Astron. J.* **116** (1998) 1009–1038, [astro-ph/9805201](#).
- [11] **Supernova Cosmology Project** Collaboration, S. Perlmutter *et al.*, “Measurements of Omega and Lambda from 42 High-Redshift Supernovae,” *Astrophys. J.* **517** (1999) 565–586, [astro-ph/9812133](#).
- [12] **WMAP** Collaboration, E. Komatsu *et al.*, “Seven-Year Wilkinson Microwave Anisotropy Probe (WMAP) Observations: Cosmological Interpretation,” *Astrophys. J. Suppl.* **192** (2011) 18, [arXiv:1001.4538](#) [[astro-ph.CO](#)].
- [13] B. A. Reid *et al.*, “Cosmological Constraints from the Clustering of the Sloan Digital Sky Survey DR7 Luminous Red Galaxies,” *Mon. Not. Roy. Astron. Soc.* **404** (2010) 60–85, [arXiv:0907.1659](#) [[astro-ph.CO](#)].
- [14] S. M. Carroll, “The cosmological constant,” [astro-ph/0004075](#).
- [15] S. M. Carroll, “Quintessence and the rest of the world,” *Phys. Rev. Lett.* **81** (1998) 3067–3070, [arXiv:astro-ph/9806099](#).
- [16] L. J. Hall, Y. Nomura, and S. J. Oliver, “Evolving dark energy with w not equal -1 ,” *Phys. Rev. Lett.* **95** (2005) 141302, [arXiv:astro-ph/0503706](#).
- [17] A. Albrecht *et al.*, “Report of the Dark Energy Task Force,” [astro-ph/0609591](#).
- [18] A. D. Sakharov, “Cosmological Transitions with a Change in Metric Signature,” *Sov. Phys. JETP* **60** (1984) 214–218.
- [19] M. B. Green, J. H. Schwarz, and E. Witten, *Superstring Theory*. Cambridge Univ. Pr., Cambridge, UK, 1987.
- [20] J. Polchinski, *String Theory*. Cambridge Univ. Pr., Cambridge, UK, 1998.

- [21] R. Bousso and J. Polchinski, “The string theory landscape,” *Sci. Am.* **291** (2004) 60–69.
- [22] W. Lerche, D. Lust, and A. N. Schellekens, “Chiral Four-Dimensional Heterotic Strings from Selfdual Lattices,” *Nucl. Phys.* **B287** (1987) 477.
- [23] M. R. Douglas and S. Kachru, “Flux compactification,” [hep-th/0610102](#).
- [24] A. N. Schellekens, “The landscape ’avant la lettre’,” [arXiv:physics/0604134](#).
- [25] R. Bousso and J. Polchinski, “Quantization of four-form fluxes and dynamical neutralization of the cosmological constant,” *JHEP* **06** (2000) 006, [hep-th/0004134](#).
- [26] S. Kachru, R. Kallosh, A. Linde, and S. P. Trivedi, “De Sitter vacua in string theory,” *Phys. Rev. D* **68** (2003) 046005, [hep-th/0301240](#).
- [27] E. Silverstein, “(A)dS backgrounds from asymmetric orientifolds,” [hep-th/0106209](#).
- [28] A. Maloney, E. Silverstein, and A. Strominger, “De Sitter space in noncritical string theory,” [hep-th/0205316](#).
- [29] F. Denef and M. R. Douglas, “Distributions of flux vacua,” *JHEP* **05** (2004) 072, [hep-th/0404116](#).
- [30] S. Coleman, “The Fate of the False Vacuum. 1. Semiclassical Theory,” *Phys. Rev. D* **15** (1977) 2929–2936.
- [31] S. Coleman and F. D. Luccia, “Gravitational effects on and of vacuum decay,” *Phys. Rev. D* **21** (1980) 3305–3315.
- [32] A. R. Brown and A. Dahlen, “Giant Leaps and Minimal Branes in Multi-Dimensional Flux Landscapes,” *Phys. Rev.* **D84** (2011) 023513, [arXiv:1010.5241](#) [[hep-th](#)].
- [33] A. H. Guth and E. J. Weinberg, “Could the universe have recovered from a slow first-order phase transition?,” *Nucl. Phys.* **B212** (1983) 321–364.
- [34] A. Linde, “Eternally Existing Selfreproducing Chaotic Inflationary Universe,” *Phys. Lett.* **B175** (1986) 395–400.
- [35] R. Bousso, B. Freivogel, and S. Leichenauer, “Saturating the holographic entropy bound,” *Phys. Rev.* **D82** (2010) 084024, [arXiv:1003.3012](#) [[hep-th](#)].
- [36] R. Bousso, “A covariant entropy conjecture,” *JHEP* **07** (1999) 004, [hep-th/9905177](#).
- [37] R. Bousso, “The holographic principle,” *Rev. Mod. Phys.* **74** (2002) 825, [hep-th/0203101](#).
- [38] R. Bousso, B. Freivogel, S. Leichenauer, and V. Rosenhaus, “A geometric solution to the coincidence problem, and the size of the landscape as the origin of hierarchy,” *Phys. Rev. Lett.* **106** (2011) 101301, [arXiv:1011.0714](#) [[hep-th](#)].

- [39] R. Bousso, R. Harnik, G. D. Kribs, and G. Perez, “Predicting the cosmological constant from the causal entropic principle,” *Phys. Rev. D* **76** (2007) 043513, [hep-th/0702115](#).
- [40] R. Bousso and R. Harnik, “The Entropic Landscape,” *Phys. Rev.* **D82** (2010) 123523, [arXiv:1001.1155 \[hep-th\]](#).
- [41] R. Bousso, “Holographic probabilities in eternal inflation,” *Phys. Rev. Lett.* **97** (2006) 191302, [hep-th/0605263](#).
- [42] S. Weinberg, “Anthropic Bound on the Cosmological Constant,” *Phys. Rev. Lett.* **59** (1987) 2607.
- [43] P. C. W. Davies and S. D. Unwin, “Why is the cosmological constant so small,” *Proc. R. Soc. Lond., A* **377** (1982) 147–149.
- [44] T. Banks, “T C P, Quantum Gravity, the Cosmological Constant and All That,” *Nucl. Phys.* **B249** (1985) 332.
- [45] J. D. Barrow and F. J. Tipler, *The Anthropic Cosmological Principle*. Clarendon Press, Oxford, 1986.
- [46] G. P. Efstathiou, “An anthropic argument for a cosmological constant,” *M.N.R.A.S.* **274** (1995) L73.
- [47] H. Martel, P. R. Shapiro, and S. Weinberg, “Likely Values of the Cosmological Constant,” [astro-ph/9701099](#).
- [48] R. Bousso, B. Freivogel, S. Leichenauer, and V. Rosenhaus, “Eternal inflation predicts that time will end,” *Phys. Rev.* **D83** (2011) 023525, [arXiv:1009.4698 \[hep-th\]](#).
- [49] B. Freivogel, M. Kleban, A. Nicolis, and K. Sigurdson, “Eternal Inflation, Bubble Collisions, and the Disintegration of the Persistence of Memory,” [arXiv:0901.0007 \[hep-th\]](#).
- [50] B. Czech, M. Kleban, K. Larjo, T. S. Levi, and K. Sigurdson, “Polarizing Bubble Collisions,” *JCAP* **1012** (2010) 023, [arXiv:1006.0832 \[astro-ph.CO\]](#).
- [51] M. Kleban, T. S. Levi, and K. Sigurdson, “Observing the Multiverse with Cosmic Wakes,” [arXiv:1109.3473 \[astro-ph.CO\]](#).
- [52] R. Gobbetti and M. Kleban, “Analyzing Cosmic Bubble Collisions,” [arXiv:1201.6380 \[hep-th\]](#).
- [53] M. Kleban, “Cosmic Bubble Collisions,” *Class. Quant. Grav.* **28** (2011) 204008, [arXiv:1107.2593 \[astro-ph.CO\]](#).
- [54] S. M. Feeney, M. C. Johnson, D. J. Mortlock, and H. V. Peiris, “First Observational Tests of Eternal Inflation,” *Phys. Rev. Lett.* **107** (2011) 071301, [arXiv:1012.1995 \[astro-ph.CO\]](#).

- [55] S. M. Feeney, M. C. Johnson, D. J. Mortlock, and H. V. Peiris, “First Observational Tests of Eternal Inflation: Analysis Methods and WMAP 7-Year Results,” *Phys. Rev. D* **D84** (2011) 043507, [arXiv:1012.3667 \[astro-ph.CO\]](#).
- [56] M. C. Johnson, H. V. Peiris, and L. Lehner, “Determining the outcome of cosmic bubble collisions in full General Relativity,” [arXiv:1112.4487 \[hep-th\]](#).
- [57] J. D. McEwen, S. M. Feeney, M. C. Johnson, and H. V. Peiris, “Optimal filters for detecting cosmic bubble collisions,” [arXiv:1202.2861 \[astro-ph.CO\]](#).
- [58] L. F. Abbott, “A Mechanism for Reducing the Value of the Cosmological Constant,” *Phys. Lett.* **B150** (1985) 427.
- [59] J. D. Brown and C. Teitelboim, “Dynamical Neutralization of the Cosmological Constant,” *Phys. Lett.* **B195** (1987) 177.
- [60] J. D. Brown and C. Teitelboim, “Neutralization of the Cosmological Constant by Membrane Creation,” *Nucl. Phys.* **B297** (1988) 787.

THE HIGH ENERGY FRONTIER PAST, PRESENT AND FUTURE

■ ROLF-DIETER HEUER

CERN – Director-General
CH-1211 Geneva 23 – Switzerland

This paper presents high-energy colliders at the energy frontier for the years to come. The immediate plans include the exploitation of the LHC at its design luminosity and energy as well as upgrades to the LHC luminosity and to its injectors. This may be complemented by a linear electron-positron collider, based on the technology being developed by the Compact Linear Collider and by the International Linear Collider, by a higher-energy LHC, by a high-energy electron-proton machine, the LHeC, and/or by a muon collider. This contribution describes the various future directions, all of which have a unique value to add to experimental particle physics, and concludes by outlining key messages for the way forward.

1 The Large Hadron Collider Physics Programme

The Large Hadron Collider (LHC) [1] is primarily a proton-proton collider (see Figure 1) with a design centre-of-mass energy of 14 TeV and nominal luminosity of $10^{34} \text{ cm}^{-2} \text{ s}^{-1}$, but also operated in heavy-ion mode. The high 40 MHz proton-proton collision rate and the tens of interactions per crossing result in an enormous challenge for the experiments and for the collection, storage and analysis of the data.

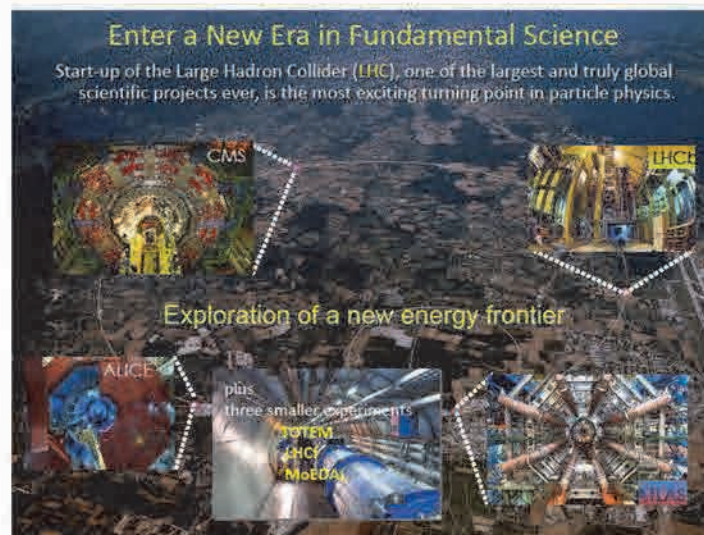


Figure 1: The LHC accelerator and the ALICE, ATLAS, CMS and LHCb experiments. There are also three smaller experiments - LHCf, MoEDAL and TOTEM.

By colliding unparalleled high-energy and high-intensity beams, the LHC is opening up previously unexplored territory at the TeV scale in great detail, allowing the experiments to probe deeper inside matter and providing further understanding of processes that occurred very early in the history of the Universe.

Of central importance to the LHC is the elucidation of the nature of electroweak symmetry breaking, for which the Higgs mechanism and the accompanying Higgs boson(s) are presumed to be responsible. In order to make significant inroads into the Standard Model Higgs Boson search, sizeable integrated luminosities of several fb^{-1} are needed. However, even with 1 fb^{-1} per experiment, discovery of the Standard Model Higgs Boson is still possible in mass regions beyond the lower limit of 114.4 GeV from direct searches at LEP2.

The LHC has provided the direct exclusion of a significant mass range unexplored until now. Exclusion limits have been placed on the Standard Model Higgs Boson by ATLAS and CMS. The mass region 146-466 GeV (except 232-256 GeV and 282-296 GeV) has been excluded by ATLAS at 95% CL while CMS has excluded the mass ranges 145-216 GeV, 226-288 GeV and 310-400 GeV.

At the initial LHC centre-of-mass energy of 7 TeV and with 1 fb^{-1} per experiment, combining the results from ATLAS and CMS would provide a 3σ sensitivity to a Standard Model Higgs Boson mass in the range 135 GeV to 475 GeV, and will exclude the Standard Model Higgs Boson between 120 GeV and 530 GeV at 95% CL. Combining the results from ATLAS and CMS at 7 TeV centre-of-mass energy and assuming about 10 fb^{-1} per experiment would exclude at 95% CL the mass range from 600 GeV down to the LEP2 lower limit and would also provide a 3σ sensitivity to a Standard Model Higgs Boson in the same mass range. Therefore, should the Standard Model Higgs Boson exist between the masses of 114 GeV to 600 GeV, it will either be discovered or ruled out by ATLAS and CMS until the end of 2012.

The reach for new physics at the LHC is considerable already at LHC start-up. In Supersymmetry (SUSY) theory, due to their high production cross-sections, squarks and gluinos can be produced in significant numbers even at modest luminosities. This would enable the LHC to start probing the nature of dark matter. No hint of SUSY particles has been observed so far, with the current lower limit being 1 TeV at 95% CL in constrained SUSY models.

Moreover, the current lower limits for new heavy bosons Z' and W' are about 2.0 TeV, while those for excited quarks are about 3 TeV.

The LHCb experiment has been studying the physics in the B-meson sector. The experiment has studied B_s oscillations and has measured a value of $\Delta m_s = 17.725 \pm 0.041 \pm 0.026 \text{ ps}^{-1}$. LHCb and CMS have also been searching for the $B_s \rightarrow \mu\mu$ decay channel. This channel is predicted to be very rare in the Standard Model but has a large sensitivity to new physics, for example to SUSY. The current results are consistent with Standard Model predictions but given that the 95% CL is still 3.4 times the value in the Standard Model, there remains plenty of room for new physics to still appear.

The LHC will also provide information on the unification of forces, the number of space-time dimensions and on matter-antimatter asymmetry. With the heavy-ion collision mode, the LHC will probe the formation of the quark-gluon plasma at the origin of the Universe.

2 LHC Machine and Experiments Performance

The main LHC achievements for 2010 and 2011 can be summarized as follows:

- Excellent performance of the LHC machine for both proton-proton and Pb-Pb runs in 2010. Beam operation availability in 2010 was 65% on average. Peak instantaneous luminosities of $2 \times 10^{32} \text{ cm}^{-2} \text{ s}^{-1}$ were attained for proton-proton collisions, which were a factor of two above the 2010 goal and which resulted in almost 50 pb^{-1} of integrated luminosity delivered to the experiments. Following a short 4-day switch-over to Pb-ion beams, peak luminosities of $3 \times 10^{25} \text{ cm}^{-2} \text{ s}^{-1}$ were attained for Pb-Pb collisions with almost $10 \text{ } \mu\text{b}^{-1}$ of integrated luminosity delivered to the experiments. This is a great achievement for the first full year of LHC operation.

The excellent performance of the LHC machine was also reported for 2011 until now. An integrated luminosity of more than 5.5 fb^{-1} has been delivered to each of the ATLAS and CMS experiments.

- All experiments took data of excellent quality and with high efficiency and they have been coping well with multiple interactions per crossing. The physics analyses re-measured the science of the Standard Model of Particle Physics, in many instances superseding limits set at the Tevatron while taking the LHC's first steps into new territory. As a result, a plethora of physics papers were published and conference presentations were made by the LHC experiments.
- The performance of the Worldwide LHC Computing Grid (WLCG) was also outstanding, exceeding the design bandwidth and allowing a very fast reconstruction and analysis of the data.

3 The LHC Consolidation and Upgrades

The coming years will lay the foundation for the next decades of high-energy physics at the LHC. The LHC research programme until around 2030 is determined by the full exploitation of its physics potential, consisting of the design luminosity and the high-luminosity upgrade (HL-LHC). Together with R&D on superconducting higher-field magnets for a higher-energy proton collider (HE-LHC), if necessitated by the physics, these initiatives will position CERN as the laboratory at the energy frontier.

3.1 LHC Consolidation

The LHC proton-proton and Pb-ion operations periods in 2011-2012 will be followed by a long shutdown in 2013 and extending well into 2014 with the following objectives:

- To repair and consolidate the inter-magnet copper-stabilizers (splices) to allow for safe operation up to 7 TeV/beam for the lifetime of the LHC.
- In the shadow of the inter-magnet copper-stabilizer work, the installation of the pressure rupture disks (DN200) will be completed and around 20 magnets which are known to have problems for high energy will be repaired or replaced. In addition, PS and SPS consolidation and upgrade work will be carried out.
- During this shutdown, the collimation system will also be upgraded at Point 3.
- The experiments will use the shutdown to implement a programme of consolidation, improvements and upgrades.

3.2 High Luminosity LHC

The strategy for the LHC for the coming years is the following:

- Exploitation of the physics potential of the LHC up to design conditions in the light of running experience and by optimizing the schedule for physics.
- Preparation of the LHC for a long operational lifetime through appropriate modifications and consolidation to the machine and detectors and through the build-up of an adequate spares inventory.
- In the years until 2018, the LHC will be operated towards 7 TeV/beam with increased intensities and luminosities.
- In 2018, a long shutdown is scheduled to connect LINAC4 [2], to complete the PS Booster energy upgrade, to finalize the collimation system enhancement and to install LHC detector improvements. After this shutdown, a further period of three years of LHC operation at 7 TeV/beam and at least the design luminosity is planned (with short technical stops around the end of each year).
- The ambitious longer-term plans include a total integrated luminosity of the order of 3000 fb^{-1} (recorded) by the end of the life of the LHC. The HL-LHC implies an annual luminosity of about $250\text{--}300 \text{ fb}^{-1}$ in the second decade of running. The HL-LHC upgrade is also required to implement modifications to elements in the insertion regions of the machine whose performance will have deteriorated due to radiation effects, such as the inner triplet quadrupole magnets. The HL-LHC upgrade is scheduled for the 2022 long shutdown.

- LHC detector R&D and upgrades to make optimal use of the LHC luminosity.

This strategy is also driven by the necessity to bring the LHC injector chain and the technical and general infrastructure up to the high standards required for a world laboratory in order to ensure reliable operation of the CERN complex.

3.3 Higher Energy LHC

Increasing the beam energy beyond the 7 TeV nominal energy of the LHC can be obtained by raising the mean field in the dipole magnets. The main parameter of the HE-LHC machine is the 16.5 TeV beam energy, and is based on the hypothesis of substituting all the present dipoles with new, more powerful ones, capable of operating at 20 T with beam. The success of the HE-LHC study depends critically on the success of the magnet R&D to reach dipole fields around 20 T in a useful bore. Despite the variety of superconducting materials and the continuous new discoveries, the practical superconductors (*i.e.* with good physics characteristics, good workability and suitability to cabling) are limited. The candidate materials are NbTi, Nb₃Sn, Nb₃Al and high-temperature superconductor (HTS). Additional open issues that require continuing R&D include high-gradient quadrupole magnets for the arcs and the interaction regions; fast-cycling superconducting magnets for a 1-TeV injector; emittance control in the regime of strong synchrotron damping; cryogenic handling of the synchrotron radiation heat load; and a study of the dynamic vacuum. The HE-LHC studies have started at CERN within an international collaboration and a first estimate provides a timeline of between 2030-2033 to start the realization of the HE-LHC machine project.

4 Colliders at the Energy Frontier beyond the LHC

Great opportunities are in store at the TeV scale and a fuller understanding of Nature will come about through a clearer insight at this energy level. The LHC will provide a first indication of any new physics at energies up to several TeV. First results from the LHC will be decisive in indicating the direction that particle physics will take in the future. Many of the open questions left by the LHC and its upgrades may be addressed best by an electron-positron collider, based on technology developed by the Compact Linear Collider (CLIC) [3] and International Linear Collider (ILC) [4] collaborations. Options for a high-energy electron-proton collider (LHeC) [5] and a muon collider [6] are also being considered. As in the past, there is a synergy between collider types that can be used to advantage. The discovery of the Standard Model over the past few decades has advanced through the synergy of hadron-hadron (e.g. SPS and the Tevatron), lepton-hadron (HERA) and lepton-lepton colliders (e.g. LEP and SLC). Such synergies should be continued in the future and thus a strategy has been developed along these lines. The above effort on accelerators should advance in parallel with the necessary detector R&D.

4.1 Linear Electron-Positron Collider

4.1.1 The Compact Linear Collider (CLIC)

The conceptual lay-out of the CLIC is shown in Figure 2. The collider is based on using lower-energy electron beams to drive high-energy electron and positron beams. The fundamental principle is that of a conventional AC transformer. The lower-energy drive beam serves as a radiofrequency source that accelerates the high-energy main beam with a high accelerating gradient. The nominal centre-of-mass energy is up to 3 TeV, the nominal luminosity exceeds $10^{34} \text{ cm}^{-2} \text{ s}^{-1}$, the main linear accelerator frequency is 12 GHz, the accelerating gradient is 100 MeV/m and the total length of the main linear accelerators is up to 48.3 km.

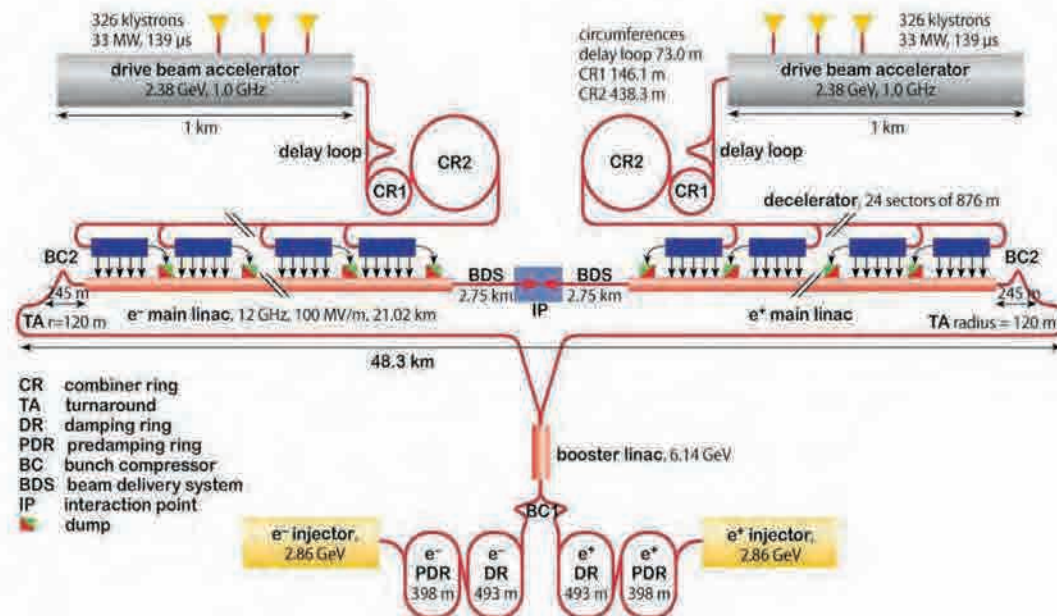


Figure 2: The CLIC general lay-out.

The CLIC project is in its R&D phase. In particular, the target accelerating gradient is considerably high and requires very aggressive performance from the accelerating structures. The nominal CLIC accelerating gradient has been exceeded in an unloaded structure with a very low breakdown probability of less than 3×10^{-7} per metre for a nominal pulse length after conditioning of the radiofrequency cavities for 1200 hours.

The mandate of the CLIC team is to demonstrate the feasibility of the CLIC concept, to be published by 2012 in a Conceptual Design Report. If this effort is successful, and if the new physics revealed by the LHC warrants, the next phase of R&D on engineering and cost issues will be launched. This would serve as the basis for a Technical Design Report and a request for project approval.

4.1.2 The International Linear Collider (ILC)

The ILC, shown in Figure 3, is an option for a linear electron-positron collider at lower energies than CLIC and is based on a more conventional design for acceleration using superconducting standing wave cavities with a nominal accelerating field of 31.5 MeV/m and a total length of 31 km at 500 GeV centre-of-mass energy. A two-stage technical design phase during 2010-2012 is presently underway, culminating in a Technical Design Report. A major contribution from Europe to the ILC Global Design Effort is the European X-ray Laser Project XFEL at DESY. The purpose of the facility is to generate extremely brilliant and ultra-short pulses of spatially-coherent X-rays. The electron energy is brought up to 20 GeV through a superconducting linear accelerator, of length one-tenth that of the ILC superconducting linear accelerator, and conveyed to long undulators where the X-rays are generated and delivered to the experimental stations. Construction of the XFEL is underway and operation is planned to start in 2015.

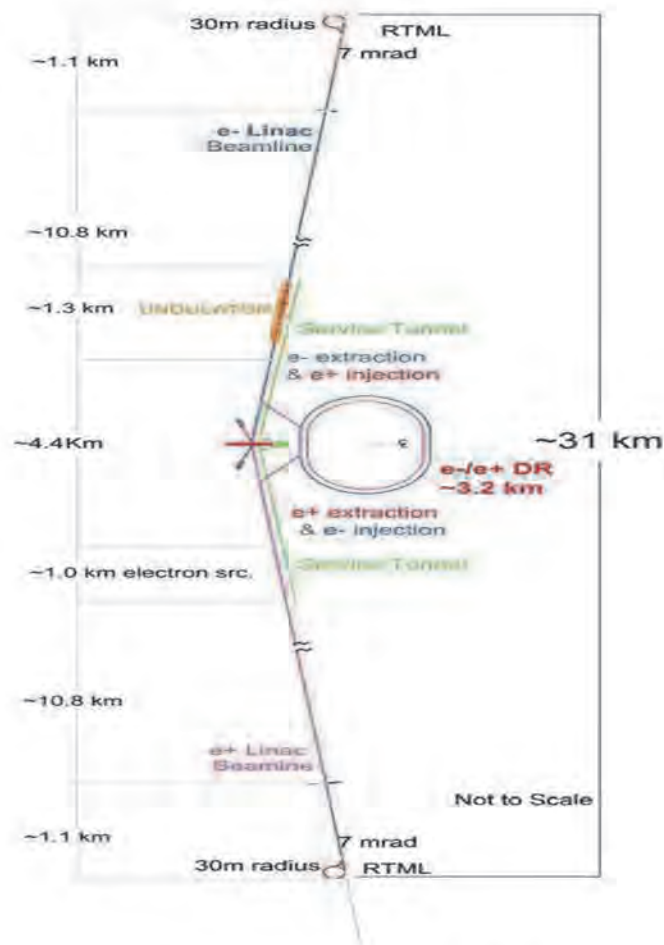


Figure 3: A schematic lay-out of the ILC.

4.1.3 Towards a Single Linear Collider Project

The strategy to address key issues common to both linear colliders involves close collaboration between ILC and CLIC. Progress has been encouraging in this respect. Such close collaboration would facilitate the exchange of concepts and R&D work between the ILC and CLIC in the future. In the meantime, items to be addressed as a matter of high priority for both linear collider projects include the construction costs, power consumption and value engineering.

4.1.4 Detector Challenges

R&D on key components of the detector for a linear collider is mandatory and is also well underway. High-precision measurements demand a new approach to the reconstruction. Particle flow, namely reconstruction of all particles, is thus proposed and requires unprecedented granularity in three dimensions of the detection channels.

4.2 Lepton-Hadron Collider

The option of a high-energy electron-proton collider - the Large Hadron Electron Collider (LHeC) - is being considered for the high-precision study of QCD and of high-density matter at the energy frontier. The LHeC design consists of an electron beam of 60 GeV (to possibly 140 GeV) colliding with protons of 7 TeV energy from the LHC. Assuming an electron-proton design luminosity of about $10^{33} \text{ cm}^{-2} \text{ s}^{-1}$, the LHeC could exceed the corresponding HERA values of integrated luminosity by two orders of magnitude and the kinematic range by a factor of 20 in the four-momentum squared Q^2 and in the inverse Bjorken x . The projected physics reach of the LHeC is shown in Figure 4. Both a ring-ring option - consisting of a new ring in the LHC tunnel with bypasses around the LHC experiments - and a linac-ring option - based on a re-circulating linac with energy recovery or on a straight linac - are being considered. The LHeC Conceptual Design Report will be completed by the end of 2011.

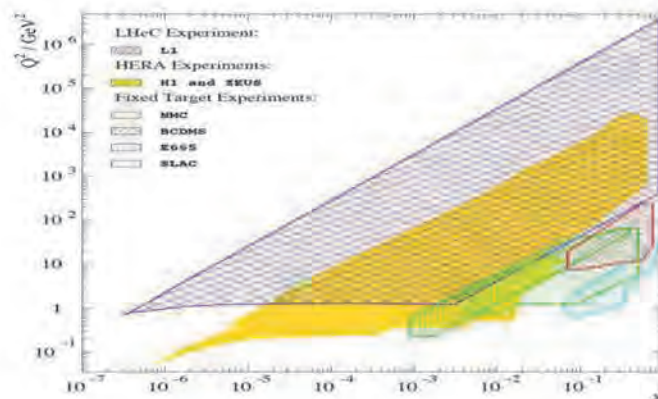


Figure 4: The projected physics reach of LHeC.

4.3 Muon Collider

Another proposal as a successor to the LHC is a muon collider [6] (Figure 5). The collider would accelerate muons, which are about 200 times heavier than electrons, into beams that would collide with each other. A benefit of muons over electrons is that, since they are heavier, they do not emit as much electromagnetic radiation in the form of synchrotron radiation (and thus lose less energy) when going around a circular accelerator ring. The muon collider would consist of a compact facility accelerating muons with re-circulating linacs. The major challenges include muon generation and cooling; cost efficient acceleration; and backgrounds from muon decays.



Figure 5: A schematic lay-out of a muon collider on the Fermilab site.

4.4 Generic Accelerator R&D

In addition to continuing focused R&D on the above collider projects, R&D should also be supported for generic accelerator studies. For example, R&D for high-power proton sources, such as the high-power superconducting proton linac (HP-SPL), in line with European participation in neutrino physics, should continue. Moreover, studies for novel acceleration techniques based on plasma acceleration is mandatory, as such machines could potentially provide the high acceleration gradients to reach the high energies required by the physics at future colliders.

5 The European Strategy for Particle Physics

European particle physics is founded on strong national institutes, universities and laboratories, working in conjunction with CERN. The increased globalization, concentration and scale of particle physics require a well-coordinated European strategy. This process started with the establishment of the CERN Council Strategy Group, which organized an open symposium in Orsay in early 2006, a final workshop in Zeuthen in May 2006 and with the strategy document being signed unanimously by Council in July 2006 in Lisbon [7]. CERN considers that experiments at the high-energy frontier to be the premier physics priority for the coming years. This direction for future colliders at CERN follows the priorities set in 2006 by the CERN Council Strategy Group. The years 2010 and 2011 are seeing the start of the LHC physics exploitation leading to important input for the update of the European strategy for particle physics planned for 2012-2013.

6 Key Messages

Particle physics will need to adapt to the evolving situation. Facilities for high-energy physics (as for other branches of science) are becoming larger and more expensive. Funding for the field is not increasing and the timescale for projects is becoming longer, both factors resulting in fewer facilities being realized. Moreover, laboratories are changing their missions.

All this leads to the need for more co-ordination and more collaboration on a global scale. Expertise in particle physics needs to be maintained in all regions, ensuring the long-term stability and support through-out. It would be necessary to engage all countries with particle physics communities and to integrate the communities in the developing countries. The funding agencies should in their turn provide a global view and synergies between various domains of research, such as particle physics and astroparticle physics, should be encouraged. Particle physics has entered a new and exciting era. The start-up of the LHC allows particle physics experiments at the highest collision energies. The expectations from the LHC are great, as it would provide revolutionary advances in the understanding of the microcosm and a fundamental change to our view of the early Universe. Due to the location of the LHC, CERN is in a unique position to contribute to further understanding of the microcosm in the long term.

Results from the LHC will guide the way in particle physics for many years. It is expected that the period of decision-making concerning the energy frontier will be in the next few years. Particle physics is now in an exciting period of accelerator planning, design, construction and running and would need intensified efforts in R&D and technical design work to enable the decisions for the future course and global collaboration coupled with stability of support over long time scales.

The particle physics community needs to define now the most appropriate organizational form and needs to be open and inventive in doing so, and it should be a dialogue between the scientists, funding agencies and politicians. It is mandatory to have accelerator laboratories in all regions as partners in accelerator development, construction, commissioning and

exploitation. Furthermore, planning and execution of high-energy physics projects today require world-wide partnerships for global, regional and national projects, namely for the whole particle physics programme. The exciting times ahead should be used to advantage to establish such partnerships.

7 Opening the Door

CERN Council opened the door to greater integration in particle physics when it recently unanimously adopted the recommendations to examine the role of CERN in the light of increasing globalization in particle physics. The key points agreed by Council include a) all states shall be eligible for CERN Membership, irrespective of their geographical location; b) a new Associate Membership status is to be introduced to allow non-Member States to establish or intensify their institutional links with CERN; and c) the participation of CERN in global projects is to be enabled wherever they are sited.

Several countries are now in the process of greater integration with CERN. Romania is a Candidate to Accession to CERN Membership; Israel is an Associate Member in the pre-stage to full Membership since October 2011; and negotiations with Cyprus, Serbia, Slovenia and Turkey for Associate Membership have started. A number of other countries have also expressed interest in Associate Membership.

8 Conclusions

In this paper, we have reported on high-energy colliders at the energy frontier for the years to come, such as the status and future plans of the LHC machine and experiments and also presented the strategy for future electron-positron linear colliders, an electron-proton collider and a muon collider. In the coming years, the priorities are the full exploitation of the LHC together with preparations for a luminosity upgrade. Moreover, studies for increasing the beam energy of the LHC are underway. It will be necessary to keep under review the physics drivers for future proton accelerator options and it will be necessary to compare the physics opportunities offered by proton colliders with those available at other colliders. The R&D associated with future colliders needs to continue in parallel.

9 Acknowledgements

I would like to thank the organizers for the invitation to make this contribution and for the excellent organization of the very interesting conference, which also provided the opportunity to present the latest developments at CERN. Many thanks go to Emmanuel Tsismelis for his assistance in preparing this contribution.

10 References

- [1] LHC Design Report, Volumes I, II and III,
<http://lhc.web.cern.ch/lhc/LHC-DesignReport.html>
- [2] LINAC4, <http://linac4.web.cern.ch/linac4/>
- [3] Compact Linear Collider, <http://cllc-study.web.cern.ch/CLIC-Study/>
- [4] International Linear Collider, <http://www.linearcollider.org/>
- [5] Large Hadron electron Collider, <http://lhec.web.cern.ch/lhec>
- [6] Muon Collider, [http://www.fnal.gov/pub/muon collider/](http://www.fnal.gov/pub/muon%20collider/)
- [7] The European Strategy for Particle Physics,
http://council-strategygroup.web.cern.ch/council-strategygroup/Strategy_Statement.pdf

HIGHLIGHTS FROM RHIC PLUS SOME EARLIER BNL HIGHLIGHTS IN SUBNUCLEAR PHYSICS

■ MICHAEL J. TANNENBAUM*

Brookhaven National Laboratory
Upton, NY 11973 USA

A new periodic table for the 21st Century

In the 20th century, the periodic table, which was invented in the 19th century, was understood using quantum mechanics, atomic, nuclear and subatomic physics; and many elements were added (Figure 1a). Also in the 20th century, the discovery of a whole new subnuclear world of physics totally changed our view of nature and led to a new periodic table to be understood (Figure 1b). The neutrons and protons, of which atomic nuclei are composed, are themselves

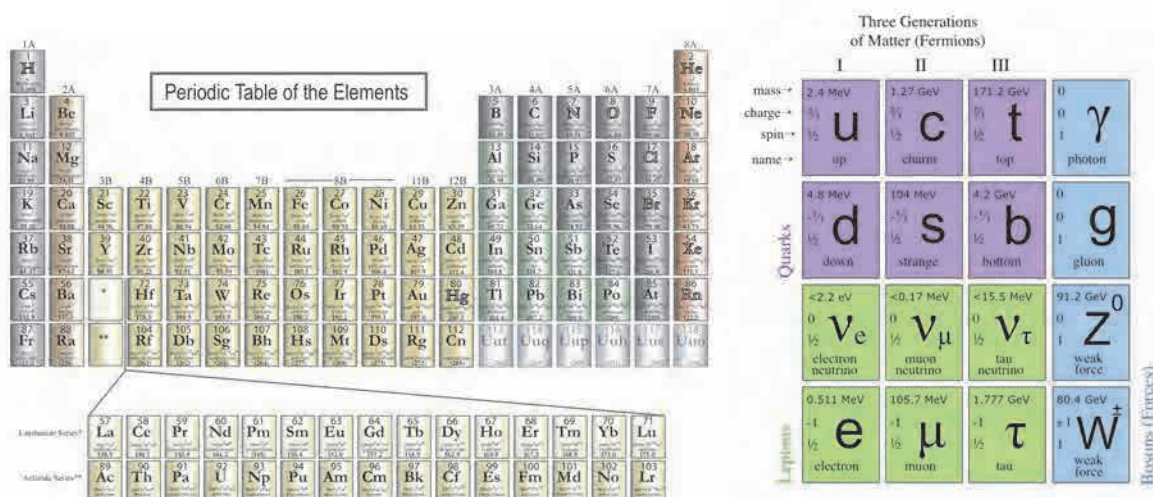


Figure 1. a) (left) Periodic Table of the Chemical Elements at end of 20th Century (LANL 2011). b) (right) 21st century periodic table of the Quarks and Leptons (Fermions) and force carriers (Bosons) (FNAL 2011)

composed of the subconstituent up (u) and down (d) quarks which are held together by gluons, the quanta of the strong interaction in a theory called Quantum Chromodynamics or QCD (QCD 1983). The quarks have electric charges which are a fraction $2/3$ (u), $-1/3$ (d) of the proton charge.

QCD has three new charges called colors, e.g. red, green, blue; and in sharp distinction to electromagnetism, whose quantum, the photon, carries no electric charge, the gluons of QCD are charged and therefore couple to each other. This provides the confinement of quarks and gluons inside nucleons as well as as a Coulomb-like $1/r^2$ short range force which can be measured. Each nucleon is composed of 3 quarks of different colors (uud for the proton and udd for the neutrons) so that the nucleons are color neutral. The nuclear force which binds neutrons and protons into nuclei is produced by a Yukawa coupling (Yukawa 1935) due to the exchange of pions which are made of quark-anti quark pairs, e.g. π^+ ($u\bar{d}$).

* Supported by the U.S. Department of Energy, Contract No. DE-AC02-98CH1-886.

Brookhaven National Laboratory (BNL)

I start with a brief description of Brookhaven National Laboratory and its contributions to the new periodic table, which concern the charm and strange quarks, the muon neutrino, and the electron neutrino. Brookhaven National Laboratory (BNL), a National Laboratory funded by the U.S. Federal Government, was founded by nine major northeastern universities in 1947 to promote basic research in the physical, chemical, biological and engineering aspects of the atomic sciences and for the purpose of the design, construction and operation of large scientific machines that individual institutions could not afford to develop on their own. It is located on Long Island roughly 100km east of New York City. In fact the Relativistic Heavy Ion Collider (RHIC) at BNL can be seen from outer space since it is not buried in a tunnel but is in an enclosure on the surface, which is covered by earth for shielding (Fig. 2).



Figure 2. NASA Infra-red photo of New York Metro Region. RHIC is the white circle in the center of Long Island below the rightmost group of clouds. Manhattan island is clearly visible on the left side.

A closer aerial view of BNL (Fig. 3) shows the Relativistic Heavy Ion Collider (RHIC), which started operations in the year 2000, as well as the two previous accelerators built for High Energy Physics (HEP): the Cosmotron, a 3.3 GeV proton accelerator, which operated from 1953—1966, and the Alternating Gradient Synchrotron (AGS), which started operation in 1960 and ended operations for HEP in 2002 but now serves as the injector to RHIC.

Major discoveries and original contributions to the new periodic table were made at BNL during both the Cosmotron and AGS era. I shall briefly review these contributions before moving on to the highlights from RHIC.



Figure 3. A closer view of RHIC at Brookhaven National Laboratory. The large circle without tree cover is excavation related to the enclosure of the RHIC machine. The labeled lines show the Linac, Booster accelerator for polarized proton injection, the tandem van de graaf accelerator and transfer line to the booster, and the AGS which accelerates the beams to an energy of 22 GeV per nucleon $\times Z/A$ where Z and A are the atomic number and weight of the nucleus.

The Cosmotron Era 1953—1966

The Cosmotron (Figs. 3,4) was the first particle accelerator to deliver beams with energy greater than 1 Billion Electron-Volts (1 GeV), with a maximum accelerated proton energy of 3.3 GeV. It was the first synchrotron with an extracted beam and the first accelerator to produce in the laboratory all the types of particles known from cosmic rays, including the strange particles, which were called strange because they were produced at a large rate, consistent with strong interactions, but decayed slowly, consistent with weak interactions. These strange particles were the first evidence for the strange (s) quark.

Some highlights of discoveries at the Cosmotron are:

- Associated production of strange particles, $\pi^- + p \rightarrow \Lambda^0 + K^0$ (Fowler 1954)¹
- Multiparticle production in a $n+p$ collision (Fowler-np1954)
- Long-lived, CP-odd, K^0_2 . Limit $K^0_2 \rightarrow \pi^+ \pi^- < 1\%$ (Lande 1956)
- ρ vector meson (Erwin 1961)

1. According to Pais (1986), “As to associated production, cosmic ray evidence seemed at first against it. ...The issue was settled when accelerators in the GeV range became available. A Cosmotron experiment [(Fowler 1954)] yielded the first convincing results.”

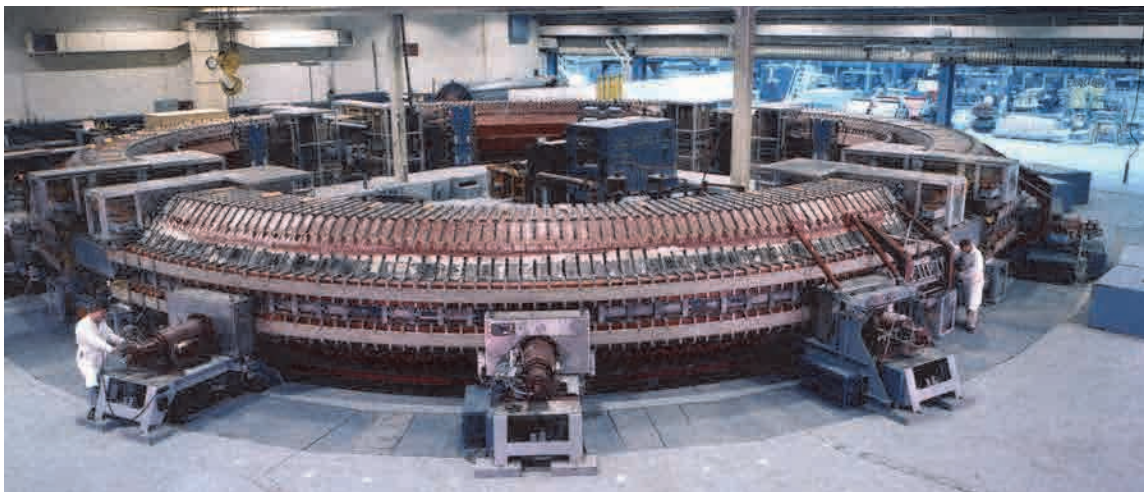


Figure 4. The Cosmotron machine. The machine is 75 feet in diameter, composed of 288 C-shaped magnets with the open gaps all facing outwards. The edge of the magnet coils are visible above and below the vacuum tank in the mid-plane, which is connected to the vacuum pumps. The machine is small enough to fit in a standard high-bay building. The machine was shielded with concrete blocks during operation.

There were also two major theory papers by BNL authors during this period:

- Gauge Field Theory. This is the basis of the standard model. (Yang-Mills 1954)
- Parity Violation in Weak Interactions? (Lee-Yang 1956) Nobel Prize 1957.

Strong Focusing, discovered in 1952, leads to the BNL-AGS (and CERN-PS).

During the last year of Cosmotron construction, a new principle of accelerator design was discovered at BNL (Courant 1952). Instead of C-magnets with their gaps all facing outwards, the orientation was alternated so that groups of magnets had gaps facing outwards and adjacent groups had gaps facing inwards. This provided, “A sequence of alternately converging and diverging magnetic lenses of equal strength [which] is itself converging, and leads to significant reductions in oscillation amplitude, both for radial and axial displacements, i.e. much smaller magnets.” (Courant 1952).

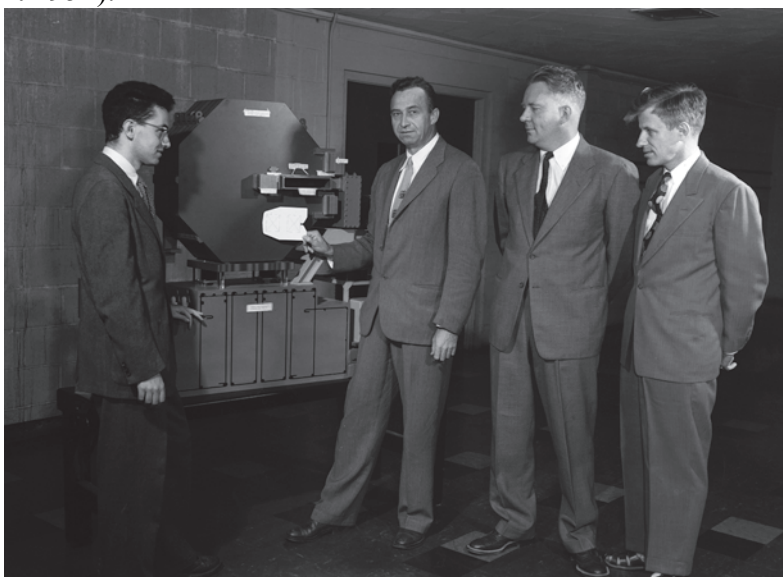


Figure 5. Courant, Livingston, Snyder and Blewett next to model of Cosmotron C-shaped magnet. Livingston holds cutout of magnet for strong focusing machine of same energy.

The Alternating Gradient Synchrotron (AGS) Era: 1960-2002 (for HEP).

The AGS is a strong focusing synchrotron which accelerates protons to an energy of 33 GeV, or ten times that of the Cosmotron. Because of the strong focusing, the magnets of the much larger AGS (Fig. 6) contained only twice as much steel as the Cosmotron.



Figure 6. View of Alternating Gradient Synchrotron (AGS) machine inside its shielding enclosure. The 33 GeV machine was the highest energy accelerator in the world until 1968. The coils of the individual out-facing magnets are visible. The AGS has accelerated protons and spin-polarized protons as well as fully stripped O, Si, Cu and Au nuclei. The AGS is now used as the injector to RHIC.

The AGS has made many major discoveries in subnuclear physics, of which three received Nobel Prizes (🏆). Some highlights are:

- 🏆 First neutrino beam experiment; discovery of μ -neutrino, ν_μ (Danby 1962)
 - ϕ -meson ($s\bar{s}$) ; Ω^- baryon (sss) (Barnes 1964).
- 🏆 CP-Violation: $K^0_2 \rightarrow \pi^+ \pi^- \approx 0.2\%$ (Christenson 1964)
 - “Drell-Yan” pairs, $p+p \rightarrow \mu^+ \mu^- + X$
- 🏆 J/Ψ ($c\bar{c}$) (Aubert 1974)

Two Other BNL Neutrino Experiments-Non Accelerator.

- ν from β -decay (actually from electron capture) is left handed (Goldhaber 1958)
- 🏆 First observation of ν from the sun (Davis 1968) Nobel Prize 2002

Figure 7a shows the entire apparatus of the experiment (Goldhaber 1958) which measured that the helicity of ν_e is left handed (i.e. its spin is opposite to its momentum) by using the reaction $e^- + \text{Eu}^{152m} \rightarrow \nu_e + \text{Sm}^{152*}$ followed by $\text{Sm}^{152*} \rightarrow \text{Sm}^{152} + \gamma$, and measuring the circular polarization of the decay γ ray by differential absorption in the magnetized iron yoke. By a clever and possibly unique choice of the isotopes used, the energy of the ν_e and γ are very close, so that the γ rays which are emitted nearly back to back from the ν_e will have the same helicity (circular polarization) as the ν_e as well as the correct energy to be ‘resonantly’ absorbed and re-emitted by a Sm^{152} nucleus at rest, $\gamma + \text{Sm}^{152} \rightarrow \text{Sm}^{152*} \rightarrow \text{Sm}^{152} + \gamma$. The Sm_2O_4 resonant-scatterer is the flower pot shaped base. The re-emitted γ rays are detected in a counter under the cone-shaped Pb shield.

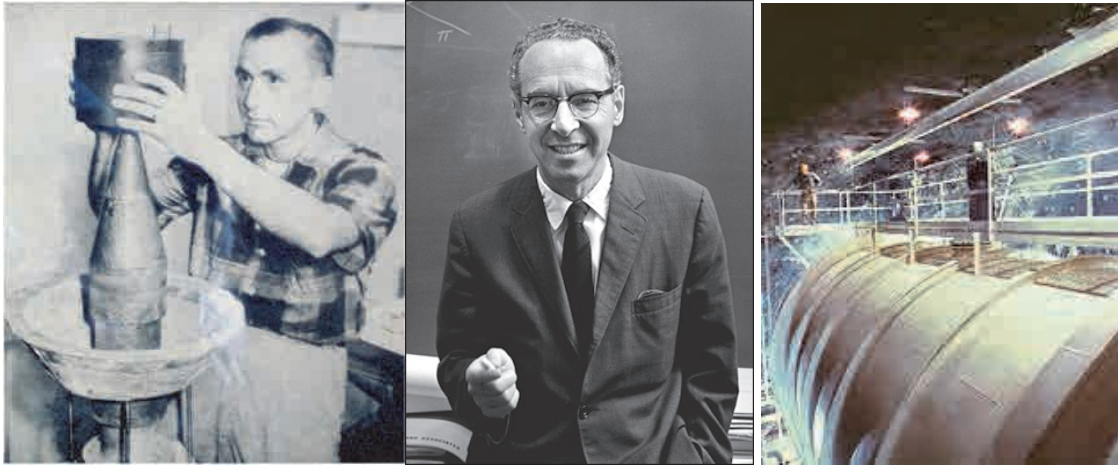


Figure 7. a) (left) Lee Grodzins c. 1957 holding the magnet of the experimental apparatus for analyzing the circular polarization of γ -rays detected by resonant scattering. The difference in counting rate due to reversing the magnetic field measures the circular polarization. The Eu_2O_3 source is inside the center of the magnet. The cone is a Pb absorber which restricts the path of the circularly polarized γ -rays from Sm^{152*} decay so that they pass through the magnetized iron on their trajectory to the basin at the bottom which is the Sm_2O_3 resonant-scatterer. The re-emitted γ -rays are detected in a scintillation counter under the Pb cone. b) (center) Maurice Goldhaber c. 1967. c) (right) Ray Davis' tank of cleaning fluid in the Homestake mine 1967. All photos courtesy BNL.

The story of Ray Davis' experiment (Figure 7c) is quicker to tell but took much longer to succeed. He put a tank of cleaning fluid (tetrachloroethylene, C_2Cl_4) into a deep mine from 1967-1988 and was the first to detect neutrinos from the sun via the reaction $\nu_e + \text{Cl} \rightarrow \text{Ar} + e^-$. He found a deficit from the theoretical predictions. This was confirmed many years later by the 'atmospheric neutrino anomaly'. Both these discoveries of a ν_e deficit shared the Nobel Prize in 2002 and were explained by neutrino oscillations.

The good old days!

The period discussed above, roughly from 1950—1970 were the good old days in Subnuclear Physics for several reasons. One such reason is that the discoveries were evident in photographs without resort to description of experimental details. Figure 8 shows photographs of associated

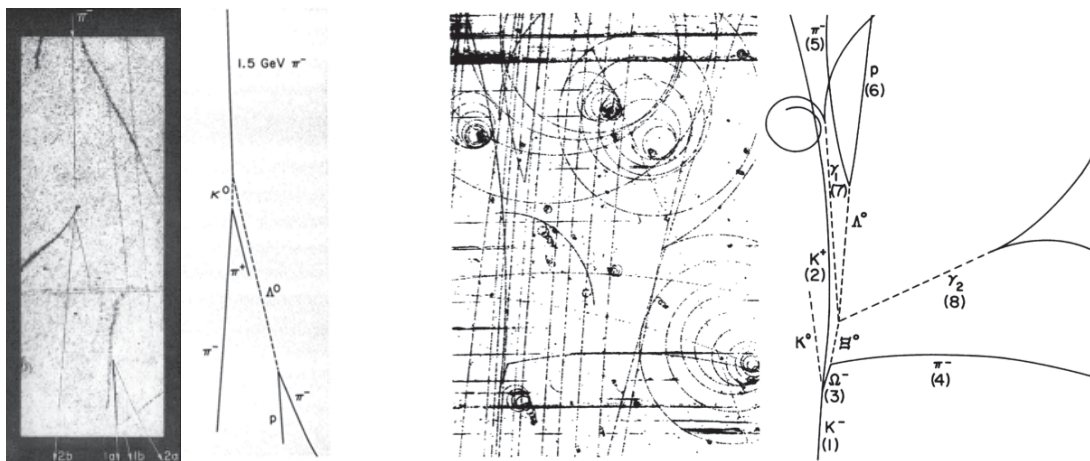


Figure 8. (left 2 panels) Hydrogen cloud chamber photograph and line diagram of event showing associated production of $\text{K}^0 \Lambda^0$ (Fowler 1954) with π^- beam entering from the top. (right 2 panels) Hydrogen bubble chamber photograph and line diagram of event showing decay of Ω^- (Barnes 1964) with K^- beam entering from the bottom.

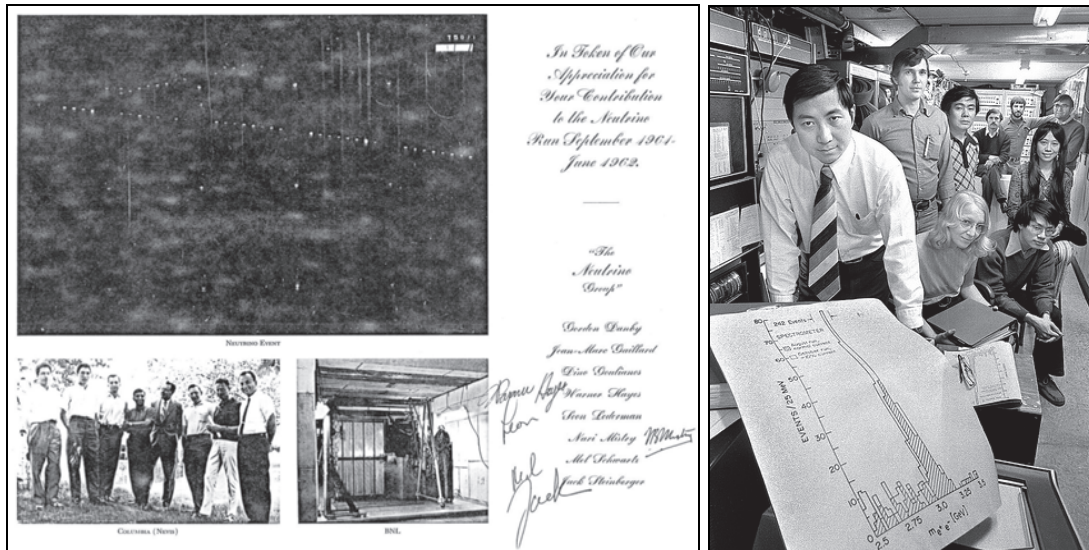


Figure 9. a) (left) Souvenir poster of the discovery of the μ -neutrino. b) (right) Prof. Ting in his counting house with members of the experiment showing a drawing of the narrow peak J which decays to an e^+e^- pair.

production of K^0 and Λ^0 and the discovery of the Ω^- which appeared in the original publications. Figure 9a shows an autographed souvenir poster of the discovery of the μ -neutrino. All 8 authors and their senior technician are in the lower left panel next to a photo of their spark chamber detector. A typical event from an exposure to a neutrino beam from π -meson decay is shown above them: a long straight track which must be a muon from the reaction $\nu + A \rightarrow \mu + A'$. No events of the type $\nu + A \rightarrow e + A'$, with a short showering track, were observed. Thus the neutrino from π decay only couples to muons. This ' μ -neutrino', or ν_μ , is different from the ν from β -decay, now called ν_e . Figure 9b shows Prof. Ting with a drawing of the very prominent and narrow peak, the J particle which decays to an e^+e^- pair. The narrow width means a long lifetime which implies a conservation law (like the strange particles), due to a new charm or c -quark. The J, now J/Ψ , is a bound state of $(c\bar{c})$, the hydrogen atom of QCD. These experiments in the 'good old days' were done by a dozen physicists or less, in contrast to modern experiments with ~ 400 to 4000 authors (Fig. 10).



Figure 10. Some members of the PHENIX experiment at RHIC, c. 2004, in front of the open PHENIX detector.

The Relativistic Heavy Ion Collider (RHIC)

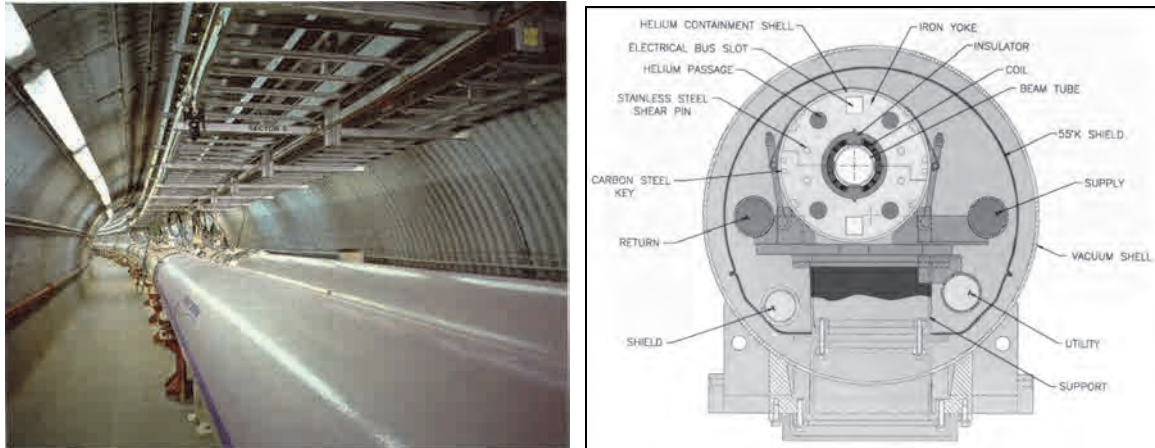


Figure 11. a)(left) Inside the RHIC enclosure—two independent rings with a total of 1740 superconducting dipole, quadrupole and corrector magnets. b)(right) Cross section of a RHIC dipole magnet viewed along the beam axis.

In the year 2000, RHIC, an accelerator-collider, with two independent rings of superconducting magnets, began operation. The Palmer magnet (Fig. 11b) used in RHIC was the basis for all post-Tevatron superconducting accelerators starting with CBA (formerly ISABELLE) including HERA, SSC, LHC: a cold iron yoke; and Cu wedges in the superconducting coils for field shaping. RHIC is a versatile accelerator which has collided Au+Au, d+Au, Cu+Cu, and polarized p-p, in runs from 2000—2011, at 12 different c.m. energies; with U+U and Cu+Au collisions scheduled for 2012.

The purpose of colliding nuclei at large nucleon-nucleon (N-N) c.m. energy ($\sqrt{s_{NN}}$) is to create nuclear matter in conditions of extreme temperature and density. At large energy or baryon density, a phase transition is expected from a nucleus as a state of nucleons containing confined quarks and gluons to a state of matter with “deconfined” (from their individual nucleons) quarks and gluons, called the quark-gluon plasma or QGP, covering a volume that is many units of the confinement length scale. The original goal of RHIC was to see whether the QGP existed and if so to measure its properties, such as phase transition temperature (T), density, equation of state, entropy, heat capacity, speed of sound, and, lately, viscosity. The experimental problems are different in A+A collisions compared to p-p because the multiplicity of soft particles is roughly A times larger in A+A than in p-p collisions, as shown with actual events in Fig. 12.

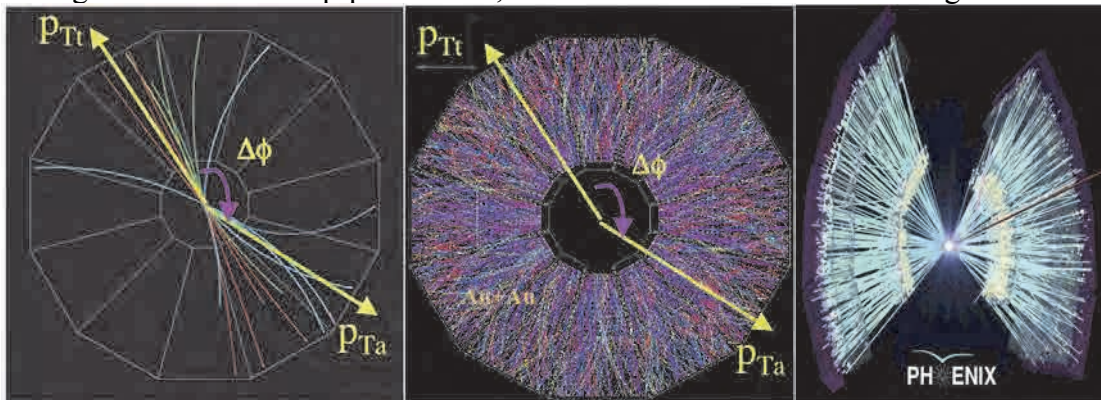


Figure 12. Collisions at nucleon-nucleon c.m. energy $\sqrt{s_{NN}}=200$ GeV a) (left) p-p collision b) (center) Au+Au central collision in the STAR detector. c) (right) Au+Au in PHENIX. Arrows p_{Tt} , p_{Ta} at angle $\Delta\phi$ represent selected particles.

Hard-scattering: Rutherford (1911) to the CERN-ISR to RHIC

Due the huge multiplicities in A+A collisions at RHIC, most of the analyses have been performed using single particle inclusive measurements ($A+A \rightarrow \pi + X$, where X represents all the other particles not detected) or two-particle correlations, as indicated by the arrows with transverse momentum p_{Tb} , p_{Ta} on Fig. 12 a,b. The value of the transverse momentum, p_T , corresponds to the closeness or ‘hardness’ of the collision, with large values of p_T indicating collisions at small distances, $p_T \approx 1/b$, where b is the impact parameter, or distance of closest

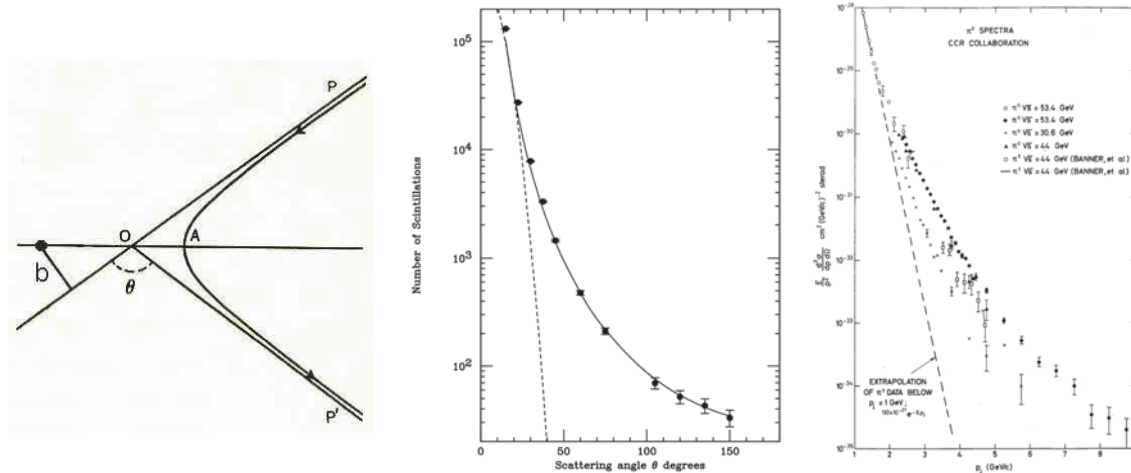


Figure 13. a) A particle P along trajectory P-O with impact parameter b from target (solid circle) scatters through angle θ [after (Rutherford 1911)]. b) (center) Rutherford scattering cross section $1/\sin^4(\theta/2)$ (solid line) measured by Geiger and Marsden (Geiger 1913) (data points); dashes indicate the expectation for a spread distribution of charge. c) (left) discovery of hard-scattering in p-p collisions at the CERN-ISR (CCR 1973), $d^3\sigma/dp^3$ of π^0 vs. p_T for several values of \sqrt{s} .

approach of the colliding particles or nuclei (Fig 13a). This was originally discovered by Rutherford (1911), Geiger and Marsden (1913), who scattered α -particles (He nuclei) on a gold foil and observed large angle scattering (Fig 13b) in agreement with Rutherford’s calculation, a power-law (solid line) if the positive charge in an atom were all located at a central point, the nucleus, rather than spread out uniformly (dashes). In Fig 13c, the discovery of production of π^0 at large p_T in p-p collisions at the CERN-ISR (CCR1973) is shown, with a power-law which depended on the c.m. energy, \sqrt{s} , and was qualitatively different from the exponential spectrum observed in cosmic rays for $p_T < 1$ GeV/c. This represented the discovery that the point-like constituents of the proton, called partons, which are the quarks and gluons of QCD, hard-scattered strongly from each other, i.e. much larger than electromagnetically.

Heavy Ion Collisions at RHIC—is the QGP produced?

At RHIC, in heavy ion collisions (Fig. 14a), hard-scattering of partons from the initial

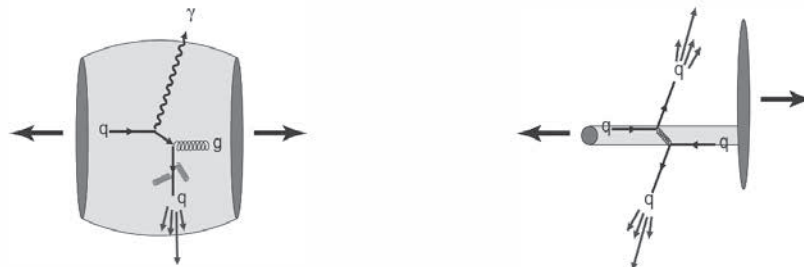


Figure 14. a) (left) Two outgoing nuclei indicated by the dark grey disks after a collision which produces a medium (light grey) in which outgoing partons from an initial hard-scattering may interact. b) (right) A p+A or d+A collision in which the medium is limited (1 nucleon wide) or non-existent, so that any interaction of outgoing partons is minimal.

collision turned out to be a valuable in-situ internal probe of the medium produced. For instance, does the quark lose energy exiting the medium as sketched in Fig. 14a? If so, exactly how? etc. A baseline for any cold-nuclear matter effects is provided by p+A (or d+A) collisions (Fig. 14b) in which no (or a very limited) medium is produced.

One of the observed distinguishing properties of the medium is that the emission of the huge number of soft particles produced is not isotropic but exhibits an asymmetry in the azimuthal distribution, $dn/dp_T d\phi = (dn/2\pi dp_T)[1 + \sum 2v_n \cos n(\phi - \Phi_R)]$, represented as an expansion in Fourier harmonics, v_n , where ϕ is the azimuthal angle in the x-y plane (Fig. 15a) of a particle relative to the impact parameter vector, the x-axis ($\Phi_R=0$). This is a collective effect, known as anisotropic

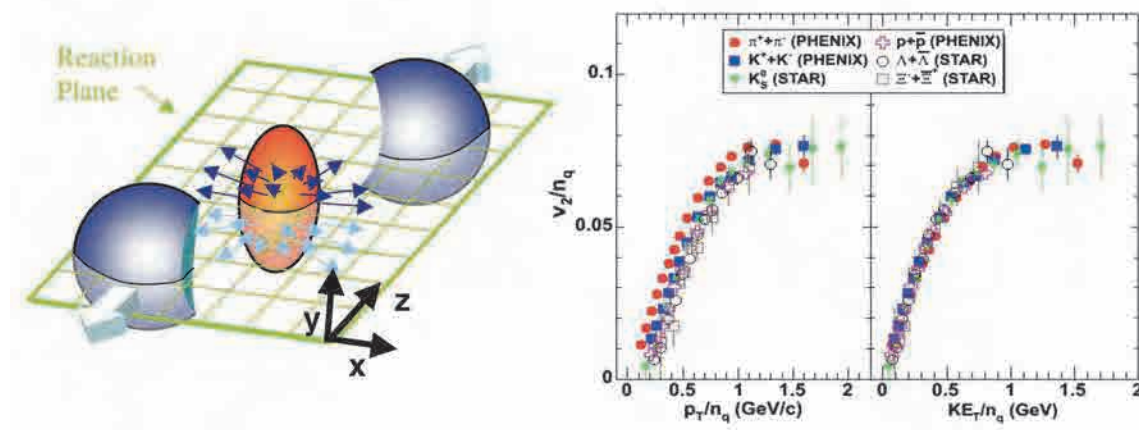


Figure 15. a) (left) Almond shaped overlap region generated just after an A+A collision where the colliding nuclei are moving along the $\pm z$ axis and the impact parameter is along the x axis. b) Measurements of elliptical flow (v_2) for identified hadrons plotted as v_2/n_q vs. p_T , or transverse kinetic energy KE_T , per constituent quark.

flow, which can not be obtained from a superposition of independent N-N collisions, but is due to the buildup of pressure in the almond shaped overlap region of the colliding nuclei. This leads to a predominant expansion of the medium in the reaction plane, which means a large v_2 called elliptical-flow (Fig. 15b). Measurements of v_2/n_q for identified hadrons, where n_q is the number of constituent quarks ($n_q=2$ for mesons, π, K ; $n_q=3$ for baryons p, Λ, Ξ), as a function of the transverse kinetic energy, $KE_T = \sqrt{p_T^2 + m^2} - m$, per constituent quark, of the particle with mass m , show a universal behavior (PHENIX v_2 2007)². The fact that flow is observed in the final state particles shows that the thermalization of the medium is rapid, so that hydrodynamic behavior can take over before the spatial anisotropy of the almond dissipates. At this early stage the hadrons are not formed so the universal behavior (Fig. 15b) suggests that it is the constituent quarks rather than the particles themselves that flow. Another crucial observation (Teaney 2003) is that the persistence of flow for $p_T > 1$ GeV/c, implies that the viscosity is small, perhaps as small as a quantum viscosity bound from string theory (Kovtun 2005), $\eta/s = 1/(4\pi)$, where η is the shear viscosity and s is the entropy density per unit volume. This has led to the description of the medium produced at RHIC as “the perfect fluid” (Rischke 2005), or the strongly interacting Quark Gluon Plasma (sQGP), which is a slight misnomer since the medium is a liquid, not a plasma (a gas of free quarks and gluons) as originally expected.

2. See Tannenbaum (2011) for a more complete list of citations to the original publications.

The major discovery at RHIC—Jet Quenching.

The discovery, at RHIC (Adcox 2002), that π^0 's produced at large $p_T > 3$ GeV/c are suppressed in central Au+Au collisions by roughly a factor of 5 compared to point-like scaling from p-p collisions is arguably the major discovery in Relativistic Heavy Ion Physics.

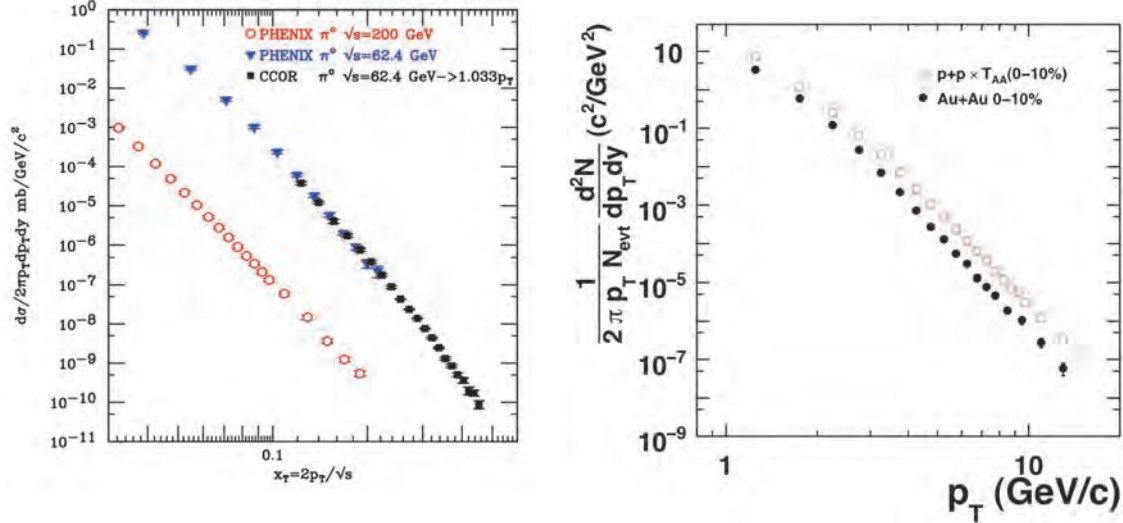


Figure 16. a) (left) Invariant cross section, $d^3\sigma/2\pi p_T dp_T dy$, where $y \approx -\ln \tan(\theta/2)$ is the rapidity, vs $x_T = 2p_T/\sqrt{s}$ for π^0 production in p-p collisions at $\sqrt{s}=62.4$ and 200 GeV at RHIC (PHENIX 2009) compared to measurements at the CERN-ISR (CCOR 1978) at $\sqrt{s}=62.4$ GeV where the absolute p_T scale has been adjusted upwards by 3.3% to agree with the RHIC data. b) (left) π^0 p-p data vs. p_T at $\sqrt{s}=200$ GeV from (a), multiplied by $\langle T_{AA} \rangle$ for Au+Au central (0-10%) collisions, compared to the measured invariant yield of π^0 in Au+Au central (0-10%) collisions at $\sqrt{s_{NN}}=200$ GeV (PHENIX 2007).

In Fig. 16a, the measurement of the invariant cross section, $d^3\sigma/2\pi p_T dp_T dy$, for π^0 production in p-p collisions at $\sqrt{s}=62.4$ GeV (PHENIX 2009) at RHIC is in excellent agreement with the CERN-ISR data (CCOR 1978). At $\sqrt{s}=200$ GeV the PHENIX π^0 data follow the same (although less steep) trend as the lower energy data, with a pure power law $1/p_T^{8.10 \pm 0.05}$ for $p_T > 3$ GeV/c. Since hard-scattering is point-like, with distance scale $1/p_T < 0.1$ fm, much less than the size of a nucleon or nucleus, the scattering cross-section in p+A collisions is simply A times larger than in p-p collisions and in A+A collisions, A^2 times larger than the p-p cross section, where A represents the number of nucleons in the nucleus. For A+A collisions in a limited range of impact parameters or “centrality” the factor is $\langle T_{AA} \rangle$, the overlap integral of the nuclear thickness functions.

In Fig. 16b, the 200 GeV p-p data, multiplied by the point-like scaling factor $\langle T_{AA} \rangle$ for central (small impact parameter) Au+Au collisions are compared to the measurement of the invariant yield of π^0 in central Au+Au collisions at $\sqrt{s}=200$ GeV (PHENIX 2007). Amazingly, the Au+Au data follow the same power-law as the p-p data but are either shifted down vertically, i.e. suppressed by a factor of ~ 5 , or shifted lower horizontally, by $\sim 20\%$ in p_T , relative to the point-like scaled p-p data. A quantitative representation of the suppression is provided by the “nuclear modification factor” $R_{AA}(p_T)$, which is defined as the measured yield in A+A collisions at a given p_T , divided by $\langle T_{AA} \rangle$ times the measured cross section in p-p collisions at the same p_T .

In order to verify that the suppression was due to the medium produced in Au+Au collisions and not an effect in the cold matter of an individual nucleus, a measurement in d+Au collisions was performed which was so definitive that all four experiments at RHIC at the time had their results displayed on the front page of Phys. Rev. Letters (Fig. 17a).

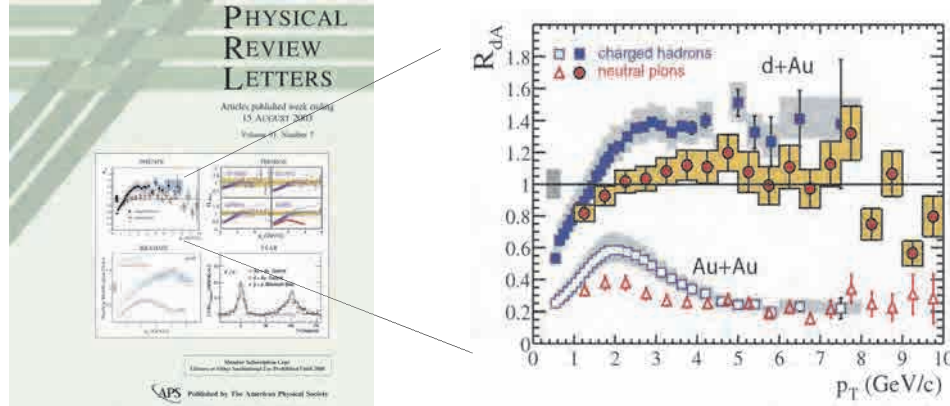


Figure 17. a) (left) Cover of Physical Review Letters of 15 August 2003 displaying the results of all 4 RHIC experiments which showed no suppression in d+Au collisions. b) (right) PHENIX results from that issue.

The conclusion from all four experiments was that there was no suppression in d+Au collisions, so that the suppression measured in A+A collisions must be due to an interaction with the medium produced, mostlikely due to radiative energy loss of the outgoing parton via gluon bremsstrahlung in the color-charged medium (Baier 2000). The PHENIX results (Fig. 17b) also showed that non-identified charged hadrons exhibited different values of $R_{AA}(p_T)$ than identified π^0 in both d+Au and Au+Au central collisions. This illustrated the importance of systematically measuring R_{AA} for identified particles.

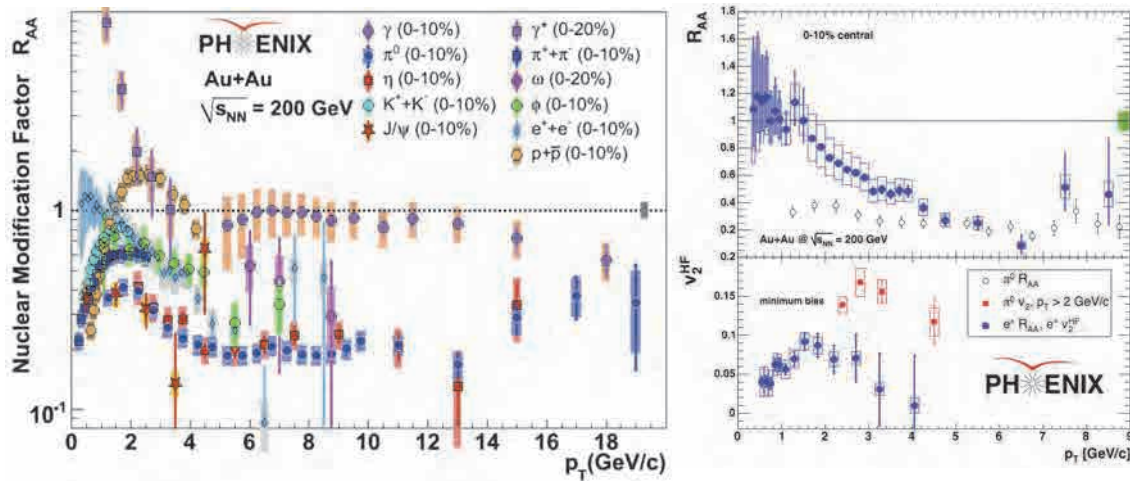


Figure 18. a) (left) PHENIX measurements of $R_{AA}(p_T)$ of the identified particles in central Au+Au collisions as indicated. b) (right) $R_{AA}(p_T)$ (top) and $v_2(p_T)$ (bottom) of single e^+ or e^- from b and c quark decay (PHENIXhq 2007).

PHENIX results from such systematic measurements proved to be both very interesting and exciting. Several important observations are evident from Fig.18a. 1) In the range $5 \leq p_T \leq 14$ GeV/c, γ -rays from the “inverse QCD Compton effect” $g+q \rightarrow \gamma+q$ (Fritzsch 1977), which do not interact with the medium since they are both electrically and color neutral, are not suppressed

($R_{AA}=1$), while π^0 , which are fragments of jets from hard-scattered u and d quarks and gluons which do interact with the medium, are suppressed by a nearly constant factor of 5 ($R_{AA}\approx 0.2$), again clearly demonstrating that suppression is a medium effect on outgoing color-charged partons; 2) γ^* (direct- γ measured by internal conversion) for $p_T < 2$ GeV/c exhibit a huge exponential enhancement over point-like scaling, shown by no other particle, which is consistent with thermal radiation from a medium with $T > 200$ MeV ($> 100,000$ times hotter than the center of the sun); 3) single e^+ or e^- from heavy b and c quark decay are suppressed the same as π^0 ($R_{AA}\approx 0.2$) for $p_T > 4$ GeV/c and exhibit flow (Fig.18b), both of which indicate a very strong interaction with the medium. This was a total surprise, a major discovery and a problem since it strongly disfavors the radiative energy loss explanation of jet-quenching because heavy quarks should radiate much less than light quarks or gluons.

One solution to this problem was offered by Professor Zichichi (2007) who proposed that the standard model Higgs Boson does not give mass to Fermions, so that “it cannot be excluded that in a QCD colored world [the sQGP] the six quarks are all nearly massless.” If this were true it would certainly explain why light and heavy quarks appear to exhibit the same radiative energy loss in the medium. This idea can in fact be tested because the energy loss of one hard-scattered parton relative to its partner, e.g. $g + g \rightarrow b + \bar{b}$, can be measured using two particle correlations by experiments, at RHIC and LHC, in which both the outgoing b and \bar{b} are identified by measurement of their displaced decay vertices in silicon vertex detectors. When such results are available, they can be compared to π^0 -charged hadron correlations from light quark and gluon jets, for which measurement of the relative energy loss has been demonstrated at RHIC (Fig. 19). In Fig.19a, the p_{Ta} spectrum of associated charged hadrons in p-p and central

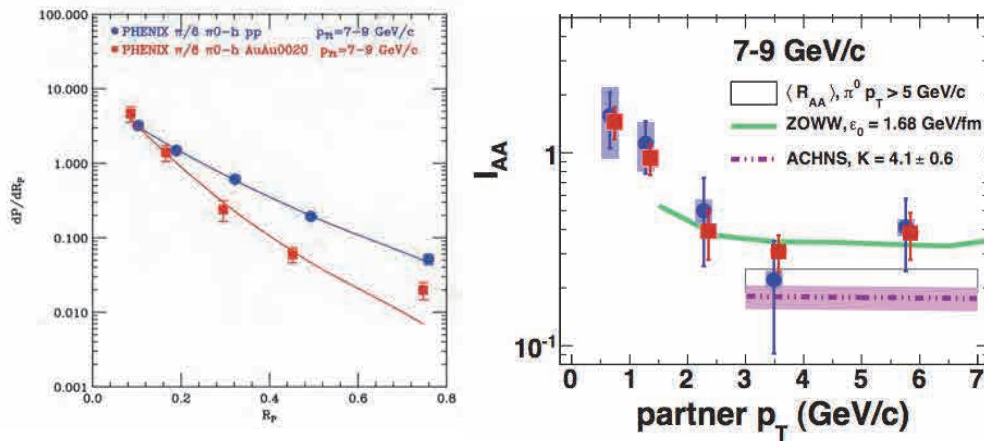


Figure 19. a) (left) $R_p = p_{Ta}/p_{Tt}$ distributions from p-p (circles) and central Au+Au collisions (squares) for $7 < p_{Tt} < 9$ GeV/c together with fits for R_J . b) (right) I_{AA} = ratio of Au+Au/pp data from (a) vs p_{Ta} (squares) (PHENIX 2010).

Au+Au collisions is presented in the variable $R_p = p_{Ta}/p_{Tt}$ for trigger π^0 's with p_{Tt} in the range 7—9 GeV/c. The energy loss is measured by the fact that the Au+Au spectrum is steeper than the p-p spectrum as more typically shown in the ratio of the spectra (Fig. 19b). The ratio of the away jet to trigger jet transverse momenta, R_J , can be found by a fit of the R_p distribution of Fig. 19a to the simple formula, $dP/dR_p = N/R_J(1+R_p/R_J)^n$, where n is the power of the p_T spectrum of the π^0 invariant yield (Fig. 16b), with result $R_J \approx 0.5$ in Fig. 19a. Zichichi's proposal could be confirmed if the same relative energy loss were also observed for b and c quarks.

Clearly, there are still exciting possibilities on the horizon in subnuclear physics.

References

- Adcox, K. *et al.*, PHENIX collaboration. (2002). Suppression of Hadrons with Large Transverse Momentum in Central Au+Au Collisions at $\sqrt{s_{NN}}=130$ GeV. *Phys. Rev. Lett.* 88, 022301.
- Aubert, J. J., Becker, U., Ting, S. C. C., Wu, S. L., *et al.* (1974). Experimental Observation of a Heavy Particle J. *Phys. Rev. Lett.* 33, 1404—1406.
- Baier, R., Schiff, D. & Zakharov, B. G. (2000). Energy Loss in Perturbative QCD. *Ann. Rev. Nucl. Part. Sci.* 50, 37—69.
- Barnes, V. E., Connolly, P. L., Samios, N. P., *et al.* (1964). Observation of a Hyperon with Strangeness Minus Three. *Phys. Rev. Lett.* 12, 204—2066.
- CCOR collaboration, Angelis, A. L. S. *et al.* (1978). A measurement of inclusive π^0 production at large p_T from p-p collisions at the CERN-ISR. *Phys. Lett. B* 79, 505—510.
- CCR collaboration, Cool, R. L. *et al.* (1973). In Jackson, J. D. & Roberts, A. (Eds.), *Proc XVI Int. Conf. High Energy Physics 1972* (Vol. 3, p. 317). Batavia, IL: NAL.
- Christenson, J. H., Cronin, J. W., Fitch, V. L. & Turlay, R. (1964). Evidence for the 2π decay of the K^0_2 meson. *Phys. Rev. Lett.* 13, 138—140.
- Courant, E. D., Livingston, M. S. & Snyder, H. S. (1952). The Strong-Focusing Synchrotron—A New High Energy Accelerator, *Phys. Rev.* 88, 1190—1196.
- Danby, G., Gaillard, J-M., Goulianos, K., Lederman, L. M., Mistry, N., Schwartz, M. & Steinberger, J. (1962). Observation ... of Two Kinds of Neutrinos, *Phys. Rev. Lett.* 9, 36.
- Davis, Jr., R., Harmer, D. S. & Hoffman, K. C. (1968). Search for Neutrinos from the Sun, *Phys. Rev. Lett.* 20, 1205—1209.
- Erwin, A. R., March, R., Walker, W. D., & West, E. (1961). Evidence for a π - π resonance in the $I=1, J=1$ state. *Phys. Rev. Lett.* 6, 628—630.

- FNAL (2011). *Standard Model of Elementary particles*. Retrieved Jan 4, 2012, from http://en.wikipedia.org/wiki/Standard_Model
- Fowler, W. B., Shutt, R. P., Thorndike, A. M. & Wittemore, W. L. (1954). Production of Heavy Unstable Particles by Negative Pions. *Phys. Rev.* 93, 861—867. Also, see Pais (1986).
- Fowler, W. B., Shutt, R. P., Thorndike, A. M. & Wittemore, W. L. (1954). Meson Production in n - p Collisions at Cosmotron Energies. *Phys. Rev.* 95, 1026—1044.
- Fritzsche, H. & Minkowski, P. (1977) Measuring QCD Compton Effects. *Phys. Lett. B* 69, 316.
- Geiger, H. & Marsden, E. (1913). The Laws of Deflexion of α Particles through Large Angles, *Phil. Mag.* 25, 604—623.
- Goldhaber, M., Grodzins, L. & Sunyar, A. W. (1958). Helicity of Neutrinos. *Phys. Rev.* 109, 1015—1017.
- Kovtun, P. K., Son, D. T. & Starinets, A. O. (2005). Viscosity in Strongly Interacting Quantum Field Theories from Black Hole Physics. *Phys. Rev. Lett.* 94, 111601.
- LANL (2011). *Periodic table of the elements*. Retrieved Jan 4, 2012, from <http://periodic.lanl.gov/images/periodictable.pdf>
- Lande, K., Booth, E. T., Impeuglia, J., Lederman, L. M., & Chinowsky, W. (1956). Observation of Long-Lived Neutral V particles. *Phys. Rev.* 103, 1901—1904.
- Lee, T. D., & Yang, C. N. (1956). Question of Parity Conservation in Weak Interactions. *Phys. Rev.* 104, 254—258.
- Pais, A. (1986). *Inward Bound—of matter and forces in the physical world*. New York, Oxford University Press.
- PHENIX collaboration, Adler, S. S. *et al.* (2007). Detailed study of high- p_T neutral pion suppression ... in Au+Au collisions at $\sqrt{s_{NN}} = 200$ GeV. *Phys. Rev. C* 76, 034904.

- PHENIX collaboration, Adare, A. *et al.* (2007). Scaling properties of Azimuthal Anisotropy (v_2) in Au+Au and Cu+Cu collisions at $\sqrt{s_{NN}} = 200$ GeV. *Phys. Rev. Lett.* **98**, 162301.
- PHENIX collaboration, Adare, A. *et al.* (2007). Energy Loss and Flow of Heavy Quarks in Au+Au Collisions at $\sqrt{s_{NN}} = 200$ GeV. *Phys. Rev. Lett.* **98**, 172301.
- PHENIX collaboration, Adare, A. *et al.* (2009). Inclusive cross section ... for π^0 production in p+ p collisions at $\sqrt{s} = 62.4$ GeV. *Phys. Rev. D* **79**, 012003.
- PHENIX collaboration, Adare, A. *et al.* (2010). Transition in Yield and Azimuthal Shape Modification in Dihadron Correlations in RHI Collisions. *Phys. Rev. Lett.* **104**, 252301.
- QCD (1983). Fritzsche, H., Gell-Mann, M. & Leutwyler, H. *Phys. Lett. B* **47**, 365. Gross, D. J. & Wilczek, F. *Phys. Rev. Lett.* **30**, 1343. Politzer, H. D. *Phys. Rev. Lett.* **30**, 1346.
- Rischke, D. & Levin, G. (Eds.) (2005). Quark-Gluon Plasma. New Discoveries at RHIC. Case for the Strongly Interacting QGP. *Nucl. Phys. A* **750**, 1—172.
- Rutherford, E. (1911). The scattering of α and β Particles by Matter and the Structure of the Atom. *Phil. Mag.* **21**, 669—688.
- Tannenbaum, M. J. (2011). Results from PHENIX at RHIC with Implications for LHC. *Int. J. Mod. Phys. A* **26**, 5299—5335. Also see <http://arxiv.org/abs/1006.5701>.
- Teaney, D. (2003). Effect of shear viscosity on spectra, elliptic flow and Hanbury Brown-Twiss radii. *Phys. Rev. C* **68**, 034913
- Yang, C. N. & Mills, R. L. (1954). Conservation of Isotopic Spin and Isotopic Gauge Invariance. *Phys. Rev.* **96**, 191—195.
- Yukawa, H. (1935). On the Interaction of Elementary Particles. I. *Proc. Phys.-Math. Soc. Japan* **17**, 48-57.
- Zichichi, A. (2007). Yukawa's gold mine. *CERN Courier*, **47(7)**, 43—46.

THE BIRTH AND DEVELOPMENT OF THE FIRST HADRON COLLIDER THE CERN INTERSECTING STORAGE RINGS (ISR)

■ K. HÜBNER, T.M. TAYLOR

CERN, 1211 Geneva 23, Switzerland

Abstract

The CERN Intersecting Storage Rings (ISR) was the first facility providing colliding hadron beams. It operated mainly with protons with a beam energy of 15 to 31 GeV. The ISR were approved in 1965 and were commissioned in 1971. This paper summarizes the context in which the ISR emerged, the design and approval phase, the construction and the commissioning. Key parameters of its performance and examples of how the ISR advanced accelerator technology and physics are given.

1. Design and approval

The concept of colliding beams was first published in a German patent by Rolf Widerøe in 1952, but had already been registered in 1943 (Widerøe, 1943). Since beam accumulation had not yet been invented, the collision rate was too low to be useful. This changed only in 1956 when radio-frequency (rf) stacking was proposed (Symon and Sessler, 1956) which allowed accumulation of high-intensity beams. Concurrently, two realistic designs were suggested, one based on two 10 GeV Fixed-Field Alternating Gradient Accelerators (FFAG) (Kerst, 1956) and one suggesting two 3 GeV storage rings with synchrotron type magnet structure (O'Neill, 1956); in both cases the beams collided in one common straight section. The idea of intersecting storage rings to increase the number of interaction points appeared later (O'Neill, 1959).

These studies have to be seen in the context of a significant activity in the field of lepton colliders at that time with the storage ring Anello Di Accumulazione (ADA) starting the successful lineage of e^+e^- colliders at the Italian National Laboratory in Frascati (Touschek, 1961) which was continued by VEPP-2 in 1964 (Auslender, 1966), ACO in 1965 (Orsay Group, 1966) and culminated in LEP at CERN in 1989 (Picasso & Plass, 1989).

At CERN, already during the construction of the 28 GeV Proton Synchrotron (PS) an accelerator research group led by A.Schoch had been formed which produced by the end of 1960 a proposal of two tangential 25 GeV proton storage rings (Hereward, 1960).

After the publication of the ISR proposal in 1960, a rather heated debate took place at CERN and in the physics community whether the next step after the PS should be a powerful synchrotron of either higher energy or of higher intensity providing more intense secondary beams, or a set of proton storage rings to investigate very high-energy phenomena.

In 1962, the intersecting ring topology was adopted for the ISR to increase the number of possible physics experiments (Johnsen, 1963). In order to channel the discussion, the European Committee for Future Accelerators (ECFA) was formed in 1963, chaired by E.Amaldi. It recommended both, the ISR fed by the PS and a 300 GeV synchrotron to compete with the US and USSR where large synchrotrons were designed, respectively under construction.

PAS Symposium Subnuclear Physics, 30 Oct.-2 Nov.2011, "Birth of the 1st Hadron Collider" KH&TMT

Although the rf stacking had been experimentally proven before (Terwilliger, 1957), CERN decided to acquire experience with these key technique for achieving high-intensity beams and, in turn, a high collider luminosity. On top of it, the ultra-high vacuum technology imperative for the ISR had to be tested. Hence, a small test ring, the CERN Electron Storage and Accumulation Ring (CESAR), was built, as shown in Fig. 1.

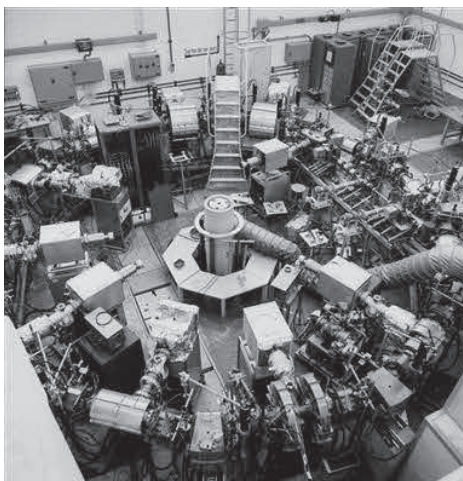


Fig. 1. The CERN Electron Storage and Accumulation Ring (CESAR).

It operated from 1963 to 1967. The beam parameters were carefully chosen so that the accumulation of a 28 GeV proton beam was faithfully simulated by a 2 MeV electron beam in a ring with 24 m circumference exhibiting virtually no radiation damping by synchrotron radiation. CESAR confirmed the rf stacking in 1964 (Hansen, 1965), which provided welcome support for the ISR-project.

The Design Reports for ISR and the 300 GeV synchrotron were published in 1964 (CERN 1964a, 1964b). The CERN directorate under V.Weisskopf decided to favour the ISR which appeared to offer more discovery potential for less cost and a shorter construction time. On top of it, a site was available for the ISR after the French government had offered land in 1962, extending suitably the Meyrin site, while one feared that the choice of the site for the 300 GeV synchrotron could be a source of tension between the CERN Member States (an apprehension which turned out to be justified in the years to come).

After considerable debate, the ISR construction was approved in principle in the framework of a Supplementary Programme, foreseen in the CERN Convention, in June 1965, and financial participation by all Member States except Greece was accepted in December of the same year. Kjell Johnsen was appointed project leader. The prevailing argument had been “to remain competitive for as low a cost possible”. However, it was also decided that the study of the 300 GeV synchrotron would be continued. A detailed account of the emergence of the ISR can be found elsewhere (Pestre, 1990).

2. Construction

The layout of the ISR with the transfer lines from the PS are shown in Fig. 2.

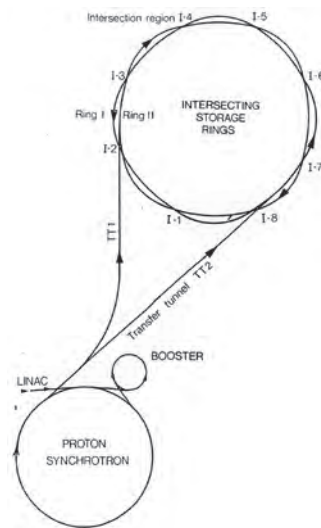


Fig. 2. Layout of ISR and of the transfer lines from the PS (Russo, 1996).

The PS and ISR sites are separated by the Swiss-French border. The maximum energy of the ISR was chosen to be 28 GeV, identical of the PS, and the orbit length was 943 m, exactly 1.5 times the PS circumference.

The main magnets were of the combined-function type, providing both a dipole field for the bending and a quadrupole component for the beam focusing. These C-shaped magnets offered a good access to the vacuum chamber, which turned out later to be decisive for the continuous up-grading of the vacuum system, and allowed for elaborate pole-face windings to fine-tune the magnetic field in the magnet gap. It was also claimed that the combined-function magnets were the cheapest option. The magnetic field was 1.33 T at 28 GeV. Fig. 3 shows a photo of the magnet during measurement.

PAS Symposium Subnuclear Physics, 30 Oct.-2 Nov.2011, "Birth of the 1st Hadron Collider" KH&TMT



Fig. 3. Combined-function magnet in the process of being measured.

A simple FODO structure was chosen as the magnet lattice after experience with the FOFDOD lattice of the PS. Here F/D stands for horizontally focusing / defocusing magnets, with a straight section O between them. The layout of an octant of the ISR around an intersection point can be seen in Fig. 4 and Fig. 5 gives a view of intersection point 5 (I5) after completion.

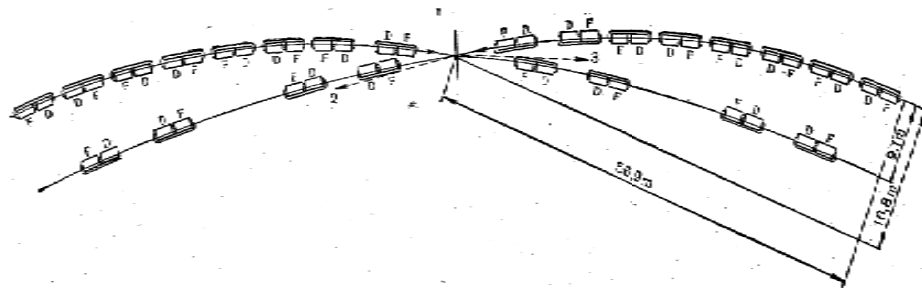


Fig. 4. One Octant of the ISR magnet lattice (Johnsen, 1963).



Fig. 5. ISR Intersection point 5.

The construction was smooth and rapid due to the excellent preparation during the design phase and due to the fact that the leading members of the team had solid experience from the construction of the PS. The earth excavation started in November 1966, only about 10 months after approval. By end of 1967, all magnets were ordered, and production of the required 11'000 t of magnet steel was complete by October 1968. In 1969, the tunnel, constructed by the cut-and-fill method with prefabricated walls, was finished, and two thirds of the magnets were installed.

3. Commissioning

Testing of the transfer lines started in April 1970, the last magnet was installed in May, and the earth shielding was complete in July. In October, a 15 GeV/c beam was injected into ring 1 and circulated immediately. Even rf stacking worked for the first time successfully leading a accumulated beam of 1 A. Ring 2 became ready in January 1971 and the first p-p collisions took place on January 27th.

The beam lifetime was as expected from the measured average vacuum pressure and rest-gas composition. This was of great relief for the team as hadron beam collisions was a new territory and some simulations had predicted a high beam decay rate brought about by beam blow-up through non-linear betatron resonances excited by the mutual interaction of the two colliding beams. This blow-up would not be counteracted by synchrotron radiation damping of particle oscillations as in e⁺e⁻ colliders since the synchrotron radiation was completely negligible, the synchrotron radiation loss per turn being only $6 \cdot 10^{-14}$ GeV for 28 GeV protons in the ISR with its bending radius of 78.6 m in the main magnets.

Regular physics runs for the experimental teams started in February with 15 GeV/c beams and collisions at 26.5 GeV/c, the highest momentum the PS was scheduled to produce, were recorded for the first time in May 1971, providing the unprecedented centre-of-mass energy equivalent to a 1500 GeV proton beam hitting a fixed target. In this first year of operation, already 1800 h could be scheduled for physics runs during which a surprising 95% availability of the accelerator was recorded (Johnsen, 1973).

4. Performance and technology

After a flying start a continuous effort was made throughout the lifetime of the ISR to improve its performance (Johnsen, 1984, 1986, 1992). The stored d.c. proton current per ring was increased from 10 A reached in the first year to typically ≤ 40 A in physics runs with 57 A as record value. The peak luminosity was steadily increasing over the years as can be seen from Fig. 6.



PAS Symposium Subnuclear Physics, 30 Oct.-2 Nov.2011, "Birth of the 1st Hadron Collider" KH&TMT

Fig. 6. Evolution of the ISR peak proton-proton luminosity (Johnsen, 1984).

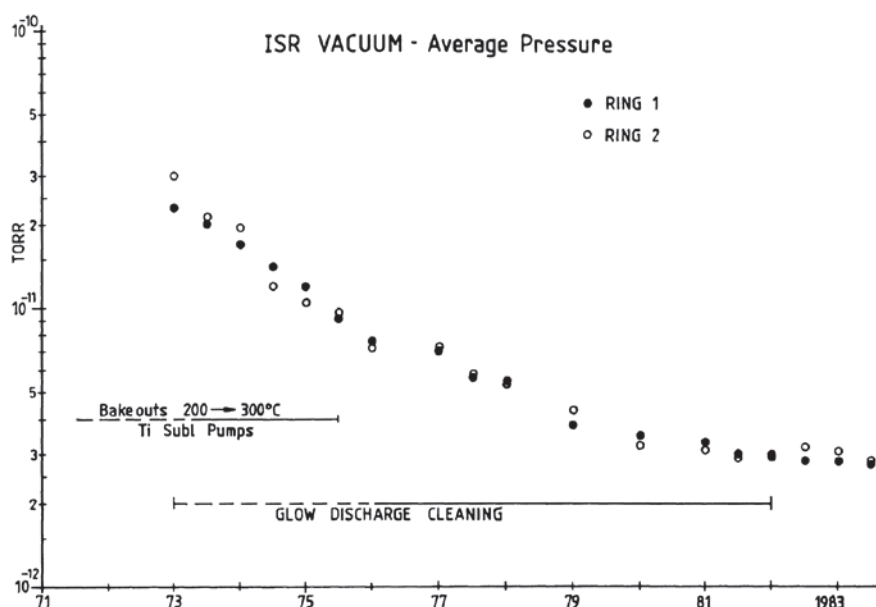
The maximum luminosity achieved was $1.4 \cdot 10^{32} \text{ cm}^{-2} \text{ s}^{-1}$ which was far above the design value of $4 \cdot 10^{30} \text{ cm}^{-2} \text{ s}^{-1}$ and which remained for a long time the world record until the trophy went to the e+e- collider at Cornell in 1991.

Of particular importance was the vacuum system as the residual gas pressure in the vacuum chamber determines the luminosity averaged over time, which is the real figure of merit of a collider. The instantaneous ISR luminosity

$$L(t) \sim \int (I_1 \cdot I_2 / h) dt \quad (1)$$

is a function of the product of the beam currents in the two rings and of the effective height of the beams in the interaction point. Since the beams crossed horizontally, the width of the beams did not affect the luminosity. The parameters in (1) are determined by the residual gas pressure and the gas composition because the beam decay is brought about by the nuclear and single Coulomb scattering of the protons on the residual gas atoms and the growth of the effective height with time is due to multiple-Coulomb scattering.

Leading-edge vacuum technology was chosen in the design phase after the successful test in CESAR which had served also for this aspect as ISR test bed. The design value for the average vacuum pressure was 10^{-9} Torr (N_2 equivalent) and 10^{-11} Torr in the interaction points to limit the background for the experiments (Fischer, 1972). As can be seen from Fig. 7 the average pressure significantly decreased over time through a continuous effort maintained with great perseverance but also because of sound initial choices.

**Fig. 7.** The average pressure of the ISR vacuum for the years 1971-1983 (Johnsen, 1984).

The key features of the vacuum system, some introduced at the design stage, some later were: stainless steel vacuum chambers of low magnetic permeability; flanges with metal seals; gas-discharge cleaning of

PAS Symposium Subnuclear Physics, 30 Oct.-2 Nov.2011, "Birth of the 1st Hadron Collider" KH&TMT

the chambers prior to installation; bake-out in situ to 300°C; sputter ion pumps (350 l/s) combined with Ti-sublimation pumps (2000 l/s) at critical places such as the interaction regions; gauges for pressures as low as $2 \cdot 10^{-13}$ Torr; clearing electrodes to remove electrons from the potential well of the proton beam; and damping resistors in cavity-like parts of the vacuum chamber to control induced electro-magnetic fields adverse for beam stability. The result was that the typical beam loss rates eventually were in the range of a few ppm/min, orders of magnitude below the design value of 0.1 %/min.

A particular challenge were the long vacuum chambers in the detectors surrounding the interaction points as scattering and loss of secondary particles had to be minimized by using very thin walls. Self-supporting chambers with wall thickness of only 0.3 mm and 0.2 mm made respectively of Ti and stainless steel were outstanding achievements (Brunet, 1979), as illustrated in Fig. 8.

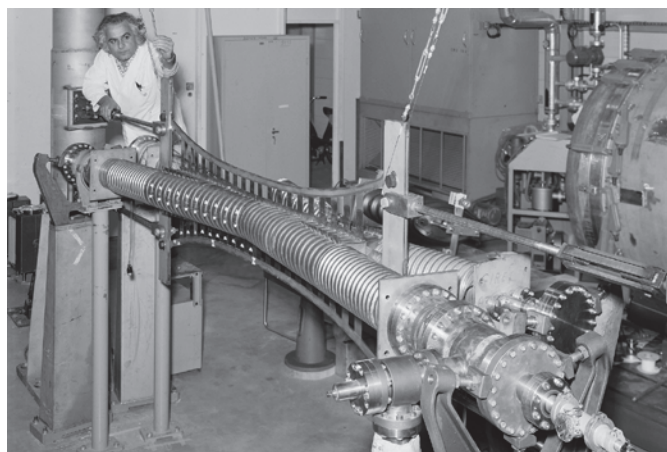


Fig. 8. Thin-walled vacuum chamber for an interaction point with its support girder.

A method had to be developed for maximizing and measuring the luminosity of the beam interaction, resulting in the establishment of the now ubiquitous method of scanning by means of controlled local bumps in the beam orbits, using small dipole correction magnets (van der Meer, 1968). In order to reduce the effective height of the beam in some interaction points and, hence, to boost the luminosity additional quadrupoles for stronger focusing of the beams, “low-beta sections”, were installed. The first one of these (Gourber, 1981) was installed in intersection I7 and later in I1. It was made up from conventional magnets while the second one (Billan, 1983) installed in I8 featured more powerful superconducting quadrupoles developed at CERN – the first time a superconducting magnet system had been used for beam handling in a working accelerator.

Some of the interaction points were equipped with large magnets for the experiments. The Split Field Magnet was the first and largest such spectrometer facility. It became operational towards the end of 1973 and was designed mainly for providing magnetic analysis in the forward region, the place of physics interest at that time. As the magnet system was acting on the ISR beams, its field was designed such as to restore the correct proton orbits. This was done by providing vertical dipole fields of opposite signs upstream and downstream of the crossing point (where it was zero), completed by 2 large and 2 small compensator magnets (Billan, 1972) as shown in Fig. 9.

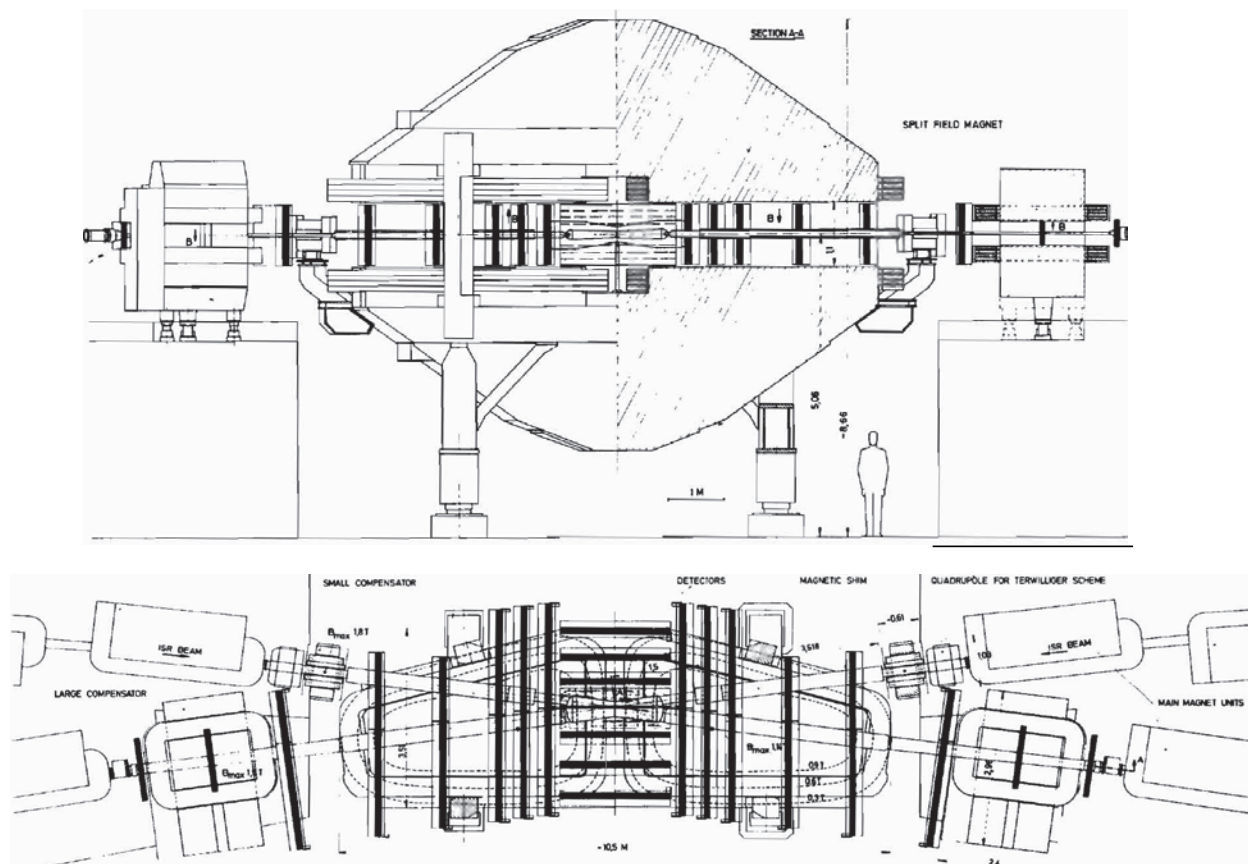


Fig. 9. Layout of the Split Field Magnet (SFM) facility. The multi-wire chambers are also shown.

The useful field volume was 28 m^3 , the maximum field 1.14 T, the gap height 1.1 m, length 10.5 m, and mass about 1000 t. The SFM detector saw the first massive application of multi-wire proportional chambers which filled the main and the large compensator magnets, and the facility was used for experiments by more than 20 collaborations.

In late 1976, a thin (1 radiation length), 3 m long, 1.5 T superconducting solenoid – one of the first of its kind – was installed at I1 (Morpurgo, 1977). With a bore of diameter 1.4 m it provided excellent capability for the study of events with large transverse momentum and several upgrades brought higher sensitivity. Good collision rates were ensured by the warm low-beta quadrupole system.

The discovery of the J/ψ in November 1974 was an important wake-up call for the community. The initial priority was to rediscover the J/ψ at the ISR, which was done soon after, but there was also a clear physics justification for a new magnetic facility with an emphasis on high- p_T phenomena, so in early 1976 the ISRC appointed a Working Party, chaired by A. Zichichi, to study the possibility. The outcome was to endorse the need, and to propose two large superconducting devices, a solenoid and a toroid. The proposal was rejected by the ISRC, but as a result of the study and a better understanding of the experimental requirements a more modest magnet based on a novel topology was proposed in early 1977. This was rapidly accepted and the Open Axial Field Magnet (OAFM) was installed and working at I8 by spring 1979 (Guignard, 1979). The 300 t magnet provided an axial field between two conical steel poles clad with copper excitation coils. It is shown in Fig. 10.



Fig.10. The Open Axial Field Magnet (OAFM) during the measurement campaign.

The result was open access to a barrel-shaped field that was favourably oriented for particles emerging from the interaction at large angles within the volume between the sides of the poles. The field at the centre was 0.5 T and the poles were hollowed out to provide space for the closest superconducting low-beta insertion magnets. Integrating innovative detectors and benefitting from increased luminosity provided by the low-beta insertion, the so-called Axial Field Spectrometer was well equipped to do excellent physics (Willis 1983, Fabjan 2011).

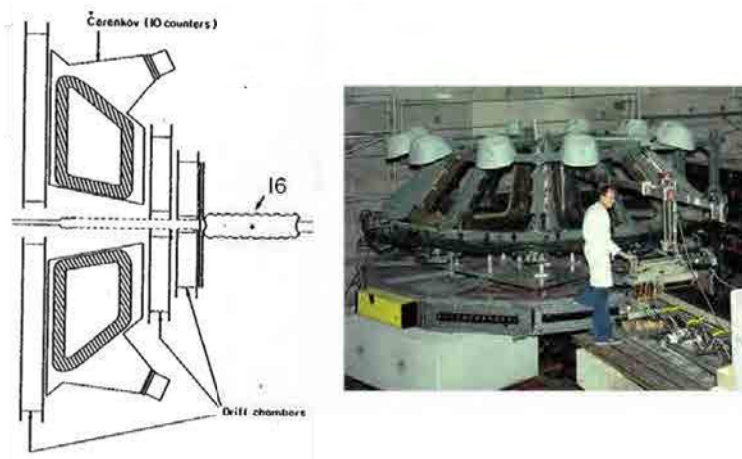


Fig. 11. The Lampshade Magnet (LSM). Left: layout at I6; right: being measured.

Other spectrometers at the ISR included the magnetized iron toroid installed at I2, used for experiments based on muon tracking, the toroidal “lampshade” magnet, shown in Fig. 11 (Giboni, 1979), and various septum magnets which shielded the beam from the analyzing field, such as the double septum magnet (Schlein, 1995) shown in Fig. 12.

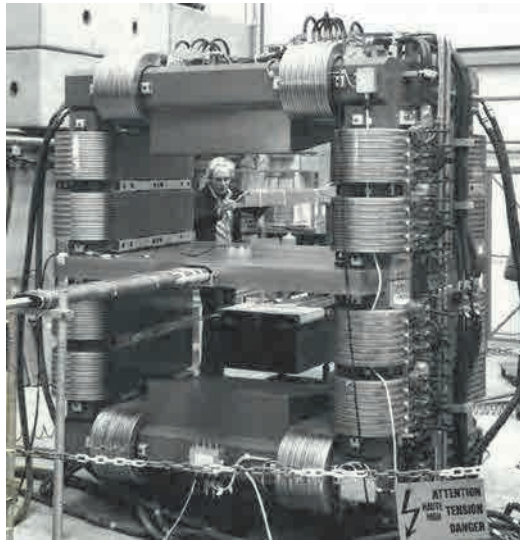


Fig. 12. The double septum magnet during the measurement campaign.

The experience with these spectrometers was instrumental in their choice for subsequent collider experiments (Taylor, 1981), and it is interesting to note that larger versions of the magnet topologies proposed by the ISR Working Party were adopted at the LHC.

A further example of a highlight in the advance of accelerator-related physics and technology was the discovery of the Schottky noise providing a non-invasive tool to monitor the position of stored beam as a function of momentum and of betatron tune in real time (Borer, 1974). The discovery was greatly facilitated by the extraordinary lifetime of the beam and it opened the door for the experimental proof of stochastic cooling of particle beams shown in Fig. 13 (Bramham, 1975). This beam cooling had been invented and suggested for the ISR to counteract beam blow-up by S.van der Meer, 1972.

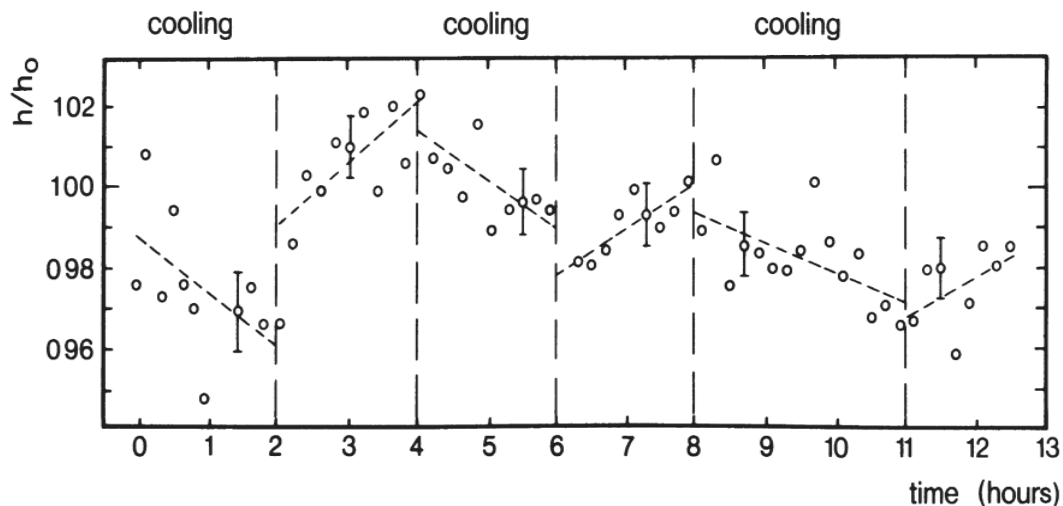


Fig. 13. Evolution of relative effective beam height as a function of time with and without stochastic cooling (Bramham, 1975)

5. Conclusion

The ISR, the first hadron collider, operating from 1971 to 1983 was a fine and unique instrument not only providing p-p collisions but also d-d, p-d, alpha-alpha, alpha-p and p-pbar collisions. It significantly advanced accelerator technology and physics. Its solid design was the broad basis for its own gradual improvement so that the design performance could be surpassed by a substantial factor, but it was also the cradle of many enabling technologies useful for the hadron colliders to come as the p-pbar collider in the SPS at CERN, the Tevatron at FNAL, RHIC at BNL, and LHC at CERN. More detailed summaries of the accelerator design and evolution can be found elsewhere (Russo, 1996), (Bryant, 2011), (Hübner 2011, 2012). The results of the experiments performed at the ISR by a vast physics community had also a considerable impact on our understanding of hadrons (Jacob 1984, Fabjan 2004, Amaldi 2011, Darriulat 2011a, 2011b). Weisskopf (1984) rightly commented at the closure ceremony of the ISR, “First considered a window into the future, but it turned out to be more”.

6. References

- Amaldi, U. (2011). Physics at small angles. *Talk given at Colloquium “40th Anniversary of the First Proton-Proton Collisions in the ISR*. January, to be published as CERN report.
- Auslender V.L. (1966). Initial experiments on Electron-Positron Storage Ring VEPP-2. In E.Crémieu-Alcan et al. (Eds), *Proc. Internat. Symposium on Electron and Positron Storage Rings, Saclay, V-4-1*.
- Billan, J., Perin R. and Sergo V. (1972). The split field magnet of the CERN intersecting storage rings. In Y.Winterbottom (Ed.), *Proc. 4th Int. Conf. on Magnet Technology, Upton, N.Y.*, 433.
- Billan J.& al. (1983). Operational experience with the superconducting high-luminosity insertion in the CERN Intersecting Storage Rings (ISR). In R.S.Taylor (Ed.), *1983 Particle Accelerator Conf., Santa Fe*, 2036.
- J.Borer & al. (1974). Non-Destructive Diagnostics of Coasting Beams with Schottky Noise. *Proc.High-Energy Accel.Conf., Stanford*, 53.
- Bramham P.& al.(1975). Stochastic cooling of a stored proton beam. *NIM* 125, 201.
- Brunet J.C. et al. (1979).The Design and Construction of Transparent Vacuum Chambers for Interaction Areas of Colliding Beam Machines. In Hendrickson (Ed.), *Proc. Particle Accelerator Conference, San Francisco*, 4063.
- Bryant P. J. (2011). The Impact of the ISR on Accelerator Physics and Technology, *Talk given at Colloquium “40th Anniversary of the First Proton-Proton Collisions in the ISR”*. January, to be published as CERN report.
- The CERN Study Group on New Accelerators (1964). Report on the Design Study of Intersecting Storage Rings (ISR) for the CERN Proton Synchrotron, *Report to Council CERN/542 and Internal Report CERN AR/Int.SG/64-9*.
- The CERN Study Group on New Accelerators (1964). Report on the Design Study of a 300 GeV Proton Synchrotron, *Report to Council CERN/563 and Internal Report AR/Int.SG/64-15*.
- Darriulat, P (2011). Physics at High Transverse Momentum, *Talk given at Colloquium “40th Anniversary of the First Proton-Proton Collisions in the ISR”*. January, to be published as CERN report.
- PAS Symposium Subnuclear Physics, 30 Oct.-2 Nov.2011, “Birth of the 1st Hadron Collider” KH&TMT

- Darriulat. P (2011). The Results Obtained with the First pp Collider ISR. *These proceedings*.
- Fabjan C.W. and McCubbin N. (2004). Physics at the CERN Intersecting Storage Rings (ISR) 1978-1983. *Physics Reports* 403-404, 165.
- Fabjan, C. (2011). Evolution and revolution: detectors at the ISR. *CERN Courier*, January.
- Fischer E. (1972). Experience Gained in the Operation of the ISR Vacuum System. *Internal Report CERN-ISR-VA/72-39 (1972)*.
- Giboni, K. & al.(1979). Diffractive production of the charmed baryon Λ^+ at the CERN ISR. *Phys. Let.*, 85B(4), 437.
- Gourber J.P., Keil E. & Pichler S.(1981) The First High-Luminosity Insertion in the ISR, In R.C.Placious (Ed.), *Proc.1981 Particle Accelerator Conference, Washington D.C.*, 1419.
- Guignard, G. and Taylor T.M. (1979). Run 1015, 22.3.79, 26 GeV/c, rings 1 and 2, Run 1017, 26.3.79, 26 GeV/c, rings 1 and 2, First running-in tests of the OAFM system. *ISR Performance Report, ISR-BOM-GG-TMT-ml*.
- Hansen S., Jones E., Koziol H. & Pentz M.J. (1965). Some Results of Stacking Experiments with the CERN Electron Storage and Accumulation Ring (CESAR), *CERN Report 65-8 (1965)*.
- Hereward H.G., Johnsen K., Schoch A. & Zilverschoon C.J. (1960). Present Ideas on 25-GeV Proton Storage Rings. *Internal Report CERN PS/Int.AR/60-35*.
- Hübner, K. (2011). Design and Construction of the ISR. *Talk given at Colloquium "40th Anniversary of the First Proton-Proton Collisions in the ISR"*. January, to be published as CERN report.
- Hübner, K. (2012). The CERN Intersecting Storage Rings (ISR). *accepted for publication in Eur.Phys.J.H*.
- Jacob M. (1984). Review of Accelerator and Particle Physics at the CERN ISR. *Report CERN 84-13, Part II*.
- Johnsen K. et al. (1963). Some Problems connected with the Use of Intersecting Proton Storage Rings. In A.A.Kolomenskij (Ed.), *Proc.4th Internat. Conf. on High-Energy Accel., Dubna*, 312.
- Johnsen K. (1973).The CERN Intersecting Storage Rings, *NIM* 108, 205.
- Johnsen K.(1973). CERN Intersecting Storage Rings (ISR), *Proc.Nat.Acad.Sci.USA*, 70, 619.
- Johnsen K.(1984). Review of Accelerator and Particle Physics at the CERN ISR. *Report CERN 84-13, part I*.
- Johnsen K.(1986). The ISR and Accelerator Physics. *Particle Accelerators* 18, 205.
- Johnsen K. (1992).The CERN Intersecting Storage Rings: the Leap into the Hadron Collider Era. In L.Hoddeson et al. (Eds.), *Third International Symposium on the History of Particle Physics at SLAC Stanford* (p. 285). Cambridge University Press.

PAS Symposium Subnuclear Physics, 30 Oct.-2 Nov.2011, "Birth of the 1st Hadron Collider" KH&TMT

- Kerst D.W (1956). Properties of an Intersecting-Beam Accelerating System. In E.Regenstreif (Ed.), *Proc.Symposium on High-Energy Accelerators and Pion Physics, Geneva, CERN, Report CERN 56-26*, 36.
- Morpurgo, M. (1977). Design and construction of a superconducting aluminium stabilized solenoid. *Cryogenics*, 17(2), 89.
- O'Neill G.K. (1956). Storage-Ring Synchrotron. In E.Regenstreif (Ed.), *Proc.Symposium on High-Energy Accelerators and Pion Physics, Geneva, CERN, Report CERN 56-26*, 64.
- O'Neill G.K. & Woods E.J. (1959). Intersecting-Beam Systems with Storage Rings. *Phys.Rev.*, 115, 659.
- The Orsay Storage Ring Group (1966). Status Report on ACO. In E.Crémieu-Alcan et al. (Eds), *Proc. Internat.Symposium on Electron and Positron Storage Rings, Saclay* II-3-1 and II-4-1.
- Pestre D. (1990). The second generation of accelerators for CERN 1956 – 1965, the decision making process. In A.Hermann et al (Eds.), *History of CERN* (Volume II 679). North Holland.
- Picasso E. & Plass G. (1989). The machine design LEP. *Europhys.News*, 20, 80.
- Russo A. (1996). The Intersecting Storage Rings: The Construction and Operation of CERN's Second Large Machine and a Survey of its Experimental Programme, In J.Knige (Ed.), *History of CERN* (Vol.III,97). Elsevier.
- Schlein, P. (1995). Evolution of forward multi-particle spectrometers at storage rings. *NIM-A*, 365, 152.
- Symon K.R. & Sessler A.M. (1956). Methods of radio frequency acceleration in fixed-field accelerators with applications to high-current and intersecting beam accelerators. In E.Regenstreif (Ed.), *Proc.Symposium on High-Energy Accelerators and Pion Physics, Geneva, CERN, Report CERN 56-26*, 44.
- Taylor, T. (1981). The choice of spectrometer magnets for LEP. *Physica Scripta*, 23, 459.
- Terwilliger K.M., Jones L.W. & Pruett C.H. (1957). Beam stacking experiments in an electron model FFAG accelerator. *Review of Scientific Instruments*, 28, 987.
- Touschek B. (1961). The Frascati storage rings. In J.S.Bell et al. (Eds.), *Proc. Internat. Conf. on Theoretical Aspects of Very High-Energy Phenomena, Geneva, CERN, Report CERN 61-22*.
- van der Meer S. (1968). Calibration of the effective beam height in the ISR. *Internal Report CERN ISR-PO/68-31*.
- van der Meer S. (1972). Stochastic damping of betatron oscillations in the ISR. *Internal Report CERN-ISR-PO-72-31*.
- Wideröe R. (1953). Anordnung zu Herbeiführung von Kernreaktionen. *Bundesrepublik Deutschland, Deutsches Patentamt Patenschrift Nr.876279*.
- Willis, W. (1983). Experience of the axial field spectrometer at the CERN ISR. In S.C.Stewart & P.Némethy (Eds.), *Proc. DPF Workshop on Collider Detectors, LBNL, report LBL-15973*, 5.

PAS Symposium Subnuclear Physics, 30 Oct.-2 Nov.2011, "Birth of the 1st Hadron Collider" KH&TMT

THE INFN CONTRIBUTION TO SUBNUCLEAR PHYSICS IN EUROPE

■ ENZO IAROCCHI

Laboratori Nazionali di Frascati – INFN
Dipartimento SBAI – Sapienza University, Rome

Abstract

The INFN contribution to subnuclear physics in Europe will be reviewed, starting with the birth of the Institute and the following creation of the Frascati Laboratory, which has been the national path to ever-lasting contributions to subnuclear physics in the field of electron-positron physics. Italy has played a leading role in the creation of CERN, and INFN has represented both the natural channel for the Italian support to its development and for the exploitation, by the Italian subnuclear physics community, of the unique opportunities offered by the European Laboratory. The participation to CERN has also facilitated the development of the INFN capacity of establishing international collaborations, which has been particularly effective in the case of the DESY Laboratory in Hamburg.

1. INFN and the Frascati National Laboratory

The roots of the *Istituto Nazionale di Fisica Nucleare* can be traced back to the pre-war years. In particular, INFN may be seen as the realization of Fermi's vision of creating a national institute, in order to establish in Italy the conditions for building accelerators, the emerging powerful tool of subatomic physics.

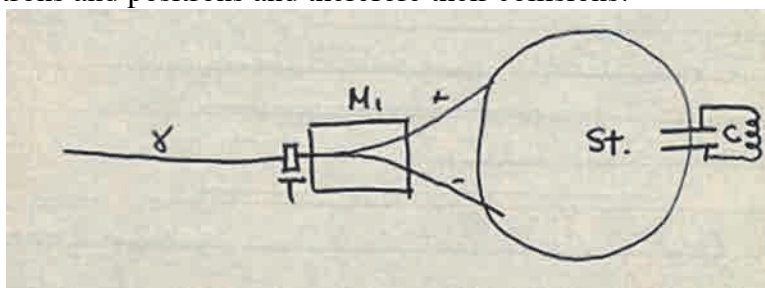
INFN was created in 1951, as the result of the joint effort of 4 University groups, from Milan, Padua, Rome, and Turin respectively. The first President was Gilberto Bernardini, who in 1954 took the decision that the first accelerator had to be a 1100 MeV electron-synchrotron – quite at the frontier in those years – to be built at Frascati, with Giorgio Salvini as director of the new laboratory.

In this way, initially, INFN consisted of 4 University *Sezioni* and one National Laboratory. The Institute grew in time according to the initial model, up to the present 20 *Sezioni* and 4 National Laboratories.

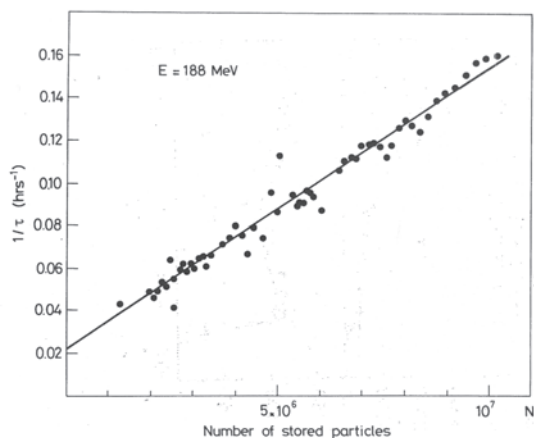
It is not easy to manage an institution combining education and research centers. In most countries, in fact, they are kept separate. INFN has succeeded in realizing the initial vision of a single integrated research community, which presently comprises around 5.000 people, from the graduate students of the universities to the engineers and technicians engaged at the laboratory infrastructures.

The Frascati electron-synchrotron started operation in 1959 giving rise to a series of experiments of international resonance. The achievement had also the merit of creating the right environment of scientific expertise and enthusiasm for the critical event in the history of Frascati, which was the conception of AdA. It was an extremely prompt decision, taken in a single meeting in February 1960, at the Frascati Laboratory, where Bruno Touschek presented his idea of a colliding beam experiment with electrons and positrons. A small team immediately formed, with the task of building a small prototype, which was ready, with beams circulating, in one year [1].

AdA, from *Anello di Accumulazione*, the Italian for Storage Ring, is a very elegant acronym, but does not reflect the original content of the idea. Actually, the idea of Storage Rings, for achieving the kinematical advantage of symmetric beam-beam collisions, was rather old: a paper by Gerard O'Neill of 1956 is usually quoted [2], although already in 1943 Rolf Wideroe had applied for patenting the idea in Germany. For instance, one would think of storing electrons in two distinct equal rings, tangent at one point, where electron-electron collisions could take place, with the total energy available for electron-electron interactions. Bruno Touschek combined the above idea, with that of colliding electrons and positrons, that is an elementary particle against its antiparticle, in order to produce time-like photons by annihilation. That meant a much more powerful instrument from the point of view of physics. At the same time, he conceived the idea of achieving such enriched physics potential in a much simpler way, by storing both beams, one against the other, in a single ring, as shown in figure 1, leaving to the CP symmetry of QED to guarantee the same equilibrium orbit for both the electrons and positrons and therefore their collisions.

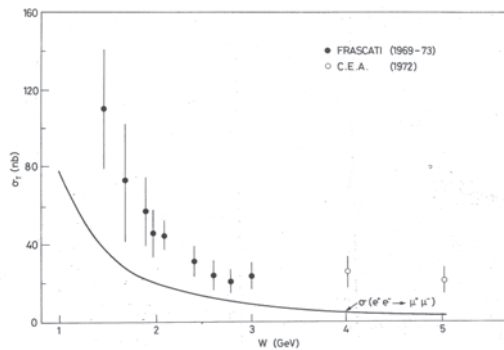


AdA was operational in one year, in February 1961 at Frascati. It consisted of a 4 meter long circular vacuum chamber and an RF cavity, mounted inside a magnet, as shown in figure 2, which allowed to store 200 MeV electrons and positrons respectively. The particles were produced through a minimal arrangement, by converting the gammas of the beam produced at the electron-synchrotron, on two small targets inside the doughnut. Storage Ring operation was demonstrated in a few months. At the very low intensities that could be achieved with the Frascati photon beam, so high a vacuum was achieved as to allow 50 hours lifetime of the circulating beams [3]. Afterwards AdA was moved to LAL at Orsay, whose LINAC allowed for higher intensities. A dependence of lifetime on intensity was discovered there, due to what today is known as Touschek effect, that is the loss of particles due to scattering between particles inside a circulating bunch. Anyhow, a lifetime of 6 hours was still available at the highest intensity, as shown in figure 3 [4]. Finally, the demonstration of collider operation was achieved in 1964 by the observation of electron-positron annihilation into electron-positron and one photon, at 400 MeV total energy and $10^{25}/\text{cm}^2\text{sec}$ luminosity [5]. This achievement started the era of electron-positron physics.

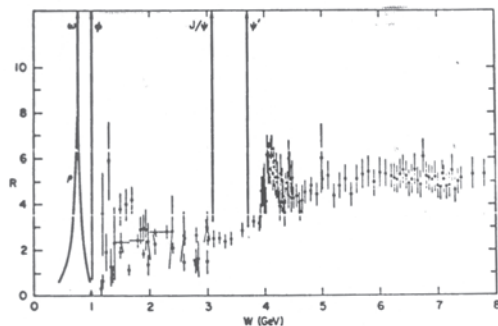


ADONE, the big AdA, was the first project to be initiated, at Frascati, actually even before the small prototype was turned on. It started operation in 1969, preceded by ACO at Orsay. There was, in fact, a rapid multiplication of successful competing initiatives, as can be seen in figure 4, so that it took less than 30 years to go from the original idea to LEP, the largest accelerator based on the AdA model. In fact the 200 GeV total energy of LEP is also the highest practically possible storage-ring collider energy, due to radiation losses. Further progress at the energy frontier is left to the linear colliders.

The ADONE experiments gained center stage when in 1972 they announced the observation of an unexpectedly large multihadronic production as compared with the muon pair production. The related overall ADONE result is reported in figure 5 [6]. The further study of this phenomenon at the other electron-positron colliders, combined with other experimental facts, led finally to establishing the colored quark model. In fact, the surprise at ADONE was about a factor of three, which is the number of quark colors.



In a couple of years, however, it became clear that the energy range chosen for ADONE had not been the most lucky, being situated just in between the ρ , ω and ϕ energy region studied in detail at ACO and, more important, the unbelievably rich region just above the ADONE maximum energy of 3 GeV, as shown in figure 6 [6], starting at 3.1 GeV, just 3% more energy, where the fundamental discovery of the J/Ψ took place in November 1974. Following the announcement, it took one day to observe it at Frascati, by pushing machine operation beyond the nominal design parameters. The combined Frascati paper was published in the same issue of December 1974 of PRL that reported the Brookhaven and SLAC discovery papers. Among the experiments at ADONE, there was also the one led by Antonino Zichichi searching for a third lepton, the heavy lepton HL, which was just another particle out of reach at the ADONE energies (see the paper by Alessandro Bettini in these same proceedings).



At ADONE there were three generations of experiments, with an inevitable progressive loss of visibility of the laboratory, a rather common fate of accelerator laboratories, which also created an unbalance between home and foreign activities of INFN.

In the 1990s the Institute caught the opportunity offered by the development of the electron-positron factories, which opened new physics prospects by advancing the luminosity frontier, aiming at high precision measurements. Such a research line was clearly favored by the increasing difficulty in the progress of the energy frontier. In 1990 INFN decided to build a ϕ -Factory at Frascati, DA ϕ NE, a 1 GeV electron-positron collider, that is 1/3 the ADONE energy, so that it could simply replace the latter in the same building, as shown in figure 7. DA ϕ NE results on kaon physics, which in particular included a very accurate measurement of the Cabibbo angle [7], brought Frascati back on the international scene of subnuclear physics. The new accelerator construction had also the merit of reviving the Frascati role in accelerator science, with the recent idea of Crab Waist, which promises a generalized advance of the collider luminosity frontier, through an improved control of instabilities of bunch crossing at an angle [8]. The method has been successfully tested on DA ϕ NE by achieving a record luminosity of $5 \cdot 10^{32} \text{cm}^{-2} \text{s}^{-1}$.

2. INFN and CERN

After having played a critical role in the creation of the European organization and its accelerator Laboratory in Geneva, Italy characterized itself, as widely recognized within the Member States community, by the positive attitude systematically expressed in the governing bodies of CERN, notably in supporting new initiatives and projects, or in facing difficult situations. It was natural for INFN, given in particular the composition of its community, to represent the overall Italian participation to CERN activities.

A constant visible presence of INFN physicists, engineers and technicians, has developed and consolidated in time in the management, theory, experiments, and infrastructures of CERN.

The most significant indication of the substantial role of INFN at CERN probably is the frequent promotion and implementation of CERN special programs.

Such front-line role was made possible by the initiative of the INFN physicists, supported by adequate financial means. In the latter respect there is a fact worth being recalled. The 5-year plan 1979-1983 marked a substantial change of pace in the funding of INFN, which was one of the achievements of Antonino Zichichi as president of the Institute in those years. The increase of funds had an obvious impact on the life of the Institute and in particular it allowed the construction of new instrumental infrastructures. As an example, in 1981 the construction of the Superconducting Cyclotron in Milan was started, which also initiated the close collaboration of INFN with Italian industries in accelerator R&D and construction. Such a promotion of industrial partnership played a key role in enhancing the INFN role as a leading partner in international projects, first of all at CERN, and also at DESY and other laboratories throughout the world.

The contribution of Italian people at CERN takes place mostly through the activity of INFN teams carrying out experiments at CERN accelerators, and also through the direct presence in the CERN staff of physicists and engineers from the INFN community. As an example in this sense one can quote the discovery of nuclear antimatter at the proton-synchrotron (see figure 8).

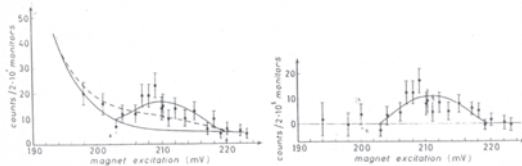
IL NUOVO CIMENTO Vol. XXXIX, N. 1 1° Settembre 1965

Experimental Observation of Antideuteron Production.

T. MASSAM, TH. MÜLLER (*), B. RIGHINI, M. SCHNEEGANS (*) and A. ZICHICH
CERN - Geneva

(ricevuto il 13 Marzo 1965)

Summary. — The results of an experiment which show the existence of antideuterons in the production process proton-beryllium are reported.



The INFN presence in CERN activities is typically very wide, as compared with other countries. In the case of the LHC experiments it is in fact the widest participation. The distinctive quality and style of the contribution of the INFN groups is influenced by the traditional engagement of its researchers in developing sub-nuclear physics techniques, which in the first place means detectors and accelerators, including all related devices and software.

INFN is probably the only institution, in the international framework, to have a research line dedicated to instrumentation R&D, along with the sub-nuclear, astro-particle, nuclear and theoretical research lines.

Such technological research line is also the natural channel for promoting the applications of the subnuclear physics techniques to other disciplines and for the related technological transfer to the industry. Autonomous special programs are set up in cases of particular relevance, such as applied superconductivity. In developing this strategy, there is a remarkable synergy with the parallel CERN effort.

In various papers in these proceedings there are many examples of detectors developed by INFN, like BOREXINO and OPERA at the Gran Sasso Laboratory, or subsystems of the LHC detectors and of the AMS detector.

Detector developments include also all those devoted to signal readout, event reconstruction and data sharing through networking. As an example for the latter case, in 1989, a few weeks before the first collisions at LEP, INFN established the first high-speed connection with CERN based on a national information network. Furthermore, when in 1990 the Web was born at CERN, the INFN group in Rome was among the first teams that dialogued with CERN. That experience was the basis for the analogous leading role of INFN in the development of the Grid at LHC, including its application to other fields.

Accelerator science and technology in the INFN started at Frascati and then diffused throughout the Institute, not only in the other two accelerator laboratories of Catania and Legnaro, but also in many university *sezioni*, like Milan, Genoa and Naples.

Since many years, the most relevant R&D activity takes place in the field of superconducting technology. Its origin may be easily situated in 1981 when, as previously recalled, the construction of a SC Cyclotron at Milan-LASA was started, with the coordinated participation of Italian industries. Once built, the Cyclotron was moved to the LNS Laboratory of INFN in Catania, where it is presently operating. The SC Cyclotron project created also the basis for the Italian contribution to HERA (see the paper by Albrecht Wagner in these proceedings).

Along the same lines in 1988 an agreement INFN-CERN was set-up, in order to promote and develop industrial partnership in superconducting technology. The most important programs

were related to the production of the LEP200 RF cavities and the LHC dipoles. It was a complex of coordinated activities, carried out by various CERN-INFN groups, of Milan-LASA, Genoa, LNL, and Naples.

One of the highlights of the program was the production of the first 15m LHC dipole prototype, shown in figure 9, which involved the coordinated participation of three Italian firms that, by the way, are the same involved twenty years before by INFN in the construction of the SC Cyclotron mentioned above.

3. INFN and DESY.

DESY was initially established, as an autonomous particle physics facility, with the aim of providing accelerator infrastructure to German universities, and the start-up project, like at Frascati, was an electron-synchrotron.

DESY rapidly became a research center of international visibility, notably with the success of the DORIS electron-positron collider, till the creation of what became known as the “HERA model” of international co-operation.

It was therefore natural for INFN to set-up with DESY a relation that was structurally analogous to the one established with CERN, concerning both experiments and infrastructures, and including industrial partnership. In particular, the INFN superconductivity program was the basis for the Italian participation to HERA, as already recalled.

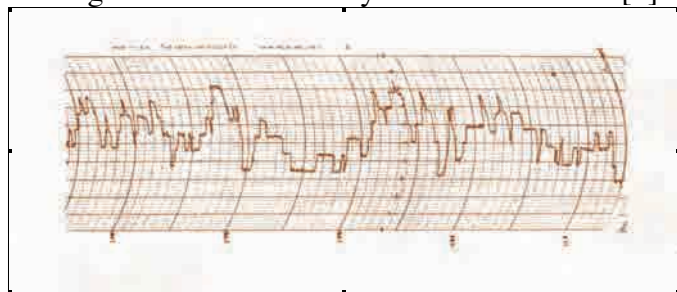
Another line of collaboration will be addressed in what follows, concerning the R&D towards the project of a new high-energy electron-positron Linear Collider, in which case the major INFN contribution came from Frascati and Milan groups.

The collaboration with DESY in this field was certainly favored by the common long-standing tradition in electron-synchrotrons and electro-positron colliders, including also their applications to photon science. Actually, those applications are an outstanding spin-off of subnuclear physics to other science fields and industry.

Let me briefly recall the crucial steps in the development of radiation sources by accelerated electrons.

In 1947 there was the first observation of the light emitted by circulating electrons, in a small electron-synchrotron, from which that light got its name.

In 1961 with AdA there was the first light from a stored beam, whose detection played a crucial role for beam diagnostics in the collider prototype: single circulating particles going in and out could be seen, as shown in figure 10, even directly by eye. In particular, the measurement of the light intensity was a crucial tool for the first luminosity measurement, although that word had not yet been introduced [5].



AdA, therefore, was also the prototype of storage ring light source. In fact, one has to notice that Synchrotron Light machines are usually synchrotrons in the accelerating phase but they

are operated as storage rings in the phase of delivering the light beams to the experimental users. ADONE and DORIS, as many other electron-positron colliders, concluded their career as the first respective national Synchrotron Light facilities.

In recent years, a third revolution in photon science has taken place, again promoted by sub-nuclear physics, which is based on the lucky technological convergence in the development of electron-positron linear colliders on the one hand and the SASE-FEL idea on the other.

In the Self-Amplified Stimulated Emission scheme, extremely short and brilliant – and at the same time rather monochromatic and coherent – radiation pulses are created, by sending an electron beam through an extremely long and fine-grained undulator. In such a layout, differently from the case of the classical Free Electron Lasers, there are no mirrors. Therefore the radiation wavelength can be in the X-ray region of the spectrum. It is worthwhile mentioning that one of the authors of the idea [9], Claudio Pellegrini, was the synchrotron radiation expert of the ADONE group.

A 20 year long collaboration with DESY has taken place within the R&D for ILC, in combination with the development of the SASE-FEL technique, which involved the Italian industry, one example being shown in figure 11. In particular the collaboration concerned, the Tesla Test Facility, which has become the FLASH SASE-FEL facility, presently operational at DESY. There are several SASE-FEL projects in the world. LCLS is already operational at SLAC in the U.S. and SPring-8 in Japan. The most ambitious project is the European X-Fel in construction at DESY, with an Italian firm as one of the SC cavity producers. A small SASE-FEL prototype, SPARC, is operating at Frascati producing light in the green region of the spectrum [10] (see figure 12).

Concluding remarks

The INFN contribution to particle physics in Europe has been addressed in this paper. One can well imagine a similar topic addressed with the subjects inverted. In other words there is a mutual value in that contribution, because of the immense return to the Institute and Italy at large, which resulted from it.

In particular, Italy profited from the combination of research and education, which is built in the INFN organization, enriched by the INFN action in promoting innovation in the national industry.

References

- Bernardini, C., Corazza G. F., Ghigo, G., Touschek, B. (1960). The Frascati Storage Ring. *Nuovo Cimento*, 18, 1293-1295.
- O'Neill, G. K. (1956). Storage-Ring Synchrotron: Device for High-Energy Research. *Physical Review*, 102, 1418-1419.
- Bernardini, C., Bizzarri, U., Corazza, G. F., Ghigo, G., Querzoli, R., Touschek, B. (1962). Progress Report on AdA (Frascati Storage Ring). *Nuovo Cimento*, 23, 202-207.
- Bernardini, C., Corazza, G. F., Di Giugno, G., Ghigo, G., Haissinsky, J., Marin, P., Querzoli, R., Touschek, B. (1963). Lifetime and beam size in a storage ring. *Physical Review Letters*, 10, 407-409.
- Bernardini, C., Corazza, G. F., Di Giugno, G., Haissinsky, J., Marin, P., Querzoli, R., Touschek, B. (1964). Measurement of the rate of interaction between electrons and positrons. *Nuovo Cimento*, 34, 1473-1493.
- Conversi, M. (1976). Electron-positron Physics. *Symposium on "Frontier Problems in High-Energy Physics"*, Pisa "Scuola Normale Superiore" 4-5 June, and CERN, Geneva, 9 September
- Bossi, F., De Lucia, E., Lee-Franzini, J., Miscetti, S., Palutan, M., and KLOE Collaboration (2008). Precision Kaon and Hadron Physics with KLOE. *Rivista del Nuovo Cimento*, 34, 531-623
- Raimondi, P., Zobov, M., Shatilov, D. (2008). Suppression of beam-beam resonances in Crab Waist collisions. *Proceedings EPAC08, Genoa, Italy (European Physical Society Accelerator Group)*, 2620.
- Bonifacio, R., Pellegrini, C., Narducci, L. (1984). Collective Instabilities and High Gain Regime Free Electron Laser. *Optics Communication*, 50, 373.

Ferrario, M. et al (2009). Recent results of the SparC-FEL Experiment. *Proceedings of the Free Electron Laser Conference (FEL 2009), Liverpool, UK*, 734.

Figure captions

1. Sketch of AdA by Bruno Touschek.
2. AdA at Frascati.
3. Inverse-lifetime $1/\tau$ (hrs^{-1}) vs N , the number of stored particles in a beam, at the energy of 188 MeV in AdA.
4. The energy and luminosity of electron-positron ring colliders (red), factories (yellow), and linear colliders (green).
5. Multihadron production as observed with ADONE.
6. Energy dependence of the ratio R between total hadronic cross-section and muon pair cross-section from electron-positron annihilation.
7. ADONE (above) and DAΦNE (below) installed in the same building.
8. The discovery of nuclear antimatter at the CERN proton-synchrotron.
9. The 15 m long LHC superconducting dipole prototype.
10. Current plot of a photomultiplier detecting the light radiated by few electrons circulating in AdA.
11. SC Cavity module, built by an Italian firm under the guidance of INFN, within the ILC R&D, installed at KEK, Japan.
12. The spectrum of SASE-FEL radiation produced in SparC, at different undulator lengths.

FROM D-BARS TO ANTIMATTER- & HYPERCLUSTERS FROM THE STARS TO FAIR IN EUROPE

■ J. STEINHEIMER¹, H. STÖCKER^{1,2,3}, ZHANGBU XU⁴

¹ FIAS, Johann Wolfgang Goethe University, Frankfurt am Main, Germany

² Institut für Theoretische Physik, Goethe-Universität, Max-von-Laue-Str. 1,
D-60438 Frankfurt am Main, Germany

³ GSI Helmholtzzentrum für Schwerionenforschung GmbH, Planckstr. 1, D-64291
Darmstadt, Germany

⁴ Physics Department, Brookhaven National Laboratory, Upton, New York 11973, USA

Abstract

The Facility for Antiproton and Ion Research FAIR at Darmstadt/Germany will provide worldwide unique accelerator and experimental facilities allowing for a large variety of unprecedented fore-front research in hadron, nuclear, and atomic physics and applied sciences which will be described in this article briefly. As an example the article presents research efforts on strangeness at FAIR using heavy ion collisions, exotic nuclei from fragmentation and antiprotons to tackle various topics in this area. In particular the creation of hypernuclei as well as metastable exotic multi-hypernuclear objects (MEMOs) and anti-matter will be investigated. While stable nuclei, such as alpha and iron, are abundant and accessible in nature, antimatter nuclei that are heavier than the antiproton have been observed only as rare products of interactions at particle accelerators. High-energy nuclear collisions recreate conditions in the universe microseconds after the Big Bang. The subsequent rapid expansion of Quark-Gluon Plasma (QGP) in nuclear collisions is significantly different from the case of the Big Bang. This decouples matter and antimatter before annihilation, and provides an ideal laboratory for producing and studying heavy antimatter. We present the recent antimatter discoveries and their implications for nuclear and astrophysics.

The FAIR Project

The Facility for Antiproton and Ion Research, FAIR (Gutbrod 2006, Henning 2008, Stöcker 2008), will provide an extensive range of particle beams from protons and their antimatter partners, antiprotons, to ion beams of all chemical elements up to the heaviest one, uranium, with in many respects world record intensities. As a joint effort of 16 countries the new facility builds, and substantially expands, on the present accelerator system at GSI, both in its research goals and its technical possibilities. Compared to

the present GSI facility, an increase of a factor of 100 in primary beam intensities, and up to a factor of 10000 in secondary radioactive beam intensities, will be a technical property of the new facility.

The start version of FAIR, the so called *Modularized Start Version* includes a basic accelerator as well as three experimental modules as it is colored illustrated in figure 1. The superconducting synchrotron SIS100 with a circumference of 1100 meters and a magnetic rigidity of 100 Tm is at the heart of the FAIR accelerator facility. Following an upgrade for high intensities, the existing GSI accelerators UNILAC and SIS18 will serve as an injector. Adjacent to the SIS100 synchrotron are two storage-cooler rings and experiment stations, including a superconducting nuclear fragment separator (Super-FRS) and an antiproton production target. By delivering first beams FAIR will supply rare isotope beams (RIBs) and antiproton beams with excellent intensity and quality. Moreover, after the start phase the facility will be upgraded by experimental storage rings enhancing capabilities of secondary beams and by the SIS300 providing particle energies 20-fold higher compared to those achieved so far at GSI as additional funds become available.

After the official launch of the project on November 7th, 2007, the FAIR scientific community, the partner countries and the host State of Hesse are now eager to see FAIR materialise. Because of the long lead times for civil-construction planning civil work for the first buildings of FAIR will start in the fourth quarter of 2010 earliest. First beams will be delivered in 2015/2016.

The Experimental Programme of FAIR

The main thrust of FAIR research focuses on the structure and evolution of matter on both a microscopic and on a cosmic scale. The approved FAIR research programme embraces 14 experiments, which form the four scientific pillars of FAIR and offers a large variety of unprecedented forefront research in hadron, nuclear, atomic and plasma physics and applied sciences. Already today, over two 2500 scientists and engineers are involved in the design and preparation of the FAIR experiments. They are organized in the experimental collaborations APPA, CBM, NuSTAR, and PANDA.

Figure 1: On the left hand side the existing GSI facility is shown. Colored displayed is the so called Modularized Start Version of FAIR including module 0, 1, 2 and 3~. Coloring: the 100 Tm superconducting synchrotron SIS100 (module 0) - green; the experimental area for CBM/HADES (module 1) - red; the NuSTAR facility including the Super-FRS (module 2) - yellow; The Antiproton facility



including the PANDA experiment (module 3) - orange. Not shown is the additional experimental area above ground for the APPA community (module 1). These colored parts are financed within the presently available firm funding commitments of about 1030 million EURO. Additional site related costs of about 100 million EURO will be covered by the Federal Government of Germany and the State of Hesse. The Modularized Start Version secures a swift start of FAIR with outstanding science potential for all scientific pillars of FAIR within the current funding commitments. After the start phase the e.g. NESR, RESR or the SIS300 will be built as additional funds become available.

APPA -- Atomic Physics, Plasma Physics and Applications

Atomic physics with highly charged ions (Stöhlker 2007) will concentrate on two central research themes: a) the correlated electron dynamics in strong, ultra-short electromagnetic fields including the production of electron-positron pairs and b) fundamental interactions between electrons and heavy nuclei – in particular the interactions described by Quantum Electrodynamics, QED. Here bound-state QED in critical and supercritical fields is the focus of the research programme. In addition, atomic physics techniques will be used to determine properties of stable and unstable nuclei and to perform tests of predictions of fundamental theories besides QED.

For Plasma physics the availability of high-energy, high-intensity ion-beams enables the investigation of High Energy Density Matter in regimes of temperature, density and pressure not accessible so far

(Lomonosov & Tahir 2006). It will allow probing new areas in the phase diagram and long-standing open questions of basic equation of state research can be addressed.

The biological effectiveness of high energy and high intensity beams was never studied in the past. It will afford to investigate the radiation damage induced by cosmic rays and protection issues for the Moon and Mars missions. Furthermore, the intense ion-matter interactions with projectiles of energies above 1 GeV/u will endorse systematic studies of material modifications.

CBM HADES – Compressed Baryonic Matter

Violent collisions between heavy nuclei promise insight into an unusual state in nature, that of highly compressed nuclear matter. In addition to its relevance for understanding fundamental aspects of the strong interaction, this form of matter may exist in various so far unexplored phases in the interior of neutron stars and in the core of supernovae. The mission of high-energy nucleus-nucleus collision experiments worldwide is to investigate the properties of strongly interacting matter under these extreme conditions. At very high collision energies, as available at RHIC and LHC, the measurements concentrate on the study of the properties of deconfined QCD matter at very high temperatures and almost zero net baryon densities.

Complementary, HADES (HADES 2009) and CBM (Senger 2008) at SIS100/300 will explore the QCD phase diagram in the region of very high baryon densities and moderate temperatures. This approach includes the study of the nuclear matter equation-of-state, the search for new forms of matter, the search for the predicted first order phase transition between hadronic and partonic matter, the QCD critical endpoint, and the chiral phase transition, which is related to the origin of hadron masses. Vector mesons decaying into di-lepton pairs, strangeness and charm are promising diagnostic tools. It is intended to perform comprehensive measurements of hadrons, electrons, muons and photons created in collisions of heavy nuclei. Most of the rare probes like lepton pairs, multi-strange hyperons and charm will be measured for the first time in the FAIR energy range. The goal of the CBM/HADES experiment is to study rare and bulk particles including their phase-space distributions, correlations and fluctuations with unprecedented precision and statistics. These measurements will be performed in nucleus--nucleus, proton--nucleus, and proton--proton collisions at different beam energies.

NuSTAR – Nuclear Structure, Astrophysics and Reactions

The main scientific thrusts in the study of nuclei far from stability are aimed at three areas of research: (i) the structure of nuclei, the quantal many-body systems built by protons and neutrons and governed

by the strong force, towards the limits of stability, where nuclei become unbound, (ii) nuclear astrophysics delineating the detailed paths of element formation in stars and explosive nucleosynthesis that involve short-lived nuclei, (iii) and the study of fundamental interactions and symmetries exploiting the properties of specific radioactive nuclei.

The central part of the NuSTAR programme at FAIR (NuSTAR 2005) is the high acceptance Super-FRS with its multi-stage separation that will provide high intensity mono-isotopic radioactive ion beams of bare and highly-ionized exotic nuclei at and close to the driplines. This separator, in conjunction with high intensity primary beams with energies up to 1.5 AGeV, is the keystone for a competitive NuSTAR physics programme. This opens the unique opportunity to study the evolution of nuclear structure into the yet unexplored territory of the nuclear chart and to determine the properties of many short-lived nuclei which are produced in explosive astrophysical events and crucially influence their dynamics and associated nucleosynthesis processes.

PANDA -- AntiProton ANnihilation in DArmstadt

The big challenge in hadron physics is to achieve a quantitative understanding of strongly interacting complex systems at the level of quarks and gluons. In p anti- p -annihilation, particles with gluonic degrees of freedom as well as particle-antiparticle pairs are copiously produced, allowing spectroscopic studies with unprecedented statistics and precision. The PANDA experiment at FAIR (Fohl 2008) will bring new fundamental knowledge in hadron physics by pushing the precision barrier towards new limits. The charmonium (c anti- c) spectroscopy will take advantage by precision measurements of mass, width, decay branches of all charmonium states. Particular emphasis is placed on mesons with open and hidden charm, which extends ongoing studies in the light quark sector to heavy quarks, and adds information on contributions of the gluon dynamics to hadron masses. The search for exotic hadronic matter such as hybrid mesons or heavy glueballs gains enormously by precise scanning of resonance curves of narrow states as well. Recently, this field has attracted much attention with the surprise observation at electron-positron colliders of the new X , Y and Z states with masses around 4 GeV. These heavy particles show very unusual properties, whose theoretical interpretation is entirely open. Additionally the precision gamma-ray spectroscopy of single and double hypernuclei will allow extracting information on their structure and on the hyperon-nucleon and hyperon-hyperon interaction.

The creation of antimatter

The history of antimatter is a brief and fascinating history of scientific discoveries. In 1928, Dirac predicted the existence of negative energy states of electrons based on the application of symmetry principles to quantum mechanics. The states were recognized as antimatter partner of electrons (positrons) discovered by Anderson in the cosmic rays in 1932. The constructions of accelerators have provided the necessary energy and luminosity for the discoveries of heavier antimatters. The extension of Dirac's theory implied the existence of antimatter protons and neutrons, and both particles were discovered at Bevatron in 1955.

The scientific investigation of antimatter has three major focuses since then:

- a) Antiparticles are produced as by-products of high-energy particle collisions. Many particle and antiparticle pairs are created in such collisions through strong or electromagnetic processes. Antiparticles are merely part of the energy and chemical (baryon, isospin or lepton) conservation laws.
- b) Precise measurements of particle and antiparticle properties, which can provide insights into the fundamental CPT conservation and baryon asymmetry in the Universe.
- c) Constructing more complex system of antimatter.

It is clear that all these three topics are related to each other with a different emphasis for each subject. Although it may sound trivial to define what antimatter is, its definition is not without controversy. There are particles and antiparticles (such as μ^- and μ^+), which annihilate when put together. However, neither of them annihilates the ordinary matter. Antonino Zichichi (2008) has argued that there is a basic difference between antiparticle and antimatter, and even anti-hydrogen is not antimatter. In this proceeding, we mainly focus on constructing more complex system of antimatter: antinuclei and antihypernuclei.

After the discoveries of antiprotons and antineutrons, one of the important questions was whether the building blocks in the antimatter world have the same force to glue together the antinucleons into nuclei and eventually anti-atoms by adding positrons. Figure 2 depicts the history of the discoveries of antimatter. We noted that the antimatter project span eight decades with four decades per step in our discoveries. There are effectively three periods in these 80 years. The first discovery was made in the cosmic ray in 1932. The second period of discovery was between 1955 to 1975 when the fixed target accelerators provided increasing intensity and energy for producing heavier and heavier antimatter. The third period was made possible with high energy relativistic heavy-ion collider at RHIC and at Large Hadron Collider. At the same time, the technology advance also enables us to decelerate antiproton beams and trap antimatter hydrogen. The necessity of the long term commitment was expressed by Walt Greiner (2001) in <<Fundamental Issues in the Physics of Elementary Matter>>: "The extension

of the periodic system into the sectors of hypermatter (strangeness) and antimatter is of general and astrophysical importance. ... The ideas proposed here, the verification of which will need the **commitment for 2-4 decades of research, could be such a vision** with considerable attraction for the best young physicists.”

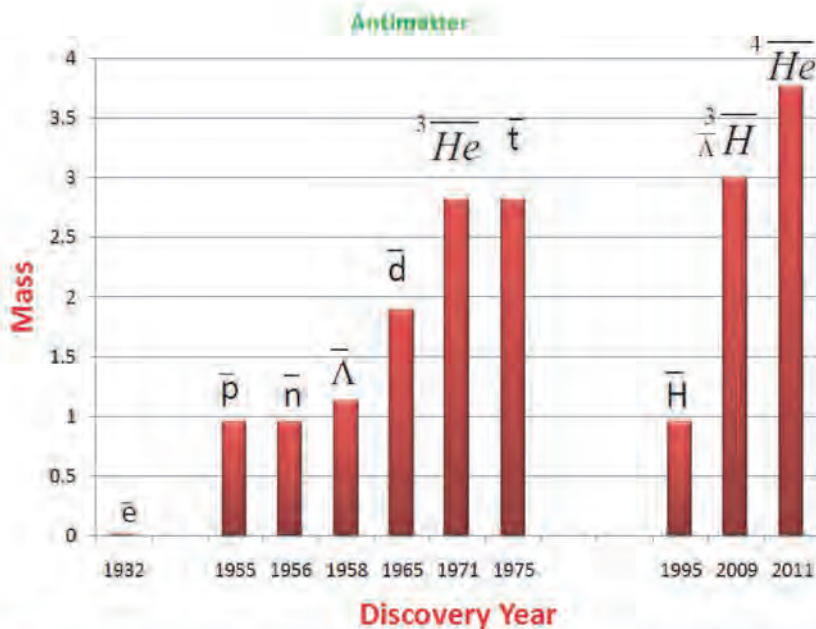


Figure 2: discovery year of the antimatter and its associated mass

Understanding the asymmetry of antimatter and matter is one of the frontiers of modern physics. Nuclei are abundant in the universe, but anti-nuclei with $|A| \geq 2$ haven't been found in nature. Relativistic heavy ion collisions, simulating the condition at the early universe, provide an environment with abundant antinucleons and antihyperons and produce antinuclei and antihypernuclei by coalescing them together (STAR 2005). This offers the first opportunity for discovery of antihypernuclei (STAR 2010) and heavier antinuclei (STAR 2011) having atomic mass number (or baryon number) $|A| > 2$. The production of antimatter nuclei can be explained by coalescence of antiprotons and antineutrons close in position and momentum. Figure 3 compiles all the antideuteron production in e^+e^- , γp , pp , pA and AA collisions (Liu & Xu 2006). The results are shown for $d\bar{b}/p\bar{b}$ ratio as a function of beam energy. One can see that this ratio increases from 10^{-5} at low energy to 10^{-3} at high energy. Each additional antinucleon into the heavier antimatter decreases its production rate by that same penalty factor. At center of mass energy of 100 GeV and above, this factor is relatively flat at slightly below 10^{-3} . It is interesting to note that this effective measure of antibaryon density shows no difference among pp , pA

and AA collisions. In heavy ion collisions, more antiprotons are produced in each collision than in pp collisions. However, if more pp collisions are collected to match the amount of antiproton yields in heavy-ion collisions, one can essentially produce same amount of heavy antimatter in pp and heavy-ion collisions. Now we understand that there are two deciding facts that RHIC discovered the last two heavy antimatters: sufficient energy to provide the highest antibaryon density for antinuclear production, and high luminosity heavy-ion collisions for effective data collection and particle identification.

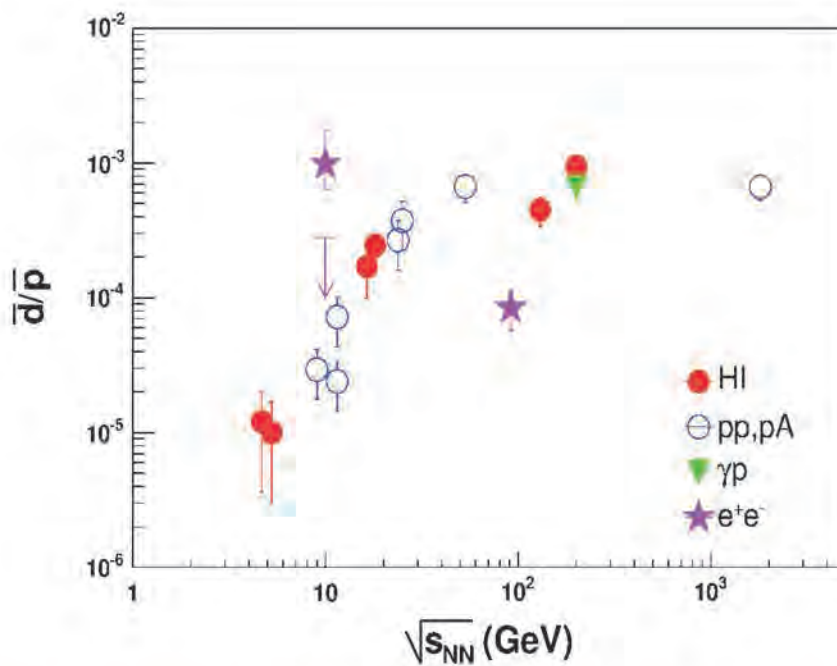


Figure 3: antideuteron and antiproton yield ratio as a function of the center of mass energy of the colliding target and projectile particles.

Figure 4 shows the matter and antimatter yields as a function of baryon numbers as measured by the STAR Collaboration at RHIC (STAR 2011). The fit lines yield the production reduction rate by a factor of 1.6×10^{-3} (1.1×10^{-3}) for matter (antimatter) for each additional nucleon (antinucleon). The sensitivity of current and planned space based charged particle detectors is below what would be needed to observe antihelium produced by nuclear interactions in the cosmos. This implies that any observation of antihelium or even heavier antinuclei in space would indicate the existence of a large amount of antimatter elsewhere in the universe. In particular, finding antimatter ${}^4\text{He}$ in the cosmos is one of the major motivations for space detectors such as the Alpha Magnetic Spectrometer (AMS 1994). We have shown that antimatter ${}^4\text{He}$ exists and provided a measure of the background rate in nuclear collisions for possible future observations in cosmic radiation.

The next stable antimatter nucleus would be $A=6$ (${}^6\bar{\text{He}}$, ${}^6\bar{\text{Li}}$). However, the penalty factor on the production rate for an additional antinucleon is about 1500 as shown in Fig. 4. This means that the $A=6$ antinuclei are produced at a rate 2×10^6 lower than that of an $A=4$ antialpha particle. Unless production mechanisms or collider technology change dramatically, it is unlikely that $A=6$ antinuclei can be produced in collider or fixed-target experiments (STAR 2011). On the other hand, the ratio of the ${}^4\bar{\text{He}}/{}^3\bar{\text{He}} = 3.1 \times 10^{-3}$ and $\text{anti-}{}^4\text{He}/\text{anti-}{}^3\text{He} = 2.4 \times 10^{-3}$. There is a factor of 2 higher yield of $|A|=4$ over $|A|=3$ than the extrapolation from the fit. The excess is visible even in a log-scale plot of 13 orders of magnitude. This ratio is also much higher than that shown in Fig.3 for the $|A|=2$ over $|A|=1$. It has been argued that a more economic way of producing heavier antimatter and/or nuclear matter containing large amount of strange quark contents is through excitation of complex nuclear structure from the vacuum or through strangeness distillation from a QGP. Is this enhanced yield an indicative of a new production mechanism or a minor deviation due to trivial configuration of nuclear binding?

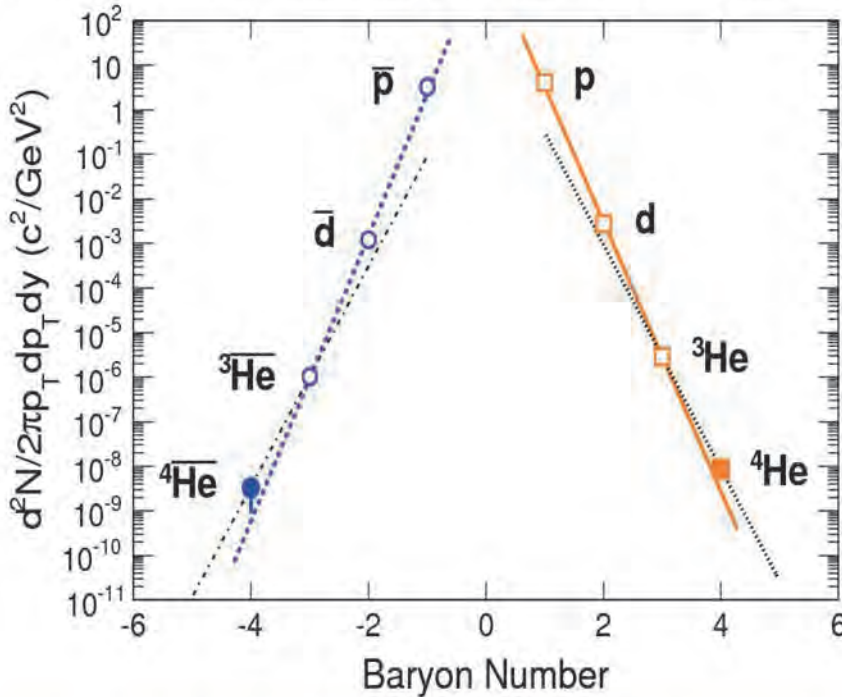


Figure 4: Matter and Antimatter invariant differential yields as a function of the baryon number. The solid and dashed lines are a fit to all the experimental data. The dotted and dotted dash lines are extrapolations from the yields of $|A|=3$ and $|A|=4$.

Where do we go from here into the future in search and construction of heavier and more exotic antimatters? The indicative enhancement of higher antialpha yields suggests that even higher enhanced yields of heavier antimatter. Besides the possible high yields of $|A|=6$ antimatter, the heaviest antimatter

that can be produced and detected with a tracking detector in high-energy accelerators are likely to be $A=4$ or 5 unstable antinuclei: ${}^4\text{He}^* \rightarrow t+p$, ${}^4\text{Li} \rightarrow {}^3\text{He} + p$, and ${}^5\text{Li} \rightarrow {}^4\text{He} + p$. New trigger scheme and high data acquisition rate have been proposed to improve the effective data taking rate by two orders of magnitude in STAR during the heavy ion collisions (STAR Decadal Plan 2011). This should confirm if the enhancement indeed exists and provide a possible path for discovering even heavier antimatter. In addition, as mentioned in previous section, the antimatter yield reduction factor is similar in p+p and AA collisions. One expects that the penalty factor to persist for antimatter heavier than antideuteron in p+p collisions. A comparison between the antimatter yields as shown in Fig.4 in p+p and A+A collisions will provide a reference for whether the enhancement seen in antialpha production in AA collisions is due to new production mechanism. Both RHIC and LHC have sufficient luminosity in p+p collisions to produce antialpha. The only experimental issue is how to trigger and identify those particles. STAR has proposed a new trigger and TPC readout schemes for heavy antimatter search by using the Electromagnetic Calorimeter (EMC) for charged hadrons and only readout small sector of TPC associated with that struck EMC.

Hypermatter

Relativistic heavy ion collisions are an abundant source of strangeness. As strange quarks have to be newly produced during the hot and dense stage of the collision, they are thought of carrying information on the properties of the matter that was created (Koch 1986).

Exotic forms of deeply bound objects with strangeness have been proposed (Bodmer 1971) as states of matter, either consisting of baryons or quarks.

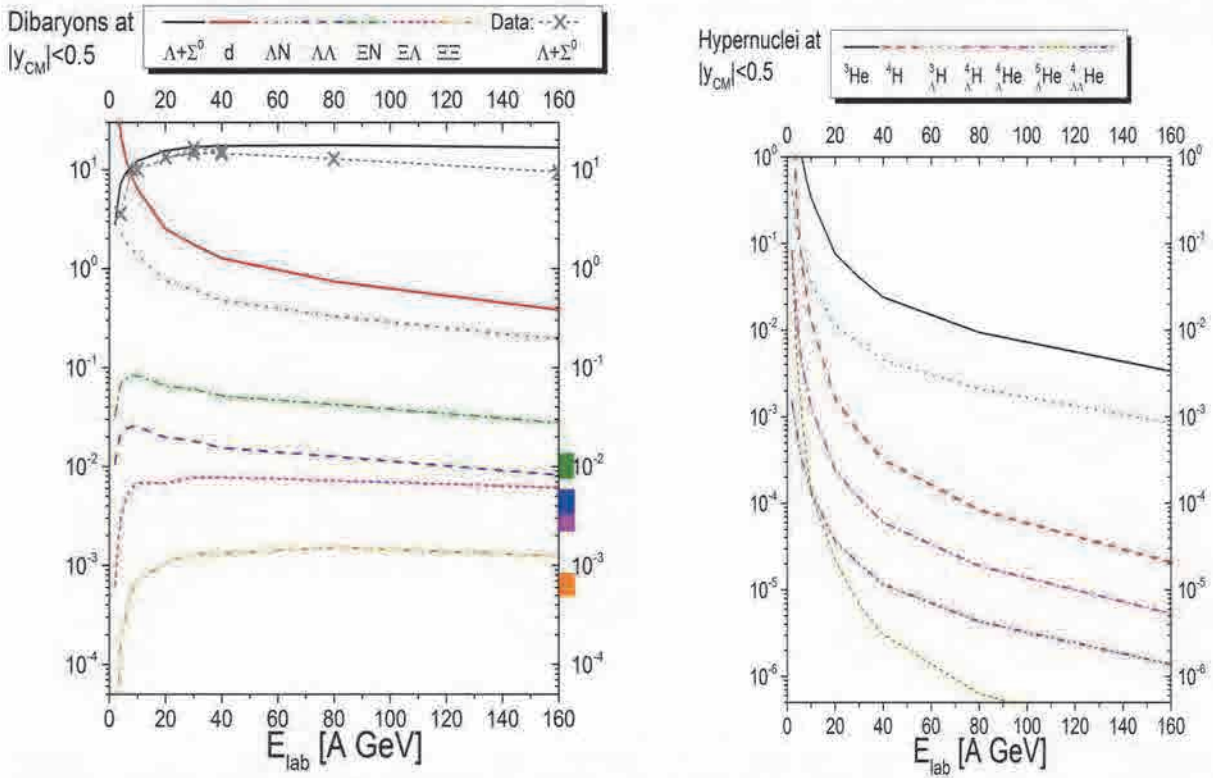
The H di-baryon was predicted by Jaffe (1977) and later, many more bound di-baryon states with strangeness were proposed using quark potentials (Goldman 1987, Goldman 1998) or the Skyrme model (Schwesinger 1995). However, the non-observation of multi-quark bags, e.g. strangelets is still one of the open problems of intermediate and high energy physics. Lattice calculations suggest that the H-dibaryon is a weakly unbound system (Wetzorke & Karsch 2003), while recent lattice studies report that there could be strange di-baryon systems including Ξ 's that can be bound (Wetzorke & Karsch 2003). Because of the size of these clusters lattice studies are usually very demanding on computational resources and have large lattice artifacts, therefore an experimental confirmation of such a state would be an enormous advance in the understanding of the hyperon interaction. Hypernuclei are known to exist and are predicted to be produced in heavy Ion collisions already for a long time (Braun-Munzinger 1995, Takahashi 2001, Andronic 2011). The recent discoveries of the first anti-hypertriton (STAR 2010) and anti-alpha (STAR 2011) (the largest anti-particle cluster ever reported) has fueled the

interest in the field of hypernuclear physics. Metastable exotic multi-hypernuclear objects (MEMOs) as well as purely hyperonic systems of Λ 's and Ξ 's were introduced in (Schaffner 1992, Schaffner 1993) as the hadronic counterparts to multi-strange quark bags (Gilson & Jaffe 1993, Schaffner-Bielich 1997). In this work we will focus on the production of hypernuclei in high energy collisions of Au+Au ions. In such systems strangeness is produced abundantly and is likely to form clusters of different sizes. Hypernuclear clusters can emerge from the hot and dense fireball region of the reaction. In this scenario the cluster is formed at, or shortly after, the (chemical-)freeze out of the system. A general assumption is, that these clusters are then formed through coalescence of different newly produced hadrons. To estimate the production yield we can employ thermal production of clusters from a fluid dynamical description to heavy ion collisions.

Though thermal production differs significantly in its assumptions from a coalescence approach one would expect to obtain different results, depending on the method used. However it has been shown that both approaches can lead to very similar results (Steinheimer 2012). More detailed information on the calculations performed for the results in this section can be found in (Steinheimer 2009)

Figures 5 and 6 show our results for the mid rapidity yields ($|y| < 0.5$) of di-baryons and hypernuclei as a function of the beam energy E_{lab} . In our calculations we considered most central ($b < 3.4$ fm) Pb+Pb/Au+Au collisions at $E_{\text{lab}} = 1 - 160$ A GeV. In addition, figure 2 shows the Λ yield (black lines and squares) for the model compared to data (NA49 2008). In these figures, the UrQMD hybrid model calculations are shown as lines. At lower energies the cluster production is should be additionally suppressed due to the non-equilibrium of strangeness. In the thermal calculations restrictions of energy and momentum conservation, resulting in a phase space reduction for produced strange particles, strongly decreases strange particle yields (Becattini 1997, Cleymans 1991, Andronic 2006). This behavior was also observed in a core-corona implementation in the hybrid model (Steinheimer 2011).

Figures 5 and 6: Yields of different di-baryons and hypernuclei in the mid rapidity region ($|y| < 0.5$) of



most central collisions of Pb+Pb/Au+Au. Shown are the results from the thermal production in the UrQMD hybrid model (lines) as compared to coalescence results with the DCM model (symbols). The small bars on the right hand axis denote results on di-baryon yields from a previous RQMD calculation at $\sqrt{s_{NN}}=200$ GeV (Schaffner-Bielich 2000). In addition, the black lines and symbols depict results for the production rate of Λ 's from both models, compared to data (grey crosses) from NA49 (2008).

Di-baryon production rates have also been calculated in a coalescence approach using the RQMD model for collisions at $\sqrt{s_{NN}}=200$ GeV of Au nuclei (Schaffner-Bielich 2000). To relate our calculations to these results, they are indicated as the colored bars on the right axis of figure 2. The RQMD model used was in particular tuned to reproduce multi strange particle yields (such as the Ξ) and the results are therefore close to the ones obtained with our thermal/hydrodynamic approach.

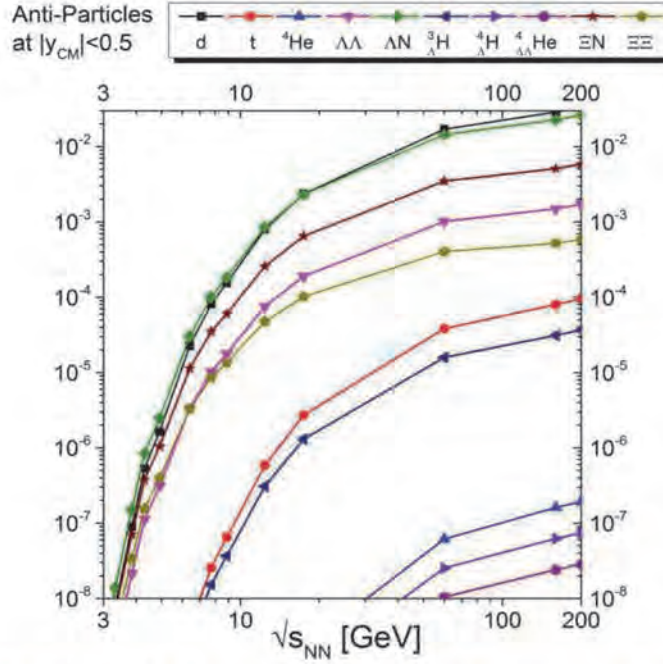


Figure 7: Yields of anti-particle clusters in the mid rapidity region ($|y| < 0.5$) of most central collisions of Pb+Pb/Au+Au as a function of the center of mass beam energy. Shown are only the results from the thermal production in the UrQMD hybrid model (lines with symbols).

When the beam energy of the collisions is increased, the system created becomes almost net-baryon free. This means that the probability to create an anti-particle cluster approaches that of the particle cluster. Figure 4 shows the results for anti-particle cluster production at mid-rapidity ($|y| < 0.5$) in collisions of Pb+Pb/Au+Au at center of mass energies of $\sqrt{s_{NN}} = 3 - 200$ GeV. The yields of the anti-particle clusters show a monotonous increase with beam energy. They show that, at the highest RHIC energy (and at the LHC) the reconstruction of anti- ${}^4\text{He}$ might be a feasible task.

Summary

FAIR will allow forefront research addressing (1) the investigation of the properties and the role of the strong (nuclear) force in shaping basic building blocks of the visible world around us and of its role in the evolution of the universe, (2) tests of symmetries and predictions of the standard model and search for physics beyond in the electro-weak sector and in the domain of the strong interaction, (3) the properties of matter under extreme conditions, both at the subatomic as well as at the macroscopic scale of matter and (4) applications of high-intensity, high-quality ion and antiproton beams in research areas that provide the basis for, or directly address, issues of applied sciences and technology. Due to the high luminosity which exceeds current facilities by up to a factor of 10000, experiments will be feasible that could not be done elsewhere. This opens the unique opportunity to study the evolution of nuclear structure into the yet unexplored 3rd dimension of the nuclear chart and to determine the properties of many short-lived hypernuclei and metastable exotic multi-hypernuclear objects. FAIR will

expand the knowledge in the various scientific fields beyond current frontiers. Moreover, there exists strong cross-topical synergies which can be exploited and promise novel insights. The discoveries of heavy antimatter have reached a new height with RHIC and LHC, and in the near future, FAIR. The potential new discoveries are: antimatter nuclei with $|A|=5,6$; antimatter muonic hydrogen and new studies on antimatter hydrogen atom and atomcules.

References

- Gutbrod (2006). H.H. Gutbrod et al. (Eds.) FAIR Baseline Technical Report, ISBN 3-9811298-0-6 Nov. 2006.
- Henning (2008). W. F. Henning, FAIR: Recent developments and status, Nucl. Phys. A 805 (2008) 502.
- Stöcker (2008). H. Stöcker, FAIR: Challenges Overcome and Still to be Met, published in Conf.Proc.C0806233:moycgm01, 2008.
- Stöhlker (2007). Th. Stöhlker et al. , Atomic physics with highly-charged ions at the future FAIR facility: A status report, Nuclear Instruments and Methods in Physics Research B 261 (2007) 234-238.
- Lomonosov & Tahir (2006). I.V. Lomonosov and N.A. Tahir, Prospects of High-Energy Density Matter Research at the Future FAIR Facility at Darmstadt, Nuclear Physics News 16 (1) (2006) 29 - 35.
- HADES (2009). G. Agakishiev et al. [HADES Collaboration], The High-Acceptance Dielectron Spectrometer HADES, Eur. Phys. J. A 41, 243 (2009)
- Senger (2008). P. Senger et al.. Compressed baryonic matter: Experiments at GSI and FAIR, Phys. Part. Nucl. 39 (2008) 1055.
- NuSTAR (2005). R. Krücken [NuSTAR Collaboration], The Nustar Facility At Fair, J. Phys. G 31 (2005) S1807.
- Rubio & Nilsson(2006). B. Rubio and T. Nilsson. Nucl. Phys. News 16 (2006) 9.
- Fohl (2008). K. Fohl et al. , The Panda Detector At The Future Fair Laboratory, Eur. Phys. J. ST 162 (2008) 213 .
- Koch (1986). P. Koch, B. Muller and J. Rafelski. Strangeness in Relativistic Heavy Ion Collisions, Phys. Rept. 142, 167 (1986).
- Bodmer (1971). A. R. Bodmer, Collapsed nuclei, Phys. Rev. D 4, 1601 (1971).
- Jaffe (1977). R. L. Jaffe. Perhaps a Stable Dihyperon, Phys. Rev. Lett. 38, 195 (1977).
- Goldman (1987). J. T. Goldman, K. Maltman, G. J. Stephenson, K. E. Schmidt and F. Wang. Strangeness -3 dibaryons, Phys. Rev. Lett. 59, 627 (1987).
- Goldman (1998). J. T. Goldman, K. Maltman, G. J. Stephenson, J. L. . Ping and F. Wang. Quark delocalization, color screening model and nucleon baryon scattering. Mod. Phys. Lett. A 13, 59 (1998)
- Schwesinger (1995). B. Schwesinger, F. G. Scholtz and H. B. Geyer. Loosely bound hyperons in the SU(3) Skyrme model. Phys. Rev. D 51, 1228 (1995)
- Wetzorke & Karsch (2003). I. Wetzorke and F. Karsch. The H dibaryon on the lattice. Nucl. Phys. Proc. Suppl. 119, 278 (2003) .
- Beane (2011). S. R. Beane et al. [NPLQCD Collaboration and NPLQCD Collaboration and NPLQCD Collaboration]. The Deuteron and Exotic Two-Body Bound States from Lattice QCD. arXiv:1109.2889 [heplat].
- Braun-Munzinger (1995). P. Braun-Munzinger and J. Stachel. Production of strange clusters and strange matter in nucleus-nucleus collisions at the AGS. J. Phys. G 21, L17 (1995).
- Ahn (2001). J. K. Ahn et al.. Production of ${}_{\Lambda\Lambda}^4\text{H}$ Hypernuclei. Phys. Rev. Lett. 87, 132504 (2001).
- Takahashi (2001). H. Takahashi et al., Observation of a ${}_{\Lambda\Lambda}^6\text{H}$ Double Hypernucleus. Phys. Rev. Lett. 87, 212502 (2001).

- Andronic (2011). A. Andronic, P. Braun-Munzinger, J. Stachel and H. Stoecker. Production of light nuclei, hypernuclei and their antiparticles in relativistic nuclear collisions. *Phys. Lett. B* 697, 203 (2011).
- Schaffner (1992). J. Schaffner, H. Stoecker and C. Greiner. Metastable exotic multihypernuclear objects. *Phys. Rev. C* 46, 322 (1992).
- Schaffner (1993). J. Schaffner, C. B. Dover, A. Gal, C. Greiner and H. Stoecker. Strange hadronic matter. *Phys. Rev. Lett.* 71, 1328 (1993).
- Gilson & Jaffe (1993). E. P. Gilson and R. L. Jaffe. Stability of very small strangelets. *Phys. Rev. Lett.* 71, 332 (1993).
- Schaffner-Bielich (1997). J. Schaffner-Bielich, C. Greiner, A. Diener and H. Stoecker. Detectability of strange matter in heavy ion experiments. *Phys. Rev. C* 55, 3038 (1997).
- Steinheimer (2012). J. Steinheimer, K. Gudima, A. Botvina, I. Mishustin, M. Bleicher and H. Stöcker, to be published.
- Steinheimer (2009). J. Steinheimer, M. Mitrovski, T. Schuster, H. Petersen, M. Bleicher and H. Stoecker, *Phys. Lett. B* 676, 126 (2009).
- NA49 (2008). C. Alt et al. [NA49 Collaboration]. Energy dependence of Λ and Ξ production in central Pb+Pb collisions at 20A,30A,40A,80A, and 158A GeV measured at the CERN Super Proton Synchrotron. *Phys. Rev. C* 78, 034918 (2008).
- Becattini (1997). F. Becattini and U. W. Heinz. Thermal hadron production in p p and p anti-p collisions. *Z. Phys. C* 76, 269 (1997) [Erratum-ibid. C 76, 578 (1997)] .
- Cleymans (1991). J. Cleymans, K. Redlich and E. Suhonen On The Phenomenology Of Deconfinement And Chiral Symmetry Restoration. *Z. Phys. C* 51, 137 (1991).
- Andronic (2006). A. Andronic, P. Braun-Munzinger and J. Stachel. Hadron production in central nucleus-nucleus collisions at chemical freeze-out. *Nucl. Phys. A* 772, 167 (2006) .
- Steinheimer (2011) J. Steinheimer and M. Bleicher. Core-corona separation in the UrQMD hybrid model. *Phys. Rev. C* 84, 024905 (2011).
- Schaffner-Bielich (2000). J. Schaffner-Bielich, R. Mattiello and H. Sorge. Dibaryons with Strangeness: Their Weak Nonleptonic Decay Using SU(3) Symmetry and How to Find Them in Relativistic Heavy-Ion Collisions. *Phys. Rev. Lett.* 84, 4305 (2000) .
- STAR (2005). STAR Collaboration, “Experimental and theoretical challenges in the search for the quark gluon plasma: The STAR Collaboration's critical assessment of the evidence from RHIC collisions”, *Nucl.Phys.A*757:102-183,2005.
- Liu & Xu (2006). Haidong Liu and Zhangbu Xu, “Universal anti-baryon density in $e^+ e^-$, gp, pp, pA and AA collisions”, e-Print arXiv: nucl-ex/0610035.
- STAR (2010). STAR Collaboration, “Observation of an Antimatter Hypernucleus”, *Science* 328 (2010) 58.
- STAR (2011). STAR Collaboration, “Observation of the antimatter helium-4 nucleus”, *Nature* 473 (2011) 353.
- Greiner (1996, 2001). “On the extension of the periodic system into the sectors of strangeness and antimatter”, *Int. J. Mod. Phys. E* 5, 1 (1996).
- AMS (1994). Ahlen, S. et al., “An antimatter spectrometer in space”, *Nucl. Instr. and Meth. in Phys. Res. A* 350, 351 (1994).
- STAR Decadal Plan 2011. [http://www.bnl.gov/npp/docs/STAR_Decadal_Plan_Final\[1\].pdf](http://www.bnl.gov/npp/docs/STAR_Decadal_Plan_Final[1].pdf)

THE MYSTERY OF NEUTRINO MIXING

■ GUIDO ALTARELLI

*Dipartimento di Fisica, Università di Roma Tre
Rome, Italy*

and

*CERN, Department of Physics, Theory Division
CH-1211 Genève 23, Switzerland*

E-mail: guido.altarelli@cern.ch

ABSTRACT

In the last years we have learnt a lot about neutrino physics. A long list of models have been formulated to understand neutrino masses and mixings. Along the way, with the continuous improvement of the data, most of the models have been discarded by experiment. At present, the surviving models still span a wide range of possibilities, going from a maximum of symmetry, described by discrete non-abelian flavour groups, to the opposite extreme of anarchy. In particular, discrete flavour groups have been studied in connection with special patterns of neutrino mixing suggested by the data, like Tri-Bimaximal mixing (groups A_4 , S_4 ...) or Bi-Maximal mixing (group S_4 ...) etc. We briefly summarize a number of models based on various patterns and symmetries and compare them with the experimental data.

1. Introduction

So far the main theoretical lessons from ν mass and mixing^{1), 2)} are that ν 's are not all massless but their masses are very small; probably their masses are small because ν 's are Majorana fermions with masses inversely proportional to the large scale M of interactions that violate lepton number (L) conservation. From the see-saw formula³⁾, the observed atmospheric oscillation frequency and a Dirac mass m_D of the order of the Higgs VEV, it follows that the Majorana mass scale $M \sim m_{\nu R}$ is empirically close to $10^{14} - 10^{15}$ GeV $\sim M_{GUT}$, so that ν masses fit well in the SUSY GUT picture. Decays of ν_R with CP and L violation can produce a sizable B-L asymmetry that survives instanton effects at the electroweak scale thus explaining baryogenesis as arising from leptogenesis. There is still no direct proof that neutrinos are Majorana fermions: detecting neutrino-less double beta decay ($0\nu\beta\beta$) would prove that ν 's are Majorana particles and that L is violated. It also appears that the active ν 's are not

a significant component of dark matter in the Universe.

2. Experimental Highlights

On the experimental side the two main recent developments were, first, that substantial evidence for a non vanishing value of the smallest mixing angle θ_{13} is building up and, second, the coming back of some hints of sterile neutrinos. As well known, the T2K run was suddenly interrupted by the devastating earthquake that hit Japan on March 11, 2011 just minutes away from the scheduled presentation of the first T2K data. Later T2K released the first publication on their data⁴⁾, reporting a 2.5σ signal for $\sin^2 2\theta_{13}$. The T2K result⁴⁾, based on the observation of 6 electron events when 1.5 ± 0.3 are expected for $\theta_{13} = 0$, is converted into a confidence interval $0.03(0.04) \leq \sin^2 2\theta_{13} \leq 0.28(0.34)$ at 90% c.l. for $\sin^2 2\theta_{23} = 1$, $|\Delta m_{23}^2| = 2.4 \cdot 10^{-3} \text{eV}^2$, $\delta_{CP} = 0$ and for normal (inverted) neutrino mass hierarchy. Also the MINOS Collaboration released⁵⁾ their corresponding 90% c.l. range as $0(0) \leq \sin^2 2\theta_{13} \leq 0.12(0.19)$, which is displaced towards smaller values with respect to that of T2K. Finally DOUBLE CHOOZ⁶⁾ finds (with only the far detector in operation): $\sin^2 2\theta_{13} = 0.085 \pm 0.051$ at 1σ . Additional input on $\sin^2 2\theta_{13}$ is derived from comparing the 3-neutrino fits with the separate 2-neutrino fits for solar and atmospheric oscillations. These results on $\sin \theta_{13}$ have very important implications on neutrino oscillation physics. First, it is very good news for the possibility of detecting CP violation in neutrino oscillations. Second, the relatively large central values for $\sin^2 \theta_{13}$ in the fits of Table 1 have a strong impact in discriminating models of neutrino mixing. In fact, these values correspond to $\sin \theta_{13} \sim 0.158$ or 0.114 , which is comparable to $\lambda_C = \sin \theta_C \sim 0.226$ or perhaps to $\lambda_C^2 \sim 0.051$.

On the evidence for sterile neutrinos a number of hints have been reported recently. They do not make yet a clear evidence but certainly pose an experimental problem that needs clarification. First, there is the MiniBooNE experiment⁷⁾ that in the antineutrino channel reports an excess of events supporting the LSND oscillation signal (originally observed with antineutrinos). The MiniBooNE best fit point falls in an excluded area but there is an overlap with the LSND signal in an allowed region. In the neutrino channel MiniBooNE did not observe a signal in the LSND domain. However, in these data there is a unexplained excess at low energy over the (reliably?) estimated background. Consequently, in the neutrino data sample, for the search of a LSND-like signal, only the events with neutrino energy above a threshold value E_{th} were used, leaving the issue of an explanation of the low energy excess unanswered. In the antineutrino channel most of the support to the LSND signal appears to arise from an excess above E_{th} but quite close to it, so that there is, in my opinion, some room for perplexity. More recently an update of the MiniBooNE data in the antineutrino channel shows less supporting evidence⁸⁾. Then there is the reactor anomaly: a reevaluation of the reactor flux⁹⁾ produced an apparent gap

between the theoretical expectations and the data taken at small distances from the reactor ($\lesssim 100$ m). The discrepancy is of the same order of the quoted systematic error whose estimate, detailed in the paper, should perhaps be reconsidered. Similarly the Gallium anomaly¹⁰⁾ depends on the assumed cross-section which could be questioned. The reactor anomaly and the Gallium anomaly do not really agree on the oscillation parameters that they point to: the Δm^2 values are compatible but the central values of $\sin^2 2\theta$ differ by about an order of magnitude, with Gallium favouring the larger angle. Cosmological data allow the existence of one sterile neutrino, while the most stringent bounds arising from nucleosynthesis disfavour two or more sterile neutrinos¹¹⁾. Over all, only a small leakage from active to sterile neutrinos is allowed by present neutrino oscillation data¹²⁾. If all the indications listed above were confirmed (it looks unlikely) then 1 sterile neutrino would not be enough and at least 2 would be needed with sub-eV masses. Establishing the existence of sterile neutrinos would be a great discovery. In fact a sterile neutrino is an exotic particle not predicted by the most popular models of new physics. A sterile neutrino is not a 4th generation neutrino: the latter is coupled to the weak interactions (it is active) and heavier than half the Z mass. A sterile neutrino would probably be a remnant of some hidden sector. The issue is very important so that new and better experimental data are badly needed.

In neutrino oscillations the leakage from the three active species towards the sterile neutrinos is any case small and, in fact, the bulk of oscillation phenomena is well described in terms of 3-neutrino models. In the following we will neglect this possible small leakage to sterile neutrinos and concentrate on 3-neutrino models. The results of two fits of all the present data are summarised in Table(1)^{13), 14)}.

Quantity	Fogli et al ¹³⁾	Schwetz et al ¹⁴⁾
Δm_{sun}^2 (10^{-5} eV ²)	$7.58^{+0.22}_{-0.26}$	$7.59^{+0.20}_{-0.18}$
Δm_{atm}^2 (10^{-3} eV ²)	$2.35^{+0.12}_{-0.09}$	$2.50^{+0.09}_{-0.16}$
$\sin^2 \theta_{12}$	$0.312^{+0.017}_{-0.016}$	$0.312^{+0.017}_{-0.015}$
$\sin^2 \theta_{23}$	$0.42^{+0.08}_{-0.03}$	$0.52^{+0.06}_{-0.07}$
$\sin^2 \theta_{13}$	0.025 ± 0.007	$0.013^{+0.007}_{-0.005}$

Table 1:

Fits to neutrino oscillation data. The results correspond to the new reactor fluxes. The fit of Schwetz et al¹⁴⁾ refers to the normal hierarchy case (in the inverse hierarchy case the main difference is that $\sin^2 \theta_{13} = 0.016 + 0.008 - 0.006$)

For the near future the most important experimental challenges on neutrino oscillation experiments are more precise measurements of the absolute scale of neutrino mass (KATRIN, MARE), the search for neutrinoless double beta decay ($0\nu\beta\beta$) (CUORE, GERDA, ...), the accurate determination of θ_{13} (from MINOS, T2K and the reactor experiments DOUBLE CHOOZ, Daya Bay and RENO) and of the shift

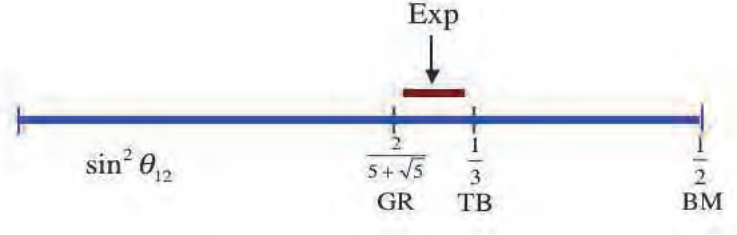


Figure 1: The values of $\sin^2 \theta_{12}$ for TB or GR or BM mixing are compared with the data

from maximal of θ_{23} , the fixing of the sign of Δm_{23}^2 (normal or inverse hierarchy) (e.g. $\text{NO}\nu\text{A}$) and the detection of CP violation in ν oscillations. Related to neutrino physics is the issue of the non conservation of the separate e , μ and τ lepton numbers. The recent new limit $\text{Br}(\mu \rightarrow e\gamma) \lesssim 2.4 \cdot 10^{-12}$ obtained by the MEG experiment¹⁵⁾ is largely satisfied in the SM but it imposes a strong constraint on SUSY-GUT models.

3. Models of Neutrino Mixing

To illustrate the impact of the new results on θ_{13} on models of neutrino mixing, we consider the case of models based on discrete flavour groups that have received a lot of attention in recent years¹⁶⁾. There are a number of special mixing patterns that have been studied in this context. These mixing matrices all have $\sin^2 \theta_{23} = 1/2$, $\sin^2 \theta_{13} = 0$ and differ by the value of $\sin^2 \theta_{12}$ (see Fig. 1). The corresponding mass matrices are 2-3 symmetric, i.e. $\mu - \tau$ symmetric (see, as examples, the early work in ref.¹⁷⁾ and the recent paper ref.¹⁸⁾). The observed value of $\sin^2 \theta_{12}$ ^{13), 14)} the best measured mixing angle, is very close, from below, to the so called Tri-Bimaximal (TB) value¹⁹⁾ which is $\sin^2 \theta_{12} = 1/3$. Alternatively it is also very close, from above, to the Golden Ratio (GR) value^{20), 21), 22)} which is $\sin^2 \theta_{12} = \frac{1}{\sqrt{5}\phi} = \frac{2}{5+\sqrt{5}} \sim 0.276$, where $\phi = (1 + \sqrt{5})/2$ is the GR (for a different connection to the GR in this context, see^{23), 24)}). Thus, a possibility is that one or the other of these coincidences is taken seriously and this leads to models where either TB or GR mixing is naturally predicted as a good first approximation. On a different perspective, one has considered models with Bi-Maximal (BM) mixing, with $\sin^2 \theta_{12} = 1/2$, i.e. also maximal, as the value before diagonalization of charged leptons. This is in line with the well known empirical observation that $\theta_{12} + \theta_C \sim \pi/4$, a relation known as quark-lepton complementarity²⁵⁾. Probably the exact complementarity relation becomes more plausible if replaced with $\theta_{12} + \mathcal{O}(\theta_C) \sim \pi/4$ (which we could call "weak" complementarity). One can think of models where, because of a suitable symmetry, BM mixing holds in the neutrino sector at leading order and the necessary, rather large, corrective terms for θ_{12} arise from the diagonalization of charged lepton masses²⁵⁾.

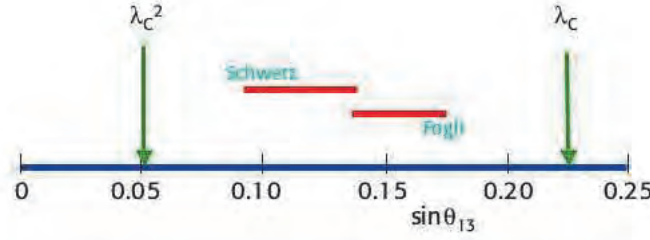


Figure 2: The experimental values of $\sin \theta_{13}$ (world averages derived from Table(1)^{13), 14)} are numerically intermediate between $\mathcal{O}(\lambda_C^2)$ and $\mathcal{O}(\lambda_C)$

Thus, a possibility is that one of these coincidences is taken seriously and this leads to models where TB or GR or BM mixing is naturally predicted as a good first approximation. In the following we will mainly refer to TB or BM mixing which are the most studied first approximations to the data. The simplest symmetry that, in leading order (LO), leads to TB is A_4 while BM can be obtained from S_4 . In the literature A_4 models have been widely studied (for a review and a list of references, see¹⁶⁾). At LO the typical A_4 model leads to exact TB mixing. The LO approximation is then corrected by non leading effects. Given the set of flavour symmetries and having specified the field content, the non leading corrections to TB mixing, arising from higher dimensional effective operators, can be evaluated in a well defined expansion. In the absence of specific dynamical tricks, in a generic model, all three mixing angles receive corrections of the same order of magnitude. Since the experimentally allowed departures of θ_{12} from the TB value, $\sin^2 \theta_{12} = 1/3$, are small, numerically not larger than $\mathcal{O}(\lambda_C^2)$, it follows that both θ_{13} and the deviation of θ_{23} from the maximal value are also expected to be typically of the same general size. The same qualitative conclusion also applies to A_5 models for GR mixing. This generic prediction of θ_{13} small, numerically of $\mathcal{O}(\lambda_C^2)$ can now be confronted with the most recent data. The central values $\sin \theta_{13} \sim 0.16$ or 0.11 that can be derived from the experimental results in the two columns of Table(1), respectively, are in between $\mathcal{O}(\lambda_C^2) \sim \mathcal{O}(0.05)$ and $\mathcal{O}(\lambda_C) \sim \mathcal{O}(0.23)$. Although models based on TB (or GR) mixing tend to lead to a rather small value of θ_{13} one can argue that they are still viable with preference for the lower side of the experimental range (see Fig. 2).

It is to be stressed in this context that, of course, one can introduce some additional theoretical input to enhance the value of θ_{13} . In the case of A_4 , one particularly interesting example is provided by the Lin version of the A_4 model²⁶⁾, formulated before the T2K, MINOS and DOUBLE CHOOZ results were known. In the Lin model

the A_4 symmetry breaking is arranged, by suitable additional Z_n parities, in such a way that, not only at LO but also at next-to-the-leading (NLO), the corrections to the charged lepton and the neutrino sectors are kept separate. Then the contributions to neutrino mixing from the diagonalization of the charged leptons can be of $\mathcal{O}(\lambda_C^2)$ while those in the neutrino sector can be of $\mathcal{O}(\lambda_C)$. In addition, in the Lin model these large corrections do not affect θ_{12} and satisfy the relation $\sin^2 \theta_{23} = 1/2 + 1/\sqrt{2} \cos \delta \sin \theta_{13}$, with δ being an unspecified phase. Thus in the Lin model the NLO corrections to the solar angle θ_{12} and to the reactor angle θ_{13} can naturally be of different orders.

Alternatively one can think of models where, because of a suitable symmetry, BM mixing holds in the neutrino sector at LO and the corrective terms for θ_{12} , which in this case are necessarily rather large, arise from the diagonalization of charged lepton masses²⁵⁾. These terms numerically of order $\mathcal{O}(\lambda_C)$ from the charged lepton sector would then generically also affect θ_{13} and the resulting value could well be compatible with the present experimental values of θ_{13} . An explicit model of this type based on the group S_4 has been developed in ref.²⁷⁾. An important feature of this model is that only θ_{12} and θ_{13} are corrected by terms of $\mathcal{O}(\lambda_C)$ while θ_{23} is unchanged at this order. This model is compatible with present data and clearly prefers the upper range of the present experimental interval for θ_{13} . Recently the model was extended to include quarks in a $SU(5)$ Grand Unified version²⁸⁾.

It is important to keep in mind that the implications of lepton flavour violating processes for the three classes of possibilities, e.g. TB mixing in a typical A_4 model, the Lin version of A_4 and BM in S_4 , are quite different and the present bounds pose severe constraints on the respective models. In particular we refer to the recent improved MEG result¹⁵⁾ on the $\mu \rightarrow e\gamma$ branching ratio and to other similar processes like $\tau \rightarrow (e \text{ or } \mu)\gamma$. It appears¹⁶⁾ that the safest class of models is one where no large corrective terms of order $\mathcal{O}(\lambda_C)$ are present in either the charged or the neutral lepton sectors. The most dangerous case is that of the models where large terms directly appear in the off diagonal terms of the charged lepton mass matrix.

We now briefly turn to models that do not take seriously any of the coincidences described above (the proximity of the data to the TB or GR patterns or the quark-lepton complementarity: these indications cannot all be relevant and it is possible that none of them is so) and are therefore based on a less restrictive flavour symmetry. There are many possible models that fit the data on mixing angles well and yet have no TB or GR or BM built in in their structure (for a largely incomplete list of examples see²⁹⁾). It is clear that the T2K hint that θ_{13} may be large is great news for the most extreme position of this type, which is "anarchy"³⁰⁾: no symmetry at all in the lepton sector, only chance. This view predicts generic neutrino mixing angles, so the largest θ_{23} should be different than maximal and the smallest θ_{13} should be as large as possible within the experimental bounds. Anarchy can be formulated in a $SU(5) \otimes U(1)$ context by taking different Froggatt-Nielsen³¹⁾ charges only for the $SU(5)$ tenplets (for example 10: (3,2,0), where 3 is the charge of the first generation, 2

of the second, zero of the third) while no charge differences appear in the $\bar{5}$: $\bar{5}$: (0,0,0). This assignment is in agreement with the empirical fact that the mass hierarchies are more pronounced for up quarks in comparison with down quarks and charged leptons. In a non see-saw model, with neutrino masses dominated by the contribution of the dimension-5 Weinberg operator ³²⁾, the $\bar{5}$ vanishing charges directly lead to random neutrino mass and mixing matrices. In anarchical see-saw models also the charges of the SU(5) singlet right-handed neutrinos must be undifferentiated. Anarchy can be mitigated by assuming that it only holds in the 2-3 sector: e.g $\bar{5}$: (2,0,0) with the advantage that the first generation masses and the angle θ_{13} are naturally small (see also the recent revisiting in ref.³³⁾). In models with see-saw one can alternatively play with the charges for the right-handed SU(5) singlet neutrinos. If, for example, we take 1: (1, -1, 0), together with $\bar{5}$: (2,0,0), it is possible to get a normal hierarchy model with θ_{13} small and also with $r = \Delta m_{solar}^2 / \Delta m_{atm}^2$ naturally small (see, for example, ref.³⁴⁾). In summary anarchy and its variants, all based on chance, offer a rather economical class of models that are among those encouraged by the new θ_{13} result.

4. Conclusion

In the last decade we have learnt a lot about neutrino masses and mixings. A list of important conclusions have been reached. Neutrinos are not all massless but their masses are very small. Probably masses are small because neutrinos are Majorana particles with masses inversely proportional to the large scale M of lepton number violation. It is quite remarkable that M is empirically not far from M_{GUT} , so that neutrino masses fit well in the SUSY GUT picture. Also out of equilibrium decays with CP and L violation of heavy RH neutrinos can produce a B-L asymmetry, then converted near the weak scale by instantons into an amount of B asymmetry compatible with observations (baryogenesis via leptogenesis)³⁵⁾. It has been established that most probably active neutrinos are not a significant component of dark matter in the Universe. We have also understood there there is no contradiction between large neutrino mixings and small quark mixings, even in the context of GUTs.

This is a very impressive list of achievements. Coming to a detailed analysis of neutrino masses and mixings a long collection of models have been formulated over the years. With continuous improvements of the data and more precise values of the mixing angles most of the models have been discarded by experiment. Still the surviving models span a wide range going from a maximum of symmetry, with discrete non-abelian flavour groups, to the opposite extreme of anarchy. By now, besides the detailed knowledge of the entries of the V_{CKM} matrix, we also have a reasonable determination of the neutrino mixing matrix U_{PMNS} . The data appear to suggest some special patterns (recall Fig. 1) like TB or GR or BM mixing to be valid in some leading approximation, corrected by small non leading terms. If

one takes these "coincidences" seriously, then non-abelian discrete flavour groups emerge as the main road to an understanding of this mixing pattern. Indeed the entries of e.g. TB mixing matrix are clearly suggestive of "rotations" by simple, very specific angles. It is remarkable that neutrino and quark mixings have such a different qualitative pattern. An obvious question is whether some additional indication for discrete flavour groups can be obtained by considering the extension of the models to the quark sector, perhaps in a Grand Unified context. The answer appears to be that, while the quark masses and mixings can indeed be reproduced in models where TB or BM mixing is realized in the leptonic sector through the action of discrete groups, there are no specific additional hints in favour of discrete groups that come from the quark sector¹⁶⁾. Further important input could come from $\mu \rightarrow e\gamma$ and in general from lepton flavour violating processes, from $b \rightarrow s\gamma$ and from LHC physics. In fact, new physics at the weak scale could have important feedback on the physics of neutrino masses and mixing.

It is expected that in the near future, we will know the value of θ_{13} with a good accuracy, from the continuation of T2K and from the reactor experiments DOUBLE CHOOZ, Daya Bay and RENO. Many existing models will be eliminated and the surviving ones will be updated to become more quantitative in order to cope with a precisely known mixing matrix. A sizable θ_{13} will encourage the planning of long baseline experiments for the detection of CP violation in neutrino oscillations. Along the way the important issue of the existence of sterile neutrinos must be clarified. The on going or in preparation experiments on the absolute value of neutrino masses, on $0\nu\beta\beta$, on $\mu \rightarrow e\gamma$, on the search for dark matter etc can also lead to extremely important developments in the near future. So this field is very promising and there all reasons to expect an exciting time ahead of us.

Finally, one could have imagined that neutrinos would bring a decisive boost towards the formulation of a comprehensive understanding of fermion masses and mixings. In reality it is frustrating that no real illumination was sparked on the problem of flavour. We can reproduce in many different ways the observations, in a wide range that goes from anarchy to discrete flavour symmetries) but we have not yet been able to single out a unique and convincing baseline for the understanding of fermion masses and mixings. In spite of many interesting ideas and the formulation of many elegant models the mysteries of the flavour structure of the three generations of fermions have not been much unveiled.

5. Acknowledgments

It is a very pleasant duty for me to most warmly thank Professors Werner Arber and Antonino Zichichi, Monsignor Marcelo Sanchez Sorondo and the whole Organising Committee for their kind invitation and for the great hospitality offered to all of us in the Vatican. I am also glad to acknowledge interesting discussions on this subject

with Ferruccio Feruglio, Davide Meloni and Luca Merlo.

6. References

- 1) G. Altarelli and F. Feruglio, *New J. Phys.* **6** (2004) 106 [ArXiv:hep-ph/0405048]; G. Altarelli, [ArXiv:1011.5342].
- 2) R. N. Mohapatra and A. Y. Smirnov, *Ann. Rev. Nucl. Part. Sci.* **56**, 569 (2006) [ArXiv:hep-ph/0603118]; W. Grimus, PoS P2GC:001,2006. [ArXiv:hep-ph/0612311]; M. C. Gonzalez-Garcia and M. Maltoni, *Phys. Rept.* **460** (2008) 1 [ArXiv:0704.1800].
- 3) P. Minkowski, *Phys. Letters B* **67** (1977)421; T. Yanagida, in *Proc. of the Workshop on Unified Theory and Baryon Number in the Universe*, KEK, March 1979; S. L. Glashow, in “Quarks and Leptons”, Cargèse, ed. M. Lévy et al., Plenum, 1980 New York, p. 707; M. Gell-Mann, P. Ramond and R. Slansky, in *Supergravity*, Stony Brook, Sept 1979; R. N. Mohapatra and G. Senjanovic, *Phys. Rev. Lett.* **44** (1980) 912.
- 4) T2K Collaboration: K.Abe et al, *Phys. Rev. Lett.* **107** (2011) 041801, [ArXiv:1106.2822].
- 5) MINOS Collaboration, P. Adamson et al, [ArXiv:1108.0015].
- 6) DOUBLE CHOOZ Collaboration, H. de Kerret, Talk at LowNu, Seoul, November 2011.
- 7) MiniBooNE Collaboration *Phys.Rev.Lett.* **105** 181801 (2010), [ArXiv:1007.1150].
- 8) Z. Djurcic, Talk at NuFact2011, Geneva, August 2011.
- 9) G. Mention et al, *Phys.Rev.D* **83**:073006,2011, [ArXiv:1101.2755; Th. A. Mueller et al, *Phys.Rev.C* **83**:054615,2011, [ArXiv:1101.2663].
- 10) P. Anselmann et al. (GALLEX), *Phys. Lett. B* **342**, 440 (1995); W. Hampel et al. (GALLEX), *Phys. Lett. B* **420**, 114 (1998); F. Kaether et al. *Phys. Lett. B* **685**, 47 (2010); J. N. Abdurashitov et al. (SAGE), *Phys. Rev. Lett.* **77**, 4708 (1996); J. N. Abdurashitov et al. (SAGE), *Phys. Rev. C* **59**, 2246 (1999); J. N. Abdurashitov et al., *Phys. Rev. C* **73**, 045805 (2006); J. N. Abdurashitov et al. (SAGE), *Phys. Rev. C* **80**, 015807 (2009).
- 11) E. Giusarma et al, [ArXiv:1102.4774].
- 12) C. Giunti, [ArXiv:1110.3914] and references therein.
- 13) G. L. Fogli et al, [ArXiv:1106.6028].
- 14) T. Schwetz, M. Tortola and J. W. F. Valle, [ArXiv:1108.1376].
- 15) MEG Collaboration, T. Mori, Talk at the EPS Conference, Grenoble, July 2011.
- 16) G. Altarelli and F. Feruglio, *Rev.Mod.Phys.* **82** (2010) 2701, [ArXiv:1002.0211].
- 17) T. Fukuyama and H. Nishiura, [ArXiv:hep-ph/9702253].

- 18) H.-J. He and F.-R. Yin, Phys.Rev. D84 (2011) 033009, [ArXiv:1104.2654].
- 19) P. F. Harrison, D. H. Perkins and W. G. Scott, Phys. Lett. B **530** (2002) 167, [ArXiv:hep-ph/0202074]; P. F. Harrison and W. G. Scott, Phys. Lett. B **535** (2002) 163, [ArXiv:hep-ph/0203209]; Phys. Lett. B **547** (2002) 219, [ArXiv:hep-ph/0210197]; Phys. Lett. B **557** (2003) 76, [ArXiv:hep-ph/0302025]; Z. z. Xing, Phys. Lett. B **533** (2002) 85, [ArXiv:hep-ph/0204049].
- 20) Y. Kajiyama, M. Raidal and A. Strumia, Phys. Rev. D **76** (2007) 117301 [ArXiv:0705.4559].
- 21) L. L. Everett and A. J. Stuart, Phys.Rev. D79:085005, 2009, [ArXiv:0812.1057], G.-J. Ding, L. L. Everett and A. J. Stuart, [ArXiv:1110.1688].
- 22) F. Feruglio and A. Paris, JHEP 1103 (2011) 101, [ArXiv:1101.0393].
- 23) W. Rodejohann, Phys. Lett. **B671** (2009) 267, [ArXiv:0810.5239 [hep-ph]].
- 24) A. Adulpravitchai, A. Blum and W. Rodejohann, New J. Phys. **11** (2009) 063026 [ArXiv:0903.0531].
- 25) M. Raidal, Phys. Rev. Lett. **93** (2004) 16180, [ArXiv:hep-ph/0404046]; H. Minakata and A. Y. Smirnov, Phys. Rev. D **70** (2004) 073009, [ArXiv:hep-ph/0405088]; H. Minakata, [ArXiv:hep-ph/0505262]; P. H. Frampton and R. N. Mohapatra, JHEP **0501**, 025 (2005), [ArXiv:hep-ph/0407139]; J. Ferrandis and S. Pakvasa, Phys. Rev. D **71** (2005) 033004, [ArXiv:hep-ph/0412038]; S. K. Kang, C. S. Kim and J. Lee, [ArXiv:hep-ph/0501029]; G. Altarelli, F. Feruglio and I. Masina, Nucl. Phys. B **689** (2004) 157 [ArXiv:hep-ph/0402155]; N. Li and B. Q. Ma, [ArXiv:hep-ph/0501226]; K. Cheung, et al, [ArXiv:hep-ph/0503122]; Z. z. Xing, [ArXiv:hep-ph/0503200]; A. Datta, L. Everett and P. Ramond, [ArXiv:hep-ph/0503222]; T. Ohlsson, [ArXiv:hep-ph/0506094]; S. Antusch, S. F. King and R. N. Mohapatra, [ArXiv:hep-ph/0504007]; M. Lindner, M. A. Schmidt and A. Y. Smirnov, [ArXiv:hep-ph/0505067]; S. F. King, JHEP **0508** (2005) 105 [ArXiv:hep-ph/0506297]; A. Dighe, S. Goswami, and P. Roy, Phys.Rev.**D73** (2006) 07130, [ArXiv:hep-ph/0602062]; B. C. Chauhan et al, Eur.Phys. **J.C50**(2007) 573, [ArXiv:hep-ph/0605032] M. A. Schmidt and A. Yu. Smirnov, Phys.Rev. **D74**(2006)113003, [ArXiv:hep-ph/0607232]; K. A Hochmuth and W. Rodejohann, Phys.Rev. **D75**(2007) 073001, [ArXiv:hep-ph/0607103]; F. Plentinger, G. Seidl and W. Winter, Nucl.Phys. **B791** (2008) 60, [ArXiv: hep-ph/0612169]; Phys.Rev. **D76** (2007)113003, [ArXiv:0707.2379]; Y. H. Ahn, H-Y. Cheng and S. Oh, Phys.Rev.D83:076012,2011, [ArXiv:1102.0879].
- 26) Y. Lin, Nucl.Phys. B824 (2010) 95, [ArXiv:0905.3534].
- 27) G. Altarelli, F. Feruglio and L. Merlo, JHEP 0905 (2009) 020, [ArXiv:0903.1940].
- 28) D. Meloni, JHEP 1110 (2011) 010, [ArXiv:1107.0221].
- 29) C. H. Albright and W. Rodejohann, Phys. Lett. B **665** (2008) 378,

- [ArXiv:0804.4581[hep-ph], G. Altarelli and G. Blankenburg, JHEP 1103 (2011) 133, [ArXiv:1012.2697.
- 30) L. J. Hall, H. Murayama and N. Weiner, Phys.Rev.Lett. 84 (2000) 2572, [ArXiv:hep-ph/9911341.
- 31) C. D. Froggatt and H. B. Nielsen, Nucl. Phys. **B147** (1979) 277.
- 32) S. Weinberg, Phys.Rev.Lett. **43** 1566 (1979).
- 33) W. Buchmuller, V. Domcke and K. Schmitz, [ArXiv:1111.3872].
- 34) G. Altarelli, F. Feruglio and I. Masina, JHEP 0301 (2003) 035, [ArXiv:hep-ph/0210342.
- 35) For a review see for example: W. Buchmuller, R.D. Peccei and T. Yanagida, Ann.Rev.Nucl.Part.Sci.55:311-355,2005. [ArXiv:hep-ph/0502169].

NOVEL PERSPECTIVES FOR HADRON PHYSICS

■ STANLEY J. BRODSKY¹

¹*SLAC National Accelerator Laboratory
Stanford University, Stanford, California 94309, USA*

I discuss several novel and unexpected aspects of quantum chromodynamics. These include: (a) the nonperturbative origin of intrinsic strange, charm and bottom quarks in the nucleon at large x ; the breakdown of pQCD factorization theorems due to the lensing effects of initial- and final-state interactions; (b) important corrections to pQCD scaling for inclusive reactions due to processes in which hadrons are created at high transverse momentum directly in the hard processes and their relation to the baryon anomaly in high-centrality heavy-ion collisions; and (c) the nonuniversality of quark distributions in nuclei. I also discuss some novel theoretical perspectives in QCD: (a) light-front holography – a relativistic color-confining first approximation to QCD based on the AdS/CFT correspondence principle; (b) the principle of maximum conformality – a method which determines the renormalization scale at finite order in perturbation theory yielding scheme independent results; (c) the replacement of quark and gluon vacuum condensates by “in-hadron condensates” and how this helps to resolve the conflict between QCD vacuum and the cosmological constant.

I. INTRODUCTION

One of the most remarkable achievements in the history of science was the development [1] of quantum chromodynamics, the renormalizable gauge theory of color-triplet quark and color-octet gluon fields. QCD is believed to be the fundamental theory of hadron and nuclear phenomena in the same sense that quantum electrodynamics provides the fundamental theory underlying all of atomic physics and chemistry. In fact, quantum electrodynamics can be regarded as the zero-color limit of quantum chromodynamics [2]

QCD predictions based on the nearly scale-invariant interactions of quarks and gluons at short distances and asymptotic freedom have been validated by many measurements, such as deep inelastic lepton scattering, electron-positron annihilation into hadrons, and quark and gluon jet production in high energy hadronic collisions. However, phenomena in the nonperturbative color-confining strong-coupling domain can be extraordinarily complex and can have unexpected features.

In this talk I will review a number of unexpected features of quantum chromodynamics, especially the novel effects arising from the heavy-quark quantum fluctuations of hadron wavefunctions. I will also discuss corrections to pQCD leading-twist scaling for inclusive reactions due to processes in which hadrons are created at high transverse momentum directly in the hard process; the baryon anomaly in high centrality heavy ion collisions; the breakdown of factorization theorems due to the lensing effects of initial- and final-state interactions; and the non-universality of quark distributions in nuclei. I will also discuss some novel theoretical perspectives in QCD: (a) light-front holography – a first approximation to QCD based on the AdS/CFT correspondence principle; (b) the principle of maximum conformality – which determines the renormalization scale order-by-order in perturbation theory yielding scheme independent results; (c) the replacement of quark and gluon vacuum condensates by “in-hadron condensates” and how this resolves the conflict between the physics of the QCD vacuum and the cosmological constant. QCD also predicts a rich array of novel hadronic and nuclear phenomena. These include the production of a quark-gluon plasma in high energy, high density heavy ion collisions, “color transparent” interactions of hadrons in nuclear reactions, and “hidden-color” degrees of freedom in nuclei.

II. INTRINSIC HEAVY QUARKS

If one follows conventional wisdom, nonvalence “sea” quarks in the proton structure functions only arise from gluon splitting $g \rightarrow Q\bar{Q}$; i.e., the proton wavefunction at an initial soft scale is assumed to only contain valence quarks and gluons. DGLAP evolution from the $g \rightarrow Q\bar{Q}$ spitting process is then assumed to generate all of the sea quarks at virtuality $Q^2 > 4m_Q^2$. If this hypothesis were correct, then the $\bar{u}(x)$ and $\bar{d}(x)$ distributions would be identical. Similarly, if sea quarks only arise from gluon splitting, one expects that the $s(x)$ and $\bar{s}(x)$ distributions will be the same and fall-off faster in x than the parent gluon distributions. However, measurements of Drell-Yan processes, deep inelastic electron and neutrino scattering, and other experiments show that these simplified predictions are incorrect.

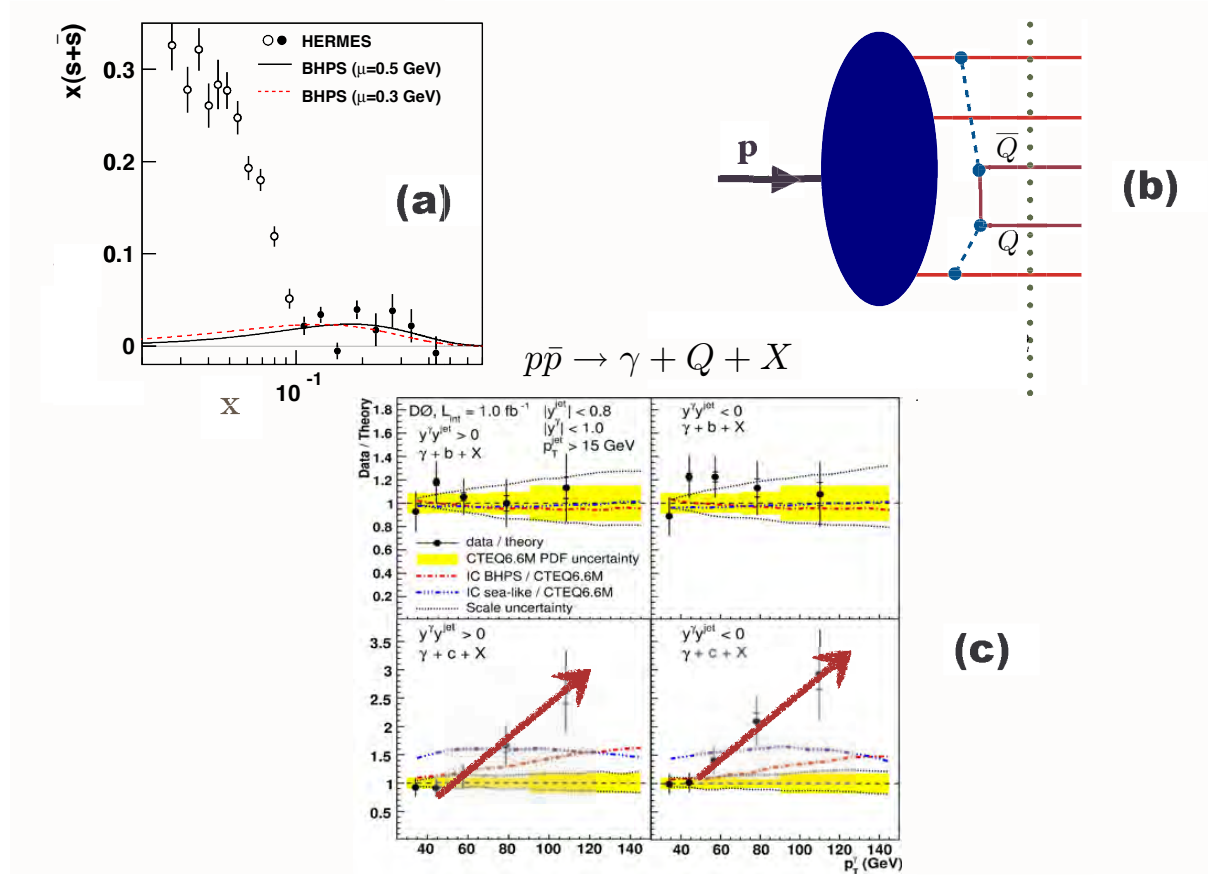


FIG. 1: (a) Intrinsic and extrinsic strangeness distribution. [8] (b) Five-quark Fock state of the proton and the origin of the intrinsic sea. (c) D0 measurement of $p\bar{p} \rightarrow \gamma + bX$ and $p\bar{p} \rightarrow \gamma + cX$.

The five-quark Fock state of the proton's LFWF $|uudQ\bar{Q}\rangle$ is the primary origin of the sea-quark distributions of the proton. Experiments show that the sea quarks have remarkable nonperturbative features, such as $\bar{u}(x) \neq \bar{d}(x)$, and an intrinsic strangeness [3] distribution $s(x)$ appearing at light-cone momentum fraction $x > 0.1$, as well as intrinsic charm and bottom distributions at large x . In fact, recent measurements from HERMES show that the strange quark in the proton has two distinct components: a fast-falling contribution consistent with gluon splitting to $s\bar{s}$ and an approximately flat component up to $x < 0.5$. See fig. 1(a).

The proton light-front wavefunction in QCD contains *ab initio* intrinsic heavy-quark Fock state components such as $|uudc\bar{c}\rangle$. [4–7] Such distributions [5, 7] favor configurations where the quarks have equal rapidity. The intrinsic heavy quarks thus carry most of the proton's momentum since this minimizes the off-shellness of the state. These configurations arise, for example, from $gg \rightarrow Q\bar{Q} \rightarrow gg$ insertions connected to the valence quarks in the proton self-energy; See Fig. 1(b). In fact, the intrinsic strangeness, charm and $\bar{u}(x) - \bar{d}(x)$ distributions fit a universal intrinsic quark model, [4] as recently shown by Chang and Peng. [8]. QCD also predicts that the heavy quark pair $Q\bar{Q}$ in the intrinsic five-quark Fock state is primarily a color-octet, and the ratio of intrinsic charm to intrinsic bottom scales as $m_c^2/m_b^2 \simeq 1/10$, as can easily be seen from the operator product expansion in non-Abelian QCD. [5, 7] Intrinsic charm and bottom thus can explain the origin of high open-charm and open-bottom hadron production at high momentum fractions, as well as the single and double J/ψ hadroproduction cross sections observed at high x_F .

In the case of a hadronic high energy proton collision, the high- x intrinsic charm quark in the proton's $|uudc\bar{c}\rangle$ Fock state can coalesce with the co-moving ud valence quarks in a projectile proton to produce a $\Lambda_c(cud)$ baryon at the combined high momentum fraction $x_F = x_u + x_d + x_c$. Similarly, the coalescence of comoving b and \bar{u} quarks from the $|uudb\bar{b}\rangle$ intrinsic bottom Fock state explains the production of the $\Lambda_b(udb)$ which was first observed at the ISR collider at CERN by Cifarelli, Zichichi, and their collaborators [9]. Furthermore, one finds that the Λ_b is produced in association with a positron from the decay of the associated high- x_F $B^0(u\bar{b})$ meson.

As emphasized by Lai, Tung, and Pumplin [10], the structure functions used to model charm and bottom quarks

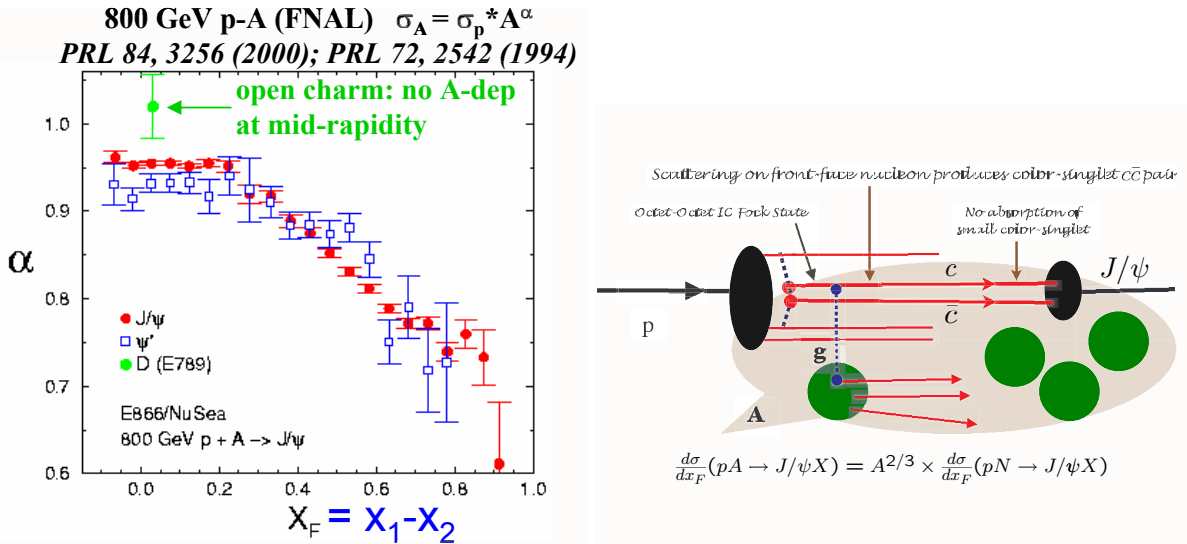


FIG. 2: (a) E866/NuSea data for the nuclear A dependence of J/ψ and ψ' hadroproduction. (b) Model for the A dependence of J/ψ hadroproduction based on color-octet intrinsic charm.

in the proton at large x_{bj} have been consistently underestimated, since they ignore intrinsic heavy quark fluctuations of hadron wavefunctions. Furthermore, the neglect of the intrinsic-heavy quark component in the proton structure function will lead to an incorrect assessment of the gluon distribution at large x if it is assumed that sea quarks always arise from gluon splitting [11]

The D0 collaboration [12] at the Tevatron has recently measured the processes $\bar{p}p \rightarrow c + \gamma + X$ and $\bar{p}p \rightarrow b + \gamma + X$ at very high photon transverse momentum: $p_T^\gamma \sim 120$ GeV/c. As seen in Fig. 1(c), the rate for $\bar{p}p \rightarrow b + \gamma X$ for bottom quark jets agrees very well with NLO PQCD predictions; however the corresponding charm jet cross section deviates strongly from the standard PQCD prediction for $p_T^\gamma > 60$ GeV/c. This photon plus charm jet anomaly can be explained if one allows for an intrinsic contribution to the charm structure function in $gc \rightarrow c\gamma$ at $Q^2 \sim 10^4$ GeV², but it requires a factor of two increase in strength compared to the CTEQ parameterization. This discrepancy could indicate that the reduction of the charm distribution due to DGLAP evolution has been overestimated.

The SELEX collaboration [13] has reported the discovery of a set of doubly-charmed spin 1/2 and spin 3/2 baryons with quantum numbers matching $|ccu\rangle$ and $|ccd\rangle$ bound states. The NA3 experiment has also observed the hadroproduction of two J/ψ s at high x_F , also a signal for seven quark Fock states like $|uudc\bar{c}\bar{c}\bar{c}\rangle$ in the proton. However, the mass splittings of the ccu and ccd states measured by SELEX are much larger than expected from known QCD isospin-splitting mechanisms. One speculative proposal [14] is that these baryons have a linear configuration $c\ q\ c$ where the light quark q is exchanged between the heavy quarks as in a linear molecule. The linear configuration enhances the Coulomb repulsion of the $c\ u\ c$ relative to $c\ d\ c$. It is clearly important to have experimental confirmation of the SELEX results.

The cross section for J/ψ production in a nuclear target is well measured. The ratio of the nuclear and proton target cross sections has the form $A^{\alpha(x_F)}$ where x_F is Feynman fractional longitudinal momentum of the J/ψ . At small x_F , $\alpha(x_F)$ is slightly smaller than one but at $x_F \sim 1$ it decreases to $\alpha = 2/3$. These results, as shown in Fig. 2(a), are surprising since (1) the value $\alpha = 2/3$ would be characteristic of a strongly interacting hadron, not a small-size quarkonium state; and (2) the functional dependence $A^{\alpha(x_F)}$ contradicts pQCD factorization predictions. This anomaly, in combination with the anomalously large and flat cross sections measured at high x_F , is consistent with a QCD mechanism based on color-octet intrinsic charm Fock states: because of its large color dipole moment, the intrinsic heavy quark Fock state of the proton: $|uud\rangle_{8_C}(c\bar{c})_{8_C}$ interacts primarily with the $A^{2/3}$ nucleons at the front surface. See Fig. 2(b). The $c\bar{c}$ color octet thus scatters on a front-surface nucleon, changes to a color singlet, and then propagates through the nucleus as a J/ψ at high x_F . Alternatively, one can postulate strong energy losses of a color octet $c\bar{c}$ state as it propagates in the nucleus but it is hard to see how this can account for the observed nearly flat behavior of the $A^{2/3}$ component as observed by NA3.

Intrinsic heavy quarks also provide a novel mechanism for the inclusive and diffractive Higgs production $pp \rightarrow ppH$, in which the Higgs boson carries a significant fraction of the projectile proton momentum. [15, 16] The production mechanism is based on the subprocess $(Q\bar{Q})g \rightarrow H$ where the Higgs acquires the momentum of the $Q\bar{Q}$ pair in the

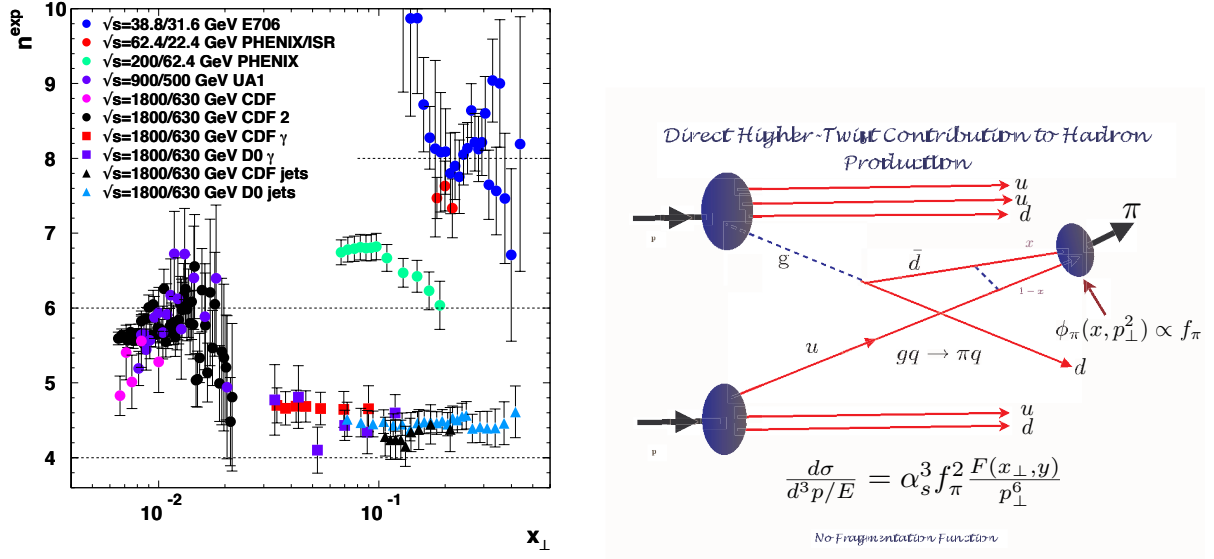


FIG. 3: (a) Scaling of inclusive cross sections for hadron, photons and jets at high p_T at fixed $x_T = 2 \frac{p_T}{\sqrt{s}}$. (b) Example of a direct QCD contribution for pion production. [18, 19].

$|uudQ\bar{Q}\rangle$ intrinsic heavy quark Fock state of the colliding proton and thus has approximately 80% of the projectile proton's momentum. The high- x_F Higgs could be accessed at the LHC using far forward detectors or arranging the proton beams to collide at a significant crossing angle. It is also possible to produce a light mass Higgs at threshold using the 7 TeV proton beam colliding with a fixed nuclear target.

III. THE UNEXPECTED ROLE OF DIRECT PROCESSES IN HIGH p_T HADRON REACTIONS

It is normally assumed that hadrons produced at high transverse momentum in inclusive high energy hadronic collisions such as $pp \rightarrow HX$ only arise from quark and gluon jet fragmentation. A fundamental test of leading-twist QCD predictions in high transverse momentum hadronic reactions is the measurement of the power-law fall-off of the inclusive cross section [17] $Ed\sigma/d^3p(AB \rightarrow CX) = F(\theta_{cm}, x_T)/p_T^{n_{\text{eff}}}$ at fixed $x_T = 2p_T/\sqrt{s}$ and fixed θ_{CM} . In the case of the scale-invariant parton model $n_{\text{eff}} = 4$. However in QCD $n_{\text{eff}} \sim 4 + \delta$ where $\delta \simeq 1.5$ is the typical correction to the conformal prediction arising from the QCD running coupling and the DGLAP evolution of the input parton distribution and fragmentation functions. [18, 19]

The usual expectation is that leading-twist subprocesses (i.e., the leading power-law contributions) will dominate measurements of high p_T hadron production at RHIC and at Tevatron energies. In fact, the data for isolated photon production $pp \rightarrow \gamma_{\text{direct}} X$, as well as jet production, agrees well with the leading-twist scaling prediction $n_{\text{eff}} \simeq 4.5$. [18] However, measurements of n_{eff} for hadron production are not consistent with the leading twist predictions. See Fig. 3(a). Striking deviations from the leading-twist predictions were also observed at lower energy at the ISR and Fermilab fixed-target experiments. [17] This deviation points to a significant contribution from direct higher-twist processes where the hadron is created directly in the hard subprocess rather than from quark or gluon jet fragmentation.

In fact, a significant fraction of high p_{\perp}^H isolated hadrons can emerge directly from hard higher-twist subprocess [18, 19] even at the LHC. An example is shown in Fig. 3(b). The direct production of hadrons can also explain [21] the remarkable “baryon anomaly” observed at RHIC: the ratio of baryons to mesons at high p_{\perp}^H , as well as the power-law fall-off $1/p_{\perp}^n$ at fixed $x_{\perp} = 2p_{\perp}/\sqrt{s}$, both increase with centrality, [24] opposite to the usual expectation that protons should suffer more energy loss in the nuclear medium than mesons. The high values n_{eff} with x_T seen in the data indicate the presence of an array of higher-twist processes, including subprocesses where the hadron enters directly, rather than through jet fragmentation. [20] Although they are suppressed by powers of $1/p_T$, the direct higher twist processes can dominate because they are energy efficient – no same side energy or momentum is lost from the undetected fragments. Thus the incident colliding partons are evaluated at the minimum possible values of light-front momentum fractions x_1 and x_2 , where the parton distribution functions are numerically large.

Normally many more pions than protons are produced at high transverse momentum in hadron-hadron collisions. This is also true for the peripheral collisions of heavy ions. However, when the nuclei collide with maximal overlap (central collisions) the situation is reversed – more protons than pions emerge. This observation at RHIC [24] contradicts the usual expectation that protons should be more strongly absorbed than pions in the nuclear medium. This deviation also points to a significant contribution from direct higher twist processes where hadrons, particularly baryons are created directly in the hard subprocess rather than from quark or gluon jet fragmentation. Since these processes create color-transparent baryons, this mechanism can explain the RHIC baryon anomaly. [21]. Evidence for color transparency [22] is particularly clear in diffractive dijet production on nuclei [23]

IV. BREAKDOWN OF PERTURBATIVE QCD FACTORIZATION THEOREMS

The factorization picture derived from the parton and pQCD has played a guiding role in virtually all aspects of hadron physics phenomenology. In the case of inclusive reactions such as $\frac{E_H d\sigma}{d^3p_H}(pp \rightarrow HX)$, the pQCD ansatz predicts that the cross section at leading order in the transverse momentum p_T can be computed by convoluting the perturbatively calculable hard subprocess quark and gluon cross section with the process-independent structure functions of the colliding hadrons with the quark fragmentation functions. The resulting cross section scales as $1/p_T^4$, modulo the DGLAP scaling violations derived from the logarithmic evolution of the structure functions and fragmentation distributions, as well as the running of the QCD coupling appearing in the hard scattering subprocess matrix element.

The effects of final-state interactions of the scattered quark in deep inelastic scattering have been traditionally assumed to either give an inconsequential phase factor or power-law suppressed corrections. However, this is only true for sufficiently inclusive cross sections. For example, consider semi-inclusive deep inelastic lepton scattering (SIDIS) on a polarized target $\ell p \rightarrow H \ell' X$. In this case the final-state gluonic interactions of the scattered quark lead to a T -odd non-zero spin correlation of the plane of the lepton-quark scattering plane with the polarization of the target proton [25] which is not power-law suppressed with increasing virtuality of the photon Q^2 ; i.e. it Bjorken-scales. This leading-twist “Sivers effect” [26] is nonuniversal in the sense that pQCD predicts an opposite-sign correlation in Drell-Yan reactions relative to single-inclusive deep inelastic scattering. [27, 28] This important but yet untested prediction occurs because the Sivers effect in the Drell-Yan reaction is modified by the initial-state interactions of the annihilating antiquark.

Similarly, the final-state interactions of the produced quark with its comoving spectators in SIDIS produces a final-state T -odd polarization correlation – the “Collins effect”. This can be measured without beam polarization by measuring the correlation of the polarization of a hadron such as the Λ baryon with the quark-jet production plane. Analogous spin effects occur in QED reactions due to the rescattering via final-state Coulomb interactions. Although the Coulomb phase for a given partial wave is infinite, the interference of Coulomb phases arising from different partial waves leads to observable effects. These considerations have led to a reappraisal of the range of validity of the standard factorization ansatz. [38]

The calculation of the Sivers single-spin asymmetry in deep inelastic lepton scattering in QCD is illustrated in Fig. 4. The analysis requires two different orbital angular momentum components: S -wave with the quark-spin parallel to the proton spin and P -wave for the quark with anti-parallel spin; the difference between the final-state “Coulomb” phases leads to a $\vec{S} \cdot \vec{q} \times \vec{p}$ correlation of the proton’s spin with the virtual photon-to-quark production plane. [25] Thus, as it is clear from its QED analog, the final-state gluonic interactions of the scattered quark lead to a T -odd non-zero spin correlation of the plane of the lepton-quark scattering plane with the polarization of the target proton. [25]

The S - and P -wave proton wavefunctions also appear in the calculation of the Pauli form factor quark-by-quark. Thus one can correlate the Sivers asymmetry for each struck quark with the anomalous magnetic moment of the proton carried by that quark, [29] leading to the prediction that the Sivers effect is larger for positive pions as seen by the HERMES experiment at DESY, [31] the COMPASS experiment [32–34] at CERN, and CLAS at Jefferson Laboratory [35, 36]

This leading-twist Bjorken-scaling “Sivers effect” is nonuniversal since QCD predicts an opposite-sign correlation [27, 28] in Drell-Yan reactions due to the initial-state interactions of the annihilating antiquark. The S - and P -wave proton wavefunctions also appear in the calculation of the Pauli form factor quark-by-quark. Thus one can correlate the Sivers asymmetry for each struck quark with the anomalous magnetic moment of the proton carried by that quark [29], leading to the prediction that the Sivers effect is larger for positive pions.

The physics of the “lensing dynamics” or Wilson-line physics [30] underlying the Sivers effect involves nonperturbative quark-quark interactions at small momentum transfer, not the hard scale Q^2 of the virtuality of the photon. It would be interesting to see if the strength of the soft initial- or final- state scattering can be predicted using the effective confining potential of QCD from light-front holographic QCD.

Measurements [37] of the Drell-Yan Process $\pi p \rightarrow \mu^+ \mu^- X$ display an angular distribution which contradicts pQCD

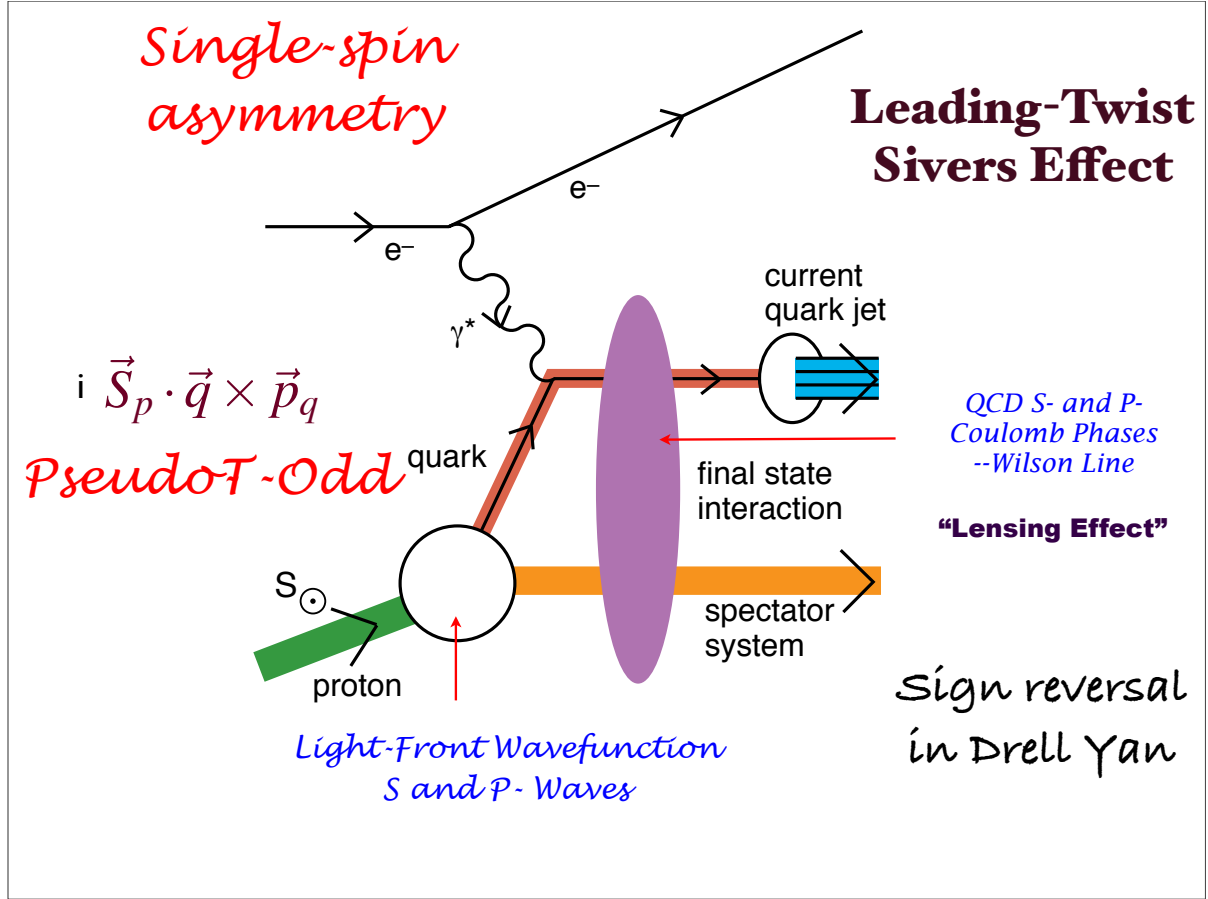


FIG. 4: Origin of the Sivers single-spin asymmetry in deep inelastic lepton scattering.

expectations. In particular one observes an anomalously large $\cos 2\phi$ azimuthal angular correlation between the lepton decay plane and its production plane which contradicts the Lam-Tung relation, a prediction of perturbative QCD factorization. [39] Such effects again point to the importance of initial and final-state interactions of the hard-scattering constituents, [40] corrections not included in the standard pQCD factorization formalism.

As noted by Collins and Qiu, [38] the traditional factorization formalism of perturbative QCD fails in detail for many hard inclusive reactions because of initial- and final-state interactions. For example, if both the quark and antiquark in the Drell-Yan subprocess $q\bar{q} \rightarrow \mu^+\mu^-$ interact with the spectators of the other hadron, then one predicts a $\cos 2\phi \sin^2 \theta$ planar correlation in unpolarized Drell-Yan reactions. [40] This “double Boer-Mulders effect” can account for the anomalously large $\cos 2\phi$ correlation and the corresponding violation [40, 41] of the Lam Tung relation for Drell-Yan processes observed by the NA10 collaboration. [37] Such effects again point to the importance of initial and final-state interactions of the hard-scattering constituents, corrections not included in the standard pQCD factorization formalism. One also observes large single spin asymmetries in reactions such as $pp \rightarrow \pi X$, an effect not yet explained. [42] Another important signal for factorization breakdown at the LHC will be the observation of a $\cos 2\phi$ planar correlation in dijet production.

The final-state interactions of the struck quark with the target spectators [43] also lead to diffractive events in deep inelastic scattering (DDIS) at leading twist, such as $lp \rightarrow l'p'X$, where the proton remains intact and isolated in rapidity; in fact, approximately 10 % of the deep inelastic lepton-proton scattering events observed at HERA are diffractive. [44, 45] This seems surprising since the underlying hard subprocess $lq \rightarrow l'q'$ is highly disruptive of the target nucleon. The presence of a rapidity gap between the target and diffractive system requires that the target remnant emerges in a color-singlet state; this is made possible in any gauge by the soft rescattering incorporated in the Wilson line or by augmented light-front wavefunctions. Quite different fractions of single $pp \rightarrow \text{Jet } p'X$ and double diffractive $p\bar{p} \rightarrow \text{Jet } p'\bar{p}'X$ events are observed at the Tevatron. The underlying mechanism is believed to be soft gluon exchange between the scattered quark and the remnant system in the final state occurring after the hard scattering occurs.

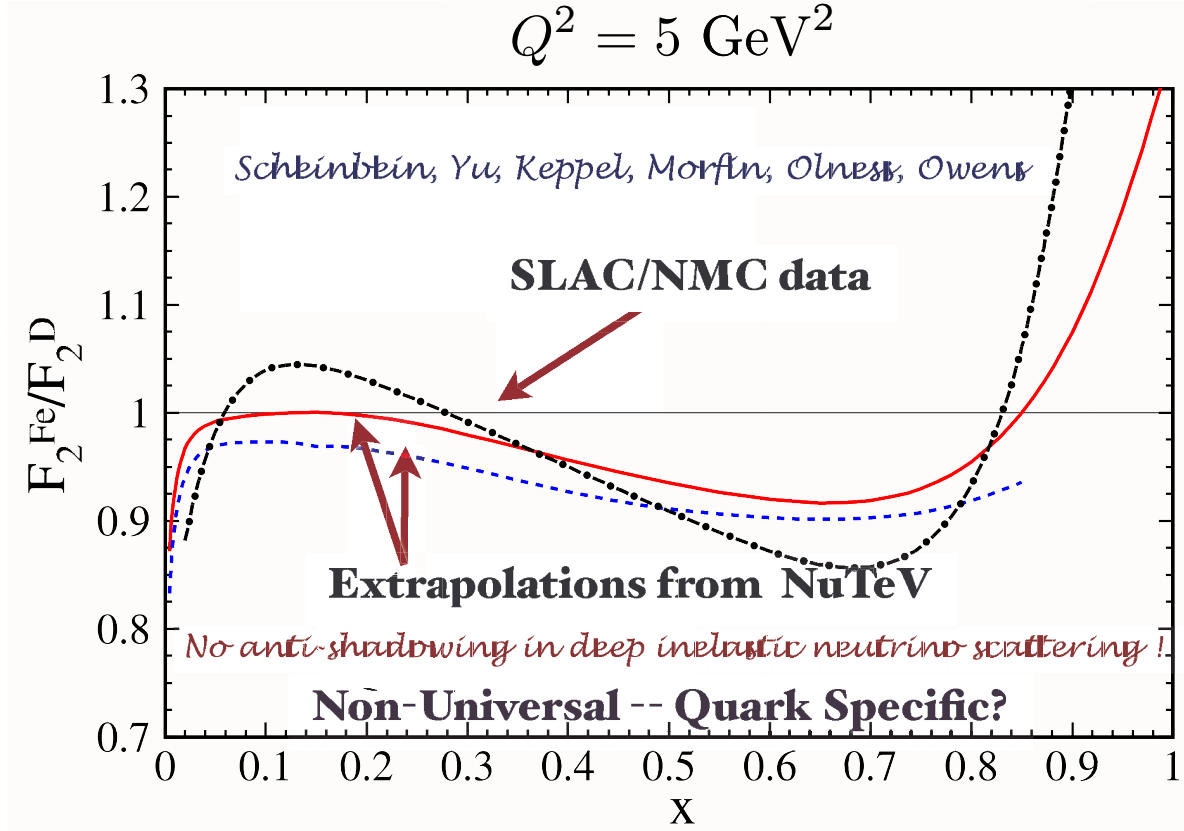


FIG. 5: Antishadowing is nonuniversal.

One can show [46] using Gribov-Glauber theory that the Bjorken-scaling diffractive deep inelastic scattering events lead to the shadowing of nuclear structure functions at small x_{Bjorken} . This is due to the destructive interference of two-step and one step amplitudes in the nucleus. Since diffraction involves rescattering, one sees that shadowing and diffractive processes are not intrinsic properties of hadron and nuclear wavefunctions and structure functions, but are properties of the complete dynamics of the scattering reaction. [47]

The CDF [49] and D0 [50] experiments at the Tevatron have recently reported that the t and \bar{t} heavy quarks do not have the same momentum distributions in $\bar{p}p \rightarrow t\bar{t}X$ events. The observed asymmetry is much larger than predicted from QCD NLO corrections to the $\bar{q}q \rightarrow t\bar{t}$ subprocess. The Tevatron $t\bar{t}$ asymmetry may indicate the importance of rescattering Coulomb-like final state interactions of the top quarks with ud and $\bar{u}\bar{d}$ remnant spectators of the colliding proton and antiproton. [48]. This effect can also lead to a $t\bar{t}$ asymmetry in $pp \rightarrow t\bar{t}X$ collisions at the LHC since the t quark can be color-attracted of one of the spectator ud diquarks produced in the $q\bar{q} \rightarrow t\bar{t}$ subprocess; however, the effect would only significant when the t and ud systems have small rapidity separation. [48]

V. NON-UNIVERSAL ANTISHADOWING

It has been conventional to assume that the nuclear modifications to the structure functions measured in deep inelastic charged lepton-nucleus and neutrino-nucleus interactions are identical. In fact, Gribov-Glauber theory predicts that the antishadowing of nuclear structure functions is not universal, but depends on the quantum numbers of each struck quark and antiquark. [52] This observation can explain the recent analysis of Schienbein *et al.* [53] which finds that the NuTeV measurements of nuclear structure functions obtained from neutrino charged current reactions differ significantly from the distributions measured in deep inelastic electron and muon scattering. See Fig. 5. This implies that part of the anomalous NuTeV result for θ_W could be due to the non-universality of nuclear antishadowing for charged and neutral currents.

The *antishadowing* of the nuclear structure functions as observed in deep inelastic lepton-nucleus scattering is particularly interesting. Empirically, one finds $R_A(x, Q^2) \equiv$

$(F_{2A}(x, Q^2)/(A/2)F_d(x, Q^2)) > 1$ in the domain $0.1 < x < 0.2$; i.e., the measured nuclear structure function (referenced to the deuteron) is larger than the scattering on a set of A independent nucleons. There are leading-twist diffractive contributions $\gamma^* N_1 \rightarrow (q\bar{q})N_1$ arising from Reggeon exchanges in the t -channel. For example, isospin-non-singlet $C = +$ Reggeons contribute to the difference of proton and neutron structure functions, giving the characteristic Kutzi-Weiskopf $F_{2p} - F_{2n} \sim x^{1-\alpha_R(0)} \sim x^{0.5}$ behavior at small x . The x dependence of the structure functions reflects the Regge behavior $\nu^{\alpha_R(0)}$ of the virtual Compton amplitude at fixed Q^2 and $t = 0$. The phase of the diffractive amplitude is determined by analyticity and crossing to be proportional to $-1 + i$ for $\alpha_R = 0.5$, which together with the phase from the Glauber cut, leads to *constructive* interference of the diffractive and nondiffractive multi-step nuclear amplitudes. The nuclear structure function is predicted [51] to be enhanced precisely in the domain $0.1 < x < 0.2$ where antishadowing is empirically observed. The strength of the Reggeon amplitudes is fixed by the fits to the nucleon structure functions, so there is little model dependence. Since quarks of different flavors couple to different Reggeons, this leads to the remarkable prediction that nuclear antishadowing is not universal; [52] it depends on the quantum numbers of the struck quark. This picture implies substantially different antishadowing for charged and neutral current reactions, thus affecting the extraction of the weak-mixing angle θ_W .

VI. DYNAMIC VERSUS STATIC HADRONIC STRUCTURE FUNCTIONS

The nontrivial effects from rescattering and diffraction highlight the need for a fundamental understanding the dynamics of hadrons in QCD at the amplitude level. This is essential for understanding phenomena such as hadronization; i.e., the quantum mechanics of hadron formation, the remarkable effects of initial and final interactions, the origins of diffractive phenomena and single-spin asymmetries, and manifestations of higher-twist semi-exclusive hadron sub-processes.

It is usually assumed – following the intuition of the parton model – that the structure functions measured in deep inelastic scattering can be computed in the Bjorken-scaling leading-twist limit from the absolute square of the light-front wavefunctions, summed over all Fock states. In fact, dynamical effects, such as the Sivers spin correlation and diffractive deep inelastic lepton scattering due to final-state gluon interactions, contribute to the experimentally observed deep inelastic lepton-hadron cross sections. Diffractive events also lead to the interference of two-step and one-step processes in nuclei which in turn, via the Gribov-Glauber theory, lead to the shadowing and the antishadowing of the deep inelastic nuclear structure functions; [52] such lensing phenomena are not included in the light-front wavefunctions of the nuclear eigenstate. This leads to an important distinction between “dynamical” vs. “static” (wavefunction-specific) structure functions. [54]

It is thus important to distinguish [54] “static” structure functions which are computed directly from the light-front wavefunctions of a target hadron from the nonuniversal “dynamic” empirical structure functions which take into account rescattering of the struck quark in deep inelastic lepton scattering. See Fig. 6. The real wavefunctions of hadrons which underly the static structure functions cannot describe diffractive deep inelastic scattering nor single-spin asymmetries, since such phenomena involve the complex phase structure of the γ^*p amplitude. One can augment the light-front wavefunctions with a gauge link corresponding to an external field created by the virtual photon $q\bar{q}$ pair current, [55, 56] but such a gauge link is process dependent, so the resulting augmented wavefunctions are not universal. [27] The physics of rescattering and nuclear shadowing is not included in the nuclear light-front wavefunctions and a probabilistic interpretation of the nuclear DIS cross section in terms of hadron structure is thus precluded in principle, although it can often be treated as an effective approximation.

VII. THE PRINCIPLE OF MAXIMUM CONFORMALITY AND THE ELIMINATION OF THE RENORMALIZATION SCALE AMBIGUITY

A key difficulty in making precise perturbative QCD predictions is the uncertainty in determining the renormalization scale μ of the running coupling $\alpha_s(\mu^2)$. It is common practice to simply guess a physical scale $\mu = Q$ of order of a typical momentum transfer Q in the process, and then vary the scale over a range $Q/2$ and $2Q$. This procedure is clearly problematic, since the resulting fixed-order pQCD prediction will depend on the choice of renormalization scheme; it can even predict negative QCD cross sections at next-to-leading-order. If one uses the criterion that one should choose the renormalization scale to have minimum sensitivity, one gets the wrong answer in QED and even in QCD. The prediction violates the transitivity property of the renormalization group; it will also depend on the choice of renormalization scheme. Worse, if one tries to minimize sensitivity, the resulting renormalization scale goes to zero as the gluon jet virtuality becomes large in $e^+e^- \rightarrow q\bar{q}g$ three-jet events. [57]

The running coupling in any gauge theory sums all terms involving the β function; in fact, when the renormalization scale is set properly, all non-conformal $\beta \neq 0$ terms in a perturbative expansion arising from renormalization are

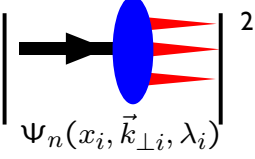
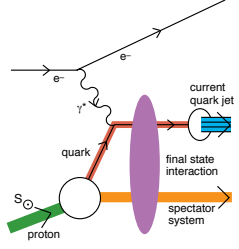
Static	Dynamic
<ul style="list-style-type: none"> • Square of Target LFWFs • No Wilson Line • Probability Distributions • Process-Independent • T-even Observables • No Shadowing, Anti-Shadowing • Sum Rules: Momentum and J^z • DGLAP Evolution; mod. at large x • No Diffractive DIS 	<ul style="list-style-type: none"> Modified by Rescattering: ISI & FSI Contains Wilson Line, Phases No Probabilistic Interpretation Process-Dependent - From Collision T-Odd (Sivers, Boer-Mulders, etc.) Shadowing, Anti-Shadowing, Saturation Sum Rules Not Proven DGLAP Evolution Hard Pomeron and Odderon Diffractive DIS
 <p>$\Psi_n(x_i, \vec{k}_{\perp i}, \lambda_i)$</p>	

FIG. 6: Static versus dynamic structure functions.

summed into the running coupling. The remaining terms in the perturbative series are then identical to those of a conformal theory; i.e., the corresponding theory with $\beta = 0$. As discussed by Di Giustino, Wu, and myself [58, 59], the resulting scale-fixed predictions using this “principle of maximum conformality” are independent of the choice of renormalization scheme – a key requirement of renormalization group invariance. In practice, the scale can often be determined from the n_f dependence of the NLO terms. The BLM/PMC scale also determines the number of effective flavors in the β -function. The results avoid renormalon resummation and agree with QED scale-setting in the Abelian limit. The PMC is the principle [58, 59] which underlies the BLM scale-setting method. [60]

Extended renormalization group equations, which express the invariance of physical observables under both the renormalization scale- and scheme-parameter transformations, provide a convenient way for analyzing the scale- and scheme-dependence of the physical process. In a recent paper [59], we have analyzed the scale-dependence of the extended renormalization group equations at the four-loop level. Using the principle of maximum conformality, all non-conformal $\{\beta_i\}$ terms in the perturbative expansion series can be summed into the running coupling, and the resulting scale-fixed predictions are verified to be independent of the renormalization scheme. Different schemes lead to different effective PMC/BLM scales, but the final results are scheme independent. Conversely, from the requirement of scheme independence, one not only can obtain scheme-independent commensurate scale relations among different observables, but also determine the scale displacements among the PMC/BLM scales which are derived under different schemes. In principle, the PMC/BLM scales can be fixed order-by-order, and as a useful reference, we present a systematic and scheme-independent procedure for setting PMC/BLM scales up to NNLO.

Thus, most important, the BLM/PMC method gives results which are independent of the choice of renormalization scheme at each order of perturbation theory, as required by the transitivity property of the renormalization group. The argument of the running coupling constant acquires the appropriate displacement appropriate to its scheme so that the evaluated result is scheme-independent. In the case of Abelian theory, the scale is proportional to the photon virtuality and sums all vacuum polarization corrections to all orders.

The elimination of the renormalization scheme ambiguity will not only increase the precision of QCD tests, but it will also increase the sensitivity of LHC experiments and other measurements to new physics beyond the Standard Model. The BLM/PMC method also provides scale-fixed, scheme-independent high-precision connections between observables, such as the “Generalized Crewther Relation”, [61] as well as other “Commensurate Scale Relations”. [62,

[63] Clearly the elimination of the renormalization scale ambiguity would greatly improve the precision of QCD predictions and increase the sensitivity of searches for new physics at the LHC.

VIII. LIGHT-FRONT QUANTIZATION

The distributions of electrons within an atom are determined in QED using the Schrödinger wavefunction, the eigenfunction of the QED Hamiltonian. In principle, one could calculate hadronic spectroscopy and wavefunctions by solving for the eigenstates of the QCD Hamiltonian: $H|\Psi\rangle = E|\Psi\rangle$ at fixed time t . However, this traditional method – called the “instant” form” by Dirac, [64] is plagued by complex vacuum and relativistic effects, as well as by the fact that the boost of such fixed- t wavefunctions away from the hadron’s rest frame is an intractable dynamical problem. However, there is an extraordinarily powerful non-perturbative alternative – quantization at fixed light-front (LF) time $\tau = t + z/c = x^+ = x^0 + x^3$ – the “front-form” of Dirac. [64] In this framework each hadron H is identified as an eigenstate of the QCD Hamiltonian $H_{LF}^{QCD}|\Psi_H\rangle = M_H^2|\Psi_H\rangle$, where $H_{LF}^{QCD} = P_\mu P^\mu = P^- P^+ - P_\perp^2$ is derived directly from the QCD Lagrangian or action. The eigenvalues of this Heisenberg equation give the complete mass spectrum of hadrons. The eigensolution $|\Psi_H\rangle$ projected on the free Fock basis provides the set of valence and non-valence light-front Fock state wavefunctions $\Psi_{n/H}(x_i, k_{\perp i}, \lambda_i)$, which describe the hadron’s momentum and spin distributions and the direct measures of its structure at the quark and gluon level. If one quantizes the gluon field in light-cone gauge $A^+ = A^0 + A^3 = 0$, the gluons have physical polarization $S^z = \pm 1$, there are no ghosts, so that one has a physical interpretation of the quark and gluon constituents. The constituents of a bound state in a light-front wavefunction are measured at the same light-front time τ – along the front of a light-wave, as in a flash picture. In contrast, the constituents of a bound state in an instant form wavefunction must be measured at the same instant time t – this requires the exact synchrony in time of many simultaneous probes.

A remarkable feature of LFWFs is the fact that they are frame independent; i.e., the form of the LFWF is independent of the hadron’s total momentum $P^+ = P^0 + P^3$ and P_\perp . The boost invariance of LFWFs contrasts dramatically with the complexity of boosting the wavefunctions defined at fixed time t . [65] Light-front quantization is thus the ideal framework to describe the structure of hadrons in terms of their quark and gluon degrees of freedom. The constituent spin and orbital angular momentum properties of the hadrons are also encoded in the LFWFs. The total angular momentum projection [66] $J^z = \sum_{i=1}^n S_i^z + \sum_{i=1}^{n-1} L_i^z$ is conserved Fock-state by Fock-state and by every interaction in the LF Hamiltonian. The constituent spin and orbital angular momentum properties of the hadrons are thus encoded in their LFWFs. The empirical observation that quarks carry only a small fraction of the nucleon angular momentum highlights the importance of quark orbital angular momentum. In fact the nucleon anomalous moment and the Pauli form factor are zero unless the quarks carry nonzero L^z .

Hadron observables, e.g., hadronic structure functions, form factors, distribution amplitudes, GPDs, TMDs, and Wigner distributions can be computed as simple convolutions of light-front wavefunctions (LFWFs). For example, one can calculate the electromagnetic and gravitational form factors $\langle p+q|j^\mu(0)|p\rangle$ and $\langle p+q|t^{\mu\nu}(0)|p\rangle$ of a hadron from the Drell-Yan-West formula – i.e., the overlap of LFWFs. The anomalous gravitomagnetic moment $B(0)$ defined from the spin-flip matrix element $\langle p+q|t^{\mu\nu}(0)|p\rangle$ at $q \rightarrow 0$ vanishes – consistent with the equivalence theorem of gravity. In contrast, in the instant form, the overlap of instant time wavefunctions is not sufficient. One must also couple the photon probe to currents arising spontaneously from the vacuum which are connected to the hadron’s constituents. The Light-Front method is directly applicable for describing atomic bound states in both the relativistic and nonrelativistic domains; it is particularly useful for atoms in flight since the LFWFs are frame-independent. It also satisfies theorems such as cluster decomposition.

One can solve the LF Hamiltonian problem for theories in one-space and one-time by Heisenberg matrix diagonalization. For example, the complete set of discrete and continuum eigensolutions of mesons and baryons in QCD(1+1) can be obtained to any desired precision for general color, multiple flavors, and general quark masses using the discretized light-cone quantized (DLCQ) method. [67, 68] The DLCQ approach can in principle be applied to QED(3+1) and QCD(3+1); however, in practice, the huge matrix diagonalization problem is computational challenging.

IX. ADS/QCD AND LIGHT-FRONT HOLOGRAPHY

A long-sought goal in hadron physics is to find a simple analytic first approximation to QCD analogous to the Schrödinger-Coulomb equation of atomic physics. This problem is particularly challenging since the formalism must be relativistic, color-confining, and consistent with chiral symmetry. de Téramond and I [69] have shown that the gauge/gravity duality leads to a simple analytical and phenomenologically compelling nonperturbative approximation to the full light-front QCD Hamiltonian – “Light-Front Holography”. [69] Light-Front Holography is in fact one of the most remarkable features of the AdS/CFT correspondence. [71] In particular the soft-wall AdS/QCD model, modified

by a positive-sign dilaton metric, leads to a simple Schrödinger-like light-front wave equation and a remarkable one-parameter description of nonperturbative hadron dynamics [69]. The model predicts a zero-mass pion for massless quarks and a Regge spectrum of linear trajectories with the same slope in the (leading) orbital angular momentum L of the hadrons and their radial quantum number N .

Light front holographic methods allow one to project the functional dependence of the wavefunction $\Phi(z)$ computed in the AdS fifth dimension to the hadronic frame-independent light-front wavefunction $\psi(x_i, b_{\perp i})$ in $3+1$ physical space-time. The variable z maps to a transverse LF variable $\zeta(x_i, b_{\perp i})$. The result is a single-variable light-front Schrödinger equation which determines the eigenspectrum and the LFWFs of hadrons for general spin and orbital angular momentum. The transverse coordinate ζ is closely related to the invariant mass squared of the constituents in the LFWF and its off-shellness in the LF kinetic energy, and it is thus the natural variable to characterize the hadronic wavefunction. In fact ζ is the only variable to appear in the relativistic light-front Schrödinger equations predicted from holographic QCD in the limit of zero quark masses. The coordinate z in AdS space is thus uniquely identified with a Lorentz-invariant coordinate ζ which measures the separation of the constituents within a hadron at equal light-front time.

The result is a semi-classical frame-independent first approximation to the spectra and light-front wavefunctions of meson and baryon light-quark bound states, which in turn predicts the behavior of the pion and nucleon form factors. The hadron eigenstates generally have components with different orbital angular momentum; e.g., the proton eigenstate in AdS/QCD with massless quarks has $L^z = 0$ and $L^z = 1$ light-front Fock components with equal probability. Thus in AdS/QCD the spin of the proton is carried by the quark orbital angular momentum: $J^z = \langle L^z \rangle = \pm 1/2$ since $\langle \sum S_q^z \rangle = 0$, [72] helping to explain the “spin-crisis”.

The AdS/QCD soft-wall model also predicts the form of the non-perturbative effective coupling $\alpha_s^{AdS}(Q)$ as shown in fig. 7(d) and its β -function in excellent agreement with JLAB measurements. [70] The AdS/QCD light-front wavefunctions also lead to a proposal for computing the hadronization of quark and gluon jets at the amplitude level. [73]

In general the QCD Light-Front Hamiltonian can be systematically reduced to an effective equation in acting on the valence Fock state. This is illustrated for mesons in fig. 7. The kinetic energy contains a term L^2/ζ^2 analogous to $\ell(\ell+1)/r^2$ in nonrelativistic theory, where the invariant $\zeta^2 = x(1-x)b_{\perp}^2$ is conjugate to the $q\bar{q}$ invariant mass $k_{\perp}^2/x(1-x)$. It plays the role of the radial variable r . Here $L = L^z$ is the projection of the orbital angular momentum appearing in the ζ, ϕ basis. In QCD, the interaction U couples the valence state to all Fock states. The AdS/QCD model has the identical structure as the reduced form of the LF Hamiltonian, but it also specifies the confining potential as $U(\zeta, S, L) = \kappa^4 \zeta^2 + \kappa^2(L + S - 1/2)$. This correspondence, plus the fact that one can match the AdS/QCD formulae for elastic electromagnetic and gravitational form factors to the LF Drell-Yan West formula, is the basis for light-front holography. The light-quark meson and baryon spectroscopy is well described taking the mass parameter $\kappa \simeq 0.5$ GeV. The linear trajectories in $M_H^2(n, L)$ have the same slope in L and n , the radial quantum number. The corresponding LF wavefunctions are functions of the off-shell invariant mass. AdS/QCD, together with Light-Front Holography [69] thus provides a simple Lorentz-invariant color-confining approximation to QCD which is successful in accounting for light-quark meson and baryon spectroscopy as well as their LFWFs. This semiclassical approximation to light-front QCD is expected to break down at short distances where hard gluon exchange and quantum corrections become important. The model can be systematically improved by Lippmann-Schwinger methods [75] or using the AdS/QCD orthonormal basis to diagonalize the LF Hamiltonian. One can also improve the semiclassical approximation by introducing nonzero quark masses and short-range Coulomb corrections, thus extending the predictions of the model to the dynamics and spectra of heavy and heavy-light quark systems. [74]

X. QCD CONDENSATES AND THE COSMOLOGICAL CONSTANT

It is conventional to assume that the vacuum of QCD contains quark $\langle 0|q\bar{q}|0\rangle$ and gluon $\langle 0|G^{\mu\nu}G_{\mu\nu}|0\rangle$ vacuum condensates. However, as reviewed by Zee [76], the resulting vacuum energy density from QCD leads to a 10^{45} order-of-magnitude or more discrepancy with the measured cosmological constant. In fact, Zee has called this conflict “one of the gravest puzzles of theoretical physics.” This extraordinary contradiction between theory and cosmology has been used as an argument for the anthropic principle. [77] The resolution of this long-standing puzzle has been suggested [84], motivated by Bethe-Salpeter and light-front analyses in which the QCD condensates are identified as “in-hadron” condensates, rather than vacuum entities, but consistent with the Gell Mann-Oakes-Renner relation. [78] See. Fig. 8. The “in-hadron” condensates become realized as higher Fock states of the hadron when the theory is quantized at fixed light-front time $\tau = t - z/c$.

Hadronic condensates have played an important role in quantum chromodynamics (QCD). Conventionally, these condensates are considered to be properties of the QCD vacuum and hence to be constant throughout space-time. Recently a new perspective on the nature of QCD condensates $\langle \bar{q}q \rangle$ and $\langle G_{\mu\nu}G^{\mu\nu} \rangle$, particularly where they have

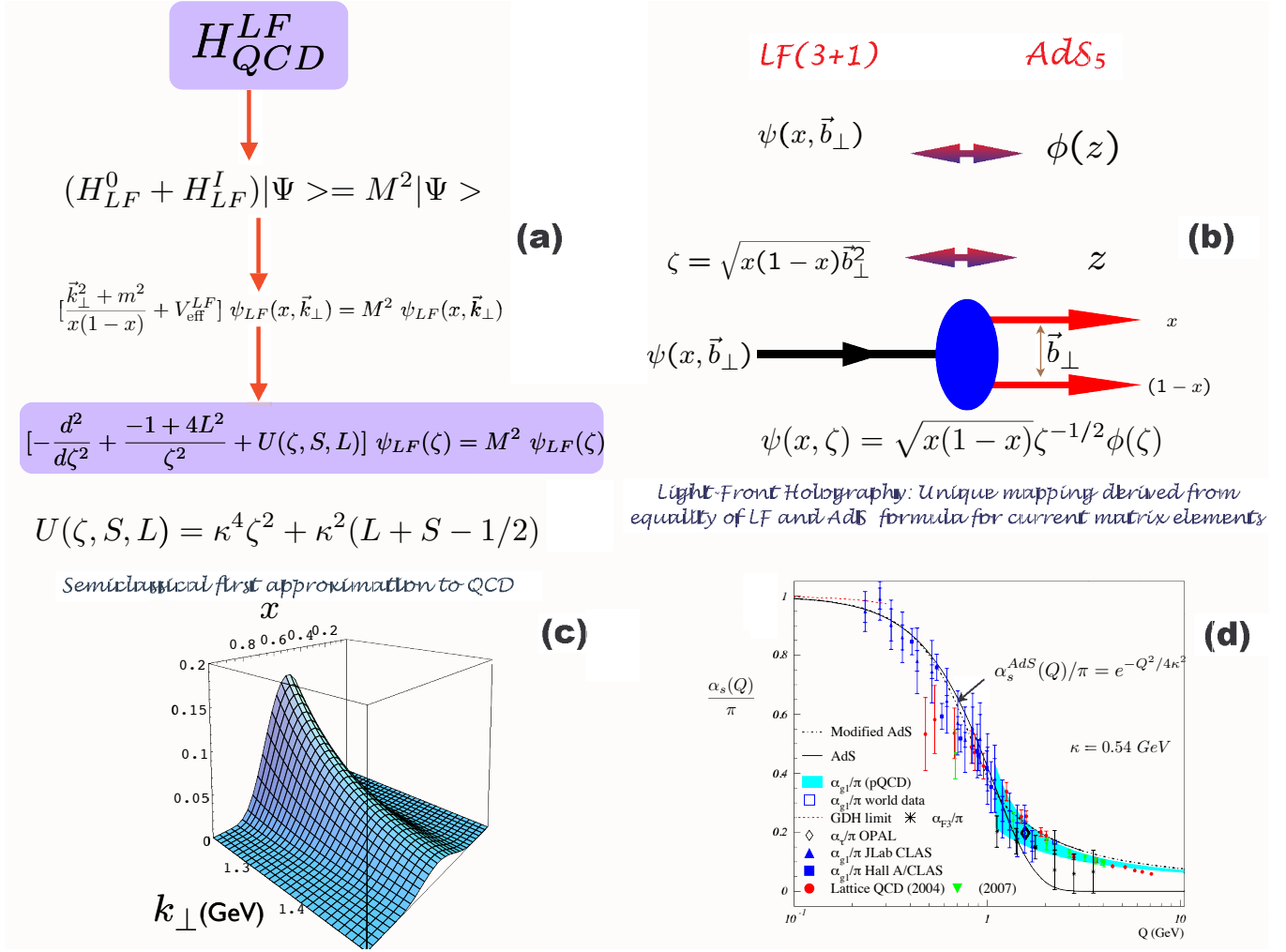


FIG. 7: (a) Reduction of the Light-Front Hamiltonian to an effective LF Schrodinger Equation for mesons. (b) Mapping of the fifth dimension coordinate z to the invariant LF separation variable ζ . The insert (c) shows the AdS/QCD – light-front holography prediction for the pion’s valence LFWF $\psi(x, \vec{k}_\perp)$. (d) The running coupling predicted by AdS/QCD normalized to $\alpha_s/\pi = 1$ compared with the effective charge defined from the Bjorken sum rule. From Ref. [69].

spatial and temporal support, has been presented. [79] A key ingredient in this approach is the use of Dirac’s “Front Form”; [64] i.e., the light-front (infinite momentum) frame to analyze the condensates. In this formulation the spatial support of condensates is restricted to the interior of hadrons, since in the LF vacuum is an empty Fock state. Thus condensates arise due to the interactions of quarks and gluons which are confined within hadrons.

Physical eigenstates are built from operators acting on the vacuum. It is thus important to distinguish two very different concepts of the vacuum in quantum field theories such as QED and QCD. The conventional instant-form vacuum is a state defined at the same time t at all spatial points in the universe. In contrast, the front-form vacuum only senses phenomena which are causally connected; i.e., or within the observer’s light-cone. The instant-form vacuum is defined as the lowest energy eigenstate of the instant-form Hamiltonian. For example, the instant-form vacuum in QED is saturated with quantum loops of leptons and photons. In calculations of physical processes one must then normal-order the vacuum and divide the S -matrix elements by the disconnected vacuum loops. In contrast, the front-form (light-front) vacuum is defined as the lowest mass eigenstate of light-front Hamiltonian defined by quantizing at fixed $\tau = t - z/c$. The vacuum is remarkably simple in light-front quantization because of the restriction $k^+ \geq 0$. For example QED vacuum graphs such as $e^+e^-\gamma$ do not arise. The LF vacuum thus coincides with the vacuum of the free LF Hamiltonian. The front-form vacuum and its eigenstates are causal and Lorentz invariant; whereas the instant form vacuum depends on the observer’s Lorentz frame. The instant-form vacuum is a state defined at the same time t at all spatial points in the universe. In contrast, the front-form vacuum only senses phenomena which

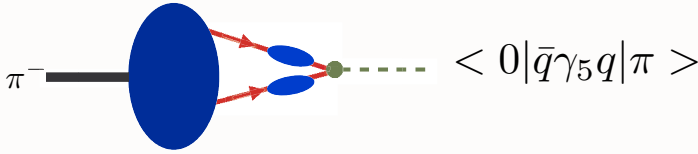
Gell-Mann Oakes Renner Formula in QCD

$$m_\pi^2 = -\frac{(m_u + m_d)}{f_\pi^2} \langle 0 | \bar{q}q | 0 \rangle$$

**current algebra:
effective pion field**

$$m_\pi^2 = -\frac{(m_u + m_d)}{f_\pi} \langle 0 | i\bar{q}\gamma_5 q | \pi \rangle$$

**QCD: composite pion
Bethe-Salpeter Eq.**



Maris, Roberts, Tandy

FIG. 8: Revised GMOR Relation.

are causally connected; i.e., or within the observer's light-cone. Causality in quantum field theory follows the fact that commutators vanish outside the light-cone. In fact in the LF analysis the spatial support of QCD condensates is restricted to the interior of hadrons, physics which arises due to the interactions of confined quarks and gluons. In the Higgs theory, the usual Higgs vacuum expectation value is replaced with a $k^+ = 0$ zero mode; [80] however, the resulting phenomenology is identical to the standard analysis.

When one makes a measurement in hadron physics, such as deep inelastic lepton-proton scattering, one probes hadron's constituents consistent with causality – at a given light front time, not at instant time. Similarly, when one makes observations in cosmology, information is obtained within the causal horizon; i.e., consistent with the finite speed of light. The cosmological constant measures the matrix element of the energy momentum tensor $T^{\mu\nu}$ in the background universe. It corresponds to the measurement of the gravitational interactions of a probe of finite mass; it only senses the causally connected domain within the light-cone of the observer. If the universe is empty, the appropriate vacuum state is thus the LF vacuum since it is causal. One automatically obtains a vanishing cosmological constant from the LF vacuum. Thus, as argued in Refs. [83, 84] the 45 orders of magnitude conflict of QCD with the observed value of the cosmological condensate is removed, and a new perspective on the nature of quark and gluon condensates in QCD is thus obtained. [79, 83, 84].

In fact, in the LF analysis one finds that the spatial support of QCD condensates is restricted to the interior of hadrons, physics which arises due to the interactions of color-confined quarks and gluons. The condensate physics normally associated with the instant-form vacuum is replaced by the dynamics of higher non-valence Fock states as shown in the context of the infinite momentum/light-front method by Casher and Susskind. [81] and Burkardt [82] In particular, chiral symmetry is broken in a limited domain of size $1/m_\pi$, in analogy to the limited physical extent of superconductor phases. This novel description of chiral symmetry breaking in terms of “in-hadron condensates” has also been observed in Bethe-Salpeter studies. [85–89] The usual argument for a quark vacuum condensate is the Gell-Mann–Oakes–Renner (GMOR) formula: $m_\pi^2 = -2m_q \langle 0 | \bar{q}q | 0 \rangle / f_\pi^2$. However, in the Bethe-Salpeter and light-front formalisms, where the pion is a $q\bar{q}$ bound-state, the GMOR relation is replaced by $m_\pi^2 = -2m_q \langle 0 | \bar{q}\gamma_5 q | \pi \rangle / f_\pi$, where $\rho_\pi \equiv -\langle 0 | \bar{q}\gamma_5 q | \pi \rangle$ represents a pion decay constant via an elementary pseudoscalar current. The result is independent of the renormalization scale. In the light-front formalism, this matrix element derives from the $|q\bar{q}\rangle$ Fock

state of the pion with parallel spin-projections $S^z = \pm 1$ and $L^z = \mp 1$, which couples by quark spin-flip to the usual $|q\bar{q}\rangle$ $S^z = 0, L^z = 0$ Fock state via the running quark mass. Thus again one finds “in-hadron condensates” replacing vacuum condensates: the $\langle 0|\bar{q}q|0\rangle$ vacuum condensate which appears in the Gell-Mann Oakes Renner formula is replaced by the $\langle 0|\bar{q}\gamma_5|\pi\rangle$ pion decay constant. This new perspective also explains the results of studies [90–92] which find no significant signal for the vacuum gluon condensate.

XI. CONCLUSIONS

In this talk, I have highlighted a number of areas where conventional wisdom in QCD and hadron physics has been challenged. These include standard assumptions such as

1. The heavy quark sea is conventionally assumed to arise only from gluon splitting and is thus confined to the low x domain; in fact, QCD also predicts intrinsic contributions [4] where the heavy quarks are multi-connected to the valence quarks and appear at the same rapidity as the valence quarks; i.e., at large light-cone momentum fractions x . This has important consequences for heavy quark phenomena at large x_F and large transverse momentum as well as in weak decays of the B -meson [93].
2. Initial-state and final-state Interactions are assumed to be power-law suppressed. This is contradicted by factorization-breaking lensing phenomena such as the Sivers effect in polarized single-inclusive deep inelastic scattering [25] as well as and the breakdown [40] of the Lam-Tung relation in Drell-Yan reactions.
3. The structure function of a hadron is usually assumed to reflect just the physics of the wavefunction of the hadron, and thus it must be process independent; in fact, the observed structure functions are sensitive to process-dependent rescattering and lensing processes at leading twist. One thus should distinguish dynamical versus static structure functions [54].
4. Antishadowing is usually assumed to be a property of the nuclear wavefunction and is thus process-independent. In fact as the NuTeV data shows [53] each quark can have its own antishadowing distribution [51, 52].
5. High-transverse momentum hadrons in inclusive reactions are usually assumed to arise only from jet fragmentation. In fact, there is a significant probability for high p_T hadrons to arise from “direct” color-transparent subprocesses. This can explain anomalies in the fixed x_T cross section and the baryon anomaly, the large proton to pion ratio observed in heavy-ion collisions at RHIC [18].
6. Conventional wisdom states that the renormalization scale in QCD cannot be fixed and can only be guessed or chosen to minimize sensitivity. In fact, it can be fixed at each order in perturbation theory using the principle of maximal conformality(PMC) [58, 59] The result is scheme-independent way and agrees with the conventional QED procedure in the Abelian limit.
7. It is standard wisdom that QCD condensates must be properties of the vacuum. In fact, one finds that vacuum condensates are replaced by hadronic matrix elements in the Bethe-Salpeter and light-front analyses. The conflict of traditional analyses with the cosmological constant highlights the need to distinguish different concepts of the vacuum: the acausal instant form vacuum versus the causal light-front definition [78].
8. Usually nuclei are regarded as composites of color-singlet nucleons; in fact, QCD predicts “hidden color” configurations of the quarks which can dominate short distance nuclear reactions. [94]
9. It is conventional to take the real part of the virtual Compton scattering amplitude to be arbitrary subtraction term; in fact, local four-point photon-quark scattering leads to a real amplitude [95], a “ $J = 0$ fixed pole” which is constant in energy and independent of the photons’ virtuality at fixed t .
10. Gluon degrees of freedom should be manifest at all scales - however, in AdS/QCD the effects of soft gluons are sublimated in favor of the QCD confinement potential [96].
11. Orbital angular momentum in the low lying hadrons is often assumed to be negligible. In fact, in AdS/QCD the nucleon eigensolutions for the light quarks have $L^z = \pm 1$ orbital components comparable in strength to the $L^z = 0$ component [72]. This observation can help to explain the empirical fact that only a small fraction of the proton’s spin is carried by quark or gluon spin.

Acknowledgments

Presented at the International Symposium on Subnuclear Physics: Past, Present and Future, held at the Pontifical Academy of Sciences in the Vatican from 30 Oct. to 2 Nov. 2011, I am grateful to Professor Antonio Zichichi, the organizer of the symposium, and Marcelo Snchez Sorondo, the Chancellor of the Pontifical Academy of Sciences at the Vatican, for their invitation to this unique and outstanding conference. I also thank my collaborators for many helpful conversations. This research was supported by the Department of Energy contract DE-AC02-76SF00515. SLAC-PUB-14865.

-
- [1] H. Fritzsch, M. Gell-Mann and H. Leutwyler, “Advantages of the Color Octet Gluon Picture,” *Phys. Lett. B* **47**, 365 (1973).
 - [2] S. J. Brodsky and P. Huet, “Aspects of $SU(N(c))$ gauge theories in the limit of small number of Phys. Lett. B **417**, 145 (1998) [arXiv:hep-ph/9707543].
 - [3] A. Airapetian *et al.* [HERMES Collaboration], “Measurement of Parton Distributions of Strange Quarks in the Nucleon from Phys. Lett. B **666**, 446 (2008) [arXiv:0803.2993 [hep-ex]].
 - [4] S. J. Brodsky, P. Hoyer, C. Peterson and N. Sakai, “The Intrinsic Charm of the Proton,” *Phys. Lett. B* **93**, 451 (1980).
 - [5] S. J. Brodsky, J. C. Collins, S. D. Ellis, J. F. Gunion and A. H. Mueller, “INTRINSIC CHEVROLETS AT THE SSC,”
 - [6] B. W. Harris, J. Smith and R. Vogt, “Reanalysis of the EMC charm production data with extrinsic and intrinsic Nucl. Phys. B **461**, 181 (1996) [arXiv:hep-ph/9508403].
 - [7] M. Franz, M. V. Polyakov and K. Goeke, “Heavy quark mass expansion and intrinsic charm in light hadrons,” *Phys. Rev. D* **62**, 074024 (2000) [arXiv:hep-ph/0002240].
 - [8] W. C. Chang and J. C. Peng, “Extraction of Various Five-Quark Components of the Nucleons,” *Phys. Lett. B* **704**, 197 (2011) [arXiv:1105.2381 [hep-ph]].
 - [9] G. Bari, M. Basile, G. Bruni, G. Cara Romeo, R. Casaccia, L. Cifarelli, F. Cindolo and A. Contin *et al.*, “The Lambda/b0 beauty baryon production in proton proton interactions at $s^{*(1/2)} = 62\text{-GeV}$: A Second observation,” *Nuovo Cim. A* **104**, 1787 (1991).
 - [10] J. Pumplin, H. L. Lai and W. K. Tung, “The Charm Parton Content of the Nucleon,” *Phys. Rev. D* **75**, 054029 (2007) [arXiv:hep-ph/0701220].
 - [11] T. Stavreva, I. Schienbein, F. Arleo, K. Kovarik, F. Olness, J. Y. Yu and J. F. Owens, “Probing gluon and heavy-quark nuclear PDFs with gamma + Q production in pA JHEP **1101**, 152 (2011) [arXiv:1012.1178 [hep-ph]].
 - [12] V. M. Abazov *et al.* [D0 Collaboration], “Measurement of gamma + b + X and gamma + c + X production cross sections in Phys. Rev. Lett. **102**, 192002 (2009) [arXiv:0901.0739 [hep-ex]].
 - [13] J. Engelfried [SELEX Collaboration], “The experimental discovery of double-charm baryons,” *Nucl. Phys. A* **752**, 121 (2005).
 - [14] S. J. Brodsky, F. -K. Guo, C. Hanhart and U. -G. Meissner, “Isospin splittings of doubly heavy baryons,” *Phys. Lett. B* **698**, 251 (2011) [arXiv:1101.1983 [hep-ph]].
 - [15] S. J. Brodsky, A. S. Goldhaber, B. Z. Kopeliovich and I. Schmidt, “Higgs Hadroproduction at Large Feynman x,” *Nucl. Phys. B* **807**, 334 (2009) [arXiv:0707.4658 [hep-ph]].
 - [16] S. J. Brodsky, B. Kopeliovich, I. Schmidt and J. Soffer, “Diffractive Higgs production from intrinsic heavy flavors in the proton,” *Phys. Rev. D* **73**, 113005 (2006) [arXiv:hep-ph/0603238].
 - [17] D. W. Sivers, S. J. Brodsky and R. Blankenbecler, “Large Transverse Momentum Processes,” *Phys. Rept.* **23**, 1 (1976).
 - [18] F. Arleo, S. J. Brodsky, D. S. Hwang and A. M. Sickles, “Higher-Twist Dynamics in Large Transverse Momentum Hadron Production,” *Phys. Rev. Lett.* **105**, 062002 (2010) [arXiv:0911.4604 [hep-ph]].
 - [19] F. Arleo, S. J. Brodsky, D. S. Hwang and A. M. Sickles, “Higher-twist contributions to large p_{\perp} hadron production in hadronic collisions,” arXiv:1006.4045 [hep-ph].
 - [20] R. Blankenbecler, S. J. Brodsky and J. F. Gunion, “Inclusive processes at high transverse momentum,” *eConf C720906V1*, 504 (1972).
 - [21] S. J. Brodsky and A. Sickles, “The Baryon Anomaly: Evidence for Color Transparency and Direct Hadron Phys. Lett. B **668**, 111 (2008) [arXiv:0804.4608 [hep-ph]].
 - [22] S. J. Brodsky and A. H. Mueller, “Using Nuclei to Probe Hadronization in QCD,” *Phys. Lett. B* **206**, 685 (1988).
 - [23] E. M. Aitala *et al.* [E791 Collaboration], “Observation of color transparency in diffractive dissociation of pions,” *Phys. Rev. Lett.* **86**, 4773 (2001) [hep-ex/0010044].
 - [24] S. S. Adler *et al.* [PHENIX Collaboration], “Scaling properties of proton and anti-proton production in $s(NN)^{*(1/2)}$ 200-GeV Au+Au collisions,” *Phys. Rev. Lett.* **91**, 172301 (2003) [arXiv:nucl-ex/0305036].
 - [25] S. J. Brodsky, D. S. Hwang and I. Schmidt, “Final state interactions and single spin asymmetries in semiinclusive deep Phys. Lett. B **530**, 99 (2002) [arXiv:hep-ph/0201296].
 - [26] D. W. Sivers, “Single Spin Production Asymmetries from the Hard Scattering of Point-Like Constituents,” *Phys. Rev. D* **41**, 83 (1990).
 - [27] J. C. Collins, “Leading twist single transverse-spin asymmetries: Drell-Yan and deep inelastic scattering,” *Phys. Lett. B*

- 536**, 43 (2002) [arXiv:hep-ph/0204004].
- [28] S. J. Brodsky, D. S. Hwang and I. Schmidt, “Initial state interactions and single spin asymmetries in Drell-Yan processes,” Nucl. Phys. B **642**, 344 (2002) [arXiv:hep-ph/0206259].
 - [29] Z. Lu and I. Schmidt, “Connection between the Sivers function and the anomalous magnetic moment,” Phys. Rev. D **75**, 073008 (2007) [arXiv:hep-ph/0611158].
 - [30] S. J. Brodsky, B. Pasquini, B. -W. Xiao and F. Yuan, “Phases of Augmented Hadronic Light-Front Wave Functions,” Phys. Lett. B **687**, 327 (2010) [arXiv:1001.1163 [hep-ph]].
 - [31] A. Airapetian *et al.* [HERMES Collaboration], “Single-spin asymmetries in semi-inclusive deep-inelastic scattering on a Phys. Rev. Lett. **94**, 012002 (2005) [arXiv:hep-ex/0408013].
 - [32] F. Bradamante [COMPASS Collaboration], “New COMPASS results on Collins and Sivers asymmetries,” arXiv:1111.0869 [hep-ex].
 - [33] M. G. Alekseev *et al.* [The COMPASS Collaboration], “Measurement of the Collins and Sivers asymmetries on transversely polarised protons,” Phys. Lett. B **692**, 240 (2010) [arXiv:1005.5609 [hep-ex]].
 - [34] F. Bradamante, “Transverse spin and transverse momentum effects at COMPASS,” Mod. Phys. Lett. A **24**, 3015 (2009).
 - [35] H. Avakian *et al.* [The CLAS Collaboration], “Measurement of Single and Double Spin Asymmetries in Deep Inelastic Pion Electroproduction with a Longitudinally Polarized Target,” Phys. Rev. Lett. **105**, 262002 (2010) [arXiv:1003.4549 [hep-ex]].
 - [36] H. Gao *et al.*, “Transverse Spin Structure of the Nucleon through Target Single Spin Asymmetry in Semi-Inclusive Deep-Inelastic ($e, e' \pi^\pm$) Reaction at Jefferson Lab,” Eur. Phys. J. Plus **126**, 2 (2011) [arXiv:1009.3803 [hep-ph]].
 - [37] S. Falciano *et al.* [NA10 Collaboration], “ANGULAR DISTRIBUTIONS OF MUON PAIRS PRODUCED BY 194-GeV/c NEGATIVE PIONS,” Z. Phys. C **31**, 513 (1986).
 - [38] J. Collins and J. W. Qiu, “ k_T factorization is violated in production of high-transverse-momentum particles in hadron-hadron collisions,” Phys. Rev. D **75**, 114014 (2007) [arXiv:0705.2141 [hep-ph]].
 - [39] C. S. Lam and W. K. Tung, “A parton model relation sans QCD modifications in lepton pair production,” Phys. Rev. D **21**, 2712 (1980).
 - [40] D. Boer, S. J. Brodsky and D. S. Hwang, “Initial state interactions in the unpolarized Drell-Yan process,” Phys. Rev. D **67**, 054003 (2003) [arXiv:hep-ph/0211110].
 - [41] D. Boer, “Investigating the origins of transverse spin asymmetries at RHIC,” Phys. Rev. D **60**, 014012 (1999) [arXiv:hep-ph/9902255].
 - [42] Z. t. Liang and T. c. Meng, “Meson production mechanisms and single spin hadron hadron collisions,” Phys. Rev. D **49**, 3759 (1994).
 - [43] S. J. Brodsky, P. Hoyer, N. Marchal, S. Peigne and F. Sannino, “Structure functions are not parton probabilities,” Phys. Rev. D **65**, 114025 (2002) [arXiv:hep-ph/0104291].
 - [44] C. Adloff *et al.* [H1 Collaboration], “Inclusive measurement of diffractive deep inelastic ep scattering,” Z. Phys. C **76**, 613 (1997) [arXiv:hep-ex/9708016].
 - [45] J. Breitweg *et al.* [ZEUS Collaboration], “Measurement of the diffractive cross-section in deep inelastic scattering Eur. Phys. J. C **6**, 43 (1999) [arXiv:hep-ex/9807010].
 - [46] L. Stodolsky, “‘Rapidity gap’ events and shadowing in deep inelastic scattering,” Phys. Lett. B **325**, 505 (1994).
 - [47] S. J. Brodsky, “Dynamic versus Static Structure Functions and Novel Diffractive Effects in AIP Conf. Proc. **1105**, 315 (2009) [arXiv:0811.0875 [hep-ph]].
 - [48] S. J. Brodsky, B. von Harling, Y. Zhao (in preparation)
 - [49] T. Aaltonen *et al.* [CDF Collaboration], “Evidence for a Mass Dependent Forward-Backward Asymmetry in Top Quark Pair Phys. Rev. D **83**, 112003 (2011) [arXiv:1101.0034 [hep-ex]].
 - [50] V. M. Abazov *et al.* [D0 Collaboration], “First measurement of the forward-backward charge asymmetry in top quark Phys. Rev. Lett. **100**, 142002 (2008) [arXiv:0712.0851 [hep-ex]].
 - [51] S. J. Brodsky and H. J. Lu, “Shadowing and Antishadowing of Nuclear Structure Functions,” Phys. Rev. Lett. **64**, 1342 (1990).
 - [52] S. J. Brodsky, I. Schmidt and J. J. Yang, “Nuclear antishadowing in neutrino deep inelastic scattering,” Phys. Rev. D **70**, 116003 (2004) [arXiv:hep-ph/0409279].
 - [53] I. Schienbein, J. Y. Yu, C. Keppel, J. G. Morfin, F. I. Olness and J. F. Owens, “Parton distribution function uncertainties and nuclear corrections for the LHC,” arXiv:0806.0723 [hep-ph].
 - [54] S. J. Brodsky, “Dynamic versus Static Hadronic Structure Functions,” Nucl. Phys. A **827**, 327C (2009) [arXiv:0901.0781 [hep-ph]].
 - [55] A. V. Belitsky, X. Ji and F. Yuan, “Final state interactions and gauge invariant parton distributions,” Nucl. Phys. B **656**, 165 (2003) [arXiv:hep-ph/0208038].
 - [56] J. C. Collins and A. Metz, “Universality of soft and collinear factors in hard-scattering factorization,” Phys. Rev. Lett. **93**, 252001 (2004) [arXiv:hep-ph/0408249].
 - [57] G. Kramer and B. Lampe, Optimized Perturbation Theory Applied to Jet Cross Sections in e^+e^- Annihilation” “OPTIMIZED PERTURBATION THEORY APPLIED TO JET CROSS-SECTIONS IN e^+e^- ANNIHILATION,” Z. Phys. C **39**, 101 (1988).
 - [58] S. J. Brodsky and L. Di Giustino, “Setting the Renormalization Scale in QCD: The Principle of Maximum Conformality,” arXiv:1107.0338 [hep-ph].
 - [59] S. J. Brodsky and X. G. Wu, “Scale Setting Using the Extended Renormalization Group and the Principle of Maximum Conformality: the QCD Coupling Constant at Four Loops,” arXiv:1111.6175 [hep-ph].

- [60] S. J. Brodsky, G. P. Lepage and P. B. Mackenzie, “On the Elimination of Scale Ambiguities in Perturbative Quantum Chromodynamics,” *Phys. Rev. D* **28**, 228 (1983).
- [61] S. J. Brodsky, G. T. Gabadadze, A. L. Kataev and H. J. Lu, “The Generalized Crewther relation in QCD and its experimental Phys. Lett. B **372**, 133 (1996) [arXiv:hep-ph/9512367].
- [62] S. J. Brodsky and H. J. Lu, “Commensurate scale relations in quantum chromodynamics,” *Phys. Rev. D* **51**, 3652 (1995) [arXiv:hep-ph/9405218].
- [63] S. J. Brodsky, E. Gardi, G. Grunberg and J. Rathsmann, “Disentangling running coupling and conformal effects in QCD,” *Phys. Rev. D* **63**, 094017 (2001) [arXiv:hep-ph/0002065].
- [64] P. A. M. Dirac, “Forms of Relativistic Dynamics,” *Rev. Mod. Phys.* **21**, 392 (1949).
- [65] S. J. Brodsky and J. R. Primack, “The Electromagnetic Interactions of Composite Systems,” *Annals Phys.* **52**, 315 (1969).
- [66] S. J. Brodsky, D. S. Hwang, B. Q. Ma and I. Schmidt, “Light cone representation of the spin and orbital angular momentum of relativistic composite systems,” *Nucl. Phys. B* **593**, 311 (2001) [arXiv:hep-th/0003082].
- [67] H. C. Pauli and S. J. Brodsky, “Discretized Light Cone Quantization: Solution to a Field Theory in One Space One Time Dimensions,” *Phys. Rev. D* **32**, 2001 (1985).
- [68] K. Hornbostel, S. J. Brodsky and H. C. Pauli, “Light Cone Quantized QCD in (1+1)-Dimensions,” *Phys. Rev. D* **41**, 3814 (1990).
- [69] G. F. de Teramond and S. J. Brodsky, “Light-Front Holography: A First Approximation to QCD,” *Phys. Rev. Lett.* **102**, 081601 (2009) [arXiv:0809.4899 [hep-ph]].
- [70] S. J. Brodsky, G. F. de Teramond and A. Deur, “Nonperturbative QCD Coupling and its β -function from Light-Front Holography,” *Phys. Rev. D* **81**, 096010 (2010) [arXiv:1002.3948 [hep-ph]].
- [71] J. M. Maldacena, “The Large N limit of superconformal field theories and supergravity,” *Adv. Theor. Math. Phys.* **2**, 231 (1998) [*Int. J. Theor. Phys.* **38**, 1113 (1999)] [arXiv:hep-th/9711200].
- [72] S. J. Brodsky and G. F. de Teramond, “Applications of AdS/QCD and Light-Front Holography to Baryon Physics,” *AIP Conf. Proc.* **1388**, 22 (2011) [arXiv:1103.1186 [hep-ph]].
- [73] S. J. Brodsky, G. de Teramond and R. Shrock, “Light-Front Holography and Hadronization at the Amplitude Level,” *AIP Conf. Proc.* **1056**, 3 (2008) [arXiv:0807.2484 [hep-ph]].
- [74] T. Branz, T. Gutsche, V. E. Lyubovitskij, I. Schmidt and A. Vega, “Light and heavy mesons in a soft-wall holographic approach,” *Phys. Rev. D* **82**, 074022 (2010) [arXiv:1008.0268 [hep-ph]].
- [75] S. S. Chabysheva and J. R. Hiller, “Application of a light-front coupled cluster method,” arXiv:1110.5324 [hep-ph].
- [76] A. Zee, “Dark energy and the cosmological constant paradox,” *Mod. Phys. Lett. A* **23**, 1336 (2008).
- [77] S. Weinberg, “Anthropic Bound on the Cosmological Constant,” *Phys. Rev. Lett.* **59**, 2607 (1987).
- [78] S. J. Brodsky, C. D. Roberts, R. Shrock and P. C. Tandy, “Essence of the vacuum quark condensate,” *Phys. Rev. C* **82**, 022201 (2010) [arXiv:1005.4610 [nucl-th]].
- [79] S. J. Brodsky and R. Shrock, “Condensates in Quantum Chromodynamics and the Cosmological Constant,” *Proc. Nat. Acad. Sci.* **108**, 45 (2011) [arXiv:0905.1151 [hep-th]].
- [80] P. P. Srivastava and S. J. Brodsky, “A Unitary and renormalizable theory of the standard model in ghost free Phys. Rev. D **66**, 045019 (2002) [arXiv:hep-ph/0202141].
- [81] A. Casher and L. Susskind, “Chiral magnetism (or magnetohydrochirons),” *Phys. Rev. D* **9**, 436 (1974).
- [82] M. Burkardt, “Much ado about nothing: Vacuum and renormalization on the light-front,” arXiv:hep-ph/9709421.
- [83] S. J. Brodsky and R. Shrock, “Maximum Wavelength of Confined Quarks and Gluons and Properties of Quantum Phys. Lett. B **666**, 95 (2008) [arXiv:0806.1535 [hep-th]].
- [84] S. J. Brodsky and R. Shrock, “Standard-Model Condensates and the Cosmological Constant,” *Proc. Nat. Acad. Sci.* **108**, 45 (2011) [arXiv:0803.2554 [hep-th]].
- [85] P. Maris, C. D. Roberts and P. C. Tandy, “Pion mass and decay constant,” *Phys. Lett. B* **420**, 267 (1998) [nucl-th/9707003].
- [86] P. Maris and C. D. Roberts, “ Π - and K meson Bethe-Salpeter amplitudes,” *Phys. Rev. C* **56**, 3369 (1997) [nucl-th/9708029].
- [87] L. Chang, C. D. Roberts and D. J. Wilson, “Hadron physics and dynamical chiral symmetry breaking,” arXiv:1201.3918 [nucl-th].
- [88] L. Chang, C. D. Roberts and P. C. Tandy, “Expanding the concept of in-hadron condensates,” *Phys. Rev. C* **85**, 012201 (2012) [arXiv:1109.2903 [nucl-th]].
- [89] L. Chang and C. D. Roberts, “Hadron Physics: The Essence of Matter,” *AIP Conf. Proc.* **1361**, 91 (2011) [arXiv:1003.5006 [nucl-th]].
- [90] B. L. Ioffe and K. N. Zyablyuk, “Gluon condensate in charmonium sum rules with three loop corrections,” *Eur. Phys. J. C* **27**, 229 (2003) [arXiv:hep-ph/0207183].
- [91] M. Davier, A. Hocker and Z. Zhang, “ALEPH Tau Spectral Functions and QCD,” *Nucl. Phys. Proc. Suppl.* **169**, 22 (2007) [arXiv:hep-ph/0701170].
- [92] M. Davier, S. Descotes-Genon, A. Hocker, B. Malaescu and Z. Zhang, “The Determination of $\alpha(s)$ from Tau Decays Revisited,” *Eur. Phys. J. C* **56**, 305 (2008) [arXiv:0803.0979 [hep-ph]].
- [93] S. J. Brodsky and S. Gardner, “Evading the CKM hierarchy: Intrinsic charm in B decays,” *Phys. Rev. D* **65**, 054016 (2002) [hep-ph/0108121].
- [94] C. -R. Ji and S. J. Brodsky, “Quantum Chromodynamic Evolution Of Six Quark States,” *Phys. Rev. D* **34**, 1460 (1986).
- [95] S. J. Brodsky, F. J. Llanes-Estrada and A. P. Szczepaniak, “Local Two-Photon Couplings and the $J=0$ Fixed Pole in Real and Virtual Compton Scattering,” *Phys. Rev. D* **79**, 033012 (2009) [arXiv:0812.0395 [hep-ph]].
- [96] S. J. Brodsky and G. F. de Teramond, “AdS/QCD, Light-Front Holography, and Sublimated Gluons,” arXiv:1112.4212 [hep-th].

BLACK HOLES IN THE SUPERWORLD

■ LAURA ANDRIANOPOLI¹, RICCARDO D'AURIA¹ AND SERGIO FERRARA²

¹ *Dipartimento di Fisica, Politecnico di Torino, Corso Duca degli Abruzzi 24, I-10129 Turin, Italy and Istituto Nazionale di Fisica Nucleare (INFN) Sezione di Torino, Italy; E-mail: laura.andrianopoli@polito.it; riccardo.dauria@polito.it*

² *Physics Department, theory Unit, CERN, 1211 Geneva 23, Switzerland and INFN LNF, Via E. Fermi 40 00044 Frascati, Italy; E-mail: sergio.ferrara@cern.ch*

Abstract

Some aspects of black holes in supersymmetric theories of gravity are reviewed and some recent results outlined.

✂ Talk given by Sergio Ferrara.

1 Introduction

Black holes are perhaps the most misterious and fascinating outcome of Einstein's theory of General Relativity (*A. Einstein, 1880-1952*). This theory was the result of a deep intuition on the implications of the equivalence principle, whilst trying to merge Newton's Law of gravitation with general relativistic covariance. Its mathematical formulation was then realized in terms of Riemannian geometry of space-time (*B. Riemann, 1826-1866*). Nowadays black holes are predicted by fundamental candidate theories of Quantum Gravity like Superstring or M-Theory and they are observed in the sky as relics of collapsing stars. They seem to encompass many of the mysteries of the evolution of our Universe from its creation to its final destiny, the so-called Big Crunch, or its eternal existence, namely an endless expansion.

Astrophysical black holes have huge masses, typically of the order of magnitude of the solar mass scale, 2×10^{30} Kg, while Quantum Gravity black holes have tiny masses, of the order of the Planck mass scale, namely 2×10^{-8} Kg. note that this is still much bigger than the typical mass of the atomic nuclei, that is from one to ten proton masses (the mass of a proton being 1.6×10^{-27} Kg).

Supergravity black holes are the black holes of the superworld [1]. Supersymmetry requires that they are extremal, that is that they have vanishing temperature, are marginally stable but carry Entropy. Actually, the black-hole Entropy makes a bridge between classical gravity and Quantum Gravity. In fact, we recall that the macroscopic definition of the black-hole entropy (Bekenstein – Hawking Entropy) [2, 3] connects its value to the black-hole horizon area A_H :

$$S_{BH}^{macro} = \frac{k_B c^3}{G \hbar} \frac{1}{4} A_H \quad (1.1)$$

The microscopic definition of the black-hole entropy, instead, relates its value to the number N_{mic} of microstates of the quantum system underlying the black hole, namely:

$$S_{BH}^{micro} = k_B \ln(N_{mic}) \quad (1.2)$$

Remarkably these formulae, computed with appropriate approximations, give the same result in Superstring Theory [4].

From now on, we generally use Natural Units, where $c = \hbar = G = k_B = 1$.

2 What is the Superworld?

In order to understand what Superworld is, one first has to introduce the notion of Superspace [6, 7]. This is a geometrical entity which extends the notion of Riemannian manifold to that of Supermanifold. A point on a D -dimensional Riemannian manifold \mathcal{M}_D , endowed with a Lorentz signature (*H. A. Lorentz, 1853-1928*), is identified by giving numerical coordinates x^μ , ($\mu = 1, \dots, D$). To identify a point in a Supermanifold we need, besides the coordinates x^μ , also a set of Grassmann (*H. Grassmann, 1809-1877*) anticommuting coordinates θ_α ($\alpha = 1, \dots, 2^{[D/2]}$) with two basic properties:

1. $\theta_\alpha \theta_\beta = -\theta_\beta \theta_\alpha$
which implies nilpotency: $\theta_\alpha^2 = 0$;
2. They transform as spinors (*E. Cartan, 1869-1951, H. Weyl, 1885-1955*) under the action of the Lorentz group and their properties are related to modules of Clifford Algebras (*W. K. Clifford, 1845-1879*) and to the Spin Group, namely the universal covering group of the D -dimensional Lorentz group [5].

Superworld is the physical entity corresponding to the mathematical concept of supermanifold, whose environment is not ordinary space but superspace. The group of motion in Superspace is supersymmetry, as much as the group of motion in ordinary space-time is the Poincaré group (*H. Poincaré, 1854-1912*). An infinitesimal supersymmetry transformation with spinorial parameter ϵ_α acts on the coordinates of superspace as follows:

$$x^\mu \rightarrow x^\mu + i\bar{\epsilon}^\alpha (\gamma^\mu)_\alpha{}^\beta \theta_\beta \Leftrightarrow \delta x^\mu = i\bar{\epsilon}^\alpha (\gamma^\mu)_\alpha{}^\beta \theta_\beta \quad (2.1)$$

$$\theta_\alpha \rightarrow \theta_\alpha + \epsilon_\alpha \Leftrightarrow \delta \theta_\alpha = \epsilon_\alpha \quad (2.2)$$

where γ^μ is a matrix satisfying the Clifford Algebra and $\bar{\epsilon}$ denotes the Dirac conjugate spinor, namely $\bar{\epsilon} = \epsilon^\dagger \gamma^0$. Commuting twice the action of such transformations with parameters ϵ_1 and ϵ_2 respectively, one finds that x^μ undergoes an infinitesimal translation:

$$[\delta_1, \delta_2]x^\mu = 2i\bar{\epsilon}_2^\alpha (\gamma^\mu)_\alpha{}^\beta \epsilon_{1\beta}. \quad (2.3)$$

The supersymmetry algebra is a graded Lie algebra [8] (*S. Lie, 1842-1899*) with basic anticommutator: [9, 10, 11]

$$\{Q_\alpha, \bar{Q}_\beta\} = 2(\gamma^\mu C)_{\alpha\beta} p_\mu \quad (2.4)$$

where the supersymmetry generators Q_α are Majorana spinors (*E. Majorana, 1906-1938*) and C denotes the charge-conjugation matrix.

The supergroup associated to the supersymmetry algebra acts on a supermanifold, denoted by $\mathcal{M}_{b,f} \equiv \mathcal{M}_{D,2^{[D/2]}}$, where b and f denote the number of bosonic and fermionic coordinates respectively. the total (graded) dimension of a supermanifold is $b + f$. As we will see in the following, the maximal possible number of coordinates of superspace is $b_{max} = 11$, $f_{max} = 32$.

Actually, one can extend the super Lie algebra by introducing N supersymmetry generators $Q_{\alpha I}$ ($I = 1, \dots, N$) acting on an N -extended superspace labeled by N Grassmannian spinor coordinates $\theta_{\alpha I}$. The basic anti-commutators now become

$$\{Q_{\alpha I}, \bar{Q}_{\beta}^J\} = 2(\gamma^\mu C)_{\alpha\beta} p_\mu \delta_I^J \quad (2.5)$$

$$\{Q_{\alpha I}, Q_{\beta J}\} = \varepsilon_{\alpha\beta} Z_{IJ} \quad (2.6)$$

where Z_{IJ} are “central terms” which commute with all the rest of the superalgebra, including the Lorentz generators. It is precisely the presence of the central charges Z_{IJ} which makes it possible the existence of supersymmetric Black Holes, as will be shown in the next section.

The interaction in the superworld are described by supersymmetric theories. It is remarkable that such theories may encompass gauge interactions, in particular Yang–Mills theories [12, 6], as well as gravitational interactions. In the latter case, the corresponding theory is called supergravity [13, 14]. However these theories exist only for few values of the number N of supersymmetries and of the space-time dimension D [15, 16]. In particular, Super Yang–Mills theories in $D = 4$ require $1 \leq N \leq 4$ and at most they live in $D = 10$ [17]. On the other hand supergravity theories at $D = 4$ require $1 \leq N \leq 8$ and at most they live in $D = 11$ dimensions [18].

3 From Schwarzschild to Reissner–Nordström: The case of extremal Black Holes.

The celebrated Black-Hole solution of pure Einstein theory looks, in a chosen frame of spherical coordinates

$$ds_{\text{Schw}}^2 = - \left(1 - \frac{2M}{r}\right) dt^2 + \left(1 - \frac{2M}{r}\right)^{-1} dr^2 + r^2 d\Omega^2 \quad (3.1)$$

where M denotes the ADM mass, that is the total energy of the black-hole configuration. The naked singularity at $r = 0$ is covered by the *event horizon* at $r = 2M$. By event horizon we mean a surface where the gravitational redshift is infinite, that is where the time intervals undergo an infinite dilation with respect to a distant observer. This is also a singularity of the metric but it is only a *coordinate* singularity which can be removed with an appropriate choice of coordinates, while the singularity at $r = 0$ is a real singularity of the theory, that is independent of the reference frame.

The generalization of the Schwarzschild solution to an electrically charged black hole in the Einstein–Maxwell theory is given by the Reissner–Nordström black hole, whose metric reads:

$$ds_{\text{RN}}^2 = - \left(1 - \frac{2M}{r} + \frac{Q^2}{r^2} \right) dt^2 + \left(1 - \frac{2M}{r} + \frac{Q^2}{r^2} \right)^{-1} dr^2 + r^2 d\Omega^2 \quad (3.2)$$

Here M denotes the ADM mass and Q the electric charge of the space-time configuration. Such configuration can be easily generalized for dyonic configurations where also a magnetic charge P is present by replacing in (3.2) Q^2 with $Q^2 + P^2$. This metric exhibits two horizons, at

$$r_{\pm} = M \pm \sqrt{M^2 - Q^2} = M \pm r_0 \quad (3.3)$$

where r_+ corresponds to the event horizon and r_- to the Cauchy horizon, together with the physical singularity at $r = 0$.

In cosmology a Cosmic Censorship Principle is postulated (see for example [19]). An event horizon should always cover the singularity at $r = 0$, so that the singularity be not accessible to an observer external to the event horizon of the black hole. This can be rephrased by saying that no "naked" singularities can exist. For the Reissner–Nordström solution the Cosmic Censorship principle requires $M \geq Q$.

As shown by Steven Hawking, black holes obey laws which are formally the same as the laws of thermodynamics, after an appropriate identification of the quantum numbers of the solution is given. In particular, the thermodynamical properties of the black holes relate the area of the event horizon to the Entropy through the Bekenstein–Hawking formula (see eq. (1.1) in Natural Units):

$$S_{BH} = \frac{1}{4} A_H = \frac{1}{4} \pi R_+^2, \quad (3.4)$$

where R_+ is the event horizon r_+ for the Reissner–Nordström black hole, while it becomes an effective radius in the presence of other black-hole attributes such as angular momentum J and/or scalar charges Σ . For instance, in the presence of the latter $R_+^2 = r_+^2 - \Sigma^2 \leq r_+^2$.

The fact that a black hole continuously increases its horizon area can be interpreted as the second law of thermodynamics if we identify the black hole entropy as proportional to the horizon area, as pointed out by S. Hawking. Further support to this interpretation is given by the other laws of thermodynamics. In particular, the 0th law of thermodynamics states that for a system in equilibrium there is a quantity, the temperature, which is constant. An analogous constant quantity exists for a black hole at equilibrium, the so-called surface gravity that for the Reissner–Nordström black hole is

$$\kappa = \frac{c}{(r_+ + r_-)r_+ - Q^2} \quad (3.5)$$

where

$$c = \frac{1}{2}(r_+ - r_-) \quad (3.6)$$

It is then possible to identify the black-hole temperature T_{BH} as

$$T_{BH} = \frac{1}{2\pi}\kappa = \frac{c}{2S_{BH}} \quad (3.7)$$

The analogy is completed by rewriting the first law of thermodynamics:

$$dE = TdS + \text{work terms} \quad (3.8)$$

as

$$dM = T_{BH}dS_{BH} + \dots = \frac{\kappa}{2\pi} \frac{A_H}{4} + \dots \quad (3.9)$$

and observing that the third law of thermodynamics, stating that it is impossible to achieve $T = 0$ by a finite number of physical processes, can be rephrased as the impossibility to achieve $\kappa = 0$ by a finite number of physical processes.

The black hole which reaches the limit equilibrium temperature $\kappa = 0$ is called extremal. This corresponds to $c = 0$, that is to $r_+ = r_-$. For the Reissner–Nordström black hole, this happens when $M = |Q|$. A supergravity black hole is supersymmetric (BPS saturated) if its ADM mass M equals the highest skew-eigenvalue of the central charge matrix $Z_{IJ} = -Z_{JI}$ evaluated

at asymptotic infinity. In the presence of scalar charges Σ , the extremality condition allows both for supersymmetric and non-supersymmetric black-hole configurations.

For stationary but non-static solutions, that is rotating black holes of angular momentum J (Kerr–Newman black holes), the horizon radii become

$$r_{\pm} = M \pm \sqrt{M^2 - Q^2 - P^2 - J^2/M^2} \quad (3.10)$$

so that for a neutral spinning black hole (Kerr black hole) we reach extremality when $M^2 = J$, that is when the extremality parameter $a^* \equiv J/(GM^2) = 1$. Kerr black holes have been observed in our galaxy, in particular **GRS 1915+105** is the heaviest of the stellar black holes so far known [20] in the Milky Way Galaxy, with 10 to 18 times the mass of the Sun and a value of spin $J \simeq 10^{78} \hbar$. It was discovered on 15 August 1992. It is a nearly extremal black hole since in this case the extremality parameter is $a^* = 0.98 \simeq 1$. It has been argued that such black hole has an exact Conformal Field Theory dual [21].

4 Black Holes and Supersymmetry

One of the main properties of supergravity is the presence of scalar fields not minimally coupled to vector fields. The typical form of the Lagrangian of a set of electromagnetic field strengths $F^\Lambda = dA^\Lambda$ (enumerated by capital Greek indices Λ, Σ) in supergravity is of the form:

$$\mathcal{L} \propto g_{\Lambda\Sigma}(\varphi) F_{\mu\nu}^\Lambda F^{\Sigma|\mu\nu} + \Theta_{\Lambda\Sigma}(\varphi) \frac{1}{2} F_{\mu\nu}^\Lambda F_{\rho\sigma}^\Sigma \epsilon^{\mu\nu\rho\sigma} \quad (4.1)$$

where the couplings $g_{\Lambda\Sigma}$ and $\Theta_{\Lambda\Sigma}$ depend on a set of scalar fields enumerated by an index s . This has the implication that the Maxwell–Einstein black hole solution gets a non-trivial modification. In particular, the metric flow of the black hole towards the horizon $r = r_H$ is accompanied by trajectories of scalar-fields evolution from asymptotic infinity to the horizon:

$$\begin{aligned} \lim_{r \rightarrow \infty} \varphi^s(r) &= \varphi_\infty^s \in \mathcal{M} \\ \lim_{r \rightarrow r_H} \varphi^s(r) &= \varphi_{crit}^s \in \mathcal{M} \end{aligned} \quad (4.2)$$

The resulting analysis exploits the *attractor mechanism* [22]. Indeed scalar fields behave as dynamical systems which, in their evolution towards the

black-hole horizon of an extremal black hole, loose memory of their initial conditions (at $\varphi = \varphi_\infty$) approaching a critical point where the first derivative vanishes:

$$\begin{aligned}\lim_{r \rightarrow r_H} \varphi^s(r) &= \varphi_{crit}^s(Q) \\ \lim_{r \rightarrow \infty} \frac{d}{dr} \varphi^s(r) &= 0,\end{aligned}\tag{4.3}$$

and whose value only depends on the set of charges Q . Consistency of the solution implies that φ_{crit} is a critical point of an *effective black-hole potential* $V_{BH}(\varphi, Q)$:

$$\lim_{r \rightarrow \infty} \frac{\partial}{\partial \varphi^s} V_{BH}|_{\varphi=\varphi_{crit}} = 0.\tag{4.4}$$

Moreover, the Bekenstein–Hawking entropy-area formula becomes [24, 25]:

$$S_{BH} = \frac{1}{4} A_H = \pi V_{BH}(Q, \varphi_{crit}(Q)).\tag{4.5}$$

Note that the critical value of the scalar fields for extremal black holes, satisfying the attractor mechanism, is given only in terms of the electric and magnetic vector of charges Q , and this explains why the entropy only depends on Q and not on the initial values of the scalar fields φ_∞ .

The attractor mechanism allows to reduce the dynamical black-hole flow to a *first-order* evolution both for supersymmetric and non-supersymmetric extremal black holes [26, 27, 28, 29]. Indeed, the black-hole potential V_{BH} may be always written for extremal black holes as

$$V_{BH} = W^2 + 2\partial_s W \partial^s W\tag{4.6}$$

where $W(\varphi, Q)$ is known as the (*fake*) *superpotential*. There are several properties of W that make it important. First of all, in terms of W , the second order equations of motion of the theory reduce to a set of first order equations. Moreover W is invariant under the electric-magnetic duality group. It has a clear meaning in the context of the Hamilton–Jacobi theory, since it allows the interpretation of the flow as an Hamiltonian flow whose Hamilton characteristic function is actually simply related to W [30, 31].

The attractor mechanism allows to classify black-hole solutions, that is critical points of the black-hole potential, through the electric-magnetic duality symmetry of the theory. For each orbit of the duality symmetry, the

fake superpotential W has a different expression. In the particular case of supersymmetric black holes, one obtains $W = |Z|$ where $|Z|$ is the highest skew-eigenvalue of the central charge matrix Z_{IJ} . The duality orbits are modules of *groups of type E_7* , as requested by the Gaillard–Zumino analysis [23] combined with the attractor mechanism. The group E_7 appears in supergravity as the duality group of the maximally extended $N = 8$ theory in four dimensions, in its symplectic 56 dimensional module relating 28 electric to 28 magnetic charges. The orbits of the **56** module classify the black-hole solutions preserving different fractions of the original $N = 8$ supersymmetry. Moreover, E_7 controls the ultraviolet divergences of perturbation theory since it is anomaly free, and its arithmetic subgroups $G \subset E_7(\mathbb{Z})$ may encode the non-perturbative quantum corrections. It happens that all the duality groups of four dimensional supergravity theories with a number of supersymmetries $N < 8$ are groups of type E_7 , that is they have symplectic representations admitting a symmetric quartic invariant polynomial, but not a quadratic one [32]. As an example, we have presented in Table 1 the possible $N = 2$ choices

	G	R module	Primitive symm. inv.
$J_3^\mathbb{O}$	$E_{7(-25)}$	56	I_4
$J_3^\mathbb{H}$	$SO^*(12)$	32	I_4
$J_3^\mathbb{C}$	$SU(3, 3)$	20	I_4
$J_3^\mathbb{R}$	$Sp(6, \mathbb{R})$	14'	I_4
\mathbb{R}	$SL(2, \mathbb{R})$	4	I_4
$\mathbb{R} \oplus \Gamma_{1,n-1}, n \in \mathbb{N}$	$SL(2, \mathbb{R}) \times SO(2, n)$	$(2, 2 + n)$	I_4
CP^n	$U(1, n)$	$(1 + n)_\mathbb{C}$	I_2

Table 1: Supergravity sequence for $N = 2$ symmetric spaces.

of groups G of the $\frac{G}{H}$ symmetric spaces and their symplectic representations R [33, 34]. The first column identifies the scalar manifold whose isometry group is G is given. In particular, for the first four entries, they are named with the Jordan algebras J_3 over octonions, quaternions, complex and real numbers respectively, to which they are related. As we see in the last column, all the duality groups listed are of Type E_7 groups [35] except the last one, which has a primitive quadratic invariant polynomial. For $N \geq 3$ supergravity theories the analogous sequence is given in Table 2. Again, all the groups appearing in the sequence are of type E_7 except the first one, which admits

a primitive symmetric invariant polynomial of order 2.

N	G	\mathbf{R}
$N = 3$	$U(3, n)$	$(\mathbf{3} + \mathbf{n})$
$N = 4$	$SL(2, \mathbb{R}) \otimes SO(6, n)$	$(\mathbf{2}, \mathbf{6} + \mathbf{n})$
$N = 5$	$SU(1, 5)$	$\mathbf{20}$
$N = 6$	$SO^*(12)$	$\mathbf{32}$
$N = 8$	$E_{7(7)}$	$\mathbf{56}$

Table 2: The supergravity sequence for $N \geq 3$

5 Future directions of research

We are just at the beginning of the exploration of the beautiful intricacy given by supergravity black-hole physics, its group-theoretical structure and quantum perspectives. It is clear that much work and effort has to be done to unveil all the physics behind their structure which are emerging from supergravity considerations. In particular, we may mention few possible future directions of research:

- Extension of black-hole solutions to multi-center configurations, the classification of their orbits and the study of their dynamics, regarding their splitting behavior and their relation to the underlying stringy microstate counting.

- Clarification of the role of the group E_7 as far as quantum corrections are concerned.
- Inclusion of the Attractor Mechanism in the presence of higher derivative modifications of gravity, as suggested by superstring theory.
- The role of $N = 8$ black holes in a perturbatively finite theory of $N = 8$ supergravity.

Acknowledgements

The work of S.F. is supported by the ERC Advanced Grant n. 226455, “Supergravity, Quantum Gravity and Gauge Fields”. This work was supported in part by the MIUR-PRIN contract 2009-KHZKRX.

References

- [1] Andrianopoli L., D’Auria R., Ferrara S. and Trigiante M. (2008). Extremal black holes in supergravity. In Gasperini M. and Maharana J. (Ed.s). *String Theory and Fundamental Interactions. Lect. Notes Phys.* **737** 661. [hep-th/0611345].
- [2] Hawking S. W. (1971). *Gravitational radiation from colliding black holes.* *Phys. Rev. Lett.* **26**, 1344.
- [3] Bekenstein J. D. (1973). *Black holes and entropy.* *Phys. Rev. D* **7**, 2333.
- [4] Strominger A. and Vafa C. (1996). *Microscopic origin of the Bekenstein-Hawking entropy.* *Phys. Lett. B* **379**, 99. [hep-th/9601029].
- [5] Deligne P. (1999). Notes on spinors. In Deligne P., Etingof P., Freed D. S., Jeffrey L. C., Kazhdan D., Morgan J. W., Morrison D. R. and Witten E. (Ed.s). *Quantum fields and strings: A course for mathematicians.* American Mathematical Society.
- [6] Salam A. and Strathdee J. A. (1975). *On Superfields and Fermi-Bose Symmetry.* *Phys. Rev. D* **11**, 1521.
- [7] Ferrara S., Wess J. and Zumino B. (1974). *Supergauge Multiplets and Superfields.* *Phys. Lett. B* **51**, 239.

- [8] Corwin L., Ne'eman Y. and Sternberg S. (1975). *Graded Lie Algebras in Mathematics and Physics (Bose-Fermi Symmetry)*. *Rev. Mod. Phys.* **47**, 573.
- [9] Wess J. and Zumino B. (1974). *Supergauge Transformations in Four-Dimensions*. *Nucl. Phys. B* **70**, 39.
- [10] Golfand Y. .A. and Likhtman E. P. On N=1 Supersymmetry Algebra And Simple Models. In Shifman, M. A. (Ed.). *The many faces of the superworld*, 54-79
- [11] Akulov V. P. and Volkov D. V. (1974). *Goldstone fields with spin 1/2*. *Theor. Math. Phys.* **18**, 28.
- [12] Ferrara S. and Zumino B. (1974). *Supergauge Invariant Yang-Mills Theories*. *Nucl. Phys. B* **79**, 413.
- [13] Freedman D. Z., van Nieuwenhuizen P. and Ferrara S. (1976). *Progress Toward a Theory of Supergravity*. *Phys. Rev. D* **13**, 3214.
- [14] Deser S. and Zumino B. (1976). *Consistent Supergravity*. *Phys. Lett. B* **62**, 335.
- [15] Gell-Mann M., Ramond P. and Slansky R. (1978). *Color Embeddings, Charge Assignments, and Proton Stability in Unified Gauge Theories*. *Rev. Mod. Phys.* **50**, 721.
Gell-Mann M., Ramond P. and Slansky R. (1979). *Complex Spinors And Unified Theories*. *Conf. Proc. C* **790927** 315.
- [16] Nahm W. (1978). *Supersymmetries and their Representations*. *Nucl. Phys. B* **135**, 149.
- [17] Brink L., Schwarz J. H. and Scherk J. (1977). *Supersymmetric Yang-Mills Theories*. *Nucl. Phys. B* **121**, 77.
- [18] Cremmer E., Julia B. and Scherk J. (1978). *Supergravity Theory in Eleven-Dimensions*. *Phys. Lett. B* **76**, 409.
- [19] Kallosh R., Linde A. D., Ortin T., Peet A. W. and Van Proeyen A. (1992). *Supersymmetry as a cosmic censor*. *Phys. Rev. D* **46**, 5278. [hep-th/9205027].

- [20] McClintock J. E., Shafee R., Narayan R., Remillard R. A., Davis S. W. and Li L. -X. (2006). *The Spin of the Near-Extreme Kerr Black Hole GRS 1915+105*. *Astrophys. J.* **652**, 518. [astro-ph/0606076].
- [21] Guica M., Hartman T., Song W. and Strominger A. (2009). *The Kerr/CFT Correspondence*. *Phys. Rev. D* **80**, 124008. [arXiv:0809.4266 [hep-th]].
- [22] Ferrara S., Kallosh R. and Strominger A. (1995). *$N=2$ extremal black holes*. *Phys. Rev. D* **52**, 5412. [hep-th/9508072].
- [23] Gaillard M. K. and Zumino B. (1981). *Duality Rotations for Interacting Fields*. *Nucl. Phys. B* **193**, 221.
- [24] Ferrara S. and Kallosh R. (1996). *Supersymmetry and attractors*. *Phys. Rev. D* **54**, 1514. [hep-th/9602136].
- [25] Ceresole A., D'Auria R. and Ferrara S. (1996). *The Symplectic structure of $N=2$ supergravity and its central extension*. *Nucl. Phys. Proc. Suppl.* **46**, 67. [hep-th/9509160].
- [26] Ceresole A. and Dall'Agata G. (2007). *Flow Equations for Non-BPS Extremal Black Holes*. *JHEP* **0703**, 110. [hep-th/0702088].
- [27] Andrianopoli L., D'Auria R., Orazi E. and Trigiante M. (2007). *First order description of black holes in moduli space*. *JHEP* **0711**, 032. [arXiv:0706.0712 [hep-th]].
- [28] Ceresole A., Dall'Agata G., Ferrara S. and Yeranyan A. (2010). *First order flows for $N=2$ extremal black holes and duality invariants*. *Nucl. Phys. B* **824**, 239. [arXiv:0908.1110 [hep-th]].
Ceresole A., Dall'Agata G., Ferrara S. and Yeranyan A. (2010). *Universality of the superpotential for $d = 4$ extremal black holes*. *Nucl. Phys. B* **832**, 358. [arXiv:0910.2697 [hep-th]].
- [29] Bossard G., Michel Y. and Pioline B. (2010). *Extremal black holes, nilpotent orbits and the true fake superpotential*. *JHEP* **1001**, 038. [arXiv:0908.1742 [hep-th]].

- [30] Andrianopoli L., D'Auria R., Orazi E. and Trigiante M. (2010). *First Order Description of $D=4$ static Black Holes and the Hamilton-Jacobi equation*. *Nucl. Phys. B* **833**, 1. [arXiv:0905.3938 [hep-th]].
- [31] Andrianopoli L., D'Auria R., Ferrara S. and Trigiante M. (2010). *Fake Superpotential for Large and Small Extremal Black Holes*. *JHEP* **1008**, 126. [arXiv:1002.4340 [hep-th]].
- [32] Ferrara S. and Kallosh R. *Creation of Matter in the Universe and Groups of Type E_7* . *arXiv:1110.4048 [hep-th]*. To appear in *JHEP*.
- [33] Gunaydin M., Sierra G. and Townsend P. K. (1984). *The Geometry of $N=2$ Maxwell-Einstein Supergravity and Jordan Algebras*. *Nucl. Phys. B* **242**, 244. Gunaydin M., Sierra G. and Townsend P. K. (1983). *Exceptional Supergravity Theories and the MAGIC Square*. *Phys. Lett. B* **133**, 72.
- [34] Cremmer E. and Van Proeyen A. (1985). *Classification Of Kahler Manifolds In $N=2$ Vector Multiplet Supergravity Couplings*. *Class. Quant. Grav.* **2**, 445.
- [35] Brown R. B. (1969). *Groups of Type E_7* . *J. Reine Angew. Math.* **236**, 79.
 Garibaldi R. S. (2001). *Groups of Type E_7 over Arbitrary Fields.*, *Commun. in Algebra* **29**, 2689.
 Meyberg K. (1968). *Eine Theorie der Freudenthalschen Triplesysteme. I, II*. *Nederl. Akad. Wetensch. Proc. Ser. A* **71**, 162.

HIGHLIGHTS FROM ATLAS

■ PETER JENNI

CERN, Switzerland

Summary

For the past two years, experiments at the Large Hadron Collider (LHC) have started exploring physics at the high-energy frontier. Thanks to the superb turn-on of the LHC already a rich harvest of initial physics results have been obtained by the general purpose experiment ATLAS, as well as its sister-experiment CMS. The initial data has allowed a test, at the highest collision energies ever reached in a laboratory, of the Standard Model (SM) of elementary particles, and to make early searches Beyond the Standard Model (BSM). Significant results have already been obtained in the search for the Higgs Boson, which would establish the postulated electro-weak symmetry breaking mechanism in the SM, as well as for BSM physics like Supersymmetry (SUSY), heavy new particles, quark compositeness, and others. The important, and successful, SM physics measurements are giving confidence that the experiment is in good shape for their journey into the uncharted territory of new physics anticipated at the LHC.

Key index words

LHC, ATLAS experiment, experimental Standard Model measurements, and experimental searches for physics Beyond the Standard Model.

1. INTRODUCTION

The first high-energy proton-proton collisions ($3.5 + 3.5$ TeV) at the LHC were registered on 30th March 2010, and since then the machine has operated in a superb way, providing the two general-purpose experiments ATLAS and CMS with data samples corresponding to an integrated luminosity of close to 5 fb^{-1} during the pp running periods in 2010 and 2011. ATLAS has recorded collision data in a very effective way, reaching a data taking efficiency of up about 94% for the luminosity delivered by LHC in stable conditions. Thanks to a very careful and rather complete commissioning of the experiment over several years with cosmic ray data, and with the lower energy LHC collision data accumulated at the end of 2009 during the initial LHC operation, ATLAS was able to quickly produce a rich harvest of early physics results. In fact, ATLAS has published more than 80 papers in scientific journals up to this Symposium.

It would be impossible to review all these results; necessarily a very restrictive selection had to be made, in the spirit of giving illustrative examples. The results will be presented, roughly speaking, following a pattern of decreasing cross-sections. This will naturally first lead to measurements of the known Standard Model (SM) particles, of which the top quark is the heaviest known, with the smallest cross-section. All SM measurements, already with considerable accuracies and details, agree so far with the most sophisticated theoretical expectations. Next will be discussed the status of the search for the still missing element of the SM, the Higgs boson as the messenger of the electro-weak symmetry breaking mechanism. Finally, several examples of searches and resulting new limits on various physics processes Beyond the Standard Model (BSM) will be reported, mostly involving heavy new particles with small

production cross-sections. For the searches the exploration at the LHC has only just begun, as much larger data samples are anticipated for the future, once the integrated luminosity will have reached the expected hundredfold increase at the end of 2012, and further on also with the full LHC collision energy of $7 + 7$ TeV for the years 2014 and beyond.

ATLAS is the result of an enormous collaborative effort that already lasts almost two decades including all its phases from conception, design, prototyping, construction, pre-assembling, installation in the underground cavern and commissioning to finally starting up operation with recording the first collisions in November 2009. There is no way that any justice can be given here to this huge scientific, technological and human undertaking; the reader is referred to [1,2] and references therein. Just as an indication of the complexity and how well the apparatus is functioning, one may note that for all different detector layers, totaling about 100 Million electronic read-out channels, typically 98% of channels are working within design specification. The Fig. 1 shows as an example the detector status in February 2007 during the peak period of the installation work.

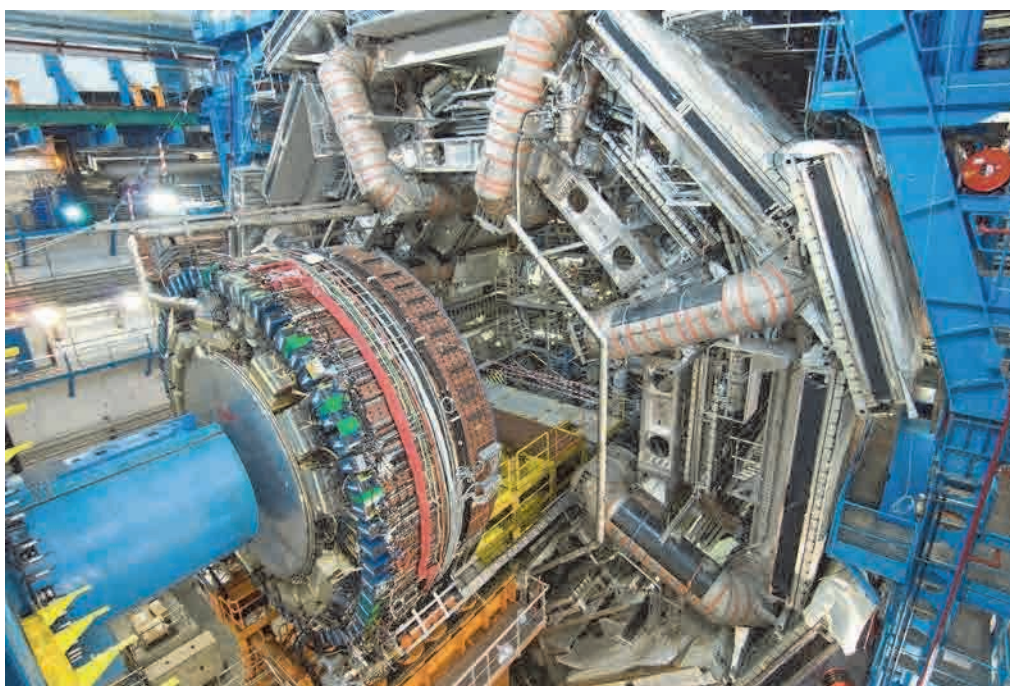


Figure 1. Photograph of one end of the ATLAS detector barrel with the calorimeter end-cap still retracted before its insertion into barrel toroid magnet structure (February 2007 during the installation phase).

The ATLAS Collaboration currently brings together about 3000 scientists in a world-wide common effort from almost 200 Universities and Laboratories located in 38 countries. About one-third of the scientists are students working on their PhD with data accumulated with the ATLAS experiment.

2. GENERAL EVENT PROPERTIES

The experiment has collected large samples of so-called minimum bias events (ordinary collision events without, or at most very minimal, selection criteria) in order to study general event properties. These

properties are interesting in their own right as the physics of soft hadronic interactions (soft QCD), and an understanding of them is a crucial input to the modeling of background events for any measurements and searches of SM and BSM physics processes. The minimum bias events also allowed the experiments to verify in great detail that the average detector responses are well described in the Monte Carlo (MC) simulations, and that the detector elements are well aligned and calibrated, most convincingly demonstrated by the reconstruction and measurement of many well-known resonances, yielding the expected mass values and resolutions.

Charged particle production properties measured by ATLAS [3] over the central region in 7 TeV centre-of-mass proton-proton collisions are shown as an example in Fig. 2. The central region is expressed as $|\eta| < 2.5$ where η is the pseudorapidity defined in terms of the polar angle θ w.r.t. the beam axis as $\eta = -\ln \tan(\theta/2)$. Figure 2a shows the number of charged particles (multiplicities) per unit η , and Fig. 2b displays the transverse momentum p_T distribution w.r.t. the beam axis. Both measurements are compared with various Monte Carlo (MC) model simulations before tuning of the latter, and as can be seen, in particular from the MC over data ratio plots, the model descriptions require adjustments to better represent the measurement.

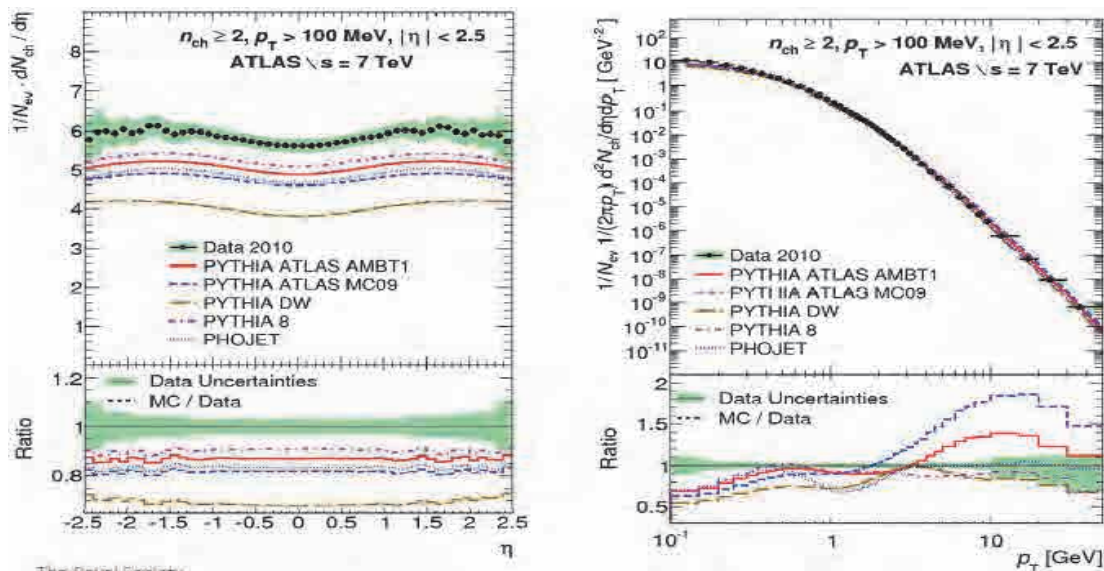


Figure 2. (a, left) Charged particle multiplicity per event and per unit η , (b, right) charged particle transverse momentum p_T distribution. The data (dots) are compared to various MC model simulations before tuning of the latter.

3. KNOWN STANDARD MODEL PHYSICS

Observing, and measuring accurately at the new collision energies, the known particles from the SM can be considered to be a necessary stepping stone towards exploring the full potential of the LHC with its many promises of possible new physics discoveries. The SM processes are often called ‘standard candles’ for the experiments. However there is much more value to measuring the SM processes than this: never before could the SM physics be studied at a hadron collider with such sophisticated and highly accurate detectors, ultimately allowing a test of detailed predictions of the SM with

unprecedented precision and minimal instrumental systematic errors, as already published for several ATLAS and CMS QCD results.

The charged and neutral Intermediate Vector Bosons (IVB) W and Z are the major benchmark measurements at the LHC [4] for demonstrating the excellent detector performance, as well as for testing model predictions to a high degree of accuracy. The Z decays into electron and muon pairs can be extracted almost free of any backgrounds, as shown in Fig. 3.

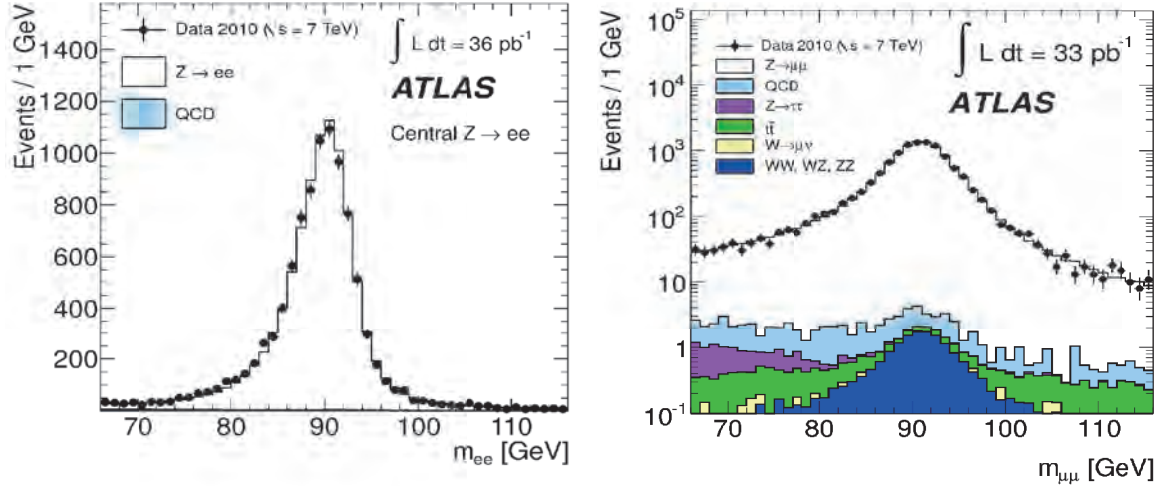


Figure 3. The electron-pair mass distribution on a linear (left) and the muon-pair mass distribution on a logarithmic (right) vertical scale, in the Z mass region. The estimated small background contributions are indicated, as well as the expected signal shape from MC simulations.

The classical W decay signatures into an electron or muon and the associated neutrino are an excellent test for the missing transverse energy (E_T^{miss}) performance of the detector due to the undetected neutrino. E_T^{miss} is inferred from the measured energy imbalance in the transverse projection of all observed signals w.r.t. the beam axis. The E_T^{miss} spectrum for events with a well-identified muon candidate is shown in Fig. 4a, and shows a clear W signal over the expected background sources. After applying a selection of events with $E_T^{\text{miss}} > 25$ GeV only a small residual background remains present under the W signal, as indicated in the transverse mass distribution (defined in [4]) given in Fig. 4b.

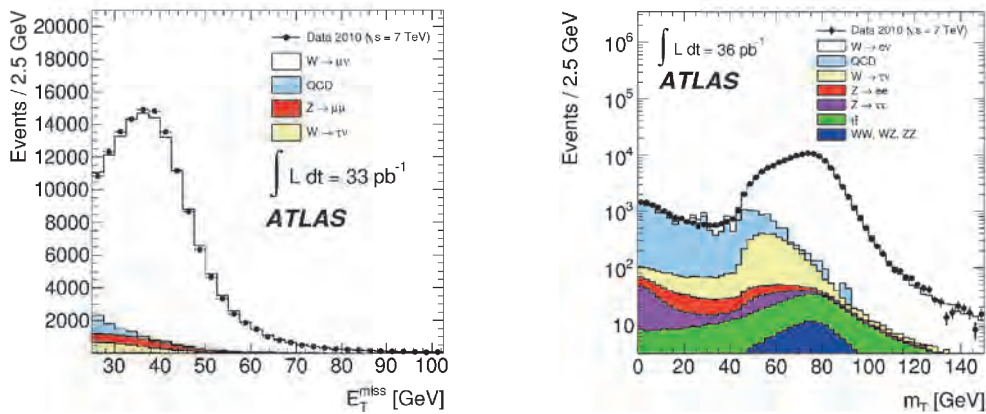


Figure 4. (a, left) Missing transverse energy distribution for events with a muon candidate. (b, right) Transverse mass distribution for W to electron decays before a cut on the transverse mass (see text). The expected background contributions are indicated as well.

The good agreement between the measured and expected cross-sections times the leptonic decay branching ratios (which is the expected rate for W bosons to be produced and then decay to leptons) is illustrated in Fig. 5. With the present data samples the experimental uncertainties still dominate, but with the addition of the 2011 data, the measurements will already constrain the theoretical model parameters. Figure 5a shows the W cross-section measurements and predictions as a function of the collision energy, whereas in (b) the W and Z cross-section results are displayed in a 2-dimensional plot including their correlated error ellipse, and compared to predictions with various parton distribution functions (describing the quark and gluon momentum distributions inside the protons). Detailed measurements of properties for IVB production and decay at the LHC have been published already, including for example the lepton charge asymmetry measurements for W decays [4] which were an important signature of the electro-weak nature of the W at the time of their discovery some 30 years ago.

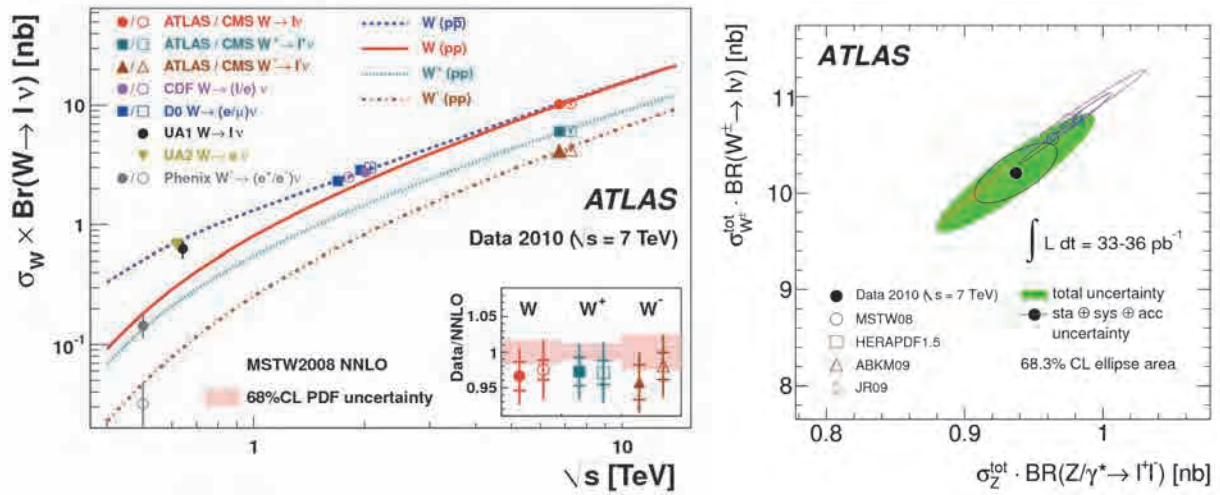


Figure 5. (a, left) W production cross-sections times leptonic branching ratio as a function of the collision energy, showing also previous measurements at lower energy colliders, (b, right) correlation of the measured (solid dot) leptonic W and Z cross-section as compared to theoretical expectations with various choices for the parton distribution functions (open dots).

Hard collisions (characterized by having final state particles with significant transverse energy) at the LHC are dominated by the production of high transverse momentum jets, which are the collimated sprays of particles from the hadronization of the initially scattered partons (quarks, gluons) in the colliding protons. At work is the strong interaction described by Quantum Chromo Dynamics (QCD). Most commonly two jets emerge at opposite azimuth with balanced transverse momenta, from an initial lowest order parton-parton scattering process. However, higher order QCD corrections alter this picture significantly, and detailed measurements of multi-jet configurations are very important to constrain the QCD descriptions of hadronic processes.

The most impressive results at this stage are the inclusive jet and the di-jet cross-section measurements [5]; an example for them is shown in Fig. 6a. These measurements cover unprecedented kinematical ranges spanning typically over jet transverse momenta from 20 GeV to 1.5 TeV, in many angular bins up to $|\eta| < 4.4$ (i.e. very close to the beam axis). The cross-sections vary over these ranges by up to 12 orders of magnitude. In general the agreement with perturbative QCD calculations including next to

leading order (NLO) corrections is well within the systematic uncertainties. This cannot be seen in Fig. 6a directly, only in ratio plots measurement/theory for a given η -interval. The systematic uncertainties in the ratios are typically only 30%, which is a great achievement compared to previous such measurements. The systematic uncertainties on the measurements are dominated by the jet energy scale uncertainty (calibration of the detectors for the energy of jets), which thanks to a considerable effort has been determined to typically better than 3% [6]. Another example of precise QCD results is displayed in Fig. 6b where the inclusive single isolated prompt photon cross-section [7] is compared to one of the most advanced QCD calculation.

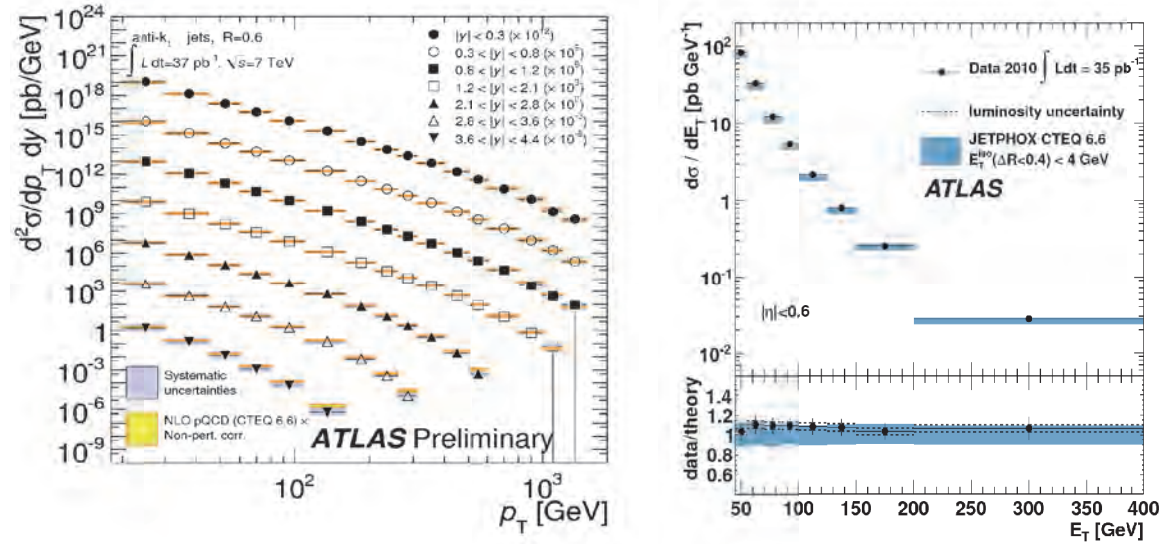


Figure 6. Inclusive jet (a, left) and single isolated prompt photon (b, right) cross-sections, compared to NLO perturbative QCD predictions.

Jets can also be produced together with W and Z bosons, so-called QCD corrections to the Intermediate Vector Boson production. First results of these processes have been published [8]. A good understanding of them is particularly important as they are, in many cases, a dominant source of backgrounds to the search for new particles, as well as to the measurements of top quark production discussed next.

The heaviest known particle in the SM is the top quark with its roughly 175 GeV mass. It decays almost exclusively into a W and a bottom quark. The measurement of top quark pair production typically requests that at least one of the W decays leptonically (also needed to trigger the events), and therefore the final states require one or two leptons (electrons or muons), $E_{T\text{miss}}$, and jets, some of which, coming from the b-quarks, can be tagged by the displaced secondary vertices due to the finite life times of b-hadrons. Whilst it is beyond the scope of this report to describe the sophisticated analyses employed, the message is that there are clear top pair signals in ATLAS [9], both in the single and two-lepton channels, when considering the correct jet topologies. The resulting cross-sections are shown in Fig. 7 which also illustrates the expected large rise of the cross-section with the collision energy increase from 2 TeV at the TeVatron to 7 TeV at the LHC. Good agreement with NLO QCD calculations is seen within the present 7% measurement errors. It can be mentioned that ATLAS has also reported first single top observations (events with just one top quark) at a rate in good agreement with QCD expectations.

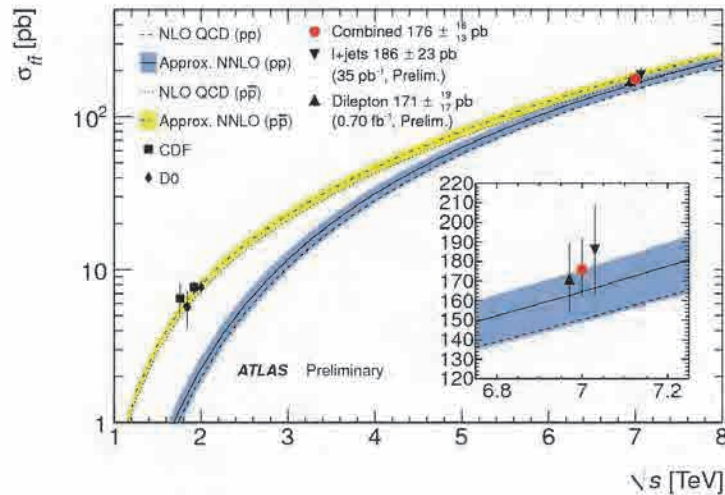


Figure 7. Top pair production cross-section as a function of the collision energy, showing the TeVatron and ATLAS LHC measurements.

A summary of many measurements of interesting Standard Model production cross-sections is given in Fig.8 which includes also the low cross-section processes of IVB pair productions.

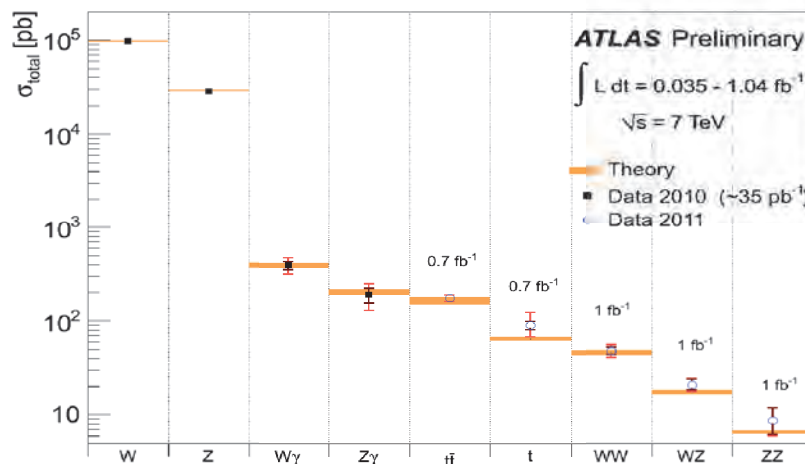


Figure 8. Summary of various Standard Model production cross-sections.

4. THE HUNT FOR THE HIGGS BOSON

The search for the Higgs boson H , as the decisive manifestation of the Brout, Englert, and Higgs mechanism for electro-weak symmetry breaking, postulated in 1961, was one of the major motivations for initiating the LHC project already more than 25 years ago. The ability to detect it unambiguously over the full possible mass range from its lower experimental limit of 114 GeV (set at the LEP collider) up to one TeV, with very different favoured final states (decay modes) at different masses, was the major benchmark in the conception of the ATLAS and CMS detector designs.

The most stringent limits at hadron colliders were set until spring 2011 by the combined Higgs search results from the TeVatron experiments CDF and D0, excluding at 95% confidence level (CL) the mass

range 157 to 173 GeV. This was achieved by combining searches for an excess of events over the SM backgrounds in several Higgs decay channels, but dominated in this mass range by $H \rightarrow W^+W^-$ decays, with the W s decaying in turn leptonically (electron, or muon plus neutrino channel). ATLAS and CMS have updated their searches in many channels for the summer conferences, extending the H exclusion limits over a significantly larger mass range.

At the time of this Symposium the public ATLAS Higgs search status [10] corresponded to the results presented at the 2011 International Symposium for Photon Lepton Interactions at High Energies. Two examples are given in Fig. 9. The first (Fig. 9a) shows the relatively straight forward search for a mass peak from the process of the H decaying into two Z 's (one might be virtual), which in turn decay into charged lepton pairs (electrons or muons in this figure). The second example (Fig. 9b) displays the search for the H decaying into WW , and each W decaying leptonically into an electron or muon and its associated neutrino. Because of the ETmiss from the neutrinos no mass peak can be reconstructed, only a broad enhancement in the transverse mass of the leptons and ETmiss can be expected. In both cases no excess is observed over the background distributions within the present data samples. The figures also illustrate the expected contributions from a Standard Model H boson.

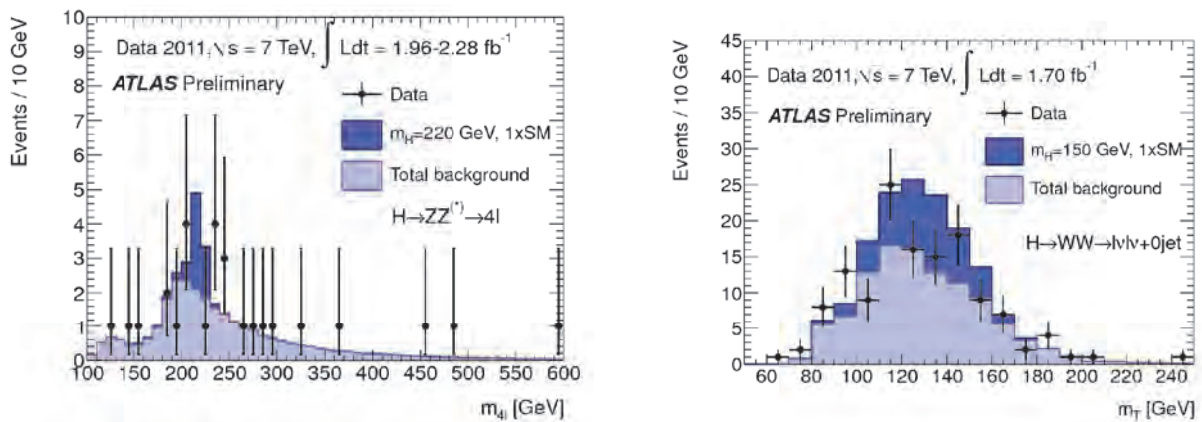


Figure 9. Examples of H search results, (a, left) in the four charged leptons channel and (b, right) in the two charged leptons plus two neutrinos channel (see text).

At this stage, the absence of any significant signal over the backgrounds in the analysis of many channels can be expressed in terms of 95% confidence level (CL) exclusion limits. For a graphical representation this is done in terms of a ratio between the limit cross-sections over the expected Standard Model H cross-sections, as shown in detail for several decay channels in Fig. 10. The mass range for which this ratio is smaller than one is then excluded at the 95% CL. Combining all analysis channels, and taking into account also possible correlations, leads to exclude at 95% CL the SM H boson in the mass ranges 146–232, 256–282 and 296–466 GeV [10].

Note, however, that much progress in the H search can be expected on the basis of already accumulated data, as well as the anticipated data from 2012. A definite statement about the existence or not of a SM H might well be in reach for the end of 2012.

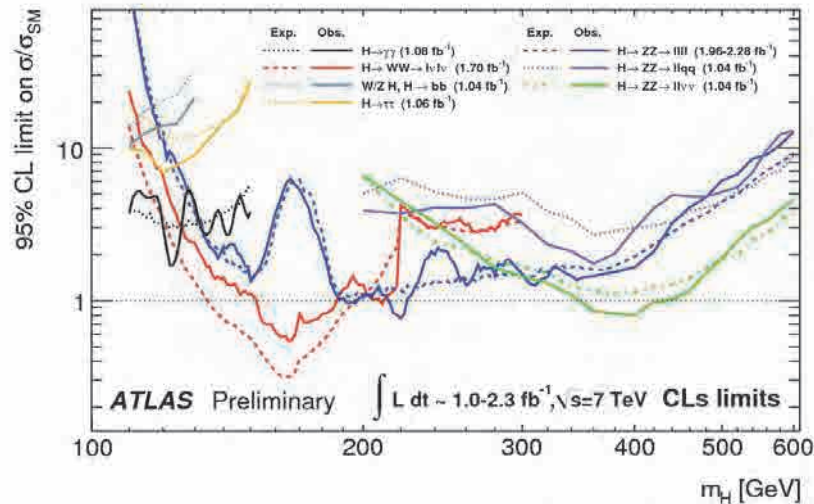


Figure 10. A summary of 95% CL limits, for various Standard Model Higgs search channels separately, as a function of the H mass (see text for explanations).

5. SEARCHES FOR PHYSICS BEYOND THE STANDARD MODEL

Besides the quest to elucidate the mechanism of the electro-weak symmetry breaking by searching for the Higgs boson, the major excitement for LHC comes from the great potential to explore uncharted territory of physics Beyond the Standard Model (BSM), thanks to its highest collision energy available in the laboratory. Since the beginning of the project, the search for Supersymmetry (SUSY) was a strong motivation, and besides the H boson it has been the other benchmark physics guiding the detector designs. However, many other hypothetical new processes can be searched for, and indeed ATLAS and CMS have already reported in many publications a very broad spectrum of searches for signatures of such processes (mass peaks for new particles or kinematical distributions with deviations from the expectations of known physics) for BSM physics. No such effect has yet been found, but all of these searches result in new exclusion limits, often well beyond the one TeV scale already. Only a few examples are shown in the following.

The most popular searches concern SUSY, which predicts additional fundamental particles. The search for SUSY is motivated in part by the prospect that the lightest stable neutral SUSY particle (LSP) could be an excellent candidate for explaining the Dark Matter (DM) in the Universe. The mysterious existence of DM was postulated by Zwicky, and rather convincingly evidenced by Rubin, both astronomers, in the 1930s and 1970s respectively. The SUSY searches at LHC are very complex as they must be sensitive to many (model-dependent) decay chains, implying a large variety of possible final state topologies. A common feature for most of them is the existence of significant missing transverse energy, $E_{T\text{miss}}$, due to the escaping LSPs (an experimental signature similar to that of the neutrinos in the W decays). Furthermore the SUSY signatures include high transverse momentum jets, some tagged as B-jets for third-generation squarks, and leptons. The expected topologies depend not only on the model parameters, but also on the mass relations between squarks and gluinos (the SUSY partners of the SM quarks and the gluons).

As an illustration of the typical data in the SUSY searches [11], Fig. 11 shows the effective mass (m_{eff}) distributions, defined as scalar sum of $E_{T\text{miss}}$ and all jet transverse momenta, for a search for SUSY in

events with at least two jets, ETmiss and no lepton. The distributions are shown in (a) for a background control region which is enhanced with QCD multi-jet events having only minimal contributions from a possible signal, and in (b) for a kinematical region where the signal would be strongest. In both distributions an expected signal for certain SUSY parameters is indicated by the dashed histogram, over the various SM backgrounds. The figure shows that the data are perfectly described at this stage with the background distributions only.

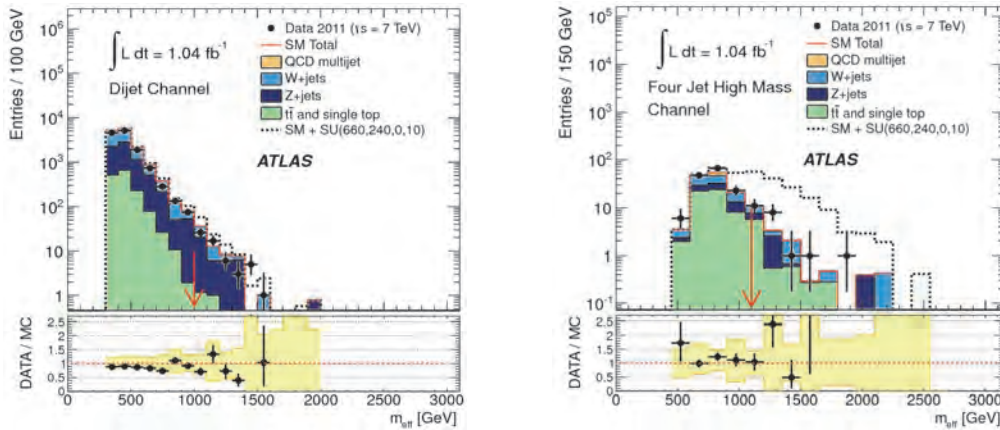


Figure 11. Typical m_{eff} distributions for (left) background enhanced and (right) signal enhanced SUSY search regions. A possible SUSY signal is indicated by the dashed histogramme (see text).

The data can then be used to extract 95% CL upper limits for the number of observable events and cross-sections independently of new physics models, in the background-only hypothesis. These cross-section limits in turn can be translated into lower limits for SUSY particle masses in SUSY models for a given set of model parameters. It is customary to represent the limits in a parameter plane correlating scalar (m_0) masses vs. gaugino ($m_{1/2}$) masses of SUSY representations [11]. The results for a simplified model are shown in Fig. 12 that assume only first- and second- generation squarks, gluinos, and massless neutralinos. Mass values smaller than indicated by the experimental limit are excluded by the data at 95% CL. It can be noted that the LHC results already extend significantly the search range from previous experiments. In this particular example, and assuming equal squark and gluino masses, their lower mass bound is 1.075 TeV at 95% CL. It is expected that the mass range will be quickly extended within more LHC running, and ultimately the LHC will be able to discover such particles up to about 2.5 TeV mass.

Classical searches for BSM physics include the exploration of IVB-like signatures in the high mass range made kinematically accessible by the high collision energy of the LHC. The searches for hypothetical heavy W' and Z' particles is rather straightforward in the lepton-pair and lepton-neutrino decay channels, extending in mass coverage the SM IVB analyses mentioned before. Such heavy resonances arise in a variety of models mostly related to hypothetical new forces, either with the same properties as the SM IVBs, in that case called sequential (and labeled as SSM), or in other models as referenced in the ATLAS publications [12].

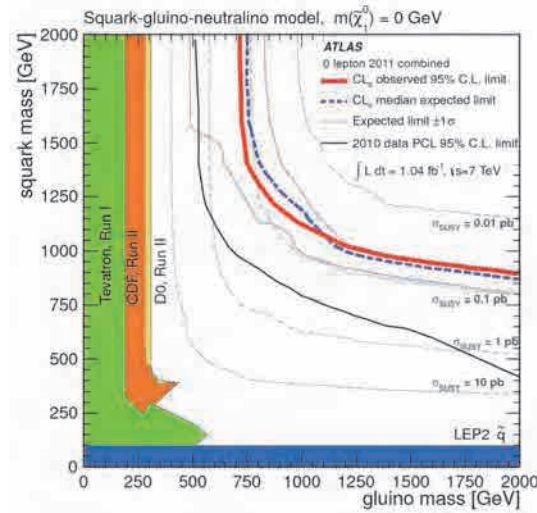


Figure 12. Example of an exclusion contour in a SUSY parameter plane of gluino mass vs. squark mass in the simplified SUSY model mentioned in the text. Lower mass values than indicated by the solid red line are excluded at 95% CL. Results from previous experiments are also indicated at lower masses.

As examples of such searches, Fig. 13 shows the Z' and W' data distributions superimposed with the expected signals for various IVB' masses. The absence of a signal in the data can be translated into 95% CL cross-section limits that are confronted with the expected theoretical cross-sections as a function of the mass of the new particles in order to establish lower mass limits. At this stage this typically leads to 95% CL lower limits for Z' and W' of 1.83 and 2.15 TeV, respectively. Ultimately, with the LHC running for several years at 14 TeV collision energy, the experiments will explore masses up to the order of 5 TeV for such particles.

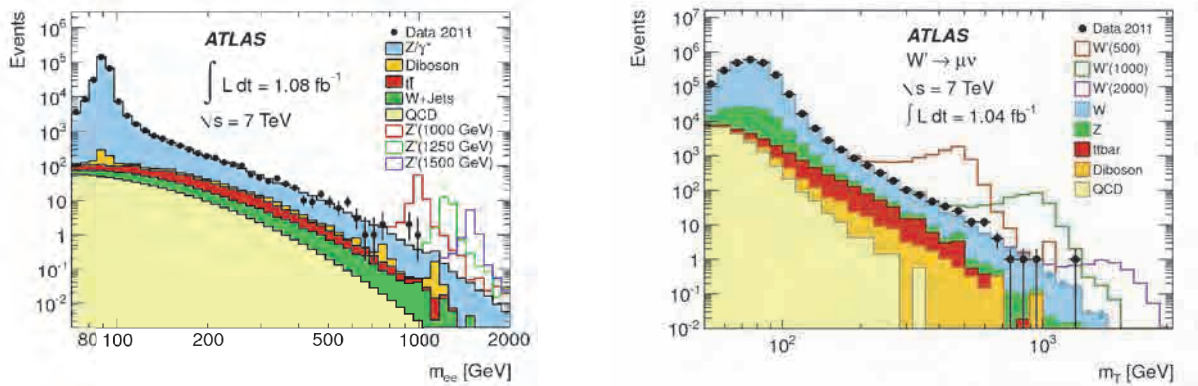


Figure 13. Examples of the di-electron mass distribution (left) and of the muon-neutrino transverse mass distribution (right) for the searches of heavy Z' and W' particles. The data are compatible with the SM backgrounds, the expected signals from hypothetical SSM signals are also indicated (see text).

Excited heavy quarks (q^*), axigluons (massive gluons) or other objects are predicted in various models that would decay into a pair of partons, manifesting themselves as resonances in the final state di-jet mass distributions above the SM QCD spectrum. Searches for such di-jet resonances have been published in [13], and Fig. 14 shows an example of how well the data are actually described by the

smooth QCD spectrum, allowing ATLAS to exclude at 95% CL typically q^* with masses below 3 TeV and axigluons below 3.3 TeV.

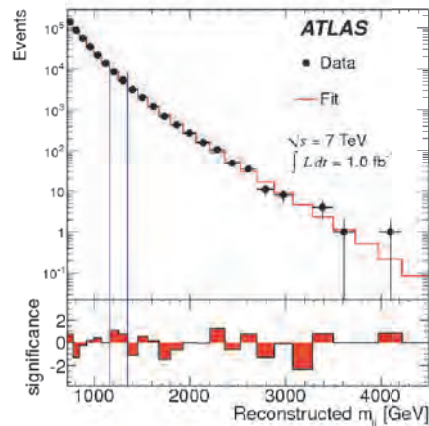


Figure 14. Example of a search for a resonance mass peak over the smooth QCD di-jet mass spectrum.

Of great interest at this new energy frontier are also searches for a possible substructure of the quarks related to a new super-strong interaction. Such a substructure, called compositeness at a scale Λ , could manifest itself by deviations from QCD in the angular distribution of high-momentum transfer, large-angle scatterings, in analogy to the famous Rutherford scattering experiment some 100 years ago. No deviations have been observed so far [14], setting a 95% CL lower limits on Λ at 6.7 TeV, significantly higher than in previous experiments. Another possibility would be the formation of new bound states containing both quark and lepton properties that would decay into quarks (resulting in jets) and leptons, so-called lepto-quarks. New limits on their existence have been established in dedicated searches.

Many other searches aimed at exploring BSM physics have been conducted, all with finding any excess of event rates over the expected backgrounds from the SM. But in essentially all cases more stringent constraints could be established compared to previous experiments at lower collision energy. A non-exhaustive summary of such 95% CL limits is displayed in Fig. 15.

6. CONCLUSIONS

After only two years of high-energy operation of the LHC, ATLAS (as well as CMS, LHCb and ALICE) has already produced a very rich harvest of physics results. This should in first place be seen as a success of the overall LHC project with its three major components having worked in an extraordinary coherent way so early on: the collider, the experiments and the novel computing grid structure wLCG.

ATLAS (as well as CMS) has already amply demonstrated that it masters the analyses of Standard Model physics, and has brought many SM measurements into domains of details and a degree of sophistication unprecedented at lower energy machines, setting a challenge for accurate theoretical descriptions. The early SM results also demonstrate that the experiment is well understood and operates at full potential to attack the main goals of LHC, namely to make the conclusive investigations of the electro-weak symmetry breaking mechanism, i.e. establish the existence, or otherwise, of the Higgs boson, and explore the physics Beyond the Standard Model. The searches for BSM physics are already exploring

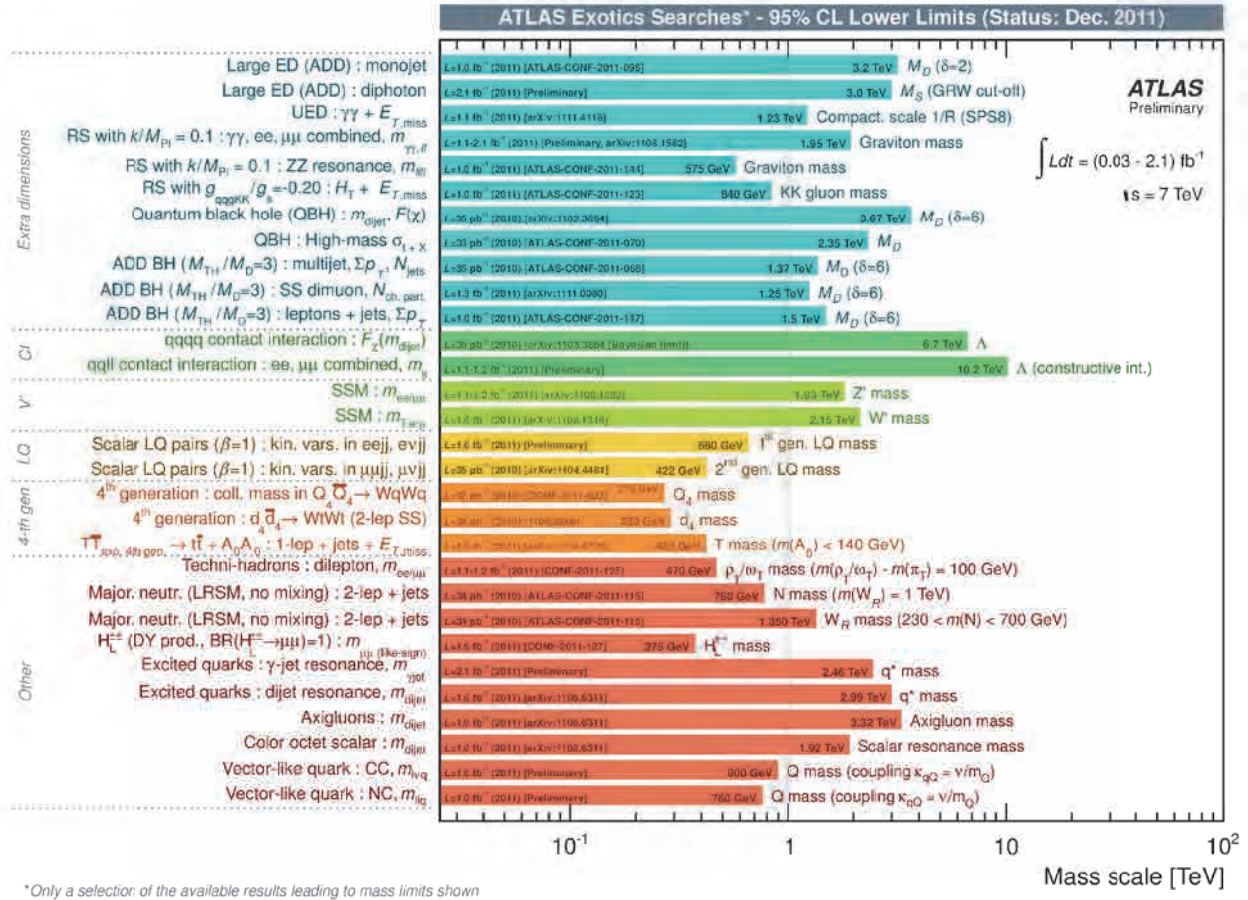


Figure 15. A non-exhaustive summary of 95% CL lower limits established so far on a variety of searches for BSM physics.

unchartered territory, thanks to the superb start-up of the collider. One should remain aware, however, that the full physics potential will only become available in future years with the machine reaching its full design luminosity and energy. But there is no doubt: particle physics has exciting times ahead with the LHC project now operational.

ACKNOWLEDGEMENT

I thank the Pontifical Academy of Sciences and Professor Antonino Zichichi for having invited me to this stimulating international Symposium, and for the generous hospitality in the Vatican City.

REFERENCES

- [1] The Large Hadron Collider: a Marvel of Technology, ed. L. Evans, EPFL Press, 2009, 182-199.
- [2] ATLAS Collaboration, The ATLAS Experiment at the CERN Large Hadron Collider, JINST 3 (2008) S08003.
- [3] ATLAS Collaboration, Charged-particle multiplicities in pp interactions measured with the ATLAS detector at the LHC, New J. Phys. 13 (2010) 053033.
- [4] ATLAS Collaboration, Measurement of the inclusive W and Z cross-sections in the electron and muon decay channels in pp collisions at 7 TeV with the ATLAS detector, arXiv:1109.5141[hep-ex], submitted to Phys. Rev. D.
- [5] ATLAS Collaboration, Measurement of inclusive jet and dijet production in pp collisions at 7 TeV using the ATLAS detector, arXiv:1112.6297[hep-ex], submitted to Phys. Rev. D.
- [6] ATLAS Collaboration, Jet energy measurement with the ATLAS detector in proton-proton collisions at 7 TeV, arXiv:1112.6426[hep-ex], submitted to Eur. Phys. J. C.
- [7] ATLAS Collaboration, Measurement of the inclusive isolated prompt photon cross-section in pp collisions at 7 TeV using 35 pb⁻¹ of ATLAS data, Phys. Lett. B706 (2011) 150.
- [8] ATLAS Collaboration, Measurement of the production cross-section for W-bosons in association with jets in pp collisions at 7 TeV with the ATLAS detector, Phys. Lett. B698 (2011) 325;
ATLAS Collaboration, Measurement of the production cross-section for Z in association with jets in pp collisions at 7 TeV with the ATLAS detector, arXiv:1111.2690[hep-ex], submitted to Phys. Rev. D.
- [9] ATLAS Collaboration, Measurement of the top quark-pair production cross-section with ATLAS in pp collisions at 7 TeV, Eur. Phys. J. C71 (2011) 1577;
ATLAS Collaboration, Measurement of the top quark-pair production cross-section in pp collisions at 7 TeV in dilepton final states with ATLAS; arXiv:1108.3699[hep-ex], submitted to Phys. Lett. B.
- [10] ATLAS Collaboration, Update of the combination of Higgs boson searches in 1.0 to 2.3 fb⁻¹ of pp collisions data taken at 7 TeV with the ATLAS experiment at the LHC, ATLAS-CONF-2011-135.
- [11] ATLAS Collaboration, Search for squarks and gluinos using final states with jets and missing transverse momentum with the ATLAS detector at 7 TeV proton-proton collisions, arXiv:1109.6572[hep-ex], submitted to Phys. Lett. B.
- [12] ATLAS Collaboration, Search for dilepton resonances in pp collisions at 7 TeV with the ATLAS detector, Phys. Rev. Lett. 107 (2011) 272002;
ATLAS Collaboration, Search for a heavy gauge boson decaying to a charged lepton and a neutrino in 1 fb⁻¹ of pp collisions at 7 TeV using the ATLAS detector, Phys. Lett. B705 (2011) 28.
- [13] ATLAS Collaboration, Search for New Physics in the dijet mass distribution using 1 fb⁻¹ of pp collision data at 7 TeV collected by the ATLAS detector, arXiv:1108.6311[hep-ex], submitted to Phys. Lett. B.
- [14] ATLAS Collaboration, Search for New Physics in dijet mass and angular distributions in pp collisions at 7 TeV measured with the ATLAS detector, New J. Phys. 13 (2011) 053044.

TQUARKS: AS CONSTITUENTS AND IN QCD

■ FRANK CLOSE

Dept of Theoretical Physics, University of Oxford
Oxford OX1 3NP; England

In the 19th century, the first clues that there is a deeper layer of structure within atoms came from the discovery of patterns among the atomic elements: Mendeleev's periodic table. This was accompanied by spectra and followed by Rutherford's direct observation of the atomic nucleus and Thomson's discovery of the electron. In the middle of the 20th century an analogous set of circumstances led to the revelation of the quark layer of reality. Strongly interacting particles – hadrons – were found to be built from quarks, the inter-quark forces being transmitted by gluons.

The analogue of Mendeleev's table was the recognition of patterns – known as the Eightfold Way - among families of hadrons (Gell-Mann, 1962). These arise from the various ways that the underlying quarks, which form those hadrons, combine (Gell-Mann 1964; Zweig 1964). In the late 1960s the presence of quarks within hadrons was directly confirmed by experiments scattering high energy beams of electrons and neutrinos from targets of protons and neutrons (Panofsky 1968). Discovery of a spectroscopy of hadrons, analogous to the spectra of atomic elements, completed the parallel.

Today the quark layer of reality is established. However, the quarks revealed by spectroscopy are not easily identified with those that are manifested by the high energy “deep inelastic scattering” experiments. The latter have almost no mass, and as such have the attributes of the basic entities in the fundamental Lagrangian of QCD, the relativistic quantum field theory of the strong force. The

Dalitz, Morpurgo and others initially to have large masses and deep binding (Dalitz 1965; Morpurgo 1965; Morpurgo 1974).

Non-relativistic constituent quarks

The non-relativistic constituent quark model worked empirically even though there was no well-defined rationale for the approach. The most dramatic success was with photoproduction, where over 100 amplitudes were well described, both in relative magnitudes and phases, a feat which no other approach then or since has matched (Copley 1969; Feynman 1971).

The success of this unfounded non relativistic model was, in many cases at least, revealed to be due to its underlying structure rather than detailed dynamics (Close 1979). A hadron has total spin J , made up of quarks with total spin S and the left over defined by L . In a specific non relativistic model, L was identified with the orbital angular momentum. However, as far as the mathematical algebra was concerned it was not necessary to make this further assumption. This reduced the amount of predictions, but made the survivors stronger. In particular relations among amplitudes survived, and proved empirically successful. Therefore it was possible that the success of the model was due to more general features, driven by the couplings of spins, rather than detailed and ill-founded, dynamics.

One of these successes concerned the photoproduction amplitudes of the prominent resonance $D(13)$ mass 1520 MeV. From proton targets a specific amplitude – when the combined helicity of photon and proton are anti-aligned to total $\frac{1}{2}$ rather than aligned to $\frac{3}{2}$ - vanishes. This was described in the model as a cancellation between electric and magnetic multipoles for this transition (Copley 1969, Feynman 1971). Fred Gilman and I then realized that, while this could be accounted for by the general mathematical algebra, without specific recourse to non-relativistic models, a change from photo to electroproduction would provide a sensitive dynamic test (Close 1972). Real quarks would respond more strongly to the magnetic rather than to the electric multipoles as the

photon became more virtual; in an algebraic approach there was no reason for such an effect.

Empirically this was verified, and remarkably so (Close 1979). The change to magnetic dominance took place almost immediately as the photon became virtual. The speed of this change was in line with the non-relativistic model. Why the model worked so well was, and remains, a mystery. However, this result proved that constituent quarks are real dynamical degrees of freedom within hadrons and are more than simply book-keeping devices for the mathematical algebra.

Bag models: relativistic quarks; glueballs and hybrids

A resolution to the dichotomy came with the Bag models, notably that of MIT (Jaffe 1978). Quarks with the characteristics of QCD, possibly even massless, were confined in a simple model where, in effect, an infinitely high potential imprisoned them within a femto-universe of about 1 fm. Quantum mechanics implies that a massless fermion confined in such a length scale gains an energy of around 350MeV. This could be identified with the effective mass of the constituent quark.

The model was never developed enough to deal with the excited states that Gilman and I had investigated. However, it had another implication: massless gluons, similarly confined, would themselves gain an energy. This enabled a tentative spectroscopy of glueballs – containing two or more gluons – and hybrids – where a gluon accompanies quarks and/or antiquarks inside the confinement bag.

This simple picture seems remarkably robust in comparison with modern understanding of the spectrum. The equations of QCD, when studied in computer simulations, which assume space-time to consist of a discrete lattice rather than a continuum (so called Lattice QCD), reveal a spectrum of states with remarkable parallels to those of the simple bag model of massless quarks and gluons.

In 1983 Barnes and I computed the spectrum of the lightest hybrid mesons and baryons, including the perturbations of energy levels (hadron masses) arising from single gluon exchanges among the constituents (Barnes 1983a,1983b). For the lightest hybrid mesons this implied that the lightest such state would be $J^{PC} = 0^{-+}$, the next being the exotic 1^{-+} , with 1^{-} and 2^{-+} heavier and completing the group. This is what modern lattice QCD finds.

We also studied the spectrum of hybrid baryons. There is a rich set of N^* and Delta excitations with positive parity and spins ranging from $\frac{1}{2}$ to $\frac{5}{2}$. The pattern here too seems to be confirmed in recent studies of lattice QCD by a group at Jefferson Lab (Dudek 2012).

The message seems to be that the simple bag picture agrees with the pattern of the real world (lattice QCD being the nearest to this that we can simulate at present.) The fact that quarks and gluons act as quasi-free particles until they hit the wall of confinement is a remarkably simple, and empirically successful, description of hadrons. Nature has turned out to be simple enough for us to decode its patterns. Obtaining a robust theoretical description though remains a challenge.

Gluonic Hadrons: a new picture

One thing is missing from all of the above: the structure of a hadron depends on the resolving power of the microscope with which it is examined. In a nutshell: the larger the resolution, or in effect, the shorter the wavelength of the probe, so the more structure is revealed. What appears as a quark at low resolution is revealed as a seed surrounded by virtual quarks and antiquarks, and gluons, at high resolution. This poses a challenge: what would a glueball look like as you power up the microscope?

Scattering electrons from a state of pure glue would not occur, as the electron needs a source of electric charge to couple to. However, as the momentum

transferred grows, the resolution improves and the target is increasingly perceived to contain quarks and antiquarks, from which the electron can scatter. The probability of scattering thereby grows.

The quantitative measure is the amount of momentum carried by electrically charged constituents – technically this is given by the integral of the inelastic structure function, $F_2(x, q^2)$, where x is the Bjorken variable and q^2 is the square of the four-momentum transfer (Close 1979). The integral will grow with q^2 . As q^2 tends to infinity, the integral tends to an asymptotic value, whose value depends on the number of flavours. Physically, this extreme is where the hadron is perceived as a plasma of quarks, antiquarks and gluons in equilibrium.

This behaviour contrasts what occurs for a hadron such as a proton, where there is electric charge available even as q^2 is small. In this case the integral of $F_2(x, q^2)$ falls to its asymptotic value.

Thus we have a well-defined way of classifying hadrons as gluonic or flavoured: the two classes correspond to the said integral rising or falling to the asymptotic limit. In other words, at small q^2 the hadron's momentum is dominantly carried by gluons or flavoured fermions.

This applies to hadrons made of the constituents as defined by the Lagrangian of QCD and revealed in deep inelastic experiments: lightweight fermions and gluons. There is an interesting question of counting of states relative to classification in the old constituent picture. In the latter, mesons can be glueball, hybrid or conventional. This involves three classes, whereas the novel approach only admits two: gluonic or fermionic. This is a question that I am currently investigating, together with that of decays, and how the concept of multiquark hadrons fits in with this scheme.

References

- Barnes (1983a) Barnes T., F.E.Close and F.de Viron, Hybrid mesons in the MIT Bag Model, *Nuclear Physics* B224, 241-264
- Barnes (1983b) Barnes T. and F.E.Close, Where are Hermaphrodite Baryons? *Physics Letters* 123B, 89-92
- Close (1972) Close F.E. and F.J.Gilman, Helicity Structure of Nucleon Resonance Electroproduction and the Symmetric Quark Model, *Physics Letters* 38B, 541-543
- Close (1979) *Introduction to Quarks and Partons* (Academic Press; New York and London)
- Copley (1969); Copley L.A., G. Karl and E.Obryk, Single Pion Photoproduction in the Quark Model, *Nuclear Physics* B13, 303-312
- Dalitz (1965); Dalitz R.H., in *High Energy Physics* (eds. C. de Witt and M.Jacob) (Gordon and Breach, New York)
- Dudek (2012) Dudek J. and R. Edwards, Hybrid Baryons in QCD <http://arxiv.org/pdf/1201.2349>
- Feynman (1971) Feynman R., M Kislinger and F Ravndal, Current Matrix Elements from a Relativistic Quark Model, *Physical Review* D3, 2706-2732
- Gell-Mann,(1962) Gell-Mann M., Symmetries of Baryons and Mesons, *Physical Review* 125, 1067-1084
- Gell-Mann (1964); Gell-Mann M., A Schematic Model of Baryons and Mesons, *Physics Letters* 8, 214-215
- Jaffe (1978). Jaffe R.L. *Proceedings of Erice School on Subnuclear Physics* (ed A.Zichichi) (Academic Press, New York and London)
- Morpurgo (1965) Morpurgo G., *Physics* 2, 95
- Morpurgo (1974) Morpurgo G., *Proceedings of Erice school on Subnuclear Physics* (ed A.Zichichi) (Academic Press, New York and London)
- Panofsky (1968) Panofsy W., *Proceedings of 14th International Conference on High Energy Physics*, Vienna, 1968 (ed J Prentki and J Steinberger), (CERN)
- Zweig (1964) Zweig G., CERN report TH 402 (1964) unpublished

TCOMPOSITE WEAK BOSONS, LEPTONS AND QUARKS

■ HARALD FRITZSCH

University of Munich
Faculty of Physics,
Arnold Sommerfeld Center for Theoretical Physics,

Abstract

The weak bosons consist of two fermions, bound by a new confining gauge force. The mass scale of this new interaction is determined. At energies below 0.5 TeV the standard electroweak theory is valid. A neutral isoscalar weak boson X must exist - its mass is less than 1 TeV. It will decay mainly into quark and lepton pairs and into two or three weak bosons. Above the mass of 1 TeV one finds excitations of the weak bosons, which mainly decay into pairs of weak bosons. Leptons and quarks consist of a fermion and a scalar. Pairs of leptons and pairs of quarks form resonances at very high energy.

In the Standard Model the leptons, quarks and weak bosons are pointlike particles. I shall assume that they are composite particles with a finite size. The present limit on the size of the electron, the muon and of the light quarks is about 10^{-17} cm.

The constituents of the weak bosons and of the leptons and quarks are bound by a new confining gauge interaction. Due to the parity violation in the weak interactions this theory must be a chiral gauge theory, unlike quantum chromodynamics.

The Greek translation of "simple" is "haplos". We denote the constituents as "haplons" and the new confining gauge theory as quantum haplodynamics (QHD). The QHD mass scale is given by a mass parameter Λ_h , which determines the sizes and the masses of the weak bosons. It must be very large, at least thousand times larger than the QCD mass scale Λ_c . A theory of this type was proposed in 1981 (ref.(1), see also ref.(2-6)).

Two types of lefthanded spin $\frac{1}{2}$ haplons are needed as constituents of the weak bosons, denoted by α and β . The doublet h of the weak isospin group $SU(2)$ is given by the two lefthanded haplon fields:

$$h = \begin{pmatrix} \alpha \\ \beta \end{pmatrix} \quad (1)$$

The three weak bosons have the following internal structure:

$$\begin{aligned} W^+ &= \bar{\beta}\alpha \\ W^- &= \bar{\alpha}\beta \\ W^3 &= \frac{1}{\sqrt{2}} (\bar{\alpha}\alpha - \bar{\beta}\beta) . \end{aligned} \quad (2)$$

We expect that in a composite model the structure of the spectral functions of the weak currents is similar to the structure of the spectral functions

in hadronic physics. At an energy of the order of Λ_c the spectral functions of the hadronic currents are dominated by the ρ -mesons. At energies much larger than Λ_c the spectral functions are given by the continuum of quark-antiquark states. Analogously we expect that at the energy of the order Λ_h the spectral functions of the weak currents are dominated by the weak bosons. At energies much larger than Λ_h the spectral functions are given by the continuum of haplon pairs.

In strong interaction physics the universality of the couplings of the ρ -mesons to the hadrons follows from the current algebra and the dominance of the matrix elements of the vector currents by the ρ -mesons. In the Standard Model the universality of the weak coupling constants is due to the gauge invariance. In a composite model of the weak bosons it follows from the algebra of the weak currents and the dominance of the weak currents by the weak bosons (ref.(3)).

In the absence of electromagnetism and the quark masses the three ρ -mesons are degenerate in mass. If the electromagnetic interaction is introduced, the neutral ρ -meson changes its mass due to a mixing with the photon. The mass shift, caused by this mixing, can be calculated. It depends on a mixing parameter μ , which is determined by the electric charge, the decay constant F_ρ and the mass of the ρ -meson:

$$\mu = e \frac{F_\rho}{M_\rho}. \quad (3)$$

One finds for the mass difference between the charged and neutral ρ -mesons:

$$M(\rho^0)^2 - M(\rho^\pm)^2 = M(\rho^\pm)^2 \left(\frac{\mu^2}{1 - \mu^2} \right). \quad (4)$$

The decay constant is measured to about 220 MeV, which gives $\mu \approx 0.09$. The mass shift due to the mixing is about 3.1 MeV.

Analogously in QHD the three weak bosons are degenerate in mass in the absence of electromagnetism. If the electromagnetic interaction is introduced, the mass of the neutral boson increases due to the mixing with the photon. The mixing between the neutral weak boson and the photon is caused by the dynamics, like the mixing between the photon and the neutral ρ -meson in QCD. It is described by a mixing parameter m , which is determined by the decay constant of the weak boson F_W , defined in analogy to the decay constant of the ρ -meson in QCD (ref.(3)):

$$\langle 0 \left| \frac{1}{2} (\bar{\alpha} \gamma_\mu \alpha - \bar{\beta} \gamma_\mu \beta) \right| Z \rangle = \varepsilon_\mu M_W F_W . \quad (5)$$

In the Standard Model the mixing is described by the weak mixing angle. In QHD the mixing is a dynamical phenomenon, and the mixing parameter m is given by the decay constant of the W -boson F_W :

$$m = e \frac{F_W}{M_W} . \quad (6)$$

In the Standard Model the mixing parameter m is given by the weak mixing angle (ref.(3)):

$$\sin \theta_w = m . \quad (7)$$

The mass difference between the Z -boson and the W -boson is determined by the mixing parameter m and the W -mass:

$$M_Z^2 - M_W^2 = M_W^2 \left(\frac{m^2}{1 - m^2} \right) . \quad (8)$$

Using the experimental values for the weak boson masses and the weak mixing angle, we find:

$$\begin{aligned} F_W &= 124 \text{ GeV} \\ m &= 0.482 . \end{aligned} \tag{9}$$

In strong interaction physics the decay constant of the ρ -meson and the QCD mass parameter Λ_c are proportional. The decay constant of the ρ -meson is measured to about 220 MeV. The QCD mass parameter Λ_c has also been measured: 217 ± 25 MeV. By accident both parameters are about equal. We expect a similar connection between the decay constant of the weak boson and the QHD mass parameter Λ_h . If the QHD gauge group would be SU(3), the ratio of Λ_h and Λ_c would be given by the measured ratio of the decay constants:

$$\frac{\Lambda_h}{\Lambda_c} \approx \frac{F_W}{F_\rho} \simeq 564. \tag{10}$$

In that case Λ_h would be 0.122 TeV. The actual value of Λ_h depends on details of the gauge group, but it should be less than 1 TeV. Thus the mass scales of QCD and QHD differ by about three orders of magnitude. The leptons, quarks and weak bosons have a size of about 10^{-17} cm. At energies below 1 TeV the standard electroweak theory is a very good approximation, but above 1 TeV it will break down.

If the weak bosons consist of the two haplons α and β , there must exist a second neutral weak boson, which is an isoscalar and has the internal structure:

$$X = \frac{1}{\sqrt{2}} (\bar{\alpha}\alpha + \bar{\beta}\beta) . \tag{11}$$

This boson is not present in the Standard Model - it will be denoted by X . Its mass must be much larger than the mass of the Z -boson. The present lower limit on the mass of the X -boson is about 0.8 TeV (see also ref.(7)).

In strong interaction physics the mass of the ρ -meson and of the ω -meson are nearly the same. One would expect that the mass of the X -boson is about the same as the mass of the Z -boson, but this is excluded by the experiments. The fact that the X -boson must be much heavier than the Z -boson might be related to the QHD analogy of the gluonic anomaly of QCD. The latter implies that the mass of the η' -meson is different from zero in the chiral limit, while the masses of the π -mesons and of the η -meson vanish.

In QHD the isospin singlet axial vector current also has an anomaly, and this might be the reason why the X -boson is very heavy. The theory of QHD is a confining chiral gauge theory, and low mass pseudoscalar bosons do not exist. The anomalous divergence of the singlet axial vector current might increase the mass of the X -boson. But details about the dynamics of chiral gauge theories are not yet known. For our further discussion we shall assume a mass of 0.8 TeV for the X -boson.

The X -boson would couple to the leptons and quarks with the same strength as the Z -boson, since they consist of the same constituents. Thus it can easily be produced at the LHC by quark-antiquark-fusion. The cross section for the production of Z -bosons at the LHC is estimated to about 60 nb. If the X -boson has a mass of 0.8 TeV, we can determine the cross section for its production at the LHC. It should be about 0.8 nb.

An important decay mode of the X -boson is the decay into lepton pairs, e.g. into muon pairs. The partial width for this decay can be estimated by comparing it with the decay of a charged weak boson into a muon and the muon antineutrino, which has a partial width of about 226 MeV. Using this result, we can calculate the partial width for the leptonic decay of the X -boson with a mass of 0.8 TeV:

$$\Gamma(X \rightarrow \mu^+ \mu^-) \approx 2.25 \text{ GeV}. \quad (12)$$

The X -boson will decay primarily into lepton pairs and quark pairs. We expect the following relations to hold between the branching fractions of the various decays:

$$\begin{aligned}
Br(X \rightarrow e^+e^-) &\cong Br(X \rightarrow \nu_e\nu_e) \\
Br(X \rightarrow \nu_e\nu_e) &\cong Br(X \rightarrow \nu_\mu\nu_\mu) \cong Br(X \rightarrow \nu_\tau\nu_\tau) \\
Br(X \rightarrow e^+e^-) &\cong Br(X \rightarrow \mu^+\mu^-) \cong Br(X \rightarrow \tau^+\tau^-) \\
3Br(X \rightarrow e^+e^-) &\cong Br(X \rightarrow \bar{u}u) \cong Br(X \rightarrow \bar{d}d) \\
Br(X \rightarrow \bar{u}u) &\cong Br(X \rightarrow \bar{c}c) \cong Br(X \rightarrow \bar{t}t) \\
Br(X \rightarrow \bar{d}d) &\cong Br(X \rightarrow \bar{s}s) \cong Br(X \rightarrow \bar{b}b).
\end{aligned} \tag{13}$$

The X -boson can also decay into weak bosons. The decay rate into a pair of weak bosons should be similar to the decay rate into muons:

$$\Gamma(X \rightarrow W^+W^-) \cong \Gamma(X \rightarrow ZZ) \simeq \Gamma(X \rightarrow \mu^+\mu^-). \tag{14}$$

For the decays of the X - boson into three and four weak bosons the following relations for the partial widths are expected:

$$\begin{aligned}
\Gamma(X \rightarrow W^+W^-Z) &\cong \Gamma(X \rightarrow ZZZ) \\
\Gamma(X \rightarrow W^+W^-W^+W^-) &\cong \Gamma(X \rightarrow W^+W^-ZZ) \\
\Gamma(X \rightarrow W^+W^-W^+W^-) &\cong \Gamma(X \rightarrow ZZZZ).
\end{aligned} \tag{15}$$

We introduce the parameters a and b :

$$\begin{aligned}
\Gamma(X \rightarrow W^+W^-Z) &= a \cdot \Gamma(X \rightarrow \mu^+\mu^-) \\
\Gamma(X \rightarrow W^+W^-W^+W^-) &= b \cdot \Gamma(X \rightarrow \mu^+\mu^-).
\end{aligned} \tag{16}$$

The parameters "a" and "b" are expected to be smaller than one. As an example we set $a=0.5$, $b=0.3$ and estimate the total width of the X -boson. There are three decay channels for the charged leptons, three channels for the neutrinos and 18 channels for the quark-antiquark pairs (including the color degree of freedom). The decays into weak bosons are added, using the parameters above. Other decays of the X - boson are expected to be small and are neglected. Then we find for the total width:

$$\Gamma(X \rightarrow all) \approx 63 \text{ GeV}. \quad (17)$$

The Z -boson has a width of 2.5 GeV - thus the width of the X -boson is about 25 times larger.

The best way to observe the X - boson in the collisions at the LHC is to find the decays into muon pairs and into electron-positron pairs. Once it has been found, one can search for the decays into quark-antiquark pairs. Two narrow quark jets should be observed with an invariant mass given by the mass of the X -boson.

The QHD mass scale Λ_h is three orders of magnitude larger than the QCD mass scale Λ_c . In strong interaction physics complexities arise at the energy of 1 GeV and above. Analogously there should be complexities due to the QHD dynamics at the energy of 1 TeV and above, and the standard electroweak theory breaks down.

In strong interaction physics there exist excited states of the vector mesons. Analogously we expect excited states of the weak bosons, with masses of the order of 1 TeV and higher. The first excited state of a charged weak boson can decay into a charged weak boson and a Z -boson or a photon. The first excited state of a Z -boson will decay mainly into two weak bosons. Decays of the excited weak bosons into quark pairs or leptons pairs are expected to be suppressed.

The weak bosons couple universally to the leptons and quarks, as the ρ -mesons to the nucleons. Inside the ρ -meson are the same quarks as inside the nucleons, and this leads to the universality of the coupling parameters. Analogously we expect from the universality of the weak coupling parameters that inside a lepton and quark the haplons α and β are also present. A bound state model of the weak bosons requires that the leptons and quarks are also composite systems.

The simplest model of composite leptons and quarks is the one discussed in ref.(4). Besides the fermions α and β four scalar haplons are needed, one scalar for the leptons, denoted by l , and three scalars for the three colors of the quarks, denoted by r , g and b :

$$h(fermion) = \begin{pmatrix} \alpha \\ \beta \end{pmatrix} , \quad (18)$$

$$h(scalar) = (l, r, g, b) . \quad (19)$$

Both the fermions and the scalars transform according to the fundamental representation of the QHD gauge group. Thus bound states of the fermions and the scalars exist - the lowest states would be the observed leptons and quarks. The leptons have the following internal structure:

$$\begin{aligned} \nu &= (\alpha l) \\ e^- &= (\beta l) \end{aligned} \quad (20)$$

The structure of the up and down quarks (with red color) is given by:

$$\begin{aligned} u &= (\alpha r) \\ d &= (\beta r) \end{aligned} \tag{21}$$

In such a model the first generation of leptons and quarks would be described by the ground states of the fermion-scalar bound states, the second and third generation must be dynamical excitations. The electron is the ground state of the charged leptons, the muon and the tau-lepton are excitations. We expect that the muon will decay into an electron and a photon. Likewise the u-quark is the ground state of the up-quarks, the c-quark and the t-quarks are excitations.

Compared to the QHD mass scale Λ_h the masses of the observed leptons and quarks are essentially zero. The number of nearly massless bound states, i.e. the number of generations, could be related to the rank of the QHD gauge group. Three generations might be obtained, if the gauge group is $SU(3)$.

The cross section in proton-proton collisions for exciting the QHD degrees of freedom can be estimated as follows. The size of the proton is about 1 Fermi. The inelastic cross section is about 60 mb. The size of a quark is about 0.001 Fermi. Thus the cross section for exciting the QHD degrees of freedom in quark-quark-collisions is about 60 nb. In the proton there are three quarks and many gluons. We estimate the cross section for exciting the QHD degrees of freedom in high energy proton-proton collisions to about 600 nb.

Of particular interest for the LHC is the scattering of a quark and the corresponding antiquark. If these quarks collide, the scalars inside the quark or antiquark collide and can form a resonance. This resonance, formed e.g. by the collision of red scalar and its antiparticle, can decay into a leptonic scalar and its antiparticle. This scalar will form together with the fermion a lepton, e.g. a muon. Thus the quark and antiquark disappear, and a muon and its antiparticle are produced, with an invariant mass, given by the mass

of the resonance. Likewise an electron and a positron can be produced, or a tau-lepton and its antiparticle. The mass of the first resonance of this type should be at about 1 TeV.

If our model is correct, the first signal of the new substructure of the weak bosons will be observed soon at the Large Hadron Collider at CERN - the discovery of the X -boson.

References

- [1] H. Fritzsch and G. Mandelbaum, Phys. Lett. B102 (1981) 319;
Phys. Lett. B 109 (1982) 224;
X. Calmet and H. Fritzsch, Phys. Lett. B496 (2000), 161.
- [2] R. Barbieri, R. Mohapatra and A. Masiero, Phys. Lett. B 105 (1981) 369.
- [3] H. Fritzsch, R. Kogerler and D. Schildknecht, Phys. Lett. B 114 (1982) 157.
- [4] L. F. Abbott and E. Farhi, Phys. Lett. B 101, 69 (1981).
- [5] T. Kugo, S. Uehara and T. Yanagida, Phys. Lett. B 147, 321 (1984).
- [6] S. Uehara and T. Yanagida, Phys. Lett. B 165, 94 (1985).
- [7] U. Baur and K. H. Schwarzer, Phys. Lett. B 180, 163 (1986).

HERA – FROM AN IDEA TO RESULTS

■ ALBRECHT WAGNER

DESY

Abstract

For many decades, deep inelastic scattering has been a key tool in the quest for the understanding of the innermost structure of matter. HERA (Hadron-Elektron-Ringanlage, or Hadron-Electron Ring Accelerator), located at DESY in Hamburg, was the first storage ring in which leptons collided with protons. Using a collider increased the centre-of-mass energy by a factor of ten over previous fixed-target experiments, thus making HERA the most powerful electron microscope in the world. Data taking at HERA began in 1992 and ended in the summer of 2007. The international collaboration on the construction of the accelerator represented a new way of jointly building large research infrastructure. Two collider experiments, H1 and ZEUS, have provided a detailed and very precise picture of the proton and the forces acting within it. Many searches for new physics were performed at the electron-proton energy frontier. Two fixed target experiments, HERMES and HERA-B which used only the electron and proton beams of HERA, respectively, studied the spin structure of the nucleon and the production of strangeness, charm, and bottom in high-energy proton collisions.

Introduction

Around 1910, E. Rutherford and his co-workers were the first to analyse the inner structure of atoms by scattering alpha-particles off a gold foil. About 60 years later, accelerator-based deep-inelastic scattering using electrons as projectiles led at the Stanford Linear Accelerator to the discovery of partons as hard, point-like constituents of the proton (Breidenbach (1969)). This discovery established lepton-proton scattering as a very powerful technique. In order to reach yet higher resolution, two paths were pursued: Using very high energy muons or neutrinos and using the collider technique, by also accelerating the protons and by colliding them with high energy leptons. The second solution was studied especially in Europe in a number of workshops and reports, leading in May 1980 to a recommendation by the European Committee for Future Accelerators, ECFA. ECFA recommended strongly the construction of an electron/positron-proton collider at DESY and welcomed the possibility of its being used by the European community. This recommendation was unanimously approved by the Plenary ECFA assembly.

In February 1981 the project was positively evaluated by a review panel of the German science ministry, in July of the same year the detailed proposal was published, followed in 1984 by the official ‘go-ahead’ from the German funding agencies, after significant contributions from international partners had been secured (see below).

Building an Accelerator in International Collaboration

The construction of HERA is an impressive example for international collaboration in particle physics. The HERA collider was the first major accelerator project at a national laboratory which was internationally funded. Previously, the construction of accelerators was funded to 100 % by the host countries, while experiments were frequently funded and built by international collaborations. The desire to use HERA was, however, so large, that many international partners declared their willingness to contribute through components and manpower to the construction. In total, more than 45 institutes from 12 countries contributed to the construction (about 22 % of the HERA construction cost of 700 Mio. € was carried by the international partners). This way of building new research infrastructures became later known as the ‘HERA-Model’.

Two elements were essential for this model to work: The personal engagement of individuals and the willingness of the German government to invest in a major facility using this model. A few individuals deserve mentioning. At DESY the driving forces behind the project were V. Soergel (Chairman of the Board of Directors), G.A. Voss (project leader for the electron ring, civil construction and infrastructure), and B. Wiik (for many years one of the leading proponents for electron-proton colliders and project leader for the proton ring). Among the international partners Italy played a special role as the largest contributor (half of the superconducting magnets were provided as in-kind contribution from Italy). The driving force behind Italy's engagement was A. Zichichi (then president of INFN), who had realised that a major engagement in the superconducting magnet construction would provide an essential boost of know-how to the Italian industry in the area of superconducting magnets to the Italian industry (Fig. 1).

The HERA Double Ring Collider

The HERA ring (Voss and Wiik (1994)) has a circumference of 6.3 km. Inside the HERA tunnel, leptons (electrons or positrons) and protons were stored in two independent storage rings. Leptons and protons were pre-accelerated in a chain of accelerators before being injected into the HERA ring, where they were accelerated to their nominal energies (most of the time 820 and 920 GeV for protons and 27.5 GeV for electrons or positrons). The lepton ring was equipped with warm magnets, while the proton ring used superconducting magnets to provide the high magnetic field needed for proton energies close to 1 TeV.

A few milestones on the way to completion were: Civil construction (1984-87), mass production of the superconducting magnets (1988-90), installation of the electron ring and in August 1988 the first stored electron beam, completion of the installation of the proton ring (September 1990), commissioning of the proton ring (April 1991). On 19 October 1991 first collisions of electrons and protons were observed.

During the HERA construction and operation substantial challenges had to be met. A few examples are the design of the superconducting magnets; the collision of different particle species (never done so far); handling a large number of colliding bunches; and the short, 96-ns bunch-repetition time, which was also a major challenge for the experiments.

The HERA Harvest

The luminosity operation and data taking of the collider experiments started in 1992 and ended in June 2007. Until 1997, HERA accelerated protons to 820 GeV and leptons to 27.5 GeV. In 1998, the beam energy for protons was increased to 920 GeV, corresponding to a centre-of-mass energy of 318 GeV and a spatial resolution of 10^{-18} m. After a significant luminosity upgrade program (2000-2001) a fourfold luminosity increase was achieved. During the last few months of operation in 2007, the proton-beam energy was lowered to 460 GeV and 575 GeV in order to measure one particular structure function. HERA operation ended in June 2007 after 15 years of data collection, having delivered its design luminosity. The total integrated collider luminosity delivered by HERA amounted to 320 pb⁻¹ (for electrons), and 460 pb⁻¹ (for positrons).

One special feature of HERA was the fact that the lepton beam became naturally transversely polarized through the emission of synchrotron radiation (Sokholov & Ternov (1964)). The characteristic build-up time of polarization in HERA was approximately 40 min. Spin rotators on both sides of the experiments (Buon & Steffen (1986)) changed the transverse polarization of the beam into a longitudinal one. The polarisation reached 65% when only one experiment used the polarised beam and decreased due to a larger beam-beam interaction to 40% when three experiments used the polarisation.

Experiments at HERA

HERA had four interaction regions used by the experiments H1, ZEUS, HERMES, and HERA-B. Of the four experiments, H1 and ZEUS used the colliding lepton and proton beams, whereas HERMES used only the leptons and HERA-B only the protons.

The H1 and ZEUS detectors were large magnetic spectrometers with nearly hermetic coverage. They were designed following similar physics considerations but with different technical solutions, both for the calorimetric and the tracking measurements. They are described in detail in (Abt (1997) and Holm (1993)).

The main component of the H1 detector was a finely segmented liquid argon calorimeter surrounded by a superconducting coil, together with an instrumented iron structure acting as both a shower tail catcher and a muon detector. Tracks in the forward direction were measured in the forward tracking detector. Fig. 2 shows a schematic view of the H1 detector with the tracks and energy deposition of an electron and a hadronic shower superimposed.

The main component of the ZEUS detector was a uranium–scintillator calorimeter. Charged particles were tracked in the central tracking detector, which operated in a magnetic field provided by a thin superconducting solenoid that was positioned inside the calorimeter. Drift chambers provided additional tracking in the forward and rear directions.

The collider experiments H1 and ZEUS had to cope with a number of considerable challenges: bunch crossings every 96 ns, currents of up to 100 mA in the proton beam, and very asymmetric energies of the colliding particles.

The HERMES experiment was designed to study the spin structure of the nucleon with collisions of longitudinally polarized electrons or positrons on the (polarised) gas jet target. A detailed description of the HERMES experiment can be found in (Ackerstaff (1998)). The HERMES detector was a forward spectrometer with a large number of tracking chambers and several particle-identification detectors. The spectrometer was constructed as two identical halves, mounted above and below the beam pipes.

HERA-B had been designed to measure all charged particles and photons produced in the central rapidity region by collisions of protons from the HERA proton ring with the nuclei of target wires positioned in the halo of the beam. It consisted of a vertex detector, followed by a magnetic spectrometer. These components were supplemented by an electromagnetic calorimeter, a ring-imaging Cherenkov detector, and a muon identifier. More details on the detector and trigger system can be found in (Abt et al. (2006)).

Physics Results from the Collider Experiments

In HERA, a point-like probe (electron or positron) collided with a complex target (proton). The principal processes of interest in these collisions are the neutral-current (NC) and charged-current (CC) interactions of the electron or positron with the proton through the exchange of a neutral or charged virtual boson. These processes are characterized by either the scattered electron/positron or a neutrino in the final state.

The following variables are used to describe the kinematics: the virtuality of the exchanged boson, $-q^2 = Q^2$, where q is the four-momentum of the boson and the so-called Bjorken scaling variable, $x = Q^2/(2p \cdot q)$, where p is the four-momentum of the proton and x the fraction of the proton momentum carried by the struck quark.

The main emphases of the collider experiments were the measure the proton structure with unprecedented precision, the study the strong force in a clean laboratory, the study the electroweak force, the exploration of the physics beyond the Standard Model which could manifest itself for example as some form of *lepton-quark* fusion and become visible through the observation of lepto-quarks.

In the following, only a few highlights among the results are being presented. A comprehensive review of collider physics results from HERA-I can be found in (Klein & Yoshida (2008)). A more recent review can be found in (Diaconu et al. (2010)).

Strong Interaction

A measure of the density of quarks and gluons in the proton is provided by the so-called *structure functions* (F_2 , F_3 , F_L). The precise knowledge of the structure functions of the proton provides important information about the features of the strong interaction (QCD) and is of vital importance for understanding the results from proton-proton collisions as measured at the Tevatron and the Large Hadron Collider LHC. The structure functions depend only on the variables x and Q^2 .

The HERA measurements of the inclusive deep-inelastic scattering (DIS) cross sections provide information on the structure of the proton in the ranges $10^{-6} < x < 0.5$ and $0.04 \text{ GeV}^2 < Q^2 < 10^5 \text{ GeV}^2$. At small Q^2 , F_2 rises moderately toward low x . The rise of F_2 with Q^2 becomes more and more pronounced as Q^2 increases. This rise is an effect of the gluon splitting into a quark-antiquark pair $g \rightarrow \text{quark pair}$. With growing Q^2 , the time resolution of the probing photon improves, leading to an increasing number of interacting partons from the gluons short time fluctuations into quarks. The “steep rise in F_2 ” with decreasing x , due to density increase of soft partons (gluon splitting), is one of the most significant discoveries of HERA (Fig. 3). This rise is also qualitatively predicted by perturbative QCD. The H1 and ZEUS Collaborations achieved a significant reduction of their systematic uncertainties by combining their independent cross-section measurements, leading to a significant part of the reduction in the uncertainties through a cross-calibration of the two detectors and reaching a level of total uncertainty reaches of about 1%. In this way the complementary design of the two experiments paid off through an increased accuracy (Fig. 4) (Aaron et al. (2010)).

The leptons do not only probe the valence quark density, but provide also a measurement of the density of heavy quarks which contribute significantly to the total cross section: charm (20%) and beauty (5%). The cross sections of heavy quark production are described by perturbative QCD and allow testing if heavy quarks result only from gluon splitting or if an intrinsic, non-perturbative gluon density in the proton exists. The measurements indicate that there is no evidence for a non-perturbative gluon component.

The structure of the proton and QCD can be measured not only through the DIS cross-section, but also in more detail through the analysis of the hadronic final states. Extensive tests of jet and particle production have shown an excellent agreement of the data with QCD.

Jets with large transverse energy result when the struck quark radiates energetic gluons. The production rate of these jets is sensitive to the strong coupling constant, α_s . Jet cross sections were measured as functions of Q^2 and *transverse energy*. The dependence of the cross sections on these variables allows measuring α_s at various energies in a single experiment. The observed decrease of α_s with increasing scale demonstrates strikingly the asymptotic freedom of QCD (Schoerner-Sadenius (2011) (Fig. 5).

Electroweak Interaction, Searches and Other Topics

The large centre-of-mass energy of HERA gave access to a measurement of the weak and electromagnetic effects in a region where the NC and CC cross sections, i.e. the electromagnetic and weak forces, are of comparable strength. In Figure 6 the NC and CC *electron- and positron- p* scattering cross sections are shown as a function of Q^2 (Chekanov et al. (2008 & 2009)). At small values of Q^2 , the NC process dominates because only electromagnetic effects contribute. When Q^2 is comparable to the mass squared of the Z^0 and W -bosons, the two cross sections are of similar magnitude. In addition, the CC cross section is much larger in e^-p than in e^+p scattering. In e^-p scattering, the exchanged W^- couples mostly to the u -valence quarks, which are approximately twice as abundant in the proton as the d -valence quarks. A similar but smaller effect can be observed in the NC cross section, where the difference between the e^+p and e^-p cross sections is due to interference

between photon and Z^0 exchange. From this difference one obtains the parity violating structure function xF_3 , which provides information about the valence quark distributions. It is impressive to see that the measured cross sections agree with the predictions of the Standard Model over 6 orders of magnitude and that the electromagnetic and weak forces become of similar strength at high energies, directly showing the unification of forces.

The availability of longitudinally polarised beams in H1 and ZEUS gave access to a measurement of the polarisation dependence of the CC cross section. This cross section depends linearly on the polarisation and will vanish for right-handed electrons or left-handed positrons. The three measurements of the CC cross sections made with un-polarised beams and with negatively and positively polarized beams lie on a straight line when plotted as a function of the beam polarization. In agreement with the Standard Model, no right handed CC events were observed. However, this measurement was less precise than from other methods.

HERA was also sensitive to many kinds of new physics – for example the production of lepto-quarks, R-violating supersymmetry, etc., allowing searches for physics beyond the Standard Model with sensitivities which for many channels were comparable to or higher than at LEP and the Tevatron. In the course of data taking some signals of unexpected physics were observed by both H1 and ZEUS. These were indications for lepto-quarks and an apparent excess of high p_T leptons. However, the signals came and went, and were statistical fluctuations which disappeared with more accumulated data (see for example Ciesielski (2009)).

The ratio of the measurements of the neutral-current cross section for e^+p and e^-p scattering has been used to determine an upper limit on the quark radius. If quarks were not point-like, the predicted Standard Model cross section at largest Q^2 would follow a form factor depending on the effective quark radius. In the measurements no deviation from the Standard Model prediction has been found, from which an upper limit for the quark radius of approximately 0.63×10^{-18} m has been determined, illustrating the power of HERA as an electron microscope (Ciesielski (2009)).

Physics Results from HERMES: What is the Origin of the Proton Spin?

The HERMES experiment was proposed after the unexpected observation by the EMC Collaboration (Ashman (1988)) that only a small fraction of the nucleon's spin could be attributed to the spins of the quarks. The primary scientific goal of HERMES was therefore the detailed investigation of the spin structure of the nucleon. Using the polarised electrons/positrons together with a polarised target, combined with a tagging of the final state quark species (as the flavour content of the final state hadrons is connected to the flavour of the struck quark), HERMES determined with high precision the contribution of different quark types to the spin of the proton to be approximately 1/3, while the rest must be attributed to gluons and orbital angular momenta. In addition, HERMES extracted a rather small value of the average gluon polarization $\Delta g/g = 0.05 \pm 0.15$ in the range $0.1 < x < 0.4$ (Airapetian (2010)). Thus, the measurements by HERMES have confirmed with high precision the contribution of quark spins to the spin of the nucleon. Yet, the full explanation of the nucleon spin still remains unclear.

The physics reach of the experiment extended well beyond the original scientific goal, and HERMES explored many details of hadron structure, hadron production, hadronic interactions, and especially hard exclusive reactions with electromagnetic probes at centre-of-mass energies of approx. 7 GeV. Many of the results published to date are discussed in (Rith (2002) and Burkardt (2010)).

Physics Results from HERA-B

The HERA-B Collaboration proposed to measure CP violation in decays of B mesons. In order to achieve the needed integrated luminosity, a collision rate of protons from HERA with the target nuclei of 40 MHz was required, which in turn required the use of radiation-hard technologies and a multilevel di-lepton trigger and data-acquisition systems. The development of the trackers needed to cope with the intense particle fluxes at HERA proved more difficult than anticipated, and in 2000 it

became apparent that HERA-B could not compete with the e^+e^- experiments. Nonetheless, the radiation issues had been overcome, and the experiment was nearing completion. The collaboration then decided to exploit the detector for a range of production studies with an emphasis on heavy-flavour production. The two principal results were the determination of the total cross section for b quark production (Abt (2007)) and the measurement of charmonium production and its dependency on the atomic number of the target nucleus.

Summary

During fifteen years of very successful operation, the electron/positron collider HERA has reached its luminosity goals and has provided a wealth of results which exceeded the expectations in terms of precision and which significantly deepened our understanding of the strong and electroweak forces, while at the same time exploring uncharted territory beyond the Standard Model. HERA became a unique probe for physics at small x and provided detailed insight into the structure of the proton. Many results are essential for the interpretation of the LHC measurements and for all other experiments in which precise knowledge of the proton structure is important. Many of the HERA results will enter the text books and remain valid for a long time, present a challenge to theorists, particularly in the field of QCD, in order to explain the measurements.

At the same time HERA became a role model for how to build large research infrastructure in a joint national and international effort.

Acknowledgements

The author would like to thank C. Diaconu, T. Haas, K. Rith and M. Medinnis for interesting discussions about the results from HERA. Special thanks go to the Pontifical Academy of Sciences for its generous hospitality in a historic setting and A. Zichichi for initiating this very interesting International Symposium on Subnuclear Physics: Past, Present and Future, which provided an excellent overview of the field.

References

The following references represent only a small sample of the full list of HERA publications. For more references the reader is referred to Diaconu et al. (2010) and the references therein.

- Aaron FD et al. (H1 and ZEUS Collab.) *JHEP*01 109 (2010) and references therein
- Abt I et al. (H1 Collab.) *Nucl. Instrum. Methods A* 386:310 (1997)
- Abt I et al. (HERA-B Collab.) *Phys. Rev. D* 73:052005 (2006)
- Abt I et al. (HERA-B Collab.) *Phys. Lett. B* 650:103 (2007)
- Ackerstaff K et al. (HERMES Collab.) *Nucl. Instrum. Methods A* 417:230 (1998)
- Airapetian A et al. (HERMES Collab.) arXiv:1002.3921 [hep-ex] (2010)
- Ashman J et al. (EMC Collab.) *Phys. Lett. B* 206:364 (1988)
- Breidenbach M et al. *Phys. Rev. Lett.* 23:935 (1969)
- Buon J, Steffen K *Nucl. Instrum. Methods A* 245:248 (1986)
- Burkardt M et al. *Rep. Prog. Phys.* 73:016201 (2010)
- Chekanov S et al. (ZEUS Collab.) *Eur. Phys. J. C* 61:223 (2008) and Chekanov S, et al. (ZEUS Collab.) *Eur. Phys. J. C* 62:625 (2009)
- Ciesielski R (for H1 and ZEUS Collab.) *PoS (EPS-HEP 2009):269 (2009)*

- Diaconu C, Haas T, Medinnis M, Rith K, and Wagner A. *Annu. Rev. Nucl. Part. Sci.* 60:101 (2010)
- Holm U ed. (ZEUS Collab.) Status rep. <http://www-zeus.desy.de/bluebook/bluebook.html> (1993)
- Klein M, Yoshida R. *Prog. Nucl. Part. Phys.* 61:334 (2008)
- Rith K. *Prog. Nucl. Part. Phys.* 49:245 (2002)
- Schoerner-Sadenius, T. arXiv:1111.7290 [hep-ex] (2011)
- Sokholov AA, Ternov M. *Sov. Phys. Dokl.* 8:1203 (1964)
- Voss GA, Wiik BH. *Annu. Rev. Nucl. Part. Sci.* 44:413 (1994)

Pictures _ HERA – from an Idea to Results (A. Wagner)



Figure 1: V. Soergel (left), A. Zichichi and the former Italian Prime Minister G. Andreotti, discussing the Italian engagement in HERA.

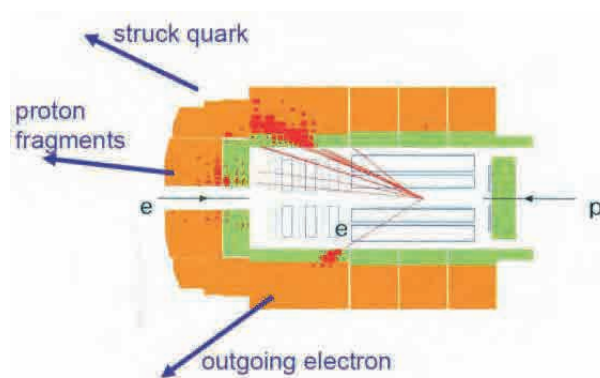


Figure 2: Schematic view of the H1 experiment and, superimposed, a neutral current event. The scattered electron, the particle shower resulting from the struck quark and traces of the proton fragments are clearly visible

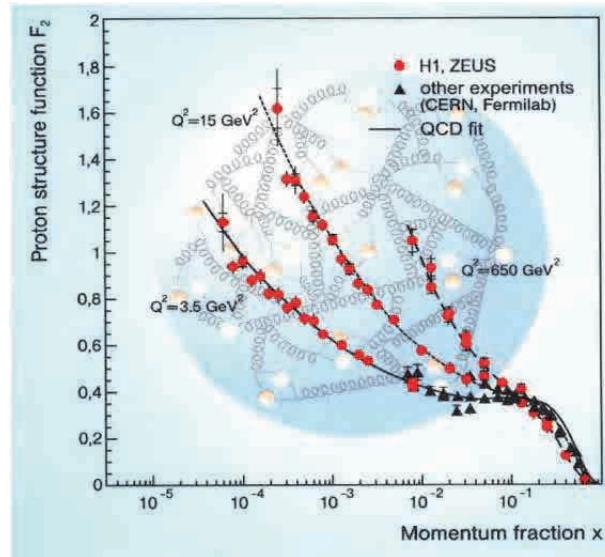


Figure 3: The proton structure function F_2 (a measure of the number of quarks and gluons in the proton) as function of the momentum fraction x , for various values of Q^2 (a measure for the special resolution). The strong rise of the parton density at low x is clearly visible, increasing with Q^2 .

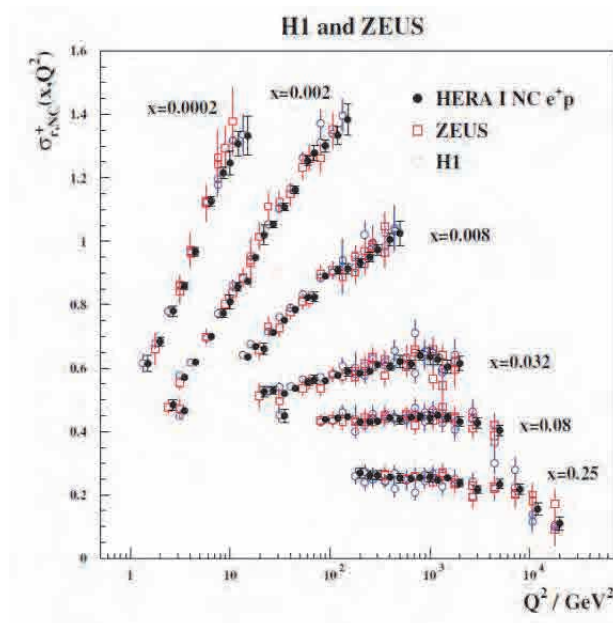


Figure 4: HERA combined NC e^+p reduced cross section as a function of Q^2 for six x -bins compared to the separate H1 and ZEUS data input to the averaging procedure. The individual measurements are displaced horizontally for better visibility.

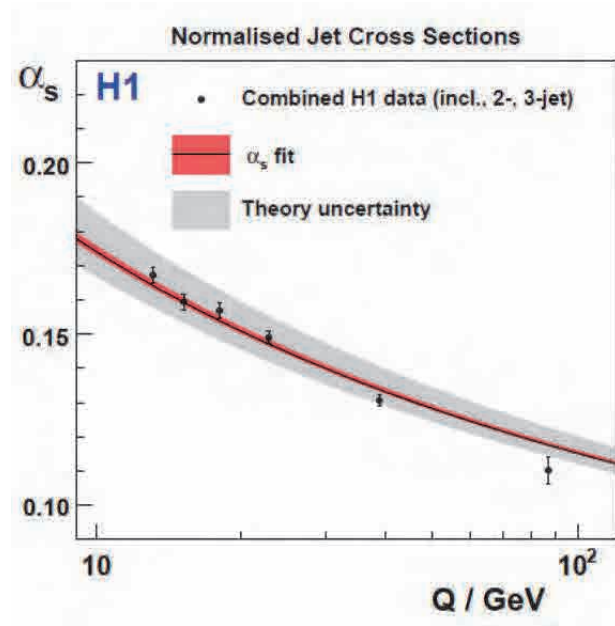


Figure 5: The value of the strong coupling constant α_s as function of energy Q , obtained by H1 by a simultaneous fit of all normalized jet cross sections.

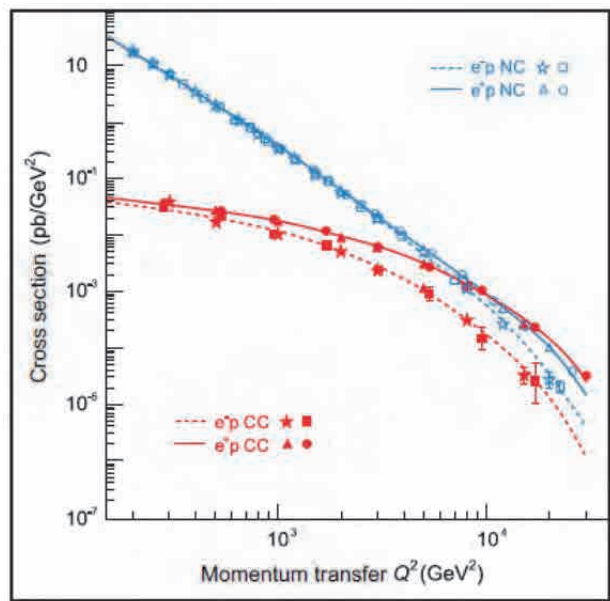


Figure 6: The cross section for deep inelastic electron- and positron-proton scattering neutral current (NC) and charged current (CC) events as function of the momentum transfer Q^2 . The lines indicate the expectations from the Standard Model.

NEW PHYSICS WITHOUT NEW ENERGY SCALE

■ MIKHAIL SHAPOSHNIKOV

Institut de Théorie des Phénomènes Physiques, École Polytechnique Fédérale de
Lausanne, CH-1015 Lausanne, Switzerland

Abstract

I will discuss the so-called “nightmare scenario” for particle physics in which the LHC finds the Higgs boson with the mass $m_{\min} < m_H < m_{\max}$ and nothing else. The boundary values of the Higgs mass are given, with several GeV uncertainties, by $m_{\min} \simeq 130$ GeV and $m_{\max} \simeq 174$ GeV. In this case the Standard Model is a valid effective field theory all the way up to the Planck scale, and no new physics between the Fermi and Planck scales is required for its consistency. I will review a proposal in which the new physics responsible for neutrino masses and oscillations, dark matter and baryon asymmetry of the Universe is associated with three new Majorana leptons with masses *below* the Fermi scale and inflation is driven by the Higgs boson of the SM.

Introduction

The mass M_H of the Higgs boson in the Standard Model (SM) is an important indicator of the presence of new energy scales in particle physics. It is well known that if $M_H < m_{\min}$, the SM ground state is unstable against decay into a deeper vacuum with the Higgs vacuum expectation value below the Planck mass (Krasnikov, 1978; Hung, 1979; Politzer & Wolfram, 1979). If $M_H > m_{\max}$ the Landau pole in the scalar self-coupling appears at energies below the Planck scale $M_P = 2.44 \times 10^{18}$ GeV (Maiani, Parisi, & Petronzio, 1978; Cabibbo, Maiani, Parisi, & Petronzio, 1979; Lindner, 1986). In other words, if the Higgs mass is too large or too small, the Standard Model is inconsistent below M_P and there *must* be a new energy scale between the Fermi $M_F \sim 100$ GeV and the Planck scales. On the contrary, in the mass interval $M_H \in [m_{\min}, m_{\max}]$, no new physics between M_F and M_P is needed, if only the self-consistency of the SM all the way up to M_P is considered. Note that M_H coinciding with m_{\min} is a *prediction* of the asymptotically safe Standard Model, see (Shaposhnikov & Wetterich, 2010). Also, m_{\min} is just few hundred *MeV* higher than the lower mass bound coming from the Higgs inflation (Bezrukov & Shaposhnikov, 2009).

So, the discovery of the Higgs boson at the LHC within this mass interval, and no any other physics beyond the SM, may lead to a pessimistic conclusion that there will be no new physics accessible for future particle experiments (that’s why “nightmare scenario”). The aim of this talk is to argue that this is not the case – new physics responsible for

neutrino masses and oscillations, dark matter and baryon asymmetry of the Universe may be associated with new particles with masses *below* the Fermi scale, which can be searched for with existing accelerators, whereas inflation can be driven by the Higgs boson of the SM.

The paper is organized as follows. First, we will discuss the value of m_{\min} and compare it with the LHC bounds. Then we will overview the observational problems of the SM and describe how the ν MSM (Neutrino Minimal Standard Model) solves them. The last section presents the conclusions.

Higgs mass bounds and the LHC

The numerical values of m_{\min} and m_{\max} can be computed in the SM with a standard technique, involving fixing the coupling constants of the SM at the Fermi scales through the physical parameters, and then running them to high energy scale with the use of renormalisation group equations (Altarelli & Isidori, 1994; Casas, Espinosa, & Quiros, 1995, 1996; Hambye & Riessellmann, 1997; Espinosa, Giudice, & Riotto, 2008).

With a good accuracy of the order of $\mathcal{O}(100)$ MeV in the Higgs mass, the value of m_{\min} can be determined as follows. Take the standard \overline{MS} definition of all coupling constants of the SM, fix all of them at the Fermi scale given the experimentally known parameters such as the mass of top quark, QCD coupling, etc, and consider the running Higgs self-coupling $\lambda(\mu)$ depending on the standard t'Hooft-Veltman parameter μ . Then m_{\min} is found the from solution of two equations:

$$\lambda(\mu_0) = 0, \quad \beta_\lambda(\lambda(\mu_0)) = 0, \quad (1)$$

which also determine the normalisation point μ_0 , coinciding with the position of the second minimum of the effective potential, $\phi \simeq \mu_0$.

The values of m_{\min} below are taken from (Bezrukov & Shaposhnikov, 2009) (see also (Ellis, Espinosa, Giudice, Hoecker, & Riotto, 2009)) ¹,

$$m_{\min} = \left[126.3 + \frac{m_t - 171.2}{2.1} \times 4.1 - \frac{\alpha_s - 0.1176}{0.002} \times 1.5 \right] \text{ GeV}, \quad m_{\max} \simeq 175 \text{ GeV}. \quad (2)$$

With experimental value of the top quark mass $m_t = 172.9 \pm 0.6(\text{stat}) \pm 0.9(\text{syst})$ GeV ((Particle Data Group), 2010 and 2011 partial update for the 2012 edition) (all experimental errors are 1σ) and the value of the strong coupling constant $\alpha_s = 0.1184 \pm 0.0007$ one gets

$$m_{\min} = [129.6 \pm 1.2(\text{stat, t-quark}) \pm 0.5(\text{stat, } \alpha_s) \pm 1.75(\text{syst})] \text{ GeV}. \quad (3)$$

The contributions from higher loops can change this value by 2.2 GeV (if uncertainties are added quadratically) or by 5 GeV (if they are summed up linearly), see (Bezrukov & Shaposhnikov, 2009) for a detailed discussion. In summary, given the present theoretical and experimental uncertainties, the value of m_{\min} can be as small as, say, 123 GeV or as large as, say, 135 GeV (in getting these numbers we took 2.2 GeV as an estimate of the theoretical error and added it linearly to 2σ experimental error).

¹They correspond to the so-called “one-loop-matching-two-loop running” procedure.

The Atlas and CMS evidence for existence of the Higgs boson with the mass $124 - 126$ GeV is thus within the interval of allowed values for m_{\min} . In other words, we are not in position yet to conclude with confidence whether there is a necessity of a new energy scale between the Fermi and the Planck scales. On the theory side, the most urgent theoretical computations would be to go one step above the current “one-loop-matching-two-loop running” computation. It should account for 2-loop strong and electroweak corrections to low energy \overline{MS} -pole matching and 3-loop running up to the Planck scale. This would allow to push down the theoretical error to ~ 0.4 GeV (Bezrukov & Shaposhnikov, 2009). These computations, together with reducing the experimental errors in the Higgs boson and top quark mass, are decisive for setting up the question about the *necessity* of new energy scale besides the two already known - the Fermi and the Planck.

Observational evidence of new physics

Even if the Higgs boson will be found with the mass within interval $M_H \in [m_{\min}, m_{\max}]$, there are no doubts that the SM is not a final theory. Indeed, it fails to explain a number of *observed* phenomena in particle physics, astrophysics and cosmology. These phenomena *beyond the SM* (BSM) are:

- (i) *Neutrino oscillations* (transition between neutrinos of different flavours).
- (ii) *Dark matter* (some 80% of all matter in the Universe consists of unknown particles).
- (iii) *Baryon asymmetry* (excess of matter over anti-matter in the Universe).
- (iv) *Inflation* (a period of the rapid accelerated expansion in the early Universe).
- (v) *Dark energy* (late time accelerated expansion of the Universe).

This list of *well-established observational* drawbacks of the SM is complete at present time. All the other BSM problems are those of theoretical fine-tuning: the “gauge hierarchy problem”, strong CP-problem, etc. There are several anomalies in particle physics experiments, such as discrepancy between experiment and theory prediction of anomalous magnetic moment of muon, LSND anomaly, evidence of the neutrinoless double decay presented by a part of the Heidelberg group, etc. However, none of these anomalies has been confirmed by other experiments.

Once the SM is not a fundamental theory, one has to ask oneself: “At what energies the SM should be superseded by some other, more fundamental theory?” The existence of gravity with the coupling related to the Planck scale $M_{Pl} = G_N^{-1/2} = 1.2 \times 10^{19}$ GeV (G_N is the Newtonian gravitational constant) implies that this certainly happens at energies $\sim M_{Pl}$. However, whether there exists any new intermediate energy scale between the Fermi and Planck scales remains unclear. I will describe below a proposal of solution of above mentioned problems (i-iv), which does not require any new energy scale, which is based on a minimal extension of the SM by three new particles. As for the problem (v), in no-new-scale proposal it may be solved if the theory is scale-invariant on the quantum level and gravity is unimodular (Shaposhnikov & Zenhausern, 2009b, 2009a; Blas, Shaposhnikov, & Zenhausern, 2011; Garcia-Bellido, Rubio, Shaposhnikov, & Zenhausern, 2011). This will not be discussed in this talk due to the lack of time.

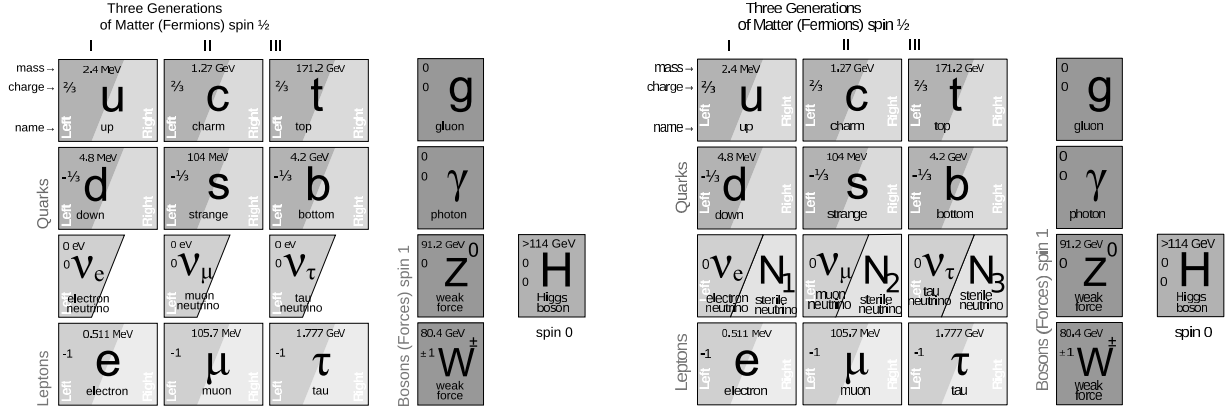


Figure 1. Particle content of the SM and its intension in neutrino sector.

The ν MSM

Let us start from the problem (i) of the SM. The success of relativistic quantum field theory, associated with the fact that the SM agrees with most experiments, strongly indicates that the origin of neutrino masses is the existence of new unseen particles and that the complete theory should be a renormalizable extension of the Standard Model. From the SM quantum numbers of active neutrinos one can identify several possible sources for neutrino masses. If no new fermionic degrees of freedom are introduced, one needs to have a Higgs triplet with weak hypercharge 2. Another option is an introduction of singlet (with respect to the SM gauge group) Majorana fermions N_I (other names for them are sterile neutrinos or heavy neutral leptons). We choose the second possibility. Since N_I are $SU(3) \times SU(2) \times U(1)$ singlets, Majorana mass terms for them are consistent with the symmetries of the SM. The number of singlet fermions cannot be deduced from symmetry principles; the minimal number is 2, to get 2 different mass square differences in active neutrino sector. We take it to be 3 in analogy with the number of generations of quarks and leptons. The new particles complement nicely the fermionic content of the SM, making it left-right symmetric in neutrino sector as well, see Fig. 1.

This extension of the SM is associated with the Lagrangian

$$L = L_{\text{SM}} + \bar{N}_I i \partial_\mu \gamma^\mu N_I - F_{\alpha I} \bar{L}_\alpha N_I \tilde{\phi} - \frac{M_I}{2} \bar{N}_I^c N_I + h.c., \quad (4)$$

where L_{SM} is the Lagrangian of the SM. This Lagrangian is usually used for the explanation of the small values of neutrino masses via the see-saw mechanism (Minkowski, 1977; Yanagida, 1980; Gell-Mann, Ramond, & Slansky, 1979; Mohapatra & Senjanovic, 1980), which *assumes* that the Yukawa coupling constants $F_{\alpha I}$ of the singlet fermions are of the order of the similar couplings of the charged leptons or quarks. We are not going to make such an assumption.

In comparison with the SM, this theory contains 18 new parameters: 3 Majorana masses of new neutral fermions N_I , and 15 new Yukawa couplings in the leptonic sector, corresponding to 3 Dirac neutrino masses, 6 mixing angles and 6 CP-violating phases. The number of parameters is almost doubled in comparison with the SM; none of them can be

determined theoretically within this model, in complete analogy with the SM parameters (which are all taken from experiment).

The new parameters can be divided in two different groups. The first one is the new mass scale - a generic value of the Majorana neutrino mass (denoted by M), and the second one is the typical amplitude of the Yukawa coupling constants Y , which may be defined as $Y^2 = \text{Trace}[F^\dagger F]$. We know very little about the actual values of Y and M . Basically, M can have any value between zero (corresponding to Dirac neutrinos) to 10^{16} GeV, whereas Y can vary from 10^{-13} (Dirac neutrino case) to 1 (the onset of the strong coupling). The admitted region is shown in Fig. 2 (left panel).

The requirement of the absence of new energy scale tells that M should be of the order of the Planck scale, or smaller than the Fermi scale. The first possibility is phenomenological unacceptable - the active neutrino masses following from the see-saw mechanism are too small in comparison with observed values. Therefore we choose the second option, in which the masses of new fermions are similar to those of ordinary quarks or charged leptons. Quite amazingly, in this case these three new Majorana leptons can explain simultaneously neutrino masses and oscillations, Dark Matter, and baryon asymmetry of the Universe, i.e. the problems (i-iii) of section (for reviews see (Shaposhnikov, 2007; Boyarsky, Ruchayskiy, & Shaposhnikov, 2009)).

Dark matter

Though the ν MSM does not have any extra stable particle in comparison with the SM, the lightest singlet fermion, N_1 , may have a life-time τ_{N_1} greatly exceeding the age of the Universe and thus play a role of a dark matter particle (Dodelson & Widrow, 1994; Shi & Fuller, 1999; Dolgov & Hansen, 2002; Abazajian, Fuller, & Patel, 2001). The following considerations determine the range of masses and couplings of the DM sterile neutrino:

- (i) Cosmological production. N_1 are created in the early Universe in reactions $l\bar{l} \rightarrow \nu N_1$, $q\bar{q} \rightarrow \nu N_1$, etc. We should get the correct DM abundance.
- (ii) Structure formation. If N_1 is too light it may have considerable free streaming length and erase fluctuations on small scales. This can be checked by the study of Lyman- α forest spectra of distant quasars and structure of dwarf galaxies.
- (iii) X-rays. N_1 decays radiatively, $N_1 \rightarrow \gamma\nu$, producing a narrow line which can be detected by X-ray telescopes (such as Chandra or XMM-Newton). This line has not been seen yet.

The summary of these constraints (see (Boyarsky, Ruchayskiy, & Iakubovskyi, 2008; Gorbunov, Khmel'nitsky, & Rubakov, 2008; Boyarsky, Ruchayskiy, & Shaposhnikov, 2009; Boyarsky, Lesgourgues, Ruchayskiy, & Viel, 2009) for more details) is presented in Fig. 2 where the mixing angle θ is the ratio of the Dirac and Majorana masses,

$$\theta = \frac{m_D}{M_1} . \quad (5)$$

The interactions of N_1 with particles of the SM is weaker than the weak interactions by a factor θ (in the amplitude). So, they fall into the SuperWIMP category of the DM particle physics candidates. It is important that the DM sterile neutrino production requires the presence of large, $\Delta L/L > 2 \times 10^{-3}$ lepton asymmetry at temperature $T \sim 100$ MeV. It can only be produced in the ν MSM (Shaposhnikov, 2008).

The constraints shown in Fig. 2 (right panel) allow to make a number of predictions for neutrino physics (Asaka, Blanchet, & Shaposhnikov, 2005; Boyarsky, Neronov, Ruchayskiy,

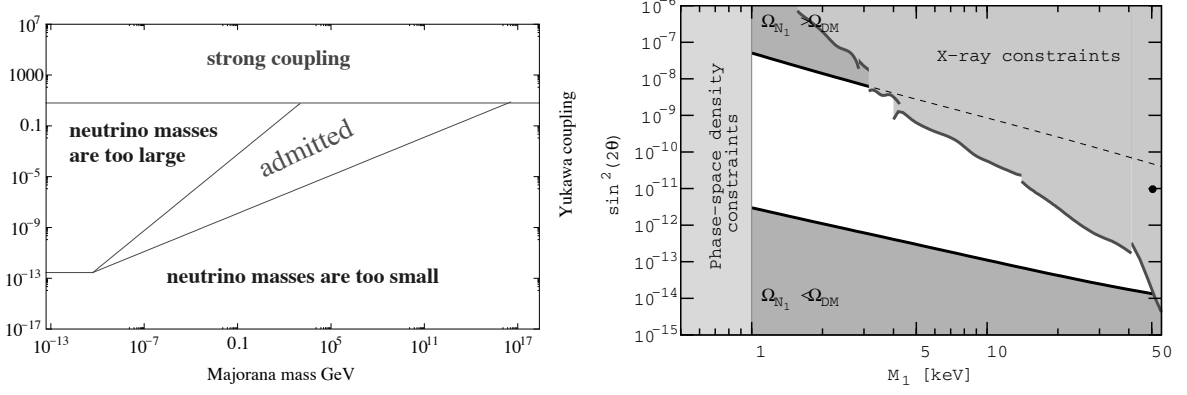


Figure 2. Left panel. The admitted values of the Yukawa couplings as a function of the Majorana fermion mass. **Right panel.** The allowed region of parameters for dark matter sterile neutrinos produced via mixing with active neutrinos (unshaded region). The two thick black lines bounding this region represent production curves for zero lepton asymmetry (upper line) and for the maximal lepton asymmetry attainable in the ν MSM. The red shaded region in the upper right corner represents X-ray constraints. The region below 1 keV is ruled out according to the phase-space density arguments. The Lyman- α constraints are in general stronger but depend essentially on lepton asymmetry. For zero lepton asymmetry the lower bound on M_1 is around 8 keV, while for large asymmetries it is as small as 2 keV.

& Shaposhnikov, 2006). The minimal number of sterile neutrinos, which can explain the dark matter in the Universe and neutrino oscillations, is $\mathcal{N} = 3$. Only one sterile neutrino can be the dark matter. Moreover, it practically decouples and does not contribute to active neutrino masses. Also, the absolute neutrino mass scale is fixed: the mass of the lightest active neutrino is bounded from above by $m_1 \leq 2 \cdot 10^{-3}$ eV. This leads to the following values of the masses of other active neutrinos: $m_2 = [9.05^{+0.2}_{-0.1}] \cdot 10^{-3}$ eV $\simeq \sqrt{\Delta m_{solar}^2}$, $m_3 = [4.8^{+0.6}_{-0.5}] \cdot 10^{-2}$ eV $\simeq \sqrt{\Delta m_{atm}^2}$ (normal hierarchy), or $m_{2,3} = [4.7^{+0.6}_{-0.5}] \cdot 10^{-2}$ eV (inverted hierarchy). Yet another prediction is the effective Majorana mass $m_{\beta\beta}$ for neutrinoless double β decay (Bezrukov, 2005): $1.3 \text{ meV} < m_{\beta\beta} < 3.4 \text{ meV}$ (normal hierarchy) and $13 \text{ meV} < m_{\beta\beta} < 50 \text{ meV}$ (inverted hierarchy). Moreover, knowing $m_{\beta\beta}$ experimentally will allow to fix Majorana CP-violating phases in neutrino mass matrix, provided θ_{13} and Dirac phase δ are known.

The strategy for search of DM sterile neutrino was discussed in a number of papers, for a review see (Boyarsky, Ruchayskiy, & Shaposhnikov, 2009). In short, one should use the X-ray telescopes (such as Chandra and XMM Newton) to look for a narrow γ line against astrophysical background. The astrophysical objects leading to the best signal to background ratio are the dwarf satellite galaxies and the Milky Way.

Baryon asymmetry

In addition to DM sterile neutrino the ν MSM contains a pair of more heavier singlet fermions, N_2 and N_3 . The parameters of these particles can be constrained from the following conditions:

- (i) BAU generation via singlet fermion oscillations (Akhmedov, Rubakov, & Smirnov, 1998;

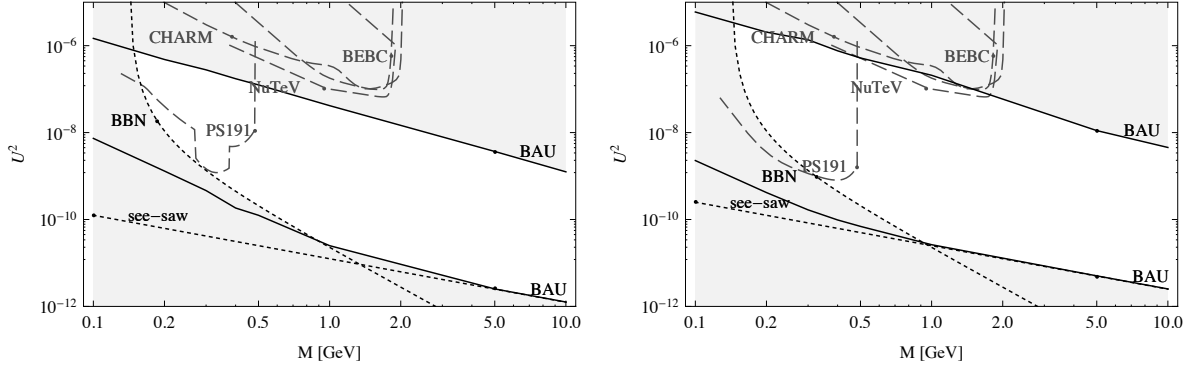


Figure 3. Constraints on U^2 coming from the baryon asymmetry of the Universe (solid lines), from the see-saw formula (dotted line) and from the big bang nucleosynthesis (dotted line). Experimental searched regions are in red - dashed lines. Left panel - normal hierarchy, right panel - inverted hierarchy.

Asaka & Shaposhnikov, 2005) requires out of equilibrium: mixing angle of $N_{2,3}$ to active neutrinos cannot be too large. In addition, due to the smallness of the Yukawa couplings, the asymmetry generation must have a resonant character, leading to the requirement that $N_{2,3}$ must be almost degenerate.

- (ii) Neutrino masses: mixing angle of $N_{2,3}$ to active neutrinos cannot be too small.
- (iii) BBN: decays of $N_{2,3}$ must not spoil Big Bang Nucleosynthesis.
- (iv) Experiment: $N_{2,3}$ have not been seen yet.

The summary of constraints derived in (Canetti & Shaposhnikov, 2010). is presented in Fig. 3 where the mixing angle U^2 is defined in full analogy with (5).

Experimental searches of $N_{2,3}$

It is an experimental challenge to detect Majorana leptons $N_{2,3}$. Indeed, the constraint from baryon asymmetry tells that these particles must interact very weakly, $U^2 \lesssim 5 \times 10^{-7} \left(\frac{\text{GeV}}{M} \right)$.

Several distinct strategies can be used for the experimental search of $N_{2,3}$ (Gorbunov & Shaposhnikov, 2007). The first one is related to their production (U^2 effect). The singlet fermions participate in all the reactions the ordinary neutrinos do with a probability suppressed roughly by a factor U^2 . Since they are massive, the kinematics of, say, two body decays $K^\pm \rightarrow \mu^\pm N$, $K^\pm \rightarrow e^\pm N$ or three-body decays $K_{L,S} \rightarrow \pi^\pm + e^\mp + N_{2,3}$ changes when $N_{2,3}$ is replaced by an ordinary neutrino. Therefore, the study of *kinematics* of rare K , D , and B meson decays can constrain the strength of the coupling of heavy leptons. This strategy has been used in a number of experiments for the search of neutral leptons in the past (Yamazaki et al., n.d.; Daum et al., 2000), where the spectrum of electrons or muons originating in decays π and K mesons has been studied. The precise study of kinematics of rare meson decays is possible in Φ (like KLOE), charm, and B factories, or in experiments with kaons where their initial 4-momentum is well known.

The second strategy is to use the proton beam dump (U^4 effect). As a first step, the proton beam heating the fixed target creates K , D or B mesons, which decay and produce

$N_{2,3}$. The second step is a search for decays of N in a near detector, looking for the processes “nothing” \rightarrow leptons and hadrons (Bernardi et al., 1986, 1988; Vaitaitis et al., 1999; Astier et al., 2001). To this end, quite a number of already existing or planned neutrino facilities (related, e.g., to CERN SPS, MiniBooNE, MINOS or J-PARC), complemented by a near *dedicated* detector, can be used. Finally, these two strategies can be unified, so that the production and the decay occurs inside the same detector (Achard et al., 2001).

For the mass interval $M_N < M_K$, both strategies can be used. According to the estimates, an upgrade of NA62 experiment at CERN would allow the finding or exclusion of singlet fermions with the mass below that of the kaon. If $m_K < M_{2,3} < m_D$, the search for the missing energy signal, potentially possible at beauty, charm, and τ factories, is unlikely to gain the necessary statistics. Thus, the search for decays of neutral fermions is the most effective opportunity. The dedicated experiments on the basis of the SPS proton beam at CERN can touch a very interesting parameter range for $M_N < 1.8$ GeV. The sensitivity is proportional to total delivered protons on target (PoT); for 2.5×10^{20} PoT the constraints shown in Fig. 3 can be improved by one order of magnitude (without accounting for improvement of experimental technique). An upgrade of the LHCb experiment, allowing to use the combination of two strategies, could potentially enter in a cosmologically interesting region for masses and mixing angles of singlet fermions. Going above D -meson but still below B -meson thresholds is very hard if not impossible with the present or planned proton machines or B-factories. To enter into a cosmologically interesting parameter space would require the increase in the present intensity of, say, CERN SPS beam by two orders of magnitude or to produce and study the kinematics of more than 10^{10} B-mesons.

Standard Model Higgs boson as inflaton

Let us turn now to the problem (iv) of section . Our Universe is flat, homogeneous and isotropic, and contains structures that were produced from initial perturbations with almost scale invariant spectrum. An elegant explanation of these facts is associated with cosmological inflation (Starobinsky, 1979, 1980; Mukhanov & Chibisov, 1981; Guth, 1981; Linde, 1982; Albrecht & Steinhardt, 1982). In inflationary cosmology (for a recent review see (Linde, 2008)) the early evolution of the Universe can be roughly divided into three parts. During the first stage, the Universe expands exponentially and becomes nearly flat. At this stage matter perturbations, leading to structure formation, are generated. During the second, reheating stage, the energy stored in the inflaton field is transferred to the fields of the Standard Model. The third stage is the radiation dominated Universe in nearly thermal equilibrium for most of the SM particles. The starting moment of this stage t_r corresponds to a maximal temperature of the Universe T_{\max} , and this is the onset of the standard hot Big Bang.

In (Bezrukov & Shaposhnikov, 2008) it was proposed that the Higgs boson of the SM can play the role of the inflaton and make the Universe flat, homogeneous and isotropic, produce the primordial fluctuations, necessary for structure formation, and heat up the Universe making the Big Bang. In other words, no new special particle is needed for inflation.

To describe the main idea of SM Higgs-inflation, let us consider Lagrangian of the

SM *non-minimally* coupled to gravity,

$$L_{\text{tot}} = L_{\text{SM}} - \frac{M^2}{2}R - \xi H^\dagger H R, \quad (6)$$

where L_{SM} is the SM part, M is some mass parameter, R is the scalar curvature, H is the Higgs field, and ξ is an extra constant, characterizing the strength of coupling of the Higgs field to gravity. The third term in (6) is in fact required by the renormalization properties of the scalar field in a curved space-time background (Birrell & Davies, 1982). If $\xi = 0$, the coupling of the Higgs field to gravity is said to be “minimal”. Then M can be identified with the reduced Planck scale M_P related to the Newton’s constant as $M_P = (8\pi G_N)^{-1/2} = 2.4 \times 10^{18}$ GeV. The parameter ξ cannot be fixed within the theory (6), it will be determined from the requirement of successful inflation.

For large Higgs backgrounds $\xi h^2 \gtrsim M_P^2$ (here $h^2 = 2H^\dagger H$) the masses of all the SM particles *and* the induced Planck mass $[M_P^{\text{eff}}]^2 = M_P^2 + \xi h^2$ are proportional to one and the same parameter, leading to independence of physical effects on the magnitude of h . In other words, the Higgs potential in the large-field region is effectively flat and can result in successful inflation. This is not the case for the theory with the minimal coupling, when $\xi = 0$.

Let us discuss the predictions of the Higgs inflation. The basic inflationary parameters, which can be extracted from the analysis of anisotropies of cosmic microwave background are:

- (i) The amplitude of the temperature fluctuation $\delta T/T$ at the WMAP normalization scale ~ 500 Mpc.
- (ii) The value of spectral index n_s of scalar density perturbations

$$\left\langle \frac{\delta T(x)}{T} \frac{\delta T(y)}{T} \right\rangle \propto \int \frac{d^3 k}{k^3} e^{ik(x-y)} k^{n_s-1}. \quad (7)$$

- (iii) The amplitude of tensor perturbations $r = \frac{\delta \rho_t}{\delta \rho_s}$.

Since in the Higgs inflation we have got one new parameter ξ , we can fix it from (i) and make predictions of n_s and r .

The analysis can be performed in standard way using the slow-roll approximation (for a review see (Lyth & Riotto, 1999)). The condition (i) leads to the relation between the Higgs mass and the parameter ξ ,

$$\xi \simeq 47000\sqrt{\lambda}. \quad (8)$$

Since the Higgs self-coupling constant is of the order of one, ξ must be large enough. As anticipated, the Higgs-inflation predicts the specific values for spectral indexes describing scalar (n_s) and tensor (r) perturbations. They are in accordance with the WMAP-5 observations, see Fig. 4 (left panel).

If tree approximation is used for computations, nothing can be said about the Higgs mass: change λ and ξ^2 in such a way that the ratio λ/ξ^2 stays constant - cosmological predictions do not change (see eq. (8)). This is not true any longer if quantum effects are taken into account. In particular, the Higgs self-coupling constant λ is not a constant as it depends on energy through renormalisation group equations. Since the typical inflationary energy scale is $M_P/\sqrt{\xi}$, for Higgs inflation to work, the SM must be a valid quantum

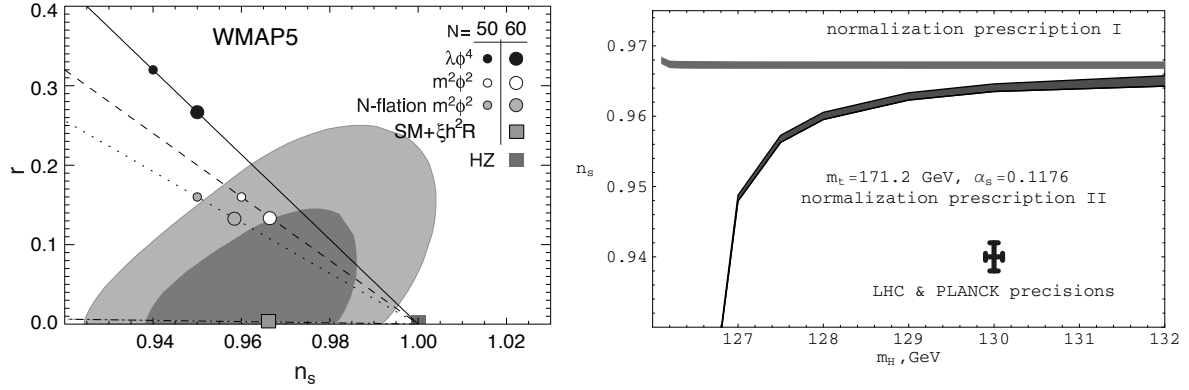


Figure 4. Left. The allowed WMAP region for inflationary parameters (r, n_s) . The green box is the prediction for Higgs inflation. Black and white dots are predictions of usual chaotic inflation with $\lambda\phi^4$ and $m^2\phi^2$ potentials, HZ is the Harrison-Zeldovich spectrum. **Right.** Dependence of the spectral index of scalar perturbations on the Higgs mass in two different renormalisation prescriptions, related to the computations in the Jordan and Einstein frames. The cross indicates the accuracy to be achieved in the measurements of the Higgs mass at the LHC and of the spectral index n_s with the Planck satellite.

field theory up to the inflation scale. The analysis of radiative corrections carried out in (Bezrukov, Magnin, & Shaposhnikov, 2009; Bezrukov & Shaposhnikov, 2009) (see also (De Simone, Hertzberg, & Wilczek, 2009; Barvinsky, Kamenshchik, Kiefer, Starobinsky, & Steinwachs, 2009; A. Barvinsky, Kamenshchik, Kiefer, Starobinsky, & Steinwachs, 2009)) lead to the conclusion that Higgs inflation works for sufficiently large Higgs masses, $M_H > m_{\min} - \Delta M$, where ΔM is typically few hundreds of MeV, slightly depending on the mass of the top quark. The inflationary range of Higgs masses lies within the region allowed the direct LEP and LHC searches for the Higgs boson. The combination of the future Planck measurements of n_s and r with the coming LHC data on the Higgs boson would allow to test the predictions of the Higgs inflation.

Remarkably, the Higgs inflation automatically solves the problem of the graceful exit from inflation. Roughly, for the Higgs fields $h > \frac{M_P}{\sqrt{\xi}}$ the Universe is inflating, for $\frac{M_P}{\sqrt{\xi}} < h < \frac{M_P}{\sqrt{\xi}}$ it is in the matter dominated phase (the role of matter is played by the oscillating Higgs field), and at $h < \frac{M_P}{\sqrt{\xi}}$ it enters into the radiation dominated phase. At $h \simeq \frac{M_P}{\sqrt{\xi}}$ the energy stored in the Higgs field is transferred rapidly to other fields of the SM, leading to the Big Bang. The detailed discussion of these processes can be found in (Bezrukov, Gorbunov, & Shaposhnikov, 2009; Garcia-Bellido, Figueroa, & Rubio, 2009).

Conclusions

The so-called “nightmare scenario” for particle physics (discovery of the Higgs boson in a specific mass interval and nothing else at the LHC) would indicate that there is no need in new scale between the Fermi and Planck energies. Quoting Hermann Nicolai, the absence of an intermediate scale will provide then a possibility to have an unobstructed view of Planck physics, otherwise impossible. The accuracy of theoretical computations

and of the experimental measurements of the top and the Higgs masses does not allow yet to conclude with confidence whether there is a necessity of a new energy scale between the Fermi and the Planck scales. However, the nearly coincidence of m_{\min} and of the experimental number 124 – 126 GeV reported recently at CERN puts a strong argument in favour of the absence of new energy scale. The following argument (quite well known, but not widely appreciated) adds an extra evidence to this conjecture.

There is a remarkable numerical coincidence of the energy scale μ_0 , defined from equations (1) with the Planck mass. This coincidence is highly non-trivial, because these equations are formulated with the use of the SM only, without inclusion of gravity. The fact that $\mu_0 \simeq M_P$ suggests that the electroweak symmetry breaking is likely to be associated with gravity. A generic new physics between the Fermi and Planck scales would remove this coincidence unless some conspiracy is taking place.

The “nightmare scenario” does not mean that no new physics can be found in future experiments: it may be very well that it exists below the electroweak scale. The fact that the universe contains different structures, but is flat, homogeneous and isotropic at large distances, may find its explanation in a non-minimal coupling of the Higgs field to gravity. Yet other problems of the SM, related to the cosmological constant puzzle, to the existence of Dark Energy (late Universe acceleration), and to the problem of stability of the Higgs mass against radiative corrections may be related to quantum scale invariance (Shaposhnikov & Zenhausern, 2009b, 2009a) and not to the existence of any intermediate energy scales between the Fermi and Planck scales. New physics, responsible for neutrino masses and mixings, for dark matter, and for baryon asymmetry of the Universe may hide itself *below* the EW scale. This possibility is offered by the ν MSM - a minimal model, explaining simultaneously a number of well-established observational drawbacks of the SM.

There are many experimental applications of no-new-scale proposal. Higgs inflation is only possible in a specific interval of the Higgs boson masses, discussed above. Moreover, the inflationary spectral indices have definite values in the Higgs inflation, what can be tested by the Planck satellite. A pair of new neutral leptons, creating the baryon asymmetry of the Universe can be searched for in dedicated experiments with the use of existing intensive proton beams at CERN, FNAL and neutrino facilities in Japan (J-PARC). To search for DM sterile neutrino in the Universe one needs an X-ray spectrometer in Space with good energy resolution $\delta E/E \sim 10^{-3} - 10^{-4}$ getting signals from our Galaxy and its dwarf satellites. The laboratory search for this particle would require an extremely challenging detailed analysis of kinematics of β -decays of different isotopes (Bezrukov & Shaposhnikov, 2007).

An indirect evidence in favour of our proposal will be given by LHC, if it discovers the Higgs boson within the mass interval discussed above and nothing else. Moreover, the ν MSM gives a hint on how and where to search for new physics in this case. It tells, in particular, that in order to uncover new phenomena in particle physics one should go towards high intensity proton beams or very high intensity charm or B-factories. At the same time, to pin down the value of m_{\min} , which can provide a non-trivial relationship between the electroweak and Planck scales making a “window” to Planck physics, one would need, besides higher order theoretical computations, a precise determination of the top quark mass. The required accuracy can hardly be reached at the LHC - an electron-positron accelerator (top-Higgs factory) would be needed.

Acknowledgements

I am grateful to the organizers of the International Symposium on Subnuclear Physics: Past, Present and Future, held at the Pontifical Academy of Sciences in the Vatican from 30 Oct. - 2 Nov. 2011 for the invitation to this outstanding meeting. This work was supported in part by the Swiss National Science Foundation.

References

- Abazajian, K., Fuller, G. M., & Patel, M. (2001). Sterile neutrino hot, warm, and cold dark matter. *Phys. Rev.*, *D64*, 023501.
- Achard, P., et al. (2001). Search for heavy neutral and charged leptons in e^+e^- annihilation at LEP. *Phys. Lett.*, *B517*, 75-85.
- Akhmedov, E. K., Rubakov, V. A., & Smirnov, A. Y. (1998). Baryogenesis via neutrino oscillations. *Phys. Rev. Lett.*, *81*, 1359-1362.
- Albrecht, A., & Steinhardt, P. J. (1982). Cosmology for grand unified theories with radiatively induced symmetry breaking. *Phys. Rev. Lett.*, *48*, 1220-1223.
- Altarelli, G., & Isidori, G. (1994). Lower limit on the Higgs mass in the standard model: An Update. *Phys. Lett.*, *B337*, 141-144.
- Asaka, T., Blanchet, S., & Shaposhnikov, M. (2005). The ν MSM, dark matter and neutrino masses. *Phys. Lett.*, *B631*, 151-156.
- Asaka, T., & Shaposhnikov, M. (2005). The ν MSM, dark matter and baryon asymmetry of the universe. *Phys. Lett.*, *B620*, 17-26.
- Astier, P., et al. (2001). Search for heavy neutrinos mixing with tau neutrinos. *Phys. Lett.*, *B506*, 27-38.
- Barvinsky, A., Kamenshchik, A., Kiefer, C., Starobinsky, A., & Steinwachs, C. (2009). Higgs boson, renormalization group, and naturalness in cosmology.
- Barvinsky, A. O., Kamenshchik, A. Y., Kiefer, C., Starobinsky, A. A., & Steinwachs, C. (2009). Asymptotic freedom in inflationary cosmology with a non- minimally coupled Higgs field. *JCAP*, *0912*, 003.
- Bernardi, G., et al. (1986). Search for neutrino decay. *Phys. Lett.*, *B166*, 479.
- Bernardi, G., et al. (1988). Further limits on heavy neutrino couplings. *Phys. Lett.*, *B203*, 332.
- Bezrukov, F. (2005). ν MSM predictions for neutrinoless double beta decay. *Phys. Rev.*, *D72*, 071303.
- Bezrukov, F., Gorbunov, D., & Shaposhnikov, M. (2009). On initial conditions for the Hot Big Bang. *JCAP*, *0906*, 029.
- Bezrukov, F., & Shaposhnikov, M. (2007). Searching for dark matter sterile neutrino in laboratory. *Phys. Rev.*, *D75*, 053005.
- Bezrukov, F., & Shaposhnikov, M. (2009). Standard Model Higgs boson mass from inflation: two loop analysis. *JHEP*, *07*, 089.
- Bezrukov, F. L., Magnin, A., & Shaposhnikov, M. (2009). Standard Model Higgs boson mass from inflation. *Phys. Lett.*, *B675*, 88-92.
- Bezrukov, F. L., & Shaposhnikov, M. (2008). The Standard Model Higgs boson as the inflaton. *Phys. Lett.*, *B659*, 703-706.
- Birrell, N. D., & Davies, P. C. W. (1982). Quantum fields in curved space. (Cambridge, Uk: Univ. Pr. (1982) 340p)
- Blas, D., Shaposhnikov, M., & Zenhausern, D. (2011). Scale-invariant alternatives to general relativity. *Phys.Rev.*, *D84*, 044001.
- Boyarsky, A., Lesgourgues, J., Ruchayskiy, O., & Viel, M. (2009). Realistic sterile neutrino dark matter with keV mass does not contradict cosmological bounds. *Phys. Rev. Lett.*, *102*, 201304.

- Boyarsky, A., Neronov, A., Ruchayskiy, O., & Shaposhnikov, M. (2006). The masses of active neutrinos in the ν MSM from x-ray astronomy. *JETP Lett.*, *83*, 133-135.
- Boyarsky, A., Ruchayskiy, O., & Iakubovskiy, D. (2008). A lower bound on the mass of Dark Matter particles.
- Boyarsky, A., Ruchayskiy, O., & Shaposhnikov, M. (2009). The role of sterile neutrinos in cosmology and astrophysics. *Ann. Rev. Nucl. Part. Sci.*, *59*, 191-214.
- Cabibbo, N., Maiani, L., Parisi, G., & Petronzio, R. (1979). Bounds on the Fermions and Higgs Boson Masses in Grand Unified Theories. *Nucl. Phys.*, *B158*, 295-305.
- Canetti, L., & Shaposhnikov, M. (2010). Baryon Asymmetry of the Universe in the ν MSM. *JCAP*, *1009*, 001.
- Casas, J. A., Espinosa, J. R., & Quiros, M. (1995). Improved Higgs mass stability bound in the standard model and implications for supersymmetry. *Phys. Lett.*, *B342*, 171-179.
- Casas, J. A., Espinosa, J. R., & Quiros, M. (1996). Standard Model stability bounds for new physics within LHC reach. *Phys. Lett.*, *B382*, 374-382.
- Daum, M., et al. (2000). The KARMEN Time Anomaly: Search for a Neutral Particle of Mass 33.9 MeV in Pion Decay. *Phys. Rev. Lett.*, *85*, 1815-1818.
- De Simone, A., Hertzberg, M. P., & Wilczek, F. (2009). Running Inflation in the Standard Model. *Phys. Lett.*, *B678*, 1-8.
- Dodelson, S., & Widrow, L. M. (1994). Sterile-neutrinos as dark matter. *Phys. Rev. Lett.*, *72*, 17-20.
- Dolgov, A. D., & Hansen, S. H. (2002). Massive sterile neutrinos as warm dark matter. *Astropart. Phys.*, *16*, 339-344.
- Ellis, J., Espinosa, J. R., Giudice, G. F., Hoecker, A., & Riotto, A. (2009). The Probable Fate of the Standard Model. *Phys. Lett.*, *B679*, 369-375.
- Espinosa, J. R., Giudice, G. F., & Riotto, A. (2008). Cosmological implications of the Higgs mass measurement. *JCAP*, *0805*, 002.
- Garcia-Bellido, J., Figueroa, D. G., & Rubio, J. (2009). Preheating in the Standard Model with the Higgs-Inflaton coupled to gravity. *Phys. Rev.*, *D79*, 063531.
- Garcia-Bellido, J., Rubio, J., Shaposhnikov, M., & Zenhausern, D. (2011). Higgs-Dilaton Cosmology: From the Early to the Late Universe. *Phys. Rev.*, *D84*, 123504.
- Gell-Mann, M., Ramond, P., & Slansky, R. (1979). *in Supergravity, ed. by D. Freedman et al., North Holland.*
- Gorbunov, D., Khmelnitsky, A., & Rubakov, V. (2008). Constraining sterile neutrino dark matter by phase-space density observations. *JCAP*, *0810*, 041.
- Gorbunov, D., & Shaposhnikov, M. (2007). How to find neutral leptons of the ν MSM? *JHEP*, *10*, 015.
- Guth, A. H. (1981). The inflationary universe: A possible solution to the horizon and flatness problems. *Phys. Rev.*, *D23*, 347-356.
- Hambye, T., & Riesselmann, K. (1997). Matching conditions and higgs mass upper bounds revisited. *Phys. Rev.*, *D55*, 7255-7262.
- Hung, P. Q. (1979). Vacuum Instability and New Constraints on Fermion Masses. *Phys. Rev. Lett.*, *42*, 873.
- Krasnikov, N. V. (1978). Restriction of the Fermion Mass in Gauge Theories of Weak and Electromagnetic Interactions. *Yad. Fiz.*, *28*, 549-551.
- Linde, A. (2008). Inflationary cosmology. *Lect. Notes Phys.*, *738*, 1-54.
- Linde, A. D. (1982). A new inflationary universe scenario: A possible solution of the horizon, flatness, homogeneity, isotropy and primordial monopole problems. *Phys. Lett.*, *B108*, 389-393.
- Lindner, M. (1986). Implications of Triviality for the Standard Model. *Zeit. Phys.*, *C31*, 295.
- Lyth, D. H., & Riotto, A. (1999). Particle physics models of inflation and the cosmological density perturbation. *Phys. Rept.*, *314*, 1-146.

- Maiani, L., Parisi, G., & Petronzio, R. (1978). Bounds on the Number and Masses of Quarks and Leptons. *Nucl. Phys.*, *B136*, 115.
- Minkowski, P. (1977). $\mu \rightarrow e \gamma$ at a rate of one out of 1-billion muon decays? *Phys. Lett.*, *B67*, 421.
- Mohapatra, R. N., & Senjanovic, G. (1980). Neutrino mass and spontaneous parity nonconservation. *Phys. Rev. Lett.*, *44*, 912.
- Mukhanov, V. F., & Chibisov, G. V. (1981). Quantum fluctuation and nonsingular universe. *JETP Lett.*, *33*, 532-535.
- (Particle Data Group), K. Nakamura et al. (2010 and 2011 partial update for the 2012 edition). *J. Phys.*, *G 37*, 075021.
- Politzer, H. D., & Wolfram, S. (1979). Bounds on Particle Masses in the Weinberg-Salam Model. *Phys. Lett.*, *B82*, 242-246.
- Shaposhnikov, M. (2007). Is there a new physics between electroweak and planck scales? *hep-th/0708.3550*.
- Shaposhnikov, M. (2008). The ν MSM, leptonic asymmetries, and properties of singlet fermions. *JHEP*, *08*, 008.
- Shaposhnikov, M., & Wetterich, C. (2010). Asymptotic safety of gravity and the Higgs boson mass. *Phys. Lett.*, *B683*, 196-200.
- Shaposhnikov, M., & Zenhausern, D. (2009a). Quantum scale invariance, cosmological constant and hierarchy problem. *Phys. Lett.*, *B671*, 162-166.
- Shaposhnikov, M., & Zenhausern, D. (2009b). Scale invariance, unimodular gravity and dark energy. *Phys. Lett.*, *B671*, 187-192.
- Shi, X.-D., & Fuller, G. M. (1999). A new dark matter candidate: Non-thermal sterile neutrinos. *Phys. Rev. Lett.*, *82*, 2832-2835.
- Starobinsky, A. A. (1979). Spectrum of relict gravitational radiation and the early state of the universe. *JETP Lett.*, *30*, 682-685.
- Starobinsky, A. A. (1980). A new type of isotropic cosmological models without singularity. *Phys. Lett.*, *B91*, 99-102.
- Vaitaitis, A., et al. (1999). Search for neutral heavy leptons in a high-energy neutrino beam. *Phys. Rev. Lett.*, *83*, 4943-4946.
- Yamazaki, T., et al. (1984). Search for heavy neutrinos in kaon decay.
(IN *Leipzig 1984, Proceedings, High Energy Physics, Vol. 1*, 262.)
- Yanagida, T. (1980). Origin of horizontal symmetry and $SU(5) \times SU(2)$ unification. *Prog.Theor.Phys.*, *63*, 354-356.

RESULTS FROM THE XENON100 DARK MATTER SEARCH EXPERIMENT

■ LAURA BAUDIS

Physics Institute, University of Zürich, CH-8057 Zürich, Switzerland

E-mail: laura.baudis@physik.uzh.ch (for the XENON collaboration)

Abstract.

XENON100 is a liquid xenon time projection chamber built to search for rare collisions of hypothetical, weakly interacting massive particles (WIMPs), which are candidates for the dark matter in our universe, with xenon atoms. Operated in a low-background shield at the Gran Sasso Underground Laboratory in Italy, XENON100 has reached the unprecedented background level of <0.15 events/(day·keV) in the energy range below 100 keV in 30 kg of target mass, before electronic/nuclear recoil discrimination. It found no evidence for WIMPs during a dark matter run lasting for 100.9 live days in 2010, excluding with 90% confidence scalar WIMP-nucleon cross sections above 7×10^{-45} cm² at a WIMP mass of 50 GeV/c². A new run started in March 2011, and more than 200 live days of WIMP-search data were acquired. Results are expected to be released in spring 2012. The construction of the ton-scale XENON1T detector in Hall B of the Gran Sasso Laboratory will start in late 2012.

1. Introduction

The XENON100 [1, 2] experiment was built to search for interactions of massive, cold dark matter particles in liquid xenon. The motivation for this search comes from our current understanding of the universe. Cosmological observations ranging from the measured abundance of primordial elements to the precise mapping of anisotropies in the cosmic microwave background, to the study of the distribution of matter on galactic, extragalactic and the largest observed scales, to observations of high-redshift supernovae, have led to a so-called standard model of cosmology. In this model, our universe is spatially flat and composed of $\sim 4\%$ atoms, $\sim 23\%$ dark matter and $\sim 73\%$ dark energy [3]. Understanding the nature of dark matter poses a significant challenge to astroparticle physics, for its solution may involve new particles with masses and cross sections characteristic of the electroweak scale. Such weakly interactive massive particles (WIMPs), which would have been in thermal equilibrium with quarks and leptons in the hot early universe, and decoupled when they were non-relativistic, represent a generic class of dark matter candidates [4]. Concrete examples are the lightest superpartner in supersymmetry with R-parity conservation [5], and the lightest Kaluza-Klein particle, for instance the first excitation of the hypercharge gauge boson, in theories with universal extra dimensions [6]. Perhaps the most intriguing aspect of the WIMP hypothesis is the fact that it is testable by experiment. WIMPs with masses around the TeV scale are within reach of high-energy colliders and of direct and indirect dark matter detection experiments [7].

2. Direct detection of WIMPs

Dark matter particles might be detected via their elastic collisions with atomic nuclei in earthbound, low-background detectors [8]. The differential rate for elastic scattering can be expressed as [9]:

$$\frac{dR}{dE_R} = N_T \frac{\rho_h}{m_W} \int_{v_{\min}}^{v_{\max}} d\vec{v} f(\vec{v}) v \frac{d\sigma}{dE_R} \quad (1)$$

where N_T is the number of the target nuclei, ρ_h is the local dark matter density in the galactic halo, m_W is the WIMP mass, \vec{v} and $f(\vec{v})$ are the WIMP velocity and velocity distribution function in the Earth frame and $d\sigma/dE_R$ is the WIMP-nucleus differential cross section. The nuclear recoil energy is $E_R = m_r^2 v^2 (1 - \cos \theta) / m_N$, where θ is the scattering angle in the center-of-mass frame, m_N is the nuclear mass and m_r is the reduced mass. The minimum velocity is defined as $v_{\min} = (m_N E_{th} / 2m_r^2)^{1/2}$, where E_{th} is the energy threshold of the detector, and v_{\max} is the escape velocity in the Earth frame. The simplest galactic model assumes a Maxwell-Boltzmann distribution for the WIMP velocity in the galactic rest frame, with a velocity dispersion of $\sigma \approx 270 \text{ km s}^{-1}$ and an escape velocity of $v_{esc} \approx 544 \text{ km s}^{-1}$. For direct detection experiments, the mass density and velocity distribution at a radius around 8 kpc are most relevant. High-resolution, dark-matter-only simulations of Milky Way-like halos find that the dark matter mass distribution at the solar position is smooth, with substructures being far away from the Sun. The local velocity distribution of dark matter particles is likewise found to be smooth, and close to Maxwellian [10]. Recent simulation of hierarchical structure formation including the effect of baryons revealed that a thick dark matter disk forms in galaxies, along with the dark matter halo [11, 12]. The dark disk has a density of $\rho_d/\rho_h = 0.25\text{--}1.5$ where the standard halo density is $\rho_h = 0.3 \text{ GeV cm}^{-3}$ and the kinematics are predicted to follow the Milky Way's stellar thick disk. At the solar neighborhood, this yields a rotation lag of $v_{lag} = 40\text{--}50 \text{ km/s}$ with respect to the local circular velocity, and a dispersion of $\sigma \simeq 40\text{--}60 \text{ km/s}$. These velocities are significantly lower than in the standard halo model and have implications for the expected rates in direct [13] and indirect [14] dark matter detection experiments.

The differential cross section for elastic scattering has two separate components: an effective scalar coupling between the WIMP and the mass of the nucleus and an effective coupling between the spin of the WIMP and the total angular momentum of the nucleus. In general, the coherent part dominates the interaction (depending however on the characteristics and composition of the dark matter particle) for target masses with $A \geq 30$ [5]. The total cross section is the sum of both contributions $\frac{d\sigma}{dE_R} \propto \sigma_{SI}^0 F_{SI}^2(E_R) + \sigma_{SD}^0 F_{SD}^2(E_R)$, where $\sigma_{SI,SD}^0$ are the spin-independent (SI) and spin-dependent (SD) cross sections in the limit of zero momentum transfer and $F_{SI,SD}^2(E_R)$ denote the nuclear form factors, expressed as a function of the recoil energy. These become significant at large WIMP and nucleus masses, leading to a suppression of the differential scattering rate at higher recoil energies.

A dark matter particle with a mass in the GeV–TeV range has a momentum of a few tens to a few hundred MeV and an energy below 100 keV is transferred to a nucleus in a terrestrial detector. Expected event rates range from one to less than 10^{-3} events per kg detector material and year. To observe a WIMP-induced spectrum, a low energy threshold, an ultra-low background noise and a large target mass are essential. In a given detector, the kinetic energy carried by the scattered nucleus is transformed into a measurable signal, such as ionization, scintillation light or phonons. The simultaneous detection of two observables yields a powerful discrimination against background events, which are mostly interactions with electrons, as opposed to WIMPs and neutrons, which scatter off nuclei. Given the size and rate of a potential dark matter signal, an absolute low background is equally relevant. It implies high material selection of detector components and specific active and passive shields against the natural radioactivity of the environment and against cosmic rays and secondary particles

produced in their interactions. Highly granular detectors and/or good timing and position resolution will distinguish localized energy depositions from multiple scatters within the active detector volume and in addition allow to intrinsically measure the neutron background. Finally, the position resolution leads to the identification of events clustered at the detector surfaces or elsewhere, which are quite unlikely to be induced by WIMP interactions.

3. Liquid xenon dark matter detectors

Liquid xenon has ideal properties as a dark matter target and is used to build massive, homogeneous and position-sensitive WIMP detectors. It has a high scintillation ($\lambda = 178\text{ nm}$) and ionization yield because of its low ionization potential of 12.13 eV [15]. Scintillation is produced by the formation and radiative decay of so-called excimers, Xe_2^* , which are bound ion-atom states. Due to the deexcitation of the singlet and triplet states of the excited dimers, the scintillation decay times have a fast ($\sim 4.2\text{ ns}$) and a slow ($\sim 22\text{ ns}$) component. Although the intensity ratio of the singlet to triplet state depends on the deposited energy density, the effect is difficult to exploit in practice, in particular at low recoil energies, because of the similar involved time scales¹. If an electric field around 1 kV/cm is applied, ionization electrons can also be detected, either directly or through the secondary process of proportional scintillation. The interaction of a WIMP results in a low-energy nuclear recoil, which loses its energy generating charge carriers and scintillation photons. Both signals are suppressed when compared to an electronic recoil of the same initial energy, but by different amounts, allowing to use their ratio to distinguish between electronic and nuclear recoils. The ionization and scintillation yields, defined as the number of produced electron-ion pairs and photons per unit of absorbed energy, depend on the drift field and on the energy of the recoil and must be known precisely down to low energies. For electronic recoils, measurements and predictions for the light yield exist down to 5 keV [16], while for nuclear recoils the light and charge yield were measured directly down to 3 keV [17, 18] and 4 keV [19], respectively. Natural xenon does not contain long-lived radioactive isotopes apart from the double beta emitter ^{136}Xe , which has a half-life of $2.1 \times 10^{21}\text{ yr}$ [20]. The trace content of ^{85}Kr , a beta emitter with an endpoint of 687 keV and a half-life of 10.76 years , has to be separated to a level of 10^{-12} mol/mol ($^{nat}\text{Kr/Xe}$) for a ton-scale experiment. It is achieved by distillation [21], which exploits the different boiling points of krypton (120 K) and xenon (165 K) at 1 atmosphere , or by adsorption-based chromatography [15]. These tiny krypton concentrations in xenon gas can be observed with the mass spectrometry technique [22], which in the future might also be used to monitor the krypton levels in a dark matter detector. The high mass of the xenon nucleus is favorable for scalar interactions and the presence of two isotopes with unpaired neutrons (^{129}Xe : spin- $1/2$, 26.4% and ^{131}Xe : spin- $3/2$, 21.2%) ensures sensitivity to axial WIMP-nuclei couplings. The high density (3 g/cm^3) and high atomic number ($Z=54$, $A=131.3$) allow to build self-shielding, compact dark matter detectors.

4. The XENON program

XENON is a phased approach to dark matter direct detection with time projection chambers (TPCs) at the 10 kg , 100 kg and 1000 kg fiducial target mass scale. An interaction within the active volume of the detector will create ionization electrons and prompt scintillation photons, and both signals are detected. The electrons drift in the pure liquid under an external electric field, are accelerated by a stronger field and extracted into the vapour phase above the liquid, where they generate proportional scintillation, or electroluminescence. Two arrays of photomultiplier tubes, one in the liquid and one in the gas, detect the prompt scintillation (S1) and the delayed proportional scintillation signal (S2). The array immersed in the liquid collects

¹ This effect is widely explored in liquid argon detectors, where the decay times of the singlet and triplet states are 7 ns and $1.6\text{ }\mu\text{s}$, respectively.

the majority of the prompt signal, which is totally reflected at the liquid-gas interface. The ratio of the two signals is different for nuclear recoils created by WIMP or neutron interactions, and electronic recoils produced by β and γ -rays, providing the basis for background discrimination. Since electron diffusion in the ultra-pure liquid xenon is small, the proportional scintillation photons carry the $x - y$ information of the interaction site. With the z -information from the drift time measurement, the TPC yields a three-dimensional event localization, enabling to reject the majority of the background via fiducial volume cuts. To test the concept and verify the achievable energy threshold, background rejection and dark matter sensitivity, a detector with a fiducial mass on the order of 10 kg (XENON10) [23, 24], was developed and operated at the Gran Sasso National Laboratory (LNGS). XENON10 excluded previously unexplored parameter space, setting 90% C.L. upper limits of $4.5 \times 10^{-44} \text{ cm}^2$ and $5 \times 10^{-39} \text{ cm}^2$ on the WIMP-nucleon spin-independent and spin-dependent cross-sections, respectively, at a WIMP mass of $30 \text{ GeV}/c^2$ [23, 25]. It found no evidence for light ($\leq 10 \text{ GeV}$) dark matter particles with scattering cross sections above 10^{-42} cm^2 [26]. The next step in this program, the XENON100 detector [2], is taking data at LNGS since 2008. I will briefly describe the experiment and its recent results in the following sections. XENON1T, with a total liquid xenon mass of 2.4 tons, is approved to be built in Hall B at LNGS, in a 9.6 m diameter and 10 m height water Cherenkov shield [27]. Construction will start in late 2012. Finally, DARWIN [28, 29, 30] is a design study for an “ultimate” noble liquid dark matter experiment, aiming to probe cross sections down to 10^{-48} cm^2 and to measure WIMP-induced nuclear recoil spectra with high-statistics, should they be discovered by an existing or near-future experiment. The goal is to determine or at least constrain WIMP properties, such as its mass, scattering cross section and possibly spin [31].

5. The XENON100 detector

XENON100 is a 161 kg double-phase xenon TPC operated at LNGS in an improved XENON10 shield [1, 2]. A total of 242 low-radioactivity, UV-sensitive photomultiplier tubes (PMTs) detect the prompt and proportional light signals induced by particles interacting in the sensitive volume, containing 62 kg of ultra-pure liquid xenon. The remaining 99 kg act as an active veto shield mostly against multiple Compton scatters. While the fiducial mass of XENON100 has been increased by a factor of 10 with respect to XENON10, its background is lower by a factor of 100 [32]. This remarkable reduction was achieved through screening and selection of ultra-low background materials for the detector and shield construction [33], by placing the cryogenic system along with its cryocooler and the high-voltage feedthroughs outside of the shield, by taking advantage of the self-shielding power of xenon and of the active xenon shield, by purifying the xenon for the radioactive ^{85}Kr with a dedicated distillation column operated underground, and by adding $\sim 5 \text{ cm}$ of electrolytic copper and 20 cm of water inside and outside of the existing shield, respectively.

6. Detector design

The design of the XENON100 detector and present performance results are detailed in [2]. The time projection chamber is close to cylindrical in shape, with 30.6 cm in diameter and 30.5 cm in height. Its walls are made of 24 interlocking polytetrafluorethylen (teflon) panels, which work as insulators and are good reflectors for the xenon scintillation light [34]. The electrical fields are created with thin metal meshes that were etched with a hexagonal pattern from stainless steel foils and spot-welded onto low-radioactivity, stainless steel rings. The cathode mesh, which is $75 \mu\text{m}$ thick and has a pitch of 5 mm , is biased with 16 kV , generating a drift field of 0.53 kV/cm across the TPC. About 5 mm below the top PMT array, the TPC is closed with a stack of three meshes: a central anode, $125 \mu\text{m}$ thick and 2.5 mm pitch is placed between two grounded meshes with a spacing of 5 mm . An electron extraction field of $\sim 12 \text{ kV/cm}$ is obtained by applying $+4.5 \text{ kV}$ to the anode. The field is sufficiently high to obtain an electron extraction efficiency

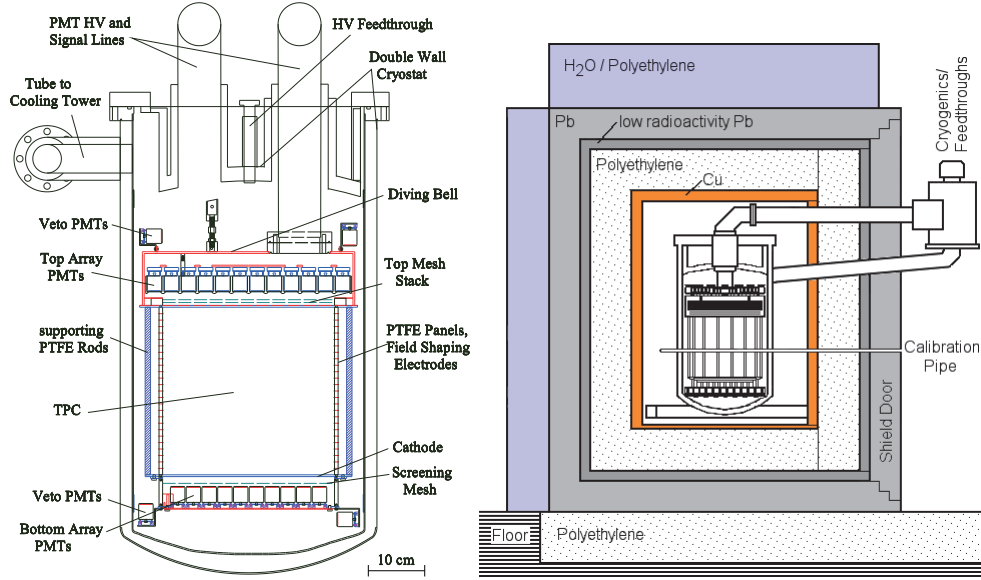


Figure 1. (Left): Drawing of the XENON100 detector. The time projection chamber contains 62 kg of liquid xenon and is surrounded by an active liquid xenon veto of 99 kg. (Right): Schematic view of XENON100 in its passive shield made of copper, polyethylene, lead and water [2].

close to 100% [35]. Averaged over all angles of incidence, the optical transparency of the top mesh stack and of cathode plus an additional screening mesh below the cathode is 47.7% and 83.4%, respectively. A homogeneous electric field across the drift region is created by 40 equidistant field shaping electrodes, connected through 700 M Ω resistors.

Two arrays of Hamamatsu R8520-06-AL 1-inch square PMTs with synthetic quartz windows and selected for low radioactivity in $^{238}\text{U}/^{232}\text{Th}/^{40}\text{K}/^{60}\text{Co}/^{137}\text{Cs}$ [33], detect the VUV scintillation light: 98 tubes are located in the vapour phase above the liquid target, arranged in concentric circles to optimize the spatial resolution of radial event-position reconstruction. While these tubes mostly see the S2 light signal, the energy threshold of the detector is determined by the much smaller S1 signal. Because of the 1.7 refractive index of LXe [36] and the resulting internal reflection at the liquid-gas interface, about 80% of the S1 signal is seen by a second PMT array immersed in the liquid below the cathode. These 80 tubes have higher quantum efficiencies compared to the ones on top, and are arranged in a closed-packed geometry, yielding optimal area coverage for efficient S1 light collection.

The TPC is enclosed in a double-walled, low-radioactivity stainless steel cryostat [33]. The detector is cooled remotely and the connection to the outside of the shield is established via three stainless steel pipes, one to the cooling system, two to the PMT feedthroughs and pumping ports. To bias the cathode and the anode, custom-made hermetic high-voltage feedthroughs, composed of a stainless steel core enclosed by a teflon insulation layer, are used. A liquid xenon layer of 4 cm thickness surrounds the TPC and is observed by 64 PMTs. The active veto is used to reject multiple-scatter events occurring within a time window of ± 20 ns, and is most effective in reducing the background from Compton scatters [32]. It is optically separated from the TPC by the interlocking teflon panels, reducing the event rate in the dark matter target and the rate of accidental coincidences to a negligible level. A drawing of the detector and a schematic view in its low-background shield are shown in figure 1.

7. Detector calibration

To characterize the detector performance and its stability in time, calibration sources are regularly inserted in the XENON100 shield through a copper tube surrounding the cryostat (visible in figure 1, right). The electronic recoil band in $\log_{10}(S2/S1)$ versus energy space defines the region of background events from β - and γ -particles. It is measured using the low-energy Compton tail from ^{60}Co and ^{232}Th calibration sources. The detector response to single-scatter nuclear recoils, the expected signature of a dark matter particle, is measured with an AmBe (α, n)-source. Besides the definition of the nuclear recoil band in $\log_{10}(S2/S1)$ and thus of the included WIMP-search region, the calibration yields gamma lines from inelastic neutron collisions, as well as from the de-excitation of xenon or fluorine (in the teflon) isomers, activated by neutron capture: 40 keV from ^{129}Xe , 80 keV from ^{131}Xe , 110 keV from ^{19}F , 164 keV from ^{131m}Xe ($T_{1/2}=11.8\text{d}$), 197 keV from ^{19}F , and 236 keV from ^{129m}Xe ($T_{1/2}=8.9\text{d}$).

The ionization and scintillation signals are anti-correlated for interactions in LXe [37, 38, 39]. The fluctuations in the sum signal are lower than in each individual signal, leading to an improved energy resolution. In XENON100, each calibration line generates an ellipse in the S2-S1 plane, that can be described with a two-dimensional Gaussian to determine the anti-correlation angle θ , as shown in figure 2, left. This angle has been determined for energies from 40 keV to 1333 keV: It is roughly constant for energies down to $\sim 100\text{ keV}$ and decreases at lower energies. The angles at 40 keV and 80 keV are smaller, since the observed energy deposition is a combination from a nuclear recoil and a subsequent, prompt gamma emission. From the mean positions and angles, the so-called combined energy scale for electronic recoils is defined, and its linearity verified by comparing the resulting spectra to Monte Carlo data. An example is shown in figure 2, right, where the measured electronic recoil spectrum from an AmBe calibration is compared to a Monte Carlo generated spectrum. This energy scale is currently used for background studies [32] alone, the WIMP search data is analyzed with an S1-based nuclear recoil energy scale [40].

The energy resolution as a function of energy, as determined for three different scales, is shown figure 3, left. At 1 MeV, the resolution is 12.2%, 5.9% and 1.9% for the S1, the S2, and the combined energy scale, respectively. Figure 3, right, illustrates the measured change in the ^{137}Cs γ -peak using the three energy scales.

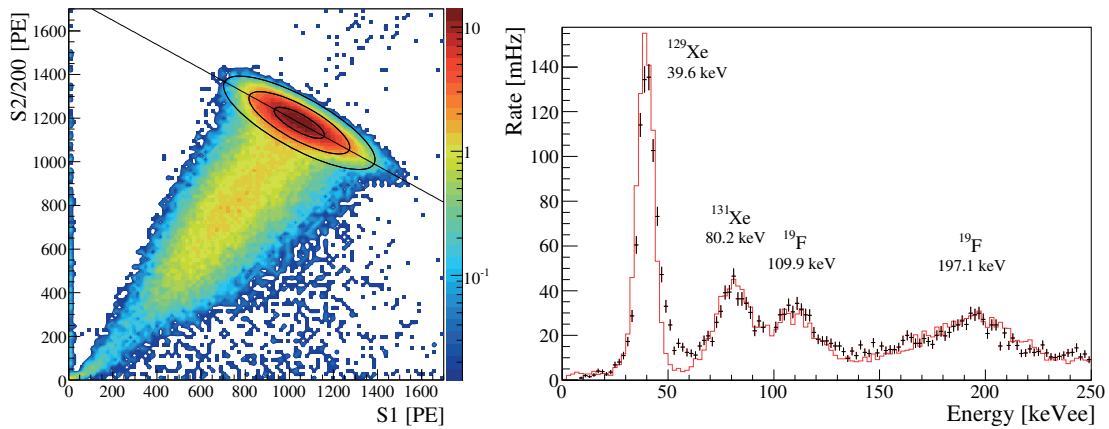


Figure 2. (Left): Data from a ^{137}Cs source in the S2-S1 parameter space. The charge and light signals are anti-correlated, a projection along the anti-correlation ellipse leads to an improved energy resolution. (Right): AmBe calibration spectrum for inelastic neutron scatter in the combined energy scale, along with Monte Carlo generated data (solid) [2].

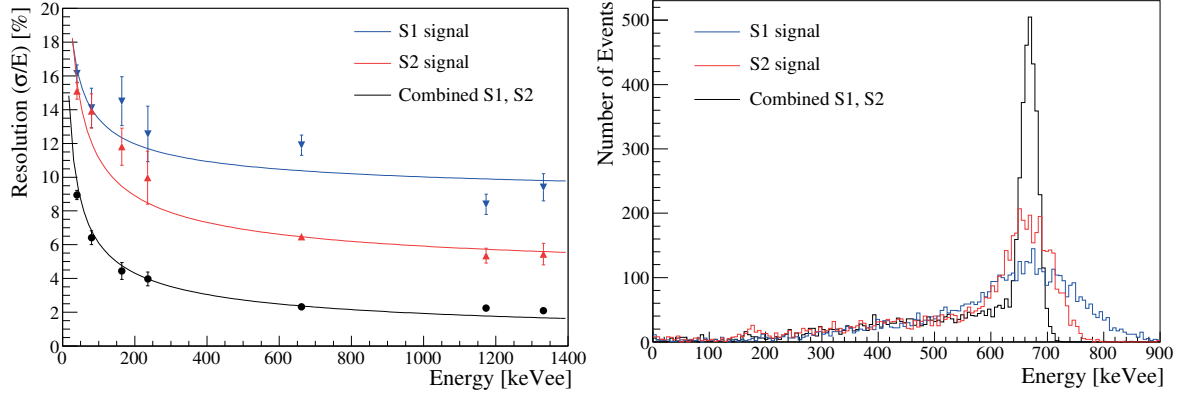


Figure 3. (Left): Measured energy resolution using γ -lines between 40 keV and 1333 keV in S1, S2, and combined energy scale, along with fits to the $1/\sqrt{E}$ dependence. (Right): Spectrum of ^{137}Cs at 662 keV. The $1\text{-}\sigma$ resolution is 12.5%, 6.5% and 2.3% for the S1, S2, and the combined scale, respectively. Shown are single-scatters surviving an active veto cut which effectively reduces the Compton continuum [2].

8. Backgrounds

The background predictions in XENON100 are based on Monte Carlo simulations of both electronic and nuclear recoil components, including the muon-induced neutron background [45] under a rock overburden of ~ 3600 m water equivalent. The simulations use as input a detailed geometry and the measured activities of all detector and shield construction materials [32]. These materials were selected for their low intrinsic radioactivity with a dedicated screening facility consisting of a 2.2 kg high-purity germanium detector in an ultra-low background copper cryostat and a Cu/Pb shield, operated underground at LNGS [41]. While the nuclear recoil background is sub-dominant at the current sensitivity level (see section 9), the electronic recoil part is dominated by interactions of γ -rays from decays of ^{238}U , ^{232}Th , ^{40}K , and ^{60}Co in detector materials, mostly in the PMTs, followed by the cryostat. The self-shielding and the active xenon veto reduce the rate significantly in the central part of the target: by a factor of ~ 20 and ~ 40 for 40 kg and 30 kg of target mass, compared to the total active xenon mass of 62 kg.

During the commissioning run in fall 2009 [42], the level of krypton in the liquid xenon has been measured with a delayed-coincidence technique using a decay channel where ^{85}Kr β -decays to $^{85\text{m}}\text{Rb}$ ($\tau = 1.46 \mu\text{s}$, $E_{\text{max}} = 173.4 \text{ keV}$), which transitions to the ground state emitting a 514 keV photon. The obtained concentration of $^{nat}\text{Kr}/\text{Xe}$ was $143_{-90}^{+130} \times 10^{-12} \text{ mol/mol}$, assuming a $^{85}\text{Kr}/^{nat}\text{Kr}$ abundance of 10^{-11} . The ^{222}Rn level in the liquid has been determined using a β - α time-coincidence analysis, where events corresponding to the decays of ^{214}Bi ($T_{1/2} = 19.7 \text{ min}$, $E_{\text{max}} = 3.27 \text{ MeV}$) and ^{214}Po ($T_{1/2} = 164 \mu\text{s}$, $E_{\alpha} = 7.69 \text{ MeV}$) are tagged. The derived upper limit on the ^{222}Rn activity in liquid xenon was $21 \mu\text{Bq/kg}$.

A comparison of the measured electronic recoil background spectrum and the Monte Carlo prediction for a central target region of 30 kg, before an active veto cut, is shown in figure 5. A zoom into the low-energy region is shown in figure 4, right. Excellent agreement of the background model with the data is observed in the energy region below 700 keV, and for the main γ -peaks. In particular, simulated and measured background spectra agree well in the energy region of interest for the dark matter search. The disagreement at higher energies is caused by non-linear effects in the PMT response, which affects the performance of the position reconstruction algorithms, changing the event rate in the fiducial volumes and leading to a degradation of the position-dependent signal corrections [32].

The total predicted rates of single-scatter electronic recoil events in the energy region of interest are 0.63 (0.24) events/(day·keV) and 0.29 (0.14) events/(day·keV) for 40 kg and 30 kg

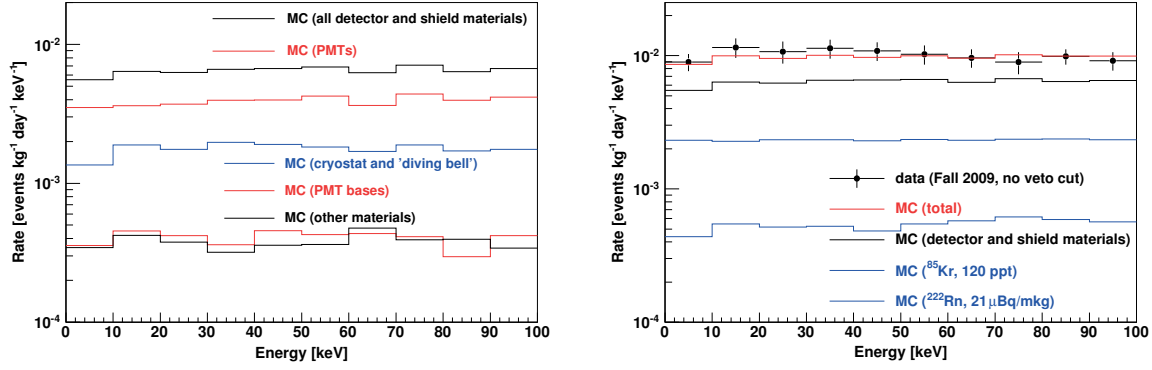


Figure 4. (Left): Predicted background from detector and shield materials (thick solid) in a 30 kg fiducial target mass without veto cut, along with individual contributions from the PMTs (solid), the cryostat (dashed-dotted), the PMT bases (long dashed), and all remaining detector components (short dashed). (Right): Zoom into the low-energy region of figure 5: measured and Monte Carlo generated background spectra in a 30 kg fiducial volume before an active veto cut [32].

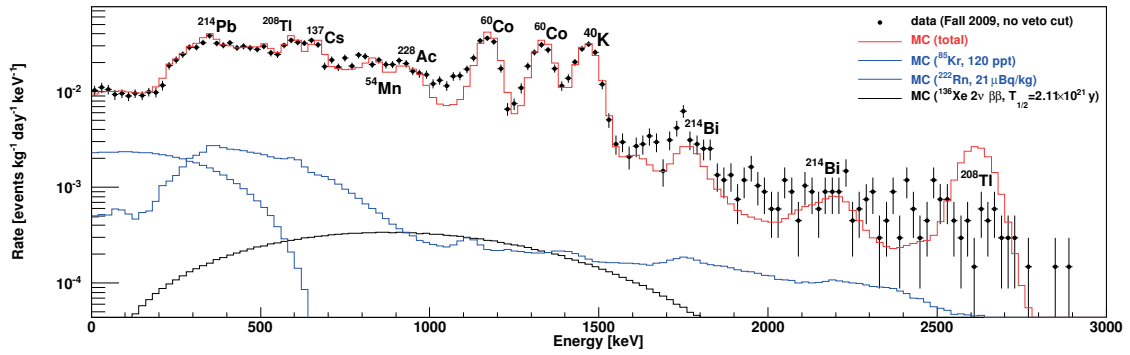


Figure 5. Measured electronic recoil background spectrum during the commissioning run [42], along with the total Monte Carlo generated spectrum (solid) in a 30 kg fiducial xenon volume before an active veto cut. The energy spectra from ^{85}Kr decays (thin solid), ^{222}Rn decays (dotted) and the recently measured 2ν double beta decay spectrum of ^{136}Xe (dashed) are also shown [32].

target mass, without (with) an active veto cut, respectively. In the 30 kg fiducial target mass, ^{85}Kr decays make about 55% of the veto-anticoincident background, while the contribution from ^{222}Rn in the liquid is $<7\%$. An electron recoil discrimination level of 99.5%, based on the $S2/S1$ -ratio, reduces this background by an additional factor of 200.

9. Science run and results

The most recent XENON100 results [40] are derived from 100.9 live days of dark matter data acquired between January and June 2010. A blind analysis, using the so-called *hidden signal box technique*, where events in and around the signal region are kept hidden until the analysis is complete, was conducted. The event selection cuts and the background predictions were fixed before the box was opened, the signal box being defined in a two-parameter space, namely $\log_{10}(S2/S1)$ versus energy, as shown in figure 8, left.

The energy of nuclear recoils is inferred from the S1 signal, as $E_{\text{nr}} = (S1/L_y)(1/\mathcal{L}_{\text{eff}})(S_{\text{ee}}/S_{\text{nr}})$.

The scintillation efficiency \mathcal{L}_{eff} of nuclear recoils relative to that of 122 keV γ -rays at zero drift field, used as a “standard candle”, is parametrized as shown in figure 6. It includes recent measurements down to 3 keV_{nr} nuclear recoil energy [17], in addition to all other direct measurements. \mathcal{L}_{eff} is logarithmically extrapolated below the lowest measured point, motivated by the trend in the data as well as phenomenological studies which simultaneously take into account light and charge signal [43]. The electric field scintillation quenching factors are $S_{\text{ee}} = 0.58$ and $S_{\text{nr}} = 0.95$ for electronic and nuclear recoils [44], and the detector’s light yield at 122 keV and drift field of 530 V/cm is $L_y = (2.20 \pm 0.09)$ photoelectrons/keV.

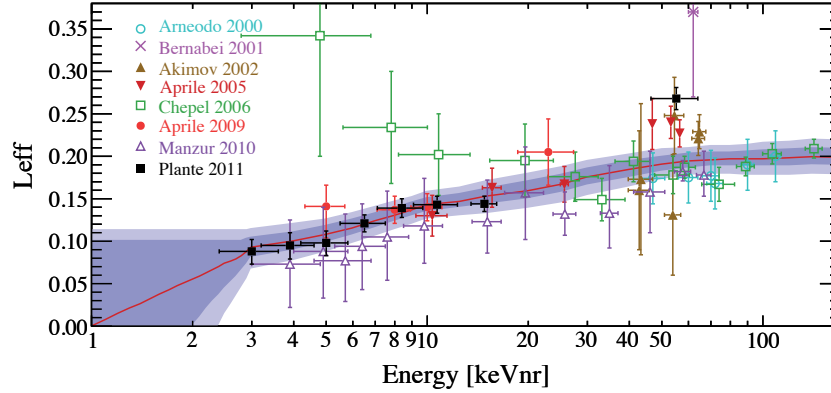


Figure 6. Direct measurements of \mathcal{L}_{eff} versus recoil energy ([17] and references therein). The data can be described by a Gaussian distribution, its mean (solid) and the 1σ and 2σ uncertainty bands are shown. Below 3 keV_{nr} the behaviour is logarithmically extrapolated to zero at 1 keV_{nr} [40].

The dark matter result was based on a profile likelihood analysis as introduced for the commissioning run in [46], taking into account the relevant backgrounds for this new dataset. The profile likelihood analysis does not employ an event selection cut based on the S2/S1-ratio; moreover, the signal and background hypothesis are tested *a priori*, regardless of the observed data. As a cross check, an analysis based on the optimum interval method [47] was performed in parallel. The restricted S2/S1-space defines a WIMP-search region which allows a direct comparison of the observed signal with the number of expected background events.

By comparing the measured background rate in this run with Monte Carlo simulations of the expected electronic recoil background components [32], a $^{nat}\text{Kr}/\text{Xe}$ concentration of $(700 \pm 100) \times 10^{-12}$ mol/mol, was inferred, which is higher than the concentration observed in the commissioning run (see section 8). The additional Kr was introduced by an air leak during maintenance work on the gas recirculation pump, prior to the start of the data-taking period. After the science run, the krypton concentration has been reduced by cryogenic distillation to the previous level, as confirmed with a β - γ -coincidence analysis.

Requirements to the quality and topology of events are designed to retain a high acceptance of the expected WIMP-induced single-scatter nuclear recoils. The majority of selection cuts were designed and fixed before unblinding the signal region, based on expected signal characteristics, on nuclear recoil data from the AmBe calibration, and on low-energy electronic recoils from Compton-scattered gammas. To satisfy the requirement of a WIMP signature to be a localized interaction, one S2 signal above 300 photoelectrons is required, corresponding to about 15 ionization electrons. The corresponding S1 signal must be above 4 photoelectrons and satisfy a two-fold PMT coincidence in a ± 20 ns window, without having a coincident signal in the LXe veto. Any other S1-like signal must be consistent with electronic noise or unrelated to the S2, based on its S2/S1-ratio. In addition, both S1 and S2 PMT hit patterns as well as

the width of the S2 pulse are required to be consistent with a single interaction vertex at the reconstructed position. The cumulative cut acceptance, used by both analyses, is shown in figure 7 and has an error of $\sim 3\%$. It is estimated based on Monte Carlo simulations, AmBe and ^{60}Co calibration data, as well as electronic recoils observed outside the WIMP search region (in so-called sidebands) during the dark matter run. It includes a WIMP mass dependent S2-acceptance which is derived from the expected recoil spectrum and the measured S2 versus S1 distribution.

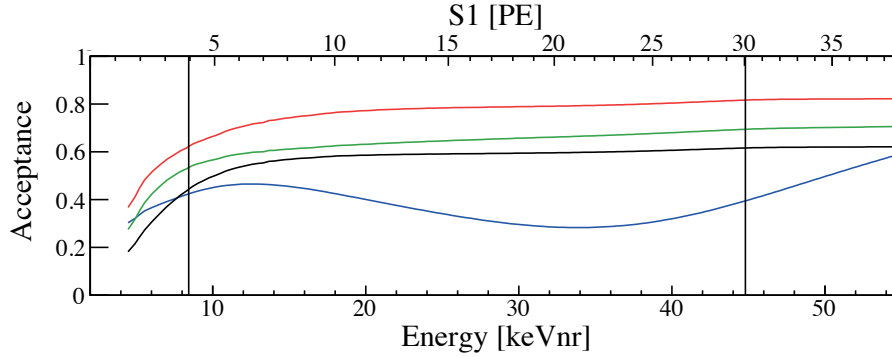


Figure 7. Acceptance of all data quality cuts for $m_W \geq 50 \text{ GeV}/c^2$ (solid), $m_W = 10 \text{ GeV}/c^2$ (dotted), $m_W = 7 \text{ GeV}/c^2$ (dash-dotted). The optimum interval analysis uses an additional event selection cut based on the S2/S1-ratio, its acceptance for nuclear recoils is shown as well (dashed) [40].

The $(8.4 - 44.6) \text{ keV}_{\text{nr}}$ energy window for the WIMP-search, corresponding to $(4 - 30)$ photoelectrons, was chosen such as to yield sufficient discrimination between genuine S1 signals and electronic noise at its lower bound, while including most of the expected WIMP signal at its upper bound. Given the homogeneously distributed ^{85}Kr background, the fiducial volume was optimized on electronic recoil background data to 48 kg. The background rejection level was set to 99.75% and its acceptance to nuclear recoils calculated using single-scatter nuclear recoils from AmBe data (shown in figure 7). The profile likelihood analysis tests the full S2/S1-space without using this additional event selection cut.

The expected background in the WIMP-search region is the sum of Gaussian leakage from electronic recoil background, of non-Gaussian leakage, and of nuclear recoils from neutron interactions. The latter, estimated by Monte Carlo simulations, takes into account neutron spectra and total production rates from (α, n) and spontaneous fission reactions in the detector and shield materials, with input from measured radioactivity concentrations [33]. The muon-induced neutrons are modeled as well, and contribute 70% to the total nuclear recoil background [45]. Considering the measured trigger efficiency and the energy threshold in the active xenon veto, the overall prediction is $(0.31^{+0.22}_{-0.11})$ single-scatter nuclear recoils in the 100.9 days data, before an S2/S1-cut, in the energy region of interest and 48 kg fiducial xenon mass, of which $(0.11^{+0.08}_{-0.04})$ are expected in the signal box.

The normalized electronic recoil band, obtained by subtracting its mean as inferred from calibration data, is well described by a Gaussian distribution in $\log_{10}(\text{S2/S1})$ space. Gaussian leakage, dominated by the ^{85}Kr background, is predicted from the number of background events outside the blinded signal region, taking into account the blinding cut efficiency and the background rejection level. It is (1.14 ± 0.48) events in the WIMP-search region. Non-Gaussian leakage, due to double-scatter gamma events with one interaction in a charge insensitive region and another in the active target, is also estimated from calibration data, yielding $(0.56^{+0.21}_{-0.27})$ events. The total background prediction in the WIMP-search region for 99.75% rejection, 100.9 days of exposure and 48 kg fiducial mass is (1.8 ± 0.6) events. The profile

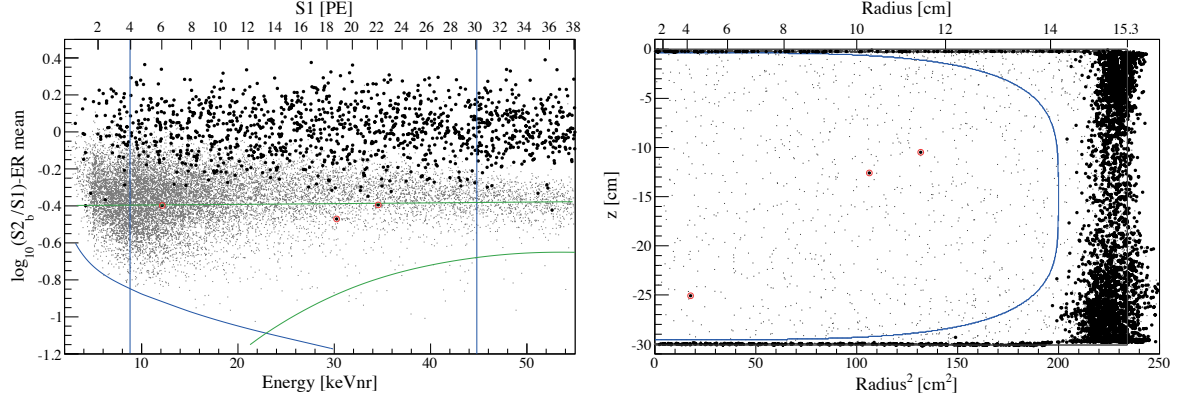


Figure 8. (Left): Event distribution in $\log_{10}(S2/S1)$ as a function of energy. Gray dots show nuclear recoils as measured with an AmBe source, black dots are the electronic recoil background. The WIMP-search region is defined by the energy window $(8.4 - 44.6) \text{ keV}_{\text{nr}}$ and the lower bound of the software threshold $S2 > 300$ photoelectrons (dashed). The optimum interval analysis additionally considers the 99.75% rejection line from above and the 3σ -contour of the nuclear recoil event distribution from below (dotted). Three events fall into the WIMP search region (circles), with (1.8 ± 0.6) events expected from background. (Right): Spatial distribution of all events (gray dots) and events below the 99.75% rejection line (black dots) in the TPC observed in the $(8.4 - 44.6) \text{ keV}_{\text{nr}}$ energy range during 100.9 live days. The 48 kg fiducial volume (dashed) and the TPC dimensions (gray) are indicated as well [40].

likelihood analysis uses identical data sets and background assumptions to obtain prediction for the Gaussian, non-Gaussian and neutron background for every point in the $\log_{10}(S2/S1)$ parameter space.

Three events, at energies of $12.1 \text{ keV}_{\text{nr}}$, $30.2 \text{ keV}_{\text{nr}}$, and $34.6 \text{ keV}_{\text{nr}}$ pass all quality criteria for single-scatter nuclear recoils in the signal region; these are shown in figure 8, left, in the normalized $\log_{10}(S2/S1)$ space. The observation does not depend on moderate variations in the definition of data quality cuts. Their spatial distribution in the TPC is shown in figure 8, right. Given a background expectation of (1.8 ± 0.6) events, no dark matter discovery can be claimed, the chance probability of the corresponding Poisson process to result in 3 or more events being 28%. Consistent with above result, the profile likelihood analysis does not see a significant signal excess, the p -value of the background-only hypothesis being 31%.

The experimental upper limit on the scalar WIMP-nucleon elastic scattering cross-section, shown in figure 9, is calculated for the standard halo model with $v_0 = 220 \text{ km/s}$, an escape velocity of $v_{\text{esc}} = (544^{+64}_{-46}) \text{ km/s}$, and a local density of $\rho_h = 0.3 \text{ GeV/cm}^3$. The S1 energy resolution, governed by Poisson fluctuations of the photoelectron generation in the PMTs, is taken into account. Uncertainties in the energy scale as indicated in figure 6, in the background expectation and in v_{esc} are profiled out and incorporated into the limit. A minimum cross section limit of $7 \times 10^{-45} \text{ cm}^2$, at 90% C.L., is reached at a WIMP mass of $50 \text{ GeV}/c^2$. The impact of \mathcal{L}_{eff} below $3 \text{ keV}_{\text{nr}}$ is negligible at a mass of $10 \text{ GeV}/c^2$. The limit at higher masses is weaker than the expected sensitivity because of the presence of two events around $30 \text{ keV}_{\text{nr}}$. Within the systematic differences of the methods, the result is consistent with the one from the optimum interval analysis, which calculates the limit based only on events in the WIMP-search region. Its acceptance-corrected exposure, weighted with the spectrum of a $100 \text{ GeV}/c^2$ WIMP, is $1471 \text{ kg} \times \text{days}$. XENON100 thus improves upon XENON10 results, and starts to probe the region where supersymmetric dark matter is accessible to the LHC [48].

The XENON100 detector is taking new dark matter data with a reduced krypton background, a lower trigger threshold and an improved performance since March 2011. More than 200 live

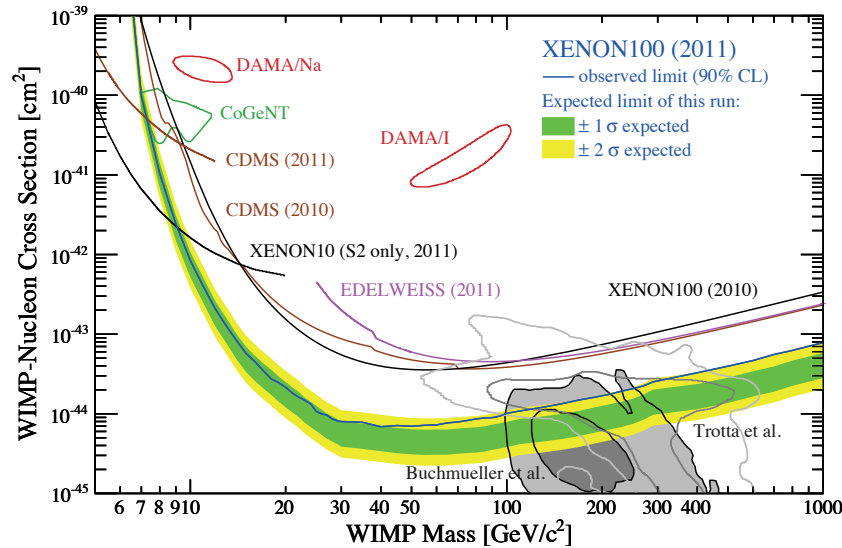


Figure 9. XENON100 limit (at 90% CL, thick line) on the spin-independent WIMP-nucleon cross-section, together with the expected sensitivity of the run (shaded bands). Previous results from XENON100, as well as from other experiments are also shown. Theoretical expectations from supersymmetry are indicated at 68% and 95% CL (shaded gray [48] and gray contour [49]) [40].

days are currently on disk, results are expected to be released in spring 2011. In parallel, the preparations for XENON1T are ongoing, and its construction at LNGS will start in late 2012.

10. Acknowledgements

This work has been supported by the National Science Foundation Grants No. PHY-03-02646 and PHY-04-00596, the Department of Energy under Contract No. DE-FG02-91ER40688, the CAREER Grant No. PHY-0542066, the Swiss National Foundation SNF Grant No. 20-118119, the Volkswagen Foundation, and the FCT Grant No. PTDC/FIS/100474/2008.

- [1] E. Aprile, L. Baudis and f. t. X. Collaboration, PoS IDM **2008** (2008) 018 [arXiv:0902.4253 [astro-ph.IM]].
- [2] E. Aprile *et al.* [XENON100 Collaboration], Astroparticle Physics **35**, 573 (2012) arXiv:1107.2155 [astro-ph.IM].
- [3] E. Komatsu *et al.* [WMAP Collaboration], Astrophys. J. Suppl. **192** (2011) 18 [arXiv:1001.4538 [astro-ph.CO]].
- [4] B. W. Lee and S. W. Weinberg, Phys. Rev. Lett. **39**, 165 (1977).
- [5] G. Jungmann, M. Kamionkowski, K. Griest, Phys. Rep. **267**, 195 (1996).
- [6] D. Hooper and S. Profumo, Phys. Rept. **453**, 29 (2007).
- [7] G. Bertone, D. Hooper and J. Silk, Phys. Rept. **405**, 279 (2005).
- [8] M. W. Goodman and E. Witten, Phys. Rev. D **31**, 3059 (1985).
- [9] J. D. Lewin and P. F. Smith, Astrop. Phys. **6**, 87 (1996).
- [10] M. Vogelsberger, A. Helmi, V. Springel, S. D. M. White, J. Wang, C. S. Frenk, A. Jenkins and A. D. Ludlow *et al.*, arXiv:0812.0362 [astro-ph].
- [11] J. I. Read, G. Lake, O. Agertz, V. P. Debattista, MNRAS **389**, 1041 (2008).
- [12] J. I. Read, L. Mayer, A. M. Brooks, F. Governato, G. Lake, MNRAS, arXiv:0902.0009v1 (2009).
- [13] T. Bruch, J. I. Read, L. Baudis, G. Lake, Astrophysical Journal **696**, 920-923 (2009).
- [14] T. Bruch, A. Peter, J. Read, L. Baudis, G. Lake, Physics Letters B **674**, 250-256 (2009).
- [15] E. Aprile, A.E. Bolotnikov, A. I. Bolozdyna, T. Doke, 'Noble Gas Detectors', Wiley-VHC, Weinheim, 2006.
- [16] M. Szydagis *et al.*, JINST **6** P10002 (2011).
- [17] G. Plante *et al.*, Phys. Rev. C **84**, 045805 (2011).

- [18] E. Aprile, L. Baudis, B. Choi, K. L. Giboni, K. Lim, A. Manalaysay, M. E. Monzani and G. Plante *et al.*, Phys. Rev. C **79** (2009) 045807 [arXiv:0810.0274 [astro-ph]].
- [19] A. Manzur *et al.*, Phys. Rev. C **81**, 025808 (2010).
- [20] N. Ackerman *et al.*, Phys Rev Lett. **107**, 212501 (2011).
- [21] K. Abe *et al.*, (XMASS Collaboration), arXiv:0809.4413v3 [physics.ins-det]
- [22] Attila Dobi, Clayton G Davis, Carter Hall, Thomas Langford, Simon Slutsky and Yung-Ruey Yen, Nucl. Instrum. Meth. A **665**, 1-6 (2011).
- [23] J. Angle *et al.* [XENON Collaboration], Phys. Rev. Lett. **100** (2008) 021303 [arXiv:0706.0039 [astro-ph]].
- [24] E. Aprile *et al.* (XENON10 Collaboration), Astroparticle Physics **34**, 679-698 (2011).
- [25] J. Angle, E. Aprile, F. Arneodo, L. Baudis, A. Bernstein, A. Bolozdynya, L. C. C. Coelho and C. E. Dahl *et al.*, Phys. Rev. Lett. **101** (2008) 091301 [arXiv:0805.2939 [astro-ph]].
- [26] J. Angle *et al.* (XENON10 Collaboration), Phys. Rev. Lett. **107**, 051301 (2011).
- [27] E. Aprile *et al.* (XENON Collaboration), XENON1T at LNGS, *Proposal*, April (2010) and *Technical Design Report*, October (2010).
- [28] L. Baudis (DARWIN Consortium), PoS(IDM2010)122 (2010), arXiv:1012.4764v1 [astro-ph.IM], TAUP 2011 proceedings, arXiv:1201.2402v1 [astro-ph.IM]
- [29] M. Schumann (DARWIN Consortium), arXiv:1111.6251v1 [astro-ph.IM].
- [30] <http://darwin.physik.uzh.ch>
- [31] M. Pato, L. Baudis, G. Bertone, R. R. de Austri, L. E. Strigari and R. Trotta, Phys. Rev. D **83**, 083505 (2011).
- [32] E. Aprile *et al.* (XENON Collaboration), Phys. Rev. D. **83**, 082001 (2011).
- [33] E. Aprile *et al.* (XENON Collaboration), Astropart. Phys. **35**, 43 (2011).
- [34] M. Yamashita *et al.*, Nucl. Instr. Meth. Phys. Res. Sect. A **535** (2004) 692.
- [35] E. Aprile *et al.*, IEEE Trans. Nucl. Sci. **51** (2004) 1986.
- [36] V.N. Solotov *et al.*, Nucl. Instr. Meth. Phys. Res. Sect. A **516** (2004) 462.
- [37] T. Shutt *et al.*, Nucl. Instr. Meth. Phys. Res. Sect. A **579** (2007) 451.
- [38] E. Aprile *et al.*, Nucl. Instr. Meth. Phys. Res. Sect. B **173** (2007) 113.
- [39] E. Aprile *et al.*, Phys. Rev. B **76** (2007) 014115.
- [40] E. Aprile *et al.* (XENON Collaboration), Phys. Rev. Lett. **107**, 131302 (2011)
- [41] L. Baudis, A.D. Ferella, A. Askin, J. Angle, E. Aprile, T. Bruch, A.Kish, M. Laubenstein, A. Manalaysay, T. Marrodan Undagoitia, M. Schumann, JINST **6** P08010, 2011.
- [42] E. Aprile *et al.* (XENON Collaboration), *Phys. Rev. Lett.* **105**, 131302 (2010).
- [43] F. Bezrukov, F. Kahlhoefer, M. Lindner, F. Kahlhoefer and M. Lindner, Astropart. Phys. **35** (2011) 119 [arXiv:1011.3990 [astro-ph.IM]].
- [44] E. Aprile, C. E. Dahl, L. DeViveiros, R. Gaitskell, K. L. Giboni, J. Kwong, P. Majewski and K. Ni *et al.*, Phys. Rev. Lett. **97** (2006) 081302 [astro-ph/0601552].
- [45] Alex Kish, PhD thesis, University of Zurich, 2011
- [46] E. Aprile *et al.* [XENON100 Collaboration], Phys. Rev. D **84** (2011) 052003 [arXiv:1103.0303 [hep-ex]].
- [47] S. Yellin, Phys. Rev. D **66** (2002) 032005 [physics/0203002].
- [48] O. Buchmueller, R. Cavanaugh, D. Colling, A. De Roeck, M. J. Dolan, J. R. Ellis, H. Flacher and S. Heinemeyer *et al.*, Eur. Phys. J. C **71** (2011) 1722 [arXiv:1106.2529 [hep-ph]].
- [49] R. Trotta, F. Feroz, M. P. Hobson, L. Roszkowski and R. Ruiz de Austri, JHEP **0812** (2008) 024 [arXiv:0809.3792 [hep-ph]].

ORIGIN AND STATUS OF THE GRAN SASSO INFN LABORATORY

■ LUCIA VOTANO

*Laboratori Nazionali del Gran Sasso
dell'Istituto Nazionale di Fisica Nucleare, Italy*

Abstract

Underground laboratories are the main infrastructures for astroparticle and neutrino physics aiming at the exploration of the highest energy scales – still inaccessible to accelerators - by searching for extremely rare phenomena. The Gran Sasso INFN Laboratory, conceived by Antonino Zichichi approximately 30 years ago, is the largest underground laboratory in the world devoted to astroparticle physics. The main characteristics of the Gran Sasso Laboratory together with an overview of its broad scientific activities will be reviewed.

A brief history of the Gran Sasso Laboratory

The proposal to build a large underground Laboratory under the Gran Sasso massif was submitted in late 1970s by the then President of INFN Antonino Zichichi. At that time the tunnel under the Gran Sasso mountain of the Rome-Teramo highway was under construction and this was a unique opportunity for the excavation of large halls of an underground laboratory at a reasonable price.

The Italian Parliament approved the ‘Gran Sasso Project’ and its funding in 1982. By 1987 the civil engineering works were completed and in 1989 the first experimental apparatus, MACRO, started its data taking. Looking back on those past thirty years, the advances we have made in understanding the fundamental laws of nature and the evolution of the universe as well as the extraordinary growth of astroparticle physics can be clearly observed.



Fig1. Excavation of the experimental halls of the Gran Sasso Underground Lab.

An ever-increasing number of physicists joined this sector, which represents one of the most fascinating and challenging deal of the physics research. Technologies developed in accelerator apparatuses were first adopted; later on the search for very rare events, the need of increasing sensitivity and efficiency and the complexity of the analysis have called for the development of ever more cutting

edge technologies. At present experimental apparatuses dedicated to astroparticle physics have mass, dimensions and technological complexity comparable to that used in the Large Hadron Collider (LHC). Astroparticle physics would not have been able to make such a massive and rapid progress without the great infrastructures necessary for this kind of study that only the facilities of underground laboratories can offer.

Having planned and built such a large and well equipped laboratory as early as the late 1970s, has brought Italy to have a leading role in this field, since then.

INFN Gran Sasso National Laboratory (LNGS) is the largest underground laboratory in the world for astroparticle physics. It is one of the four INFN National Laboratories and it is an international facility housing twenty experiments. Located between L'Aquila and Teramo, the underground structures are on one side of the highway tunnel (10 km long) which crosses the Gran Sasso massif (A24 Teramo-Rome Highway) and consist of three huge experimental halls (each one 100 m long, 20 m large and 18 m high) linked by service tunnels, for a total volume of $\sim 180.000 \text{ m}^3$ and a surface of $\sim 18.000 \text{ m}^2$.

The 1400 metre-rock thickness above provides a cosmic ray flux reduction by one million times; moreover, due to the very small amount of uranium and thorium of the Dolomite calcareous rock of the mountain, the flux of neutrons in the underground halls is about thousand times less than on the surface.

Outside, next to the highway tollgate of Assergi, an area of more than 23 acres hosts the external laboratories, the Computing Centre, the Directorate and various Offices. Presently LNGS staff consists of about 90 people; besides, more than 950 scientists from 29 different Countries take part in its experimental activities.

Neutrino Physics

The study of the intrinsic properties of neutrino is of prime interest in particle physics and one of the main research topics of the present scientific program of the Laboratory where various neutrino sources, both natural (the Sun, stars and the Earth) and artificial (particle accelerators) are used.

Solar neutrinos

The Borexino experiment at LNGS detects low energy solar neutrinos by means of their elastic

scattering on electrons in a large volume liquid scintillator apparatus. Collecting the scintillation light with a large set of photomultipliers makes real-time detection of all events. The very low intrinsic radioactivity of the scintillator and of the materials surrounding it allows a clean spectral separation between the neutrino signals and the residual background.

While the main goal is the detection of the monochromatic ${}^7\text{Be}$ neutrinos, Borexino is now able to explore the 1-2 MeV region of the solar neutrino spectrum with unprecedented sensitivity and to study other components, such as the CNO, pep and pp. In 2011 Borexino measured the ${}^7\text{Be}$ solar neutrino rate with accuracy better than 5%, rejecting the hypothesis of no oscillation for ${}^7\text{Be}$ solar neutrinos at 4.90 C.L. More recently they have published the first observation of solar neutrinos from the basic pep reaction and the upper limit, the lowest ever published, for the CNO production in a star has been established.

Borexino is a very sensitive detector for geo-neutrinos too. Geo-neutrinos are electron antineutrinos produced in β decays of ${}^{40}\text{K}$ and of several nuclides in the chains of long-lived ${}^{238}\text{U}$ and ${}^{232}\text{Th}$ present in the Earth crust and mantle. They are direct messengers of the abundances and distribution of radioactive elements within our planet.

CNGS project

The CNGS (Cern Neutrino Gran Sasso) project consists of an artificial neutrino beam produced by the protons accelerator SPS of CERN and directed towards Gran Sasso. The main experiment of Gran Sasso National Laboratory devoted to CNGS neutrino detection is OPERA. The goal of the experiment is the detection of neutrino oscillations in direct appearance mode through the study of $\nu_\mu \leftrightarrow \nu_e$ channel; The challenge of the OPERA experiment is, in fact, the seeking of tau neutrinos in the beam CNGS originally constituted by muon neutrinos only, providing the first direct evidence of the so called ‘oscillation’ mechanism of these particles.

The detector consists of 150.000 ‘bricks’ made up of lead layers interleaved with nuclear emulsions, historically called Emulsion Cloud Chamber (ECC) and electronic detectors to localize neutrino interactions within the target. The observation of a first ν_e candidate event in the experiment has been reported in June 2010, followed by a second candidate in 2012 and the third one in March 2013.

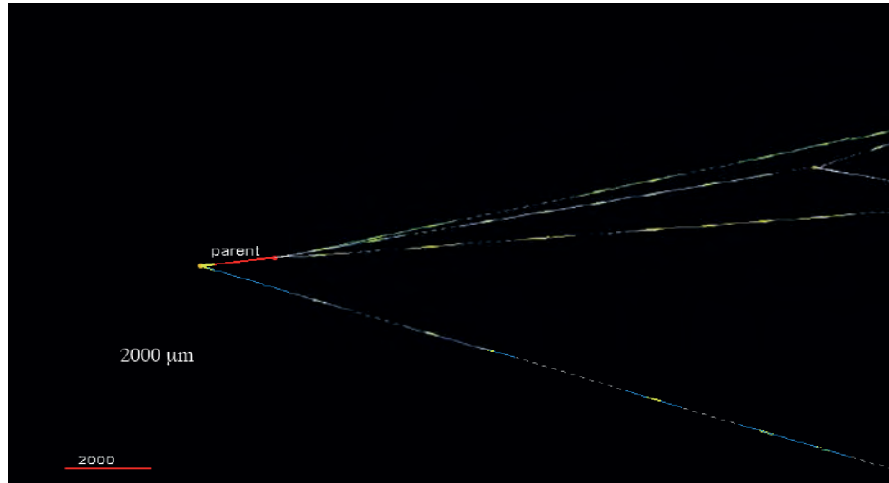


Fig 2. Second observation of tau neutrino in the OPERA experiment – April 2011

Another experiment able to detect CNGS beam is ICARUS, an innovative apparatus consisting of a big mass (about 600 tons) of liquid Argon, at a temperature of -186°C . In particular conditions and by means of proper devices this liquefied gas is able to act as an extraordinary particle detector, allowing a 3D reproduction of any interactions of charged particles inside its volume. The commissioning of ICARUS was successfully completed in 2010 and in May the first CNGS neutrino events were recorded. ICARUS is now continuously collecting data from CNGS.

Such a massive liquid argon experiment running in an underground laboratory is, so far, the most important milestone for the LAr-TPC technology towards the design of a much more massive multikiloton LAr detector.

Neutrino less Double-Beta Decay

Neutrino less double-beta decay is a process by which two neutrons in a nucleus undergo beta decay by exchanging a virtual Majorana neutrino, emitting an electron each. This would violate lepton number conservation ($\Delta L = 2$) and would necessarily require neutrinos to be Majorana particles; therefore this represents a unique tool to test this hypothesis and nowadays, thanks to the discovery of neutrino oscillations, this makes it the object of a renewed interest. The LNGS program exploits complementary approaches concerning isotopes and technique.

GERDA experiment

GERDA (The GERmanium Detector Array) is designed to search for $2\beta 0\nu$ -decay of ^{76}Ge using an array of high-purity germanium detectors, enriched ($\sim 85\%$) in ^{76}Ge , directly immersed in LAr, which acts both as shield and as cooling medium. The cryostat is located in a stainless steel water tank providing an additional shield against external background. GERDA is presently operating eight enriched coaxial detectors (approximately 15 kg of ^{76}Ge). Moreover five new enriched BEGe detectors have been tested and deployed in GERDA at the beginning of July 2012. The background reached is approximately 17×10^{-3} cts/(keV kg y), which is about a factor of 10 lower than for previous experiment HdM and close to the design goal of 10×10^{-3} cts/(keV kg y). About 30 new custom-made enriched BEGe detectors will be deployed in the next phase (additional 20 kg of ^{76}Ge).

CUORE experiment

The CUORE experiment (Cryogenic Underground Detector for Rare Events) aims at the detection of $2\beta 0\nu$ -decay through TeO_2 crystals acting as bolometer detectors: the energy from particle interactions is converted into heat and measured via the resulting rise in temperature. Recently the Laboratory has received additional 120 lead bricks (4 tons) from an ancient Roman ship that sunk off the coast of Sardinia 2.000 years ago. CUORE is in the construction phase at LNGS and is expected to start operation in 2015. The first tower CUORE-0 has been recently commissioned.

Dark Matter search at Gran Sasso

There are compelling evidence from astrophysical and astronomical observations that about one-quarter of the energy density in the universe is composed of non-baryonic and non-relativistic (cold) massive component larger than the one observable through telescopes, due to a not-yet-identified particle. It is called Dark Matter because it neither emits nor absorbs radiation and thus it is invisible to our eyes and instruments. It is supposed to be five times more abundant than ordinary matter, which only constitutes 5% of our Universe.

One of the most well known hypotheses is that these massive particles constitute a widespread halo permeating our galaxy as well as others. There are different techniques that could be able to discover Dark Matter. One of the most common candidate for CDM are Weakly Interactive Massive

Particles (WIMPs) predicted by super symmetric theories (SUSY), searched for at LHC looking for their appearance in collisions; while space-experiments are looking for the detection of CDM by looking for WIMP annihilation signatures from the centre of the Sun or from the centre of the galaxy, the direct detection of DM candidates is only possible in underground laboratories.

LNGS houses experiments devoted to search for dark matter candidates through their direct detection. These experiments put Gran Sasso Laboratory at the forefront of this kind of study.

DAMA/LIBRA experiment

The DAMA/LIBRA experiment is mainly based on the development and use of low background scintillators and the main aim is the direct detection of DM particles in the galactic halo by investigating the model independent annual modulation signature.

The experiment has been operational since 2003 with 250 kg of extremely radio-pure NaI (TI) crystals. The most recent published results confirmed the annual modulation of the very low energy signals induced in the detector, already observed in the previous lower mass experiment DAMA. Such modulation is identical to the one that the relative motion of the Earth through the huge amount of dark matter halo of our galaxy is supposed to cause. The interesting result has produced a lively debate inside the scientific community as well as the production of theoretical models able to conciliate such results with the absence of positive signals by other experiments.

XENON100 experiment

After the successful results of the 10 kg scale detector XENON10, a second-generation experiment exploiting the two-phase time projection chamber (TPC) technique based on liquid xenon (LXe) is now operating at LNGS. The two-phase detector XENON100 experiment contains 170 kg of xenon, 65 kg of which constitute the active part while the remaining acts as a shield. A key feature of the detector is its ability to localize events with millimetre resolution in 3 dimensions, which further allows selecting only the innermost 48 kg as ultra-low background.

After the result published in 2011 from 100.9 live days of data, the present improved running

conditions of XENON100 allowed to further push the sensitivity of XENON100 that smoothly continues data taking. Recently the XENON collaboration has published the analysis of 225 more days of data accumulated in 2011 and 2012. They see no evidence for the existence of WIMPs: the two candidate events being observed are statistically consistent with one event being expected from background radiation. Compared to their previous 2011 result, the world-leading sensitivity has again been improved by a factor ~ 5 .

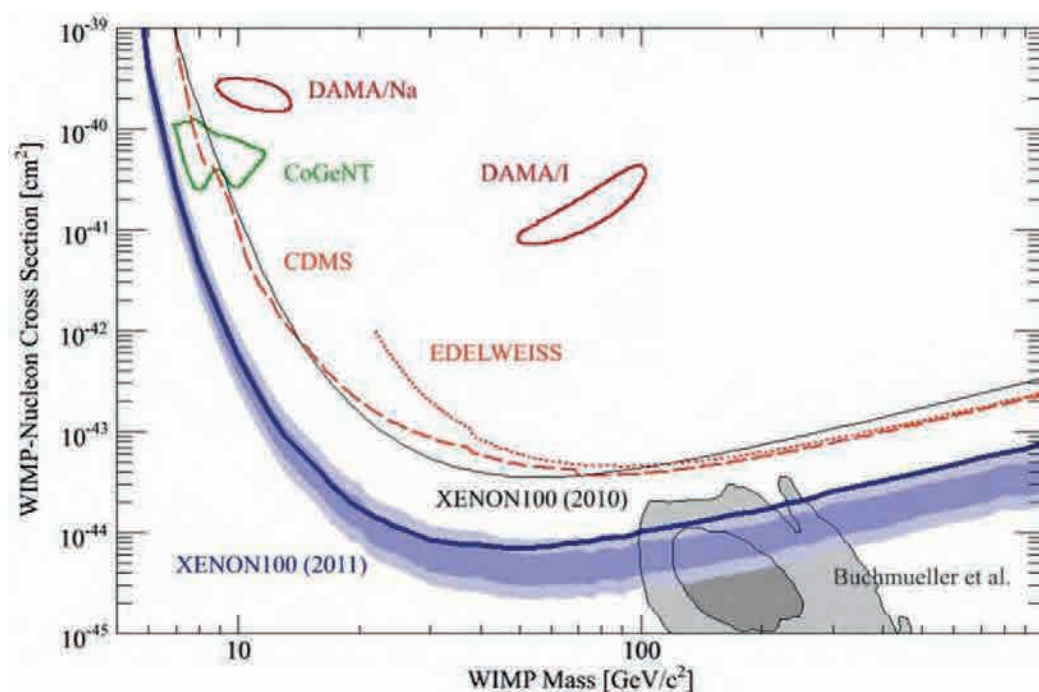


Fig 3. 2011 results: XENON100 Dark Matter Limit (90% CL)

In order to reach a lower sensitivity of about $5 \times 10^{-47} \text{ cm}^2$ and/or to confirm a possible detection in XENON100, the collaboration will continue the Xenon program at LNGS with the XENON 1T detector having a total mass of 2.4 tons of LXe

XENON1T will be installed in the Hall B of the underground Laboratory and the construction should start in summer 2013.

CRESST experiment

The CRESST (Cryogenic Rare Event Search with Superconducting Thermometers) experiment is based on the bolometer technique with $CaWO_4$ crystals at a temperature of few mK as well as on the simultaneous detection of scintillation light and the heat resulting by the interaction of a particle with the crystals. One advantage of the cryogenic detectors developed for CRESST consists on the fact that they can measure the deposited energy calorimetrically, independently on the type of interaction. Combining the calorimetric measurement of the deposited energy with a measurement of scintillation light, a potentially high discrimination of the nuclear recoils from radioactive background can be obtained and the type of recoiling nucleus can be determined in a multi atomic target.

In 2011 CRESST has completed a long run and has submitted a paper with the analysis of data with a total exposure of 730 kg days. An excess of events has been found in the acceptance region where a WIMP signal would be expected. A new run with several detector improvements aimed at a reduction of the overall background is expected to be started soon.

Conclusion

The Gran Sasso National Laboratory of INFN, the largest underground laboratory in the world, holds the leadership in massive experiments with record performance and low-level background. The present scientific program of LNGS includes a very broad spectrum of competitive experiments (astroparticle, particle and nuclear physics), including the world-leading ones in the fields of solar neutrinos, accelerator neutrinos, double beta decay, dark matter and nuclear astrophysics.

References

- G. Bellini et al., Phys. Rev. Lett. 108 (2012) 051302
- Agafonova, N., Aleksandrov, A., Altinok, O., et al.(2010). Observation of a first ν candidate event in the OPERA experiment in the CNGS beam. Phys. Lett. B 691 (pp.138–145).
- Bernabei, R., Belli, P., Cappella, F., et al. (2011). Particle Dark Matter in the galactic halo: recent results from DAMA/LIBRA. Nucl. Phys. B (Proc. Suppl.) (pp. 212-213).
- XENON100 Collaboration arXiv:1207.5988v1

THE PROTON BEAM FOR THE NEUTRINO VELOCITY MEASUREMENT WITH OPERA

■ LYNDON EVANS

Imperial College, London/ CERN, Geneva

1. Introduction

Since the announcement of the measurement of neutrino velocity with the OPERA detector in the CNGS beam [1] much effort has been devoted to searching for possible sources of error in the experiment. This paper concerns the time structure of the primary proton beam striking the neutrino target. With this beam it is not possible to make direct time-of-flight measurement. Instead, the distribution in time of the OPERA neutrino events is fitted to the averaged time structure of the proton beam. Fitting the leading edge of the distribution is crucial to the analysis. Possible sources of error with this procedure are discussed.

A much better beam for the purpose of time-of-flight measurement can be derived from the beam prepared for injection into the LHC. With this beam, all possible sources of error concerning the proton time structure are eliminated. It should make possible a precise and direct time-of-flight measurement with very few neutrino events recorded in the detector.

2. The neutrino beam

The layout of the CNGS beam is shown in Figure 1 [2]. The proton beam is accelerated to 400 GeV in the SPS and extracted with a fast kicker magnet and transported 800m to the production target. Downstream of the target is the standard horn and reflector for focussing the pions and kaons which travel about 100m to the one kilometre long evacuated decay tube. Upstream the production target a fast Beam Current Transformer (BCT) captures the time structure of the proton beam.

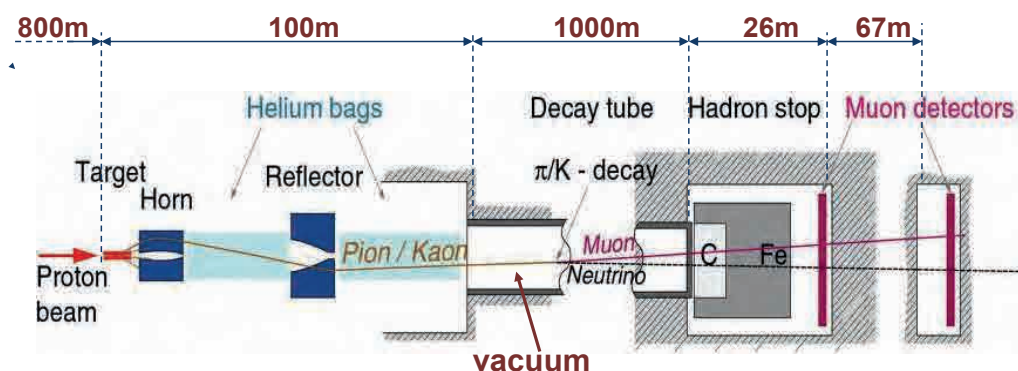


Figure 1
Schematic layout from production target to hadron stop

The proton beam itself is designed to maximise the number of protons on target. The time structure is formed in the CPS where the beam is accelerated to 14 GeV/c and then debunched. Extraction is made by peeling off the beam over 5 turns on an electrostatic septum [3], the so-called continuous transfer, giving a 10 microsecond long pulse. The leading edge of this pulse is not sharp due to the finite rise time of the closed orbit bump in the CPS and the intensity distribution between the turns is not very uniform. Two successive CPS cycles with 1.2 sec separation are injected into the SPS flat bottom at 14 GeV. Figure 2

shows an SPS super cycle with the long flat-top for the slow spill into the SPS North area is followed by 5 successive cycles for CNGS. The two separate PS injections on each cycle can be clearly seen as well as the losses at the beginning of acceleration. This beam must be taken through “transition” which occurs at around 21 GeV in the SPS. The total intensity per cycle is around $3 \cdot 10^{13}$ protons with about 10^{10} protons per bunch.

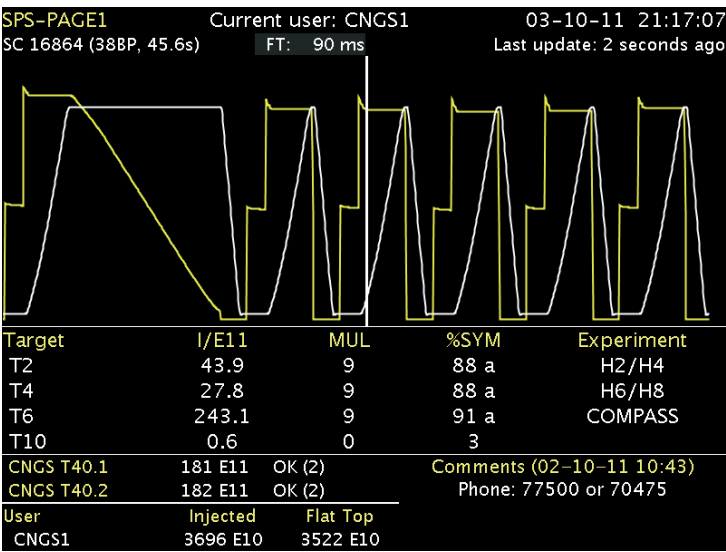


Figure 2
An SPS supercycle with 5 cycles to the neutrino target

Figures 3 and 4 show the intensity distribution of the two CPS “batches” in the SPS. The leading edge can easily be observed as well as the uneven intensity distribution along the batch. It can also be observed that the intensity distribution in the two batches is quite different. The two batches are extracted with a fast kicker separated by 50 ms.

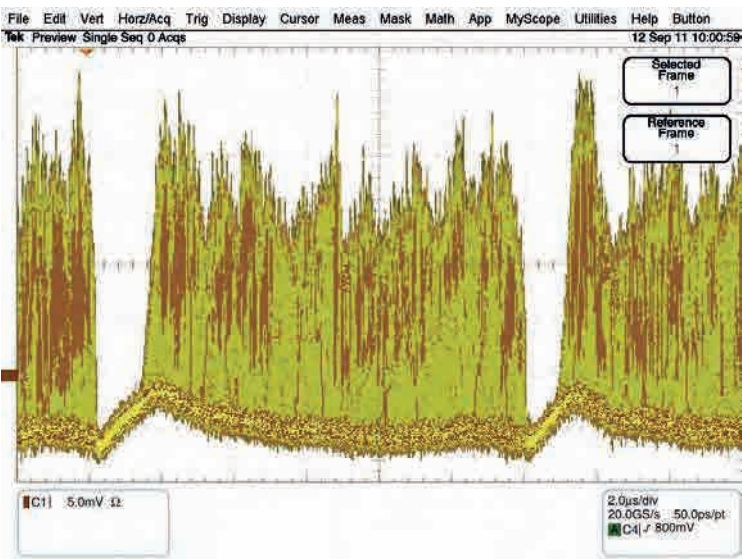


Figure 3
The two batches in the SPS

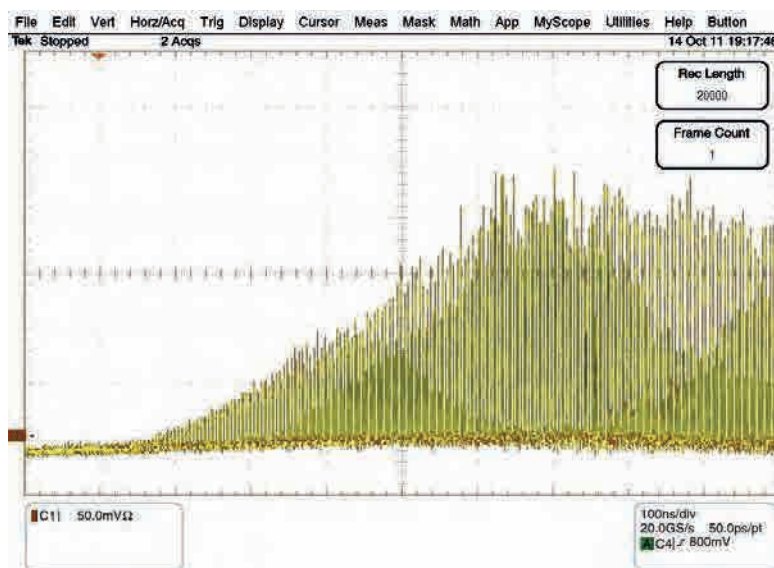


Figure 4
The leading edge of the first batch

At least three possible sources of error concerning the method of neutrino velocity measurement can be identified.

1. Pulse-to-pulse variations in intensity distribution in the CPS.
2. The rising edge of the SPS extraction kicker cuts into the leading edge of the beam. Jitter in the kicker timing can cause variations in intensity of the leading edge.
3. The finite frequency response of the fast BCT, in particular the low frequency response due to dispersion in the cables from the BCT to the electronics can distort the leading edge.

All three of these can be removed by using a very different beam, effectively the one injected into the LHC.

3. The LHC beam

The nominal LHC beam has an order of magnitude higher intensity per bunch with a larger bunch spacing than the CNGS beam. The problem of accelerating very high intensity bunches was studied [4] in the late 1970's in the context of the PPBAR Project. It was shown that the passage through transition energy with such intense bunches was impossible due to two instabilities, the transverse "head-tail" instability and the longitudinal "negative mass" instability. The solution adopted was to inject into the SPS above transition at 26 GeV. This is not possible for the continuous transfer process due to hardware limitations and increased cycle time.

For the LHC, the nominal bunch spacing is 25 ns but a very flexible and elegant [5] bunch splitting method has been developed in the CPS to allow many different bunch separations. It consists of a set of harmonic Radiofrequency cavities that allow bunches to be split by varying adiabatically the voltages at the different harmonics. Figure 5 shows such a process producing 25 ns bunch separation.

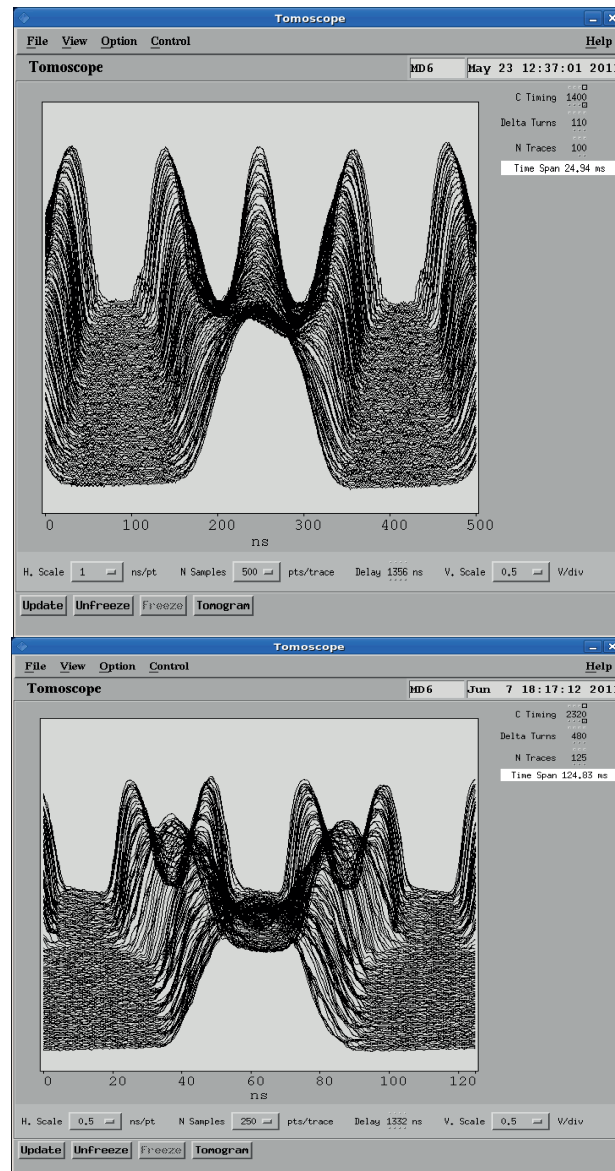


Figure 5

The “mountain range” displays show the bunch shape turn by turn with the time axis moving vertically. First (upper) a single booster bunch is split into 3 on the CPS injection plateau followed by a quadruple split on the 26 GeV CPS flat top. This beam can then be cleanly transferred into waiting RF “buckets” in the SPS. Figure 6 shows the bunch distribution using the same monitor as Figures 3 and 4. The leading edge is now perfectly defined.



Figure 6
Bunch distribution of the LHC beam in the SPS

Figure 7 shows a single bunch 2 ns duration and with an intensity of 3.10^{11} protons, 30 times the nominal bunch intensity of the CNGS beam.

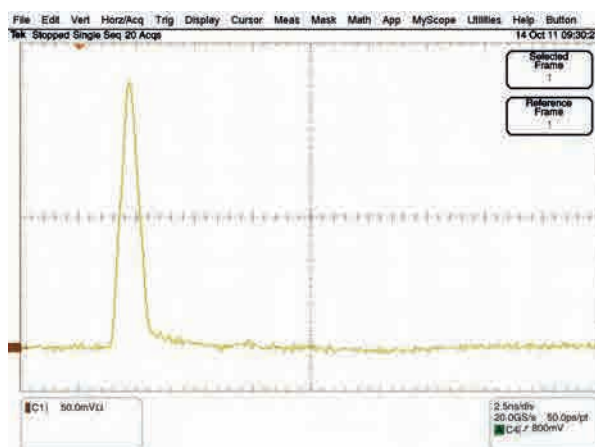


Figure 7

This beam is not suitable for Tau physics at OPERA since the total intensity is about 30 times lower than the normal beam. However, each neutrino event is very precisely defined in time so an accurate time-of-flight measurement can be made with very few events. A number of options have been studied including 25 and 50 ns bunch separation. However in these cases the intensity is limited to about $1.5 \cdot 10^{11}$ protons per bunch. It is of interest to have the highest possible bunch intensity. A good compromise has been found with 4 bunches each of 3.10^{11} protons per bunch separated by 524 ns per SPS cycle. This beam will give a few neutrino events per day in OPERA.

4. Conclusions

A dedicated “LHC type” beam removes the uncertainties inherent in the normal proton beam to CNGS. It will allow a precise neutrino velocity measurement with very few events.

Acknowledgements

I am indebted to the CERN neutrino team for very useful discussions.

References

- [1] T. Adam et al, Measurement of the neutrino velocity with the OPERA detector in the CNGS beam, Paper submitted to the Journal of High Energy Physics (17 November 2011), arXiv:1109.4897v2
- [2] E. Gschwendtner et al, First operational experience with the CNGS facility, AIP Conf Proc, 981 (2008) 23
- [3] C. Bovet et al, The fast shaping ejection for beam transfer from the CPS to the CERN 300 GeV machine. Proc 1973 Particle Accelerator Conference, San Francisco, IEEE Trans Nucl Sci, 20 (1973) 438
- [4] D. Boussard et al, Acceleration and storage of a dense single bunch in the CERN SPS. IEEE Trans Nucl Sci, NS-26, No 3 (1979) 3484
- [5] R. Garoby et al, Demonstration of bunch triple splitting in the CERN PS, CERN/PS-2000-038(RF)

CAN THE NEUTRINO SPEED ANOMALY BE DEFENDED?

■ JÜRGEN KNOBLOCH

CERN

Abstract

The OPERA collaboration reported [1] a measurement of the neutrino velocity exceeding the speed of light by 0.025%. For the 730 km distance from CERN in Geneva to the OPERA experiment an early arrival of the neutrinos of 60.7 ns is measured with an accuracy of ± 6.9 ns (stat.) and ± 7.4 ns (sys.). A basic assumption in the analysis is that the proton time structure represents exactly the time structure of the neutrino flux. In this manuscript, we challenge this assumption. We identify two main origins of systematic effects: a group delay due to low pass filters acting on the particular shape of the proton time distribution and a movement of the proton beam at the target during the leading and trailing slopes of the spill.

Introduction

In a speed measurement there are two major elements: distance and time. In the OPERA analysis there is, however, a third element that did not give rise to detailed consideration in [1]: The measurement of the time structure or Particle Density Function (PDF) of the neutrinos emanating from the CERN CNGS (CERN Neutrinos to Gran Sasso) system. The proton extraction lasts for 10.5 μ s and there are 16111 neutrino events in OPERA used in the analysis. The statistical accuracy (for a rectangular PDF) would be $\Delta = 10.5 \mu\text{s} / \sqrt{12} * \sqrt{16111} = 24$ ns. The claimed anomaly of 60.7 ns is, however, measured more precisely with an accuracy of ± 6.9 ns (stat.) and ± 7.4 ns (sys.). Therefore the leading and trailing edges of the neutrino time distribution play an important role in the analysis. OPERA assumes that the proton PDF is measured correctly and that it represents exactly the neutrino PDF. In the following, we argue that both assumptions can be questioned and that systematic effects of the order of the observed anomaly have been neglected.

The neutrino beam

In the CERN Super Proton Synchrotron (SPS), 400 GeV protons complete one round trip in 23 μ s. The ring is filled with two proton batches of 10.5 μ s separated by two gaps of 1 μ s. The batches are extracted spaced by 50 ms. The extraction of each batch is initiated by a kicker magnet powered up with a 1.1 μ s rise time during the 1 μ s gap. Once the kicker magnet strength reaches 80% of the maximum, the beam trajectory is inside the gap of a magnetic septum at the beginning of a beam line leading to a 4 mm (and 5 mm) diameter carbon target where charged mesons are produced that are subsequently charge selected and focused by a magnetic horn/reflector system. In a 1 km decay tunnel the mesons decay into muons and muon neutrinos targeted at the OPERA experiment 730 km away. Just after the septum, 743 m upstream of the target, a beam current transformer (BCT) measures the proton flux in a coil coaxial with the beam. The signal of the BCT is amplified and transported by a 140 m long cable to a precision waveform analyser (WFA).

Correct measurement of the proton PDF

In a thesis [2], additional details of the analysis are given. For certain run periods, the digitizer did not perform correctly by either saturating the signal or by inducing oscillations. These periods have been removed from the analysis. Assuming that all such periods could be traced, there remains, however, an oscillating 30 and 60 ns structure in the measured waveforms, most pronounced during the last quarter of the extractions and in particular over the falling edge of the proton spill, see Fig. 8.4 of [2].

Such oscillations are still visible after summing 16111 individual measurements.

In the analysis described in [2], the oscillations are eliminated by a low-band software filter of 8 MHz. A low-pass filter not only attenuates the noise but also inflicts a frequency dependent group delay. The filter algorithm used was not specified; therefore we have evaluated the group delay curve for several low-pass filters using FilterDesignLab II-R [3]. As example Fig. 1 shows the group delay curve for an 8 MHz Butterworth low-pass filter.

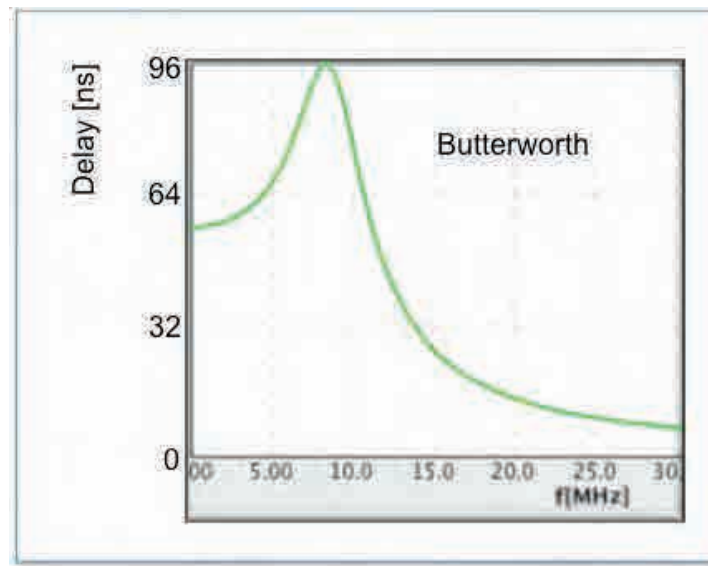


Figure 1: Group delay for 8 MHz low-pass filter

The proton PDF has a leading edge rise time of about 800 ns and a trailing edge fall time of about 400 ns (see Fig. 12 of [1]) and a more or less flat top of 9300 ns in between. The characteristic frequency of such a pulse shape is given by the rise and fall time $\tau \approx 600$ ns and amounts to $f = 1/(2\pi\tau) \approx 0.3$ MHz. In the group delay curve in Fig. 1 this frequency is at the left side of the distribution and leads to a group delay of about 60 ns. Note that a nanosecond short pulse would be located at the right side of the distribution and leads to a comparatively small group delay. Different kinds of 8 MHz low-pass filters (Chebychev-1, Chebychev-2, elliptic) have been evaluated yielding group delays between 30 and 60 ns.

A similar, though smaller, effect can impede the measurement of the time delay from the BCT to the waveform digitizer. The system BCT-amplifier-transmission cable constitutes a low-pass filter with a cut-off frequency of about 80 MHz [4]¹. The delay is measured using either a 1 PPS pulse from a Cs4000 oscillator or, with better precision, short (nanosecond) proton bunches. Both signals have short (< 5 ns) rise times. For such signals the high-frequency part of the group delay curve is relevant. The proton waveform is located at lower frequencies of 0.3 MHz. The net delay due to this effect is of the order of 10 ns.

¹ The low pass filter effect can also be seen in Fig. 4 of [1] where the 200 MHz SPS RF structure is attenuated by 70% corresponding to a 10.5 dB attenuation.

Broadening of the PDF

The proton PDF is a sum of the individual BCT measurements that are coincident with neutrino events in OPERA. In the summing process, the time alignment of the individual distributions is based on the trigger signal of the kicker magnet MKE. The timing of this trigger (kick delay) is occasionally optimized (in steps of 100 ns) in order to minimize beam loss, in particular in the septum magnet. After such optimization or after a machine development period this delay may not come back to the previous value. If this would happen during the yearly data taking, some fraction of the proton distributions would be shifted by e.g. 100 ns. Such effect would lead to a broadening of the summed PDF. It can therefore not be excluded that the widths of the used proton PDF and the neutrino event distribution are different. An indication of such broadening could be that the single waveform in Fig. 4 of [1] appears to have steeper edges than the sum shown in Fig. 12 of [1]. One may argue that this broadening would not change the mean of the distribution and therefore not impact the result. As mentioned above, however, the leading and trailing slopes differ by about a factor 2. As the steeper slope will have a larger impact on the fit result, this will lead to a shift in the final measurement. Visually, Fig. 12 of [1] does not allow excluding a broadening of the PDF by the order of 40 ns.

Differences between proton and neutrino PDF

The proton PDF is measured with a BCT 730 m upstream of the target. The neutrino PDF is proportional to the proton PDF only if all the protons measured in the BCT actually hit the target and if the position of the beam at the target does not move during the spill. The gap of 1 μ s between the proton batches in the SPS is not completely void of protons and therefore during the final 20% of the kicker magnet ramp, where the beam is within the acceptance of the neutrino beam line, protons are extracted and counted in the BCT (see [5] and [6]). The 20% kicker variation translates to a 10 mm beam movement at the septum. This can lead to a beam movement at the target of about 2 mm. The beam position stability at the target is claimed to be 50 μ m r.m.s. in the vertical plane and 100 μ m r.m.s. in the horizontal plane [7]. Due to long integration time of the beam monitors, however, this measurement reflects the beam properties during the 9.3 μ s long spill plateau and cannot account for deviations at the leading and trailing edges. The beam spot is 0.5 mm rms. The effect on the neutrino flux of a beam displacement at the target has been studied [7] and is shown in Figure 2. From this figure it is clear that a 1.5 to 2 mm displacement will lead to a significant reduction of the neutrino yield during the leading and trailing edges of the PDF and therefore distort their shapes.

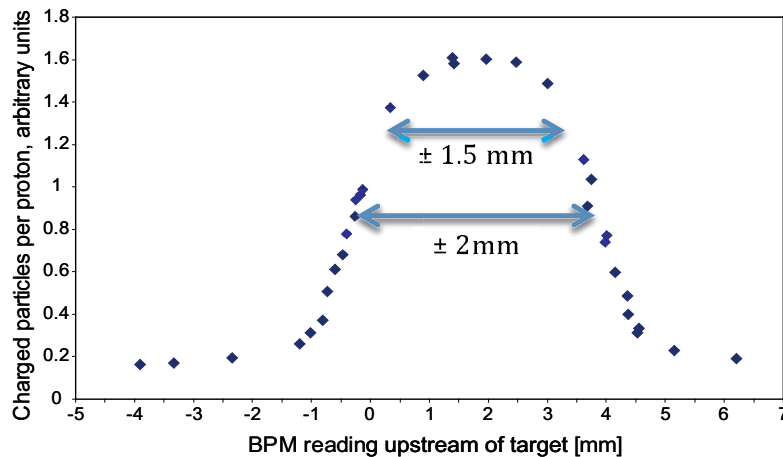


Figure 2: Horizontal proton position scan: number of charged particles in arbitrary units produced for different proton beam positions onto the target, as read by the BPM upstream of the target. (Data presented in [7]).

Conclusion and outlook

We have seen that

- The OPERA result critically depends on the edges of the PDF.
- The measurement of the proton PDF is subject to bandwidth limitation or low-pass filtering leading to group velocity delay.
- The leading slope of the individual proton time distribution is steeper than that of the final PDF.
- During the final 20% of the ejection kicker ramp up there are already protons ejected.
- The variation of kicker strength leads to 10 mm movement of the beam in the CNGS beam line
- The movement may displace the beam at the target by 1-2 mm.
- These effects act predominantly on the leading and trailing edges of the PDF

We conclude that a difference between the proton and neutrino PDF was not sufficiently considered in evaluating the systematic uncertainties summarized in Table 2 of [1]. The effects discussed in this present manuscript amount to a significant fraction of the observed anomaly. Therefore a conclusive deviation of the neutrino velocity from the speed of light has not yet been demonstrated in [1].

A new measurement of the neutrino speed is being conducted using 2 ns long bunches spaced by 500 ns from the CNGS beam [8]. In such a measurement the effects discussed here would no longer apply.

Acknowledgements

The author thanks F. Dydak for useful comments and encouragement. D. Belohrad has provided details of the BCT and I. Efthymiopoulos has discussed details of the neutrino beam. In the preparation of this manuscript, slides of presentations by J. Wenninger and E. Gschwendtner were most useful. Not least, the hospitality of the Pontifical Academy of Sciences and the support of A. Zichichi have made this work possible.

References

- [1] T. Adam et al., Measurement of the neutrino velocity with the OPERA detector in the CNGS beam, <http://arxiv.org/abs/1109.4897>
- [2] G. Brunetti, Neutrino velocity measurement with the OPERA experiment in the CNGS beams, PhD thesis, in joint supervision from Université Claude Bernard Lyon-I and Università di Bologna, 2011.
http://operaweb.lngs.infn.it:2080/Opera/ptb/theses/theses/Brunetti-Giulia_phdthesis.pdf
- [3] FilterDesignLab-IIR, <http://www.mtk-digital.com/>, Mac App Store
- [4] D. Belohrad, CERN, Private communication.
- [5] G. Arduini et al., Aperture and beam loss during extraction from the SPS and injection into the CNGS beam line., CERN AB-Note-2006-015 (ABP)
- [6] V. Kain et al., Commissioning of the CNGS Extraction in SPS LSS4, CERN AB-Note-2007-007 OP
- [7] M. Meddahi et al., CERN Neutrinos To Gran Sasso (CNGS): Results From Commissioning, Proceedings of PAC07, Albuquerque, New Mexico, USA
- [8] CERN Bulletin No. 45-46/2011

THE ORIGIN AND STATUS OF THE THIRD NEUTRINO

■ ALESSANDRO BETTINI

University of Padua. Department of Physics; INFN. Padua division (Italy)
Laboratorio Subterráneo de Canfranc (Spain)

bettini@pd.infn.it
bettini@lsc-canfranc.es

1. The three lepton families

The elementary particles known today fall in two categories: twelve spin $\frac{1}{2}$ particles (fermions), the building blocks of matter, and twelve spin 1 particles (bosons), which are the mediators of all the forces but gravity. The last element in the Standard Model is a spin 0 particle, thought to be at the origin of the masses and called the “Higgs” after the name of one of the discoverers of the theory. Not yet detected, it is searched for at the new CERN LHC collider.

The fermions come in three different groups, called families, of identical structure. The reason for that is unknown. Each family is made of a doublet of quarks, of charge $+2/3 q$ and $-1/3 q$ (q is the proton charge), and a doublet of leptons, one of charge $-q$ and one neutral. The neutral leptons are collectively called neutrinos, but are three different particles, distinguished by an additive quantum number called “lepton flavour”. The electron (e^-) and the electron-neutrino (ν_e) have one unit of electronic flavour (-1 their antiparticles); the muon (μ^-) and the muon-neutrino (ν_μ) have one unit of muonic flavour and similarly for the tau (τ^-) and the tau-neutrino (ν_τ).

The charged leptons are distinguished by their masses (increasing with the family number) and lifetimes, neutrinos only by their lepton flavours. Neutrinos are produced in states of definite flavour, as ν_e , ν_μ or ν_τ , in pairs with an antiparticle of the same and opposite flavour. Elementary interactions conserve flavours. So that, by definition, the electron-neutrino (ν_e) is the neutral lepton produced with a positron (e^+), the ν_μ is the one produced with a μ^+ and the ν_τ is the one produced with a τ^+ . And electron-anti-neutrino is the neutral particle produced with an e^- , etc.

Neutrinos cannot be detected directly. However, when one of them interacts with the matter producing a charged lepton, the latter can be detected. The identification of the charged lepton gives the flavour of the neutrino: if it is an electron (e^-) it was a ν_e etc.

Experiments show that neutrinos born with a flavour produce charged leptons of the same flavour, provided the ratio L/E between distance from production to interaction points and neutrino energy is not very large, namely if the oscillation phenomenon has no time to develop. Indeed, experiments in underground laboratories have shown that neutrinos do not behave as assumed in the Standard Model, they do change, “oscillate”, between one flavour and another. The evidence has gradually grown in the last four decades, by studying the ν_e s produced by the fusion reactions in the core of the Sun and the ν_μ s indirectly produced by the cosmic rays collisions in the atmosphere. Confirmations came by experiments with artificial neutrino sources: proton accelerators (producing mainly ν_μ) and nuclear power reactors ($\bar{\nu}_e$). There two types of experiments. In a disappearance experiment the flux of neutrinos of a certain flavour is known at production; if the flux is measured at a (large) distance and found to be less than expected, the oscillation to another flavour is inferred. In an appearance experiment a flavour not present at production is searched.

Oscillations happen because neutrinos of definite flavour are not stationary states (mass eigenstates). The latter, ν_1 , ν_2 and ν_3 , do not change and have definite masses, m_1 , m_2 and m_3 . The two basis are linked by an orthogonal transformation that can be expressed in terms of three rotations, through angles that we shall call θ_{12} , θ_{23} and θ_{13} , and of phase factors. If neutrinos are Dirac particles, as assumed in the Standard Model, all but one of the phase factors can be absorbed, as in the case of quarks, in the wave functions of the states. However, neutrino and antineutrino might be two states of

In conclusion, writing $c_{ij}=\cos\theta_{ij}$, and $s_{ij}=\sin\theta_{ij}$, the unitary transformation $\nu_l = \sum_{i=1}^3 U_{li} \nu_i$ is

$$\begin{pmatrix} \nu_e \\ \nu_\mu \\ \nu_\tau \end{pmatrix} = \begin{pmatrix} 1 & 0 & 0 \\ 0 & c_{23} & s_{23} \\ 0 & -s_{23} & c_{23} \end{pmatrix} \begin{pmatrix} c_{13} & 0 & s_{13}e^{i\delta} \\ 0 & 1 & 0 \\ -s_{13}e^{-i\delta} & 0 & c_{13} \end{pmatrix} \begin{pmatrix} c_{12} & -s_{12} & 0 \\ s_{12} & c_{12} & 0 \\ 0 & 0 & 1 \end{pmatrix} \begin{pmatrix} 1 & 0 & 0 \\ 0 & e^{i\alpha/2} & 0 \\ 0 & 0 & e^{i\beta/2} \end{pmatrix} \begin{pmatrix} \nu_1 \\ \nu_2 \\ \nu_3 \end{pmatrix}$$

Notice that Majorana phases are irrelevant for the oscillation and matter effects. They are observable in an extremely rare, not yet observed phenomenon, the neutrino-less double beta decay (see §6).

The above-mentioned experiments have measured cross sections and energy spectra relevant for the oscillation phenomena. The frequency of the oscillation in vacuum is proportional to the absolute value of the squares of two neutrino masses. The flavour conversion in matter, in the Sun in particular, depends also on the sign of the difference. A global fit to these measurements, e.g. Fogli et al. (2011), allows the extraction of the mixing angles and of the differences between the squares of the masses. Specifically, the information on θ_{12} is mainly due to solar neutrinos and reactor antineutrinos, that on θ_{23} to atmospheric neutrinos, reactor antineutrinos and accelerator neutrinos. The third angle, θ_{13} , is small, almost compatible with zero with the present uncertainties. The values are

$$\sin^2 \theta_{12} = 0.306_{-0.015}^{+0.018}, \quad \sin^2 \theta_{23} = 0.42_{-0.03}^{+0.08}, \quad \sin^2 \theta_{13} = 0.021_{-0.08}^{+0.07}$$

For the square mass differences we have

$$|\Delta m^2| = \left| m_3^2 - \left(\frac{m_1 + m_2}{2} \right)^2 \right| = 2350_{-90}^{+120} \text{ meV}^2; \quad \delta m^2 = m_2^2 - m_1^2 = 75.8 \pm_{2.6}^{2.2} \text{ meV}^2$$

Fig. 1 shows schematically the neutrino square-mass spectrum. It consists of a singlet (ν_3) and a doublet (ν_1, ν_2). The approximate flavour composition of the eigenstates is also shown. We do not know either the absolute scale or whether the mass of the singlet is larger or smaller than that of the doublet.

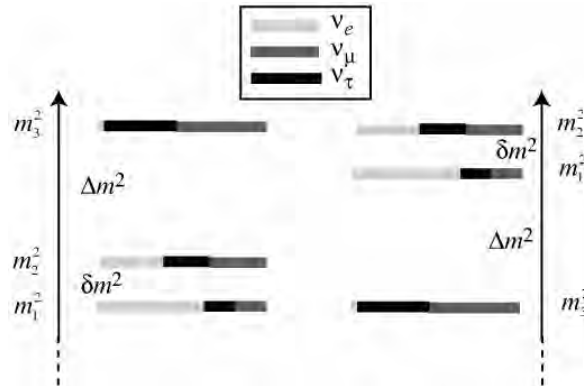


Fig. 1. Neutrino square-mass spectrum. The flavour contents of the eigenstates are also shown

2. Lepton identification

As mentioned above, the definition of the flavour of a neutrino requires experimentally the identification of the nature of the charged particle it produces and of the other particles that are also present in the final state of the interaction.

There are different types of detectors. The main categories are the trackers, which show, within a range of resolutions, the images of the tracks of the charged particles that go through, and the calorimeters that absorb and measure all the energy of the particle.

Electrons and pions produce very similar tracks, but can be distinguished by the different shape of the “shower” they produce. An electron penetrating in a dense medium will soon radiate a photon, which in turn will convert in electron-positron pair, which will radiate more photons, etc. A pion will behave similarly, but producing a shower containing also hadrons on top of electrons and photons. The difference in shape between the two showers can be enhanced and detected with proper techniques, as

we shall see, particularly in their initial phases. A high discriminating power is needed to reliably identify the electrons that are produced very rarely compared to the pions.

Muons can be distinguished from hadrons due to their much higher penetrating power. Differently from pions, muons go through metres of material without interacting, leaving a long, straight track.

Tau leptons have a lifetime much shorter than the more common hadrons, about 0.3 ps; at the energies of a few GeV energy, which are typical in the experiments under discussion, the lengths of their tracks between production and decay points, are of the order of hundreds micrometres. Consequently, extremely high spatial resolution, of the order of a micrometre is needed, as provided by nuclear emulsions. Moreover, also large target masses are necessary to secure an appreciable rate of neutrino interactions. A powerful technique, known as emulsion cloud chamber (ECC), has been developed by the Nagoya group initially lead by K. Niu. Fig. 2 shows, as an example, the configuration in the DONUT experiment that we shall discuss later. One mm thick Fe sheets, providing the mass, are interleaved with emulsion sheet pairs, providing the images of the track segments. A short track, a kink between the mother and the daughter, is the signature of the tau lepton. Short lifetime hadrons, such as the charmed ones, give the same topology, but are much rarer than the pions.

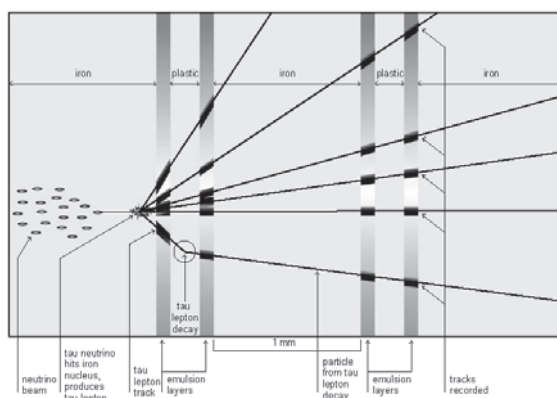


Fig. 2. The Emulsion Cloud Chamber (ECC) of the DONUT experiment at FermiLab

3. The history of the third lepton family

In 1897 J. J. Thomson (1897) discovered the electron, the first elementary particle, by developing the technique of deflecting charged particles in a magnetic field in a vacuum and building the first mass spectrometer, and in 1932 he detected the positron.

Fifty years later, J. Street and E. Stevenson (1937) and C. Anderson and S. Neddermeyer (1936) discovered a penetrating component in the cosmic rays. Surprisingly, it was not the mediator of the nuclear forces, the pion, predicted by Yukawa, but was a lepton, as experimentally shown by M. Conversi, E. Pancini and O. Piccioni (1947). I. I. Rabi will comment these completely unexpected results by asking: “Who ordered that?”

Almost another decennium later, F. Reines (Cowan, C. L. et al. 1956), using the Savannah River power reactor as a source, finally discovered “the” neutrino that had been introduced as a “desperate hypothesis” by Pauli back in 1930, when only the electron was known, to explain the apparent non-conservation of energy in beta decay. It became later known that it was the “anti” of “one” of the three neutrinos (electron-anti-neutrino).

In 1962 M. Schwartz, L. Lederman, J. Steinberger et al. (Danby et al. 1962) discovered the muon-neutrino at BNL AGS proton accelerator.

In the same years, A. Zichichi (Conversi, M. 1963) developed the PAPLEP (Proton-AntiProton into LEpton Pairs) experiment at the CERN Proton Synchrotron (PS). It was the beginning of the search for the 3rd sequential lepton family, imagined as a replica of the first two, made of a “Heavy Lepton” (HL) and its neutrino (ν_{HL}). For a complete history see Wu et al. (1997). The idea was to look for lepton pairs of opposite sign. These can be produced directly or result from the decays of a HL anti-HL pair, produced by the reaction $p + \bar{p} \rightarrow HL^+ + HL^-$, shortly followed by the decays $HL^+ \rightarrow e^+ \nu_e \bar{\nu}_e$ or $HL^+ \rightarrow \mu^+ \nu_\mu \bar{\nu}_\mu$ and $HL^- \rightarrow e^- \bar{\nu}_e \nu_e$ or $HL^- \rightarrow \mu^- \bar{\nu}_\mu \nu_\mu$. The presence of the intermediate Heavy Leptons can be inferred when one of these decays is into an electron the other into

a muon, while in the direct production the leptons have the same flavour. A further signature, due to the presence of undetected neutrinos, is the “acoplanarity”, meaning that the plane defined by the momenta of the detected leptons does not contain the direction of the beam.

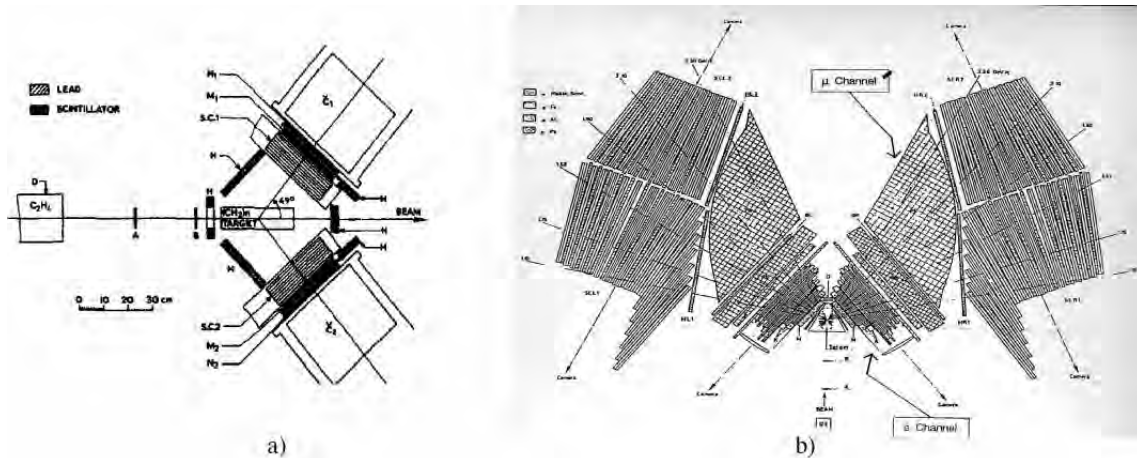


Fig. 3. a) The principle of the double arm spectrometer. b) the full design of PAPLEP

Having that stated, the experimental challenges were several.

- The detector should have had a large acceptance to collect a good fraction of the expectedly rare process: a large solid angle double arm spectrometer was built
- The very rare electrons had to be discriminated from the hadrons with high efficiency: the pre-shower was developed (Massam et al. 1965)
- The very rare muons had to be discriminated from the hadrons with high efficiency: the hadrons punch through phenomenon leading to the penetration, like the muons, of the Fe absorber was preliminarily investigated (Buhler et al. 1965).

The PAPLEP principles are shown in Fig. 3a), while Fig. 3b) shows its design. Fig. 4 is a photo of PAPLEP, a very large device for the time.

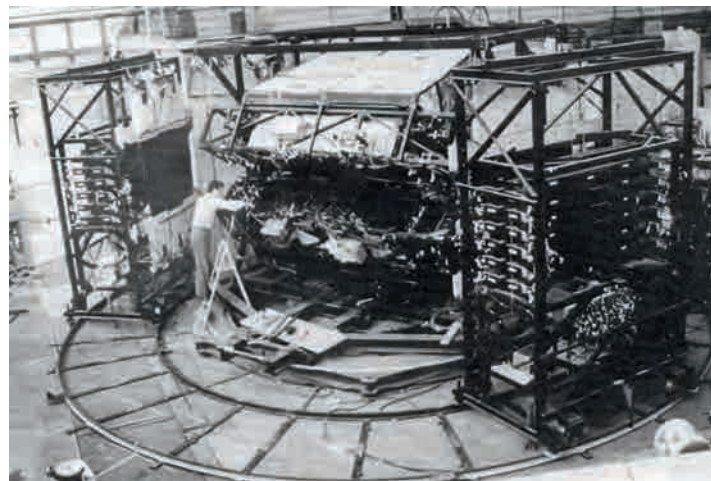


Fig. 4. The PAPLEP apparatus at the CERN PS. Circa 1963

The detector elements closest to the target in both arms are two equal copies of the early development of the shower, or pre-shower, apparatus. As shown in Fig. 5, it is a sandwich of five repeated elements, each composed of Pb layer controlling the early development of the shower, a plastic scintillator sampling the energy deposit and an Al-plates spark chamber visualizing the tracks. The novel method combines in this way visual and non-visual approaches, each providing 10^{-2} rejection to obtain an overall rejection of the pions of a few 10^{-4} (Massam et al. 1965).

PAPLEP did not find the HL, but produced important results based on the lepton pairs detection, in particular on the time-like nuclear form factor (Conversi et al. 1964 and 1965)

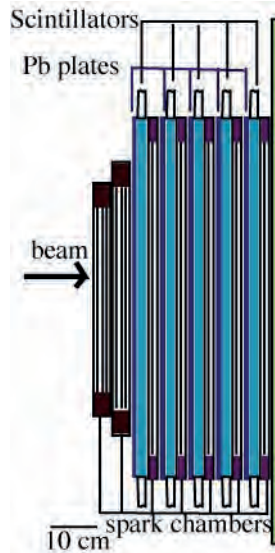


Fig. 5. The pre-shower scheme

A reason for the non-observation of the HL might have been the non point-like structure of the proton. Consequently, the next step of Zichichi was to move the search to the highest energy e^+e^- collider available, ADONE at Frascati. (Bernardini M. et al. 1967). The apparatus, shown in Fig. 6 employs all the technologies for electron/pion and muon/pion discrimination developed in PAPLEP, adapted to the collider situation. The two equal arms are now on opposite sides of the collision point.

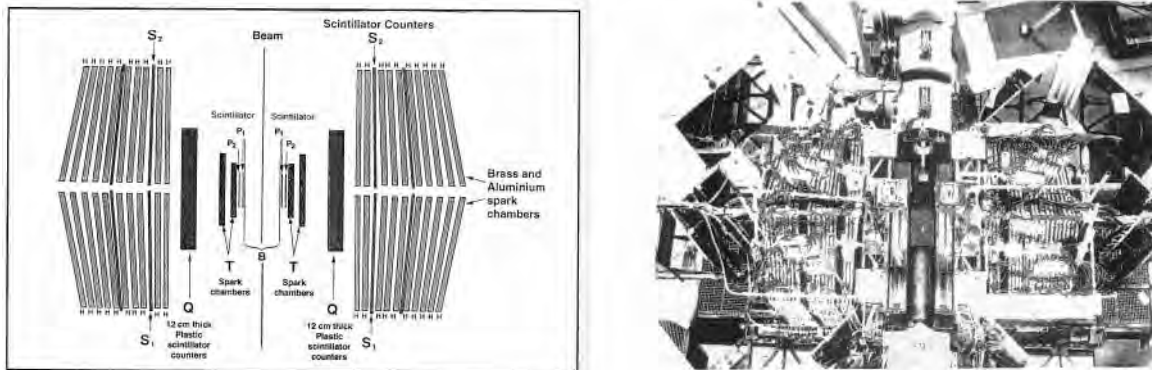


Fig. 6. The apparatus to search for Heavy Lepton at ADONE. Left: schematic. Right: a picture

Once more, the HL was not found, and only a lower limit of 1 GeV could be established for its mass, as shown in Fig. 7 (Alles Borelli et al. 1970). The reason is that the HL mass is 1.777 GeV, too large to be produced at ADONE, which had a maximum energy of 3 GeV.

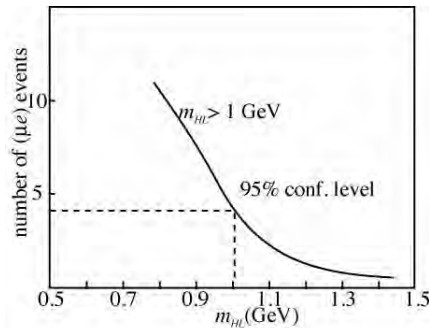


Fig. 7. Limits on the HL mass. Simplified from Alles Borelli et al. 1970

In 1974 a new e^+e^- collider, SPEAR at SLAC, had reached steady operation at 4.8 GeV, together with the detector shown in Fig. 8 left. The apparatus, which became later known as MARK I (after the construction of its successor MARK II), had been built as a general purpose one with a broad physics programme, which were to discover a gold mine (the charm). Four layers of cylindrical wire chambers provided tracking in magnetic field produced by a solenoid. Outside the coils, lead-scintillator electromagnetic shower counters and tracking chambers for the muons were located.

As part of the facility programme, M. Perl and collaborators started searching for HL looking for acoplanar $e\mu$ pairs. However, the general-purpose detector had not been conceived with the necessary particle identification capability. A track was defined as an “electron” if it released more than four times the ionization minimum in a lead-scintillator sandwich. A “muon” was defined as a track penetrating 20 cm of Fe absorber. The resulting samples had estimated hadron contaminations of 18% and 20% respectively.

Under these conditions, the analysis had to rely on a statistical selection on acoplanarity. A statistically significant effect was found, published by Perl et al. (1975) with the conclusion: “We have found 64 events of the form $e^+ + e^- \rightarrow e^\pm + \mu^\mp + \geq 2$ undetected particles, of which we have no conventional explanation”. Once more, the HL had escaped discovery, this time due to the insufficient particle identification.

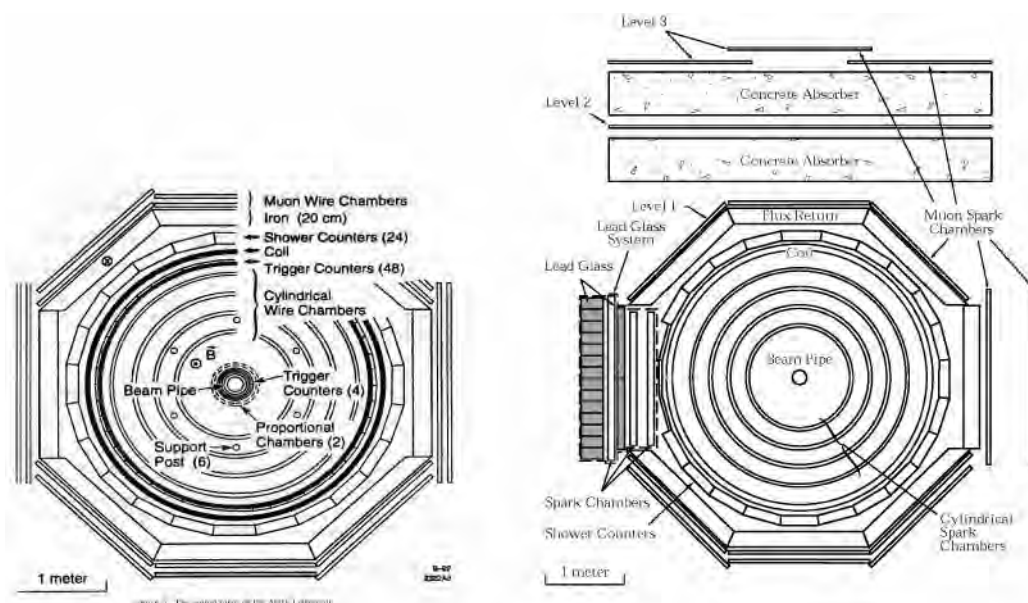


Fig. 8. The MARK I detector at the SPEAR collider at SLAC (sections perpendicular to the beams). Left: initial configuration in 1974. Right: with the additions of the hadron filter on top and the Pb glass wall on the left side

Already in the summer 1974 the muon identification was substantially improved, in a fraction of the solid angle, by adding thick concrete absorbers to filter the muons above the apparatus, and in 1976 a new “lead glass wall” photon detector was added by L. Barbaro Galtieri and her group to substantially improve the electron identification (Fig. 8 right). In their second article, Perl et al (1976) could reach the conclusion: “We present the properties of 105 events of the form $e^+ + e^- \rightarrow e^\pm + \mu^\mp + \text{missing energy}$ The simplest hypothesis compatible with all data is that these events come from the production of a pair of heavy leptons, the mass of the lepton being in the range 1.6 to 2.0 GeV”. Finally, the discovery was consolidated in a third paper, one year later (Perl et al. 1977), titled “Properties of the proposed τ charged lepton”. Notice that in this article, the name is changed from heavy lepton to tau, the initial letter of *τριτων*, “the third” in Greek, on the suggestion of P. Rapidis.

Soon, two other experiments, PLUTO and DASP at the e^+e^- DORIS collider at DESY confirmed the discovery.

The discovery of the other member of the 3rd lepton family, the tau-neutrino, had to wait another quarter of a century. As already discussed, the detector must have a large mass, because neutrino

cross-sections are small and micrometre level spatial resolution, provided by emulsion techniques (Fig. 2).

In the DONUT experiment at Fermilab, the neutrino beam was produced using 800 GeV protons from the Tevatron interacting in a one-metre long tungsten “beam dump”, which was 36 m upstream from the emulsion target. All the hadrons produced in the dump are absorbed, with the exception of those that decay within a picosecond or so. The latter are mainly charmed mesons. The primary source of ν_τ is the leptonic decay of a D_s meson into τ and ν_τ .



Fig. 9. Basic topologies of a) ν_μ interaction b) ν_τ interaction

The signature of the τ is a track with a kink, signifying a decay characterized by a large transverse momentum. Fig. 9 shows the difference between ν_τ and ν_μ interaction topologies. The already mentioned ECC technique was used. A charged particle spectrometer with electron and muon identification capabilities provided additional information.

A drawback of the ECC technique is the large amount of work needed at the microscope to extract the relevant information from the emulsion sheets after having exposed them to the beam and chemical develop. First, the sheet must be scanned to find the interesting tracks, then these tracks must be followed to check if they originate from an interesting vertex, finally all the tracks of the event must be accurately measured. Automatic techniques were continually developed by the Nagoya group lead by K. Niwa to cope with the large amount of emulsion sheets of the DONUT experiment.

Kodama (2001) published the discovery of the tau neutrino based on the observation of four ν_τ interactions with an estimated background of 0.34 events. Fig. 10 shows one of them. The short track of the τ is clearly resolved.

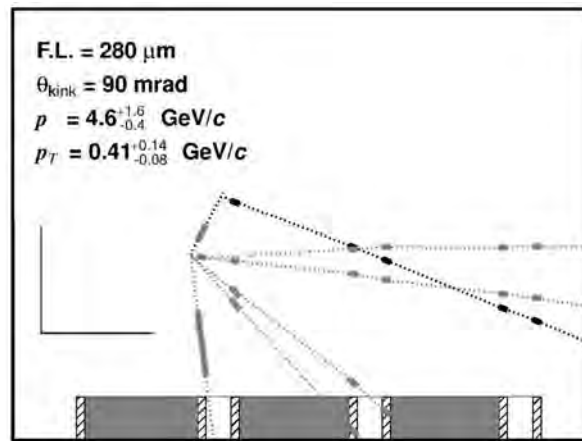


Fig. 10. A 3rd neutrino, producing a τ lepton, whose short track is detected in the DONUT experiment

4. The third neutrino appearance

As we have seen, more than one century, from 1887 to 2001, was needed to discover the six leptons of the three families. During this period, neutrinos gave many surprises. Neutrinos are the only known particles that do not behave as foreseen by the Standard Model: they have non-zero mass and they can change flavour in the oscillation phenomena. In other words, neutrinos do not belong to a family forever; as time goes by they change family. We have also mentioned that different experiments have now clarified many aspects of neutrino physics. However, several unknowns remain. One of these is the following. Experiments on atmospheric and accelerator ν_μ s have proven that they disappear over long distances. All the evidence is that they change flavour almost exclusively into ν_τ , but the experimental proof still lacks. The OPERA experiment at LNGS is searching for that.

The history starts three decades ago.

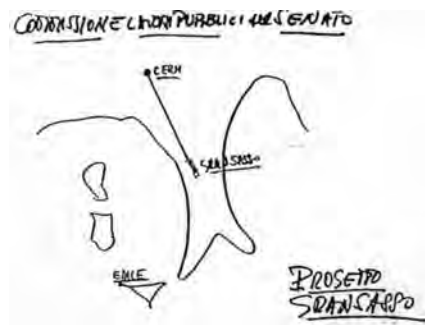


Fig. 11. Sketch of the neutrino beam from CERN to Gran Sasso by A. Zichichi (1979)

In 1979, A. Zichichi, then president of INFN, presented to the Italian Senate the Gran Sasso Project, to build a large, technologically advanced, laboratory under the Gran Sasso massive. The Project was soon approved with a first appropriation to ANAS (the Italian Government Road Department) in 1982 (a second followed in 1984). By 1987 ANAS had completed the civil engineering works and the first experiments had begun to be commissioned. The laboratory halls were oriented, in particular, toward CERN, in order to be able in a future to host experiments on a neutrino beam from those accelerators. The draft presented by Zichichi to the Senate is shown in Fig. 11.

The latter vision started to become reality around 1997. Recalling that accelerators produce (almost pure) ν_μ beams, the alternative ν_μ disappearance vs. ν_μ appearance was open. Notice that the two require different characteristics both for the beam and the experiments. Vivid discussions started in the community leading to proposals for both options. In particular, in that year Ereditato, Niwa and Strolin (1997) proposed the OPERA experiment. It was as an appearance experiment based on the ECC technique. The study of the proposals led to a common decision by the CERN Director General, L. Maiani, the INFN President, E. Iarocci, and the LNGS Director, myself, for the more risky, but much more rewarding in case of success, appearance experiments. We took into account that two disappearance experiments were under way, K2K under construction in Japan (run started in 1999) and MINOS, planned at Fermilab in the USA (run started in 2005) and of the specific characteristics of the CERN accelerators complex. A joint CERN-INFN team was charged to design a new neutrino beam, aiming at Gran Sasso (CERN Neutrinos to Gran Sasso, CNGS) optimised for ν_μ appearance. The Technical Design Report (Elsner 1998) was ready in 1998.

The INFN and CERN Councils approved the project in 1999. The civil engineering works at CERN and the construction of the beam took place between Autumn 2000 and Summer 2004; the following delicate and complex phases of testing and commissioning were completed by the Spring 2006. In the August of the same year the large detectors at LNGS, LVD, OPERA and BOREXINO detected the first events produced by the neutrino beam.

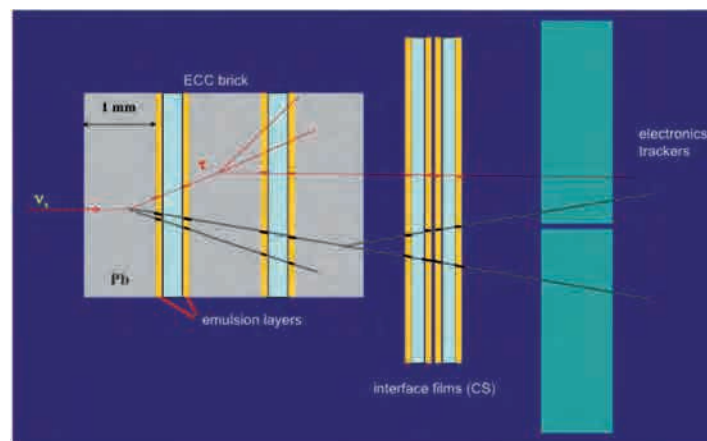


Fig. 12. The neutrino interaction detection principle of OPERA. Electronic trackers are used to identify the brick containing the interaction, which is then removed and processed.

As mentioned, the beam produced at CERN is mainly composed of ν_μ with no ν_τ . Consequently, the observation of any ν_τ at LNGS must be due to the appearance in the oscillation phenomenon. As already discussed, the two types of neutrinos can be distinguished, when they produce a charged lepton: a ν_μ produces a μ and a ν_τ produces a τ (Fig. 9).

As in DONUT, in OPERA an ECC tracking target is followed by a magnetic spectrometer. A very large target mass is necessary, because, even a distance of 732 km from CERN to Gran Sasso the appearance probability is small, because the corresponding 2.5 ms flight time is only a small fraction of the oscillation period. Consequently, only 1-2% of neutrinos are expected to “oscillate”. Considering in addition the very small neutrino cross section the conclusion is reached that the detector target mass needs to be considerably larger than 1000 t.

Fig. 12 shows schematically the components of each spectrometer. The OPERA ECC is composed of “bricks”. Each brick is a sandwich of 1 mm thick Pb sheets and double, thin (50 μm) emulsion sheets on the two sides of a plastic sheet on each side of the lead. Overall, OPERA is made of 150 000 bricks, including about 110 000 m^2 emulsion films and 105 000 m^2 lead plates, for a total of about 1250 t. The automatic emulsion read-out techniques had to be further developed.

OPERA is collecting and analysing data since 2008 and is planned to continue till the end of 2012. Already one candidate ν_τ was found (Agafonova et al. 2010). It is shown in Fig. 13. The τ lepton is the short red track. It decays in a charged hadron, presumably a pion and a π^0 , which in turn decays into 2 gammas, which are detected. Even if the calculated probability for any background to simulate a τ is only 0.045 ± 0.020 , it is too early to claim the discovery of the appearance phenomenon. But a few other similar events will hopefully lead to the ν_τ discovery in the next years.

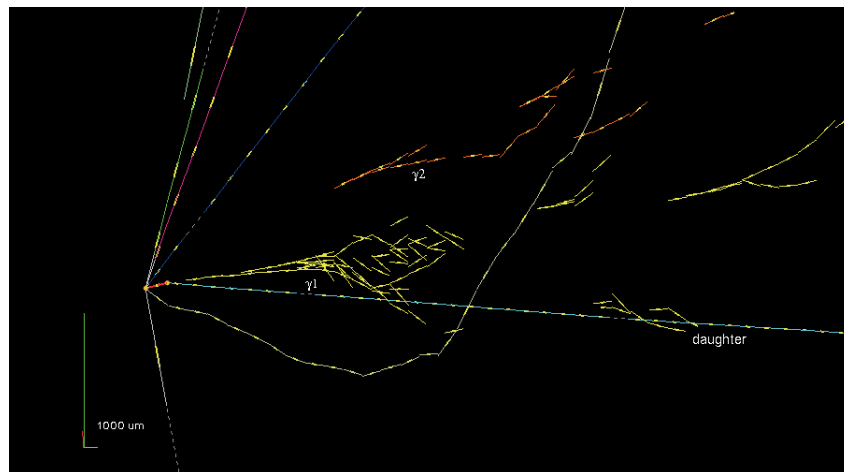


Fig. 13. The first ν_τ to ν_μ oscillation candidate. Notice the different scales on the two axes. Picture OPERA

5. Are neutrinos and antineutrinos different particles?

The Standard Model assumes neutrino masses to be zero, but as we have discussed, they are not, it assumes flavour lepton numbers to be conserved, but the oscillation phenomena show that this is not true. These facts make it plausible that even the total lepton number might not be absolutely conserved. Being the lepton number the only quantum number that distinguishes neutrinos from antineutrinos, neutrino and antineutrino may be the same particle, as predicted by Majorana (1937).

Let me recall that, in any case, the V-A structure of the charged current weak interactions (maximum parity violation) implies that only the negative chirality projection of the four-component spinor neutrino field appears in the weak charged current (in the interaction Lagrangian). In case of massless particles, as the SM neutrinos, the negative chirality field generates neutrinos in the helicity eigenstate with eigenvalue -1 and antineutrinos with eigenvalue $+1$. When a neutrino hitting a nucleus produces a charged lepton l , the V-A nature of the current implies its helicity to be negative, which in turn implies it being a \bar{l} . As a consequence, the lepton number appears to be conserved (see Fig. 14a).

The situation changes if neutrinos are, as they do, massive. There are two possibilities, corresponding to the lepton number being conserved (neutrinos obey Dirac equation, Fig. 14b) or not (neutrinos obey the Majorana equation, Fig. 14c). In both cases the particles generated by the negative chirality field are no more in a helicity eigenstate, even if they are, in practice, “almost” so. Neutrinos of mass m ,

energy E_ν and momentum p_ν have a component of positive (“wrong”) helicity of amplitude $\frac{1}{2}\left(1 - \frac{p_\nu}{E_\nu + m}\right)$ (see for example Bettini 2008). This amplitude is in the laboratory frame always extremely small, being the neutrino masses of the order of 100 meV and their energies of the order of the MeV or GeV. (Notice, however, that the relic neutrinos that fill the Universe are non relativistic). Under these condition, with a very good approximation

$$\frac{1}{2}\left(1 - \frac{p_\nu}{E_\nu + m}\right) \approx \frac{m}{4E_\nu}$$

It is however the effect of this tiny component that distinguishes the Dirac from the Majorana cases. If lepton number is conserved, this component produces leptons of the same sign as the dominant one (Fig. 14b). On the contrary, a Majorana particle produces charged leptons of both signs, negative if its helicity is negative, positive if it is positive. Having those produced in the weak interactions a dominant helicity component, we call “neutrino” the one with dominant negative helicity, “antineutrino” the one with dominant positive helicity. The situation is pictured in Fig. 14c). Calculation shows (Kayser 2008) that the probability amplitude to produce a positive lepton in the collision of a neutrino with a fixed target is proportional to m/E_ν .

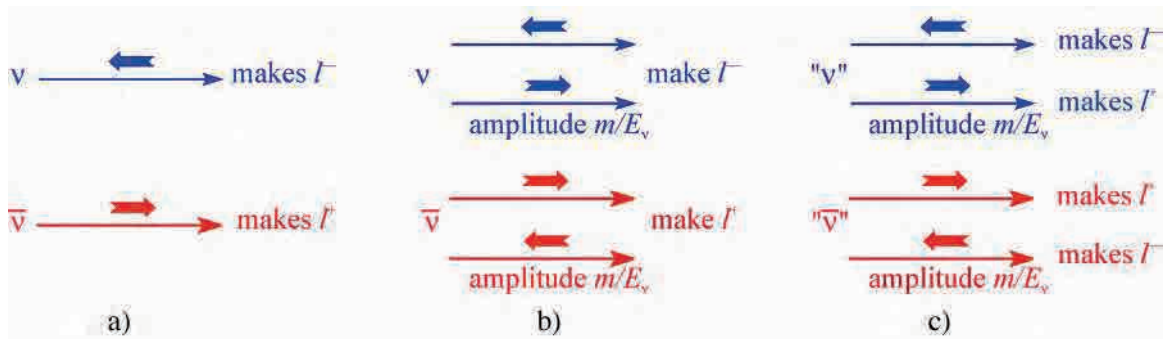


Fig. 14. Scheme of neutrino & antineutrino states in the target at rest frame. Long arrow = velocity direction, thick arrow = spin direction. a) massless neutrinos. b) Dirac massive neutrinos. c) Majorana neutrinos

In principle, one might investigate whether neutrinos are Majorana particles searching for reactions like $\nu_\mu + N \rightarrow \mu^+ + N'$. However, the factor $(m/E_\nu)^2$ in the cross section, for energies of the order of GeV (to be above threshold) is as small as 10^{-20} , making the detection impossible. There is however a possibility, the neutrino-less double-beta decay.

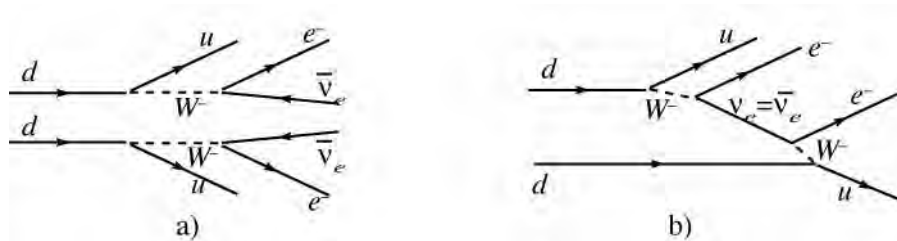


Fig. 15. Feynman diagrams for a) the $2\nu 2\beta$ decay and b) $0\nu 2\beta$ decay

As it is well known, beta decay is energetically forbidden for even-even nuclei. The open channel is a second order weak process, the two-neutrino double beta ($2\nu 2\beta$) decay, in which two nucleons experience beta decay contemporarily, $(A, Z) \rightarrow (A, Z+2) + 2\bar{\nu}_e + 2e^-$. The underlying process at the quark level is shown in Fig. 15a).

The extremely long $2\nu 2\beta$ half-lives of several nuclei have been measured. For example, it is for ^{76}Ge $150 \pm 10 \cdot 10^{19}$ yr, for ^{100}Mo , $0.71 \pm 0.04 \cdot 10^{19}$ yr and for ^{130}Te , $90 \pm 10 \cdot 10^{19}$ yr.

If neutrinos are Majorana particles, the neutrino-less double beta ($0\nu 2\beta$) decay, $(A, Z) \rightarrow (A, Z+2) + 2e^-$, is possible. It is shown at the quark level in Fig. 15b). The process violates the lepton number by two units.

The matrix element in Fig. 15b) can be reliably calculated in terms of the relevant element of the mass matrix of the three neutrinos, called Majorana mass, M_{ee}

$$M_{ee} = \sum_i U_{ei}^2 m_i = c_{13}^2 c_{12}^2 m_1 + c_{13}^2 s_{12}^2 m_2 e^{i\alpha} + s_{13}^2 m_3 e^{i\beta}$$

It is the sum of three addenda, one for each neutrino mass eigenstate. Notice that cancellations may happen between them due to the (unknown) phase factors.

The measured quantity is the half-life, related to the Majorana mass by the equation

$$T_{1/2}^{-1} = G_Z(Q_{\beta\beta}) |M^{0\nu}|^2 M_{ee}^2$$

where G_Z is the phase space volume, depending on the nucleus, which is calculated without uncertainties and $M^{0\nu}$ is the “nuclear matrix element”. Much progress has recently been done in understanding the nuclear physics effects and the present uncertainties have been reduced to a factor 2-3.

Notice that the differences between initial and final nuclear levels have been accurately measured. Consequently, the sum of the two electrons energies, called $Q_{\beta\beta}$ (which is typically a few MeV), is known, usually within a fraction of a keV.

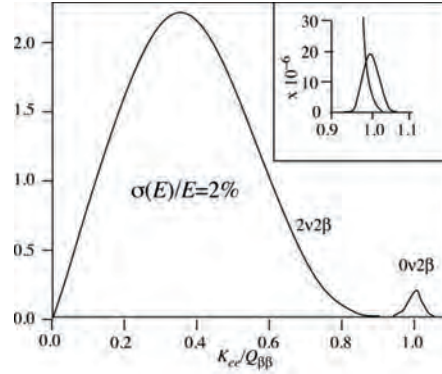


Fig. 16. Sum energy spectrum in the double beta decay

Fig. 16 shows schematically the spectrum of the sum energy: the continuous part is the $2\nu 2\beta$ decay, the small peak the $0\nu 2\beta$, if it exists. Clearly, its size is not known, but its position is. In practice, other backgrounds are present. The “background index” b , in the region of interest, is the number of counts per unit exposure time, per unit detector mass and unit energy interval. The lowest background index in the last generation experiments has been $b=10^{-1} \text{ yr}^{-1} \text{ kg}^{-1} \text{ keV}^{-1}$. The present generation aims to improve to $b=10^{-2}-10^{-3} \text{ yr}^{-1} \text{ kg}^{-1} \text{ keV}^{-1}$.

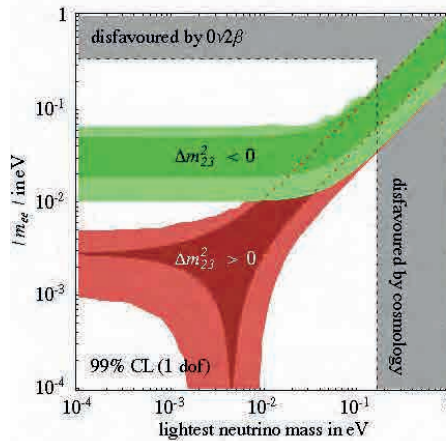


Fig. 17. M_{ee} vs. lightest neutrino mass

The sensitivity of an experiment with background index b , sensitive mass M , live time T and energy resolution (FWHM) ΔE to M_{ee} scales as the figure of merit $F_M = \left(\frac{MT}{b\Delta E} \right)^{1/4}$. The fourth-root dependence implies that to gain, for example, an order of magnitude in the Majorana mass the sensitive mass must be increased by four orders of magnitude, if the background index is constant! If however the background is zero (or almost so), the figure of merit scales as $F_M \propto \sqrt[4]{MT}$. Another important parameter is the energy resolution. The region of interest of the spectrum has a width of the order of ΔE .

Moreover, the energy resolution is the only way to reduce the tail of the $2\nu 2\beta$ decay under the peak, as shown in the insert of Fig. 16. It can be shown that, for a given ratio of the two half lives, the signal to

(this) background ratio is $\frac{S}{B} \approx \frac{m_e Q_{\beta\beta}^5}{7(\Delta E)^6} \frac{T_{1/2}^{2\nu}}{T_{1/2}^{0\nu}}$, which depends on the 6th power of the energy resolution.

In conclusion, background free condition and energy resolution are the key features.

Fig 17 shows M_{ee} as a function of the lightest neutrino mass as calculated by Feruglio, Strumia & Vissani (2002) for the two signs of Δm^2 .

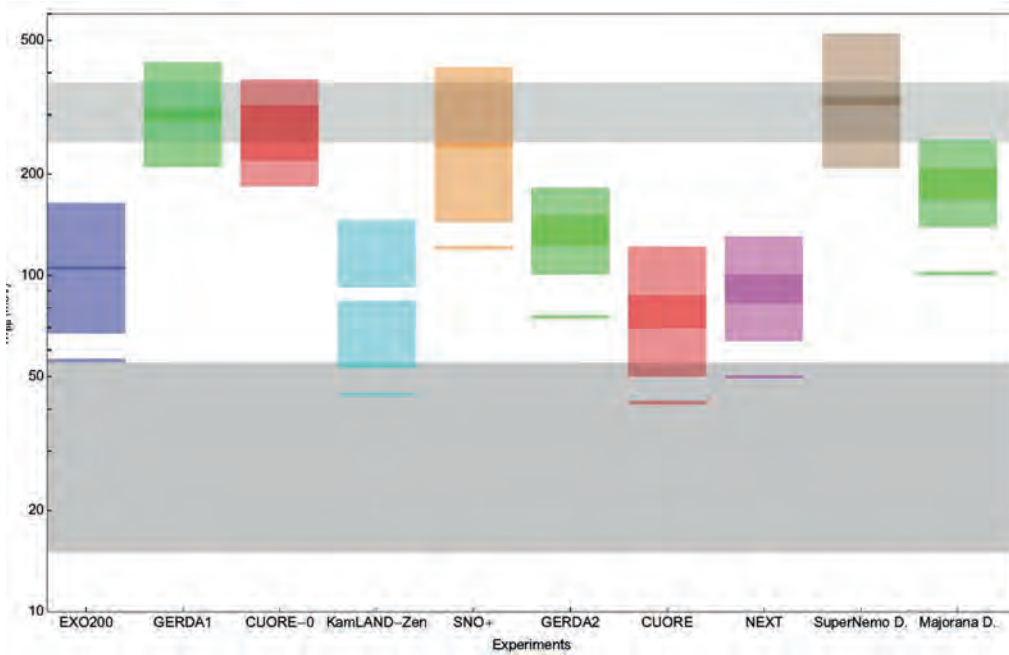


Fig. 18. From Gómez-Cadenas et al (2012). Sensitivity of the different experiments to M_{ee} computed assuming a 5 years exposure, proper intervals for the nuclear matrix elements and for both “optimistic” and “pessimistic” experimental parameters (see reference). A sensitivity line corresponding to a 10 years exposure, and to the most optimistic NME and experimental parameter set, is also shown

To fix the orders of magnitude consider the three nuclei employed by the experiments that just started running, EXO and KAMLand-Zen with (85%) enriched ^{136}Xe , GERDA-1 with (85%) enriched ^{76}Ge , or ready to do so, CUORE-0 with natural TeO_3 (the active ^{130}Te isotope abundance is 34%). At $M_{ee}=50$ meV, even with a very large exposure of 1 t yr, the numbers of expected signal events are small: 4.3, 4 and 2.5 respectively. These numbers should be compared with the expected background in the region of interest, namely the product $b \Delta E$. ΔE is 100 keV for EXO, 250 keV for KAMLand-Zen, 5 keV for CUORE and 4 keV for GERDA-1. The background indexes are not yet well known, given the initial phases of all the experiments; estimates range, in units $10^{-3}/(\text{kg keV yr})$, between 1 and 300.

A review of the present status of the search for double beta decay by Gómez Cadenas et al. (2012) has been recently published. Fig. 18 gives their estimate of the sensitivities of the next generation experiments, within a range of uncertainty due to both experimental unknown parameters and nuclear matrix elements.

6. Conclusions

More than half a century is passed since the discovery of the first neutrino and more than 80 since the desperate hypothesis of Pauli. When the second neutrino was discovered, 50 years ago, the search for the third lepton family started. I hope to have given some flavour of the fascinating discoveries in neutrino physics.

Neutrinos are indeed the most elusive of the known particles and have always in store for us unpredicted properties. The first window on new physics, beyond the Standard Model, was opened in neutrino physics. It started in underground laboratories in the late 1960s with the solar neutrino puzzle, even before the Standard Model was established.

On the other hand, the difficulties of neutrino experiments have often induced premature enthusiasms, under evaluating the systematic uncertainties, over stressing the statistical significance, un-accounting for hidden experimental effects, etc. Examples are the 17 keV neutrino, the negative electron neutrino mass squared, the eV mass neutrinos, the recent two-sigma-or-so effects leading to sterile neutrinos, and more, till now.

Neutrino experiments are very difficult, but we have still a lot to learn from them.

References

- Agafonova, N. et al. Observation of a first ν_τ candidate in the OPERA experiment in the CNGS beam. *Phys. Lett. B* **691** 138-145 [arXiv: 1006.1623v1]
- Alles Borelli, V. et al. (1970). Limits on electromagnetic production of heavy leptons; *Nuovo Cimento Lett.* **4** 1156
- Anderson, C. D. & Neddermeyer, S. H. (1937); Note on the nature of cosmic particles. *Phys. Rev.* **51** 884; Cosmic-ray particles of intermediate mass. *Phys. Rev.* **54** (1938) 88
- Bernardini, M. et al. (1967); A proposal to search for leptonic quarks and heavy leptons produced by ADONE. INFN/AE-67/1, 20 March 1967
- Bettini, A. (2008). Introduction to elementary particle physics. Cambridge University Press. Cambridge UK
- Buhler, A. (1965). Range measurements for muons in the GeV region. *Nuovo Cimento* **35** 759
- Conversi, M. et al. (1947); On the disintegration of negative mesons; *Phys. Rev.* **71** 209 (L)
- Conversi, M. et al. (1963); Search for time-like structure of the proton. *Phys. Lett.* **5** (1963) 195
- Conversi, M. et al (1964). Proton antiproton annihilation into muon pairs. *Proceedings of the International Conference on High Energy Physics 1964*. Atomizdat, Moskow, 1966. Vol I, 857
- Conversi, M. et al (1965), The leptonic annihilation modes of the proton antiproton system at 6.8 (GeV/c)^2 time-like four-momentum transfer. *Nuovo Cimento* **40** 690
- Cowan, C. L. et al. (1956). Detection of the Free Neutrino: A Confirmation, *Science* **124**, 103
- Danby, G. et al. (1962); Observation of High-Energy Neutrino Reactions and the Existence of Two Kinds of Neutrinos. *Phys. Rev. Lett.* **9** 36
- Elsner, K. et al. (1998). The CERN neutrino beam to Gran Sasso (NGS): conceptual technical design. CERN-98-02 ; INFN-AE-98-05
- Ereditato, A, Niwa, K. and Strolin, P. (1997), INFN/AE-97/06, DPNU-97-07; H. Shibuya et al., CERN-SPSC-97-24, LNGS-LOI-8-97
- Feruglio, F., Strumia, A. and Vissani, F.; Neutrino oscillations and signals in β and $0\nu 2\beta$ experiments. *Nucl. Phys. B* **637** (2002) 345
- Fogli, G.L., et al. (2011). Evidence of $\theta_{13} > 0$ from global neutrino data analysis. *Phys. Rev. D* **84** 053007 (ArXiv: 1106.6028 v2)
- Gómez-Cadenas, J. J. (2012). The search for neutrinoless double beta decay. *Riv. Nuovo Cimento* **35** 29
- Kayser, B. (2008). Neutrino mass, mixing and flavour change; arXiv hep-ph 0211134
- Kodama, K. et al. (2001); Observation of tau neutrino interactions. *Phys. Lett. B* **504** 218
- Majorana, E. (1937). Teoria simmetrica dell'elettrone e del positrone *Nuovo Cimento*, **5** 171
- Massam, T. (1965). A new electron detector with high rejection power against pions. *Nuovo Cimento* **39** 464. See also CERN-63-26. Nuclear Physics Division, June 27, 1963
- Perl, M. L. et al. (1975); Evidence for anomalous lepton production in e^+e^- annihilation. *Phys. Rev. Lett.* **35** 1489
- Perl, M. L. et al. (1976); Properties of anomalous $e\mu$ events produced in e^+e^- annihilation. *Phys. Lett.* **63B** 466
- Perl, M. L. et al. (1977); Properties of the proposed τ charged lepton. *Phys. Lett.* **70B** 487
- Street, J. C. & Stevenson, E. C. (1937); New Evidence for the Existence of a Particle of Mass Intermediate Between the Proton and Electron. *Phys. Rev.* **52** 1003 (L)
- Thomson, J. J. (1897). Cathode rays. *Phil. Mag.* **44**, 293
- C.S.Wu et al. (1997); The Origin of the Third Family, *World Scientific Series in 20th Century Physics – Vol.20* In Honour of A. Zichichi on the XXX Anniversary of the Proposal to Search for the Third Lepton at ADONE.

STATUS AND RESULTS OF THE LVD EXPERIMENT

■ PAOLO GIUSTI

1 Introduction and generalities

The sudden appearance of a new bright star in the otherwise immutable sky was observed since ancient times. The study of historical records worldwide allows to identify 6 such events as supernova explosions occurred in our Galaxy, the first one recorded by Chinese astronomers in 185 AD, the last one observed in Europe in 1604 and studied in detail by Kepler.

In the XXth century nuclear and particle physics made possible the early recognition of the role of nuclear fusion reactions and neutrinos in the stellar evolution and in particular in the gravitational core collapse of massive stars where neutrinos are thought to be the instrumental in causing the final supernova explosion.

Stars are maintained in a quasi equilibrium state by the opposite effects of the gravity's pull and of the energy released by the nuclear reaction that fuse the hydrogen in the star core into helium. When most of the hydrogen in the core has been burned the fusion reaction stops, the core contracts and its temperature increases. If the star is massive enough the core temperature become so high that the fusion of helium into carbon starts and the quasi equilibrium state is reconstituted. Massive stars, $M > (6 \div 10) M_{\text{SUN}}$, can repeat this process in a succession of increasingly shorter and more violent steps, producing heavier and heavier elements until they reach a structure where an iron core is surrounded by shells of lighter elements. Since ^{56}Fe is the most stable nucleus no further exothermic nuclear fusion reactions are possible. The iron core contracts and if its mass overcomes the Chandrasekhar limit it collapses until nuclear matter density is reached. The collapse gets halted and a rebound shock wave is generated that propagates outward through the core and eventually causes the supernova explosion leaving a remnant neutron star. From the start of the collapse to the cooling of the resulting neutron star the most of the gravitational binding energy (a few 10^{53} erg) is carried away by neutrinos and antineutrinos of all species in a time interval estimated to be a few tens of seconds. That's why neutrinos are thought to have a fundamental role in causing the supernova explosion.

At 7:36 (UT) of 23 February 1987 a neutrino signal from a stellar core collapse occurred 170.000 years ago in the Large Magellanic Cloud (an irregular small galaxy not too far from the Milky Way) was detected by several experiments: Kamiokande II (20 events), IMB (8 events), Baksan (6 events) and perhaps LSD (Costantini et al. 2004).

As the cross section of the reaction ($\bar{\nu}_e p, n e^+$) is by far the largest of those detectable by the experiments one can assume that basically all the observed events were due to $\bar{\nu}_e$. Neglecting neutrino oscillation effects the SN1987A observation suggests a reasonable agreement with theoretical expectations in terms of the duration of emission, the total amount of energy released in $\bar{\nu}_e$ and their mean energy.

However, due to a number of puzzling features present in the data, no firm conclusions can be drawn from this first landmark observation of extragalactic neutrinos, the only one detected so far.

On the other hand also the theoretical models need to be improved since they have problems in reproducing the supernova explosion (the shock wave dissipates most of its energy in the photodisintegration of the iron core) and the production of elements heavier than iron.

The experimental data needed to improve the theoretical understanding have to come from the measurements performed in the occasion of the next galactic gravitational stellar collapse. Considering the expected rate of these events ($2 \pm 1 / 100$ years) and the experimental difficulties in measuring the energy, flux, flavor of the neutrinos in the various phases of the collapse, this is not an easy task and certainly different experiments using different neutrino detection techniques are required. Table I shows the experiments capable to detect a galactic supernova presently in operation; the neutrino detection techniques are also shown together with mass, expected events number and status.

Detector	Type	Location	Mass (kton)	Events @ 8 kpc	Status
Super-K	Water	Japan	32	8000	Running (SK IV)
LVD	Scintillator	Italy	1	300	Running
KamLAND	Scintillator	Japan	1	300	Running
Borexino	Scintillator	Italy	0.3	100	Running
IceCube	Long string	South Pole	600	10^6	Running
Baksan	Scintillator	Russia	0.33	50	Running
Mini-BOONE	Scintillator	USA	0.7	200	Running
Icarus	Liquid argon	Italy	0.6	60	Running

Table I: Presently running experiment with supernova neutrino detection capabilities.

2 The LVD experiment

The Large Volume Detector (LVD), installed in the INFN Gran Sasso National Laboratory (Assergi, Italy) at a depth of 3600 m.w.e., is a 1 kt liquid scintillator detector whose main purpose is to detect and study neutrino bursts from galactic gravitational stellar core collapses. The experiment started taking data in June 1992 (Aglietta et al. 1992) and has continued without interruptions up to this date.

The LVD apparatus, schematically shown in Fig. 2.1, consists of 840 liquid scintillation counters, 1.5 m^3 each. Clusters of 8 counters are hosted into an iron support module which is in turn inserted in the overall LVD mechanical structure (not shown in figure). The 105 modules are distributed in the structure to form 3 separate identical arrays (named “towers”) each comprising 35 modules arranged in a matrix of 7 rows and 5 columns. Each tower has independent power supply, trigger and data acquisition systems.

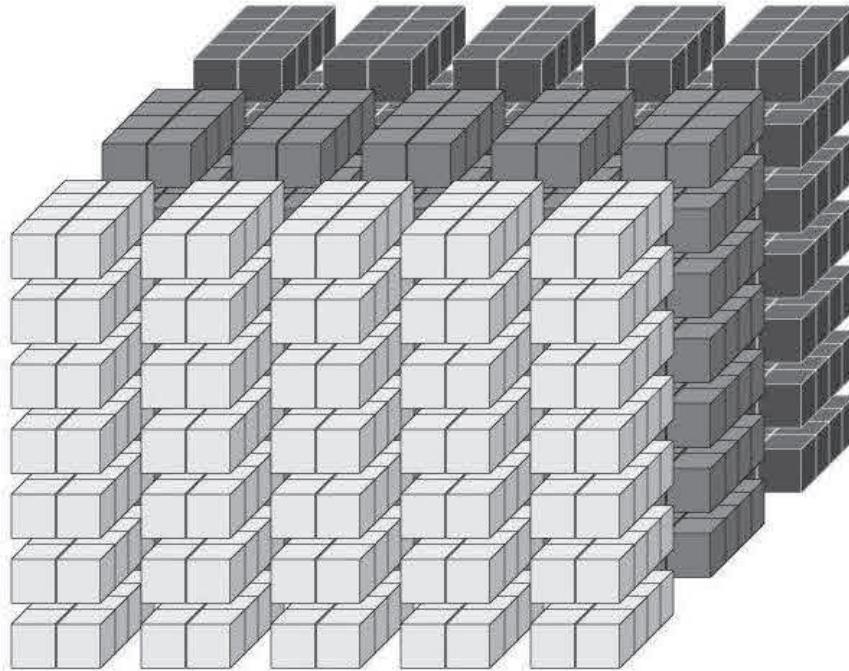


Fig. 2.1 Schematic view of the LVD apparatus.

Each counter is viewed from the top by three $\Phi=15$ cm photomultiplier tubes (PMTs) FEU49 or FEU125. The liquid scintillator is C_nH_{2n} with $\langle n \rangle = 9.6$ doped with 1g/l of PPO (scintillation activator) and 0.03 g/l of POPOP (wavelengthshifter). The liquid scintillator density is $\rho = 0.8 \text{ g/cm}^3$.

In addition to the liquid scintillator also the iron of the counters hosting modules (0.9 kt) contributes to the active mass of LVD since neutrino interactions in the iron can be detected in the scintillation counters.

The signals from the three PMTs of a counter are summed and the sum charge is digitized by a non linear 12 bit ADC (conversion time $1\mu\text{s}$). The time is measured with a relative granularity of 12.5 ns and an absolute one of 100 ns.

The modularity of the apparatus allows for calibration, maintenance and repair interventions without major negative interference with data taking and detector sensitivity. Fig. 2.2 shows the duty cycle (black) and the trigger active mass (red) of LVD from June 1992 to March 2011. From 2001 the experiment has been in very stable conditions with duty cycle $\geq 99\%$ and slightly increasing active mass. The active trigger mass limit (300 t) at which LVD can monitor the whole Galaxy for gravitational core collapses, is also shown (blue).

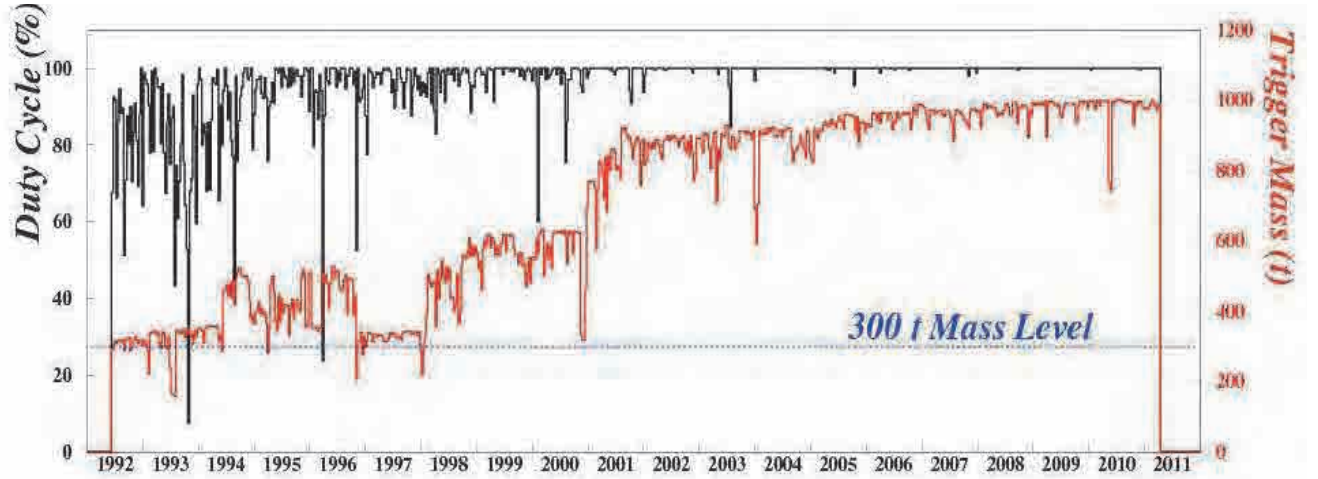


Fig. 2.2 – LVD Duty Cycle and Active Mass in the period June 1992 – June 2011.

The main LVD reaction is the inverse beta decay ($\bar{\nu}_e p, n e^+$) which gives two signals: a prompt one due to the e^+ followed by the signal from the neutron capture reaction ($np, d\gamma$) with mean capture time of about $185 \mu\text{s}$ and $E_\gamma = 2.2 \text{ MeV}$.

Charged and neutral current reactions due to the three neutrino species provide astrophysical informations on the nature of the collapse and are sensitive to intrinsic neutrino properties. They can give an important contribution to define some of the neutrino oscillation properties (Agafonova et al. 2007).

The trigger logic is optimized for the detection of both products of the inverse beta decay reaction and is based on the three-fold coincidence of a counter PMTs. Each PMT is discriminated at two different levels, $E_{\text{High}} \cong 4 \text{ MeV}$ and $E_{\text{Low}} \cong 0.5 \text{ MeV}$, resulting in two possible levels of coincidence between the three PMTs: High Energy Threshold (HET) and Low Energy Threshold (LET).

A HET coincidence signal in any counter represents the trigger condition for the 8 counters in the module. Once the trigger counter has been identified the charge of the 3 PMTs summed signals and the time of their coincidence are stored in a memory buffer. For all LET coincidences occurring in anyone of the 8 counters in the same module of the trigger counter within 1 ms from the trigger, the charge of the three PMTs summed signals and the coincidence time are also recorded.

Starting 1 ms after the occurrence of a trigger, the read out of the memory buffers, one per module, containing the charge and time information of both HET and LET signals, is performed independently on the three towers without introducing any dead time.

3 The LVD search for gravitational core collapses

To ensure the efficient monitoring of gravitational core collapses even in regions obscured to optical observation the LVD detector capability to identify a neutrino burst in the absence of an external trigger has been investigated. If optical observation is possible the prompt identification of the neutrino burst could then alert the astronomical community and allows the observation of a supernova explosion as near as possible to the onset.

The basis of the on-line search for neutrino bursts with LVD is the identification of clusters of HET triggers in a 10 s wide time window (Agafonova et al. 2008). As a first step the on-line monitor applies the following cuts to the data. The energy E of the scintillation counter pulses must be in the range $E_{\text{cut}} \leq E \leq 100 \text{ MeV}$, with two values for E_{cut} : 7 MeV and 10 MeV.

Events with signals in time coincidence within 200 ns in 2 or more counters are identified as muons and rejected.

Not properly working counters identified by their response to atmospheric or CNGS muons, are rejected. These counters are usually less the 5% and represent a steady loss of active mass requiring a maintenance intervention typically on the associated PMTs, ADC or TDC.

Counters with background rate $R \geq 3 \cdot 10^{-3} \text{ s}^{-1}$ for $E \geq 7 \text{ MeV}$ during the last two hours of operation are rejected as noisy. These counters are usually less than 2%. The problem is cured by maintenance intervention on the electronics or a new energy calibration.

The effect of the cuts on counters is to adjust dynamically the LVD active mass which is, as shown in Fig. 2.2, quite stable starting from 2001 when the detector reached its final configuration.

The average background counting rate of the whole LVD array is then typically $f_{\text{bk}} = 0.2 \text{ Hz}$ with $E_{\text{cut}} = 7 \text{ MeV}$ and $f_{\text{bk}} = 0.03 \text{ Hz}$ with $E_{\text{cut}} = 10 \text{ MeV}$.

After this selection procedure the time distribution of the HET triggers is well described by the Poisson statistics as can be seen in Fig. 3.1, where the time difference between successive signals is shown and in Fig. 3.2 which shows the fluctuations f_5 of the 5 m counting rate, s_5 , with respect to the average value measured in a time interval of 40 min, in units of the expected error σ_{exp} calculated assuming pure Poisson fluctuations:

$$f_5 = \frac{s_5 - \bar{s}_5}{\sigma_{\text{exp}}}$$

The experimental distribution, obtained during 100 days of operation is fitted with a Gaussian with mean equal zero and $\sigma = 1.01$ showing that the residual non-Poisson contribution to the fluctuations,

$$\sigma_{\text{res}} = \sqrt{\sigma^2 - 1}$$

is less than 15%.

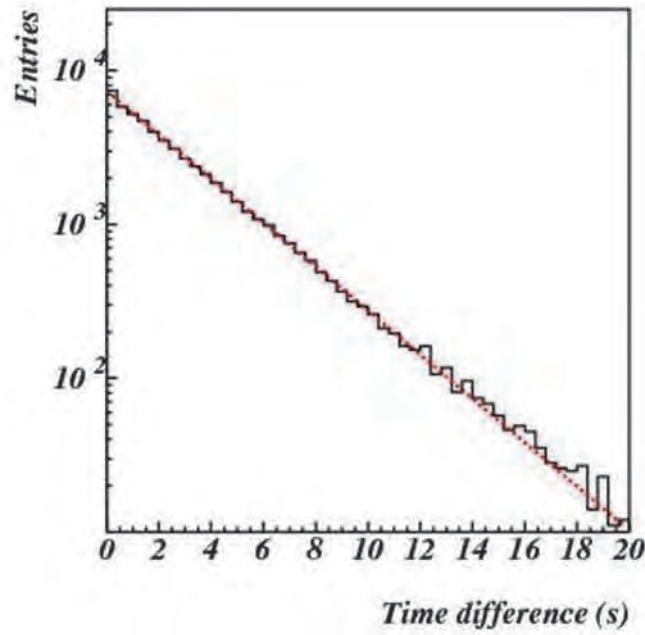


Fig. 3.1 Distribution of the difference of the arrival time between successive signals compared with Poisson expectations (red dotted line).

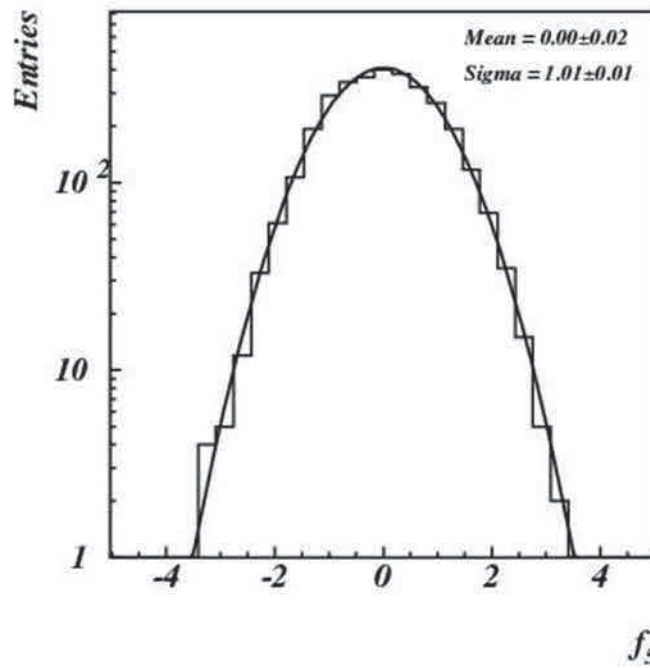


Fig. 3.2 Distribution of the fluctuations of the 5 minutes counting rate. The superimposed curve is the free parameter Gaussian fit.

As the time distribution of the background is purely statistical the candidate neutrino burst is simply characterized by the multiplicity of HET triggers detected in a time window, Δt . All other characteristics as detailed time structure, energy spectra, topological distribution of signals inside the detector can be left to a subsequent off-line analysis.

Each data period, T , is scanned through a “sliding window” with duration $\Delta t = 20$ s and is divided into $N = 2 \cdot T/\Delta t - 1$ intervals, each one starting in the middle of the previous one so that the unbiased time window is 10 s. The frequency of clusters of duration 20 s and multiplicity $\geq m$, i.e. the imitation threshold due to background is:

$$F_{im}(m, f_{bk}, 20) = N \cdot \sum_{k \geq m}^{\infty} P(k; 20 \cdot f_{bk}) \text{ events} \cdot \text{day}^{-1}$$

Where f_{bk} is the background counting rate (in Hz) of the detector for $E \geq E_{cut}$, $P(k; 20 \cdot f_{bk})$ is the Poisson probability to have clusters of multiplicity k if $(20 \cdot f_{bk})$ is the average background multiplicity and N is the number of trials per day.

As mentioned above the on-line search for neutrino burst candidates is performed for two values of the energy cut: $E_{cut} \geq 7$ MeV (with a corresponding $f_{bk} = 0.2$ Hz) and : $E_{cut} \geq 7$ MeV (with a corresponding $f_{bk} = 0.03$ Hz).

When LVD operates in standalone the imitation frequency threshold to identify on-line a cluster as a neutrino burst candidate is set to 1 event in 100 years. Since 2005 LVD participates to the Supernova Early Warning System (SNEWS) an international collaboration including several experiments sensitive to galactic stellar gravitational core collapses (LVD, Borexino, SuperKamiokande, Ice-Cube) aiming to provide the worldwide network of observatories with a prompt and reliable alert generated by the coincidence of at least two of the participating experiments. In the framework of the SNEWS project the LVD imitation frequency threshold may then be relaxed to 1 event per month.

Less sensitive thresholds on F_{im} are used for monitoring purposes and as a test of the stability of the overall procedure. Fig 3.3 shows the rate of clusters with $F_{im} = 1/\text{day}$ as measured in the 5 years period from 2006 to 2010.

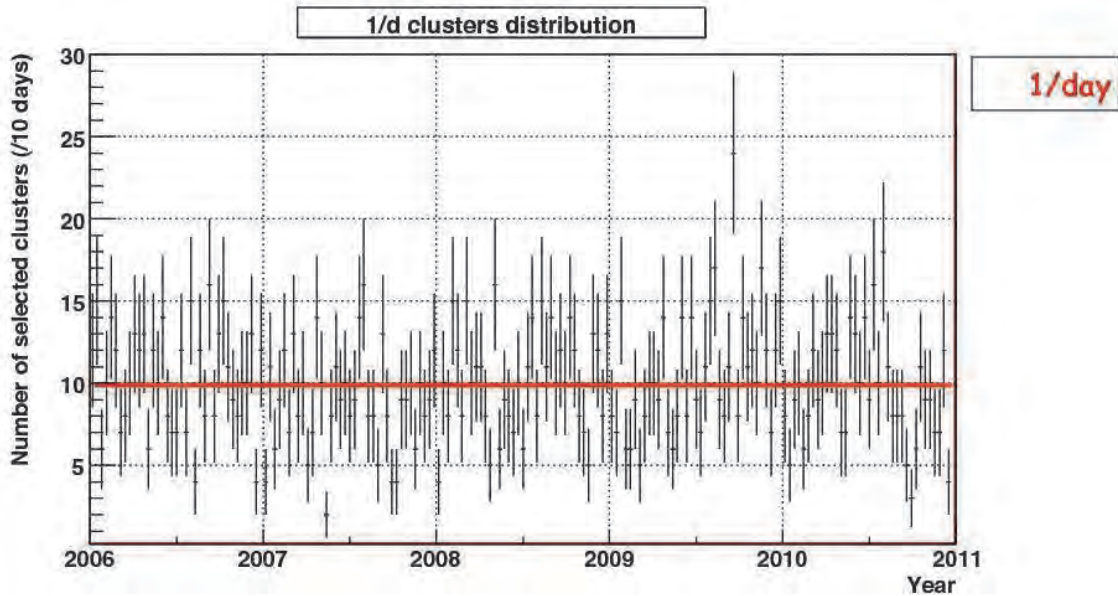


Fig. 3.3 The rate of clusters with 1/day imitation frequency from 2006 to 2010.

To determine the LVD on-line trigger efficiency we proceed as follows. For known values of f_{bk} , Δt and of the selected imitation frequency threshold, F_{im}^{thr} , we derive the minimum multiplicity value m_{min} of a cluster to be identified as a neutrino burst. The difference $(m_{min} - f_{bk} \cdot \Delta t)$ represents therefore the minimum number of neutrino interactions to produce a supernova alarm at the selected imitation frequency threshold. Assuming a model for the neutrino emission and propagation and taking into account the apparatus detection efficiency, we calculate the number of observed interactions and the detector trigger efficiency as a function of the source distance or as emitted neutrino flux can be derived.

As the astrophysical parameters of the Supernova mechanism are still not well defined we have adopted the following conservative values (Pagliaroli et al. 2009): average $\bar{\nu}_e$ energy $\langle E_{\bar{\nu}_e} \rangle = 14 \text{ MeV}$; total gravitational binding energy $E_b = 2.4 \cdot 10^{53} \text{ erg}$ and average non-electron neutrino energy 20% higher than $\bar{\nu}_e$.

Concerning neutrino oscillations we conservatively considered normal mass hierarchy and non-adiabaticity. Taking into account Poisson fluctuations in the cluster multiplicity, we derived the trigger efficiency shown in Fig. 3.4 as a function of the distance for LVD working in standalone and in Fig. 3.5 for LVD working in coincidence with other detectors.

We can conclude that, without introducing any further check on the time structure, energy spectra and neutrino flavor content of the signals in the cluster (which are postponed to the off-line analysis), LVD with an energy cut of $E_{cut} \geq 7 \text{ MeV}$ and $F_{im}^{thr} = \frac{1}{100} \text{ y}^{-1}$ is able to identify on-line neutrino bursts from gravitational stellar collapses occurring in the whole Galaxy ($D \leq 20 \text{ kpc}$) with efficiency $> 90\%$. Such a sensitivity is preserved in the same conditions even if the detector is running with only one third of its total mass. Due to the better signal to noise ratio introducing a cut on the visible energy at 10 MeV, the 90% LVD on-line trigger efficiency extends up to 50 kpc (corresponding to the Large Magellanic Cloud).

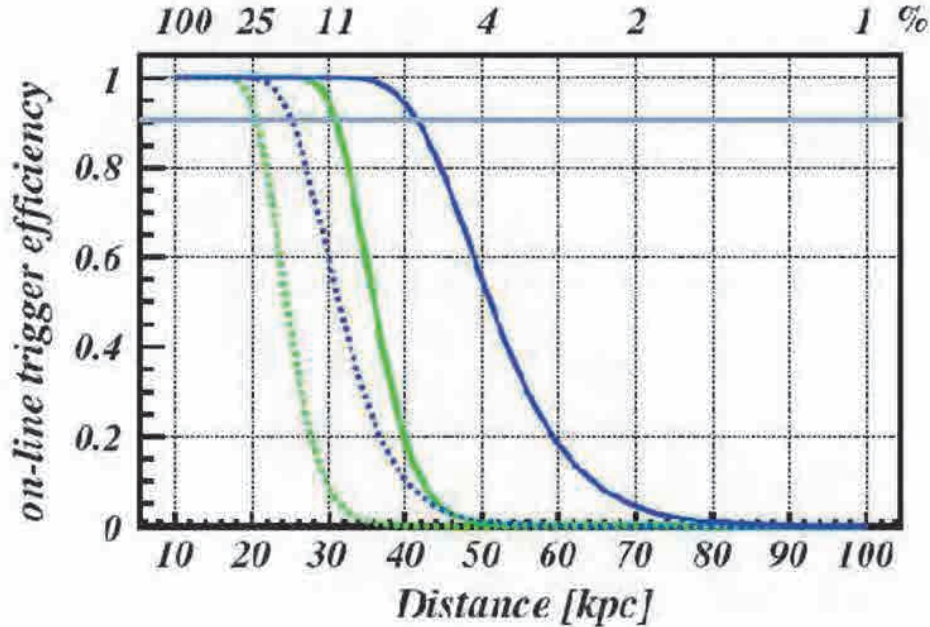


Fig. 3.4 Trigger efficiency versus distance (lower scale) and percentage of SN1987A signal at 10 kpc (upper scale) for $E_{cut} = 7 - 10 \text{ MeV}$ (light green and dark blue lines, respectively) $M = 300 \text{ t}$ (dotted) and 1000 (continuous) for LVD standalone ($F_{im} = 0.01/\text{year}$).

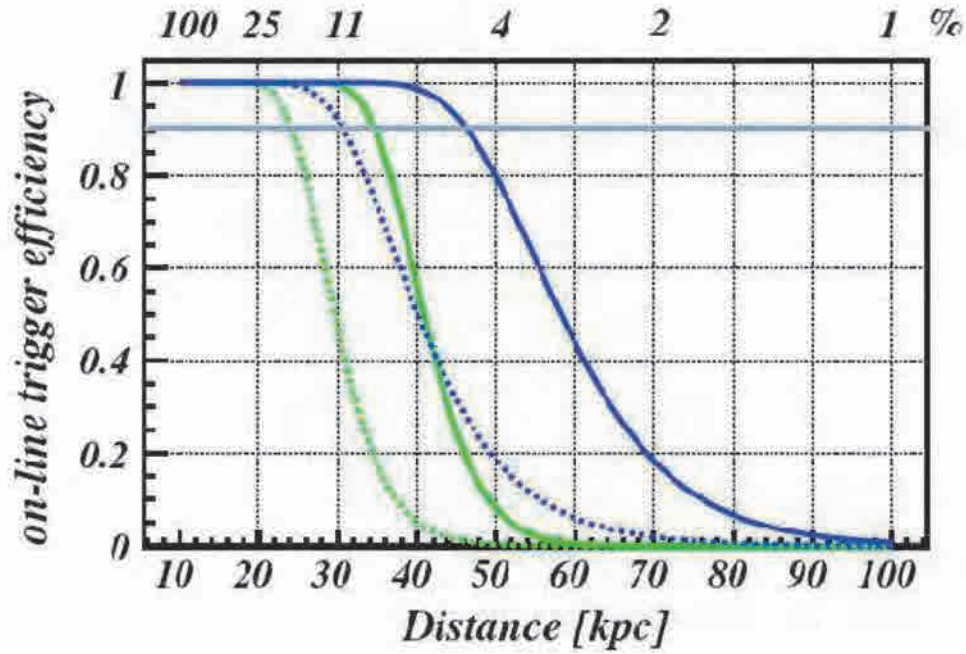


Fig. 3.5 Trigger efficiency versus distance (lower scale) and percentage of SN1987A signal at 10 kpc (upper scale) for $E_{\text{cut}} = 7 - 10$ MeV (light green and dark blue lines, respectively) $M=300$ t (dotted) and 1000 (continuous) for LVDin SNEWS ($F_{\text{im}} = 1/\text{month}$).

For what concerns the off-line analysis in addition to the selections already made at the on-line level applied with more refined calibrations, we search for clusters in time windows starting at each HET trigger and with a variable width (from 10 up to 100 s) and determine their imitation frequency F_{im} .

For all clusters with $F_{\text{im}} \leq 1/\text{day}$ a complete analysis is performed to test their consistency with a neutrino burst in terms of the topological distribution inside the LVD array, energy spectrum and time distribution of the HET signals in the cluster and time distribution of delayed LET pulses, signature of $\bar{\nu}_e$ interactions.

No candidates have been found since 1992, see detail in table II. The resulting LVD 90% c.l. upper limit to the rate of gravitational stellar collapses in the Galaxy ($D \leq 20$ kpc) is therefore 0.13 y^{-1} .

RUN	SINCE	TO	LIVETIME	DUTYCYCLE	MASS
1	06/06/1992	05/31/1993	285 days	60%	310 t
2	08/04/1993	03/11/1995	397 days	74%	390 t
3	03/11/1995	04/30/1997	627 days	90%	400 t
4	04/30/1997	03/15/1999	685 days	94%	415 t
5	03/16/1999	12/11/2000	592 days	95%	580 t
6	12/12/2000	03/24/2003	821 days	98%	842 t
7	03/25/2003	02/04/2005	666 days	>99%	881 t
8	02/04/2005	05/31/2007	846 days	>99%	936 t
9	05/31/2007	04/30/2009	669 days	>99%	967 t
10	05/01/2009	03/27/2011	696 days	>99%	981 t
Σ	06/06/1992	03/27/2011	6314 days		

Table II: LiveTime, Duty Cycle and Active Mass for the 10 LVD data taking runs from June 1992 to March 2011.

References

- Agafonova, N. Yu. et al. - LVD Collaboration. (2007). Study of the effect of neutrino oscillations on the supernova neutrino signal in the LVD detector. *Astroparticle Physics*, 27(4), 254-270.
- Agafonova, N. Yu. et al. - LVD Collaboration. (2008). On-line recognition of supernova neutrino bursts in the LVD detector. *Astroparticle Physics*, 28(6), 516-522.
- Aglietta, M., et al. - LVD Collaboration. (1992). The most powerful scintillator supernovae detector : LVD. *Nuovo Cimento A*, 105, 1793-1804.
- Costantini, M. L., Ianni, A. and Vissani, F. (2004). SN1987A and the properties of the neutrino burst. *Physical Review D*, 70(4), 043006-1,10.
- Pagliaroli, G., Vissani, F., Costantini, M. L., and Ianni, A. (2009). Improved analysis of SN1987A antineutrino events. *Astroparticle Physics*, 31(3), 163-176.

ORIGIN AND STATUS OF LUNA AT GRAN SASSO

■ CARLO BROGGINI

INFN – Padua, LUNA Collaboration

Abstract

The ultimate goal of nuclear astrophysics, the union of nuclear physics and astronomy, is to provide a comprehensive picture of the nuclear reactions which power the stars and, in doing so, synthesize the chemical elements. Deep underground in the Gran Sasso Laboratory the key reactions of the proton-proton chain and of the carbon-nitrogen-oxygen cycle have been studied down to the energies of astrophysical interest. The main results obtained in the past 20 years are reviewed and their influence on our understanding of the properties of the neutrino, the Sun, and the Universe itself is discussed. Finally, future developments of underground nuclear astrophysics beyond the study of hydrogen burning are outlined.

Introduction

Only hydrogen, helium and lithium are synthesized in the first minutes after the big-bang. The other elements of the periodic table are produced in the thermonuclear reactions taking place inside the stars. Nuclear astrophysics studies these reactions which provide also the power that allows the stars to shine over their lifetimes. In particular, the knowledge of the reaction cross-section at the stellar energies is the heart of nuclear astrophysics.

The reaction rate in the hot plasma of a star, with temperatures in the range of tens to hundreds of millions degrees, is obtained by weighting the reaction cross section $\sigma(E)$ with the energy distribution of the colliding nuclei: a Maxwell-Boltzmann $\Phi(E)$ peaked at energies of 1-10 keV. The product between $\Phi(E)$ and $\sigma(E)$ identifies the energy window where the reaction occurs in the star: the Gamow peak. At lower energies the cross section is too small, whereas at higher energies the nuclei in the tail of the Maxwell-Boltzmann are too few.

Inside the Gamow peak, which is far below the Coulomb energy arising from the repulsion between nuclei, the reaction can take place only due to the quantum mechanical tunnel effect and, as a consequence, the reaction cross section $\sigma(E)$ drops nearly exponentially with decreasing energy:

$$\sigma(E) = \frac{S(E)}{E} e^{-2\pi\eta(E)}$$

where $S(E)$ is the astrophysical factor (which contains the nuclear physics information) and $\eta(E)$ is the Sommerfeld parameter, given by $2\pi\eta = 31.29 \cdot Z_1 \cdot Z_2 \cdot (\mu/E)^{0.5}$. Z_1 and Z_2 are the charges of the interacting nuclei, μ is the reduced mass (in units of amu), and E is the center of mass energy (in units of keV). At low energies the cross sections are extremely small, because of the small probability to go through the Coulomb barrier. Such smallness makes the star life-time of the length we observe, but it also makes impossible the direct measurement in the laboratory.

The rate of the reactions, characterized by a typical energy release of a few MeV, is too low, down to a few events per year, in order to stand out from the laboratory background. Instead, the observed energy dependence of the cross-section at high energies is extrapolated to the low energy region, leading to substantial uncertainties. LUNA, Laboratory for Underground Nuclear Astrophysics, started twenty years ago to run nuclear physics experiments in an extremely low-background environment, the Gran Sasso Laboratory (LNGS), to reproduce in the laboratory what Nature makes inside the stars. As a matter of fact, the dolomite rock of Gran Sasso provides a natural shielding equivalent to at least 3800 meters of water which reduces the muon and neutron fluxes by a factor 10^6 and 10^3 , respectively.

LUNA at Gran Sasso

Two electrostatic accelerators able to deliver hydrogen or helium beam have been installed underground: first a compact 50 kV "home made" machine [1] and then a commercial 400 kV one [2]. Common features of the two accelerators are the high beam current, the long term stability and the precise beam energy determination. The first feature maximizes the reaction rate, the second is demanded by the long time typically needed for a cross section measurement, and the third is important because of the exponential energy dependency of the cross section.

In particular, the 400 kV accelerator is embedded in a tank, a cylinder of 0.9 m diameter and 2.8 m long, filled with an insulating mixture of N_2/CO_2 gas at 20 bar. The high voltage is generated by an inline Cockcroft-Walton power supply located inside the tank. The radio frequency ion source directly mounted on the accelerator tube can provide beams of 1 mA hydrogen and 500 μA He^+ over a continuous operating time of 40 days. The ions can be sent into one of two different, parallel beam lines (Fig.1), allowing the installation of two different target setups. In the energy range between 150 and 400 keV, the accelerator can provide up to 500 μA of hydrogen and 250 μA of helium at the target stations, with 0.3 keV accuracy on the beam energy, 100 eV energy spread, and 5 eV h^{-1} long-term stability.

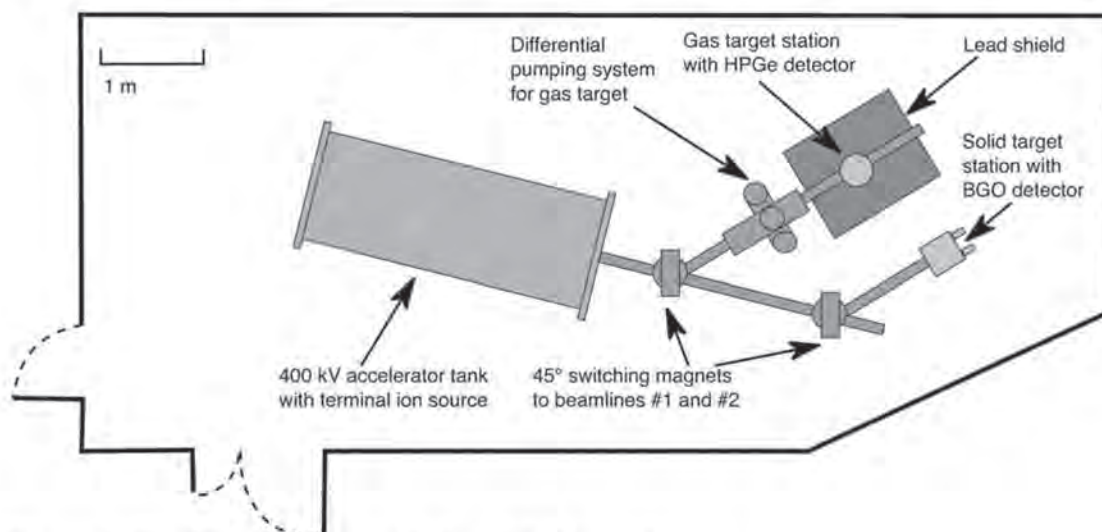


Figure 1: The LUNA set-up with the 400 kV accelerator.

Hydrogen Burning in the Sun

As the Sun mass contracted from an initially large gas cloud, half of the gravitational energy released was radiated into the space and half was converted into the kinetic energy of hydrogen and helium nuclei, thereby increasing the temperature of the system. At the central temperature of approximately 10 million degrees the kinetic energy of the hydrogen nuclei was high enough to penetrate the Coulomb barrier with significant probability and to switch on the hydrogen burning: $4^1\text{H} \rightarrow ^4\text{He} + 2e^+ + 2\nu_e$.

Since the mass of the helium nucleus is lower than four times the proton mass, approximately 0.7% of the hydrogen rest mass is converted into energy in each of the transmutations. Hydrogen fusion supplies the necessary energy to halt the contraction, it provides all the energy required for the long life of the Sun, and it produces neutrinos detectable on Earth.

The Sun is a middle-aged main-sequence star which began to burn hydrogen approximately 4.5 billion years ago. In another 5 billion years it will begin burning helium and will eventually turn into a celestial body consisting mainly of carbon and oxygen. In the central region of the Sun, at the temperature of 15 million degrees and at the density of 150 g cm^{-3} , hydrogen burning does not take place in one step but rather

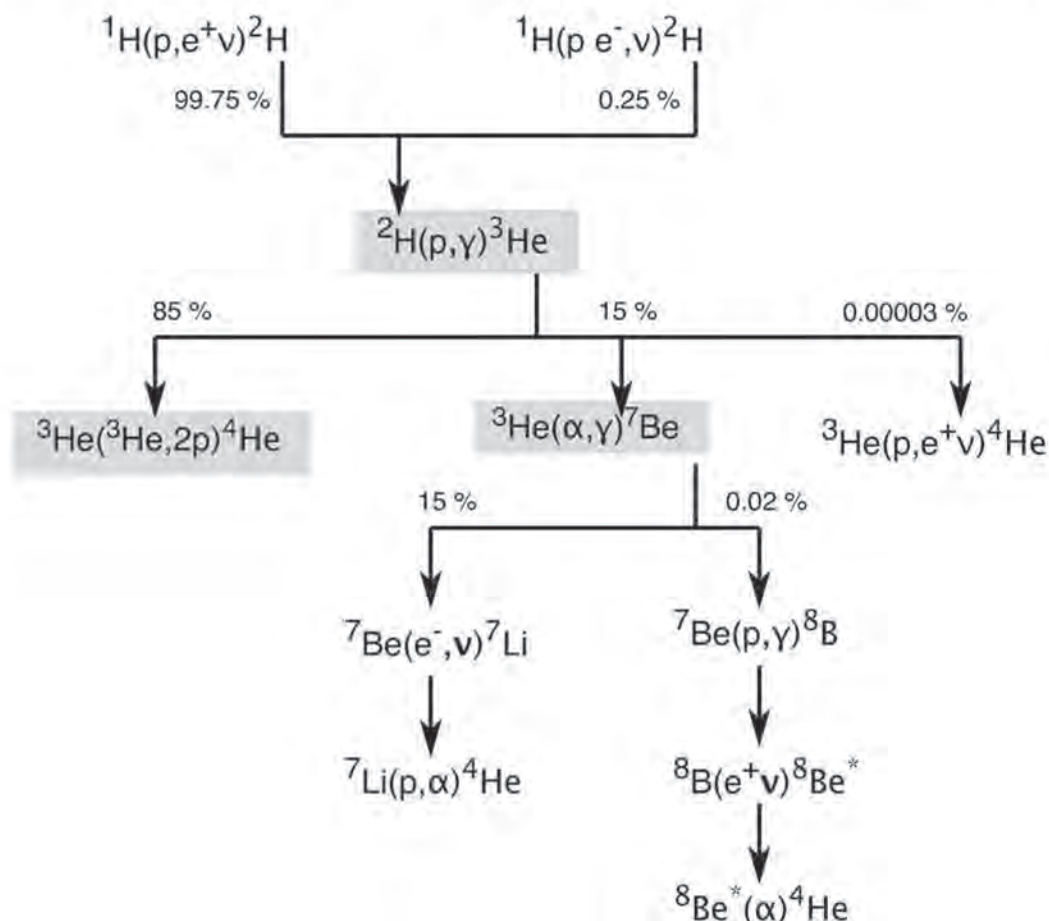


Figure 2: The proton-proton chain (pp) with the different branching ratios. The reactions studied by LUNA are highlighted.

proceeds through a sequence of two-body reactions: the proton-proton chain (Fig.2) and the CNO cycle. The relative importance of the different reactions is determined by the abundance of the nuclear species fusing together and by their fusion cross section at the Gamow peak energy. In particular, the pp chain is responsible for more than 99% of the luminosity of the Sun, whereas the CNO cycle accounts for less than 1% of nuclear energy production.

In 1964 both J.N. Bahcall and R. Davis proposed the detection of solar neutrinos in order to directly verify the hypothesis of nuclear-energy generation in stars and to study the inner region of the Sun.

The Solar Neutrino Problem and the Narrow Resonance

The initial activity of LUNA has been focused on the ${}^3\text{He}({}^3\text{He},2p){}^4\text{He}$ cross section measurement within the solar Gamow peak (15-27 keV). Such a reaction has a Q-value of 12.86 MeV and it is a key one of the pp chain. As a matter of fact, it is the most probable fate of ${}^3\text{He}$ in the Sun (85% of the fusions).

The hypothesis of a narrow (\sim keV) resonance in the cross section of ${}^3\text{He}({}^3\text{He},2p){}^4\text{He}$ at low energy was advanced at the beginning of the seventies as a solution to the solar neutrino problem. Such a resonance would have explained the observed ${}^8\text{B}$ solar neutrino flux, about a factor 3 lower than the predicted one. Fewer than 1 neutrino in 10000 comes from the ${}^8\text{B}$ decay. However, their relatively high end-point energy (about 15 MeV) makes their detection much less difficult; unsurprisingly, ${}^8\text{B}$ neutrinos are the best studied neutrinos from the Sun. The resonance would have further enhanced the relative contribution of ${}^3\text{He}({}^3\text{He},2p){}^4\text{He}$, and the flux of the ${}^8\text{B}$ neutrinos, generated in the branch starting with ${}^3\text{He}(\alpha,\gamma){}^7\text{Be}$, would have been suppressed.

The final set-up was made of eight 1 mm thick silicon detectors of $5\times 5\text{ cm}^2$ area placed around the beam inside the windowless target chamber filled with ${}^3\text{He}$ at the pressure of 0.5 mbar. The simultaneous detection of two protons has been the signature which unambiguously identified a ${}^3\text{He}({}^3\text{He},2p){}^4\text{He}$ fusion reaction.

Figure 3 shows the results from LUNA [3] together with the ones from a recent higher energy measurements. For the first time a nuclear reaction has been measured in the laboratory at the energy occurring in a star. Its cross section varies by more than two orders of magnitude in the measured energy range. In particular, at the lowest energy of 16.5 keV it has the value of 0.02 pbarn, which corresponds to a rate of about 2 events/month, rather low even for the "silent" experiments of underground physics.

No narrow resonance has been found within the solar Gamow peak and the astrophysical solution to the solar neutrino problem based on its existence has been definitely ruled out. We now know that the solution to the problem lies in the nature of the neutrino itself: it oscillates. Produced inside the Sun as an electron neutrino it may become a muon or tau neutrino by the time it reaches the Earth.

${}^3\text{He}(\alpha,\gamma){}^7\text{Be}$ (Q-value: 1.586 MeV), the competing reaction for ${}^3\text{He}$ burning, has been also studied in LUNA. The cross section of this reaction can be obtained by using two different experimental approaches: the measurement of the prompt γ rays and the detection of the delayed γ rays from ${}^7\text{Be}$ decay. Both techniques have been simultaneously employed underground, obtaining results in excellent agreement with each other. Thanks to the LUNA measurement the uncertainty on the ${}^7\text{Be}$ solar neutrino

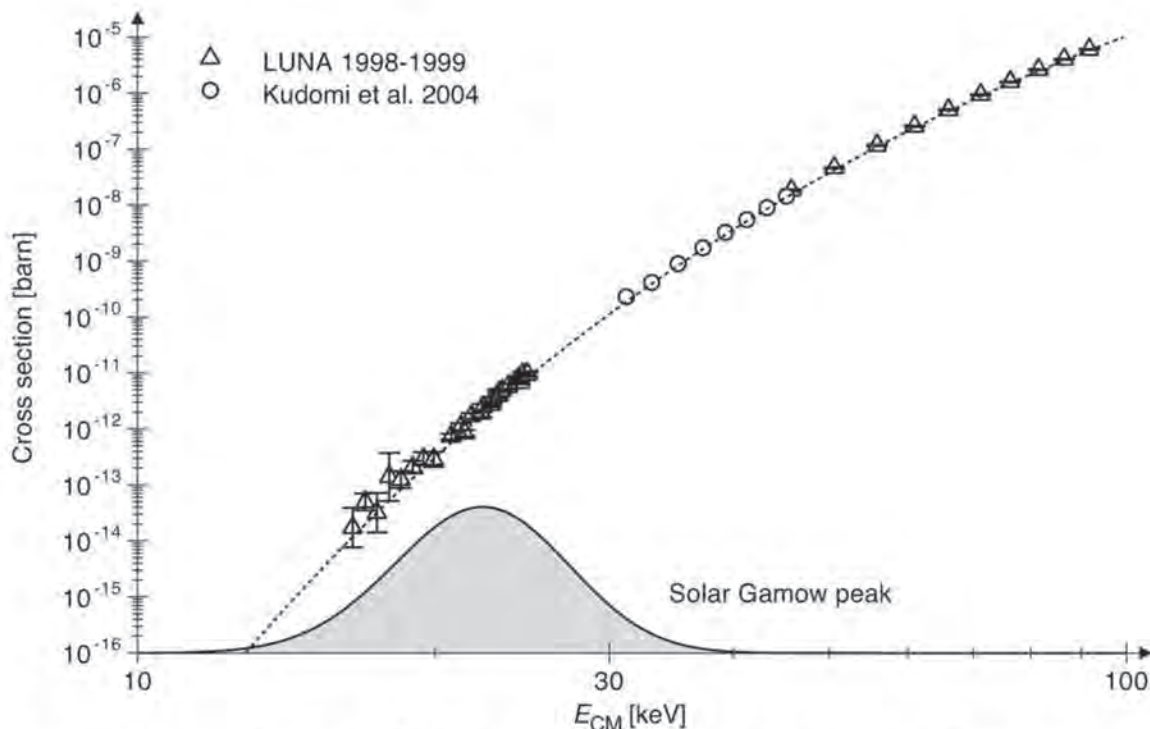


Figure 3: The cross section of ${}^3\text{He}({}^3\text{He},2p){}^4\text{He}$ as function of the centre of mass energy.

flux went from 9.4% down to 5.5% [4,5]. The 0.86 MeV ${}^7\text{Be}$ neutrinos are the second largest component of the spectrum, amounting to 7% of the total and they have been very recently measured by Borexino with 5% error. The dominant component of the total neutrino flux (92%) are the neutrinos coming from ${}^1\text{H}(p,e^+\nu){}^2\text{H}$. However, their continuous spectrum has an end-point energy of 0.42 MeV, which makes their detection extremely difficult and only possible, till now, in the radiochemical experiments with Gallium (Gallex/GNO and Sage).

The Metallicity of the Sun and the Age of the Universe

In the CNO cycle the conversion of hydrogen into helium is achieved with the aid of carbon and nitrogen previously synthesized in older stars (Fig.4). Carbon and nitrogen work as catalysts and they are not destroyed. ${}^{14}\text{N}(p,\gamma){}^{15}\text{O}$ (Q-value: 7.297 MeV) is the bottleneck reaction of the cycle and it rules its energy production rate. In particular, it is the key reaction to know the ${}^{13}\text{N}$ and ${}^{15}\text{O}$ solar neutrino flux, which depends almost linearly on its cross section. The CNO neutrinos have end-point energies of 1.20 MeV (${}^{13}\text{N}$) and 1.73 MeV (${}^{15}\text{O}$) and they are a fraction of the total neutrino flux equal to the relative contribution of the CNO cycle to the luminosity of the Sun (less than 1%).

In the first phase of the LUNA study, data have been obtained down to 119 keV energy with solid targets of TiN and a germanium detector. This way, the five different radiative capture transitions which contribute to the cross section of ${}^{14}\text{N}(p,\gamma){}^{15}\text{O}$ at low energy were measured. The total cross section was then studied down to very low energy in the second phase of the experiment by using the 4π BGO summing detector placed around a windowless gas target filled with nitrogen at 1 mbar pressure.

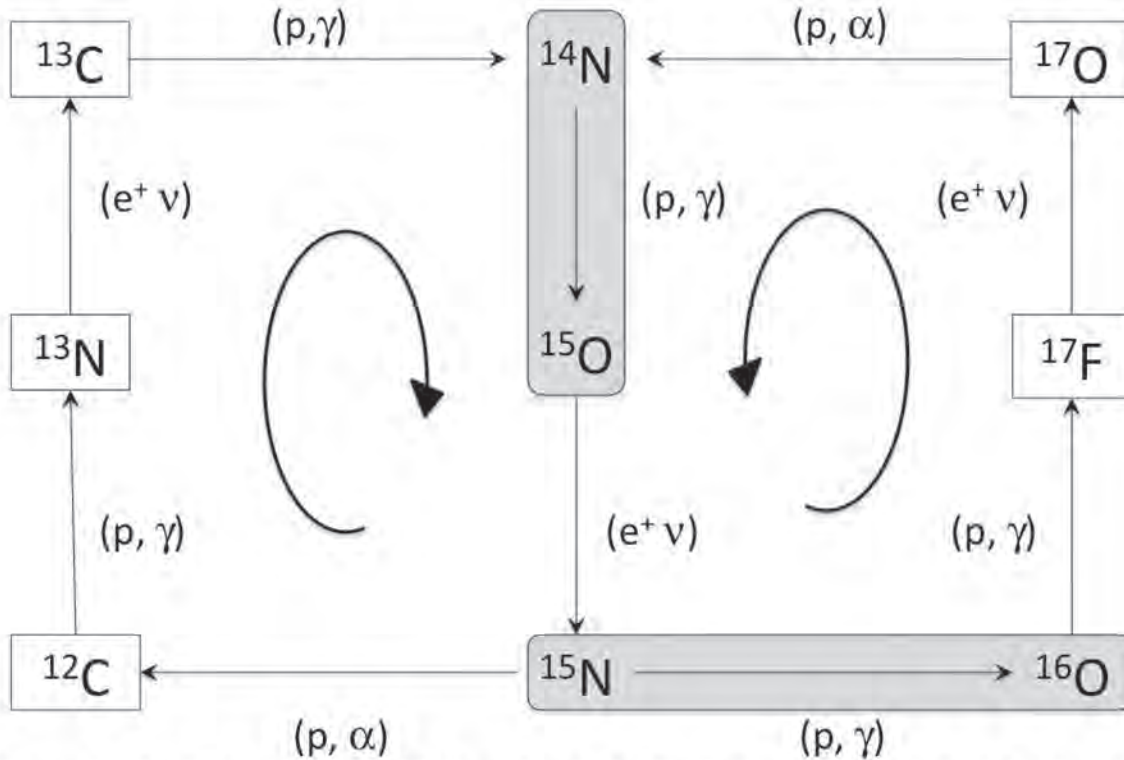


Figure 4: The first and second CNO cycles. Only the first cycle is important for the Sun because $^{15}\text{N}(p,\gamma)^{16}\text{O}$ has a cross section which is a factor 2000 lower than $^{15}\text{N}(p,\alpha)^{12}\text{C}$. The reactions studied by LUNA are highlighted.

At the lowest center of mass energy of 70 keV a cross section of 0.24 pbarn was measured, with an event rate of 11 counts/day from the reaction. The results obtained both with the germanium detector [6] and with the BGO set-up [7] were about a factor two lower than the existing extrapolation [8] from previous data at very low energy (Fig.4). As a consequence, the CNO neutrino yield in the Sun is decreased by about a factor two.

In order to provide more precise data for the ground state capture, the most difficult one to be measured because of the summing problem, we performed a third phase of the $^{14}\text{N}(p,\gamma)^{15}\text{O}$ study with a composite germanium detector. This way the total error on the S-factor has been reduced to 8%: $S_{1,14}(0)=1.57\pm0.13$ keV barn [9]. This is significant because, finally solved the solar neutrino problem, we are now facing the solar composition problem: the conflict between helioseismology and the new metal abundances (i.e. the amount of elements different from hydrogen and helium) that emerged from improved modeling of the photosphere [10].

Thanks to the relatively small error on $S_{1,14}$, it will be possible in the near future to measure the carbon and nitrogen content of the Sun core by comparing the predicted CNO neutrino flux with the measured one. As a matter of fact, the CNO neutrino flux, which almost linearly depends on the carbon and nitrogen content of the solar core where fusion reactions take place, is decreased by about 30% in going from the high to the new low metallicity scenario. This way it will be possible to test whether the early Sun was chemically homogeneous [11], a key assumption of the standard solar model.

$^{14}\text{N}(p,\gamma)^{15}\text{O}$ plays also a key role in determining the age of the globular clusters, which are the oldest stellar populations of a galaxy. The age is obtained from the luminosity of the turn off point in the Hertzsprung-Russell diagram of the cluster, which in turn depends on the $^{14}\text{N}(p,\gamma)^{15}\text{O}$ cross section (a star at the turn off is burning hydrogen through the CNO cycle). The age of the clusters give then a lower limit to the age of the Universe. In particular, this limit is increased by 0.7-1 billion years [12] up to 14 billion year as a consequence of the factor 2 reduction measured by LUNA on the $^{14}\text{N}(p,\gamma)^{15}\text{O}$ cross section.

The lower cross section also affects stars that are much more evolved than the Sun. In particular, the dredge up of carbon to the surface of asymptotic giant branch stars is much more efficient [13].

$^{14}\text{N}(p,\gamma)^{15}\text{O}$ is an excellent example to explain why physicists have been studying for years these reactions which have such extremely small cross sections. From the nuclear point of view they are often of modest interest. It is the application to astrophysics, and to so many different astrophysical scenarios, which makes them so fascinating.

Hydrogen Burning at High Temperature

The solar phase of LUNA has reached the end. A new and rich program of nuclear astrophysics mainly devoted to CNO, Mg-Al and Ne-Na cycles has already started with the measurement of $^{15}\text{N}(p,\gamma)^{16}\text{O}$ [14] and $^{25}\text{Mg}(p,\gamma)^{26}\text{Al}$ [15]. Due to the higher Coulomb barrier of the reactions involved, these cycles become important at temperature higher than the one of our Sun: hydrogen burning in the shell of massive stars and Novae explosions. Relatively unimportant for energy generation, these cycles are essential for

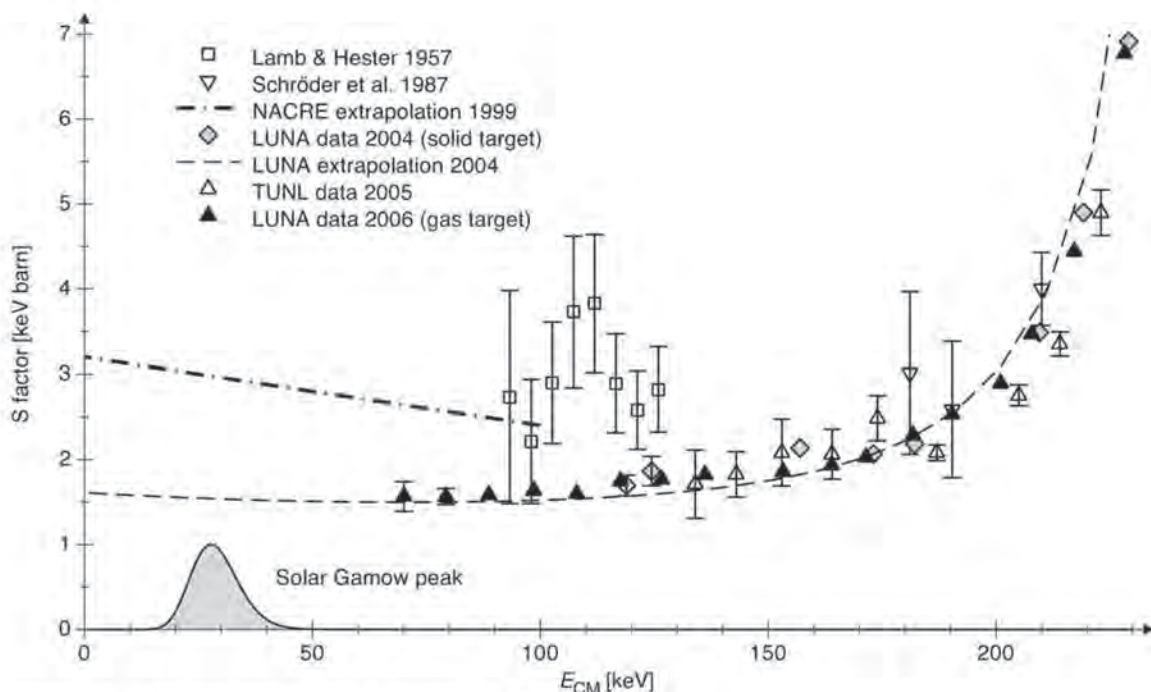


Figure 5: The astrophysical S factor of $^{14}\text{N}(p,\gamma)^{15}\text{O}$.

the synthesis of the different isotopes. In particular, LUNA is now measuring $^{17}\text{O}(p,)^{18}\text{F}$, the bridge reaction connecting the second to the third CNO cycle, and $^2\text{H}(\alpha,\gamma)^6\text{Li}$, the key reaction of big-bang nucleosynthesis which determines the amount of primordial ^6Li in the Universe.

The Future: Helium Burning

LUNA has shown the advantages of the low background environment on the study of the hydrogen burning processes at the stellar energies. Natural evolution is the exploitation of the underground environment to study the next step in the fusion chain towards ^{56}Fe (the element with the highest binding energy per nucleon): the helium burning. In particular, $^{12}\text{C}(\alpha,\gamma)^{16}\text{O}$ is the most important reaction of nuclear astrophysics and it determines the abundance ratio between carbon and oxygen, the two key elements to the development of life. This abundance ratio shapes the nucleosynthesis in massive stars up to the iron peak and the properties of supernovae.

Of great significance are also $^{13}\text{C}(\alpha,n)^{16}\text{O}$ and $^{22}\text{Ne}(\alpha,n)^{25}\text{Mg}$, the stellar sources of the neutrons which synthesize most of the trans-iron elements through the S-process: neutron captures followed by β decays. This exciting and ambitious program requires a dedicated space of about 150 m^2 where to install a 3.5 MV accelerator in an underground laboratory. A possible place to host the accelerator has been already identified in Gran Sasso. In the next two decades underground nuclear astrophysics will significantly improve the picture of stellar nucleosynthesis by studying the key processes of the helium burning.

Conclusions

Twenty years ago, LUNA started underground nuclear astrophysics in the core of Gran Sasso and it still remains the only facility of this kind in the world. The extremely low background has allowed experiments with count rates as low as a few events per year. For the first time, the important reactions which are responsible for the hydrogen burning in the Sun have been studied down to the relevant stellar energies. As a consequence, 50 years after the first pioneering cross section measurements, nuclear physics is no longer the dominant error source of the solar model. In particular, solar neutrinos can now be exploited to probe the deep interior of the Sun. When applied to the study of globular clusters, our results also increase the limit on the age of the Universe up to 14 billion years. Since a few years LUNA is not focused anymore on the Sun and it is studying those reactions which are responsible for the abundance of the chemical elements into the Cosmos. I'm sure that the key topic of underground nuclear astrophysics for the future will be the study of helium burning in the stars.

References

- [1] Greife, U., et al. (1994). Laboratory for Underground Nuclear Astrophysics (LUNA). *Nucl. Instrum. Methods A* 350. 327-337.
- [2] Formicola, A., et al. (2003). The LUNA II 400 kV accelerator. *Nucl. Instrum. Methods A* 507. 609-616.
- [3] Bonetti, R., et al. (1999). First measurement of the ${}^3\text{He}({}^3\text{He},2p){}^4\text{He}$ cross section down to the lower edge of the solar Gamow peak. *Phys. Rev. Lett.* 82. 5205-5208.
- [4] Bemmerer, D., et al. (2006). Activation Measurement of the ${}^3\text{He}(\alpha,\gamma){}^7\text{Be}$ Cross Section at Low Energy. *Phys. Rev. Lett.* 97. 122502-1-5.
- [5] Confortola, F., et al. (2007). Astrophysical S factor of the ${}^3\text{He}(\alpha,\gamma){}^7\text{Be}$ reaction measured at low energy via detection of prompt and delayed γ rays. *Phys. Rev. C* 75. 065803-1-4.
- [6] Formicola, A., et al. (2004). Astrophysical S-factor of ${}^{14}\text{N}(\text{p},\gamma){}^{15}\text{O}$. *Phys. Lett. B* 591. 61-68.
- [7] Lemut, A., et al. (2006). First measurement of the ${}^{14}\text{N}(\text{p},\gamma){}^{15}\text{O}$ cross section down to 70 keV. *Phys. Lett. B* 634. 483-487.
- [8] Angulo, C., et al. (1999). A compilation of charged-particle induced thermonuclear reaction rates. *Nucl. Phys. A* 656. 3-183.
- [9] Marta, M., et al. (2008). Precision study of ground state capture in the ${}^{14}\text{N}(\text{p},\gamma){}^{15}\text{O}$ reaction. *Phys. Rev. C* 78. 022802(R)-1-4.
- [10] Serenelli, A. M. (2009). New solar composition: the problem with solar models revisited. *Astrophys. J. Lett.* 705. L123-L127.
- [11] Haxton, W. C., & Serenelli, A. M. (2008). CN cycle solar neutrinos and the Sun's primordial core metallicity. *Astrophys. J.* 687. 678-691.
- [12] Imbriani, G. et al. (2004). The bottleneck of CNO burning and the age of Globular Clusters. *Astron. & Astrophys.* 420. 625-629.
- [13] Herwig, F., & Austin, S. M. (2004). Nuclear reaction rates and carbon star formation. *Astrophys. J.* 613. L73-76.
- [14] Caciolli, A., et al. (2011). Revision of the ${}^{15}\text{N}(\text{p},\gamma){}^{16}\text{O}$ rate and oxygen abundance in H-burning zones. *Astron. & Astrophys.* 533. A66-71.
- [15] Strieder, F., et al. (2012). The ${}^{25}\text{Mg}(\text{p},\gamma){}^{26}\text{Al}$ reaction at low astrophysical energies. *Phys. Lett. B* 707. 60-65.

THE ORIGIN AND STATUS OF SPONTANEOUS SYMMETRY BREAKING

■ FRANÇOIS ENGLERT

*Service de Physique Théorique
Université Libre de Bruxelles, Campus Plaine, C.P.225
and
The International Solvay Institutes, Campus Plaine C.P. 231
Boulevard du Triomphe, B-1050 Bruxelles, Belgium
fenglert@ulb.ac.be*

Abstract

From its inception in statistical physics to its role in the construction and in the development of the Brout-Englert-Higgs mechanism in quantum field theory, the notion of spontaneous symmetry breaking permeates contemporary physics. The discovery at the LHC of the BEH boson would confirm the mechanism and promote the quest for unified laws of nature. These topics are reviewed with particular emphasis on conceptual issues.

1 Introduction

Physics, as we know it, is an attempt to interpret the diverse phenomena as particular manifestations of general laws. This vision of a world ruled by *testable* laws is relatively recent. Essentially it started at the Renaissance and experienced a rapid development. The crucial ingredient was the inertial principle, initiated by Galileo (1564-1642), which essentially states that the uniform motion of a system does not affect the physics within the system and hence cannot be detected by an experiment performed within the system. This is a profound idea: the very fact that we do not feel such a motion confirms the universality of the Galilean physics approach to the understanding of nature in the sense that we ourselves are viewed as a physical system.

Starting from the inertial principle, Newton formulated at the end of the 17th Century the celebrated universal law of gravitation. He envisaged the world as composed of small interacting entities, which we now call elementary particles. In the 19th century, Maxwell established the

¹Contribution to “Past , Present and Future”, The Pontifical Academy of Science.

general laws of electromagnetism explaining electric and magnetic phenomena as well as the propagation of light. These laws were expressed in terms of a field, that is an object filling an extended region of space, propagating like a wave with the velocity of light and transmitting electric and magnetic interactions. The notions of particles and waves were unified in a subtle manner during the first decades of the 20th Century in Quantum Mechanics and the inertial principle was extended by Einstein to electromagnetism in the theory of Relativity. On the other hand the Newtonian law of gravitation was generalized by Einstein in 1915. The new theory of gravity, called General Relativity, opened to scientific investigation the cosmological expansion of the universe. These impressive developments in the first half of the 20th Century made it conceivable that all phenomena, from the atomic level to the edge of the visible universe, be governed solely by the known laws of classical general relativity and quantum electrodynamics, the quantum version of Maxwells electromagnetic theory .

Gravitational and electromagnetic interactions are long range interactions, meaning they are felt by objects, no matter how far they are separated from each other. But the discovery of subatomic structures revealed the existence of other fundamental interactions that are short range, being negligible at larger distance scales. In the beginning of the 60s, the theoretical interpretation of short range fundamental interactions seemed to pose insuperable obstacles.

It is the notion of spontaneous symmetry breaking (SSB) as adapted to gauge theory that provided the clue for solving the problem.

This notion finds its origin in the statistical physics of phase transitions [1]. There, the low temperature ordered phase of the system can be asymmetric with respect to the symmetry principles that govern its dynamics. This is not surprising since more often than not energetic considerations dictate that the ground state or low lying excited states of a many body system become ordered. A collective variable such as magnetization picks up expectation value, which define an order parameter that otherwise would vanish by virtue of the dynamical symmetry (isotropy in the aforementioned example). More surprising was the discovery by Nambu in 1960 [*Nobel prize 2008*] that the vacuum and the low energy excitations of a relativistic field theory may bare the mark of SSB [2, 3]: The chiral symmetry of massless fermion fields is broken by a spontaneous generation of their mass. The breaking give rise to massless pseudoscalar modes, which Nambu identified with the massless limit of pion fields. In absence of massless *gauge fields* characteristic of hitherto known fundamental interactions, such *massless Nambu-Goldstone bosons* (NG) and the concomitant vacuum degeneracy are general features of spontaneous symmetry breaking of a continuous group. The occurrence of SSB, either of a continuous or a discrete group, is also marked by fluctuations of the order parameter described

by generically *massive scalar bosons*.

Introducing the massless gauge fields renders local in space-time the otherwise global dynamical symmetry and leads to dramatic effects. While the massive scalar bosons survive, the massless NG bosons disappear as such but provide a longitudinal polarization for the gauge fields, which therefore become massive. The essential degeneracy of the vacuum is removed and local symmetry is preserved despite the gauge field masses.

This way of obtaining massive gauge fields and hence short-range forces out of a fundamental massless Yang-Mills gauge field Lagrangian was proposed in 1964 by Brout and Englert in quantum field theoretic terms [4] and then by Higgs in the equations of motion formulation [5]. Roughly this BEH mechanism [*R. Brout, F. Englert, P.W. Higgs - Wolf Prize 2004*] works as follows. We introduced scalar fields (i.e. having no spatial orientation) which acquire, in analogy with the ferromagnet, an average value pervading space. These scalar fields interact with a subset of long range forces, converting those to short range ones. We also showed that this mechanism can survive in absence of elementary scalar fields.

The preservation of local symmetry in the BEH mechanism makes the theory renormalizable, that is tames divergent quantum fluctuations. This was a feature of quantum electrodynamics but that is what was missing in previous failed attempts to cope with short range fundamental interactions. We suggested this property [6] in 1966 and its proof was achieved in the remarkable work of 't Hooft and Veltman [7] [*G. 't Hooft, M. Veltman - Nobel Prize 1999*]. The renormalizability made entirely consistent the electroweak theory, proposed by Weinberg in 1967 [*S.L. Glashow, A. Salam, S. Weinberg - Nobel Prize 1979*], related to a group theoretical model of Glashow and to the dynamics of the BEH mechanism.

The mechanism is well established by the discovery of the Z and W bosons in 1983 [*C. Rubbia, S. van der Meer - Nobel Prize 1984*] and by the detailed field theoretic computations confirming the electroweak theory within its suspected domain of validity. If the LHC discovers the massive scalar (BEH) boson of the electroweak theory, it would confirm the mechanism in its simplest form. More elaborate realizations of the BEH mechanism are possible, involving many such BEH bosons or new dynamics with composite scalars. Hopefully the LHC will tell.

The BEH mechanism thus unifies in the same consistent theoretical framework short- and long-range forces, became the cornerstone of the electroweak theory and opened the way to a modern view on unified laws of nature.

2 Spontaneous breaking of a global symmetry

2.1 Spontaneous symmetry breaking in phase transitions

Consider a condensed matter system, whose dynamics is invariant under a continuous symmetry acting globally in space and time. As the temperature is lowered below a critical one, the symmetry may be reduced by the appearance of an ordered phase. The breakdown of the original symmetry is always a discontinuous event at the phase transition point but the order parameters may set in continuously as a function of temperature. In the latter case the phase transition is second order. Symmetry breaking in a second order phase transition occurs in particular in ferromagnetism, superfluidity and superconductivity. I discuss here the ferromagnetic phase transition which illustrates three general features of global SSB: ground state degeneracy, the appearance of a “massless mode” when the dynamics is invariant under a continuous symmetry, and the occurrence of a “massive mode”.

Below the Curie point T_C , in absence of external magnetic fields and of surface effects, the exchange potential between neighboring atomic spins induces in a ferromagnet a globally oriented magnetization. The dynamics of the system is clearly rotation invariant. This is SSB.

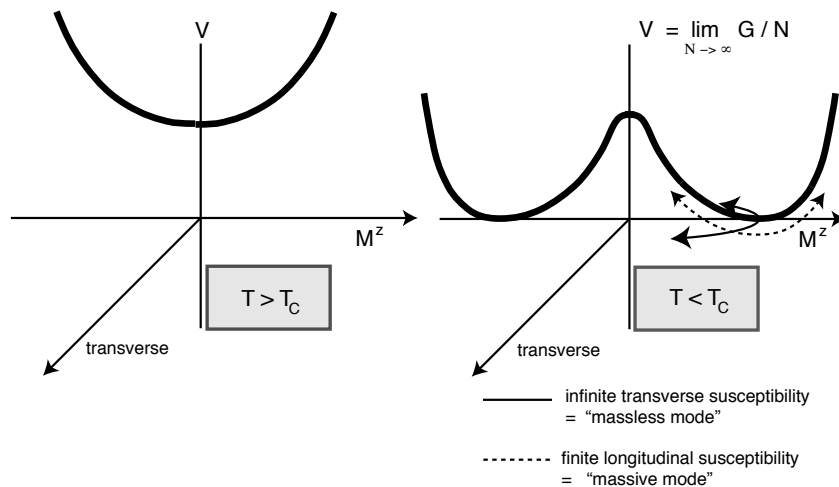


Figure 1: Effective potential of a typical ferromagnet.

The effective potential (i.e. the Gibbs free energy per spin) below the Curie point, depicted in

Fig.1, displays the essential features of SSB. At a given minimum, say, $\vec{M} = M^z \vec{1}_z$, the curvature of the effective potential measures the inverse susceptibility which determines the energy for infinite wavelength fluctuations, in other words, the “mass”. The inverse susceptibility is zero in directions transverse to the order parameter and positive in the longitudinal direction. One thus gets, even at non-zero temperature, a “massless” transverse mode characteristic of broken continuous symmetry and we learn that there is also a (possibly unstable) “massive” longitudinal mode which corresponds to fluctuations of the order parameter. The latter mode is present in any spontaneous broken symmetry, continuous or even discrete. Such generically massive mode characterize any ordered structure, be it the broken symmetry phase in statistical physics, the vacuum of the global SSB in field theory presented in Section 2.2 or of the BEH mechanism discussed in Section 3. The mass of such longitudinal mode measures the rigidity of the ordered structure.

These general features of global SSB are common to nearly all second order phase transitions. However, in superconductivity, as a consequence of the long-range Coulomb interactions, the massless mode disappears by being absorbed by electron density oscillations, namely into a massive plasma mode [8, 9]. This effect can be viewed as a non-relativistic precursor of the BEH mechanism.

2.2 Broken continuous symmetry in field theory

Spontaneous symmetry breaking was introduced in relativistic quantum field theory by Nambu in analogy with the BCS theory of superconductivity. The problem studied by Nambu [2] and Nambu and Jona-Lasinio [3] is the spontaneous breaking of the chiral symmetry of massless fermions due to the invariance of the relative (chiral) phase between their decoupled right and left constituent neutrinos. Fermion mass cannot be generated perturbatively from a chiral invariant interaction but may arise dynamically from of a self-consistent fermion condensate. This breaks the chiral symmetry spontaneously.

The “massless mode” of SSB in phase transitions becomes a genuine *massless boson*, which is here a pseudoscalar boson coupled to the axiovector current. This is interpreted as the chiral limit of the (tiny on the hadron scale) pion mass. Such interpretation of the pion mass constituted a breakthrough in our understanding of strong interaction physics. The *massive scalar boson* measuring the rigidity of the condensate also occurs as a bound states of fermions.

Let us illustrate the occurrence of massless and massive SSB bosons in the simple model of a complex scalar field with $U(1)$ symmetry introduced by Goldstone [10]. The Lagrangian

density,

$$\mathcal{L} = \partial^\mu \phi^* \partial_\mu \phi - V(\phi^* \phi) \quad \text{with} \quad V(\phi^* \phi) = -\mu^2 \phi^* \phi + \lambda (\phi^* \phi)^2, \quad \lambda > 0, \quad (2.1)$$

is invariant under the $U(1)$ group $\phi \rightarrow e^{i\alpha} \phi$. The global $U(1)$ symmetry is broken by a vacuum expectation value of the ϕ -field given, at the classical level, by the minimum of $V(\phi^* \phi)$. Writing $\phi = (\phi_1 + i\phi_2)/\sqrt{2}$, one may choose $\langle \phi_2 \rangle = 0$. Hence $\langle \phi_1 \rangle^2 = \mu^2/2\lambda$ and we select, say, the vacuum with $\langle \phi_1 \rangle$ positive. The potential $V(\phi^* \phi)$ is depicted in Fig.2. It is similar to the effective potential below the ferromagnetic Curie point shown in Fig.1 and leads to similar consequences.

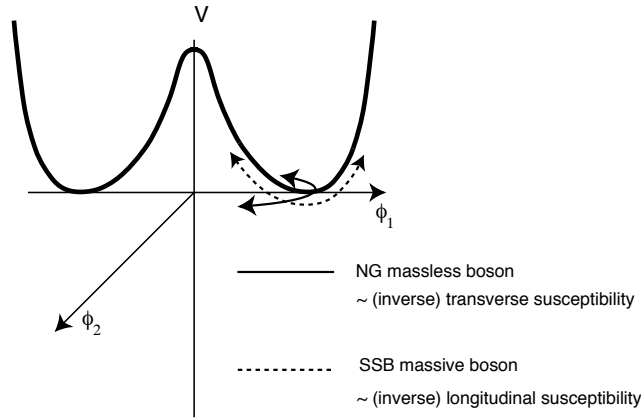


Figure 2: Spontaneous breaking of a continuous symmetry by scalar fields.

In the unbroken vacuum the field ϕ_1 has negative mass and acquires a positive mass $2\mu^2$ in the broken vacuum where the field ϕ_2 is massless. The latter is the *massless Nambu-Goldstone (NG) boson* of broken $U(1)$ symmetry and is the analog of the “massless mode” in ferromagnetism. The *massive scalar boson* describes the fluctuations of the order parameter $\langle \phi_1 \rangle$ and is the analog of the “massive mode” in the ordered phase of a many-body system.

The origin of the massless NG boson is, as in the ferromagnetism phase, a consequence of the vacuum degeneracy. The vacuum characterized by the order parameter $\langle \phi_1 \rangle$ is rotated into an equivalent vacuum by an operator proportional to the field ϕ_2 at zero space momentum. Such rotation costs no energy and thus the field ϕ_2 at space momenta $\vec{q} = 0$ has $q_0 = 0$, and hence is indeed massless.

3 The BEH mechanism

3.1 From global to local symmetry

The global $U(1)$ symmetry in Eq.(2.1) is extended to a local one $\phi(x) \rightarrow e^{i\alpha(x)}\phi(x)$ by introducing a vector field $A_\mu(x)$ transforming as $A_\mu(x) \rightarrow A_\mu(x) + (1/e)\partial_\mu\alpha(x)$. The corresponding Lagrangian density is

$$\mathcal{L} = D^\mu\phi^* D_\mu\phi - V(\phi^*\phi) - \frac{1}{4}F_{\mu\nu}F^{\mu\nu}, \quad (3.2)$$

with covariant derivative $D_\mu\phi = \partial_\mu\phi - ieA_\mu\phi$ and $F_{\mu\nu} = \partial_\mu A_\nu - \partial_\nu A_\mu$.

Local invariance under a semi-simple Lie group \mathcal{G} is realized by extending the Lagrangian Eq.(3.2) to incorporate non-abelian Yang-Mills vector fields A_μ^a

$$\mathcal{L}_\mathcal{G} = (D^\mu\phi)^{*A}(D_\mu\phi)^A - V - \frac{1}{4}F_{\mu\nu}^a F^{a\mu\nu}, \quad (3.3)$$

$$(D_\mu\phi)^A = \partial_\mu\phi^A - eA_\mu^a T^{aAB}\phi^B \quad F_{\mu\nu}^a = \partial_\mu A_\nu^a - \partial_\nu A_\mu^a - ef^{abc}A_\mu^b A_\nu^c. \quad (3.4)$$

Here, ϕ^A belongs to the representation of \mathcal{G} generated by T^{aAB} and the potential V is invariant under \mathcal{G} .

The local abelian or non-abelian gauge invariance of Yang-Mills theory hinges *apparently* upon the massless character of the gauge fields A_μ , hence on the long-range character of the forces they transmit, as the addition of a mass term for A_μ in the Lagrangian Eq.(3.2) or (3.3) destroys gauge invariance. But short-range forces such as the weak interaction forces, seem to be as fundamental as the electromagnetic ones despite the apparent departure from exact conservation laws. To reach a basic description of such forces one is tempted to link this fact to gauge fields masses arising from spontaneous broken symmetry. However the problem of SSB is very different for global and for local symmetries.

Consider the Yang-Mills theory defined by the Lagrangian Eq.(3.3). To exhibit the similarities and the differences between spontaneous breaking of a global symmetry and its local symmetry counterpart, it is convenient to choose a gauge which preserves Lorentz invariance and a residual global \mathcal{G} symmetry. This can be achieved by adding to the Lagrangian a gauge fixing term $(2\eta)^{-1}\partial_\mu A^{a\mu}\partial_\nu A^{a\nu}$. The gauge parameter η is arbitrary and is not observable.

In such gauges the global symmetry can be spontaneously broken for suitable potential V by non zero expectation values $\langle\phi^A\rangle$ of scalar fields. In Fig.3 we have represented motions of this parameter in the spatial q -direction and in a direction B of the coset space \mathcal{G}/\mathcal{H} where \mathcal{H} is the unbroken subgroup. Fig.3a pictures the spontaneously broken vacuum of the gauge fixed

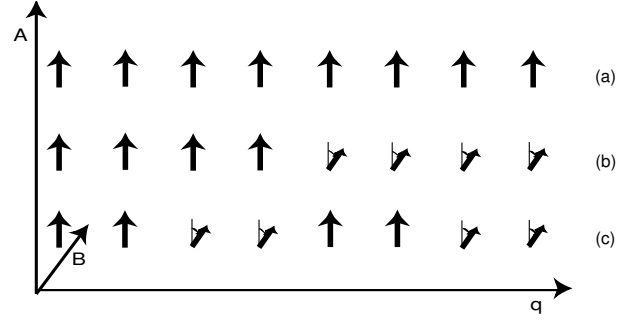


Figure 3: The disappearance of the massless NG boson in a gauge theory.

Lagrangian. Fig.3b and Fig.3c mimic motions in the coset with decreasing wavelength l . Clearly, as $l \rightarrow \infty$, such motions can only induce global rotations in the internal space. In absence of gauge fields, they would give rise, as in spontaneously broken global continuous symmetries, to massless NG modes generating the coset in the limit $l = \infty$. In a gauge theory, transverse fluctuations of $\langle \phi^A \rangle$ are just local rotations in the internal space and thus are unobservable gauge motions. Hence the would-be NG bosons induce only gauge transformations and their excitations disappear from the physical spectrum. A formal proof of the absence of the NG boson in gauge theories can be found in [11, 12] and will be further discussed in the following section.

But what makes local internal space rotations unobservable in a gauge theory is precisely the fact that they can be absorbed by the Yang-Mills fields. The absorption of the NG fields renders massive the gauge fields living in the coset \mathcal{G}/\mathcal{H} by transferring to them their degrees of freedom which become longitudinal polarizations.

We shall see in the next sections how these considerations are realized in relativistic quantum field theory and give rise to vector masses in the coset \mathcal{G}/\mathcal{H} , leaving long-range forces only in a subgroup \mathcal{H} of \mathcal{G} . Despite the unbroken local symmetry, the group \mathcal{G} appears broken to its subgroup \mathcal{H} in the asymptotic state description of field theory, and I shall therefore often term SSB such a Yang-Mills phase. The onset of SSB will now be described in detail mostly in lowest order perturbation theory around the self-consistent vacuum. This contains already the basic ingredients of the phenomenon.

3.2 The field theoretic approach

In this section, I will follow the method of reference [4]

$\alpha)$ *Breaking by scalar fields*

Let us first examine the abelian case as realized by the complex scalar field ϕ exemplified in Eq.(3.2). The interaction between the complex scalar field ϕ and the gauge field A_μ is

$$-ie (\partial_\mu \phi^* \phi - \phi^* \partial_\mu \phi) A^\mu + e^2 A_\mu A^\mu \phi^* \phi. \quad (3.5)$$

The SSB Yang-Mills phase is realized by a non vanishing expectation value for $\phi = (\phi_1 + i\phi_2)/\sqrt{2}$, which we choose to be in the ϕ_1 -direction. Thus $\phi_1 = \langle \phi_1 \rangle + \delta\phi_1$ and $\phi_2 = \delta\phi_2$; $\delta\phi_2$ and $\delta\phi_1$ are respectively as in Section 2.2 the NG massless boson and the massive scalar boson. In the covariant gauges, the free propagator of the field A_μ is

$$D_{\mu\nu}^0 = \frac{g_{\mu\nu} - q_\mu q_\nu / q^2}{q^2} + \eta \frac{q_\mu q_\nu / q^2}{q^2}, \quad (3.6)$$

where η is the gauge parameter.

The polarization tensor $\Pi_{\mu\nu}$ of the gauge field in lowest order perturbation theory around the self-consistent vacuum is given by the tadpole graphs of Fig.4,

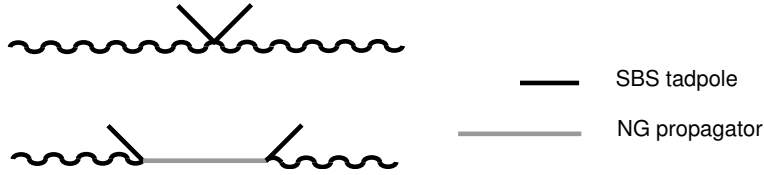


Figure 4: Tadpole graphs of SBS. Abelian gauge theory.

We see that, as a consequence of the contribution from the NG boson, the polarization tensor is transverse

$$\Pi_{\mu\nu} = (g_{\mu\nu} q^2 - q_\mu q_\nu) \Pi(q^2), \quad (3.7)$$

and yields a singular polarization scalar $\Pi(q^2)$ at $q^2 = 0$

$$\Pi(q^2) = \frac{e^2 \langle \phi_1 \rangle^2}{q^2}. \quad (3.8)$$

From Eqs.(3.6), (3.7) and (3.8), the dressed gauge field propagator becomes

$$D_{\mu\nu} = \frac{g_{\mu\nu} - q_\mu q_\nu / q^2}{q^2 - \mu^2} + \eta \frac{q_\mu q_\nu / q^2}{q^2}, \quad (3.9)$$

which shows that the A_μ -field gets a mass

$$\mu^2 = e^2 \langle \phi_1 \rangle^2. \quad (3.10)$$

The transversality of the polarization tensor Eq.(3.7) results from the contribution of the NG boson and agrees with a Ward identity which guarantees that gauge invariance is preserved [6]. This means not only that the gauge field mass is gauge invariant but also that the gauge invariant vacuum is unbroken, as discussed in the previous section. Therefore there cannot be a NG boson in the physical spectrum.

The generalization of these results to the non abelian case described by the action Eq.(3.3) is straightforward. Writing the generators in terms of the real components of the fields, one gets the mass matrix

$$(\mu^2)^{ab} = -e^2 \langle \phi^B \rangle T^{aBC} T^{bCA} \langle \phi^A \rangle, \quad (3.11)$$

and the dressed gauge boson propagators have the same form as Eq.(3.9) in terms of the diagonalized mass matrix. As in the abelian case, the would-be NG bosons disappear from the physical spectrum and generate gauge invariant masses for the gauge fields in \mathcal{G}/\mathcal{H} . Long-range forces only survive in the subgroup \mathcal{H} of \mathcal{G} which leaves invariant the non vanishing expectation values $\langle \phi^A \rangle$.

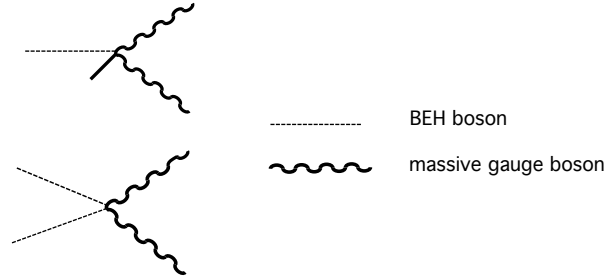


Figure 5: Coupling of BEH bosons to massive gauge bosons from Fig.4.

Note that the explicit form of the scalar potential V does not enter the computation of gauge field propagators which depend only on the expectation values at its minimum. This is because trilinear terms arising from covariant derivatives can only couple the tadpoles to the would-be NG bosons. Hence the massive scalar bosons decouple from the tadpoles in the gauge field propagators at the tree level considered here. Of course in the BEH mechanism the massive scalar (BEH) bosons couple to the massive gauge bosons already at the tree level. This is obvious from the diagrams of Fig 4 which defines the vertices coupling the BEH bosons to two massive gauge boson. These are depicted in Fig.5.

β) Dynamical symmetry breaking

The symmetry breaking giving mass to gauge vector bosons may arise from the fermion condensate. If a spontaneously global symmetry is extended to a local one by introducing gauge fields, the NG bosons are absorbed in massive gauge fields and disappear as such from the physical spectrum.

3.3 The renormalization issue

The interest in the BEH mechanism stems from the fact that it provides, as does quantum electrodynamics, a taming of quantum fluctuations. This allows the computation of the quantum effects necessary to cope with precision experiments. In other words, the theory is “renormalizable”, in contradistinction to the theory of genuine non-abelian massive vector fields. A glimpse into this issue appears by comparing our field-theoretic approach [4] with the equation of motion approach of Higgs [5].

The massive vector propagator Eq.(3.9), which is also valid in the non-abelian case by diagonalizing the mass matrix Eq.(3.11), differs from a conventional free massive propagator in two respects. First the presence of the unobservable longitudinal term reflects the arbitrariness of the gauge parameter η . Second the NG pole at $q^2 = 0$ in the transverse projector $g_{\mu\nu} - q_\mu q_\nu / q^2$ is unconventional. Its significance is made clear by expressing the propagator of the A_μ field in Eq.(3.9) as (putting η to zero)

$$D_{\mu\nu} \equiv \frac{g_{\mu\nu} - q_\mu q_\nu / q^2}{q^2 - \mu^2} = \frac{g_{\mu\nu} - q_\mu q_\nu / \mu^2}{q^2 - \mu^2} + \frac{1}{\mu^2} \frac{q_\mu q_\nu}{q^2}. \quad (3.12)$$

The first term in the right hand side of Eq.(3.12) is the conventional massive vector propagator, while the second term is a pure gauge propagator due to the NG boson. The decomposition Eq.(3.9) corresponds to the Higgs' transformation [5]

$$A_\mu = B_\mu + \frac{1}{e\langle\phi_1\rangle} \partial_\mu \phi_2 \quad (3.13)$$

which absorbs explicitly the NG boson in a redefined gauged field B_μ which behaves as a conventional massive gauge vector field.

The propagator Eq.(3.9) which appears in the field theoretic approach contains thus, in the covariant gauges, the transverse projector $g_{\mu\nu} - q_\mu q_\nu / q^2$ in the numerator of the massive gauge field A_μ propagator. This is in sharp contradistinction to the numerator $g_{\mu\nu} - q_\mu q_\nu / \mu^2$ characteristic of the conventional massive vector field B_μ propagator. It is the transversality of the polarization tensor in covariant gauges, which led in the tree approximation to the transverse

projector in Eq.(3.9). As mentioned above, the transversality of the polarization tensor is a consequence of a Ward identity and therefore does not rely on the tree approximation [6]. The importance of this fact is that transversality in covariant gauges determines the power counting of irreducible diagrams. It is then straightforward to verify that the quantum field theory formulation has the required power counting for a renormalizable field theory. On this basis it was suggested that it indeed was renormalizable [6].

However power counting is not enough to prove the renormalizability of a theory with local gauge invariance. To be consistent, the theory must also be unitary, a fact which is not apparent in “renormalizable” covariant gauges but is manifest in the “unitary gauge” defined in the free theory by the B_μ -field introduced in Eq.(3.13). In the unitary gauge however, power counting requirements fail. The equivalence between the A_μ and B_μ free propagators, *which is only true in a gauge invariant theory* where their difference is the unobservable NG propagator appearing in Eq.(3.12), is a clue of the consistency of the BEH theory. It is of course a much harder and subtler affair to proof that the full interacting theory is both renormalizable and unitary. This was achieved in the work of ’t Hooft and Veltman [7], which thereby established the consistency of the BEH mechanism.

4 The electroweak theory and its BEH boson

I first review very briefly the basic elements of the electroweak theory.

In the electroweak theory for weak and electromagnetic interactions, the gauge group is taken to be $SU(2) \times U(1)$ with corresponding generators and coupling constants $gA_\mu^a T^a$ and $g'B_\mu Y'$. The $SU(2)$ acts on left-handed fermions only. The scalar field ϕ is a doublet of $SU(2)$ and its $U(1)$ charge is $Y' = 1/2$. Breaking is characterized by $\langle \phi \rangle = 1/\sqrt{2} \{0, v\}$ and $Q = T^3 + Y'$ generates the unbroken subgroup. Q is identified with the electromagnetic charge operator. The only residual massless gauge boson is the photon and the electric charge e is usually expressed in terms of the mixing angle θ as $g = e/\sin \theta$, $g' = e/\cos \theta$.

Using Eqs.(3.10) and (3.11) one gets the mass matrix

$$|\mu^2| = \frac{v^2}{4} \begin{vmatrix} g^2 & 0 & 0 & 0 \\ 0 & g^2 & 0 & 0 \\ 0 & 0 & g'^2 & -gg' \\ 0 & 0 & -gg' & g^2 \end{vmatrix}$$

whose diagonalization yields the eigenvalues

$$M_{W^+}^2 = \frac{v^2}{4}g^2 \quad M_{W^-}^2 = \frac{v^2}{4}g^2 \quad M_Z^2 = \frac{v^2}{4}(g'^2 + g^2) \quad M_A^2 = 0. \quad (4.14)$$

This permits to relate v to the the four Fermi coupling G , namely $v^2 = (\sqrt{2}G)^{-1}$.

The electroweak theory has been amply verified by experiment but the existence of its massive BEH boson presently search for at the LHC has, as yet, to be confirmed. Although the mechanism itself is well established by the discovery of the Z and W bosons and by the precision experiments, the discovery of the BEH boson would nevertheless constitute a direct proof of its validity. In addition, its properties would yield basic information which is crucial for further developments of elementary particle physics. First, one might get a better understanding of its structure, namely whether it would appear as a composite of higher energy elements or as an elementary object, in which case it might be related to supersymmetric multiplets: supersymmetry is indeed a natural framework for fundamental scalar bosons, which otherwise can easily arise as phenomenological constructs of complex structures. Second, the main content of the BEH mechanism is a consistent theory of charged Yang-Mills field, but its application to the electroweak theory is also used for generating all elementary fermion masses (a feature already possible from global SSB). The unification of such fermion mass generation with those of the gauge fields is an important experimental issue.

5 Concluding remarks

A prominent question is thus the existence of supersymmetry at the TeV scale for the reason just mentioned. In addition, supersymmetry would give more credence to searches for Grand Unification groups containing the subgroup $SU(2) \times U(1) \times SU(3)$ [13], where $SU(3)$ is the group of the strong interaction physics mediated by its quark confining gauge fields. Indeed, in minimal supersymmetric extensions of the Standard Model, renormalization group computations render more plausible the merging of these three groups at very high energies, namely at scales comparable with the expected onset of quantum gravity effects [14]. Supersymmetry and unification at such scales would favor the approach to quantum gravity by something akin to superstring theories.

These speculations have led to the unification paradigm whose ultimate realization would be a “theory of everything” including quantum gravity in the framework of some “M-theory”. However a word of caution is perhaps in order. Quite apart from the obvious philosophical questions raised by such quest in the present framework of theoretical physics, the transition

from perturbative string theory to its elusive M-theory generalization hitherto stumbles on the treatment of non-perturbative gravity. This might well be a hint that new conceptual elements have to be found to cope with the relation between gravity and quantum theory and which may well be unrelated to a unification program.

Addendum

Since this paper was written, a dramatic event has occurred: the BEH boson has been found at the LHC at CERN and appears to be an elementary object (at the energy scale considered) consistent with the electroweak theory.

As discussed in Section 4, this provides a direct confirmation of the validity of the BEH mechanism. But more than that, the elementary character of the scalar boson appears to dispose of complicated dynamical schemes such as “extended technicolor” or “walking technicolor” needed when the simple “natural” technicolor scheme for generating gauge vector boson masses is extended to cope with dynamical elementary fermion masses. This is a welcome result but as pointed out in Section 4, it seems to suggest that (broken) supersymmetry be a likely generalization of the Standard Model. Although there is at present no experimental indication of such supersymmetric partners, we have to wait for further datas to ensure that supersymmetry is present or not at available energies. As pointed out in Section 5, in the latter case, the occurrence of supersymmetry at higher scale (and possibly only at scales close to the Planck scale) will in the foreseeable future remain a purely speculative issue.

References

- [1] L.D. Landau, *On the theory of phase transitions I*, Phys. Z. Sowjet. **11** (1937) 26 [JETP **7** (1937) 19].
- [2] Y. Nambu, *Axial vector current conservation in weak interactions*, Phys. Rev. Lett. **4** (1960) 380.
- [3] Y. Nambu and G. Jona-Lasinio, *Dynamical model of elementary particles based on an analogy with superconductivity I, II*, Phys. Rev. **122** (1961) 345; Phys. Rev. **124** (1961) 246.
- [4] F. Englert and R. Brout, *Broken symmetry and the mass of gauge vector mesons*, Phys. Rev. Lett. **13** (1964) 321.

- [5] P.W. Higgs, *Broken symmetries and the masses of gauge bosons*, Phys. Rev. Lett. **13** (1964) 508.
- [6] F. Englert, R. Brout and M. Thiry, *Vector mesons in presence of broken symmetry*, Il Nuovo Cimento **43A** (1966) 244; Proceedings of the 1997 Solvay Conference, *Fundamental Problems in Elementary Particle Physics*, Interscience Publishers J. Wiley and Sons, p 18.
- [7] G. 't Hooft, *Renormalizable Lagrangians for massive Yang-Mills fields*, Nucl. Phys. **B35** (1971) 167; G. 't Hooft and M. Veltman, *Regularization and renormalization of gauge fields*, Nucl. Phys. **B44** (1972) 189.
- [8] P.W. Anderson, *Random-phase approximation in the theory of superconductivity*, Phys. Rev. **112** (1958) 1900.
- [9] Y. Nambu, *Quasi-particles and gauge invariance in the theory of superconductivity*, Phys. Rev. **117** (1960) 648.
- [10] J. Goldstone, *Field theories with “superconductor” solutions*, Il Nuovo Cimento **19** (1961) 154.
- [11] P.W. Higgs, *Broken symmetries, massless particles and gauge fields*, Phys. Lett. **12** (1964) 132.
- [12] G.S. Guralnik, C.R. Hagen and T.W.B. Kibble *Global conservation laws and massless particles*, Phys. Rev.Lett. **13** (1964) 585.
- [13] H. Georgi, H.R. Quinn and S. Weinberg, *Hierarchy of interactions in unified gauge theories*, Phys. Rev. Lett. **33** (1974) 451.
- [14] S. Pokorski, *Status of low energy supersymmetry*, Act. Phys. Pol. **B30** (1999) 1759.

Detailed reference for all the 1964 papers quoted in the text

	Article	Reception date	Publication date
1	F. Englert and R. Brout <i>Phys.Rev.Letters</i> 13 -[9] (1964) 321	26/06/1964	31/08/1964
2	P.W. Higgs <i>Phys. Letters</i> 12 (1964) 132	27/07/1964	15/09/1964
3	P.W. Higgs <i>Phys.Rev.Letters</i> 13 -[16] (1964) 508	31/08/1964	19/10/1964
4	G.S. Guralnik, C.R. Hagen and T.W.B. Kibble <i>Phys.Rev.Letters</i> 13 -[20] (1964) 585	12/10/1964	16/11/1964

STUDY OF LOW ENERGY NEUTRINOS FROM SUN AND EARTH WITH BOREXINO

■ GIANPAOLO BELLINI

Universita' degli Studi di Milano

Istituto Nazionale di Fisica Nucleare

Abstract

The Borexino is a unique detector able to study neutrino interactions with a threshold below 1 MeV thanks to the unprecedented radiopurity reached by it. So it has been possible to measure for the first time the solar neutrino fluxes from the ${}^7\text{Be}$ and pep nuclear reactions and consequently to study the neutrino oscillation in vacuum and in the transition region. The neutrinos from ${}^8\text{B}$ with a lower threshold down to 1 MeV has been also measured and an upper limit of the flux from the CNO cycle has been reached. The measurement of these fluxes allowed a good check of the Solar Standard Model predictions.

Finally Borexino has obtained evidence of geoneutrinos with 4.2 sigma confidence level.

1. Why the solar neutrinos ?

I would like first of all to set the study of the solar neutrinos within the physics framework and to explain why this issue has been and is so important in order to understand two crucial problems in the astro-particle physics: the *Sun physics* and the *Neutrino physics*.

During about 40 years John N. Bahcall and various coworkers have developed the Standard Solar Model (SSM), which describes the Sun structure and behavior. The SSM seems very robust also because it agrees with phenomena, which take place in the Sun [1]. One of them is the helioseismology, which studies solar disruptions producing longitudinal waves which propagate within the Sun. The behaviors connected with these phenomena well agree with the SSM previsions. Of course some open problems still remain and I will discuss them later.

The SSM predicts also the neutrino fluxes emitted by the nuclear fusion reactions, which take place within the Sun, and are responsible of the Sun shining.

Despite the very low probability of the neutrinos to interact with matter, it is possible to detect them by means of experiments properly designed.

The first experiment, which measured the solar neutrino flux, has been Homestake, installed in the Homestake mine in South Dakota, which has taken data from 1970 until 1994. It was a radiochemical experiment: the solar neutrinos (all belonging to the electronic family-see later) strike Chlorine nuclei producing Argon nuclei, which decay back to Chlorine, emitting electrons. These reactions can take place only if the incident neutrino pertains to the electronic family (see later). The result of this experiment has been that the measured flux is definitively smaller that what expected by the SSM [2].

This discrepancy between model and experimental data produced what has been called the “*Solar Neutrino Problem (SNP)*”. Other radiochemical experiments, as e.g. Gallex (1991-1997) confirmed the Homestake result [3].

The cause of the SNP could be twofold: either in the SSM there is some wrong assumption and therefore the neutrino flux is lower than predicted, or there is some new

effect in the neutrino physics, beyond the prevision of the paradigmatic Standard Model of the elementary particles.

Later real time experiments detecting the Cherenkov light produced by the neutrino interactions in water, as Superkamiokande in Japan and SNO (Sudbury Neutrino Observatory) in Canada, have been carried out. These experiments studied the solar neutrino flux with a threshold > 5 MeV, recently reduced by SNO to 4.2 MeV of the neutrino energy. The difference between the radiochemical experiments and the real time experiments is that the first ones are unable to measure the energy of the incident neutrino and therefore they can measure only the total neutrino flux integrated from the threshold, while the real time experiments can measure separately the neutrino fluxes produced by the different solar nuclear reactions.

In 2001 SNO succeeded to demonstrate experimentally that the SSM previsions on the neutrino flux are correct and that the SNP is due to a new phenomenon beyond the elementary particle Standard Model, i.e. the neutrino *oscillation* [4]. I will give later a short outline of this phenomenon, which is described in the Altarelli's talk in this meeting. Here I want only to emphasize that the neutrino oscillation clashes with the Standard Model for two aspects: the neutrino mass is not zero and the neutrino family mark (so called *flavor*) can be violated.

The Cherenkov experiments, SNO and SuperKamiokande, due to the high threshold, succeeded to study only 1/10000 of the solar neutrino flux, corresponding to the highest part of the neutrino energy spectrum; therefore the by far largest part of the solar neutrino flux was remaining unexplored. This implies in addition a further limitation.

The oscillation can take place in vacuum and in matter: in vacuum in the travel between Sun and Earth (so called “just so”), in matter escaping from the Sun through the solar matter. No evidence has been observed until now that neutrinos are oscillating in the Sun-Earth travel, while SNO reached evidence that the neutrinos with energy > 5 MeV oscillate in the Sun matter. But when the energy of the solar neutrinos is below 0.8-1.0 MeV, the mechanism of the oscillation in vacuum prevails. Therefore, depending on the neutrino energy, three behaviors are possible in the neutrino oscillations: in vacuum, in matter and in a transition region between the two previous regimes. SNO and Superkamiokande, with a threshold >5 MeV can explore only the oscillation mechanism in matter.

It is evident at this point that another experiment was needed, able to study the solar neutrinos at very low energy, hopefully below 1 MeV. This was a very challenging enterprise because the natural radioactivity of any materials emits photons and particles which produce much more interactions in a detector than the rare neutrino interactions, thus fully hidden them. Therefore the first and more important effort has been to reduce the interactions due to the radiation emitted by the radioactive decay from any source to levels comparable to the neutrino rate. Thus Borexino is born and, as I will describe shortly in the following headings, the Borexino collaboration succeeded to reach an unprecedented radiopurity, allowing a very good success.

2. A brief recall of the neutrino properties.

The neutrinos (ν) are elementary particles having no charge and very small mass. In addition they interact with matter via weak interactions: their cross section is very small

and therefore the neutrinos can cross the Sun, the Earth and the Universe without to be perturbed. As a consequence the neutrinos are remarkable probes to study regions not reachable otherwise: just an example, the photons produced in the central region of the Sun need ~ 100000 years to escape, while to neutrinos few seconds are enough.

The neutrinos are *leptons*, one of the two families of the elementary particles. The leptons are divided in three sub-families; each of them contains one lepton and one neutrino, which is produced either with or from the decay of this lepton of its own subfamily. Therefore there are three different types of neutrino: electron neutrino (ν_e) produced together the electron in the beta decay, muon neutrino (ν_μ) which is one of the decay product of the lepton called muon, and finally the tau neutrino (ν_τ) also produced in the tau decay. Of course, as for all particles, to each lepton corresponds its antiparticle. Therefore the positron e^+ is the anti-electron, the $\bar{\nu}_e$ is the anti-neutrino electron, etc..

The lepton maintains its sub-family mark (called *flavour*) in its interactions and decays without exceptions: this was what the physicists believed until some years ago, before the discovery of the phenomenon called “neutrino *oscillation*”. In this phenomenon the neutrino can change its flavor during its travel between the production and the detection points (see the Altarelli’s talk in this conference). It can arrive in vacuum and in matter.

In the oscillation phenomenon the probability of transition from a flavor to another one depends on the ratio L/E , where L is the distance between the production site and the detector, and E is the neutrino energy: higher L/E , greater the probability. Therefore, the solar neutrinos are an ideal tool to study the neutrino oscillation, because L is very large and E is very small (from a few keV to ~ 16 MeV).

In the oscillation and in particular in the effect so called MSW (from the authors: Mikheiev, Smirnov, Wolfenstein) [5] the oscillation is vacuum driven or matter enhanced depending on the product $n_e E$, where n_e is the electron density of the matter crossed by the neutrinos and E is the neutrino energy. If $n_e E$ is high, the oscillation in matter is dominant, while if this product is small the oscillation is vacuum driven. In the Sun n_e can be considered constant and therefore the oscillation regime (vacuum or matter) depends only on the neutrino energy.

The previsions of the oscillation model [5,6], adopted now as paradigmatic, for the ν_e survival probability is shown in figure 1; three regions are shown: the vacuum dominated region at low neutrino energy, the matter enhanced at higher energy, and a transition region in between.

The main parameters of the oscillation are the difference of masses squared between neutrinos (really between the mass eigenstates) and an angle, called “mixing angle”.

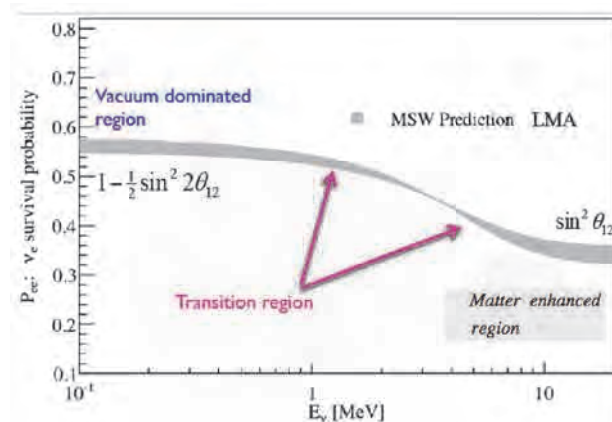


Figure 1. The ν_e survival probability as foreseen by the oscillation model MSW (see text)

3. The Solar neutrinos

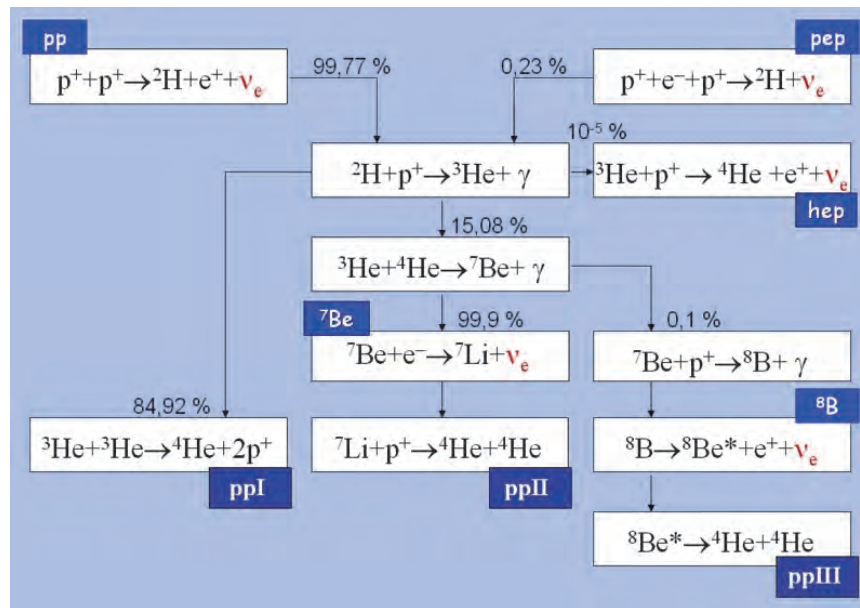


Figure 2 Nuclear reaction sequence within the Sun.

The Sun emits a huge amount of electron-neutrinos. Their flux on the Earth is about 60 billion per cm^2 per second. They are produced by two chains of nuclear fusion reactions, the dominant one (99.77%) starting with the fusion of two Hydrogen nuclei. In figure 2 the solar reaction chains are shown. We can observe that the reactions called: *pp*, *pep*, *hep*, ${}^7\text{Be}$, ${}^8\text{B}$ produce ν_e s

In addition a cycle, called *CNO*, which in the Sun produces <1% of the total energy, is considered dominant in the massive stars (with a mass >10-15 Sun masses) by the astrophysicists, but experimental proof of it never has been reached.

The energy spectrum of the solar neutrinos (figure 3) ranges from 0 to ~18 MeV, but the by far highest flux is concentrated below 1 MeV.

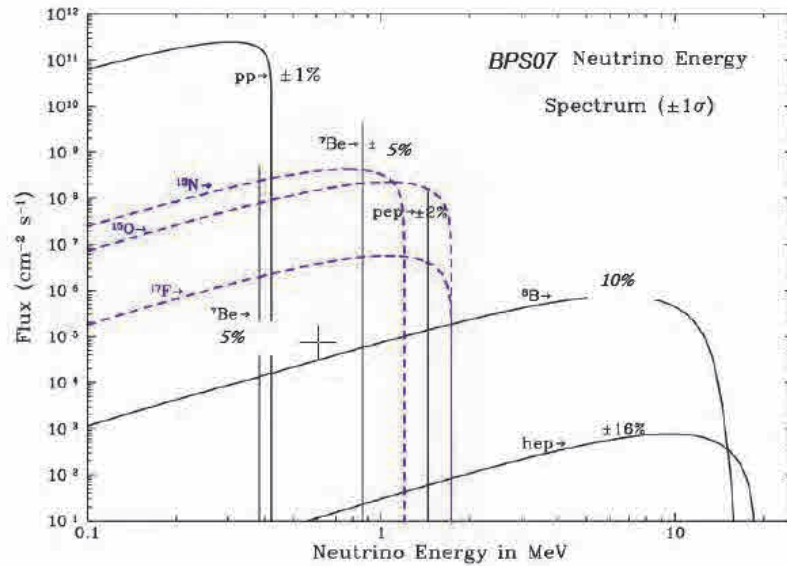


Figure 3 Energy spectrum of the solar neutrinos

The Sun mechanisms have been studied by the Standard Solar Model (SSM), developed during the last 30-40 years. The father of this model is the US physicist John N. Bahcall. The SSM is now very robust; nevertheless some problem are still present. One of them is the so called “*metallicity puzzle*”.

Solar surface abundances are determined from analyses of photosphere atomic and molecular spectral lines. The associated solar atmosphere modeling has been done in one dimension in a time-independent hydrostatic analysis that incorporates convection (GS98). A much improved 3D model of the solar atmosphere has been developed later, which better reproduces line profiles and brings the Solar abundances into better agreement with other stars in the neighborhood (AGS05). Due to this improved analysis, the solar surface contains 30-40% less carbon, nitrogen, oxygen, neon and argon than previously believed.

But, where the problem is? The one dimensional approach is in excellent agreement with the study of the so called *helioseismology*, while the three dimensional approach is in disagreement. The helioseismology, as already said in the paragraph 1, is the study of the propagation of the longitudinal waves produced by important disruptions taking place in the Sun.

The two different approaches GS98 (high metallicity) and AGS09 (low metallicity) have some influences also on the solar neutrino fluxes (Table 1). We can observe that the cycle CNO shows the highest difference and the ${}^7\text{Be}$ and ${}^8\text{B}$ fluxes have a $\sim 10\%$ and $\sim 20\%$ of discrepancy, respectively between high and low metallicity [6]. Therefore precise experimental measurements of the solar neutrino fluxes can help in fixing this SSM puzzle.

Table 1. Solar neutrino fluxes following the GS98 (high metallicity) and AGS09 (low metallicity) approaches

ν flux	GS98	AGS09	$\text{cm}^{-2} \text{s}^{-1}$
pp	5.98 (1 \pm 0.006)	6.03 (1 \pm 0.006)	$\times 10^{10}$
pep	1.44 (1 \pm 0.012)	1.47(1 \pm 0.012)	$\times 10^8$
hep	8.04 (1 \pm 0.30)	8.31 (1 \pm 0.30)	$\times 10^3$
${}^7\text{Be}$	5.00 (1 \pm 0.07)	4.56 (1 \pm 0.07)	$\times 10^9$
${}^8\text{B}$	5.58 (1 \pm 0.14)	4.59 (1 \pm 0.14)	$\times 10^6$
${}^{13}\text{N}$	2.96 (1 \pm 0.14)	2.17 (1 \pm 0.14)	$\times 10^8$
${}^{15}\text{O}$	2.23 (1 \pm 0.15)	1.56 (1 \pm 0.15)	$\times 10^8$
${}^{17}\text{F}$	5.52 (1 \pm 0.17)	3.40 (1 \pm 0.16)	$\times 10^6$

The solar neutrinos are also an ideal tool to measure the survival probability of the electron-neutrino. In fact their spectra cover the three oscillation regions as shown in figure 4.

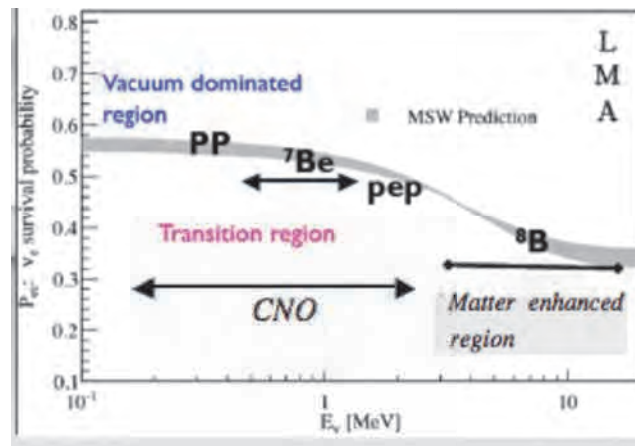


Figure 4 ν_e survival probability compared with the energy ranges of the neutrino fluxes produced in the various nuclear reactions in the Sun.

The measure of the shape of the transition region is important also because this shape is very sensitive to possible Non Standard Neutrino Interactions, a model developed by the theorists also in order to explain the neutrino oscillations.

3. The Borexino experiment

The Borexino detector has been designed with the aim to study the solar neutrinos below 1 MeV. As already said in the paragraph 1, the other experiments in real time defined a threshold much higher; the reason of the high threshold was due to the natural radioactivity, which is present everywhere, in the environment, in the construction materials used in the detector. The highest energy reached by the natural radioactivity is about 3 MeV (Tallium nuclides) and, taking into account also the resolution of the reconstruction energy, a setting of the threshold at ~ 5 MeV is a proper choice.

Therefore the first worry of the Borexino designers has been the background due to the natural radioactivity; a second worry concerned the resolution reachable in the reconstruction of the neutrino event energy and position. To fulfill the second worry liquid scintillator has been chosen as detecting material due to its high light yield which allows good measurement resolutions.

For what concerns the background we can note that one ton of liquid scintillator collects about 0.5 neutrino events/day of the ^7Be flux, corresponding to an activity of $\approx 5 \cdot 10^{-9} \text{ Bq/kg}$. The regular air and water show a radioactivity level of 10-20 Bq/kg, and the rocks, 100-1000 Bq/kg. Therefore a gain of 10-11 orders of magnitudes was required!

To be shielded from the cosmic rays the detector is installed in the Gran Sasso underground laboratory in the Italian Apennines, with $\sim 1400 \text{ m}$ of rock overburden. 1.2 cosmic muons per m^2 and per hour, in addition to the neutrinos, survive traveling across the mountain.

The structure of the detector is shown in figure 5. A big Water Tank (Diameter: 18m; Height: 16.5 m) contains 2100 m^3 of highly purified water and a stainless steel sphere (SSS) with 13.7 m of diameter. The water functions as a shield with respect to the radiations (gammas and neutrons) emitted by the rocks and the air of the underground laboratory. In the water tank a muon veto is installed (Outer Detector) with 208 photomultipliers.

The SSS functions as a support of 2212 photomultipliers and contains 1300 m^3 of a liquid aromatic compound (pseudocumene): in the centre of it, 300 m^3 of this compound, added with a 1.4 g/l of a so called fluor, is contained in a very transparent nylon vessel

(Inner Detector), 125 μm thick. The 300 m^3 are a two component liquid scintillator, which is the actual detecting material.

The more external 1000 m^3 contained in the SSS are added with a quencher to avoid light emission when particles are crossing them; their role is to equal the scintillator density in order to produce a negligible buoyancy on the very thin nylon vessel. The choice of a so thin nylon walls is due to the need to reduce as much as possible the radiation emission from the residual radioactivity present in the nylon. Nevertheless, to study the neutrino interactions, a smaller Fiducial Volume, 100 m^3 of volume, is defined to shield the residual background and in particular the one emitted by the vessel walls. A vessel balloon is installed between the Inner vessel and the photomultipliers as a barrier against the radon emitted by them and by the stainless steel of the SSS.

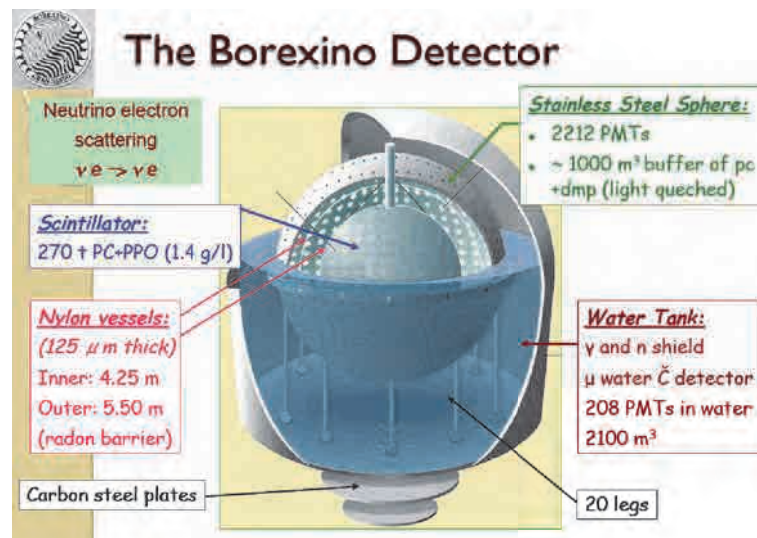


Figure 5 A dummy of the Borexino detector.

The Borexino collaboration in five years of research succeeded to develop new technologies to purify the scintillator from the radioactive elements. These technologies

allowed to achieve an unprecedented low radioactive level. Also the Nitrogen used to strip the noble gasses from the scintillator, as for instance the Radon, has been purified reaching a very low percentage of Radon, Argon and Krypton, always present in air. In addition special procedures have been adopted during the detector installation: the fabrication and the installation have been carried out in clean rooms, the detector itself has been equipped as a clean room, the plants have been assembled in Nitrogen or in Argon atmosphere, all components have been developed on purpose or very carefully selected; for the scintillator the crude oil has been taken only from very old layers, to have very low ^{14}C content.

All these efforts have been very successful: the radio-purities so obtained are a record in the world research. The results are presented in Table 2, where they are compared with the regular unpurified components.

Table 2 Radiopurity levels reached in Borexino (last column) compared with the regular ones.

	Material	Typical conc. of the unpurified materials	Final radiopurity levels
^{14}C	scintillator	$^{14}\text{C}/^{12}\text{C} < 10^{-12}$	$^{14}\text{C}/^{12}\text{C} \sim 2 \cdot 10^{-18}$
$^{238}\text{U}, ^{232}\text{Th}$ equiv.	- Hall C dust - stainless. steel - nylon	$10^{-5} - 10^{-6} \text{ g/g}$	$10^{-17}/10^{-18} \text{ g/g}$
K_{nat}	Hall C dust	$\sim 10^{-6} \text{ g/g}$	$< 3 \cdot 10^{-14} \text{ g/g}$
^{222}Rn	- external air. - air underground	$\sim 20 \text{ Bq/m}^3$ $\sim 40 - 100 \text{ Bq/m}^3$	$< 1 \text{ mBq/m}^3$
^{85}Kr ^{39}Ar	in N_2 for stripping	$\sim 40 \text{ ppt}$ $\sim 10 \text{ ppm}$	$\sim 0.16 \text{ mBq/m}^3$ $\sim 0.5 \text{ mBq/m}^3$
- ^{222}Rn - $^{238}\text{U}, ^{232}\text{Th}$ equiv. - ^{226}Ra	LNGS - Hall C water	Few kBq/m^3 $\sim 10^{-10} \text{ g/g}$ 2 Bq/m^3	$\sim 30 \text{ mBq/m}^3$ $\sim 10^{-14} \text{ g/g}$

The neutrino interactions detected in Borexino are the elastic scattering $\nu_e + e^- \rightarrow \nu_e + e^-$. The hardware threshold is fixed at ~ 60 keV, while the software one is defined between 160 and 200 keV of the electron recoiled energy. These very low thresholds are allowed by the very low radioactivity levels of the detector.

The light yield of the scintillator is very good : 10^4 photons/MeV, corresponding to ~ 500 photoelectrons/MeV if we take into account the optical coverage and the photomultiplier quantum efficiencies. The resolution of the energy reconstruction is

$\frac{5\%}{\sqrt{E(\text{MeV})}}$ from 200 keV to 2 MeV; the position of the events within the detector is reconstructed via the photomultiplier timing with an uncertainty: $\Delta(x,y,z) = 10 - 12 \text{ MeV}$.

For further details of the Borexino detector see reference [7].

4. Results on solar neutrinos

In fig. 6 the energy spectrum of the collected events is shown. The raw data are plotted, once the cosmic muons and the muon induced events are rejected, and a cut on the fiducial volume has been introduced at $R=3$ m from the centre of the detector ($\sim 100 \text{ m}^3$ of scintillator). The various contributions are also shown as they result from a global fit. We can observe that, in addition to the neutrinos from the nuclear reactions in the Sun (^7Be , pp, pep, CNO), also residues of radioactive contaminants are present (^{85}Kr , ^{210}Bi , ^{210}Po , ^{11}C). It has to be noted that the fit shown in figure 6 is devoted to ^7Be ; therefore pp, pep and CNO are fixed at the SSM expectations. The ^7Be and pep nuclear reactions produce mono-energetic neutrinos and, as a consequence, the recoiled electrons from the

ν -e elastic scattering show the typical Compton edge, a shoulder at the end of their energy distribution.

Various tools are available to fight against these residual contaminants. Alpha particles are identified by means of the property of the scintillator molecules to decay more slowly in case of alphas than in case of electrons and gammas. Therefore the nuclides, as ^{210}Po , which are alpha emitters, can be rejected.

The ^{11}C is continuously produced by the residual cosmic muons crossing the overburden. It decays into $^{11}\text{B} + e^+ + \nu_e$ with a lifetime of 29.4 minutes. It can be rejected via a threefold coincidence among the incident muon, the positron emitted in the ^{11}C decay and a neutron (s) which is produced in the muon interaction: it loses energy traveling in matter and after $\sim 250 \mu\text{s}$ is captured by a proton, producing a deuteron with the emission of 2.2 MeV gamma.

Finally the ^{85}Kr fitted rate can be checked by identifying the following decay:

$^{85}\text{Kr} \rightarrow ^{85}\text{Rb}^* \rightarrow ^{85}\text{Rb}$ with the emission of a 173 keV β and a 514 keV γ with a delay of

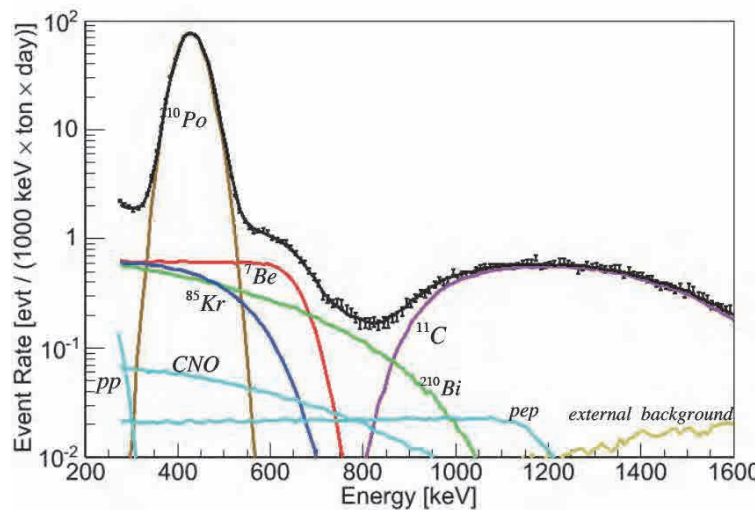


Figure 6. Spectrum of the raw data collected by Borexino, once rejected the muons and the events muon induced. Fiducial volume: $R < 3\text{m}$.

1.464 μs . Unfortunately this decay has a branching ratio of only 0.46%; therefore a high statistics has to be collected to have a good check.

In three years of data taking Borexino has reached the following results:

- i) a precise measurement of the solar neutrino flux from ^7Be at 862 keV. The rate is 46.0 ± 1.50 (stat.) ± 1.55 (syst.) counts/day and 100 tons. The first error is the statistical error obtained by the fit, the second one is the systematic error due to the uncertainties introduced by the cuts, the fitting methods, the energy scale. The corresponding unoscillated flux is: $\Phi(^7\text{Be}) = (3.1 \pm 0.25) 10^9 \text{ cm}^{-2} \text{ s}^{-1}$; the ratio to the SSM prevision is: $f_{\text{Be}} = 0.97 \pm 0.05 \pm 0.07$ [8].
- ii) for the ^7Be flux also the day/night effect has been investigated. This effect is due to the following mechanism: the solar ν_e s traveling within the solar matter are partially converted into ν_μ and ν_τ ; during the night they cross the Earth to reach the detector and some part of them can be reconverted into ν_e . In the ^7Be case this effect is null: the result obtained by Borexino is: $A_{\text{ND}} = -0.001 \pm 0.012$ (stat.) ± 0.007 (syst.) [9]

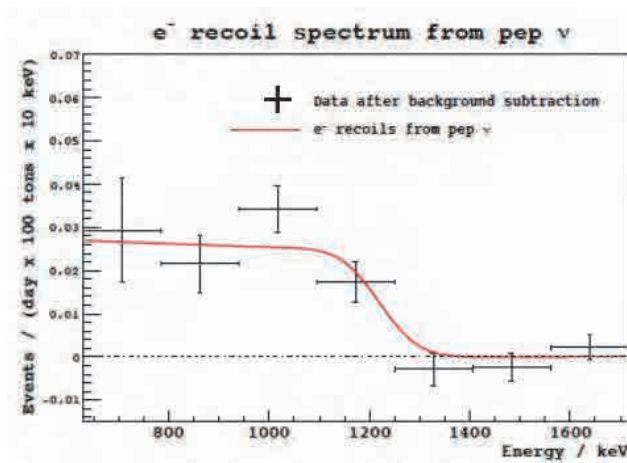


Figure 7. Energy spectrum of the neutrino interactions in the pep region once the backgrounds subtracted.

iii) Borexino succeeded to measure also the flux from the pep reaction. This is particularly difficult due to the rate, which is less than 1/10 of the ${}^7\text{Be}$ one. A very refined analysis was needed. In figure 7 the experimental data, once the background subtracted (crosses), are fitted with a continuous line: the Compton edge of the pep recoiling electrons is evident. The measured rate is: $3.13 \pm 0.05(\text{stats.}) \pm 0.23(\text{syst.})$ cpd/100 tons, the un-oscillated flux, $\Phi(\text{pep}) = (1.6 \pm 0.3) 10^8 \text{ cm}^{-2} \text{ s}^{-1}$, and the ratio to the SSM expectation, $f_{\text{pep}} = 1.1 \pm 0.2$ [10].

iv) the analysis of the neutrinos produced by the CNO cycle is very hard because its energy spectrum has a shape similar to the ${}^{210}\text{Bi}$ one. Borexino succeeded to disentangle a stringent upper limit : rate(CNO) < 7.6 cpd/100 tons, $\Phi(\text{CNO}) < (7.4 10^8 \text{ cm}^{-2} \text{ s}^{-1})$, $f_{\text{CNO}} < 1.4$ [10].

v) Borexino has measured also the neutrinos from ${}^8\text{B}$, with a lower energy threshold down to 3.0 MeV (3.2 MeV neutrino energy), obtaining a total flux of 2.4 ± 0.4 (stat.) $\pm 0.1(\text{syst.}) 10^6 \text{ cm}^2 \text{ s}^{-1}$ [11].

5. Impact of Borexino results on the neutrino and Sun physics.

I discuss here only two important insights in the neutrino physics due to the Borexino results on solar neutrinos.

The first concerns the survival probability of the electron-neutrino. In the figures 8a and 8b the ν_e survival probability is shown before (a) and after (b) Borexino. Before Borexino only the high energy region of the solar neutrino spectrum was measured, corresponding to the oscillation in matter. At lower energy only two scattered points with

large errors are plotted: they have been obtained by subtracting the ^8B flux from the integrated flux measured by the radiochemical experiments.

In figure 8b the same plot includes the Borexino data. Borexino has measured the survival probability in vacuum regime via the ^7Be flux, constraining also the pp expectation. Both ^7Be and pp show small errors and validate the prevision of the oscillation model (MSW).

At high energy two points are plotted, one is an average of SNO and Superkamiokande results over 5 MeV of threshold; the second one, the average of Borexino and SNO (>3.2 and >4.2 MeV neutrino energy, respectively). Using the Borexino results we can calculate the ratio between the survival probability in vacuum

and in matter: $\frac{P_{ee}^{vac}}{P_{ee}^{matter}} = 1.62 \pm 0.26$

Finally Borexino started the study of the transition region with the pep flux and the low threshold ^8B measurements. Unfortunately the statistics is still not enough to understand if the shape of the survival probability in this energy range is close to the prediction of the MSW model.

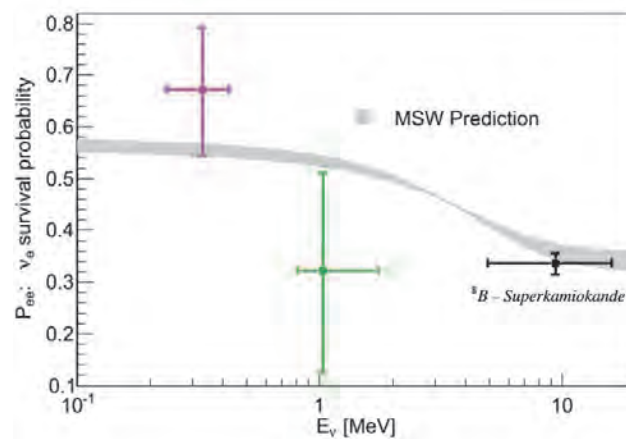


Figure 8a. ν_e survival probability before Borexino

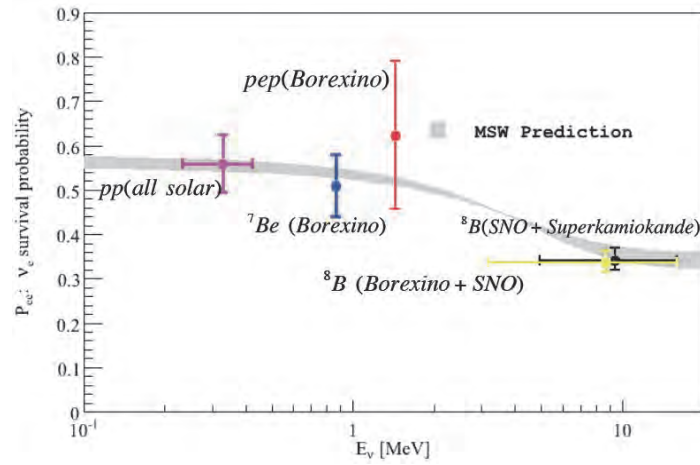


Figure 8b. ν_e survival probability after Borexino

The best fit values of the oscillation parameters, the mass difference Δm^2 and the mixing angle θ , using all solar experiments before Borexino plus the Kamland results on reactor antineutrinos succeed to isolate a parameter range called “Large Mixing Angle (LMA)”. This operation needs the assumption that neutrinos and antineutrinos have the same behavior. Adding the Borexino data it is possible to isolate the LMA region without the antineutrino data thus without any assumption (CPT conservation).

The results of Borexino give also a good validation of the SSM, because the measured fluxes are in agreement, within the errors, with its previsions. Unfortunately the experimental errors and the uncertainties of the solar model do not allow yet to discriminate between high and low metallicity.

6. Geoneutrinos

The geoneutrinos are antineutrinos emitted in radioactive decays taking place in the Earth interior. The radioactive nuclei present in the Earth are the Uranium and Thorium decay chains and the ^{40}K nuclide. In each decay of these radioactive elements antineutrinos and radiation energy are emitted; this energy is fully converted in heat. It is important to know how much of the total Earth heat is due to the radioactive decays and how many of them take place in the Crust and how many in the Mantle.

The geoneutrino flux is very low (~ 1.5 events every two months in Borexino) and therefore its measurement is hard; on the other hand the antineutrino interactions are very well tagged (inverse beta decay) and so it is possible to discriminate them with respect to the background due to the natural radioactivity and to the neutrino interactions. But another background is due to the antineutrinos produced by the nuclear reactors, which show an energy spectrum partially superimposed to the geoneutrino energy. Borexino is well favored because at the Gran Sasso site the flux from reactor antineutrinos is relatively small.

A first hint on the existence of the geoneutrinos has been obtained by KamLAND with an evidence of ~ 2 sigma. Later Borexino reached the first actual evidence a ~ 4.2 sigma [12], followed more recently by KamLAND with a similar evidence [13]. A joint analysis of Borexino and KamLAND results give the indication that the radioactive decays can produce about $\frac{1}{2}$ of the total Earth heat.

7. Conclusions

In three years of data taking Borexino obtained the first measurement of the solar neutrino fluxes from the ^7Be and pep reactions. In addition a stringent upper limit for the

neutrinos from CNO has been reached. In this way the oscillation in vacuum has been studied and the MSW oscillation model has been validated in that regime.

The pep flux measurement and the ^8B neutrinos studied by Borexino with a lower threshold down to 3.2 MeV, neutrino energy, are a starting point for the study of the transition region shape. Unfortunately the statistics is not yet enough to check the possible existence of non standard neutrino interactions. On the other hand the Borexino results are in excellent agreement with the expectations of the Standard Solar Model.

The day/night effect is null in the ^7Be region following the Borexino data and this allows the isolation of the oscillation parameters without taking into account the reactor antineutrino results and therefore without the assumption of no CPT violation in the neutrino sector.

Borexino is now proceeding to a re-purification campaign to reach a radiopurity even better of the present one. A further data collection during 3-4 years would allow to reduce the error of the pep and ^8B over 3 MeV fluxes, allowing a good study of the transition region. In addition the present goal is addressed to obtain the experimental proof of the existence of the CNO cycle, which will allow also the solution of the metallicity puzzle.

Finally Borexino reached the experimental evidence of geoneutrinos at 4.2 sigma of confidence level. Further data will allow a better evaluation of the Earth heat produced by the radioactive α decays in the Earth interior.

References

- [1] see for example: Bahcall, J.N., Status of Solar models, 1997, Proceed. of the XVII Int. Conf. on Neutrino Physics and Astrophysics, 56-70
- [2] Cleveland, B.T., et al., 1998, Ap.J. **496**, 505
- [3] Hampel W. et al., 1999, Phys. Lett.B **447**, 127
- [4] Ahmad Q.R. et al, 2001 Phys. Rev. Lett. **87**, 071301
- [5] Mikheyev S.P. and Smirnov A.Yu., 1985 Sov. J.Nucl. Phys. **42**, 913; Wolfenstein L., 1978, Phys. Rev. D **17**, 2369
- [6] Serenelli A.M. et al., 2010, arXiv:1104.16.39v1 [astro-ph]
- [7] Alimonti G. et al., 2009 Nucl. Instrum. and Meth A **600**, 58
- [8] Bellini G. et al., 2011 Phys. Rev. Lett. **107**, 141302
- [9] Bellini G. et al, 2012 Phys. Lett. B, **707**, 22
- [10] Bellini G. et al, arXiv: 1110.3230[hep-ex], accepted for publication on Phys. Rev. Lett.
- [11] Bellini G. et al, 2010 Phys. Rev.D **82**, 033006
- [12] Bellini G. et al, 2010 Phys. Lett.B **683**, 299
- [13] Gando A et al. 2011 nature geo-science. Ngeo **1205** 1

THE LITTLE BANG IN THE LABORATORY: HEAVY IONS @ LHC WITH ALICE

■ PAOLO GIUBELLINO

INFN Torino and CERN Geneva

E-mail: paolo.giubellino@CERN.ch

The LHC has delivered for the first time collisions of Nuclei in November 2010, at an energy of 2.76 TeV per nucleon pair, which represents a jump of more than an order of magnitude over the highest energy nuclear collisions ever studied before. The high energy, the quality of the state-of-the art detectors, and the readiness of the experimental collaborations at the LHC have allowed a rich harvest of important scientific results in a very short time. In this paper a short overview will be given of how the results from the LHC, and in particular from the ALICE experiment, have provided new insight on the properties of matter under extreme conditions of temperature and pressure, analogous to the conditions present in the early phases of the evolution of the Universe.

*Symposium of Subnuclear Physics at the Pontifical Academy of Sciences,
Vatican ,2011*

1. Why high-energy Heavy-Ion Collisions

Collisions between very high-energy nuclei, normally referred to as Heavy-Ions since they are atoms stripped of their electrons to allow acceleration, produce each a huge number of particles, over ten thousand in a single event at the LHC. A typical event is shown in Fig. 1. The study of such extremely complex events poses a formidable challenge both to the detection systems and to the software and analysis methods to be used to treat and eventually understand the data. So, it is legitimate to ask first of all the question of why experimenters are willing to face such extreme problems, what are the underlying questions which we aim to answer.

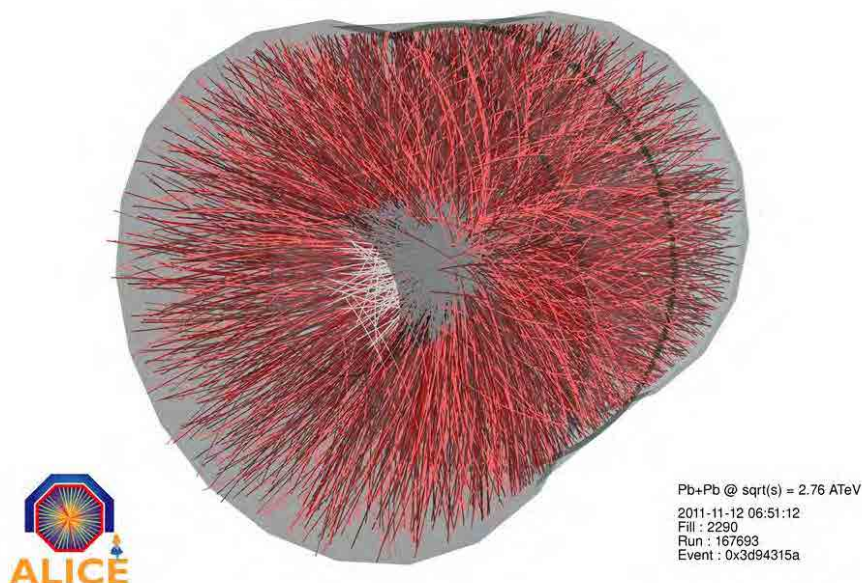


Fig. 1 A collision of two Lead Nuclei as seen by the ALICE detector at the LHC.
 (CERN-EX-1111290 04)

The strong force, which holds together the nucleons, protons and neutrons, in nuclei and the quarks within the nucleons, is described to great precision by a very successful theory, called Quantum Chromo Dynamics (QCD), in which the quarks possess a color charge and interact exchanging force carriers, the gluons, which are also colored. A fundamental feature of the interaction is the fact that it grows with the distance between the quarks, much like a spring connecting two balls. Therefore, any attempt to isolate a quark are in vain, since the energy stored in the spring will eventually be more than the mass of a quark-antiquark pair: the spring will break generating a pair, and the quarks will not be isolated. This property is called “confinement” and has major consequences. In particular, most of the mass of the hadrons is to be attributed to this feature: more technically, one can say that the mass is acquired dynamically because of the interaction between the quarks, whose Higgs mass would account for just a small fraction, about 1%, of the mass of the light hadrons as shown in Fig. 2. Therefore, since the mass of the matter around us is essentially the mass of the nuclei of the atoms, it can be said

that, while the Higgs mechanism is at the base of the masses of the quarks, strong interaction is at the origin of most of the mass of ordinary matter.

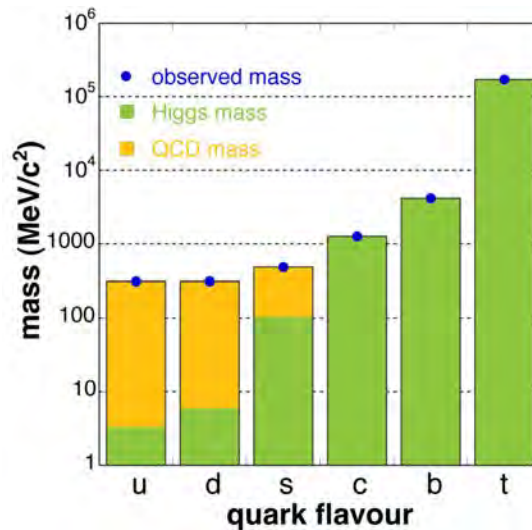


Fig. 2 QCD and Higgs mass components for the light and heavy quarks from Ref [1]

The method of colliding high-energy nuclei to heat and compress hadronic matter dates from the early eighties, but the path had been indicated already several years before. It was in 1975 that T.D. Lee pronounced the famous sentence "it would be interesting to explore new phenomena by distributing a high amount of energy or high nuclear density over a relatively large volume", and the idea of deconfinement had been around for some time. Already in 1965 Hagedorn had observed that the mass spectrum of hadronic states led naturally to the concept of a "limiting" or "critical" temperature beyond which the concept of hadron would cease to make sense. In 1973 the development of QCD as the theory describing strong interactions introduced the concept of asymptotic freedom[3][4]: at small distances quarks and gluons would be loosely interacting, or quasi-free.

In 1975, N. Cabibbo and G. Parisi[5] proposed for the first time the existence of a "different phase of the vacuum in which quarks are not confined", and drew the first schematic diagram of hadronic matter with temperature and baryonic density as axes. Two regions were defined: at low-T and low baryonic density, ordinary hadrons, at high-T, high- μ_B a deconfined state: a new field of research was born! In the same year, J.C. Collins and M.J. Perry[6] developed the idea that matter under extreme density conditions, as in neutron star cores and in the early universe, is made of quarks instead of hadrons, which overlap and lose their identity. Their argument was based on the fact that quarks interact weakly when they are close together, and therefore at high densities could be described as a gas of free massless quarks. Finally, in 1980 E. Shuryak introduced [7] the term quark gluon plasma (QGP) to describe the state of nuclear matter in which quarks are deconfined, stressing the analogy between a classical plasma made by ionized atoms and the state made of colored strongly interacting objects.

In a nucleus-nucleus collision the energy of the incoming projectiles is dissipated in the relatively large volume defined by the overlap region of the two colliding nuclei, thus creating the conditions for a phase transition to deconfined quark matter by heating.

So, by colliding nuclei at high energies we compress and heat a system with a large number of quarks, to form a “bubble” of deconfined strongly-interacting matter, which in a very short time, of the order of 10^{-23} s, expands and cools until ordinary hadrons reconstitute, just as they did in the evolution of primordial Universe, some 10 millionth of a second after the Big Bang.

Over the last three decades, a vigorous experimental program, carried both in Europe and in the United States, has dramatically increased our understanding of nuclear matter under extreme conditions of temperature and density, allowing a real exploration of the phase diagram of strongly interacting matter. Our current understanding is graphically summarized in Fig. 3, with the trajectories allowed by the most important accelerators in operation or under construction: the two colliders LHC (in Europe) and RHIC (in the USA) and the fixed-target high-luminosity facility FAIR under construction in Germany.

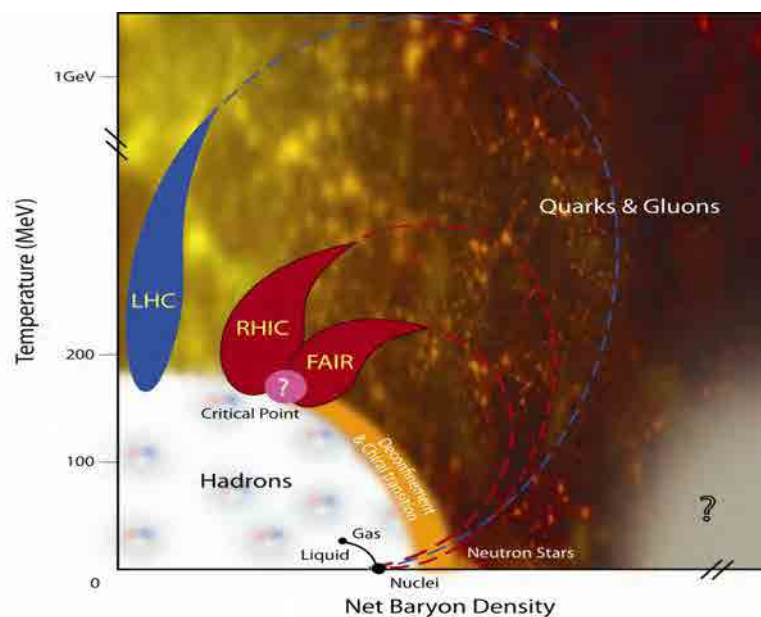


Fig.3 The phase diagram of nuclear matter, from Ref[1]

Together, these programs aim at providing answers to questions such as:

What are the properties of matter at the highest temperatures and densities?

What is the QCD equation of state? How can we test it?

What are the dominant microscopic mechanisms of QCD non-equilibrium dynamics and thermalization?

How does hadronization proceed dynamically? How is it changed in dense QCD matter?

How can the QCD phase diagram be efficiently explored?

Clearly, a comparison of the experimental results with theory is not a trivial task. Since the transition to the deconfined phase is outside the limits of validity of the perturbative QCD, a number of different approaches has been developed to derive the equation of state and the transition temperature. Only at the LHC some aspects of the interactions will be accessible with perturbative methods. Effective lagrangians have been extensively used, and also potential models, and even calculations based on the AdS/CFT correspondence have been providing a fresh look and new insight. Still, the most important and widely used are QCD calculations on a space-time lattice. They generally predict a phase transition to occur, and are able to determine its temperature. Current results indicate a critical temperature around $T_c \sim 170$ MeV, or about 10^{12} K, 100000 times higher than at the center of the Sun, corresponding to a critical energy density of $\epsilon_c \sim 700$ MeV/fm³.

In the following, I will give a brief overview of the main experimental results obtained so far at the LHC, just little over one year after the very first collision of Lead Nuclei was recorded in the experiments. Three experiments joined in this pioneering work: ALICE [9], a dedicated experiment specifically designed to study nuclear collisions, and both ATLAS [10] and CMS [11], the two general-purpose experiments of the LHC, primarily designed for the study of high- p_T processes in pp collisions. I will focus mostly on the ALICE results.

While I will not describe the experimental apparatus, I would like to remind here that ALICE has a very different optimization compared to the other LHC experiments. For the understanding of nuclear collisions it is essential that as many of the produced particle as possible are measured and identified, for the widest possible range of transverse momenta (typically from 0.1 to 100 GeV/c) and for all particle types: electrons, muons, photons and hadrons. So, the two guiding principles in the ALICE design have been robust tracking, able to handle the very large number of tracks which characterize Heavy Ion Collisions, and Particle Identification capability. The first is provided by very high granularity tracking detectors providing 3-Dimensional space points (several hundred millions of points) operating in a moderate magnetic field and with very low material. To identify leptons, photons and hadrons, including short-lived particles, such as hyperons, D and B mesons, ALICE features essentially all known techniques: dE/dx, Cherenkov & Transition radiation detectors, Time Of Flight, calorimeters, muon filter and topology (secondary vertices, kinks).

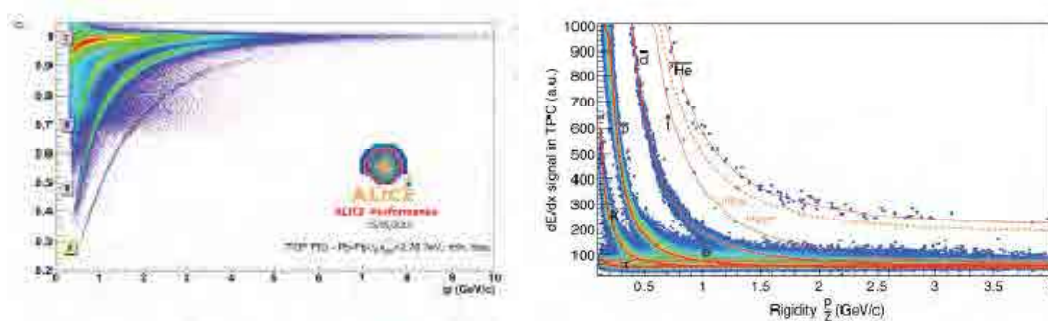


Fig. 4: PID in ALICE with TOF (left panel) and TPC (right panel) from ref.[12]

As an example of the ALICE PID capability, Fig. 4 shows the performance of the Time Of Flight (TOF) and of the Time Projection Chamber (TPC)'s energy loss measurement. Both are performing better than originally specified, a remarkable result in detector systems of such complexity observing events with thousands of tracks! The TOF has provided a time resolution below 100 picoseconds, and the TPC an energy loss measurement with a precision better than 6%.

In figure 5 (left panel) the momentum coverage of the various ALICE PID detectors is shown, demonstrating the extent of the coverage achieved. In addition, short-lived particles are identified through their decay topologies: in the right panel of figure 5 the impact parameter resolution expected in ALICE is shown, which is adequate for the measurement of D and B meson decays. K and Λ decays can be efficiently reconstructed for transverse momenta up to more than 10 GeV/c. The very fine granularity of the tracking detectors, providing a large number of space points per track, provides high efficiency tracking for charged particles even at the highest particle multiplicities foreseen at the LHC with Pb beams, with a lower limit in momentum lower than 200 MeV/c. The very long track length measured allows ALICE to achieve an excellent momentum resolution ($\delta p/p < 5\%$ at 100 GeV/c). Several smaller detectors (ZDC, PMD, FMD, T0 and V0) used for global event characterization and triggering are located at small angles. The combination of the central and forward detectors provides coverage for the measurement of charged multiplicity which extends from -3.4 to +5 in pseudorapidity. An Electromagnetic Calorimeter, EMCal, covers about a third of the azimuth and provides improved energy resolution and triggering for jets. A high-resolution crystal photon spectrometer, PHOS, is placed at a very large radial distance from the interaction point (4.6 m). The muon spectrometer covers the forward rapidities, between -2.5 and +4, and features a complex arrangement of absorbers, starting very close to the interaction point (90cm) to minimize muon background from weak hadronic decays, and fourteen planes of tracking and triggering chambers, using 2-D pad readout to handle the high multiplicities.

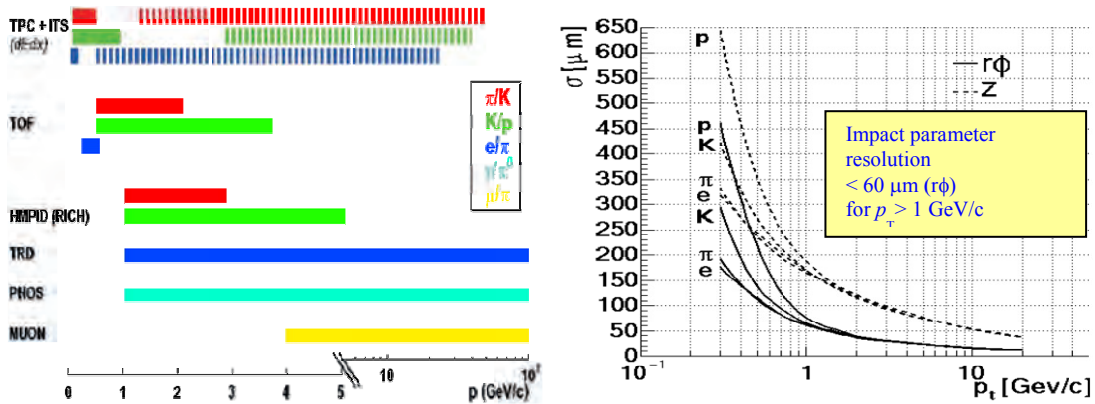


Figure 5: Left: particle identification in ALICE: momentum range and detectors used. Topological identification, not included in this plot, can reach over 10 GeV/c for K and Λ . Right: ALICE impact parameter resolution as a function of transverse momentum.

The hardware trigger in ALICE combines the input from detectors with fast trigger capability (T0, V0, ZDC, SPD, TOF, PHOS, EMCal, Muons, ACORDE). It operates at several levels (pretrigger, L0, L1 and L2) to satisfy the individual timing requirements of the different detectors, as the ALICE electronics is in general not pipelined. In addition, a software based High-Level Trigger (HLT) using a farm of up to 1000 multiprocessor PCs performs a preprocessing of the data allowing for a compression of the data volume by a factor of 3.5. It also allows real time data quality monitoring.

2. ALICE results

The first LHC heavy-ion results were already published during the 2010 lead–lead run, lasting for a month. In fact, there were three papers submitted almost simultaneously: the multiplicity measurement [13] and the measurement of v_2 coefficient of the azimuthal anisotropy [14] by ALICE, and by the ATLAS collaboration a paper on jet-energy imbalance [15]; these appeared together in one issue of Phys. Rev. Lett. One of the most spectacular findings at RHIC was that the matter generated in heavy-ion collisions flows like a liquid with very low viscosity, almost at the limit of what is allowed for any material in nature. This tells us that the constituents of this QGP are quite different from freely interacting quarks and gluons, and led to the definition of the matter under study as sQGP, for strongly interacting Quark Gluon Plasma, a liquid very different from the expected gas of quasi-free quarks and gluons. The first LHC azimuthal anisotropy measurement [14] confirms the RHIC results: elliptic flow of particles with the same transverse momenta is almost identical at the two energies. The nearly-perfect fluid has been found to be opaque to even the most energetic partons (quarks and gluons), which appear as jets of particles from the collisions, an effect known as jet quenching. This is an interpretation of the reported strong jet-energy imbalance [15]. However, the physical mechanisms underlying these phenomena are not well understood. Another manifestation of jet quenching manifests is a reduced yield of high-transverse-momentum-particle in central collisions compared to that expected from the measurements in proton–proton reactions. To express such reduction a properly normalized ratio of yields in heavy-ion and in proton–proton interactions – the nuclear modification factor R_{AA} – is used. Since proton-proton collisions are rescaled according to the number of binary collisions, R_{AA} should be well below one at low transverse momentum, where particle production is rather proportional to the number of participant nucleons, and grow toward one for increasing transverse momenta. The suppression pattern observed by ALICE [16] gives factor about 7 ($= 1/R_{AA}$) lower charged-particle production in lead–lead collisions at transverse momentum around 6 GeV/c, a striking evidence of the energy loss in the extreme density matter.

The size of the pion-emitting source in central lead-ion collisions is deduced from the shape of the Bose-Einstein peak in the two-pion correlation functions [17]. The collective flow makes the size of the system appear smaller with increasing momentum of the pair. This behaviour is clearly visible for the radii measured in the ALICE experiment. The results for measurements of the radius of the pion source in three dimensions indicate a short duration for the emission,

hence an “explosive” emission. Time when the emission reaches its maximum is 10–11 fm/c, significantly longer than it is at RHIC, see fig. 6 (left side). Moreover, the product of the three components at low pair-momentum, an estimate of the homogeneity volume of the system at decoupling, is twice as large as at RHIC, see fig. 6 (right side).

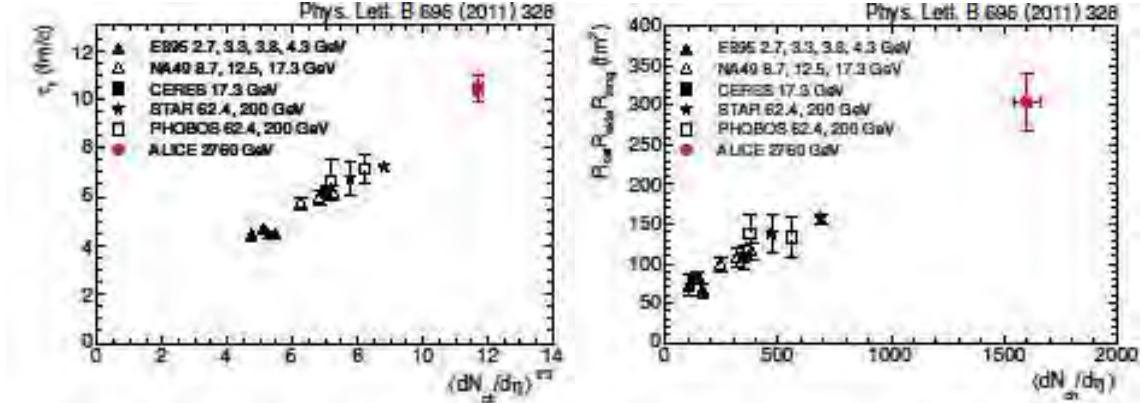


Figure 6. Bose–Einstein pion-interferometry results from different experiments [17]. Estimate of lifetime of emitting source as a function of cube root of particle density (left side). Volume of homogeneity region as a function of particle density (right side).

One of the crucial measurements for the characterization of the fireball produced in heavy-ion collisions are the spectra of identified hadrons, which encode the collective expansion velocity developed in the QGP and in hadronic stages. Moreover, the overall abundances of identified hadrons are believed to be fixed at hadronization, thus they indicate the temperature when chemical composition was established. The measured spectra [18] show an increase of about 10% in the radial-flow velocity when compared to RHIC results. At present, however, the yield ratios observed by ALICE seem to challenge both previous experiments and theory. While the K/π , Ξ/π and Ω/π ratios are compatible with the expectations from the thermal model with a temperature for the “chemical freeze-out” of about 165 MeV, as in previous observations, the p/π ratio points to a significantly lower temperature. On the experimental side, there are indications of a similar effect at lower energies, which call for further investigations. On the theoretical side, a number of different possibilities are being investigated, none of them conclusive at the moment.

As mentioned above, the first results on elliptic flow were published [14] during the initial Pb–Pb run. Flow is a fundamental observable since it carries information on the equation of state and the transport properties of matter created in a heavy-ion collision. This observable relates final state anisotropies with features of the initial one, thus allowing study of the medium response and characteristics. The azimuthal anisotropy in particle production is a clear experimental signature of collective flow. It is caused by multiple interactions between the constituents of the created matter and the initial asymmetries in the spatial geometry of a non-central collision. The amount of elliptic flow measured by the v_2 coefficient, integrated over transverse momentum, increases by 30% compared to RHIC energies. However, this increase is entirely a consequence of the growth in transverse momenta. The overall azimuthal distribution of particles emitted in a heavy-ion collision can be described with a Fourier expansion, whose

coefficients relate to different aspects of the initial state. ALICE measured also the higher harmonic coefficients of azimuthal distribution [19]; they exhibit much shallower centrality dependence than v_2 , and the symmetry planes of v_2 and v_3 coefficients are uncorrelated (see fig. 7, left side). These observations point to fluctuations in the initial geometry as the origin of higher-order azimuthal asymmetries. The flow coefficients can also be studied with a different approach, using two-particle correlations in azimuthal angle [20]. A Fourier decomposition of the correlation function gives squares of different v coefficients, and describes well the structures seen in azimuthal correlations, see fig. 7 (right side), such as the “long-range ridge” (a small angle correlation between particles distanced in longitudinal direction) and the “Mach cone” (a correlation on two sides of back-to-back direction). The collective response to initial spatial anisotropy that causes elliptic flow economically explains these puzzling features, once event-by-event initial-state density fluctuations are considered. The ALICE experiment has analyzed azimuthal asymmetry also separately for different particle species, which constrains models incorporating a realistic initial state and hydrodynamic evolution.

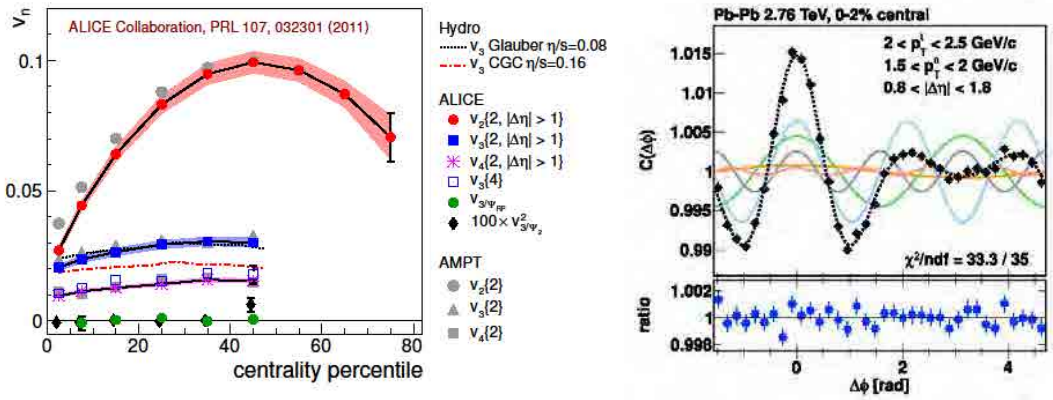


Figure 7. Measurements of azimuthal anisotropy in lead–lead collisions at LHC. Dependence of different v_n coefficients (see legend) on collision centrality [19] (left). Fourier decomposition of two-particle azimuthal correlation function in 2% most central collisions [20] (right).

The two-particle azimuthal correlations at higher transverse momenta measure particle-yield modifications in jet-like structures [21]. When compared to the expectation from proton–proton interactions, the observed yield around high-transverse-momentum particle is slightly higher, while the yield on the opposite side is reduced. This measurement assists the understanding of jet-quenching phenomena. The ALICE collaboration continues to contribute to this topic by studying reconstructed jets, underlying event fluctuations, modifications of jet-fragmentation function, jet-particle composition and providing detailed studies of the dependence of the energy loss on the parton traversing the QGP.

Heavy-flavour particles are recognized to be effective probes of a very dense and hot medium formed in nucleus–nucleus collisions; they are expected to be sensitive to its energy density, through the mechanism of in-medium energy loss. At LHC energies, heavy-flavour particles are copiously produced and thus provide ideal tools for QGP studies. The nuclear modification factor R_{AA} is well established as a sensitive observable for the study of the interaction of hard partons with the medium. Parton energy-loss is caused by the strong interaction, hence the

amount of energy loss depends on colour charge of parton. Therefore, quarks are predicted to lose less energy than gluons. In addition, heavy quarks (up to some high momentum), which are slower than light, cannot emit gluons within the so-called “dead-cone” around their trajectory; this effect is expected to reduce the energy loss of heavy quarks with respect to light ones. Thus, a pattern of gradually decreasing suppression (i.e. increasing R_{AA}) should emerge when going from the light-flavour hadrons (e.g. pions), which mainly come from gluons, to the heavier D and B mesons: $R_{AA}(\pi) < R_{AA}(D) < R_{AA}(B)$. The measurement and comparison of these different probes provides, therefore, a test of the colour-charge and mass dependence of parton energy-loss. The ALICE collaboration has measured the production of the charmed mesons D^0 and D^+ , detecting their hadronic decays in lead–lead collisions [22]. In central collisions a large suppression with respect to expectations at large transverse momentum was found, indicating that charm quarks undergo a strong energy loss in the hot and dense state of strongly-interacting matter formed at the LHC. This is the first time that D meson suppression has been measured directly in central nucleus–nucleus collisions. The results show a suppression by a factor 4–5, almost as large as for charged pions, above 5 GeV/c (see fig. 8). At lower momenta, there is an indication of smaller suppression for D than for π mesons.

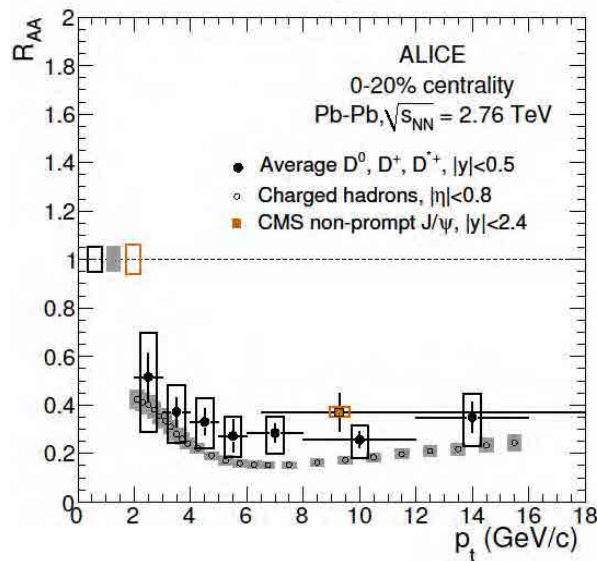


Figure 8. Charmed-meson nuclear modification factor as a function of transverse momentum compared to that of charged hadrons and of non-prompt (mostly from B-decays) J/ψ mesons (as measured by CMS).

Suppression of charmonium production was for a long time considered as one of the main probes for a deconfined medium. At large enough temperatures bound charm–anticharm states are supposed to be dissolved due to Debye screening. However, at LHC energies, new mechanisms of charmonium production in the QGP could occur because of a large number of charm quarks. Around one hundred charm–anticharm pairs are expected to be produced in a central lead–lead collision. Several dynamical transport models predict that charm and anticharm quarks could combine at later stages of the interaction, leading to an enhancement of

charmonium production in the most central collisions. ALICE detects charmonium down to very low transverse momentum in two different regions: the central barrel in the dielectron channel and the forward muon arm in the dimuon channel. The detection at low transverse momentum is crucial because the recombination of the charm and anticharm quarks is expected to be the main production mechanism for charmonium below 3 GeV/c. The different regions allow for the study of QGP with different charm densities. ALICE has studied the nuclear modification factor R_{AA} for J/ψ mesons as a function of collision centrality [23]. The results indicate that the J/ψ nuclear modification factor shows little dependence on centrality (see fig. 9), a trend that is different from that observed at lower energies. For central and mid-central collisions the J/ψ R_{AA} is larger at the LHC than that measured at RHIC. In a complementary study, the CMS collaborations at the LHC have measured a smaller value for the J/ψ nuclear modification factor at transverse momenta above 6.5 GeV/c. These observations hint at the recombination of charm and anticharm quarks in the QGP as the main mechanism for J/ψ production in central lead–lead collisions at LHC energies.

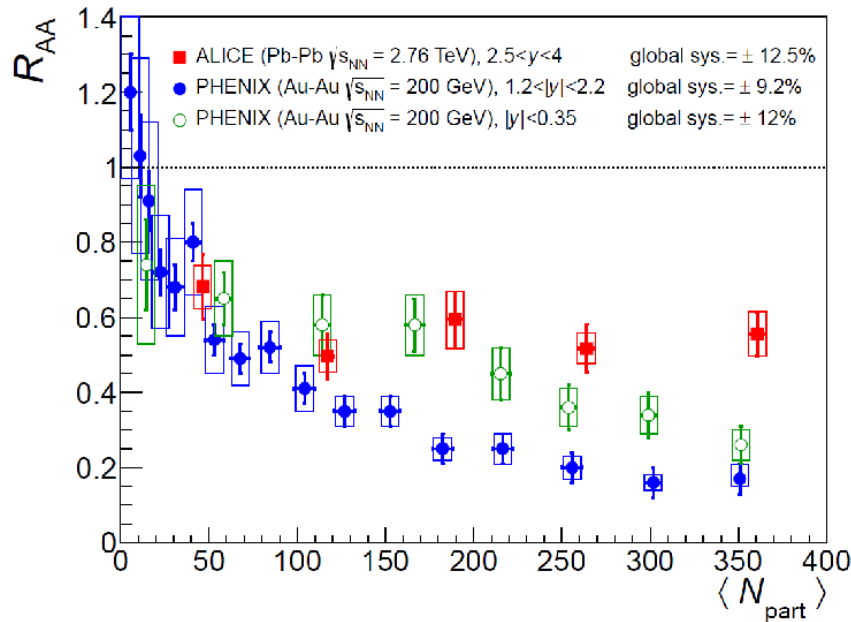


Figure 9. Nuclear modification factor for J/ψ as a function of collision centrality, expressed as number of participants. ALICE data are compared to those from the PHENIX experiment at RHIC.

It is clear from these first results that a coherent picture of the characteristics of the extreme density matter of which our Universe was made of in the first microseconds of its existence. Even more, the tool chosen to study it, heavy-ion collisions at the world’s most powerful accelerator, has proven to be the right one, allowing for a continuous improvement of our understanding. The results shown here are but a small subset of the wealth of results obtained so far, and a mere hint to the ones coming. It is indeed a very exciting time for the physics of the Quark-Gluon Plasma.

3. The future of ALICE

In 2010 the ALICE detector collected with a minimum-bias trigger about 30 million of lead–lead collisions at centre-of-mass energy of 2.76TeV per nucleon pair. In 2011 there was a short period of proton–proton running at the same energy at the start of the LHC operation, to gather comparison data; these were used for normalization in practically all measurements described above. The rest of the proton running proceeded at (a standard) energy of 7TeV. At the end of the year, the LHC switched again to the heavy-ion mode. This time the instant luminosity grew to above $10^{26}\text{cm}^{-2}\text{s}^{-1}$, and was above the design value for energy 2.76TeV per nucleon pair. ALICE used triggers for different types of lead–lead collisions: central, semi-central, dimuons, photons, jets, ultraperipheral, and others, and collected about 100 million events, inspecting over 0.1nb^{-1} of integrated luminosity.

The coming Heavy-Ion period, due for the beginning of 2013, will be dedicated to proton–lead collisions, to improve the baseline comparison, taking into account modifications of structure functions in nuclei. We expect to collect at least 0.03nb^{-1} of luminosity in the four weeks of pA running. Then the LHC operation will be paused for an upgrade necessary to increase the collision energy. After the restart the ALICE collaboration aims to complete its approved programme, collecting 1nb^{-1} of heavy-ion collisions at the higher collision energy (5.5TeV per nucleon pair in the centre of mass, being the design value). The intention is to achieve a significant part of this agenda before the second long shutdown for the preparation of the LHC luminosity increase, planned for 2018. Under discussion is an ALICE detector upgrade allowing for high-luminosity heavy-ion running after this period. The extended physics program justifying the LHC operation in heavy-ion mode beyond 2020, which would imply collecting over 10nb^{-1} of data, is being prepared.

After having confirmed the main discoveries obtained at RHIC, ALICE has entered an exciting phase of new measurements, allowing a much broader and deeper study of the QGP. At the same time, ALICE is already preparing, on the basis of what has been learnt so far, a next step in more detailed characterization of the extreme state of matter produced at LHC; new, unexpected discoveries may come!

References

- [1] NUPECC Long Range Plan 2010: Perspectives of Nuclear Physics in Europe, published by the European Science Foundation
- [2] R. Hagedorn, *NuovoCim. Suppl.* 3 (1965) 147-186
- [3] D.J. Gross and F. Wilczek *Phys. Rev. D* 8(1973) 3633—3652.
- [4] H. D. Politzer *Phys. Rev. Lett.* 30 (1973) 1346-1349.
- [5] N. Cabibbo and G. Parisi *Phys. Lett. B* 59 (1975) 67-69
- [6] J.C. Collins and M.C. Perry~M.C. *Phys. Rev. Lett.* 34(1975) 1352—1356.
- [7] E.V. Shuryak *Phys. Rept.* 61 (1980) 71—158
- [8] B. Muller and J. Nagle, *Ann. Rev. Nucl. and Part. Phys.* **56** (2006) 93
- [9] ALICE Collaboration, Aamodt K, et al., *JINST* 3:S08002 (2008).
- [10] ATLAS Collaboration, Aad G, et al., *JINST* 3:S08003 (2008).
- [11] CMS Collaboration, Adolphi R, et al., *JINST* 3:S08004 (2008).
- [12] A. Kalweit for the ALICE Collaboration, *J.Phys.G* G38 (2011) 124073.
- [13] K. Aamodt et al. (ALICE collaboration), *Phys. Rev. Lett.* **105** 252301 (2010).

- [14] K. Aamodt et al. (ALICE collaboration), Phys. Rev. Lett. **105** 252302 (2010).
- [15] G. Aad et al. (ATLAS collaboration), Phys. Rev. Lett. **105** 252303 (2010).
- [16] K. Aamodt et al. (ALICE collaboration), Phys. Lett. **B696** 30 (2011).
- [17] K. Aamodt et al. (ALICE collaboration), Phys. Lett. **B696** 328 (2011).
- [18] M. Floris for the ALICE collaboration, J. Phys. **G38** 124025 (2011).
- [19] K. Aamodt et al. (ALICE collaboration), Phys. Rev. Lett. **107** 032301 (2011).
- [20] K. Aamodt et al. (ALICE collaboration), Phys. Lett. **B708** 249 (2012).
- [21] K. Aamodt et al. (ALICE collaboration), Phys. Rev. Lett. **108** 092301 (2011).
- [22] B.Abelev et al. (ALICE collaboration), JHEP **1209** 112 (**2012**)
- [23] B.Abelev et al. (ALICE collaboration), Phys.Rev.Lett. **109** 072301 (**2012**)

AN INTERESTING RESULT IN PP COLLISIONS AT 7 TeV

■ A. AGOSTINELLI^{1,4}, A. ALICI³, P. ANTONIOLI², S. ARCELLI¹, R. BALDINI FERROLI³,
F. BELLINI^{1,4}, G. CARA ROMEO², L. CIFARELLI^{1,3,4}, M. COLOCCI¹, A. DE CARO³,
D. DE GRUTTOLA^{4,5}, S. DE PASQUALE⁵, M. FUSCO GIRARD⁵, B. GUERZONI^{1,4}, D. HATZIFOTIADOU²,
A. MARGOTTI², R. NANIA², F. NOFERINI³, P. PAGANO⁵, A. PESCI², R. PREGHENELLA³,
E. SCAPPARONE², G. SCIOLI^{1,4}, M.C.S. WILLIAMS^{2,4}, C. ZAMPOLLI^{2,4}, A. ZICHICHI^{1,4}

¹ Dipartimento di Fisica dell'Università e Sezione INFN, Bologna

² Sezione INFN, Bologna

³ Centro Fermi – Centro Studi e Ricerche e Museo Storico della Fisica “Enrico Fermi”, Roma

⁴ CERN, Geneva

⁵ Dipartimento di Fisica “E.R. Caianiello” dell'Università e Gruppo Collegato INFN, Salerno

In this work we explore the possibility to perform ‘effective energy’ studies in very high energy collisions at the CERN Large Hadron Collider (LHC). In particular, we focus on the measurement of the ‘quantum number flow’ in pp collisions with the ALICE experiment, exploiting the capability of the Zero Degree Calorimeters (ZDCs) to measure the energy of the leading baryons in the very forward region with respect to the beam axis. Similar studies performed at lower centre-of-mass energies have shown that, once the appropriate physical variables are chosen, particle production is characterized by universal properties: no matter the nature of the interacting particles, the final states have identical features.

Introduction

In high-energy particle collisions, bulk event properties like the average charged particle multiplicity are regarded as experimental observables of fundamental interest, providing important information on the dynamics of the interaction. In particular, the average charged particle multiplicity in multihadronic final states has been measured in many different interacting systems (e^+e^- and $pp(\bar{p})$ collisions, DIS processes, etc.) and over a wide range of centre-of-mass energies. The data show a dependence on \sqrt{s} which is apparently characteristic of the specific initial state under consideration. This kind of dependence disappears if the ‘effective energy’ is considered to characterize the system as proved in the past in a CERN ISR (Intersecting Storage Rings) experiment [1-6], performed using the SFM (Split Field Magnet) facility at energies of tens of GeV. The aim of this work is to address the possibility to carry out a similar study at energies of several TeV at the LHC and to measure the energy distribution of the so called ‘quantum number flow’ (QNF) particles, with the ALICE experiment [7-9]. In this respect ALICE (A Large Ion Collider Experiment) has excellent capabilities, thanks to the presence of several detectors for the measurement of particle multiplicity over a wide rapidity range [10,11]. Moreover, on both sides of the interaction point, the experiment is equipped with very forward hadronic calorimeters, the Zero Degree Calorimeters (ZDCs) [12], which allow to derive the effective energy on an event-by-event basis by detecting the outgoing leading nucleons.

Quantum number flow in pp collisions

The global properties of the final state in high-energy collisions are governed by the non-perturbative regime of QCD. This means that if the energy is high enough particles produced in the collision should not care about the nature of the colliding system but only on the energy effectively available for particle production. In e^+e^- collisions the annihilation process makes all the centre-of-mass energy available for the production of final state particles. In other systems, like pp or $p\bar{p}$ collisions, the main process is constrained by the conservation of the initial quantum numbers. We call quantum number flow (QNF) the component of the final state particles which conserves these numbers and therefore removes a sizeable fraction of the total centre-of-mass energy. In particular, in pp collisions, the initial non-zero baryon flow is expected to be manifest in the very forward rapidity region, where high (longitudinal) momentum and energy QNF baryons, often called leading baryons, can be detected. In this case it is necessary to define an effective energy to describe the system subtracting the QNF energy to the initial centre-of-mass energy (\sqrt{s}). For each hemisphere, defined with respect to the plane transverse to the beam axis, this effective energy is:

$$E_{had} = E_{inc} - E_{leading} \quad (1)$$

where $E_{inc} = \sqrt{s}/2$ and $E_{leading}$ equals the energy of the outgoing QNF particle in one hemisphere.

Once the proper variable is defined it is then possible to characterize the products of a collision in terms of the available energy of the system. It was demonstrated at ISR that the charged particle multiplicity measured in pp collisions is in very good agreement with the one measured in e^+e^- collisions when the effective energy is considered, as shown in Fig. 1 [5].

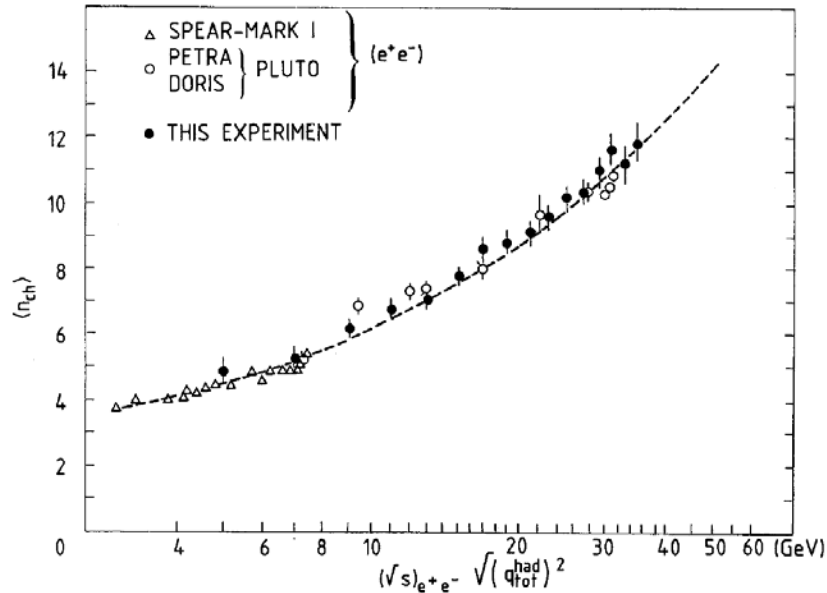


Fig. 1. Average charged multiplicity $\langle n_{ch} \rangle$ as a function of the effective energy (here indicated as $\sqrt{(q_{had}^{tot})^2}$, as measured in minimum bias pp collisions collected by the SFM experiment at the CERN ISR (full circles). The data from e^+e^- experiments are also shown (open circles and triangles) in terms of \sqrt{s} . A fit to ISR pp data is superimposed.

At the ISR it was also proved that the QNF effect happens in both hemispheres independently, as shown in Fig. 2 [6] for leading protons, where in each hemisphere their Feynman-x can be defined as $x_F^i = \frac{E_{leading}^i}{E_{inc}}$, with $i = 1, 2$.

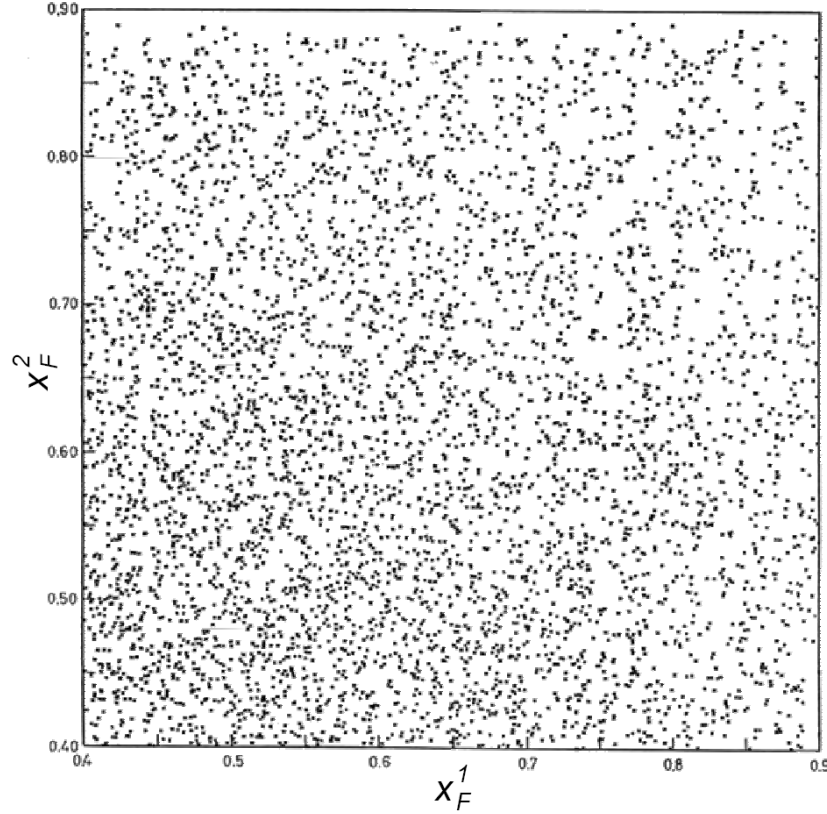


Fig. 2. Independency of the two hemispheres as seen in pp ($\sqrt{s} = 62$ GeV) at ISR, in terms of x_F^1 vs. x_F^2 for leading baryons (protons). The data correspond to about 2×10^5 pp events.

For this reason it is also possible to define a global effective energy involving both hemispheres:

$$q_{had}^{tot} = \sqrt{s(1 - x_F^1)(1 - x_F^2)}. \quad (2)$$

It has been demonstrated at the ISR that using both $2E_{had}$ and q_{had}^{tot} leads to the same observations in terms of particle production in a wide range of \sqrt{s} and x_F values. It should be stressed here that, from the experimental point of view, using the first definition (Eq. 1) allows to collect larger statistics as only one leading QNF particle needs to be detected. However, using the second approach (Eq. 2) does not require to distinguish particles in the two hemispheres.

This important results was recently reviewed on the occasion of the 40th anniversary of the ISR [13] and it will be further studied at the LHC in a new energy domain by the ALICE experiment, as foreseen in the ALICE Physics Performance Report in 2007 [10, 11] and as described in the next sections.

The ALICE Zero Degree Calorimeter

Although the programme of the ALICE experiment has its main focus on heavy-ion physics, the detector has also excellent capabilities to study pp collisions. In particular, this applies to the analysis we are presenting in this paper.

The ALICE experiment started collecting data at the end of 2009 and both pp and PbPb data are available. pp data have been collected by ALICE with full-apparatus data acquisition at the energies of 900 GeV, 2.76 TeV and 7 TeV. A small sample of events was collected in 2009 at a centre-of-mass energy of 2.36 TeV but only few subdetectors were included in the data taking. Also PbPb collisions were collected in ALICE at the energy of 2.76 TeV per nucleon pair. In this paper we will focus on pp collisions at 7 TeV.

In Fig. 3 a summary of centre-of-mass energies with respect to effective energy ranges accessible by ALICE is reported and compared with the one corresponding to the ISR.

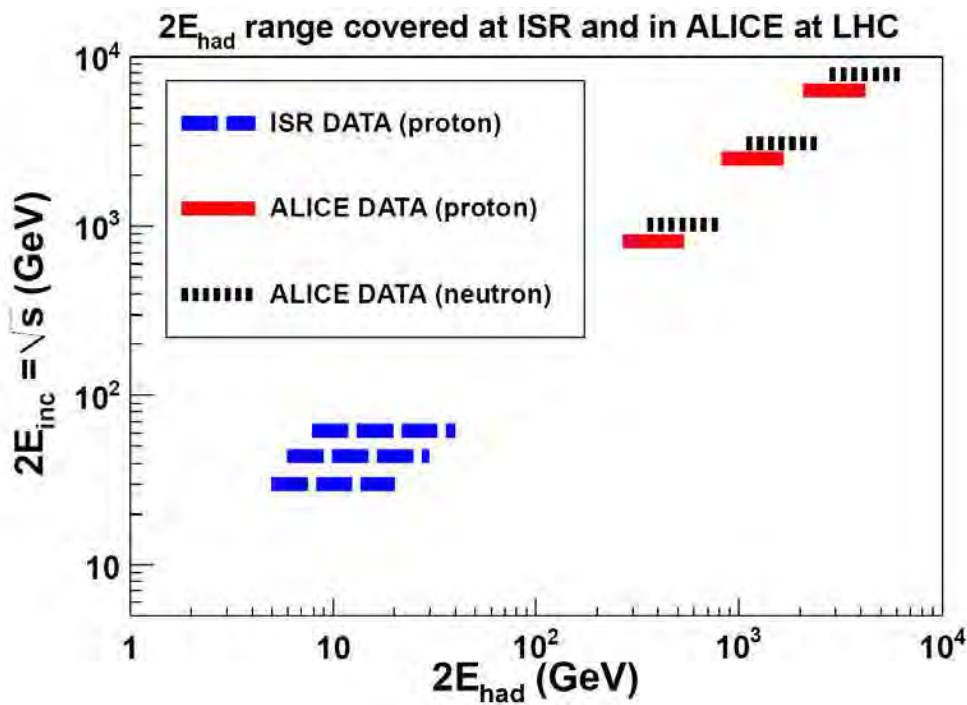


Fig. 3. Effective energy range (here indicated as $2E_{had}$ range) covered at ISR and LHC as a function of \sqrt{s} .

Two sets of Zero Degree Calorimeters (ZDCs) are located in the very forward region on both sides (called side A and side C) of the interaction point. They have been designed to provide a measurement of the centrality of nuclear collisions by measuring the energy of the spectator nucleons not participating in the collision. The same apparatus can be used in pp collisions to detect the leading baryons, both charged and neutral, thus allowing the measurement of the QNF energy on an event-by-event basis.

A scheme of the ZDC apparatus is shown in Fig. 4; it consists of two identical sets of detectors, placed on both sides of the interaction vertex at a distance of 116 m. Each set consists of two calorimeters, one for leading

neutrons (ZDCN) and one for leading protons (ZDCP). Charged particles produced at very forward rapidity (leading protons) are slightly deflected by the LHC optics, therefore only those produced with $0.30 < x_F < 0.64$ actually impinge on the ZDCP. For neutral particles such constraints are not present. Each calorimeter is segmented in 4 towers and two different geometries are used for ZDCN and ZDCP: 4 quadrants for the former and for 4 towers placed along the horizontal axis orthogonal to the beam direction for the latter. A more detailed description of the calorimeters is given elsewhere [12].

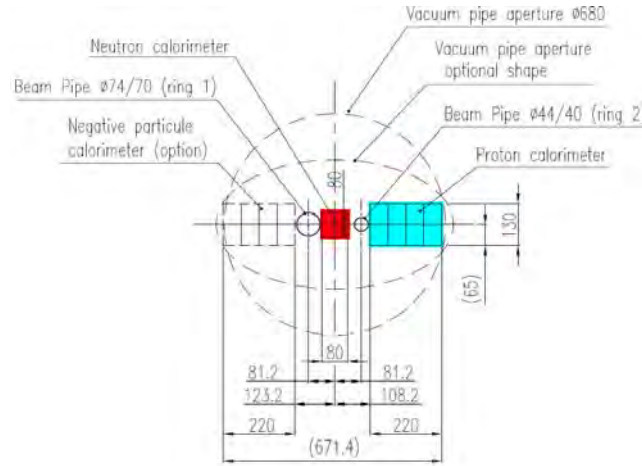


Fig. 4. Transverse section of the LHC beam line at a distance of 116 m from the interaction vertex. The location of the two ZDC calorimeters for protons and neutrons is also shown.

Because of the presence of two beam collimators in front of the ZDC neutron calorimeters, the experimental setup conditions in 2010 and 2011 pp data were not optimized. In this particular configuration an accurate estimate of the acceptance could not be achieved. In view of 2012 pp data taking, these two collimators have been moved behind the ZDCs and this will provide a cleaner experimental environment. For these reasons the results presented hereafter are not corrected for acceptance and efficiency factors, which will instead be possible with the forthcoming 2012 data.

In the next section we focus on the feasibility of the effective energy study in pp interactions at LHC using Monte Carlo simulations and we report the first results which are observed to be only weakly dependent on the acceptance corrections.

The analysis scheme and a first interesting result

The performance of the ALICE ZDC calorimeters was first checked through detailed Monte Carlo simulations using the PYTHIA generator [14] to mimic the physics expected in pp collisions. More detail on the leading baryon behaviour described by PYTHIA can be found in a previous study in [15].

As already mentioned, due to the beam optics the ZDC acceptance is restricted to protons with energies in the range $1.1 < E < 2.25$ TeV, while in the case of neutrons the whole range of energy is accessible. The GEANT3

[16] package and the ALICE simulation and reconstruction software, AliRoot [17], were used for the simulation of the detector response, and to perform realistic digitization and reconstruction in the ZDC calorimeters.

The full simulation allows to estimate the energy responses of the calorimeters for the different components (photons, baryons, etc.) and the corresponding resolutions. As mentioned before the estimate of the acceptance is still problematic because of the current difficulties in describing the influence of the beam collimator in a satisfactory way.

In Fig. 5 the neutral leading distribution is reported, in terms of x_F , for one tower of the ZDCN. The black points represent the reconstructed distribution including all detector effects. As it can be noted the ‘measured’ distribution is non-zero also for x_F larger than one because of resolution effects. Actually the energy resolution at the highest energy is about 20%. The red line is a global function used to fit the distribution. Two components are used in the fit: the baryon component which is described by a polynomial Legendre function convoluted with the detector resolution, and the photon component which is represented by an exponential convoluted with the detector resolution. Both the components are forced to be zero for $x_F = 0$ according to the expected acceptance behaviour. This model fits the data very well, thus allowing to extract separately the baryon and photon distributions already unfolded from resolution effects. The ‘reconstructed’ distributions, respectively blue and green line for baryon and photon components, are compared with the ‘true’ ones (open squares), as generated by the Monte Carlo enabling to validate the procedure. A good agreement is obtained, although the method can be further refined, which shows that the technique is very promising to perform such a measurement.

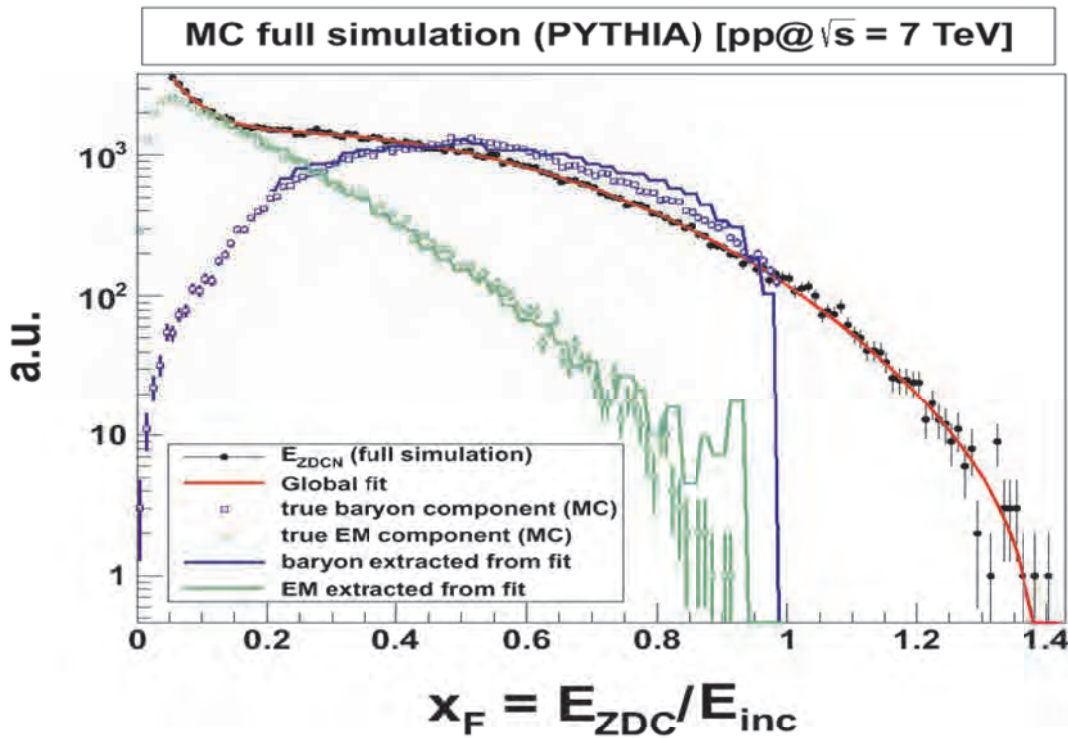


Fig. 5. Global fit to the leading neutron x_F distribution in Monte Carlo (MC) simulations. This procedure allows to disentangle the photon and baryon components and to remove the ZDC resolution effect through a deconvolution.

The same procedure has to be applied to the data and therefore a calibration of the ZDC channels is needed to convert the ADC charge into the energy of particle hits the calorimeter.

A very clean signal to calibrate the ZDC is provided by electromagnetic dissociation processes in PbPb collisions. To this purpose the data sample at $\sqrt{s} = 2.76$ GeV has been used. These processes consist in the emission of one or more nucleons which escape from the nucleus and continue to propagate approximately with the same energy (1.38 TeV). The signal expected in the calorimeter has a discrete spectrum of Gaussians corresponding to the case of 1, 2 or more nucleons recovered, as clearly visible in Fig. 6 where each peak corresponds to a known value of the energy.

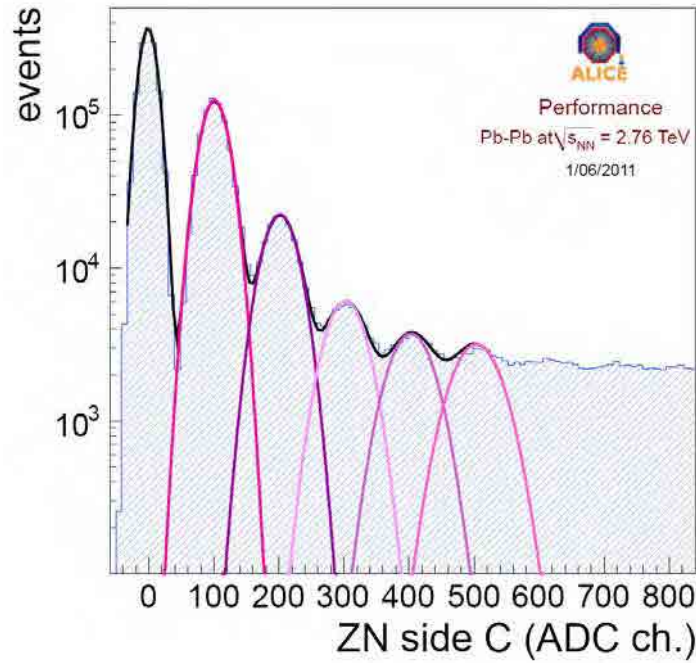


Fig. 6. Fit to the ZDCN (C side) energy distribution for electromagnetic dissociation processes in PbPb collisions ($\sqrt{s_{NN}} = 2.76$ TeV).

This technique allows to calibrate the common channel (i.e. corresponding to the OR of all single-tower signals of the calorimeter) and after that the relative calibration of the single-tower channels can be obtained with respect to the common one. Therefore, even if it is not possible at the moment to derive a QNF energy distribution from the data because of the still large uncertainties in the acceptance, there are some observations that can be already made. In fact the correlation between the QNF energies of the two hemispheres can be investigated and this is one of the key features in the particle production mechanism as observed in the past at ISR.

The question is whether the independency of the two hemispheres still holds true when moving at much higher energy above $\sqrt{s} = 62$ GeV. We performed this measurement at the maximum LHC energy available so far, i.e. $\sqrt{s} = 7$ TeV, using the neutral component of the QNF in order to cover the same x_F range as in the ISR experiment. In Fig. 7 and Fig. 8 (right panel) the independency of the QNF in the two hemispheres is clearly

visible for $0.4 < x_F < 0.9$, thus established at an unprecedented centre-of-mass energy. Furthermore, by comparing the data at \sqrt{s} values which differ by more than a factor 10^2 , one can clearly see (Fig. 8) that this non-correlation of the two hemispheres is energy independent. It should be noted that although the LHC data were not corrected for acceptance and efficiency, such a correction is negligible in the x_F range considered in this analysis. This result opens the way to a detailed study of a phenomenology similar to what observed at the ISR.

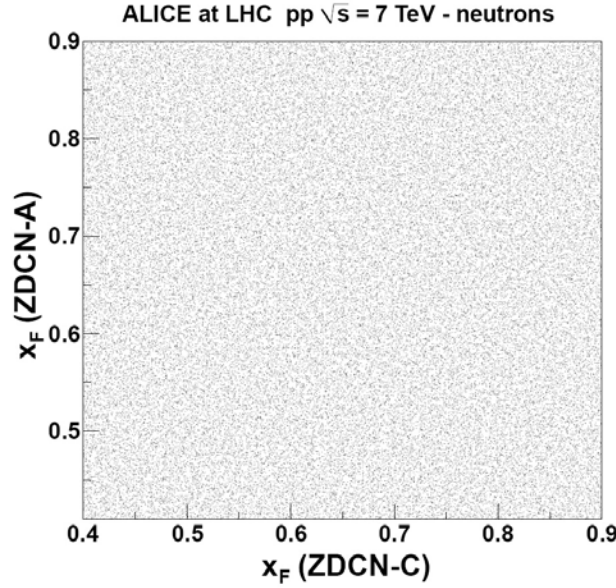


Fig. 7. Independency of the two hemispheres as seen in pp ($\sqrt{s} = 7$ TeV) by ALICE at LHC, in terms of x_F^1 vs. x_F^2 for leading baryons (neutrons). The data correspond to about 2×10^7 pp events.

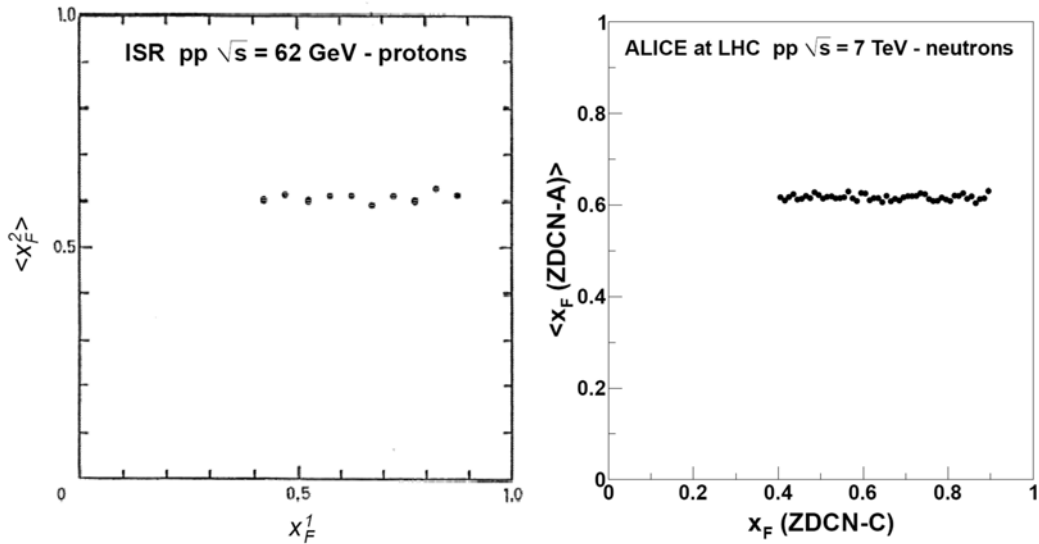


Fig. 8. Independency of the two hemispheres as seen at ISR (left panel) and by ALICE at LHC (right panel), for leading baryons (i.e. protons and neutrons, respectively). These plots are obtained by slicing those shown in Fig. 2 and Fig. 7.

Conclusion

In this work we have shown the feasibility to extend the ISR physics programme up to LHC energies with the ALICE detector and its capability to detect final state baryons in the very forward region. Following the ISR guide lines, the properties of pp collisions and in particular of multihadron production will be soon characterized using the effective energy approach (QNF effect subtracted), for three new values of energy: $\sqrt{s} = 0.9, 2.76, 7$ TeV. The measurement of the QNF neutron and proton distribution is ongoing. The independence of the two hemispheres is now proved also at LHC energies similarly to ISR observation. These results represent a further interesting frontier of the LHC research programme.

References

1. M. Basile *et al.*, Phys. Lett. B **92** (1980) 367
2. M. Basile *et al.*, Phys. Lett. B **95** (1980) 311
3. M. Basile *et al.*, Nuovo Cim. A **67** (1982) 244
4. M. Basile *et al.*, Nuovo Cim. A **79** (1984) 1
5. M. Basile *et al.*, Lett. Nuovo Cim. **38** (1983) 359
6. M. Basile *et al.*, Nuovo Cim. A **73** (1983) 329
7. ALICE Collaboration, "ALICE: Technical Proposal for A Large Ion Collider Experiment at the CERN LHC" CERN/LHCC 95–71 (1995)
8. ALICE Collaboration, "ALICE: Technical Proposal for A Large Ion Collider Experiment at the CERN LHC (addendum 1)" CERN/LHCC 96–32 (1996)
9. ALICE Collaboration, "ALICE: Technical Proposal for A Large Ion Collider Experiment at the CERN LHC (addendum 2)" CERN/LHCC 99–13 (1999)
10. F. Carminati *et al.*, J. Phys. G **30** (2004) 1517
11. F. Carminati *et al.*, J. Phys. G **32** (2006) 1295
12. ALICE Collaboration, "ALICE Technical Design Report of the Zero Degree Calorimeter (ZDC)" CERN/LHCC 99–5 (1999)
13. A. Zichichi, Nuovo Saggiatore **27** n. 3-4 (2011) 48
14. T. Sjostrand, S. Mrenna and P. Skands, JHEP **605** (2006) 826
15. A. Akindinov *et al.*, Eup. Phys. J. C **50** (2007) 341
16. R. Brun, F. Bruyant, M. Maire, A. C. McPherson and P. Zancarini, "GEANT3" CERN-DD/EE 84–1 (1987)
17. ALICE Collaboration, <http://aliweb.cern.ch/Offline/>

PERTURBATIVE QUANTUM GRAVITY FROM GAUGE THEORY

■ ZVI BERN

Department of Physics and Astronomy
UCLA, Los Angeles, CA
90095-1547, USA

Abstract

In this talk we give an overview of some recent developments in gauge and gravity theories, focusing on a new duality between color and kinematics. This duality allows us to construct gravity amplitudes by a simple replacement of color factors by kinematic numerator factors. Applications of these ideas for determining the ultraviolet compatibility of supersymmetric versions of Einstein gravity with quantum mechanics are explained.

1 Overview

Recent years have seen remarkable progress in understanding scattering processes of elementary particles in gauge and gravity theories, both for phenomenological and theoretical purposes. In this talk, we will focus on recent theoretical progress in quantum gravity. In particular, we will describe a surprising relation between gauge theory—used to describe nuclear forces—and gravity theories. For nearly 30 years, physicists have been convinced that point-like theories of gravity along the lines of Einstein’s theory are incompatible with quantum field theory because they lead to ultraviolet infinities. These infinities in turn lead to a loss of predictive power at ultra-high energies. Here we will describe how the new ideas relating gauge and gravity theories make it possible to challenge these beliefs by giving us the ability to carry out the required calculations.

Although gravity and gauge theories have obvious superficial similarities their detailed dynamics is rather different. Nevertheless we know from the celebrated AdS/CFT correspondence [1] between gauge and gravity theories that there is an equivalence between the weak coupling in one theory and strong coupling in the other. Here we will describe a different connection, purely at weak coupling, showing that in a precise sense gravity is a double copy of gauge theory. We write this schematically as

$$\text{gravity} \sim (\text{gauge theory}) \times (\text{gauge theory}). \quad (1)$$

This was first understood at tree level over 25 years ago using string theory [2], but today we have a much simpler description [3], allowing for a straightforward extension to loop level [4].

This new understanding of gravity has allowed us to probe the ultraviolet properties of gravity theories via explicit calculations at a level deeper than has been possible previously [5, 6, 7, 8]. Conventional wisdom holds that it is impossible to construct point-like ultraviolet finite quantum field theories of gravity (see *e.g.* ref. [9]).

This has been taken as a sign of a fundamental incompatibility between quantum field theory and gravity. Indeed, simple power-counting arguments show the difficulty of doing so. In a classic paper, 't Hooft and Veltman demonstrated that gravity coupled to matter generically diverges at the first quantum loop order in four dimensions [10, 11]. Due to the dimensionful nature of the coupling, the divergences cannot be absorbed by a redefinition of the original parameters of the Lagrangian, rendering the theory non-renormalizable. Pure Einstein gravity does not possess a one-loop divergence [10, 12]. The two-loop divergence of pure Einstein gravity was established by Goroff and Sagnotti and by van de Ven through direct computation [13, 14]. Unfortunately, supersymmetry offers a mechanism for delaying the onset of divergences in gravity theories. No supergravity theory can diverge until at least three loops [9]. However, supersymmetry alone cannot eliminate the ultraviolet divergences in gravity theories because of the increasingly worse divergences at each loop order in gravity theories. This leads to the general question for supergravity theories of whether a given potential divergence identified by power counting and symmetry arguments alone is actually present. Here we will explain how the double-copy property (1) is helping us to resolve this question.

2 The on-shell philosophy

In recent years there has been a fundamental shift in how we view scattering amplitudes. In the traditional Feynman diagram approach one starts from an off-shell (i.e. one where states do not satisfy the Einstein relation $p^2 = m^2$) Lagrangian and constructs Feynman diagrams according to a set of rules. The diagrams encode algebraic expressions describing the scattering process. The diagrams depend on the gauge and field variable choices. Gauge invariance is restored only at the end of a computation, when one puts all external states on shell and all pieces are added together. The lack of gauge invariance for the individual diagrams can lead to enormously complicated expressions, which simplify only after a nontrivial effort to combine terms. In numerical approaches, it also exacerbates numerical instabilities.

In contrast, on-shell methods construct new amplitudes directly from simpler gauge-invariant on-shell amplitudes. Since the simpler amplitudes are already gauge invariant they can be greatly simplified before being used in the construction of more complex amplitudes. The two basic on-shell methods are on-shell recursion [15] and the unitarity method [16]. For studying multiloop gravity, the current method of choice is the unitarity method. This method was originally developed in the context of one-loop supersymmetric amplitudes [16], but with further refinements [17, 18, 19, 20, 21, 6, 22, 23], it offers a powerful formalism for any massless theory at any loop order, including non-planar contributions. This method has been reviewed numerous times [24, 25, 26], so here we give only a brief outline.

Unitarity has been a basic principle in quantum field theory since its inception. For a description of unitarity during the 1960's see ref. [27]. However, a variety of difficulties prevented its widespread use as a means of constructing amplitudes, especially after the rise of gauge theories in the 1970's. These difficulties include non-convergence of dispersion relations and its inapplicability to massless particles. It was also unclear how

one could fully reconstruct loop amplitudes beyond four points from their unitarity cuts. The modern unitarity method overcomes these difficulties, allowing for the complete construction of loop amplitudes at any loop order. It does so by avoiding dispersion relations, and instead using the existence of an underlying covariant Feynman diagram representations to fully reconstruct amplitudes. By construction the obtained Feynman-like integrands have the correct analytic properties in all channels.

Over the years there have been a number of important refinements to the unitarity method [16]. Generalized unitarity [27] (where multiple internal lines are placed on shell, subdividing a loop amplitude into more than two pieces) was successfully applied in ref. [18] as a means for greatly simplifying loop calculations. An important more recent development is the use of complex momenta [13] by Britto, Cachazo and Feng [19], leading to the realization that at one loop in four dimensions, quadruple cuts directly determine the coefficients of all box integrals by freezing the loop integration. Powerful new methods for dealing with triangle and bubble integrals at one loop, as well as rational terms have also been developed [17, 21, 28, 23, 29]. (These have been described in other recent reviews [30].) At higher loops, efficient means of constructing the integrands of amplitudes, including non-planar contributions, have also been devised [20, 6, 22, 31].

Although the unitarity method applies just as well to supersymmetric and non-supersymmetric theories, it is usually much simpler to deal with the supersymmetric cases because they have a simpler analytic structure. Indeed, the original application of the unitarity method was to construct one-loop supersymmetric amplitudes with arbitrary numbers of external legs [16].

3 Comparing Gravity to Gauge Theory

We start by comparing gravity to gauge theory using off-shell methods. The Feynman rules are generated starting from the Einstein-Hilbert and Yang-Mills Lagrangians,

$$\mathcal{L}_{\text{YM}} = -\frac{1}{4}F_{\mu\nu}^a F^{a\mu\nu}, \quad \mathcal{L}_{\text{EH}} = \frac{2}{\kappa^2}\sqrt{-g}R. \quad (2)$$

From the viewpoint of Feynman diagrams, these two Lagrangians have rather different properties. With standard gauge choices gauge theories have three- and four-point interactions, while gravity has an infinite number of contact interactions. Perhaps more striking than the infinite number of interactions is the remarkably complexity of these interactions.

To be more concrete, consider the three-gluon vertex in Feynman gauge,

$$V_{3\mu,\nu,\sigma}^{abc}(k_1, k_2, k_3) = g f^{abc} \left[(k_1 - k_2)_\sigma \eta_{\mu\nu} + \text{cyclic} \right], \quad (3)$$

where g is the coupling, f^{abc} the usual group theory structure constants, $\eta_{\mu\nu}$ the flat metric and the k_i the momenta of the vertex. This vertex is relatively simple. We may compare this to the three-graviton interaction in, for example, de Donder gauge,

$$G_{3\mu\alpha,\nu\beta,\sigma\gamma}(k_1, k_2, k_3) = i\frac{\kappa}{2} \left[-\frac{1}{2}k_1 \cdot k_2 \eta_{\mu\alpha} \eta_{\nu\beta} \eta_{\sigma\gamma} - \frac{1}{2}k_{1\nu} k_{1\beta} \eta_{\mu\alpha} \eta_{\sigma\gamma} + \dots \right], \quad (4)$$

where we have displayed two terms out of about 100. Here the coupling κ is related to Newton's constant by $\kappa^2 = 32\pi^2 G_N$. The precise form of the vertex depends on the gauge, but in any case the three vertex is a rather involved and unenlightening object. The complete expression can be found in refs. [32, 10].

Comparing the vertex in eq. (3) to the one in eq. (4), it certainly would appear that gravity is much more complicated than gauge theory. Moreover, there does not appear to be any simplicity or obvious relation between the gauge and gravity vertices. The former leads to complicated diagrams, but the latter appears hopelessly complicated. One can do somewhat better with special gauge choices and appropriate field redefinitions [14, 33], considerably simplifying the Feynman rules. Still, multiloop Feynman diagram calculations in (super) gravity are extremely difficult, and generally out of reach using even the most powerful supercomputers.

Now let us reconsider the same process but from the on-shell vantage point. If we take the three-graviton vertex in eq. (4) and dot the three legs with physical polarizations tensors satisfying the physical state conditions, $k_i^2 = 0$, $\varepsilon_i^{\mu\nu} k_{i\mu} = \varepsilon_i^{\mu\nu} k_{i\nu} = \varepsilon_i^\mu{}_\mu = 0$, we obtain a greatly simplified vertex,

$$G_3(k_1, k_2, k_3) = -i\kappa \varepsilon_1^{\mu\alpha} \varepsilon_2^{\nu\beta} \varepsilon_3^{\sigma\gamma} \left[(k_1)_\sigma \eta_{\mu\nu} + \text{cyclic} \right] \left[(k_1)_\gamma \eta_{\alpha\beta} + \text{cyclic} \right]. \quad (5)$$

Remarkably, up to overall factors, this is just a double copy of the kinematic part of the on-shell Yang-Mills vertex,

$$V_3^{abc}(k_1, k_2, k_3) = 2\varepsilon_1^\mu \varepsilon_2^\nu \varepsilon_3^\sigma g f^{abc} \left[(k_1)_\sigma \eta_{\mu\nu} + \text{cyclic} \right], \quad (6)$$

where the polarization vector satisfies $\varepsilon_i^\mu k_{i\mu} = 0$. To make the comparison, we identify the graviton polarization tensor as a product of gluon polarization vectors, $\varepsilon_i^{\mu\nu} = \varepsilon_i^\mu \times \varepsilon_i^\nu$. Similar considerations allow us to express all three-point vertices in supergravity as products of super-Yang-Mills vertices. Using BCFW recursion [15], these three vertices are sufficient to construct any tree-level gauge or gravity amplitude. The unitarity method then allows us to construct any loop amplitude.

Clearly, there is a rather striking relationship between gravity and gauge theory, but to make it visible we need to keep external states on shell. As we shall see below, the double-copy structure in eq. (5) is not accidental, but appears likely to extend to all loop orders. As such, it reflects a profound and important property of quantum gravity, pointing to unification of the two theories, perhaps along the lines of string theory.

Along these lines, we now discuss the recently discovered duality between color and kinematics [3, 4]. In general, we can write any n -point tree-level gauge-theory amplitude with all particles in the adjoint representation as,

$$\mathcal{A}_n^{\text{tree}}(1, 2, 3, \dots, n) = \sum_i \frac{n_i c_i}{\prod_{\alpha_i} p_{\alpha_i}^2}, \quad (7)$$

where the sum runs over the set of n -point L -loop diagrams with only cubic vertices. These include distinct permutations of external legs. We have suppressed factors of

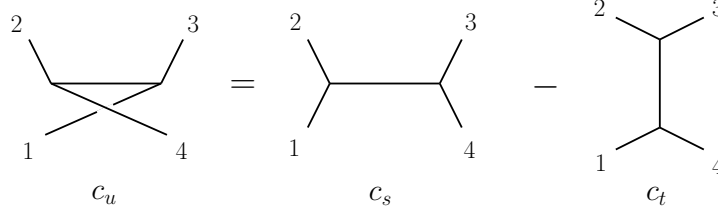


Figure 1: The Jacobi relation for at four points for the three channels labeled by s , t and u .

the coupling constant for convenience. The product in the denominator runs over all propagators of each cubic diagram. The c_i are the color factors obtained by dressing every three vertex with an $\tilde{f}^{abc} = i\sqrt{2}f^{abc}$ structure constant, and the n_i are kinematic numerator factors depending on momenta, polarizations and spinors. The form (7) can be obtained straightforwardly, for example, from Feynman diagrams, by representing all contact terms as inverse propagators in the kinematic numerators that cancel propagators. For supersymmetric amplitudes expressed in superspace, there will also be Grassmann parameters in the numerators.

The duality conjectured in ref. [3] requires there to exist such a transformation from any valid representation to one where the numerators satisfy equations in one-to-one correspondence with the Jacobi identity of the color factors,

$$c_i = c_j - c_k \Rightarrow n_i = n_j - n_k. \quad (8)$$

This duality is conjectured to hold to all multiplicity at tree level in a large variety of theories, including supersymmetric extensions of Yang-Mills theory. In fig. 1 we display the Jacobi relation at four points. The duality conjecture states there exists representations of the amplitude, such that the color factors and numerators of the diagrams satisfy the relations.

At tree level, a consequence of this duality is non-trivial relations between the color-ordered partial tree amplitudes of gauge theory [3, 34, 35]. The duality has also been studied in string theory [36, 37] and in terms of Lagrangians [38]. An alternative trace-based representation of the duality (8) was recently given in ref. [39], emphasizing the underlying group theoretic structure of the duality. In the self-dual case, underlying group theoretic structure has been made explicit [40].

Perhaps more remarkable than the duality itself is a related conjecture that once the gauge-theory amplitudes are arranged into a form satisfying the duality (8), corresponding gravity amplitudes can be obtained simply by replacing the c_i color factor in eq. (7) with a second copy of a numerator factor \tilde{n}_i [3, 4],

$$-i\mathcal{M}_n^{\text{tree}}(1, 2, \dots, n) = \sum_i \frac{n_i \tilde{n}_i}{\prod_{\alpha_i} p_{\alpha_i}^2}, \quad (9)$$

The sum runs over the same set of diagrams with cubic vertices, as in eq. (7). This is expected to hold in a large class of gravity theories, including theories that are the low-energy limits of string theories. (As for the gauge-theory case, we suppress factors of the coupling constants.) At tree level, this double-copy property encodes what are known as

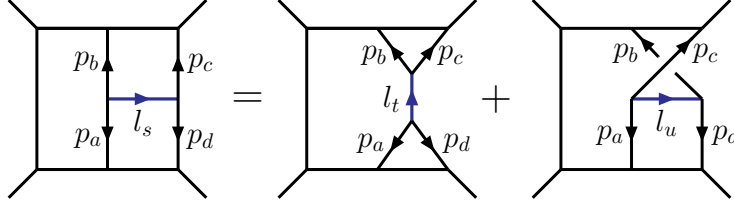


Figure 2: An example of a duality relation satisfied by numerators for diagrams of the three-loop four-point amplitude. Both color factors and numerator factors satisfy these relations.

KLT relations between gravity and gauge-theory tree amplitudes [2]. The double-copy formula (9) has been proven via on-shell recursion [15] for pure gravity and for $\mathcal{N} = 8$ supergravity tree amplitudes, whenever the duality (8) holds in the corresponding gauge theories [38].

More recently, the above conjectures have been extended to loop level [4], so that at any loop order L ,

$$\mathcal{A}_m^{\text{loop}} = \sum_j \int \prod_{l=1}^L \frac{d^D p_l}{(2\pi)^D} \frac{1}{S_j} \frac{n_j c_j}{\prod_{\alpha_j} p_{\alpha_j}^2}, \quad \mathcal{M}_m^{\text{loop}} = \sum_j \int \prod_{l=1}^L \frac{d^D p_l}{(2\pi)^D} \frac{1}{S_j} \frac{n_j \tilde{n}_j}{\prod_{\alpha_j} p_{\alpha_j}^2}, \quad (10)$$

where $\mathcal{A}_n^{\text{loop}}$ and $\mathcal{M}_n^{\text{loop}}$ are L -loop gauge and gravity amplitudes. As before we removed factors of the coupling constants. The sums now run over all distinct m -point L -loop diagrams with cubic vertices. These include distinct permutations of external legs, and the S_j are the symmetry factors of each diagram. As at tree level, at least one family of numerators (n_j or \tilde{n}_j) for gravity must be constrained to satisfy the duality (8). (For pure gravity, extra projectors are needed to obtain loop-level amplitudes from the direct product of two pure Yang-Mills theories.) A three-loop example of a duality relation for numerators factors is displayed in fig. 2. For the duality (8) to hold, the duality relation for every propagator in all diagrams must be enforced.

This loop-level extension has been tested in the rather nontrivial case of three- and four-loop four-point amplitudes [4, 8] and two-loop five point amplitude [41] of $\mathcal{N} = 4$ super-Yang-Mills theory and $\mathcal{N} = 8$ supergravity. It has also been tested in one and two-loop gravity examples in cases with fewer supersymmetries than the maximum [42].

4 Ultraviolet properties of gravity

Today, our most powerful tool for explicitly determining the ultraviolet properties of gravity theories is the double-copy property used in tandem with the unitarity method, as described in a very recent paper [8]. The best theories to study are the maximally supersymmetric ones, because of their technical simplicity and because supersymmetry tends to mitigate ultraviolet divergences. $\mathcal{N} = 4$ super-Yang-Mills theory was proven to be ultraviolet finite in four dimensions long ago [43]. The ultraviolet behavior of

$\mathcal{N} = 8$ supergravity [44] in four dimension is, however, still under study. Recent reviews discussing the ultraviolet properties of $\mathcal{N} = 8$ supergravity in more detail are given in refs. [45].

Because of the complexity of explicit calculations, people normally resort to power counting arguments. These arguments assume that all symmetries and relevant properties are known and accounted for. For the case of $\mathcal{N} = 8$ supergravity we know that there are unexpected ultraviolet cancellations in the theory to all loop orders [46, 47], though it is still not clear if these are powerful enough to render the theory finite to all loop orders. (These cancellations are related to a well studied property of one-loop $\mathcal{N} = 8$ amplitudes: in four dimensions triangle and bubble integrals drop out of the amplitudes, when expressed in a basis of scalar integral in four dimensions [48].) Some hints also follow from string-theory dualities [49]. We also know that gravity loop amplitudes are much more closely tied to better behaved gauge-theory amplitudes than had been believed [4]. While these arguments do not offer a proof of finiteness, they do suggest that it would be wise to reexamine the ultraviolet properties of gravity theories. For other approaches to trying to make quantum field theories of gravity sensible in the ultraviolet see refs. [50].

Motivated by the hint of high-loop cancellations, explicit calculations were carried out in refs. [5, 6, 7, 8] to directly investigate the ultraviolet properties of $\mathcal{N} = 8$ supergravity. These calculations definitively rule out the expected potential three-loop divergence in four space-time dimensions. Although no potential divergence exists at four loops in four dimensions (because of an “accidental” cancellation similar to the one preventing a pure gravity divergence at one loop), direct calculation establishes that the four-loop four-point amplitude of $\mathcal{N} = 8$ supergravity has the same power counting in D dimensions as $\mathcal{N} = 4$ super-Yang-Mills theory (which is known to be finite in $D = 4$).

The result of direct calculation [7, 8] is that the four-loop four-point amplitude of $\mathcal{N} = 8$ supergravity is of the form,

$$M_4^{4\text{-loop}} \sim D^8 R^4 \times \text{loop integrals} \quad (11)$$

where the $D^8 R^4$ factor corresponds to 16 powers of momentum in the numerators of the integrals coming out as external momentum. This factor is a shorthand for covariant derivatives acting on four Riemann tensors with their Lorentz indices contracted in an appropriate way. If we assume that no further ultraviolet cancellations exist, and that no further powers of loop momenta can come out of the integrals as external momenta as the loop order increases, simple power counting shows that in four dimensions the first divergence would occur at seven loops.

This is in line with recent comprehensive studies of the potential divergences in $\mathcal{N} = 8$ supergravity [51, 52, 53, 54], showing that no divergence is compatible with the known symmetries until seven loops. Based on these studies, a consensus has formed that symmetry constraints alone cannot prevent divergences in four space-time dimensions starting at seven loops and that the theory will likely diverge at this loop order. There is, however, a more optimistic view [55]. (We note that the previously claimed delay until nine loops of potential ultraviolet divergences in $\mathcal{N} = 8$ supergravity [56] has now been retracted [52].)

Is it possible that there are further symmetries or structures that prevent the widely

expected seven loop divergences? Powercounting arguments using symmetries to rule out potential divergences can, of course, never prove the existence of divergences, only that protection against divergences holds to a certain level; if a symmetry or structure is missed then it may turn out the bound is too loose. More generally, the only way we can be certain that the coefficient of a potential divergence respecting the known symmetries is non-zero is to carry out the explicit calculation to show that the numerical value is nonzero.

Today, even with all the advances, it is not yet practical to carry out a seven-loop computation. However, a simple way to lower the loop order in which a given potential divergence can occur is to work in higher space-time dimensions higher dimensions. By increasing the dimension, $\mathcal{N} = 4$ super-Yang-Mills is no longer ultraviolet finite, allowing this theory to be used as a playground for sharpening our understanding of divergences in maximally supersymmetric theories [6, 57, 22]. Explicit calculations [58, 20, 5, 6, 7, 22] show that at least for four-point amplitudes through four loops, both $\mathcal{N} = 8$ supergravity and $\mathcal{N} = 4$ super-Yang-Mills theory are ultraviolet finite for

$$D < \frac{6}{L} + 4 \quad (L > 1), \quad (12)$$

where D is the dimension of space-time and L the loop order. (The case of one loop, $L = 1$, is special, with the amplitudes finite for $D < 8$, not $D < 10$.) For $\mathcal{N} = 4$ super-Yang-Mills this bound was proposed in ref. [58] and has been confirmed in ref. [59] using superspace techniques. Explicit computations summarized below demonstrate this bound is saturated in $\mathcal{N} = 4$ super-Yang-Mills theory through at least four loops [60, 58, 46]. For $\mathcal{N} = 8$ supergravity we know that the bound (12) is saturated through four loops [58, 5, 6, 7, 8].

5 Outlook

In this talk we described a surprising relation between gravity and gauge theories, stemming from a gauge-theory duality between color and kinematics [3, 4]. Although the duality still has the status of a conjecture at loop level, we can exploit it to streamline loop computations based on the unitarity method. These types of computations have been successfully used to probe the ultraviolet properties of supergravity theories.

The current consensus in the community is that the standard symmetries of $\mathcal{N} = 8$ supergravity cannot protect the theory against divergences, starting at seven loops [51, 52] (though there is at least one contrary opinion [55]). If divergence do appear at seven loop, then we should see indications starting at five loops, albeit in higher space-time dimensions. To test this, it would be of crucial importance to directly determine the ultraviolet properties of $\mathcal{N} = 8$ supergravity as a function of dimension at five loops. If this calculation can be completed, it should greatly clarify the ultraviolet behavior of $\mathcal{N} = 8$ supergravity in four dimensions, checking the hypothesis that it is an ultraviolet finite theory. As recently discussed in some detail in ref. [8], the duality between color and kinematic numerators and the associated double-copy property of gravity offers a

promising approach to solve this problem. We can look forward to many new exciting results in the coming years based on these developments.

Acknowledgments

We thank S. Davies, L. J. Dixon, J. J. M. Carrasco, T. Dennen, H. Johansson, Y.-t. Huang, H. Ita, D. A. Kosower, and R. Roiban for many enlightening discussions and collaboration on work described in this lecture. This work was supported by the US Department of Energy under contract DE-FD03-91ER40662. I wish to thank the organizers for inviting me to such a wonderful conference.

References

- [1] J. M. Maldacena, Adv. Thew. Math. Phys. **2**, 231 (1998) [Int. J. Theor. Phys. **38**, 1113 (1999)] [hep-th/9711200]; S. S. Gubser, I. R. Klebanov and A. M. Polyakov, Phys. Lett. B **428**, 105 (1998) [hep-th/9802109].
- [2] H. Kawai, D. C. Lewellen and S. H. H. Tye, Nucl. Phys. B **269**, 1 (1986); Z. Bern, Living Rev. Rel. **5**, 5 (2002) [gr-qc/0206071].
- [3] Z. Bern, J. J. M. Carrasco and H. Johansson, Phys. Rev. D **78**, 085011 (2008) [arXiv:0805.3993 [hep-ph]].
- [4] Z. Bern, J. J. M. Carrasco and H. Johansson, Phys. Rev. Lett. **105**, 061602 (2010) [arXiv:1004.0476 [hep-th]].
- [5] Z. Bern, J. J. Carrasco, L. J. Dixon, H. Johansson, D. A. Kosower and R. Roiban, Phys. Rev. Lett. **98**, 161303 (2007) [hep-th/0702112].
- [6] Z. Bern, J. J. M. Carrasco, L. J. Dixon, H. Johansson and R. Roiban, Phys. Rev. D **78**, 105019 (2008) [arXiv:0808.4112 [hep-th]].
- [7] Z. Bern, J. J. Carrasco, L. J. Dixon, H. Johansson and R. Roiban, Phys. Rev. Lett. **103**, 081301 (2009) [arXiv:0905.2326 [hep-th]].
- [8] Z. Bern, J. J. M. Carrasco, L. J. Dixon, H. Johansson and R. Roiban, arXiv:1201.5366 [hep-th].
- [9] M. T. Grisaru, Phys. Lett. B **66**, 75 (1977); E. T. Tomboulis, Phys. Lett. B **67**, 417 (1977); S. Deser, J. H. Kay and K. S. Stelle, Phys. Rev. Lett. **38**, 527 (1977); S. Ferrara and B. Zumino, Nucl. Phys. B **134**, 301 (1978); P. S. Howe and K. S. Stelle, Phys. Lett. B **137**, 175 (1984). P. S. Howe and K. S. Stelle, Int. J. Mod. Phys. A **4**, 1871 (1989); N. Marcus and A. Sagnotti, Nucl. Phys. B **256**, 77 (1985).
- [10] G. 't Hooft and M. J. Veltman, *Annales Poincare Phys. Theor.* A **20**, 69 (1974);

- [11] S. Deser and P. van Nieuwenhuizen, *Phys. Rev. D* **10**, 411 (1974); S. Deser, H. S. Tsao and P. van Nieuwenhuizen, *Phys. Rev. D* **10**, 3337 (1974).
- [12] R. E. Kallosh, *Nucl. Phys. B* **78**, 293 (1974); P. van Nieuwenhuizen and C. C. Wu, *J. Math. Phys.* **18**, 182 (1977).
- [13] M. H. Goroff and A. Sagnotti, *Phys. Lett. B* **160**, 81 (1985); *Nucl. Phys. B* **266**, 709 (1986).
- [14] A. E. M. van de Ven, *Nucl. Phys. B* **378**, 309 (1992).
- [15] R. Britto, F. Cachazo, B. Feng and E. Witten, *Phys. Rev. Lett.* **94**, 181602 (2005) [hep-th/0501052].
- [16] Z. Bern, L. J. Dixon, D. C. Dunbar and D. A. Kosower, *Nucl. Phys. B* **425**, 217 (1994) [hep-ph/9403226]; *Nucl. Phys. B* **435**, 59 (1995) [hep-ph/9409265].
- [17] Z. Bern and A. G. Morgan, *Nucl. Phys. B* **467**, 479 (1996) [hep-ph/9511336]; Z. Bern, L. J. Dixon, D. C. Dunbar and D. A. Kosower, *Phys. Lett. B* **394**, 105 (1997) [hep-th/9611127]; Z. Bern, L. J. Dixon and D. A. Kosower, *JHEP* **0001**, 027 (2000) [hep-ph/0001001].
- [18] Z. Bern, L. J. Dixon and D. A. Kosower, *Nucl. Phys. B* **513**, 3 (1998) [hep-ph/9708239]; Z. Bern, L. J. Dixon and D. A. Kosower, *JHEP* **0408**, 012 (2004) [hep-ph/0404293]; Z. Bern, V. Del Duca, L. J. Dixon and D. A. Kosower, *Phys. Rev. D* **71**, 045006 (2005) [hep-th/0410224].
- [19] R. Britto, F. Cachazo and B. Feng, *Nucl. Phys. B* **725**, 275 (2005) [hep-th/0412103].
- [20] Z. Bern, J. J. M. Carrasco, H. Johansson and D. A. Kosower, *Phys. Rev. D* **76**, 125020 (2007) [arXiv:0705.1864 [hep-th]].
- [21] C. Anastasiou, R. Britto, B. Feng, Z. Kunszt and P. Mastrolia, *Phys. Lett. B* **645**, 213 (2007) [hep-ph/0609191]; R. Britto and B. Feng, *JHEP* **0802**, 095 (2008) [arXiv:0711.4284 [hep-ph]]; R. Britto and B. Feng, *Phys. Rev. D* **75**, 105006 (2007) [hep-ph/0612089]; G. Ossola, C. G. Papadopoulos and R. Pittau, *Nucl. Phys. B* **763**, 147 (2007) [hep-ph/0609007]; R. Britto, B. Feng and P. Mastrolia, *Phys. Rev. D* **78**, 025031 (2008) [arXiv:0803.1989 [hep-ph]]; D. Forde, *Phys. Rev. D* **75**, 125019 (2007) [arXiv:0704.1835 [hep-ph]]; S. D. Badger, *JHEP* **0901**, 049 (2009) [arXiv:0806.4600 [hep-ph]]; H. Ita and K. Ozeren, arXiv:1111.4193 [hep-ph].
- [22] Z. Bern, J. J. M. Carrasco, L. J. Dixon, H. Johansson and R. Roiban, *Phys. Rev. D* **82**, 125040 (2010) [arXiv:1008.3327 [hep-th]].
- [23] Z. Bern, J. J. Carrasco, T. Dennen, Y. t. Huang and H. Ita, *Phys. Rev. D* **83**, 085022 (2011) [arXiv:1010.0494 [hep-th]].
- [24] Z. Bern, L. J. Dixon and D. A. Kosower, *Ann. Rev. Nucl. Part. Sci.* **46**, 109 (1996) [hep-ph/9602280]; Z. Bern, L. J. Dixon and D. A. Kosower, *Annals Phys.* **322**, 1587 (2007) [arXiv:0704.2798 [hep-ph]].

- [25] Z. Bern and Y. t. Huang, J. Phys. A **44**, 454003 (2011) [arXiv:1103.1869 [hep-th]].
- [26] J. J. M. Carrasco and H. Johansson, J. Phys. A **44**, 454004 (2011) [arXiv:1103.3298 [hep-th]].
- [27] R. J. Eden, P. V. Landshoff, D. I. Olive, J. C. Polkinghorne, *The Analytic S Matrix* (Cambridge University Press, 1966).
- [28] Z. Bern, L. J. Dixon and D. A. Kosower, Phys. Rev. D **71**, 105013 (2005) [hep-th/0501240]; Phys. Rev. D **72**, 125003 (2005) [hep-ph/0505055]; Phys. Rev. D **73**, 065013 (2006) [hep-ph/0507005]; D. Forde and D. A. Kosower, Phys. Rev. D **73**, 065007 (2006) [hep-th/0507292]; Phys. Rev. D **73**, 061701 (2006) [hep-ph/0509358]; C. F. Berger, Z. Bern, L. J. Dixon, D. Forde and D. A. Kosower, Phys. Rev. D **75**, 016006 (2007) [hep-ph/0607014].
- [29] A. Brandhuber, D. Korres, D. Koschade and G. Travaglini, JHEP **1102**, 077 (2011) [arXiv:1010.1515 [hep-th]].
- [30] Z. Bern, L. J. Dixon and D. A. Kosower, Annals Phys. **322**, 1587 (2007) [arXiv:0704.2798 [hep-ph]]; C. F. Berger and D. Forde, Ann. Rev. Nucl. Part. Sci. **60**, 181 (2010) [arXiv:0912.3534 [hep-ph]]; R. Britto, J. Phys. A **44**, 454006 (2011) [arXiv:1012.4493 [hep-th]]; H. Ita, J. Phys. A **44**, 454005 (2011) [arXiv:1109.6527 [hep-th]].
- [31] N. Arkani-Hamed, J. L. Bourjaily, F. Cachazo, S. Caron-Huot and J. Trnka, arXiv:1008.2958 [hep-th]; N. Arkani-Hamed, J. L. Bourjaily, F. Cachazo and J. Trnka, arXiv:1012.6032 [hep-th].
- [32] B.S. DeWitt, Phys. Rev. 162:1239 (1967); M. Veltman, in *Les Houches 1975, Proceedings, Methods In Field Theory*, eds. R. Balian and J. Zinn-Justin (North-Holland, Amsterdam, 1976); S. Sannan, Phys. Rev. D34:1749 (1986).
- [33] Z. Bern and A. K. Grant, Phys. Lett. B **457**, 23 (1999) [hep-th/9904026].
- [34] N. E. J. Bjerrum-Bohr, P. H. Damgaard and P. Vanhove, Phys. Rev. Lett. **103**, 161602 (2009) [arXiv:0907.1425 [hep-th]]; S. Stieberger, arXiv:0907.2211 [hep-th].
- [35] B. Feng, R. Huang and Y. Jia, Phys. Lett. B **695**, 350 (2011) [arXiv:1004.3417 [hep-th]].
- [36] N. E. J. Bjerrum-Bohr, P. H. Damgaard, T. Sondergaard and P. Vanhove, arXiv:1003.2403 [hep-th]; C. R. Mafra, JHEP **1011**, 096 (2010) [arXiv:1007.3639 [hep-th]].
- [37] S. H. Henry Tye and Y. Zhang, JHEP **1006**, 071 (2010) [arXiv:1003.1732 [hep-th]].
- [38] Z. Bern, T. Dennen, Y. t. Huang and M. Kiermaier, Phys. Rev. D **82**, 065003 (2010) [arXiv:1004.0693 [hep-th]].
- [39] Z. Bern and T. Dennen, arXiv:1103.0312 [hep-th].

- [40] R. Monteiro and D. O’Connell, JHEP **1107**, 007 (2011) [arXiv:1105.2565 [hep-th]].
- [41] J. J. Carrasco and H. Johansson, Phys. Rev. D **85**, 025006 (2012) [arXiv:1106.4711 [hep-th]].
- [42] Z. Bern, C. Boucher-Veronneau and H. Johansson, Phys. Rev. D **84**, 105035 (2011) [arXiv:1107.1935 [hep-th]].
- [43] S. Mandelstam, Nucl. Phys. B **213**, 149 (1983); P. S. Howe, K. S. Stelle and P. K. Townsend, Nucl. Phys. B **214**, 519 (1983); L. Brink, O. Lindgren and B. E. W. Nilsson, Phys. Lett. B **123**, 323 (1983).
- [44] E. Cremmer, B. Julia and J. Scherk, Phys. Lett. B **76**, 409 (1978); E. Cremmer and B. Julia, Phys. Lett. B **80**, 48 (1978); Nucl. Phys. B **159**, 141 (1979).
- [45] Z. Bern, J. J. M. Carrasco and H. Johansson, arXiv:0902.3765 [hep-th]; H. Nicolai, Physics, **2**, 70, (2009); R. P. Woodard, Rept. Prog. Phys. **72**, 126002 (2009) arXiv:0907.4238 [gr-qc]; L. J. Dixon, arXiv:1005.2703 [hep-th]; Z. Bern, J. J. Carrasco, L. Dixon, H. Johansson and R. Roiban, arXiv:1103.1848 [hep-th]; H. Elvang, D. Z. Freedman and M. Kiermaier, J. Phys. A **44**, 454009 (2011) [arXiv:1012.3401 [hep-th]].
- [46] Z. Bern, L. J. Dixon and R. Roiban, Phys. Lett. B **644**, 265 (2007) [hep-th/0611086].
- [47] Z. Bern, J. J. Carrasco, D. Forde, H. Ita and H. Johansson, Phys. Rev. D **77**, 025010 (2008) [arXiv:0707.1035 [hep-th]].
- [48] Z. Bern, L. J. Dixon, M. Perelstein and J. S. Rozowsky, Nucl. Phys. B **546**, 423 (1999) [hep-th/9811140]; Z. Bern, N. E. J. Bjerrum-Bohr and D. C. Dunbar, JHEP **0505**, 056 (2005) [hep-th/0501137]; N. E. J. Bjerrum-Bohr, D. C. Dunbar and H. Ita, Phys. Lett. B **621**, 183 (2005) [hep-th/0503102]; N. E. J. Bjerrum-Bohr, D. C. Dunbar, H. Ita, W. B. Perkins and K. Risager, JHEP **0612**, 072 (2006) [hep-th/0610043]; N. E. J. Bjerrum-Bohr and P. Vanhove, JHEP **0804**, 065 (2008) [arXiv:0802.0868 [hep-th]]; JHEP **0810**, 006 (2008) [arXiv:0805.3682 [hep-th]]; N. Arkani-Hamed, F. Cachazo and J. Kaplan, JHEP **1009**, 016 (2010) [arXiv:0808.1446 [hep-th]].
- [49] G. Chalmers, hep-th/0008162; M. B. Green, J. G. Russo and P. Vanhove, JHEP **0702**, 099 (2007) [hep-th/0610299].
- [50] S. Weinberg, in *Understanding the Fundamental Constituents of Matter*, ed. A. Zichichi (Plenum Press, New York, 1977); S. Weinberg, in *General Relativity*, S. W. Hawking and W. Israel (Cambridge University Press, 1979) p. 700; M. Niedermaier and M. Reuter, Living Rev. Rel. **9**, 5 (2006); P. Horava, Phys. Rev. D **79**, 084008 (2009) [arXiv:0901.3775 [hep-th]].
- [51] G. Bossard, P. S. Howe and K. S. Stelle, JHEP **1101**, 020 (2011) [arXiv:1009.0743 [hep-th]]; H. Elvang, D. Z. Freedman and M. Kiermaier, JHEP **1011**, 016 (2010) [arXiv:1003.5018 [hep-th]]; N. Beisert, H. Elvang, D. Z. Freedman, M. Kiermaier, A. Morales and S. Stieberger, Phys. Lett. B **694**, 265 (2010) [arXiv:1009.1643 [hep-th]].

- [52] M. B. Green, J. G. Russo and P. Vanhove, JHEP **1006**, 075 (2010) [arXiv:1002.3805 [hep-th]]; P. Vanhove, arXiv:1004.1392 [hep-th]; J. Bjornsson and M. B. Green, JHEP **1008**, 132 (2010) [arXiv:1004.2692 [hep-th]].
- [53] R. Kallosh and P. Ramond, arXiv:1006.4684 [hep-th].
- [54] H. Elvang and M. Kiermaier, JHEP **1010**, 108 (2010) [arXiv:1007.4813 [hep-th]].
- [55] R. Kallosh, JHEP **1012**, 009 (2010) [arXiv:1009.1135 [hep-th]]; R. Kallosh, arXiv:1103.4115 [hep-th].
- [56] M. B. Green, J. G. Russo and P. Vanhove, Phys. Rev. Lett. **98**, 131602 (2007) [hep-th/0611273].
- [57] G. Bossard, P. S. Howe and K. S. Stelle, Phys. Lett. B **682**, 137 (2009) [arXiv:0908.3883 [hep-th]]; N. Berkovits, M. B. Green, J. G. Russo and P. Vanhove, JHEP **0911**, 063 (2009) [arXiv:0908.1923 [hep-th]]; G. Bossard, P. S. Howe, U. Lindstrom, K. S. Stelle and L. Wulff, JHEP **1105**, 021 (2011) [arXiv:1012.3142 [hep-th]].
- [58] Z. Bern, L. J. Dixon, D. C. Dunbar, M. Perelstein and J. S. Rozowsky, Nucl. Phys. B **530**, 401 (1998) [hep-th/9802162].
- [59] P. S. Howe and K. S. Stelle, Phys. Lett. B **554**, 190 (2003) [hep-th/0211279].
- [60] Z. Bern, J. S. Rozowsky and B. Yan, Phys. Lett. B **401**, 273 (1997) [hep-ph/9702424].

HIGH ENERGY PHYSICS: SCIENCE AND TECHNOLOGY BENEFITING HUMANITY

■ HARVEY B. NEWMAN

Professor of Physics

Charles C. Lauritsen Laboratory of High Energy Physics
California Institute of Technology
Pasadena, California 91125, USA

1. Introduction

Over the 80 years, particle physicists exploring the fundamental nature of matter, spacetime and the early universe at the highest available energies have invented, developed, or pushed the limits of a wide range of new technologies to make their scientific discoveries possible. From the earliest days of high energy physics in the 1930s to the latest 21st-century initiatives, the bold and innovative ideas and technologies of particle physics have entered the mainstream of society to transform the way we live. Many of these developments, from particle accelerators and ion beams [1] to particle detectors [2] and superconducting wire [3] to the World Wide Web [4] global Computing Grid systems [5] and data networks [6] have brought profound benefits to society and in some cases, such as the Web, have formed the basis of large and pervasive sectors of our modern life.

Beyond the specific technologies, the challenge of particle physics and the fascination of some of Nature's most fundamental questions has continued to attract the best and the brightest young scientists and students, who have learned to work cooperatively across international boundaries to build and successfully operate successive generations of accelerators and experiments, along with their particle detectors, high speed electronics and computing and communications systems, including the LHC and its experiments that are among the most complex instruments mankind has ever built. The impact of these scientists and engineers on society has been very great, as most have moved on from particle physics to other fields of scientific or biomedical research, medical practice, and industries where their work on accelerators, electronics, particle detection and other instrumentation, and information technologies, as well as their analytical methods and problem-solving approaches and capabilities have been widely felt.

2. Accelerator Applications

In 1930, Ernest O. Lawrence, the father of particle accelerators, built the first hand-held cyclotron at Berkeley, California. Larger and more powerful accelerators followed [7], with each generation of particle accelerators and detectors building on the previous one, raising the potential for discovery as the attainable energies have progressed by an order of magnitude roughly every 6 years, and pushing the level of technology ever higher.

After a day's research, Lawrence often operated the Berkeley cyclotrons through the night to produce medical isotopes for research and treatment. In 1938, Lawrence's mother became the first cancer patient to be treated successfully with particles from cyclotrons.

Doctors now use particle beams for the diagnosis and healing of millions of patients.

There are now an estimated 30,000 accelerators in industry, at hospitals and research centers, most of them only room-sized or smaller, which serve as essential tools for biomedical and materials research, for diagnosing and treating illnesses, and for a growing host of tasks in manufacturing, in energy and environmental technology, and in homeland security. The wide range of applications, as well as their use in research, is summarized in Figure 1 [8]:

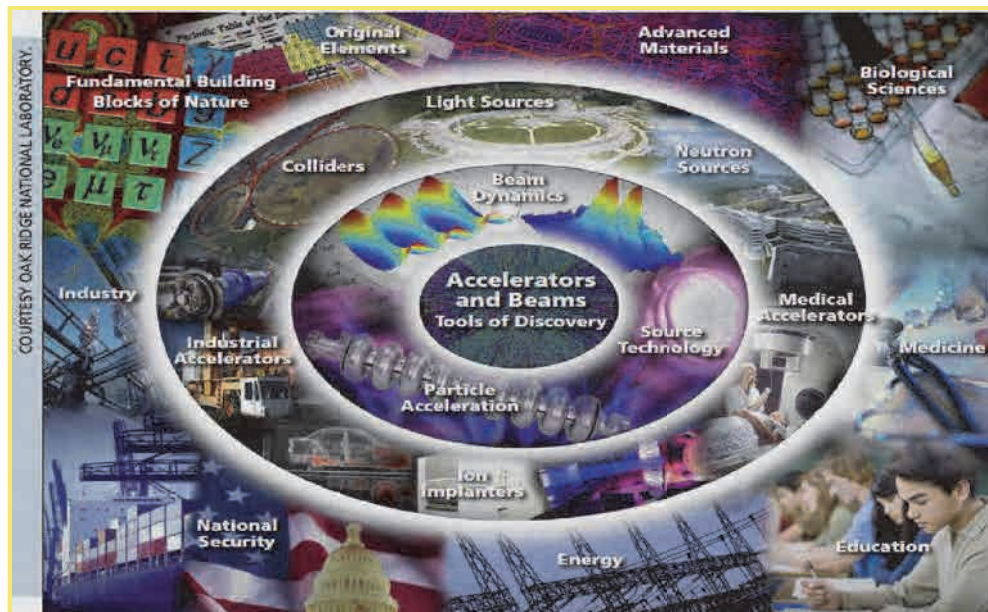


Figure 1. Illustration of the aspects and wide range of application of accelerator technologies, from Reference [8].

Accelerators today are used in a very wide range of research areas and industrial manufacturing areas from food and materials processing, to electronics manufacture to security. Some of the applications of beams of appropriate particle types and energies include:

- Detect and help diagnose, or shrink a tumor
- Design a new drug, map a protein, molecule or DNA using synchrotron radiation; find new ways to prevent or cure disease
- Make a better radial tire, or a heat-resistant automotive cable
- Harden metal surfaces to provide better bearings, make longer lasting machine and surgical tools, as well as artificial hip or knee joints
- Produce cleaner (fusion) energy through heavy ion induced fusion
- Spot suspicious cargo or luggage by scanning with neutrons
- Implant ions to dope semiconductors
- Prospect for oil
- Clean up drinking water
- Reduce pollutants in flue gases from factories and power plants
- Reduce nuclear waste
- Detect an art forgery, or discover a hidden art treasure

- Date an archaeological find
- Package food using shrink wrap that is produced by cross-linking polymers in plastics using electron beams

Medical Applications

Beams of X-rays, protons or carbon ions are used to treat tens of thousands of cancer patients daily, and proton beams are used to produce short-lived radioisotopes which are used in more than 10 million diagnostic medical treatments and 100 million laboratory tests each year. Nuclear diagnostic medicine and radiation therapy together save countless lives. Over the last two decades the use of protons and more recently heavy ions (such as carbon) are increasingly used since the beam can be tuned to deposit most of its energy at the site of a tumor, with less damage to surrounding tissue. A leading example is the Loma Linda University proton therapy center [9] whose accelerator was built at Fermilab. A leading cancer treatment center using heavy ions is at the Darmstadt Technical University [10].

Small electron accelerators are used worldwide for dental and chest X-rays.

Industrial and Environmental Applications of Electron Beams

Approximately 1700 high-current electron-beam accelerators are used worldwide for a wide range of industrial processing applications [11, 12].

The largest industrial use of these is to modify polymers by cross-linking, which forms three-dimensional chemical links among nearby polymer segments. Cross-linking makes materials insoluble in solvents that would otherwise dissolve them. Surface curing with low-energy electron beams (70 to 300 keV) is the fastest growing use, because of the improved energy efficiency of these high-speed processes and their elimination of volatile organic solvents that make the manufacturing process more environmentally friendly.

Cross-linked polymers are used for heat-shrinkable tubing for protecting electrical wire and cable connections, since this makes the insulation more flame retardant for automotive wiring under the hood and other applications. Cross-linking of heat-shrinkable films, widely used in food packaging extend the shelf life of meat, produce, poultry and dairy products and provide tamper-resistant packaging. Cross-linked polyethylene foam cushions the interior of automobile roof liners and door panels. The tire industry uses electron-beam processing to partially cure the rubber in order to stabilize the tire cord placement and to produce better-balanced tires.

Electron-beam curing of inks, coatings and adhesives eliminates the use of volatile organic compounds, enabling manufacturers to attain high production speeds with reduced energy consumption and reduced environmental impact. In these applications, “green” electron-beam technology yields as much as a 90 percent reduction in power consumption compared to conventional thermal drying and curing.

The manufacture of hydrogels for wound and burn treatment employs electron-beam technology. High-energy electron beams and x-rays derived from electron-beam systems sterilize medical equipment. A small number of service centers around the world use electron beams for food irradiation. Ionizing radiation eliminates food-borne pathogens, such as *E. coli*, *Salmonella* and *Listeria*, from meats, poultry and other food products, and disinfects grains and spices. Other industrial uses for electron-beam technology include degradation of Teflon®, for manufacturing micronized lubricants, grafting of filter membranes and battery separators; and enhancement of

polyethylene water pipes. The use of electron beams to treat seeds and soil shows promise for increasing crop yields.

Electron-beam treatment can disinfect and decontaminate both waste water and drinking water [11]. Projects in Boston and in Florida have shown the feasibility of disinfecting municipal waste water, and also breaking down water-borne organic toxins. An existing full-scale facility in Korea uses electron beams from an accelerator provided by Russia's Budker Institute to break down residual dyes from a fabric plant before discharge into a river.

Electron beam processing [12] is important for automobile production, where such systems are used to make gears and to weld and harden camshafts and tie-rod ends. In EB welding, precise energy deposition makes very deep welds possible. Complicated weld patterns can be produced using electromagnetic beam-deflection techniques. In EB drilling, rapid computer-controlled beam deflection allows "on-the-fly" drilling of thousands of holes per second in precise, repeatable patterns.

Industrial and Research Applications of Ion Beams

Ion-beam accelerators using boron, phosphorus, arsenic or other ions are essential for the the global semiconductor industry. About 10,000 ion-beam accelerators are used worldwide to "dope" the silicon or germanium chip used to manufacture computer and other electronics chips. Ion implantation also is used to transform the near-surface region of the base material into a fully or partially amorphous state, providing a method for fabricating strained and relaxed crystalline, polycrystalline, or amorphous structures during integrated circuit device fabrication. Because all digital electronics depend on ion implanters, they have a profound economic impact, and their use extends far beyond the semiconductor industry. Besides their role in CMOS, ion implanters are used in many other industrial applications, such as cleaving silicon; micro-electro-mechanical-systems (MEMS) fabrication; hardening of the surfaces of metals and ceramics for high-speed cutting tools and artificial human joints; and modification of the optical properties of materials.

Beyond semiconductor manufacture, other areas of ion implantation application include catalysis, solar energy and optical materials development, and fundamental science investigations associated with radiation effects in materials proposed for nuclear-waste stabilization and the next generation of highly resistant materials for nuclear reactors.

Ion implantation treatment of metal surfaces also is essential for the success of joint replacements.

Ion beams also are widely used in nondestructive elemental analysis by scattering of MeV ion-beam particles, by inducing nuclear reactions, or by using particle-induced x-ray and gamma-ray analysis. These methods are used to analyze materials in many fields including semiconductor research, environmental monitoring, geological and oceanographic studies, biomedical science and even art authentication. Ion-beam accelerators are also configured to be the most sensitive mass spectrometers for measuring trace radioisotope concentrations, including precise measurement of the Carbon 14 to Carbon 12 ratio for dating artifacts. This is an essential tool in geology, archaeology, drug discovery and climate studies. MeV ion accelerators have contributed to the fundamental understanding of high-density memory devices, silicon-based light amplifiers for fiber-optic communication, and the diagnosis of disease.

Ion Beams Producing Neutrons

A small but expanding use of ion beams is the production of neutrons for neutron-activation analysis and other analysis techniques in industry [13]. The use of accelerators for this purpose

rather than radioactive sources is driven in the U.S. by new regulations imposed in response to security and health concerns associated with the use and storage of radioactive materials. The majority of accelerator-based “neutron generators” are used for oil and gas exploration and borehole monitoring, mineral detection, and monitoring of various industrial processes including: on-line analysis of gold, cement, and scrap metal; radiography of manufactured parts; and determination of trace elements in biological and environmental materials. Neutron generators are also increasingly used for nondestructive examinations in the nuclear-waste and homeland-security fields, where security monitors search for concealed plastic and conventional high explosives, fissionable materials, and chemical weapons.

The accelerators most often used for neutron applications are small sealed-tube, high-voltage acceleration-gap devices which produce neutrons by accelerating deuterons and using them to initiate fusion reactions in a deuterium or tritium target. Compact sealed-tube generators such as those developed at LBNL [14] produce fluxes ranging from 10^6 to 10^{11} neutrons per second, while radiofrequency quadrupole (RFQ) deuteron and proton linacs [12] (the same type used as injectors into the proton accelerators used for high energy physics research today) have been commercially developed in recent years for applications requiring higher neutron yields or specific beam characteristics not achievable with sealed tubes, with fluxes up to 10^{13} neutrons per second.

Heavy Ion Beams for Nuclear Fusion

In the mid-1970s, A. Maschke of Brookhaven Lab suggested that heavy-ion beams, rather than laser beams, could be used to implode inertial-fusion targets for commercial generation of electrical power. The beams would deliver the kinetic energy to the surface of a capsule containing deuterium and tritium, with the resulting ablation driving compression and heat to drive nuclear fusion. Heavy ions have the advantage that the energy deposition is more local than photons. Many of the key accelerator components and subsystems have already been demonstrated to have long life, a sufficiently high pulse repetition rate and high electrical efficiency.

In the US, researchers from three laboratories – LBNL, LLNL and PPPL (Princeton) formed the US Heavy-Ion Fusion Virtual National Laboratory (HIF-VNL) to coordinate their work on heavy-ion fusion [15, 16]. Figure 2 shows an artist's concept of a heavy ion driven fusion power plant [15]. Other efforts aimed at both accelerator physics and studying the interaction of heavy ions with hot matter exist at GSI (Germany) [17], RIKEN (Japan), Orsay (France) and ITEP (Russia).

Sub-Nanometer Ion Beams

A striking development highlighted at the Symposium was a commercial sub-nm Helium ion beam by Zeiss [18], which enables the 3D nanofabrication of sub-10 nm structures for the first time. Important fields of application of this 0.35 nm short-range beam include (1) fabrication of molecular scale devices, (2) plasmonic sensors that could be pivotal in future generations of computers and communications systems, and (3) fabrication of solid state nanopores for single-molecule studies in biophysics and biotechnology, as well as studying a wide range of phenomena in DNA, RNA and proteins.

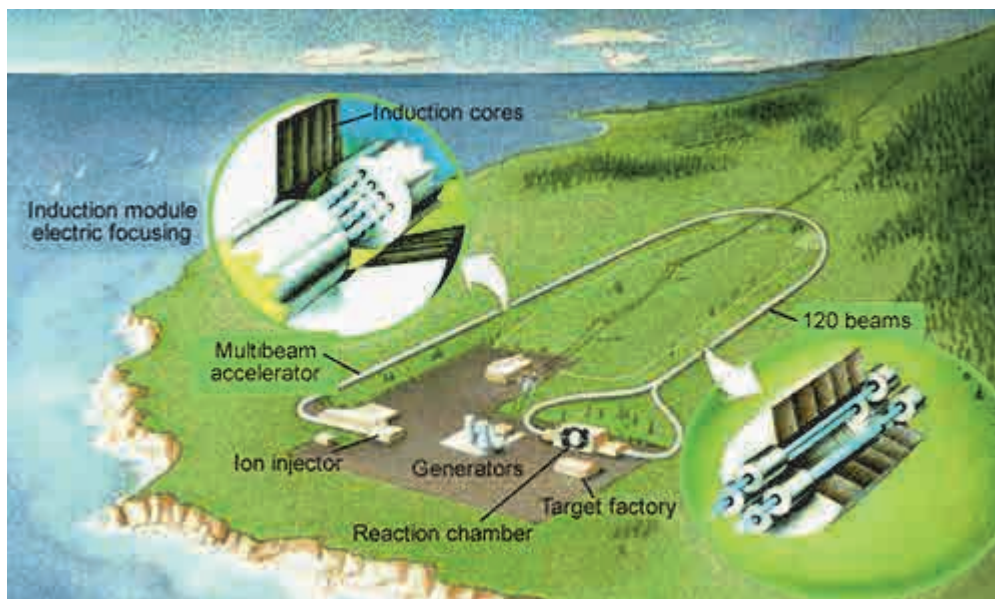


Figure 2. An artist's conception of a commercial heavy-ion fusion power facility: a load of water suitable for fueling such a fusion power plant could be carried in a pickup truck, supplying a year's worth of electrical power to a city like San Francisco.

Synchrotron Radiation

The intense, high brightness beams of photons emitted from electron accelerators are used in a vast range of research applications [19] in areas from condensed matter physics to material research, to protein structures and the functioning of normal and diseased biological systems in humans and animals, to pharmaceutical research and cultural heritage. Areas of application include:

Life Sciences

Pharmaceutical companies and medical researchers are making increasing use of macromolecular crystallography. Improvements in the speed of data collection and solving structures mean that it is now possible to obtain structural information on a timescale that allows chemists and structural biologists to work together in the development of promising compounds into drug candidates. The development of both the anti-flu drug Tamiflu and Herceptin – to treat advanced breast cancer – benefited from synchrotron experiments. Using infrared synchrotron light, research is underway to developing new cancer therapies tailored to the individual patient.

Engineering

Synchrotron X-ray beams allow detailed analysis and modelling of strain, cracks and corrosion as well as *in situ* study of materials during production processing. This vital to the development of high-performance materials and their use in innovative products and structures.

Environmental science

Synchrotron-based techniques have made a major impact in environmental science in the last 10 years. High brightness allows high-resolution study of ultra-dilute substances, the identification of species and the ability to track pollutants as they move through the environment. Synchrotrons have been used to develop more efficient techniques for hydrogen storage and to study the way in which depleted uranium disperses into the local environment.

Condensed Matter Physics and Materials Science

Determining the properties and morphology of buried layers and interfaces is an important area in solid-state science with synchrotrons driving the state-of-the-art in theory by providing high-precision experimental results. Structural studies of *in situ* processing of semiconducting polymer films are likely to be an important area of growth in the coming decade. Diffraction of high-intensity X-ray beams is a leading method to study spin, charge and orbital ordering in single-crystal samples to understand high-temperature superconductivity. Synchrotrons also were used to study giant magneto-resistance (GMR), which is now used in billions of computer disks and other electronic devices worldwide.

Cultural heritage

Scientists are using non-destructive synchrotron techniques to find answers to big questions in paleontology, archaeology, art history and forensics. Scientists in the UK have used synchrotrons to study samples from a Tudor warship and learn to enhance their conservation techniques for historical artifacts, and to study insects more than 100 million years old preserved in amber.

Current and Future Developments

The demand for synchrotron light has meant that third-generation machines are being built around the world, and existing machines continue to be developed to provide brighter X-rays, increased user hours and more flexible experimental stations. Recently developed fourth-generation sources such as the Linac Coherent Light Source (LCLS) X-ray laser at SLAC (Palo Alto) [20], and the free-electron laser European XFEL project now under construction at DESY (Hamburg) [21] generate shorter, femtosecond pulses but with the same intensity in each peak as synchrotron sources emit in one second, producing X-rays that are millions of times brighter in each pulse than the most powerful synchrotrons. These won't replace third-generation synchrotron machines, but will provide facilities that enable studies in the femtosecond range at higher peak brightness.

3. Knowledge and Technology Transfer

High energy physics has an extensive record of knowledge transfer to and from industry, commerce, and society at large. This is catalyzed by the need for state of art technologies and methods, including new materials for detector construction, radiation hard electronics, the highest speed global communications systems spanning continental and transoceanic distances, and many others, as well as cryogenics, vacuum, superconducting magnets, electronics and radiofrequency power systems, distributed computing and storage systems, and other engineering and control systems of unprecedented scale and scope. These needs for components and systems of a basically new kind or a new level of performance are sometimes met by industry, sometimes by the high energy physics community itself, and sometimes by joint-development projects between the scientific community and industry.

This is a long and deep tradition, highlighted by many articles in scientific and technical journals as well as the press over the years, and institutionalized through the U.S. funding agencies' Small Business Innovation Research (SBIR) and Small Business Technology Transfer (STTR) programs [22], as well as such laboratory based programs such as CERN's extensive Knowledge Transfer program [23]. An early example of this partnership is given in an article in the *New Scientist* about CERN in 1974 (four to five accelerator generations ago) entitled "Fallout from Smashing Atoms" [24]. The article covers an event when the laboratory opened its doors "to allow engineers from industry to see some of its advanced engineering components and design techniques." While the exceptional engineering and scientific achievements of the LHC today are

recognized worldwide, the achievements of CERN's Intersecting Storage Rings in 1974 were no less impressive, including the first large scale deployment of a cryogenic vacuum system in a 2 kilometer beam pipe reaching 10^{-12} to 10^{-13} Torr in the experimental straight sections of the pipe (less than atmospheric on the moon on some occasions), and electro-polishing of the RF cavities used to accelerate the beams to nanometer surface quality, construction of the then-largest superconducting magnet (1300 tons) for the 3.7 meter European Bubble Chamber. Last but not means least was the then-recent invention by Charpak of the Multiwire Proportional Chamber (MWPC) and associated particle detection technologies, for which he received the 1992 Nobel Prize in physics [25], which has led to a wide range of applications in biomedical imaging and research as well as high energy physics.

Technology Transfer

The Technology Transfer Office within CERN's Knowledge Transfer Program [26] now manages a diverse portfolio of technologies available for licensing and/or research collaborations with industry or institutes, in several domains:

Accelerators, Magnets and Cryogenic Technology

The extreme conditions of the LHC have led to the developments of many breakthroughs in the domains of underlying technologies such as accelerators, magnets and cryogenics and pushed existing technologies to its limits.

Detectors and Instrumentation

In experimental and applied particle physics, particle detectors are used to detect, track, and/or identify and measure the energy of particles. Driven by needs of many different experiments carried out over the last 50 years and in particular for the LHC, forefront detector technology developments are now available for many applications inside and outside high energy physics.

Some of the most important detector technologies available to biomedicine, materials research and other private sector areas include:

- The Gas Electron Multiplier (GEM) [27]: a proven amplification technique for position and ionization detection of charged particles, X-rays, photons and neutrons in gas detectors at high rates
- PHOSWICH: a gamma camera with depth-of-interaction reconstruction capability, for use in Positron Emission Tomography (PET) scanners
- Quantum Dosimetry: a novel invention comprising a method, software and apparatus to determine the dose, dose rate and composition of radiation.

Many of the key inventions and developments in detector technologies, from particle type identification to position measurements and tracking and energy measurement (calorimetry) in large area detectors have been carried out by Professor A. Zichichi and his teams over the last five decades. Many of these are summarized in a commemorative book "From the Preshower to New Technologies for Supercolliders: in Honour of Antonino Zichichi" [28], published shortly after the untimely passing of then-DESY Director Bjorn Wiik, one of the editors.

Electronics

Current accelerator systems and particle physics experiments at CERN are extremely challenging in terms of handling huge amounts of data in a very short time under difficult radiation conditions. In particular for the LHC, that has led to the development of extremely fast radiation sensors and

readout electronics, resulting in chip and sensor technologies available for use outside high energy physics such as medical imaging, material research and instrumentation for the life sciences.

Information Technology

CERN and its partners throughout the US and Europe have been the driving force for many Information and Communications Technology (ICT) developments over the last few decades, such as the handling of huge amounts of data across global networks using Grid and advanced network technologies and the World Wide Web. The invention of the World Wide Web at CERN has without doubt had the greatest impact on society. The modern Web and the technologies and structures that use it as a base, from e-banking to e-government and e-health, are now essential elements of the global economy. Indeed the Web has become one of the principal pillars of modern life in the developed world, and gateway to economic advancement, quality of life, access to knowledge, and the gateway to an equitable standard of living in the underdeveloped regions of the world.

Materials Science

The multidisciplinary technology context of CERN and the extremely challenging operational conditions of accelerators and physics experiments in particular for the LHC required and still require the development of innovative solutions for the treatment and processing of materials, to reach particular properties unachievable with methods available from outside.

Mechanics

The design and the construction of accelerator elements or components of particle physics experiments in particular for the LHC are often accompanied by the development of specific mechanical systems or tools that also can provide solutions for many engineering problems outside of high energy physics.

Networks of Experts

Knowledge transfer activities generate networks of people [29], research institutes, and companies through which technical, scientific and managerial expertise is exchanged. CERN engages in the creation, coordination and participation of several knowledge exchange networks including: the ***CERN Global Network*** that connects all the key individuals or organizations players in the knowledge exchange process, the ***HEPTech Network*** providing technology transfer opportunities involving leading HEP technologies, the ***Enterprise Europe Network (EEN)*** helping small businesses make the most of the European marketplace and many others.

Life Sciences

CERN also is involved in a range of activities connected to life sciences [30], including medical imaging, particle therapy, radiobiology, e-health and training of young researchers in these multidisciplinary fields. It also provides advice to the CERN community on these topics, and is actively involved in various projects, and promotes public awareness of its initiatives in the life sciences domain.

Crystal Scintillators

Fast, high density crystal scintillators comprise a special area of detector development, where high energy physics has had a leading role for the last 20 years [31, 32], notably driven by the Crystal Laboratory at Caltech and the Crystal Clear Collaboration at CERN. The use of crystal calorimeters with a crystal volume of as much as 9 cubic meters (in the case of the CMS experiment at the LHC) is important for precise measurements of electrons and photons, and has been a key factor in the search for new physics processes, including the ongoing search for the Higgs boson. There are a wide range of applications of these scintillators, including:

- Radiation detector modules for medical imaging
- Computed Tomography (CT) in medicine and industry
- Positron emission tomography (PET)
- Security scanning
- Oil well logging

Recent developments and areas of investigation include the development of LYSO ($\text{Lu}_{1.8}\text{Y}_{0.2}\text{SiO}_5(\text{Ce})$), an exceptionally radiation-hard, bright and fast scintillator suitable for the High Luminosity LHC, Lanthanum Bromide ($\text{LaBr}_3(\text{Ce})$) that is a very bright scintillator suitable for security scanning applications, and a new range of scintillating ceramics [33].

4. International Networks and Global Grid Systems

The fact that major high energy physics experiments are carried out by large international collaborations, combined with the need to process, distribute, access and analyze massive sets of data at sites around the world, has led to high energy physicists becoming leading developers as well as users of continental and transoceanic networks [34].

International networking for high energy physics was initiated by the author in 1982, and his group at Caltech has been responsible for transatlantic networking by the U.S. high energy community since then, with a current focus on support for the LHC program over the US LHCNet network.

In 1999 the author and collaborators proposed and designed the hierarchical worldwide grid system that is now used (in an evolved form with less hierarchical data flows in some cases) by the LHC experiments. The concept, known as the MONARC Model after the project [35] that developed the idea of a worldwide ensemble of national ("Tier1") and regional ("Tier2") computing and storage facilities, complemented by smaller ("Tier3") computing clusters serving individual physics groups at universities and small laboratories, is shown in Figure 3. The use of such a globally distributed model of computing and storage implied the intensive use of data networks, and so in the late 1990's high energy physicists, computer scientists and network engineers at Caltech and SLAC, CERN and at soon at many other sites in North America, Europe, Asia and Latin America began to engage in the development of data transfer applications designed and tuned to provide high throughput over long distance networks.

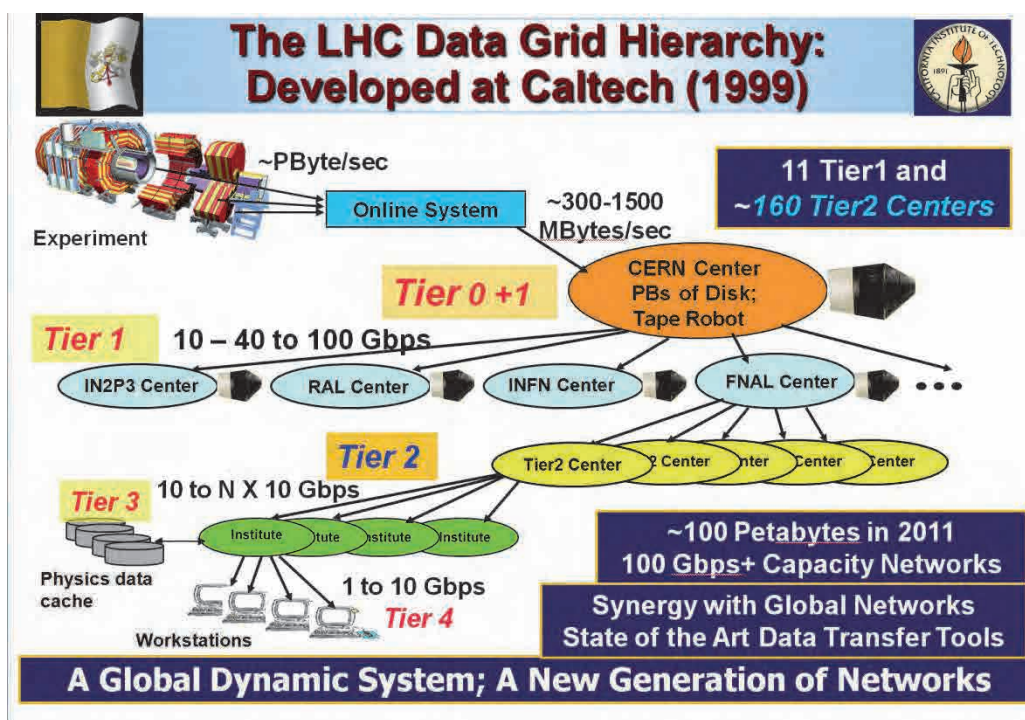


Figure 3. An illustration of the "MONARC" hierarchical grid computing model developed by the author and collaborators in 1999.

As the data volumes to be handled grew from Terabytes/year the 1990's to Petabytes (thousands of Terabytes) per year in the 2000's and hundreds of Petabytes per year now, the applications developed to fully matching the capacity of the networks. The exponential growth of the capacity of long range network links is noteworthy, rising from 2 megabits/sec (Mbps) in 1990, 1 gigabit/sec (Gbps) starting in 2000, and 10 Gbps from 2005. As of this writing, the major national and continental networks, such as Internet2 [36] and ESnet [37] in the US, and Geant [38] in Europe are undergoing a transition to the next generation of 100 Gbps networks, and transoceanic networks such as US LHCNet [39] are expected to follow as links of 40 and 100 Gbps between continents become widely available by approximately 2015. High energy physicists' use of the networks is equally noteworthy, as its historical growth trend has been at the rate of a factor of ten every 4 years, reaching a total of more than 100 Petabytes transported over networks during 2011.

State of the Art Network Applications

The ability to match current and next-generation networks, using mass-market computing equipment and open-source applications developed by high energy physics, such as Caltech's Fast Data Transfer (FDT) [40] has been demonstrated each year for the last decade, at the annual SuperComputing conferences as well as other events. The latest demonstrations [41] between the SC11 conference in Seattle and the University of Victoria in Canada achieved a sustained throughput of 186 Gbps using a single 100 Gbps link in both directions at once, between small ensembles of servers with next-generation 40 Gbps Ethernet interfaces. The methods used in these demonstrations have been adopted, on a smaller scale, by other fields of science and engineering, as well as users in the Library of Congress in the U.S., and the Amazon EC2 Cloud.

The most extensive applications developed by high energy physicists and their partners in this field are the grid software stacks of the LHC Worldwide Computing Grid (WLCG) [42] led by CERN, and the Open Science Grid in the U.S. [43]. Other key technologies developed by high energy physicist in this field include Caltech's MonALISA system that monitors and in some cases automates operations for global Grid and network systems [44], and Caltech's EVO (Enabling Virtual Organizations) system [45] that is used for videoconferencing and daily collaboration by the LHC and LIGO communities, as well as many other communities in research and education throughout the world.

ICFA Standing Committee on Inter-regional Connectivity (SCIC)

Given the importance of networks for the major collaborations in high energy physics, the International Committee on Future Accelerators (ICFA) comprised of laboratory directors and other leaders of the field of high energy physics drew the field's attention to the issue with a visionary statement in 1996 [46]:

"ICFA urges that all countries and institutions wishing to participate even more effectively and fully in international high energy physics collaborations should:

- *review their operating methods to ensure that they are fully adapted to remote participation*
- *strive to provide the necessary communication facilities and adequate international bandwidth."*

Following the formation of a Network Task Force in 1997-8, ICFA formed a Standing Committee on Inter-regional Connectivity (SCIC) [47] that the author has chaired since 2002.

The SCIC and the Digital Divide

The SCIC prepares detailed reports annually [48] which it presents to ICFA, on the state of the world's networks, with a focus on the networks used by high energy physics, as well as the use for other fields of science and for research and education in general. One important activity of the SCIC is monitoring the world's networks through its Monitoring Working Group [49]. The SCIC's main theme for the last decade has been its work to reduce and eventually eliminate the Digital Divide that separates the underdeveloped regions of the world, and the scientists and students living in those countries, from those living in the technologically and economically more advanced countries.

The SCIC has worked to lessen the Divide in nations in many regions – from central and eastern Europe to Latin America, South Asia and the Middle East, as well as many countries in Africa – by sharing information and knowledge on network and grid system technologies and applications, and working to encourage the local and regional development of the telecommunications and Grid infrastructures that will enable the disadvantaged science communities to participate more effectively in the LHC and other major programs of high energy physics.

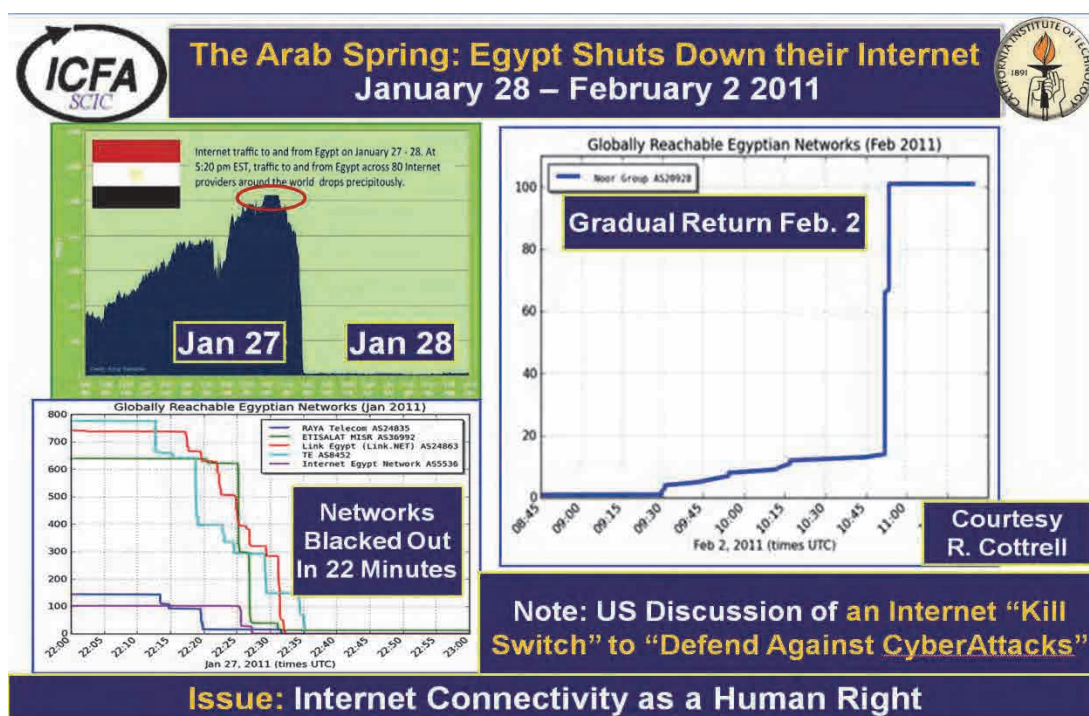


Figure 4. The abrupt cutoff and gradual return of Internet connectivity in Egypt, January 27 - February 2, also highlighting the concept of Internet connectivity as a human right.

Internet Connectivity as a Basic Human Right

The SCIC monitoring results have been used to allow the scientific community and government in each disadvantaged country to objectively gauge where it stands with respect to its neighboring countries, and its peers in other regions, and to illustrate how infrastructure improvements at moderate cost can bring rapid improvements: both technically and in the ability to collaborate effectively. The monitoring results have enabled our field to track and understand the effect of disruptions to Internet connectivity, as occurred in the Mediterranean in 2008 and 2009 due to undersea cable cuts (ascribed to earthquakes). And importantly, the real-time acquisition of this data has enabled us to track government actions to cut off access to the Internet, as occurred for example in Egypt at the start of Arab Spring in 2011, as shown in Figure 4.

The work of the SCIC towards equality in the scientific community, and the principle of Internet connectivity as a basic human right is fully in line with the *Erice Declaration on Principles for Cyber Stability and Cyber Peace* [50] that was adopted by the Plenary of the World Federation of Scientists on the occasion of the 42nd Session of the International Seminars on Planetary Emergencies in Erice (Sicily) on August 20, 2009. Some of the key provisions of this declaration are reproduced below:

ICTs support tenets of human rights guaranteed under international law, including the *Universal Declaration of Human Rights* (Articles 12, 18 and 19) and the *International Covenant on Civil and Political Rights* (Articles 17, 18, and 19). Disruption of cyberspace (a) impairs the individual's right to privacy, family, home, and correspondence without interference or attacks, (b) interferes with the right to freedom of

thought, conscience, and religion, (c) abridges the right to freedom of opinion and expression, and (d) limits the right to receive and impart information and ideas to any media and regardless of frontiers.

ICTs can be a means for beneficence or harm, hence also as an instrument for peace or for conflict. Reaping the benefits of the information age requires that information networks and systems be stable, reliable, available, and trusted. Assuring the integrity, security, and stability of cyberspace in general requires concerted international action.

THEREFORE, we advocate the following principles for achieving and maintaining cyber stability and peace:

1. All governments should recognize that international law guarantees individuals the free flow of information and ideas; these guarantees also apply to cyberspace. Restrictions should only be as necessary and accompanied by a process for legal review.
2. All countries should work together to develop a common code of cyber conduct and harmonized global legal framework, including procedural provisions regarding investigative assistance and cooperation that respects privacy and human rights. All governments, service providers, and users should support international law enforcement efforts against cyber criminals.
3. All users, service providers, and governments should work to ensure that cyberspace is not used in any way that would result in the exploitation of users, particularly the young and defenseless, through violence or degradation.
4. Governments, organizations, and the private sector, including individuals, should implement and maintain comprehensive security programs based upon internationally accepted best practices and standards and utilizing privacy and security technologies.
5. Software and hardware developers should strive to develop secure technologies that promote resiliency and resist vulnerabilities.
6. Governments should actively participate in United Nations' efforts to promote global cyber security and cyber peace and to avoid the use of cyberspace for conflict.

Conclusion

As high energy physics have pursued their investigations of the nature of matter and spacetime at the most fundamental level, they have grappled with some of the most difficult applied problems, invented, developed or extended the use of a wide range of new technologies, methods and systems, and devised some of the most complex instruments in the history of mankind in the service of their science. These developments have been made available to the world at large, and applied globally in medicine, electronics, energy, materials, security, and many other fields of industry and commerce, resulting in a worldwide beneficial impact on society. Many of the developments derived from the use of accelerators and particle detectors have directly benefitted the health, well-being and quality of life of the world's populations, while others have paved the way to succeeding generations of information and communications technologies that have increasingly defined the way humankind lives, learns and operates as a society.

As a field, many physicists have understood the obligation to use their capabilities to help address some of the world's most important human issues, such as the Digital Divide and the human right of access to Internet connectivity, as the means to knowledge, mutual understanding, equality of opportunity, and worldwide progress.

References

- [1] CERN, *Introduction to Particle Accelerators*. Retrieved January 15, 2012 from
<https://indico.cern.ch/getFile.py/access?contribId=2&resId=0&materialId=slides&confId=76283>

- [2] Grupen, C., Schwarz, B. (2008) *Particle Detectors, 2nd Edition*. Cambridge: University Press.

- [3] National High Magnetic Field Laboratory. *Superconducting Wire*. Retrieved January 15, 2012
 from <http://www.magnet.fsu.edu/education/tutorials/gallery/scwire.html>;
 Matteri, D. and Futino, L., Editors (2010). *Superconductivity and Superconducting Wires
 (Horizons in World Physics) Volume 267*. Nova Science Publishers.

- [4] Berners-Lee, Tim (2000). *Weaving the Web : The Original Design and Ultimate Destiny of
 The World Wide Web by its Inventor*. New York: Harper Collins Publishers.

- [5] Foster, I., Kesselman, C., Editors (1999). *The Grid: Blueprint for a New Computing
 Infrastructure*. San Francisco: Morgan Kaufmann Publishers;
 Berman, F., Fox, G., and Hey, T., Editors (2003) *Grid Computing: Making the Global
 Infrastructure a Reality* includes Data Intensive Grids for High Energy Physics (Chapter
 39) by Bunn, J. and Newman, H., Hoboken: Wiley

- [6] Kurose, J. and Ross, K. *Computer Networking: A Top Down Approach, 5th Edition*. New
 York: Addison-Wesley.

- [7] *Benefits to Society*. [http://www.fnal.gov/pub/science/benefits/Deconstructing the Livingston Plot](http://www.fnal.gov/pub/science/benefits/Deconstructing%20the%20Livingston%20Plot), Symmetry Magazine, Volume 6, Issue 5, October 2009. Retrieved January 12, 2012 from <http://www.symmetrymagazine.org/cms/?pid=1000756>
- [8] Malamud, E., Editor, *Accelerators and Beams: Tools of Innovation and Discovery*, APS Division of Particles and Beams. <http://www.aps.org/units/dpb/upload/brochure.pdf>
- [9] *The James M. Slater, M.D. Proton Treatment and Research Center at Loma Linda University in Southern California*. Visited online January 15, 2012: www.protons.com
- [10] The Darmstadt Technical University Heavy Ion Cancer Therapy Center. Visited online January 15, 2012: http://www.fkp.tu-darmstadt.de/groups/ag_durante/dur/cancer/index.en.jsp
- [11] U.S. Department of Energy Report: *Accelerators for America's Future*. Retrieved October 1, 2011 from <http://www.acceleratorsamerica.org/files/Report.pdf>
- [12] Hamm, R.W. and Hamm, M.E. *The Beam Business: Accelerators in Industry*. Physics Today, Volume 64, Issue 6, June 2011, p. 46.
- [13] Chichester, D. L., Simpson, J. D. *The Industrial Physicist*, December 2003/January 2004, p. 22.

- [14] Leung, K. N. et al., *Compact Neutron Generators, Lawrence Berkeley National Lab Technology Transfer and Intellectual Property Management, Available Technologies, IB-1764*. Visited online January 15, 2012: <http://www.lbl.gov/tt/techs/lbnl1764.html>
- [15] Yarris, C. et al., *Heavy Ion Fusion: Squeezing the Beams (June, 2005)*. Retrieved January 15, 2012 from: <http://www.lbl.gov/Science-Articles/Archive/sabl/2005/June/01-HIF.html>
- [16] *HIFS - Heavy Ion Fusion Science* (<http://hif.lbl.gov/>) and the *HIF Virtual National Laboratory*. <http://hif.lbl.gov/VNLOverview.html>. Recent progress (December 2010) is summarized in: http://hifnews.lbl.gov/HIFSNewsNo4_10.pdf
- [17] *The Other Route to Nuclear Fusion*, GSI Helmholtz Center for Heavy Ion Research. http://www.gsi.de/portrait/Broschueren/Wunderland/09_e.html
- [18] Maas, D. et al. (2009). *Nanofabrication with a Helium Ion Nanoscope*, Proc. of the International Society for Optics and Photonics (SPIE) Vol. 7638 763814
- [19] *Synchrotron Light*, Institute of Physics, 2010. Retrieved January 15, 2012 from: http://www.iop.org/publications/iop/2011/file_47457.pdf
- [20] *SLAC Laser Coherent Light Source (LCLS)*. https://slacportal.slac.stanford.edu/sites/lcls_public/Pages/Default.aspx
- [21] *European X-ray Laser (XFEL) Project*. <http://xfel.eu>

- [22] *U.S. DOE's Small Business Innovation Research (SBIR) and Small Business Technology Transfer (STTR) programs*. <http://science.energy.gov/sbir/about>
- [23] *CERN's Knowledge Transfer Program*. <http://knowledgetransfer.web.cern.ch/>
- [24] *Fallout from Smashing Atoms*, New Scientist Volume 62, p. 306, 9 May 1974.
Visited online on January 10, 2012 at:
http://books.google.com/books/about/New_scientist.html?id=fDMeAQAAMAAJ
- [25] *Nobel Lectures, Physics 1991-1995*, Editor Ekspöng, Gösta (1997). Singapore: World Scientific Publishing; *1992 Nobel Prize Lecture in Physics*. Visited online January 10, 2012 at:
http://www.nobelprize.org/nobel_prizes/physics/laureates/1992/charpak-lecture.html
- [26] *CERN's Technology Transfer Office*.
<http://knowledgetransfer.web.cern.ch/technology-transfer>
- [27] CERN Gas Detectors Development section. <http://gdd.web.cern.ch/GDD/>
- [28] Wiik, B., Wagner, A. and Wenniger, H. (Editors), *From the Preshower to New Technologies for Supercolliders: in honour of Antonino Zichichi*. World Scientific Series in 20th Century Physics, Volume 31, 2002.
http://books.google.com/books/about/From_the_preshower_to_the_new_technologi.html?id=o0tEjm2BgCgC; <http://www.amazon.com/Preshower-New-Technologies-Supercolliders-Scientific/dp/9812381996>

[29] CERN Knowledge Transfer, networks of people section.

<http://knowledgetransfer.web.cern.ch/networks>

[30] CERN Knowledge Transfer Life Sciences section.

<http://knowledgetransfer.web.cern.ch/life-sciences>

[31] Gratta, G., Newman, H., Zhu, R. *Crystal Calorimeters in Particle Physics*. Annu. Rev. Nucl. Part. Sci. 1994. 14:453-500.

[32] For an overview see for example: "Crystal Calorimeters in the Next Decade", Talk at the International Conference on Calorimetry in Particle Physics, May 2008.

http://www.hep.caltech.edu/~zhu/talks/ryz_080526_calor.pdf

[33] See for example Cherepy, N. J. et al. (2010) *Transparent Ceramic Scintillators for Gamma Spectroscopy and Radiography*, Proc. SPIE 7805, 78050I

[34] Newman, H. (October 2010), *A New Generation of Networks and Computing Models for High Energy Physics in the LHC Era*. Proceedings of the Computing for High Energy Physics Conference, Taipei. Journal of Physics: Conference Series, Volume 331, 2011. Available online at: <http://dx.doi.org/10.1088/1742-6596/331/1/012004>

[35] Newman, H. (Spokesperson) et al. (1998-2000). *Models of Networked Analysis at Regional Centers for LHC Experiments (MONARC)* <http://monarc.web.cern.ch/MONARC/>

[36] Internet2 is an advanced networking consortium led by the U.S. research and education community. <http://www.internet2.edu>

- [37] The U.S. Energy Sciences Network (ESnet). <http://www.es.net>
- [38] GÉANT is the pan-European data network dedicated to the research and education community. <http://www.geant.net>
- [39] USLHCNet provides transatlantic connections of the LHC Tier1 computing facilities at Fermilab and Brookhaven with the Tier0 and Tier1 facilities at CERN as well as Tier1s elsewhere in Europe and Asia, as well as connections between the Tier2 centers and the Tier1s as needed. <http://lhcnnet.caltech.edu>
- [40] Legrand, I. et al. *Fast Data Transfer (FDT)*. FDT is an open source Java application capable of reading and writing at disk speed over wide area networks, with standard TCP, that runs on all major platforms. <http://monalisa.caltech.edu/FDT/>
- [41] *High Energy Physicists Set Record for Network Data Transfer* (December 13, 2011). <http://supercomputing.caltech.edu/> and http://media.caltech.edu/press_releases/13477
- [42] The Worldwide LHC Computing Grid (WLCG) is a global collaboration of more than 140 computing centres in 35 countries, the 4 LHC experiments, and several national and international grid projects. <http://lcg.web.cern.ch/lcg/>
- [43] The Open Science Grid is a U.S. national computing grid for data-intensive research. <http://www.opensciencegrid.org>
- [44] *Monitoring Agents using a Large Integrated Services Architecture (MonALISA)*. <http://monalisa.caltech.edu>

- [45] *EVO - The Worldwide Collaboration Network*. <http://evo.caltech.edu>
- [46] *ICFA Statement on Communications in International High Energy Physics Collaborations* (October 17, 1996). http://www.fnal.gov/directorate/icfa/icfa_communicaes.html
- [47] *International Committee for Future Accelerators (ICFA) Standing Committee on Inter-Regional Connectivity (SCIC)*. <http://icfa-scic.web.cern.ch/ICFA-SCIC/>
- [48] *ICFA SCIC Annual Reports and Presentations, and Monitoring Reports*.
<http://icfa-scic.web.cern.ch/ICFA-SCIC/meetings.html>
- [49] Cottrell, R. (SLAC) et al. *Internet End-to-end Performance Monitoring*.
<http://www-iepm.slac.stanford.edu/>
- [50] Barletta, W. A., Westby, J. eProceedings of the International Seminar on Nuclear War and Planetary Emergencies, 42nd Session, 119-120.
<http://www.ewi.info/system/files/Erice.pdf>

BLUEPRINTS OF THE NO-SCALE MULTIVERSE AT THE LHC

■ TIANJUN LI, JAMES A. MAXIN, DIMITRI V. NANOPOULOS, JOEL W. WALKER

Introduction

Contemporary times have witnessed a revolution in string phenomenology, the culmination of decades of enterprise toward the comprehension of a fundamental high energy theory capable of describing the evolution of our observable universe. An unwavering theme that has emerged from this century of innovation is nature's persistent rejection of an intransigent conception of the macrocosm, of which we are just a simple element. Nature's truths have been revealed in pieces and in paradoxes, and have stymied every effort to claim mastery over her mysteries. Whether it be relativistic space and time, quantum entanglement, or black hole event horizons, we have become acclimated to radical revisions in our sense of reality, recognizing that the course of time may force all to acquiesce to axioms initially seeming exotic and fantastic, if they be first synthesized upon rigorous physical maxims.

Progress in the understanding of consistent, meta-stable vacua of string, M- or (predominantly) F-theory flux compactifications has inspired dramatic challenges to the perspective of our prominence in the cosmos. Case in point, it has been postulated that a vast landscape of an astonishing 10^{500} [1, 2] vacua can manifest plausible phenomenology in general. This suggestion implores inquiry as to why our peculiar vacuum transpired out of the landscape. One prevalent philosophy contends that any physically existent universe, whether latent or mature, should correspond to an extremization of probability density in the primordial quantum froth. Known as the *Anthropic Principle*, this idea implies that our universe, due to its natural existence and presumed singularity, occupies a statistical zenith. Consequently though, this doctrine becomes incurably burdened with fine-tuning complications of the physical properties of our universe. Motivated by the string landscape and other cosmological scenarios, the speculation of a Multiverse germinated as a strategy for overcoming those obstacles endemic to fine-tuning.

In our contemporary *Multiverse Blueprints* [3] we advanced an alternate perspective of our cosmological origins. We suggested that a mere non-zero probability for a universe featuring our measured physical parameters is the necessary and sufficient condition. An observer may inhabit a universe bearing simply a probability of existence which is greater than zero, and not inevitably that

which is most probable. Moreover, we argued for the significance of No-Scale Supergravity as a universal foundation allowing for the spontaneous quantum emergence of a cosmologically flat universe. Experimental validation of a No-Scale \mathcal{F} - $SU(5)$ structure for our own universe at the LHC could thus reinforce the role of string, M- and F-theory as a master theory of the Multiverse, with No-Scale supergravity providing an essential model building infrastructure.

We now undertake a first task of engineering in association with our Blueprints [3], considering the possibility of Multiverse model building, or *universe building*. We employ a precision numerical analysis to derive and subsequently classify the features of the No-Scale \mathcal{F} - $SU(5)$ Multiverse, within some local neighborhood of our own universe's phenomenology. By secondarily minimizing each model's scalar Higgs potential minima, under application of the dynamic Super No-Scale condition [3–5], only legitimate electroweak symmetry breaking (EWSB) vacua are viable elements of the solution space. The dynamically selected EWSB vacuum at this point of secondary minimization, which is in correspondence with the stabilization of a string-theoretic modulus, will be identified as the *minimum minimorum* (MM). Thereupon, *all* MM realize our minimal specifications for a greater than zero probability of emerging from the landscape. Hence, we conclude that a contiguous hyperspace of MM in No-Scale \mathcal{F} - $SU(5)$ may fulfill the intended goal of constructing the set of locally adjacent Multiverse constituents, endogenous to the plausible solution set of M- and F-Theory flux compactifications. We stress that application of the dynamic MM vacuum selection criterion elevates the conceptual Multiverse design presented here above a mere scan of the parameter space. We suggest that the resulting construction might rather be regarded to represent a local dominion of independent universes.

Our paper is organized as follows. First, we shall discuss No-Scale \mathcal{F} - $SU(5)$ in M- and F-Theory flux compactifications, presenting our \mathcal{F} - $SU(5)$ M(ultiverse)-Theory. Next, we engage in a brief review of \mathcal{F} - $SU(5)$, the Super No-Scale condition, and our secondary minimization procedure. In the latter half of our work, we shall demonstrate the minimization of discrete elements within the model space, and extrapolate the results to construct a hyperspace of MM, interpreting the solution space in terms of our local community of universes within the Multiverse. We then present phenomenology of a distinctive universe within the larger Multiverse structure that can explain tantalizing experimental hints of the Higgs boson and supersymmetry within our own universe.

The \mathcal{F} - $SU(5)$ M(ultiverse)-Theory

The Standard Model has been confirmed as a correct effective field theory valid up to about 100 GeV. Nonetheless, problems exist, such as the gauge hierarchy problem, charge quantization, and an excessive number of parameters, etc. Moreover, the Standard Model excludes gravity. An elegant solution to the gauge hierarchy problem is supersymmetry. In particular, gauge coupling unification can be realized in the supersymmetric SM (SSM), which strongly implies the Grand Unified Theories (GUTs). In the GUTs, not only can we explain the charge quantization, but also reduce the Standard Model parameters due to unification. Therefore, the interesting question is whether there exists a fundamental quantum theory or a final theory that can unify the SSM/GUTS and general relativity?

The most promising candidate for such a theory is superstring theory. Superstring theory is anomaly free only in ten dimensions, hence the extra six space dimensions must be compactified. As portrayed in Fig. 1, there are five consistent ten-dimensional superstring theories: heterotic $E_8 \times E_8$, heterotic $SO(32)$, Type I $SO(32)$, Type IIA, and Type IIB. Though, this leaves open the question of final unification. Interestingly, Witten pointed out that this distinction is an artifact of perturbation theory, and non-perturbatively these five superstring theories are unified into an eleven-dimensional M-theory [6]. In other words, the five superstring theories are the different perturbative limits of M-theory. Moreover, the twelve-dimensional F-theory can be considered as the strongly coupled formulation of the Type IIB string theory with a varying axion-dilaton field [7], as shown in Fig. 1.

The goal of string phenomenology is to construct the realistic string vacua where the SSM/GUTs can be realized and the moduli fields can be stabilized. Such constructions will give us a bridge between the string theory and the low energy realistic particle physics, such that we may test the string models at the Large Hadron Collider (LHC). Initially, string phenomenology was studied mainly in the weakly coupled heterotic string theory. On the other hand, we illustrate in Fig. 1 that in addition to its perturbative heterotic string theory corner, M-Theory unification possesses the other corners such as perturbative Type I, Type IIA and Type IIB superstring theory, which should provide new potentially phenomenologically interesting four-dimensional string models, related to the heterotic models via a web of string dualities. Most notably, with the advent of D-branes [8], we can construct the phenomenologically interesting string models in Type I, Type IIA and Type IIB string theories. Recall that there are five kinds of string models which have been studied extensively: (1) Heterotic $E_8 \times E_8$ string model building. The supersymmetric SM and GUTs can be constructed via the

orbifold compactifications [9–11] and the Calabi-Yau manifold compactifications [12, 13]; (2) Free fermionic string model building. Realistic models with clean particle spectra can only be constructed at the Kac-Moody level one [14–20]. Note that the Higgs fields in the adjoint representation or higher cannot be generated at the Kac-Moody level one, so only three kinds of models can be constructed: the Standard-like models, Pati-Salam models, and flipped $SU(5)$ models [14–20]. (3) D-brane model building from Type I, Type IIA, and Type IIB theories. There are two major kinds of such models: (i) Intersecting D-brane models or magnetized D-brane models [21–32]; (ii) Orientifolds of Gepner models [33,34]. (4) M-theory on G_2 manifolds [35,36]. Those models can be dual to the heterotic models on Calabi-Yau threefolds or to some Type II orientifold models. (5) F-theory GUTs [37–42]. The $SU(5)$ gauge symmetry can be broken down to the SM gauge symmetries by turning on the $U(1)_Y$ fluxes, and the $SO(10)$ gauge symmetry can be broken down to the flipped $SU(5) \times U(1)_X$ gauge symmetries and the $SU(3)_C \times SU(2)_L \times SU(2)_R \times U(1)_{B-L}$ gauge symmetries by turning on the $U(1)_X$ and $U(1)_{B-L}$ fluxes respectively.

To stabilize the moduli fields, the string theories with flux compactifications have also been studied [43–48], in which there intriguingly exist huge meta-stable flux vacua. For example, in the Type IIB theory with RR and NSNS flux compactifications, the number of the meta-stable flux vacua can be of order 10^{500} [1, 2]. With a weak anthropic principle, this may provide a solution to the cosmological constant problem and could explain the gauge hierarchy problem as well.

For our work here in this paper, we study only the flipped $SU(5) \times U(1)_X$ models, and we now shall provide a brief review of the minimal flipped $SU(5) \times U(1)_X$ model [49–51]. The gauge group of the flipped $SU(5)$ model is $SU(5) \times U(1)_X$, which can be embedded into $SO(10)$. We define the generator $U(1)_{Y'}$ in $SU(5)$ as

$$T_{U(1)_{Y'}} = \text{diag}\left(-\frac{1}{3}, -\frac{1}{3}, -\frac{1}{3}, \frac{1}{2}, \frac{1}{2}\right) \quad (1)$$

The hypercharge is given by

$$Q_Y = \frac{1}{5}(Q_X - Q_{Y'}) \quad (2)$$

In addition, there are three families of SM fermions whose quantum numbers under the $SU(5) \times U(1)_X$ gauge group are

$$F_i = (10,1), \bar{f}_i = (\bar{5}, -3), \bar{l}_i = (1,5) \quad (3)$$

where $i=1,2,3$.

To break the GUT and electroweak gauge symmetries, we introduce two pairs of Higgs fields

$$\begin{aligned} H &= (10,1), \bar{H} = (\bar{10}, -1) \\ h &= (5, -2), \bar{h} = (\bar{5}, 2) \end{aligned} \quad (4)$$

Interestingly, we can naturally solve the doublet-triplet splitting problem via the missing partner mechanism [51], and then the dimension five proton decay from the colored Higgsino exchange can be highly suppressed [51]. The flipped $SU(5) \times U(1)_X$ models have been constructed systematically in the free fermionic string constructions at Kac-Moody level one previously [14–16, 19, 51], and in the F-theory model building recently [37–42], and we represent the flipped $SU(5) \times U(1)_X$ models as one pillar of the foundation for \mathcal{F} - $SU(5)$ in Fig. 2. In the flipped $SU(5) \times U(1)_X$ models, there are two unification scales: the $SU(3)_C \times SU(2)_L$ unification scale M_{32} and the $SU(5) \times U(1)_X$ unification scale $M_{\mathcal{F}}$. To separate the M_{32} and $M_{\mathcal{F}}$ scales and obtain true string-scale gauge coupling unification in free fermionic string models [19, 52] or the decoupling scenario in F-theory models [41, 42], we introduce vector-like particles which form complete flipped $SU(5) \times U(1)_X$ multiplets, and we insert the vector particles and F-Theory as a second pillar in Fig. 2, and also integrate their presence into Fig. 1. In order to avoid the Landau pole problem for the strong coupling constant, we can only introduce the following two sets of vector-like particles around the TeV scale [52]

$$Z1: XF = (10,1), \bar{X}\bar{F} = (\bar{10}, -1) \quad (5)$$

$$Z2: XF, \bar{X}\bar{F}, Xl = (1, -5), \bar{X}\bar{l} = (1,5) \quad (6)$$

where

$$XF \equiv (XQ, XD^c, XN^c), \bar{X}\bar{l}_{(1,5)} \equiv (XE^c) \quad (7)$$

In the prior, XQ, XD^c, XE^c, XN^c have the same quantum numbers as the quark doublet, the right-handed down- type quark, charged lepton, and neutrino, respectively. Such kind of the models have been constructed systematically in the F-theory model building locally and dubbed \mathcal{F} - $SU(5)$ within that context [41,

42]. In this paper, we only consider the flipped $SU(5) \times U(1)_X$ models with $Z 2$ set of vector-like particles. The discussions for the models with $Z 1$ set and heavy threshold corrections [41, 42] are similar.

Recently, both ATLAS and CMS Collaborations announced the suggestive events for the Higgs particle with mass around 125 GeV, with each around 2σ significance over background [53, 54]. However, careful numerical analysis of the viable No-Scale \mathcal{F} - $SU(5)$ parameter space yields a prediction for m_h in the range of 119.0 GeV to 123.5 GeV [55], consistent with limits from the CMS [56], ATLAS [57, 58], CDF and DØ Collaborations [59]. To increase the lightest CP-even Higgs boson mass, we consider the Yukawa interaction terms between the MSSM Higgs and the vector-like particles in the superpotential

$$W = \frac{1}{2}Y_{xd}XF XF h + \frac{1}{2}Y_{xu}\overline{XF} \overline{XF} \overline{h} \quad (8)$$

After the $SU(5) \times U(1)_X$ gauge symmetry is broken down to the SM, the relevant Yukawa couplings are

$$W = Y_{xd}XQ XD^c H_d + Y_{xu}XQ^c XD H_u \quad (9)$$

Interestingly, we can increase the lightest CP-even Higgs boson mass by around 3-4 GeV via quantum corrections from vector-like particle Yukawa couplings.

Super No-Scale Supergravity

We now turn to the third and final pillar of the \mathcal{F} - $SU(5)$ foundation in Fig. 2, that of No-Scale supergravity. In the traditional framework, supersymmetry is broken in the hidden sector, and then its breaking effects are mediated to the observable sector via gravity or gauge interactions. In GUTs with gravity mediated supersymmetry breaking, also known as the minimal supergravity (mSUGRA) model, the supersymmetry breaking soft terms can be parameterized by four universal parameters: the gaugino mass $M_{1/2}$, scalar mass M_0 , trilinear soft term A , and the ratio of Higgs VEVs $\tan \beta$ at low energy, plus the sign of the Higgs bilinear mass term μ . The μ term and its bilinear soft term B_μ are determined by the Z -boson mass M_Z and $\tan \beta$ after the electroweak (EW) symmetry breaking.

To solve the cosmological constant problem, No-Scale supergravity was proposed [60-64]. No-scale supergravity is defined as the subset of supergravity models which satisfy the following three constraints [60-64]: (i) The vacuum energy vanishes automatically due to the suitable Kahler potential; (ii) At the

minimum of the scalar potential, there are flat directions which leave the gravitino mass $M_{3/2}$ undetermined; (iii) The super-trace quantity $\text{Str}M^2$ is zero at the minimum. Without this, the large one-loop corrections would force $M_{3/2}$ to be either zero or of Planck scale. A simple Kahler potential which satisfies the first two conditions is

$$K = -3\ln(T + \bar{T} - \sum_i \bar{\Phi}_i \Phi_i) \quad (10)$$

where T is a modulus field and Φ_i are matter fields. The third condition is model dependent and can always be satisfied in principle [65]. We emphasize that No-Scale supergravity can be realized in the compactification of the weakly coupled heterotic string theory [66] and the compactification of M-theory on S^1/Z_2 at the leading order [67]. The scalar fields in the above Kahler potential parameterize the coset space $SU(N_C + 1, 1)/(SU(N_C + 1) \times U(1))$, where N_C is the number of matter fields. Analogous structures appear in the $N \geq 5$ extended supergravity theories [68], for example, $N_C = 4$ for $N = 5$, which can be realized in the compactifications of string theory [66, 67]. The non-compact structure of the symmetry implies that the potential is not only constant but actually identical to zero. In fact, one can easily check that the scalar potential is automatically positive semi-definite, and has a flat direction along the T field. It is interesting that for the simple Kahler potential in Equation (10), we obtain the simplest No-Scale boundary condition $M_0 = A = B_\mu = 0$, while $M_{1/2}$ may be non-zero at the unification scale, allowing for low energy SUSY breaking.

The single relevant modulus field in the simplest string No-Scale supergravity is the Kahler modulus T , a characteristic of the Calabi-Yau manifold, the dilaton coupling being irrelevant. The F-term of T generates the gravitino mass $M_{3/2}$, which is proportionally equivalent to $M_{1/2}$. Exploiting the simplest No-Scale boundary condition at $M_{\mathcal{F}}$ and running from high energy to low energy under the RGEs, there can be a secondary minimization, or MM, of the minimum of the Higgs potential V_{\min} for the EWSB vacuum. Since V_{\min} depends on $M_{1/2}$, the gaugino mass $M_{1/2}$ is consequently dynamically determined by the equation $dV_{\min}/dM_{1/2} = 0$, aptly referred to as the Super No-Scale mechanism [3–5]. In this paper, we shall define the universe as the MM of the effective Higgs potential for a given set of input parameters.

The \mathcal{F} -Landscape

The methodology of Refs. [3, 5] for computing the MM had only been applied to a single point within the viable \mathcal{F} - $SU(5)$ parameter space in our previous work. We now seek to originate a full *landscape* of the local \mathcal{F} - $SU(5)$ model space by calculating the MM for a discrete set of points representative of the neighboring model space that presently subsists in the vicinity of the experimental uncertainties of our own universe [69]. Subsequently, we extrapolate the sampled findings to estimate a hypervolume of solutions for a more comprehensive panorama of the model space. We shall then interpret this landscape in the context of the *Multiverse Blueprints* [3], designating this subdivision as our local Multiverse community. In a broader sense, the Multiverse landscape is, of course, not limited to that zone which lies within our experimental uncertainty, though our purpose here is only initially to seek the prospective structure of an \mathcal{F} - $SU(5)$ local Multiverse, within an acceptable introductory level of precision. Each point within this No-Scale \mathcal{F} - $SU(5)$ Multiverse landscape of solutions, which we shall heretofore refer to as the \mathcal{F} -Landscape, can be interpreted as a distinct universe within our regional dominion of universes. With application of rigorous numerics, we shall demonstrate the resulting solution space. As elaborated in [3], testing of the No-Scale \mathcal{F} - $SU(5)$ framework at the LHC is in some sense likewise a broader test of the framework of the String Landscape and the Multiverse of plausible string, M- and F-theory vacua. One can boldly speculate that substantiation of a No-Scale \mathcal{F} - $SU(5)$ configuration for our universe at the LHC offers indirect support for a local dominion of \mathcal{F} - $SU(5)$ universes.

A modest sampling of satisfactory \mathcal{F} - $SU(5)$ points are extracted from the experimentally viable parameter space that satisfies the “bare-minimal” constraints of [5], in order to compute the MM in conformity with our conventional methodology. With the vector-like particle contributions to the Higgs boson mass, we present the updated viable parameter space in Fig. (3). The outermost borders of the experimentally viable parameter space presented in [5] are circumscribed from the bare-minimal constraints, though these constraints in principle are applicable only to our universe and not the Multiverse in general. Nevertheless, the model space persisting within this constrained perimeter presents a generous supply of archetype universes to explore and accordingly construct a hypervolume of solutions. To recapitulate, the bare-minimal constraints for our universe are defined by compatibility with the world average top quark mass $m_t = 173.3 \pm 1.1$ GeV [70], the prediction of a suitable candidate source of cold dark matter (CDM)

relic density matching the upper and lower thresholds $0.1088 \leq \Omega_{CDM} \leq 0.1158$ set by the WMAP-7 measurements [71], a rigid prohibition against a charged lightest supersymmetric particle (LSP), compatibility with the precision LEP constraints on the lightest CP-even Higgs boson ($m_h \geq 114$ GeV [72, 73]) and other light SUSY chargino, stau, and neutralino mass content, and a self-consistency specification on the dynamically evolved value of B_μ measured at the boundary scale $M_{\mathcal{F}}$. An uncertainty of ± 1 GeV on $B_\mu = 0$ is allowed, consistent with the induced variation from fluctuation of the strong coupling within its error bounds and the expected scale of radiative electroweak (EW) corrections. The lone constraint above that is necessarily mandatory for the Multiverse is that of the condition on the B-parameter at the $M_{\mathcal{F}}$ scale, since there is certainly no prerequisite for any of these other constrained parameters to inhabit within or even adjacent to the experimentally established uncertainties for our universe, although for our study here we prefer to remain nearby the local experimental ambiguities. The cumulative effect of these bare-minimal constraints distinctively shapes the experimentally viable parameter space germane to our universe into the uniquely formed profile situated in the $(M_{1/2}, M_V)$ plane exhibited in Fig. 3, from a tapered light mass region with a lower bound of $\tan \beta = 19.4$ into a more expansive heavier region that ceases sharply with the charged stau LSP exclusion around $\tan \beta \approx 23$. Correspondingly, we shall not journey too far afield from this narrow region of $\tan \beta$ or the world average top quark periphery.

The production of the hypervolume of solutions is initiated by mining the bare-minimally constrained wedge region in Fig. 3 for prospective universes from which to compute $V_{min}(h)$, carrying precision equivalent to the LEP constraints on the electroweak scale M_Z . In [3, 5], we executed the minimization procedure for a single specific fixed numerical value of μ only, so in essence, here we are broadening the blueprint of [3, 5] to encompass an extensive range of μ , utilizing our prescribed freedom of the numerical parameter. The secondary minimization procedure is thus enlarged by an order of cardinality, such that we may position the numerical value of μ to any figure we require, essentially dynamically determining in principle all $M_{1/2}$, $\tan \beta$, and M_Z for any preset permutation of M_V and m_t . This prescription can be replicated for an indefinite quantity of regional points within the model space in order to extrapolate the outcome to an estimated hypervolume comprising our local dominion of universes. A logically sequenced rendering of the prescription for dynamically determining a Multiverse is illustrated in Fig. 4, with the top half of the Fig. 4 space elucidating the minimization procedure for a unique predetermined duo of M_V and m_t , while the bottom half of the plot space reveals a depiction of the conjectural hypervolume of

universes.

Explicitly, the flow demonstrated in Fig. 4, after selection of a fixed combination of M_V and m_t , proceeds first to pinpoint $\tan\beta$ at the minimum of the 1-loop Higgs potential $V_{min}(h)$ for a precise numerical value of μ , as depicted in the upper left element, which is now deemed the MM. The curved grid surfaces illustrated in the top half of the Fig. 4 space characterize the hypersurface of $B_\mu = 0$ solutions. The effect of the ± 1 GeV induced electroweak scale variations on the $B_\mu = 0$ condition translates into a small thickness of the $B_\mu = 0$ hypersurfaces in the top half of the Fig. 4 space, though we suppress this in the diagrams here for simplicity. At first glance, $\tan\beta$ at the MM appears to be constant in Fig. 4, though in fact it is not, as $\tan\beta$ at the MM experiences a slight gradual continuous variation as the numerical value of μ is continuously adjusted. Once $\tan\beta$ at the MM for our selection of μ is discovered, we can then resolve the corresponding M_Z and $M_{1/2}$ at this MM by analyzing the center and right plots in the top half of the Fig. 4 space. We have in no way up to this point deviated from the methodology of Refs. [3, 5]. We have only demonstrated that guidelines established in Refs. [3, 5] can be broadened to incorporate the selection of any μ , such that the freedom on the bilinear μ parameter can in some sense be envisioned as a dial that can “tune” $M_{1/2}$, $\tan\beta$, and M_Z to that of any distinctive universe, for any and all prescribed sets of M_V and m_t , traversing the $B_\mu = 0$ hypersurfaces.

The multistep minimization procedure is copied for a sizable quantity of points in the model space, generating the solution space in the lower half plot of Fig. 4 through an extrapolation of the discrete returns. Only those sub one GeV perturbations about the minimum of the 1-loop Higgs potential are preserved, which we judge to be comparable in scale to the QCD corrections to the Higgs potential at the second loop. This constraint confines the value of $\tan\beta$ at the MM to live within an expected ± 1.5 deviation around the absolute minimum of $V_{min}(h)$. Consequently, we can project the ensuing variation in M_Z to be about ± 0.12 GeV at the MM. Thusly, over and above the freedom in μ to select different universes by “tuning” $M_{1/2}$, $\tan\beta$, and M_Z along a continuous string of MM, we must further recognize the indeterminate nature of these parameters at the MM from the QCD fluctuations providing some discretion on confinement of the MM to this theoretic one-dimensional string. Yet, it is essential to bear in mind that altering any one of these parameters will demand a compensating adjustment in one or more of the remaining parameters in order to transit along the $B_\mu = 0$ direction, engendering an additional unique point in the hypervolume of solutions, i.e. a unique universe in the Multiverse. These small fluctuations about the MM induce the diagrammed thickness of the hypervolume advertised in Fig. 4, where each singular point in the

illustrated hypervolume exemplifies an individual universe in the Multiverse.

The points employed in the compilation of the $B_\mu = 0$ hypersurface and hypervolume of Multiverse solutions in Fig. 4 were extracted from the experimentally viable parameter space delineated in Fig. 3 where the contours of $\tan\beta$ defining those regions consistent with the WMAP-7 relic density measurements progressively scale with both $M_{1,2}$ and M_ν . As noted earlier, the WMAP-7 experimentally allowed parameter space spans from $\tan\beta = 19.4$ to around $\tan\beta \simeq 23$, enveloping those regions of the model space regarded as credible contenders for our universe from a bottom-up experimental perspective. From a Multiverse frame of reference, the WMAP-7 region is extraneous, as any universe within the \mathcal{F} -Landscape may possess an intrinsic “WMAP” dark matter density, so to speak. In the process of dynamically determining the $M_{1,2}$, $\tan\beta$, and M_Z at the MM, relevant to the top-down theoretical perspective, there is little reason to anticipate (at least not from the point of view of an island universe) that the bottom-up and top-down techniques should be self-consistent at more than just a single point. Nevertheless, this remarkable correspondence is unquestionably what is discovered, prompting curiosity at whether the correlation stems from a deep physical motivation. In particular, the parallel transport of parameterization freedom exhibited by the phenomenological and dynamical treatments appears to support the conjectural application of this framework to a continuum of locally adjacent universes, each individually seated at its own dynamic MM.

LHC Search

We have carefully studied the expected $\mathcal{F}SU(5)$ production excesses in the high multiplicity jet channels [78,82], undertaking a detailed and comprehensive Monte Carlo simulation, employing industry standard tools [83,87]. We have painstakingly mimicked [78, 82] the leading multi-jet selection strategies of the CMS [77] and ATLAS [76] collaborations, using a post-processing script of our own design [88]. All 2-body SUSY processes have been included in our simulation. Our conclusion is that the best fit to the jet production excesses observed at both detectors occurs in the vicinity of the $M_{1,2} = 518$ GeV strip of Fig. 3. Lighter values of $M_{1,2}$ will allow for lighter vector-like particles and a heavier top quark, and thus also a heavier Higgs. However, values much below about $M_{1,2} = 480$ GeV are considered to be excluded for over-production of SUSY events. Values of $M_{1,2}$ much larger than the target range will have some difficulty achieving a sufficiently large Higgs mass. For specificity, we consider a benchmark point with inputs $M_{1,2} = 518$ GeV, $M_\nu = 1640$ GeV, $m_t = 174.4$ and $\tan\beta = 20.65$ [89]. The SUSY spectrum for this benchmark is presented in Table I.

In particular, the lightest CP-even Higgs boson mass can be lifted from 121.4 GeV up to 125.4 GeV.

TABLE I: Spectrum (in GeV) for $M_{1/2} = 518$ GeV, $M_V = 1640$ GeV, $m_t = 174.4$ GeV, $\tan\beta = 20.65$. Here, $\Omega_\chi = 0.1155$ and the lightest neutralino is 99.9% Bino. The partial lifetime for proton decay in the leading $(e|\mu)^+ \pi^0$ channels falls around 4×10^{34} Y [74, 75].

$\tilde{\chi}_1^0$	99	$\tilde{\chi}_1^\pm$	216	\tilde{e}_R	196	\tilde{t}_1	558	\tilde{u}_R	1053	m_h	125.4
$\tilde{\chi}_2^0$	216	$\tilde{\chi}_2^\pm$	900	\tilde{e}_L	570	\tilde{t}_2	982	\tilde{u}_L	1144	$m_{A,H}$	972
$\tilde{\chi}_3^0$	896	$\tilde{\nu}_{e/\mu}$	565	$\tilde{\tau}_1$	108	\tilde{b}_1	934	\tilde{d}_R	1094	m_{H^\pm}	976
$\tilde{\chi}_4^0$	899	$\tilde{\nu}_\tau$	551	$\tilde{\tau}_2$	560	\tilde{b}_2	1046	\tilde{d}_L	1147	\tilde{g}	704

TABLE II: Projections for the ATLAS and CMS signal significance at 5 fb^{-1} of integrated luminosity, in the ultra-high jet multiplicity channels. Event counts for $\mathcal{F}\text{-}SU(5)$ are based on our own Monte Carlo of the $M_{1/2} = 518$ GeV, $M_V = 1640$ GeV benchmark. SM backgrounds are scaled up from official collaboration estimates [76, 77].

	CMS 5 fb^{-1}					ATLAS 5 fb^{-1}				
	9j	10j	11j	12j	$\geq 9j$	7j	8j	9j	10j	$\geq 7j$
$\mathcal{F}\text{-}SU(5)$	14.0	4.5	1.4	0.3	20.3	7.3	1.8	0.4	0.1	9.6
SM	14.0	1.2	0.4	0.0	15.6	4.7	0.3	0.0	0.0	4.9
$S/\sqrt{B} + 1$	3.6	3.0	1.2	0.3	5.0	3.1	1.6	0.4	0.1	3.9

In Figs. 5 and 6, we overlay counts for the No-Scale $\mathcal{F}\text{-}SU(5)$ jet production (summed with the official SM backgrounds) onto histograms illustrating the current status of the LHC multi-jet SUSY search, representing just over 1.1 fb^{-1} of luminosity integrated by the ATLAS [76] and CMS [77] experiments, respectively. The statistical significance of the ATLAS overproduction, as gauged by the indicator of signal (observations minus background) to background ratio $S/\sqrt{B} + 1$, is quite low for ≥ 7 jets in the search strategy of Fig. 5, somewhat greater than 1.0, although the CMS overproduction significance for ≥ 9 jets in the search strategy of Fig. 6 is just above 2.0.

Conclusions

We evolved our *Multiverse Blueprints* to characterize our local neighborhood of the String Landscape and the Multiverse of plausible string, M- and F-theory vacua. Considering Super No-Scale \mathcal{F} - $SU(5)$, we demonstrated the existence of a continuous family of solutions which might adeptly describe the dynamics of distinctive universes. This Multiverse landscape of \mathcal{F} - $SU(5)$ solutions, which we referred to as the \mathcal{F} -Landscape, accommodates a subset of universes compatible with the presently known experimental uncertainties of our own universe. We showed that by secondarily minimizing the minimum of the scalar Higgs potential of each solution within the \mathcal{F} -Landscape, a continuous hypervolume of distinct *minimum minimorum* can be engineered which comprise a regional dominion of universes, with our own universe cast as the bellwether. In addition, we pointed out that our model can be tested at the early LHC run, and conjectured that an experimental signal at the LHC of the No-Scale \mathcal{F} - $SU(5)$ framework's applicability to our own universe might sensibly be extrapolated as corroborating evidence for the role of string, M- and F-theory as a master theory of the Multiverse, with No-Scale supergravity as a crucial and pervasive reinforcing structure.

Acknowledgements

This research was supported in part by the DOE grant DE-FG03-95-Er-40917 (TL and DVN), by the Natural Science Foundation of China under grant numbers 10821504 and 11075194 (TL), by the Mitchell-Heep Chair in High Energy Physics (JAM), and by the Sam Houston State University 2011 Enhancement Research Grant program (JWW). We also thank Sam Houston State University for providing high performance computing resources.

References

- [1] F. Denef, M. R. Douglas, and B. Florea, JHEP 0406, 034 (2004), hep-th/0404257.
- [2] F. Denef, M. R. Douglas, and S. Kachru, Ann. Rev.Nucl.Part.Sci. 57, 119 (2007), hep-th/0701050.
- [3] T. Li, J. A. Maxin, D. V. Nanopoulos, and J. W. Walker, Phys. Rev. D84, 056016 (2011), 1101.2197.
- [4] T. Li, J. A. Maxin, D. V. Nanopoulos, and J. W. Walker, Phys. Lett. B 703, 469 (2011), 1010.4550.
- [5] T. Li, J. A. Maxin, D. V. Nanopoulos, and J. W. Walker (2011), 1105.3988.
- [6] E. Witten, Nucl.Phys. B443, 85 (1995), hep-th/9503124.
- [7] C. Vafa, Nucl.Phys. B469, 403 (1996), hep-th/9602022.

- [8] J. Polchinski, Phys.Rev.Lett. 75, 4724 (1995), hep-th/9510017.
- [9] W. Buchmuller, K. Hamaguchi, O. Lebedev, and M. Ratz, Phys.Rev.Lett. 96, 121602 (2006), hep-ph/0511035.
- [10] O. Lebedev, H. P. Nilles, S. Raby, S. Ramos-Sanchez, M. Ratz, et al., Phys.Lett. B645, 88 (2007), hep-th/0611095.
- [11] J. E. Kim and B. Kyae, Nucl.Phys. B770, 47 (2007), hep-th/0608086.
- [12] V. Braun, Y.-H. He, B. A. Ovrut, and T. Pantev, Phys.Lett. B618, 252 (2005), hep-th/0501070.
- [13] V. Bouchard and R. Donagi, Phys.Lett. B633, 783 (2006), hep-th/0512149.
- [14] I. Antoniadis, J. R. Ellis, J. Hagelin, and D. V. Nanopoulos, Phys. Lett. B205, 459 (1988).
- [15] I. Antoniadis, J. R. Ellis, J. S. Hagelin, and D. V. Nanopoulos, Phys. Lett. B208, 209 (1988).
- [16] I. Antoniadis, J. R. Ellis, J. Hagelin, and D. V. Nanopoulos, Phys. Lett. B231, 65 (1989).
- [17] A. E. Faraggi, D. V. Nanopoulos, and K.-j. Yuan, Nucl.Phys. B335, 347 (1990).
- [18] I. Antoniadis, G. Leontaris, and J. Rizos, Phys.Lett. B245, 161 (1990).
- [19] J. L. Lopez, D. V. Nanopoulos, and K.-j. Yuan, Nucl. Phys. B399, 654 (1993), hep-th/9203025.
- [20] G. Cleaver, A. Faraggi, D. V. Nanopoulos, and J. Walker, Nucl.Phys. B620, 259 (2002), hep-ph/0104091.
- [21] M. Berkooz, M. R. Douglas, and R. G. Leigh, Nucl.Phys. B480, 265 (1996), hep-th/9606139.
- [22] L. E. Ibanez, F. Marchesano, and R. Rabadan, JHEP 0111, 002 (2001), hep-th/0105155.
- [23] R. Blumenhagen, B. Kors, D. Lust, and T. Ott, Nucl.Phys. B616, 3 (2001), hep-th/0107138.
- [24] M. Cvetič, G. Shiu, and A. M. Uranga, Phys.Rev.Lett. 87, 201801 (2001), hep-th/0107143.
- [25] M. Cvetič, G. Shiu, and A. M. Uranga, Nucl.Phys. B615, 3 (2001), hep-th/0107166.
- [26] M. Cvetič, I. Papadimitriou, and G. Shiu, Nucl.Phys. B659, 193 (2003), hep-th/0212177.
- [27] M. Cvetič, T. Li, and T. Liu, Nucl.Phys. B698, 163 (2004), hep-th/0403061.
- [28] M. Cvetič, P. Langacker, T.-j. Li, and T. Liu, Nucl.Phys. B709, 241 (2005), hep-th/0407178.
- [29] C.-M. Chen, G. Kraniotis, V. Mayes, D. V. Nanopoulos, and J. Walker, Phys.Lett. B611, 156 (2005), hep-th/0501182.
- [30] C.-M. Chen, G. Kraniotis, V. Mayes, D. V. Nanopoulos, and J. Walker, Phys.Lett. B625, 96 (2005), hep-th/0507232.
- [31] C.-M. Chen, T. Li, and D. V. Nanopoulos, Nucl.Phys. B732, 224 (2006), hep-th/0509059.
- [32] R. Blumenhagen, M. Cvetič, P. Langacker, and G. Shiu, Ann.Rev.Nucl.Part.Sci. 55, 71 (2005), hep-th/0502005.
- [33] T. Dijkstra, L. Huiszoon, and A. Schellekens, Phys.Lett. B609, 408 (2005), hep-th/0403196.
- [34] T. Dijkstra, L. Huiszoon, and A. Schellekens, Nucl.Phys. B710, 3 (2005), hep-th/0411129.
- [35] B. S. Acharya and E. Witten (2001), hep-th/0109152.
- [36] T. Friedmann and E. Witten, Adv.Theor.Math.Phys. 7, 577 (2003), hep-th/0211269.
- [37] C. Beasley, J. J. Heckman, and C. Vafa, JHEP 01, 058 (2009), 0802.3391.
- [38] C. Beasley, J. J. Heckman, and C. Vafa, JHEP 01, 059 (2009), 0806.0102.
- [39] R. Donagi and M. Wijnholt (2008), 0802.2969.
- [40] R. Donagi and M. Wijnholt (2008), 0808.2223.
- [41] J. Jiang, T. Li, D. V. Nanopoulos, and D. Xie, Phys. Lett. B677, 322 (2009).
- [42] J. Jiang, T. Li, D. V. Nanopoulos, and D. Xie, Nucl. Phys. B830, 195 (2010), 0905.3394.
- [43] R. Bousso and J. Polchinski, JHEP 06, 006 (2000), hep-th/0004134.

- [44] S. B. Giddings, S. Kachru, and J. Polchinski, Phys. Rev. D66, 106006 (2002), hep-th/0105097.
- [45] S. Kachru, R. Kallosh, A. D. Linde, and S. P. Trivedi, Phys. Rev. D68, 046005 (2003), hep-th/0301240.
- [46] L. Susskind (2003), hep-th/0302219.
- [47] F. Denef and M. R. Douglas, JHEP 0405, 072 (2004), hep-th/0404116.
- [48] F. Denef and M. R. Douglas, JHEP 0503, 061 (2005), hep-th/0411183.
- [49] S. M. Barr, Phys. Lett. B112, 219 (1982).
- [50] J. P. Derendinger, J. E. Kim, and D. V. Nanopoulos, Phys. Lett. B139, 170 (1984).
- [51] I. Antoniadis, J. R. Ellis, J. S. Hagelin, and D. V. Nanopoulos, Phys. Lett. B194, 231 (1987).
- [52] J. Jiang, T. Li, and D. V. Nanopoulos, Nucl. Phys. B772, 49 (2007), hep-ph/0610054.
- [53] T. C. Collaboration (2011), CMS-PAS-HIG-11-032, URL <http://cdsweb.cern.ch/>.
- [54] T. A. Collaboration (2011), ATLAS-CONF-2011-163, URL <https://atlas.web.cern.ch/>.
- [55] T. Li, J. A. Maxin, D. V. Nanopoulos, and J. W. Walker, Phys.Lett.B, In Press (2012), 1109.2110.
- [56] CMS (2011), CMS-PAS-HIG-11-022, URL <http://cdsweb.cern.ch/>.
- [57] ATLAS (2011), ATLAS-CONF-2011-135, URL <https://atlas.web.cern.ch/>.
- [58] ATLAS (2011), 1108.5895.
- [59] CDF/D0 (2011), 1107.4960.
- [60] E. Cremmer, S. Ferrara, C. Kounnas, and D. V. Nanopoulos, Phys. Lett. B133, 61 (1983).
- [61] J. R. Ellis, A. B. Lahanas, D. V. Nanopoulos, and K. Tamvakis, Phys. Lett. B134, 429 (1984).
- [62] J. R. Ellis, C. Kounnas, and D. V. Nanopoulos, Nucl. Phys. B241, 406 (1984).
- [63] J. R. Ellis, C. Kounnas, and D. V. Nanopoulos, Nucl. Phys. B247, 373 (1984).
- [64] A. B. Lahanas and D. V. Nanopoulos, Phys. Rept. 145, 1 (1987).
- [65] S. Ferrara, C. Kounnas, and F. Zwirner, Nucl. Phys. B429, 589 (1994), hep-th/9405188.
- [66] E. Witten, Phys. Lett. B155, 151 (1985).
- [67] T.-j. Li, J. L. Lopez, and D. V. Nanopoulos, Phys.Rev. D56, 2602 (1997), hep-ph/9704247.
- [68] E. Cremmer and B. Julia, Nucl.Phys. B159, 141 (1979).
- [69] T. Li, J. A. Maxin, D. V. Nanopoulos, and J. W. Walker (2011), 1111.0236.
- [70] (2010), 1007.3178.
- [71] E. Komatsu et al. (WMAP), Astrophys.J.Suppl. 192, 18 (2010), 1001.4538.
- [72] R. Barate et al. (LEP Working Group for Higgs boson searches), Phys. Lett. B565, 61 (2003), hep-ex/0306033.
- [73] W. M. Yao et al. (Particle Data Group), J. Phys. G33,1 (2006).
- [74] T. Li, D. V. Nanopoulos, and J. W. Walker, Nucl. Phys. B846, 43 (2011), 1003.2570.
- [75] T. Li, J. A. Maxin, D. V. Nanopoulos, and J. W. Walker, Nucl.Phys. B848, 314 (2011), 1003.4186.
- [76] G. Aad et al. (Atlas) (2011), 1110.2299.
- [77] (2011), CMS PAS SUS-11-003, URL <http://cdsweb.cern.ch/record/1370596>.
- [78] T. Li, J. A. Maxin, D. V. Nanopoulos, and J. W. Walker, Phys.Rev. D84, 076003 (2011), 1103.4160.
- [79] T. Li, J. A. Maxin, D. V. Nanopoulos, and J. W. Walker (2011), 1107.2375.
- [80] T. Li, J. A. Maxin, D. V. Nanopoulos, and J. W. Walker (2011), 1107.3825.
- [81] T. Li, J. A. Maxin, D. V. Nanopoulos, and J. W. Walker (2011), 1108.5169.

- [82] T. Li, J. A. Maxin, D. V. Nanopoulos, and J. W. Walker (2011), 1111.4204.
- [83] T. Stelzer and W. F. Long, *Comput. Phys. Commun.* 81, 357 (1994), hep-ph/9401258.
- [84] J. Alwall et al., *Madgraph/madevent collider event simulation suite* (2011), URL <http://madgraph.hep.uiuc.edu/>.
- [85] J. Alwall et al., *JHEP* 09, 028 (2007), 0706.2334.
- [86] T. Sjostrand, S. Mrenna, and P. Z. Skands, *JHEP* 05, 026 (2006), hep-ph/0603175.
- [87] J. Conway et al., *Pgs4: Pretty good (detector) simulation* (2009), URL <http://www.physics.ucdavis.edu/~conway/research/>.
- [88] T. Li, J. A. Maxin, D. V. Nanopoulos, and J. W. Walker, *Cutlhco: A tool for detector selection cuts* (2011), URL http://www.joelwalker.net/code/cut_lhco.tar.gz.
- [89] T. Li, J. A. Maxin, D. V. Nanopoulos, and J. W. Walker (2011), 1112.3024.

BLACK HOLES AND QUBITS

■ MICHAEL J. DUFF

Blackett Laboratory, Imperial College London

Abstract

Quantum entanglement lies at the heart of quantum information theory, with applications to quantum computing, teleportation, cryptography and communication. In the apparently separate world of quantum gravity, the Hawking effect of radiating black holes has also occupied centre stage. Despite their apparent differences, it turns out that there is a correspondence between the two.

Introduction

Whenever two very different areas of theoretical physics are found to share the same mathematics, it frequently leads to new insights on both sides. Here we describe how knowledge of string theory and M-theory leads to new discoveries about Quantum Information Theory (QIT) and vice-versa (Duff 2007; Kallosh and Linde 2006; Levey 2006).

Bekenstein-Hawking entropy

Every object, such as a star, has a critical size determined by its mass, which is called the Schwarzschild radius. A black hole is any object smaller than this. Once something falls inside the Schwarzschild radius, it can never escape. This boundary in spacetime is called the event horizon. So the classical picture of a black hole is that of a compact object whose gravitational field is so strong that nothing, not even light, can escape.

Yet in 1974 Stephen Hawking showed that quantum black holes are not entirely black but may radiate energy, due to quantum mechanical effects in curved spacetime. In that case, they must possess the thermodynamic quantity called entropy. Entropy is a measure of how organized or disorganized a system is, and, according to the second law of thermodynamics, it can never decrease. Noting that the area of a black hole's event horizon can never decrease, Jacob Bekenstein had earlier suggested such a thermodynamic interpretation implying that black holes must have entropy. This Bekenstein-Hawking black hole entropy is in fact given by one quarter the area of the event horizon. This is a remarkable fact relating a thermodynamic quantity, entropy, with a quantum mechanical origin, to a purely geometrical quantity, area, that is calculated in Einstein's classical theory of gravity.

Entropy also has a statistical interpretation as a measure of the number of quantum states available. However, it was not until 20 years later that

string theory, as a theory of quantum gravity, was able to provide a microscopic explanation of this kind.

Bits and pieces

A classical bit is the basic unit of computer information and takes the value 0 or 1. A light switch provides a good analogy; it can either be off, denoted 0, or on, denoted 1. A quantum bit or "qubit" can also have two states but whereas a classical bit is either 0 or 1, a qubit can be both 0 and 1 until we make a measurement. In quantum mechanics, this is called a superposition of states. When we actually perform a measurement, we will find either 0 or 1 but we cannot predict with certainty what the outcome will be; the best we can do is to assign a probability.

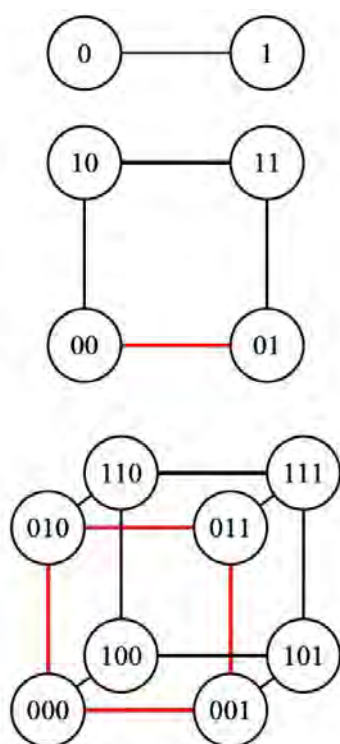


Figure 1: A single qubit is represented by a line; two qubits by a square and three qubits by a cube. up 10 and Alice-spin-down-Bob-spin-down 11, represented by the square in figure 1.

There are many different ways to realize a qubit physically. Elementary particles can carry an intrinsic spin. So one example of a qubit would be a superposition of an electron with spin up, denoted 0, and an electron with spin down, denoted 1. Another example of a qubit would be the superposition of the left and right polarizations of a photon. So a single qubit state, usually called Alice, is a superposition of Alice-spin-up 0 and Alice-spin-down 1, represented by the line in figure 1. The most general two-qubit state, Alice and Bob, is a superposition of Alice-spin-up-Bob-spin-up 00, Alice-spin-up-Bob-spin-down 01, Alice-spin-down-Bob-spin-up 10 and Alice-spin-down-Bob-spin-down 11, represented by the square in figure 1.

Consider a special two-qubit state which is just $00 + 01$. Alice can only measure spin up but Bob can measure either spin up or spin down. This is called a separable state; Bob's measurement is uncorrelated with Alice's. By contrast consider $00 + 11$. If Alice measures spin up, so must Bob and if she measures spin down so must he. This is called an entangled state; Bob cannot help making the same measurement. Mathematically, the square in figure 1 forms a 2×2 matrix and a state is entangled if the matrix has a nonzero determinant.

This is the origin of the famous Einstein-Podolsky-Rosen (EPR) paradox put forward in 1935. Even if Alice is in Geneva and Bob is millions of miles away in Alpha Centauri, Bob's measurement will still be determined by Alice's. No wonder Albert Einstein called it "spooky action at a distance". EPR concluded rightly that if quantum mechanics is correct then nature is nonlocal and if we insist on local "realism" then quantum mechanics must be incomplete. Einstein himself favoured the latter hypothesis. However, it was not until 1964 that CERN theorist John Bell proposed an experiment that could decide which version was correct, and it was not until 1982 that Alain Aspect actually performed the experiment. Quantum mechanics was right, Einstein was wrong and local realism went out the window.

As QIT developed, the impact of entanglement went far beyond the testing of the conceptual foundations of quantum mechanics. Entanglement is now essential to numerous quantum information tasks such as quantum cryptography, teleportation and quantum computation.

Cayley's hyperdeterminant

As a high-energy theorist involved in research on quantum gravity, string theory and M-theory, I paid little attention to all this, even though as a member of staff at CERN in the 1980s my office was just down the hall from Bell's.

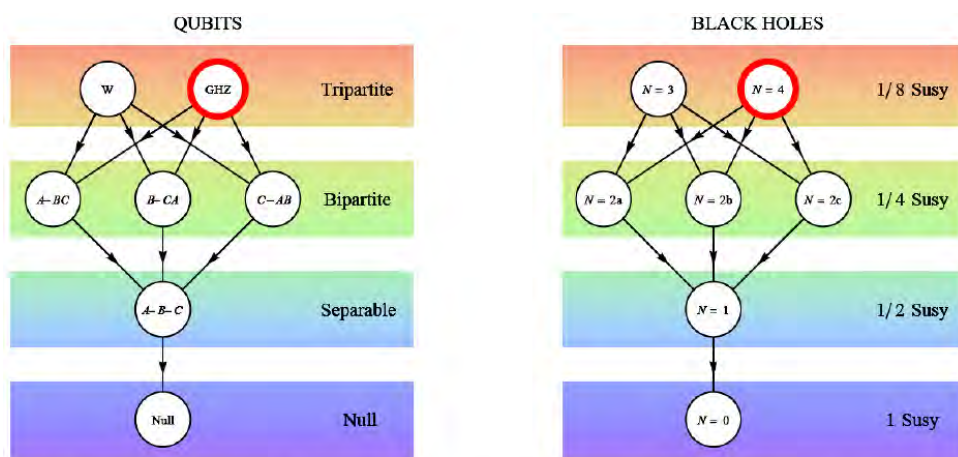


Figure 2: The classification of three qubits (left) exactly matches the classification of black holes from N wrapped branes (right). Only the GHZ state has a nonzero 3-tangle and only the $N = 4$ black hole has nonzero entropy.

My interest was not aroused until 2006, when I attended a lecture by Hungarian physicist Peter Levay at a conference in Tasmania. He was talking about three qubits Alice, Bob and Charlie where we have eight possibilities 000, 001, 010, 011, 100, 101, 110, 111, represented by the cube in figure 1. Wolfgang Dür and colleagues at the University of Innsbruck have shown that that three qubits can be entangled in several

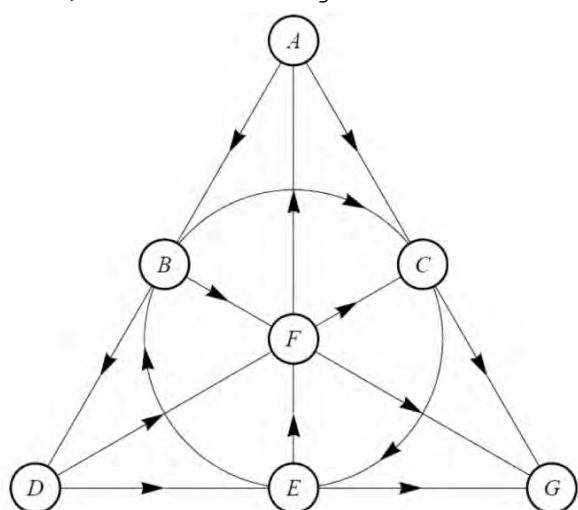
physically distinct ways: tripartite GHZ (Greenberger-Horne-Zeilinger), tripartite W, biseparable A-BC, separable A-B-C and null, as shown in the left hand diagram of figure 2 (Dür et al. 2000).

The GHZ state is distinguished by a nonzero quantity known as the 3-tangle, which measures genuine tripartite entanglement. Mathematically, the cube in figure 1 forms what in 1845 the mathematician Arthur Cayley called a $2 \times 2 \times 2$ hypermatrix and the 3-tangle is given by the generalization of a determinant called Cayley's hyperdeterminant. The reason this sparked my interest was that Levay's equations reminded me of some work I had been doing on a completely different topic in the mid 1990s with my collaborators Joachim Rahmfeld and Jim Liu (Duff et al. 1996). We found a particular black hole solution that carries eight charges (four electric and four magnetic) and involves three fields called S, T and U. When I got back to London from Tasmania I checked my old notes and asked what would happen if I identified S, T and U with Alice, Bob and Charlie so that the eight black-hole charges were identified with the eight numbers that fix the three-qubit state. I was pleasantly surprised to find that the Bekenstein-Hawking entropy of the black holes was given by the 3-tangle: both were described by Cayley's hyperdeterminant. This turned out to be the tip of an iceberg and there is now a growing dictionary between phenomena in the theory of black holes and phenomena in QIT.

Octonions

According to supersymmetry, for each known boson (integer spin 0, 1, 2 and so on), there is a fermion (half-integer spin $1/2$, $3/2$, $5/2$ and so on), and vice versa. CERN's Large Hadron Collider will be looking for these superparticles. The number of supersymmetries is denoted by N and ranges from 1 to 8 in four spacetime dimensions.

CERN's Sergio Ferrara and I have extended the STU model example, which has $N=2$, to the most general case of black holes in $N=8$ supergravity. We



have shown that the corresponding system in quantum information theory is that of seven qubits (Alice, Bob, Charlie, Daisy, Emma, Fred and George), undergoing at most a tripartite entanglement of a very specific kind as depicted by the Fano plane of figure 3 (left).

The Fano plane has a strange mathematical property: it describes the multiplication table of a particular kind of number: the octonion. Mathematicians classify numbers into four types: real numbers, complex

numbers (with one imaginary part A), quaternions (with three imaginary parts A, B, D) and octonions (with seven imaginary parts A, B, C, D, E, F, G). Quaternions are non-commutative because AB does not equal BA . Octonions are both noncommutative and non-associative because $(AB)C$ does not equal $A(BC)$.

Real, complex and quaternion numbers show up in many physical contexts. Quantum mechanics, for example, is based on complex numbers and Pauli's electron spin operators are quaternionic. Octonions have fascinated mathematicians and physicists for decades but have yet to find any physical application. In recent books both Roger Penrose and Ray Streater have characterized octonions as one of the great "lost causes" in physics. So we hope that the tripartite entanglement of seven qubits (which is just at the limit of what can be reached experimentally) will prove them wrong and provide a way of seeing the effects of octonions in the laboratory (Duff and Ferrara 2007; Borsten et al. 2009a).

Implications for M-theory

We have also learned things about M-theory from QIT. The Fano plane suggests a whole new way of studying its symmetries based on the 7 imaginary octonions (completely different from the Jordan algebra approach that uses all 8 split octonions). Such expectations have recently been strengthened by the discovery of four supergravities with $16+16$, $32+32$, $64+64$, $128+128$ degrees of freedom displaying some curious properties (Duff and Ferrara 2011a). In particular they reduce to $N = 1; 2; 4; 8$ theories all with maximum rank 7 in $D=4$ which correspond to 0, 1, 3, 7 lines of the Fano plane and hence admit a division algebra $(\mathbf{R}; \mathbf{C}; \mathbf{H}; \mathbf{O})$ interpretation consistent with the black-hole/qubit correspondence. They exhibit unusual properties. For example they are all "self-mirror" with vanishing trace anomaly (Duff and Ferrara 2011b).

Superqubits

In another development, QIT has been extended to super-QIT with the introduction of the superqubit which can take on three values: 0 or 1 or $\$$. Here 0 and 1 are "bosonic" and $\$$ is "fermionic" (Borsten et al. 2009b). Such values can be realised in condensed matter physics, such as the excitations of the t-J model of strongly correlated electrons, known as spinons and holons. The superqubits promise totally new effects, for example, could they be even more non-local than ordinary bits (Borsten et al 2012)? Super quantum computing is also being investigated (Castellani et al. 2010).

Wrapped branes as qubits

If current ideas are correct, a unified theory of all physical phenomena will require some radical ingredients in addition to supersymmetry. For

example, there should be extra dimensions: supersymmetry places an upper limit of 11 on the dimension of spacetime. The kind of real, four-dimensional world that supergravity ultimately predicts depends on how the extra seven dimensions are rolled up, in a way suggested by Oskar Kaluza and Theodor Klein in the 1920s. In 1984, however, 11-dimensional supergravity was knocked off its pedestal by superstring theory in 10 dimensions. There were five competing theories: the $E_8 \times E_8$ heterotic, the $SO(32)$ heterotic, the $SO(32)$ Type I, and the Type IIA and Type IIB strings. The $E_8 \times E_8$ seemed, at least in principle, capable of explaining the elementary particles and forces, including their handedness. Moreover, strings seemed to provide a theory of gravity consistent with quantum effects.

However, the spacetime of 11 dimensions allows for a membrane, which may take the form of a bubble or a two-dimensional sheet. In 1987 Howe, Inami, Stelle and I were able to show that if one of the 11 dimensions were a circle, we could wrap the sheet around it once, pasting the edges together to form a tube. If the radius becomes sufficiently small, the rolled-up membrane ends up looking like a string in 10 dimensions; it yields precisely the Type IIA superstring. In a landmark talk at the University of Southern California in 1995, Ed Witten drew together all of this work on strings, branes and 11 dimensions under the umbrella of M-theory in 11 dimensions. Branes now occupy centre stage as the microscopic constituents of M-theory, as the higher-dimensional progenitors of black holes and as entire universes in their own right.

Such breakthroughs have led to a new interpretation of black holes as intersecting black-branes wrapped around the seven curled dimensions of M-theory or six of string theory. Moreover, the microscopic origin of the Bekenstein-Hawking entropy is now demystified. Using Polchinski's D-branes, Andrew Strominger and Cumrun Vafa were able to count the number of quantum states of these wrapped branes (Strominger and Vafa 1996). A p -dimensional D-brane (or D_p -brane) wrapped around some number p of the compact directions ($x^4, x^5, x^6, x^7, x^8, x^9$) looks like a black hole (or D_0 -brane) from the four-dimensional (x^0, x^1, x^2, x^3) perspective. Strominger and Vafa found an entropy that agrees with Hawking's prediction, placing another feather in the cap of M-theory. Yet despite all these successes, physicists are glimpsing only small corners of M-theory; the big picture is still lacking. Over the next few years we hope to discover what M-theory really is. Understanding black holes will be an essential prerequisite.

The partial nature of our understanding of string/M-theory has so far prevented any kind of smoking-gun experimental test. This has led some critics of string theory to suggest that it is not true science. This is easily refuted by studying the history of scientific discovery; the 30-year time lag between the EPR idea and Bell's falsifiable prediction provides a nice example. Nevertheless it cannot be denied that such a prediction in string theory would be very welcome. Here we describe a prediction, not in the fields of particle physics and cosmology, but in quantum information theory.

Repurposing string theory

In the forty years since its inception, string theory has undergone many changes of direction, in the light of new evidence and discovery:

1970s: Strong nuclear interactions

1980s: Quantum gravity; ``theory of everything''

1990s: AdS/CFT: QCD (revival of 1970s); quark-gluon plasmas

2000s: AdS/CFT: superconductors

2000s: Cosmic strings

2010s: Fluid mechanics

2010s: Black hole/qubit correspondence: entanglement in Quantum Information Theory

For example, by stacking a large number of branes on top of one another, Juan Maldacena (Maldacena 1998) showed that a $(D+1)$ -dimensional spacetime with all its gravitational interactions, may be dual to a non-gravitational theory that resides on its D -dimensional boundary. If this so-called holographic picture is correct, our universe maybe like Plato's cave and we are the shadows projected on its walls. Its technical name is the ADS/CFT correspondence. Maldacena's 1998 ADS/CFT paper has garnered an incredible 7000+ citations. Interestingly enough, this is partly because it has found applications outside the traditional ``theory of everything'' milieu that one normally associates with string and M-theory. These, frequently serendipitous, applications include quark-gluon plasmas, high temperature superconductors and fluid mechanics. ADS/CFT is not the only branch of string/M-theory that has found applications in different areas of physics. After all, as shown in the table, string theory was originally invented in the 1970s to explain the behaviour of protons, neutrons and pions under the influence of the strong nuclear force.

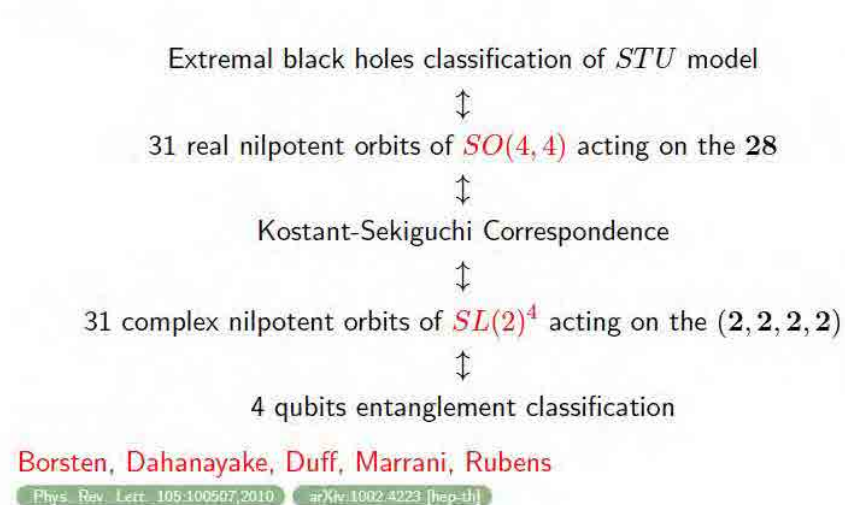
Four qubit entanglement: a falsifiable prediction

More recently the author and his graduate students Leron Borsten, Duminda Dahanayake, William Rubens at Imperial College teamed up with Alessio Marrani at CERN. We invoked this black hole-qubit/correspondence to predict a new result in quantum information theory. Noting that the classification of stringy black holes puts them in 31 different families, we predicted that four qubits can be entangled in 31 different ways (Borsten 2010). (By the way, this particular aspect of the correspondence is not a guess or a conjecture but a consequence of the Kostant-Sekiguchi

theorem. See figure 4). This can, in principle, be tested in the laboratory and we are urging our experimental colleagues to find ways of doing just that.

So the esoteric mathematics of string and M-theory might yet find practical applications.

EXTREMAL BLACK HOLE / 4 QUBIT CORRESPONDENCE



Acknowledgements

I am grateful to my collaborators Leron Borsten, Duminda Dahanayake, Sergio Ferrara, Hajar Ibrahim, Alessio Marrani and William Rubens for their part in this research and especially to Leron Borsten for help with the manuscript.

References

- E Bergshoeff et al. 1997 *Nucl. Phys.* B494, 119.
- L Borsten et al. 2008 *Phys. Rev. Lett.* 100 251602.
- L Borsten et al. 2009a *Phys. Rep.* 471 113.
- L Borsten et al. 2009b *Phys. Rev.* D81 105023.
- L Borsten et al. 2010 *Phys. Rev. Lett.* 105 100507.
- L.Borsten et al. 2012 (to appear)

- L Castellani et al. 2010 arXiv:1001.3753 [hep-th].
- M J Duff et al. 1996 *Nucl. Phys.* B459 125.
- M J Duff 2007 *Phys. Rev.* D76 025017.
- M J Duff CERN Courier May 2010
- M J Duff and S Ferrara 2007 *Phys. Rev.* D76 025018.
- M J Duff and S Ferrara 2011a *Phys. Rev.* D83 046007.
- M J Duff and S Ferrara 2011b *Class.Quant.Grav.*28:065005
- W Dür et al. 2000 *Phys. Rev.* A62 062314.
- R Kallosh and A Linde 2006 *Phys. Rev.* D73 104033.
- P Levay 2006 *Phys. Rev.* D7 015017.
- P Levay 2010 *Phys. Rev.* D82 026003.
- J M Maldacena 1998 *Adv. Theor. Math. Phys.* 2 231-252.
- A Strominger and C Vafa 1996 *Phys. Lett.* B379 99.

TESTING STRINGS AT THE LHC?^{*}

■ IGNATIOS ANTONIADIS[†]

Department of Physics, CERN – Theory Unit

Abstract

Lowering the string scale in the TeV region provides a theoretical framework for solving the mass hierarchy problem and unifying all interactions. The apparent weakness of gravity can then be accounted by the existence of large internal dimensions, in the submillimeter region, and transverse to a braneworld where our universe must be confined. I review the main properties of this scenario and its experimental implications.

1 Introduction

During the last few decades, physics beyond the Standard Model (SM) was guided from the problem of mass hierarchy. This can be formulated as the question of why gravity appears to us so weak compared to the other three known fundamental interactions corresponding to the electromagnetic, weak and strong nuclear forces. Indeed, gravitational interactions are suppressed by a very high energy scale, the Planck mass $M_P \sim 10^{19}$ GeV, associated to a length $l_P \sim 10^{-35}$ m, where they are expected to become important. In a quantum theory, the hierarchy implies a severe fine tuning of the fundamental parameters in more than 30 decimal places in order to keep the masses of elementary particles at their observed values. The reason is that quantum radiative corrections to all masses generated by the Higgs vacuum expectation value are proportional to the ultraviolet cutoff which in the presence of gravity is fixed by the Planck mass. As a result, all masses are “attracted” to about 10^{16} times heavier than their observed values.

Besides compositeness, there are two main theories that have been proposed and studied extensively during the last years, corresponding to different approaches of dealing with the mass hierarchy problem. (1) Low energy supersymmetry with all superparticle masses in the TeV region. Indeed, in the limit of exact supersymmetry, quadratically divergent corrections to the Higgs self-energy are exactly cancelled, while in the softly broken case, they are cutoff

^{*}Presented at the International Symposium on *Subnuclear Physics: Past, Present and Future*, Pontifical Academy of Sciences, Vatican, 30 Oct - 2 Nov 2011.

[†]On leave from CPHT (UMR CNRS 7644) Ecole Polytechnique, F-91128 Palaiseau.

by the supersymmetry breaking mass splittings. (2) TeV scale strings, in which quadratic divergences are cutoff by the string scale and low energy supersymmetry is not needed. Both ideas are experimentally testable at high-energy particle colliders and in particular at LHC.

2 Strings and extra dimensions

The appropriate and most convenient framework for low energy supersymmetry and grand unification is the perturbative heterotic string. Indeed, in this theory, gravity and gauge interactions have the same origin, as massless modes of the closed heterotic string, and they are unified at the string scale M_s . As a result, the Planck mass is predicted to be proportional to M_s :

$$M_P = M_s/g, \quad (1)$$

where g is the gauge coupling. In the simplest constructions all gauge couplings are the same at the string scale, given by the four-dimensional (4d) string coupling, and thus no grand unified group is needed for unification. In our conventions $\alpha_{\text{GUT}} = g^2 \simeq 0.04$, leading to a discrepancy between the string and grand unification scale M_{GUT} by almost two orders of magnitude. Explaining this gap introduces in general new parameters or a new scale, and the predictive power is essentially lost. This is the main defect of this framework, which remains though an open and interesting possibility.

The other other perturbative framework that has been studied extensively in the more recent years is type I string theory with D-branes. Unlike in the heterotic string, gauge and gravitational interactions have now different origin. The latter are described again by closed strings, while the former emerge as excitations of open strings with endpoints confined on D-branes [1]. This leads to a braneworld description of our universe, which should be localized on a hypersurface, i.e. a membrane extended in p spatial dimensions, called p -brane (see Fig. 1). Closed strings propagate in all nine dimensions of string theory: in those extended along the p -brane, called parallel, as well as in the transverse ones. On the contrary, open strings are attached on the p -brane. Obviously, our p -brane world must have at least the three known dimensions of space. But it may contain more: the extra $d_{\parallel} = p - 3$ parallel dimensions must have a finite size, in order to be unobservable at present energies, and can be as large as $\text{TeV}^{-1} \sim 10^{-18} \text{ m}$ [2]. On the other hand, transverse dimensions interact with us only gravitationally and experimental bounds are much weaker: their size should be less than about 0.1 mm [3]. In the following, I review the main properties and experimental signatures of low string scale models [4].

2.1 Framework of low scale strings

In type I theory, the different origin of gauge and gravitational interactions implies that the relation between the Planck and string scales is not linear as (1) of the heterotic string. The requirement that string theory should be weakly

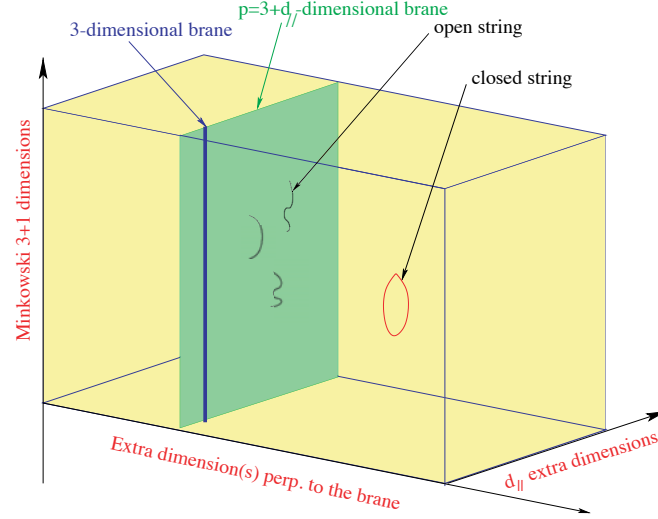


Figure 1: D-brane world universe in type I string framework.

coupled, constrain the size of all parallel dimensions to be of order of the string length, while transverse dimensions remain unrestricted. Assuming an isotropic transverse space of $n = 9 - p$ compact dimensions of common radius R_\perp , one finds:

$$M_P^2 = \frac{1}{g_s^2} M_s^{2+n} R_\perp^n, \quad g_s \simeq g^2. \quad (2)$$

where g_s is the string coupling. It follows that the type I string scale can be chosen hierarchically smaller than the Planck mass [5, 4] at the expense of introducing extra large transverse dimensions felt only by gravity, while keeping the string coupling small [4]. The weakness of 4d gravity compared to gauge interactions (ratio M_W/M_P) is then attributed to the largeness of the transverse space R_\perp compared to the string length $l_s = M_s^{-1}$.

An important property of these models is that gravity becomes effectively $(4+n)$ -dimensional with a strength comparable to those of gauge interactions at the string scale. The first relation of Eq. (2) can be understood as a consequence of the $(4+n)$ -dimensional Gauss law for gravity, with $M_*^{(4+n)} = M_s^{2+n}/g^4$ the effective scale of gravity in $4+n$ dimensions. Taking $M_s \simeq 1$ TeV, one finds a size for the extra dimensions R_\perp varying from 10^8 km, .1 mm, down to a Fermi for $n = 1, 2$, or 6 large dimensions, respectively. This shows that while $n = 1$ is excluded, $n \geq 2$ is allowed by present experimental bounds on gravitational forces [3, 6]. Thus, in these models, gravity appears to us very weak at macroscopic scales because its intensity is spread in the “hidden” extra dimensions. At distances shorter than R_\perp , it should deviate from Newton’s law, which may be possible to explore in laboratory experiments.

3 Large number of species

Here, we open a parenthesis to describe that low scale gravity with large extra dimensions is actually a particular case of a more general framework, where the ultraviolet (UV) cutoff is lower than the Planck scale due to the existence of a large number of particle species coupled to gravity [7]. Indeed, it was shown that the effective UV cutoff M_* is given by

$$M_*^2 = M_P^2/N, \quad (3)$$

where the counting of independent species N takes into account all particles which are not broad resonances, having a width less than their mass. The derivation is based on black hole evaporation but here we present a shorter argument using quantum information storage [8]. Consider a pixel of size L containing N species storing information. The energy required to localize N wave functions is then given by N/L , associated to a Schwarzschild radius $R_s = N/LM_P^2$. The latter must be less than the pixel size in order to avoid the collapse of such a system to a black hole, $R_s \leq L$, implying a minimum size $L \geq L_{min}$ with $L_{min} = \sqrt{N}/M_P$ associated precisely to the effective UV cutoff $M_* = L_{min}$ given in eq. (3). Imposing $M_* \simeq 1$ TeV, one should then have $N \sim 10^{32}$ particle species below about the TeV scale!

In the string theory context, there are two ways of realizing such a large number a particle species by lowering the string scale at a TeV:

1. In large volume compactifications with the SM localized on D-brane stacks, as described in the previous section. The particle species are then the Kaluza-Klein (KK) excitations of the graviton (and other possible bulk modes) associated to the large extra dimensions, given by $N = R_\perp^n l_s^n$, up to energies of order $M_* \simeq M_s$.
2. By introducing an infinitesimal string coupling $g_s \simeq 10^{-16}$ with the SM localized on Neveu-Schwarz NS5-branes in the framework of little strings [9]. In this case, the particle species are the effective number of string modes that contribute to the black hole bound [10]: $N = 1/g_s^2$ and gravity does not become strong at $M_s \sim \mathcal{O}(\text{TeV})$.

Note the both TeV string realizations above are compatible with the general expression (2), but in the second case there is no relation between the string and gauge couplings.

4 Experimental implications in accelerators

We now turn to the experimental predictions of TeV scale strings. Their main implications in particle accelerators are of three types, in correspondence with the three different sectors that are generally present:

1. New compactified parallel dimensions; In this case $RM_s \gtrsim 1$, and the associated compactification scale R_\parallel^{-1} would be the first scale of new physics

that should be found increasing the beam energy [2, 11]. The main consequence is the existence of KK excitations for all SM particles that propagate along the extra parallel dimensions. These can be produced on-shell at LHC as new resonances [12].

2. New extra large transverse dimensions and low scale quantum gravity,. The main experimental signal is gravitational radiation in the bulk from any physical process on the world-brane [13]. The resulting bounds are given in Table 1.

Table 1: Limits on R_\perp in mm.

Experiment	$n = 2$	$n = 4$	$n = 6$
LEP 2	5×10^{-1}	2×10^{-8}	7×10^{-11}
Tevatron	5×10^{-1}	10^{-8}	4×10^{-11}
LHC	4×10^{-3}	6×10^{-10}	3×10^{-12}

3. Genuine string and quantum gravity effects. Direct production of string resonances in hadron colliders leads generically to a universal deviation from Standard Model in jet distribution [14]. In particular, the first Regge excitation of the gluon has spin 2 and a width an order of magnitude lower than the string scale, leading to a characteristic peak in dijet production; similarly, the first excitations of quarks have spin 3/2. Concerning possible micro-black hole production, note that a string size black hole has a horizon radius $r_H \sim 1$ in string units, while the Newton's constant behaves as $G_N \sim g_s^2$. It follows that the mass of a d -dimensional black hole is [15]: $M_{\text{BH}} \sim r_H^{d/2-1}/G_N \simeq 1/g_s^2$. Using the value of the SM gauge couplings $g_s \simeq g^2 \sim 0.1$, one finds that the energy threshold M_{BH} of micro-black hole production is about four orders of magnitude higher than the string scale, implying that one would produce 10^4 string states before reaching M_{BH} .

Acknowledgments

Work supported in part by the European Commission under the ERC Advanced Grant 226371 and the contract PITN-GA-2009-237920.

References

- [1] C. Angelantonj and A. Sagnotti, *Phys. Rept.* **371** (2002) 1 [Erratum-ibid. **376** (2003) 339] [arXiv:hep-th/0204089].
- [2] I. Antoniadis, *Phys. Lett. B* **246** (1990) 377.
- [3] D. J. Kapner, T. S. Cook, E. G. Adelberger, J. H. Gundlach, B. R. Heckel, C. D. Hoyle and H. E. Swanson, *Phys. Rev. Lett.* **98** (2007) 021101.

- [4] N. Arkani-Hamed, S. Dimopoulos and G. R. Dvali, *Phys. Lett. B* **429** (1998) 263 [arXiv:hep-ph/9803315]; I. Antoniadis, N. Arkani-Hamed, S. Dimopoulos and G. R. Dvali, *Phys. Lett. B* **436** (1998) 257 [arXiv:hep-ph/9804398].
- [5] J. D. Lykken, *Phys. Rev. D* **54** (1996) 3693 [arXiv:hep-th/9603133].
- [6] J.C. Long and J.C. Price, *Comptes Rendus Physique* **4** (2003) 337; R.S. Decca, D. Lopez, H.B. Chan, E. Fischbach, D.E. Krause and C.R. Jamell, *Phys. Rev. Lett.* **94** (2005) 240401; R.S. Decca et al., arXiv:0706.3283 [hep-ph]; S.J. Smullin, A.A. Geraci, D.M. Weld, J. Chiaverini, S. Holmes and A. Kapitulnik, arXiv:hep-ph/0508204; H. Abele, S. Haeßler and A. Westphal, in 271th WE-Heraeus-Seminar, Bad Honnef (2002).
- [7] G. Dvali, arXiv:0706.2050 [hep-th]; *Int. J. Mod. Phys. A* **25** (2010) 602 [arXiv:0806.3801 [hep-th]]; G. Dvali and M. Redi, *Phys. Rev. D* **77** (2008) 045027 [arXiv:0710.4344 [hep-th]]; R. Brustein, G. Dvali and G. Veneziano, *JHEP* **0910** (2009) 085 [arXiv:0907.5516 [hep-th]].
- [8] G. Dvali and C. Gomez, *Phys. Lett. B* **674** (2009) 303.
- [9] I. Antoniadis and B. Pioline, *Nucl. Phys. B* **550** (1999) 41; I. Antoniadis, S. Dimopoulos and A. Givon, *JHEP* **0105** (2001) 055 [arXiv:hep-th/0103033]; I. Antoniadis, A. Arvanitaki, S. Dimopoulos and A. Givon, arXiv:1102.4043.
- [10] G. Dvali and D. Lust, arXiv:0912.3167 [hep-th]; G. Dvali and C. Gomez, arXiv:1004.3744 [hep-th].
- [11] I. Antoniadis and K. Benakli, *Phys. Lett. B* **326** (1994) 69.
- [12] I. Antoniadis, K. Benakli and M. Quirós, *Phys. Lett. B* **331** (1994) 313 and *Phys. Lett. B* **460** (1999) 176; P. Nath, Y. Yamada and M. Yamaguchi, *Phys. Lett. B* **466** (1999) 100 T. G. Rizzo and J. D. Wells, *Phys. Rev. D* **61** (2000) 016007; T. G. Rizzo, *Phys. Rev. D* **61** (2000) 055005; A. De Rujula, A. Donini, M. B. Gavela and S. Rigolin, *Phys. Lett. B* **482** (2000) 195.
- [13] G.F. Giudice, R. Rattazzi and J.D. Wells, *Nucl. Phys. B* **544** (1999) 3; E.A. Mirabelli, M. Perelstein and M.E. Peskin, *Phys. Rev. Lett.* **82** (1999) 2236; T. Han, J.D. Lykken and R. Zhang, *Phys. Rev. D* **59** (1999) 105006; K. Cheung, W.-Y. Keung, *Phys. Rev. D* **60** (1999) 112003; C. Balázs et al., *Phys. Rev. Lett.* **83** (1999) 2112; J.L. Hewett, *Phys. Rev. Lett.* **82** (1999) 4765.
- [14] L.A. Anchordoqui, H. Goldberg, D. Lust, S. Nawata, S. Stieberger and T.R. Taylor, *Phys. Rev. Lett.* **101** (2008) 241803 [arXiv:0808.0497 [hep-ph]].
- [15] G.T. Horowitz and J. Polchinski, *Phys. Rev. D* **55** (1997) 6189.

THE LAA PROJECT AND THE CONSEQUENCES ON LHC

■ HORST WENNINGER

CERN

The International Symposium on “Subnuclear Physics: Past, Present and Future”, held at the Pontifical Academy of Sciences from 30 October to 2 November 2011, provided an excellent occasion to highlight the achievements of an important project at CERN: **the LAA project**.

The LAA project was initiated by Prof. A. Zichichi and implemented at CERN in 1986 as „another CERN program of activities“ ¹⁾. The goal of the project was to prove the feasibility of new detector technologies that could be used in future multi-TeV hadron colliders.

To appreciate the importance of the LAA project for CERN we need to look back to the 1980th, when CERN envisaged to enter the era of lepton collider physics. Indeed, in April 1980, a progress report, published by the ECFA – LEP Working Group²⁾, chaired by Professor A ZICHICHI, was handed over to the CERN Management.

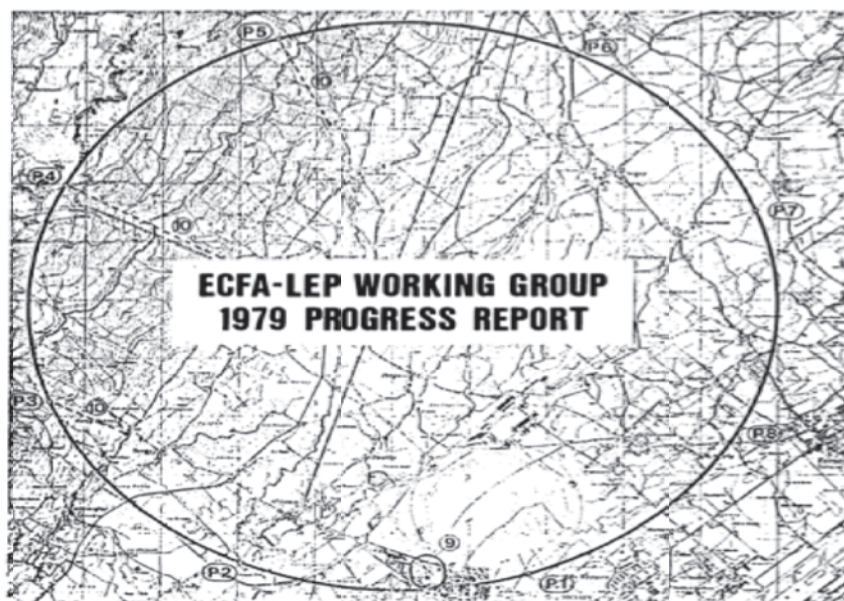
CERN LIBRARIES, GENEVA



CM-P00100391

ECFA/79/39
15/4/1980

ECFA EUROPEAN COMMITTEE FOR FUTURE ACCELERATORS



Edited by
A. Zichichi, Chairman
ECFA-LEP Working Group

In this Report it was recommended to construct a 27 km accelerator ring-tunnel adjacent to CERN between the French Jura and Geneva airport (see cover-page of the ECFA report above).

This tunnel infrastructure paved the way for 50 years of world-class subnuclear physics experiments by allowing to install high performance colliders, first LEP then LHC.

Within its constant funding levels from 1980 to 1989, CERN's resources were mainly dedicated to the SPS proton-antiproton program and to the LEP project. Not much was left for other activities: the ISR experiments, all bubble chambers and many fixed target experiments had to be closed down to free resources for LEP construction.

It was at that time when Prof. Zichichi proposed to CERN the LAA project permitting to invest in the future beyond LEP. The project allowed the recruitment of 40 staff-members (technicians-engineers-physicists) dedicated to research, innovation and development. The LAA project was open to all physicists and engineers and in the end over 80 scientists worked for LAA. The project was presented in an open meeting at CERN in June 1987 and subsequently to CERN's Research Board.

All aspects of an LHC detector layout were considered in the project and, in view of the demands of the collider, special attention was paid to hermeticity, radiation hardness, rate capability, and momentum resolution of the detector assemblies. The LAA Project consisted of sub-projects (*High precision tracking, calorimetry, large area muon detection devices, leading particle detection, data acquisition and analysis*).

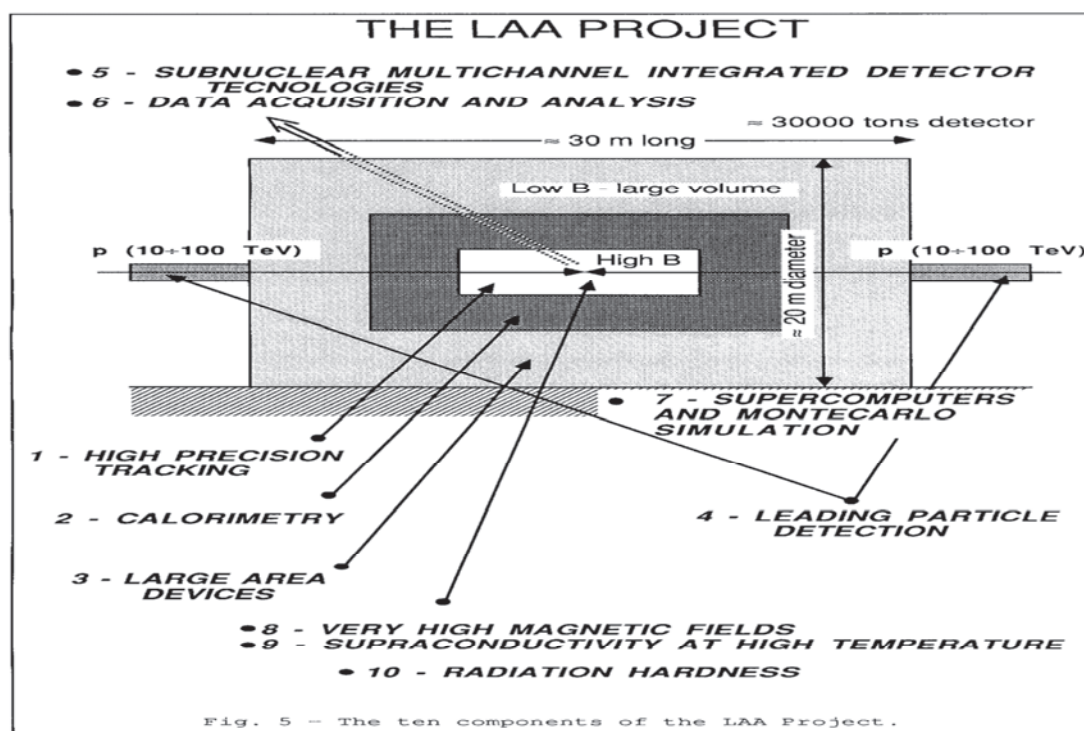


Figure 2: the ten components of the LAA project.

Main achievements are described in CERN reports³⁾ and highlighted in a book with the title: “From the Preshower to the New Technologies for Supercolliders“, dedicated to Antonino Zichichi⁴⁾.

Although some detector solutions adopted for the LHC experiments were finally different from those developed during the R&D phase, the LAA work had a great influence and measurable impact on the design of the actual LHC detectors. The LAA R&D started 10 years before technical choices were approved for LHC detectors and over 20 years before LHC detector operation started for physics. Technical solution adopted by collaborations, clearly depended also on factors such as specific know-how and competences existing in those Institutes, which took the responsibility to build and finance the detector components.

Nevertheless, the LAA technologies had an impact on LHC: examples are the spaghetti electromagnetic calorimeter, multi-drift chambers, scintillation fiber trackers, micro-strip detectors, precision tracking and read-out electronics, IPSA tube (Imaging Silicon Pixel Array), silicon pixels detectors, CMOS chips and ASIC/VLSI chip detector read-out. In addition engineers, physicists, technicians, recruited for the LAA activities, helped LHC experiments and participate in the experiments still today.

I present below a specific example to demonstrate the importance of the LAA project for CERN in preparation for the Large Hadron Collider experiments:

Example: MICRO-ELECTRONICS, a technology strengthened at CERN thanks to the resources of the LAA project which allowed to built-up the know-how within the CERN Experimental Facility Division with the recruitment of trained electronic engineers. LAA allowed to finance experts staff, hardware & software tools, which were essential for the development and design of microelectronics, silicon strip and pixel detectors.

A recent article in the IEEE Solid-State Circuits Society News⁵⁾, published by Erik Heijne, physicist from CERN, outlines that the design of custom chips for silicon detector readout was started at SLAC in 1981 and in 1986 at CERN mainly thanks to the LAA project.

A first application of microelectronics tools at CERN was leading to the construction of a hermetic silicon detector for the UA2 collider experiment. The AMPLEX chip⁶⁾, developed by Pierre Jarron at CERN in collaboration with A. Gößling from the University of Dortmund, was used to read-out the silicon pad detectors signals.

Another more recent example is the so-called NINO chip⁷⁾ for the ALICE Time-of-Flight ASIC front end. This chip is also interesting for medical applications of PET detectors, equipment developed for subnuclear physics experiments and now used in most hospitals.

A complete and detailed description of the LAA achievements has been published by the World Scientific Series in 20th Century Physics entitled: “SUBNUCLEAR PHYSICS the first 50 years Highlights from ERICE to ELN” , Antonino Zichichi⁸⁾.

From 1990 to 1996, the LAA project was complemented by a CERN Detector R&D program. LAA R&D groups participated in eight major proposals approved by the CERN DRDC ⁹⁾. Activities of the LAA R&D have been published in more than 350 papers and journals.

A most recent achievement of LAA teams concern the development of the MPRC (MULTIGAP RESISTIVE PLATE CHAMBER) for the ALICE Time of Flight systems ¹⁰⁾.

Furthermore, an educational spin-off program using LAA technology, initiated by Prof. A. Zichichi, has been implemented in schools all over Italy. The EEE (Extreme Energy Events) project ¹¹⁾, proposed by collaborator and team leader Crispin Williams, who is responsible for this R&D works, allows Italian pupils to construct themselves large area physics detectors to monitor cosmic ray showers and combine local results via Grid computing with schools in other locations.



Figure 3: Location of schools all over Italy where large area physics detectors have been installed to monitor cosmic ray showers as part of the *Extreme Energy Events* Project– to bring pupils in touch with real physics experiments

Future technological developments concentrate on an ambitious new project, which was proposed by Prof Zichichi at the International School of Subnuclear Physics at ERICE, the ISSP 2006 ¹²⁾.

The proposal is to probe a plasma of free quarks and gluons - the Quark–Gluon–Colored–World – produced in heavy ion collisions of extreme energies at LHC, by injecting beams of particles and photons to observe the different interaction results. The Quark–Gluon–Colored–World (QGCW) is expected to be totally different from our world made of QCD colorless baryons and mesons. The physics and details of this proposed project are outlined in a contribution by A. Zichichi to a conference in honour of MURRAY GELL-MANN'S 80th birthday ¹³⁾.

The QGCW project aims at experiments to probe the quark gluon colored world. Figure 4 illustrates schematically the idea of the experiment.

We need timing and synchronization between: colliding heavy ions, forming the quark gluon colored world, and bombarding particle, simultaneously injected to probe the QGCW, and detectors, triggering on the emerging particles

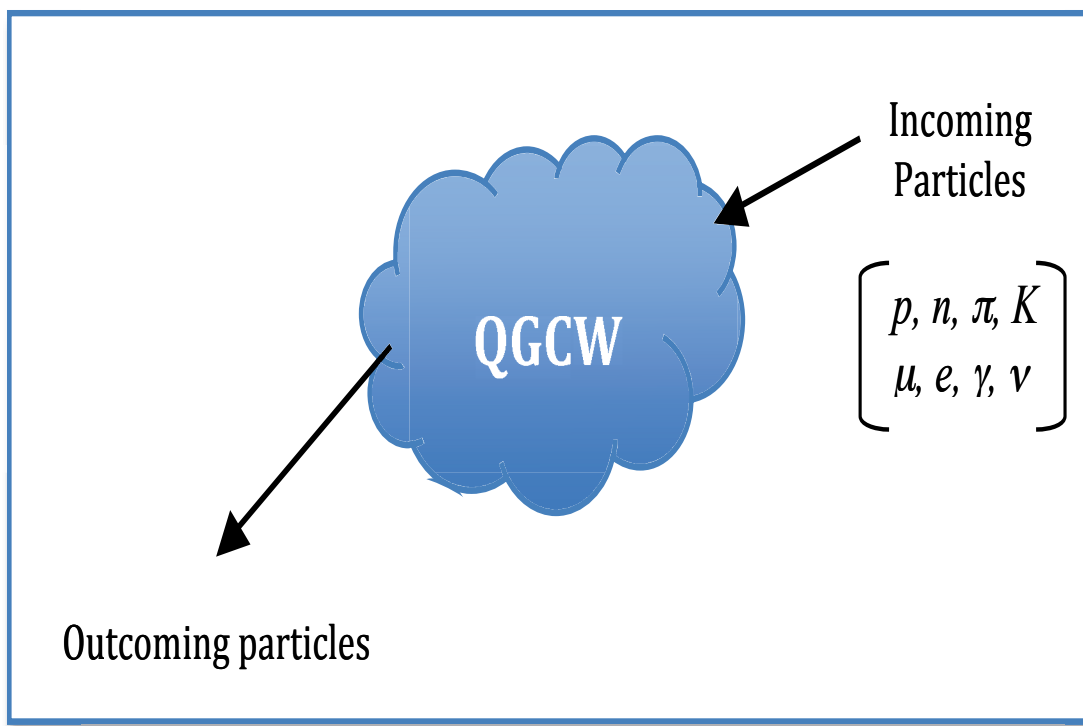


Figure 4: Schematic illustration of the way how to probe the QGCW

Advanced R&D has started all around Europe to prepare for the FAIR¹⁴⁾ project at GSI¹⁵⁾ and at CERN¹⁶⁾ for the LHC upgrade program, and this R&D allows to chose eventually the suitable technology for the preparation of future experiments to explore the entirely new world of states formed by free quarks in the QGCW.

Examples of R&D work proposed to prepare the future of the QGCW project:

The “Bunch-phase Timing System (BuTiS)” for FAIR concentrates on research of thermal stability properties of optical fibers¹⁷⁾, which are essential to carrying control and monitor signals between complex accelerator equipment.

Also in the LHC tunnel optical fibers are used for fast signal transmission through large distances to synchronize the accelerators, to take measurements of the beams, and to send controls to the LHC. “Over the past 7 years, CERN has developed special optical fibers that can resist the radiation levels of the LHC¹⁸⁾”.

Intensive R&D on the detector to obtain an improvement of timing for the Time of Flight system using the MRPC combined with the NINO readout electronics¹⁹⁾.

Beams to inject probing particles into the heavy ion collision experiment pit 2 at LHC have to be studied in parallel with the LHC upgrade program. Included in this are the development of superconducting magnets for LHC and for FAIR²⁰⁾.

In the past, focused R&D for specific experiments was performed in well defined laboratories, e.g.: for the UA, LEP and LHC experiments at CERN, for PETRA experiments at DESY, and for the future of FAIR experiments at GSI. This R&D works was in general reviewed by teams in the host laboratories. The LAA project belongs to this category of R&D programs.

Today, accelerator and detector development projects are often organized in large world-wide collaborations and funded by the EU Framework programs. This creates overheads and inefficiencies but also competition and challenges.

The QGCW project is ambitious but meets a lot of interest. “We do not know what will be the final outcome of all theoretical ideas intended to make predictions and of possible experiments to probe nature. What we know is that the world appears to be complex at every scale. Therefore we must expect a series of surprises that cannot be predicted.” (A. Zichichi, 2008). With this statement by A. Zichichi during his ERICE lectures in our minds, we are continuing to follow attentively the current efforts to find innovative ideas and develop technologies allowing to design such a challenging experiments for LHC in the future – which was and is still the spirit of the LAA project.

Acknowledgements

It is a pleasure to thank Professor Antonino Zichichi and the organizers of the Colloquium for having permitted me to present the LAA project achievements.

References

- 1) CERN Council document (December 1986), *Resolution on the LAA programme of Activities*. CERN/1642.
- 2) A. Zichichi Chairman, ECFA – LEP Working Group Progress Report (1979) *ECFA European Committee for Future Accelerators*, ECFA /79/39.
- 3) CERN Internal Reports (1988-1989), *LAA Progress Report*, CERN/EF 89-14 & CERN/ LAA/SD 89-1.
CERN Internal Report (1991), *The achievements of LAA* , CERN/ LAA/ 91-1
- 4) Wiik B., Wagner A., Wenninger H . (2002) In honour of Antonino Zichichi, “From the Preschower to the New Technologies for Supercolliders” *World Scientific Series in 20th Century Physics*, Vol 31.

- 5) Heijne, E.H.M. (2008), Gigasensors for an Attoscope: Catching Quanta in CMOS, *IEEE Solid-State Circuits society news*, Fall 2008, Vol.13, N0.4 500
- 6) Pierre Jarron, AMPLEX chip 1986 – 1988, *private communication*, Erik Heijne
- 7) Anghinolfi F., Jarron P., Martemiyarov, A.N., Usenko E., Wenninger H., Williams Zichichi A., M.C.S., (2004) NINO: an ultra-fast and low-power front-end amplifier /discriminator ASIC designed for the multigap resistive plate chamber, *Nucl. Instrum. Methods Phys. Rev. A* 533, 183-187
- 8) Zichichi A. Subnuclear Physics The First 50 Years : Highlight from Erice to ELN Edited by O. Barbabeï, P. Pupillo & F. Roversi Monaco, *World Scientific Series in 20th Century Physics* – Vol. 24
- 9) CERN Detector R&D Committee (DRDC), Retrieved October 2011, from web CERN <http://committees.web.cern.ch/Committees/DRDC/Projects.html>
- 10) Williams, M.C.S., (2011) Development of High Time Resolution Multi-gap RPCs for the TOF Detector of AILCE, *Proceedings of the 7th International Conference on Advanced Technology*, page 563
- 11) Zichichi, A., CENTRO FERMI, *The EEE Extreme Energy Events*, Retrieved October 2011, from <http://www.centrofermi.it/eee.html>
- 12) Zichichi A., (2006) Erice: *International School of Subnuclear Physics (ISSP 6)* Retrieved 2011, from <http://www.ccsem.infn.it/issp2006/index.html>
- 13) Zichichi, A., (2010) Murray Gell-Mann and the Last Frontier of LHC Physics: The QGCW Project Proceedings of the Conference in honour of Murray Gell-Mann's 80th Birthday, *Quantum Mechanics, Elementary Particles, Quantum Cosmology & Complexity*, Nanyang Technological University, Singapore, 24–26 February 2010, World Scientific books
- 14) FAIR (Facility for Antiproton and Ion Research) at GSI Darmstadt, Germany, Retrieved from <http://www.fair-center.de/index.php?id=1&L=1>
- 15) GSI (Helmholtzzentrum für Schwerionenforschung) Darmstadt, Germany Retrieved from <http://www.gsi.de/portrait/index.html>
- 16) CERN (European Organization for Nuclear Research) , Geneva, Switzerland Retrieved from <http://public.web.cern.ch/public/>
- 17) D.Beck, Campus-Wide Time Synchronization System-„BuTiS“, 2011 Retrieved from <https://www-acc.gsi.de/wiki/Timing/TimingSystemButisInterface>
- 18) TIPP 2011, *2nd International Conference on Technology and Instrumentation in Particle Physics* Retrieved 2011 from <http://conferences.fnal.gov/tipp11/>
- 19) Report and talk by Crispin Williams at this conference “ *Improve MPRC* “ Retrieved 2011 from crispin.williams@cern.ch - Indico - CERN
- 20) Joint sc magnet R&D EU project and Pulsed Magnets with Curved Shape Fabbriatore et al. INFN Genova, Lucio Rossi / CERN, *private communication* Retrieved 2011 from <http://eucard.web.cern.ch/eucard/index.html>

LATTICE FIELDS IN THE LHC ERA

■ RICHARD KENWAY

*School of Physics & Astronomy
The University of Edinburgh
Edinburgh, UK*

Lattice QCD

Lattice field theory was invented by Wilson (1974) to try to explain how the strong force, described by Quantum Chromodynamics (QCD), binds quarks permanently into the observed hadrons. He replaced space-time by a regular four-dimensional lattice with quark fields at the sites and gluon fields on the links between neighbouring sites, retaining the local gauge invariance of the theory at the sites. This controls the infinities of the quantum field theory by defining it as the zero-lattice-spacing, or “continuum”, limit of the lattice theory. The number of degrees of freedom is proportional to the number of sites and hence is finite on a finite-volume lattice, permitting physical quantities to be computed within a fully controlled approximation, if the volume is large enough. QCD is “asymptotically free” – its beta function is negative and has a fixed point at zero gauge coupling the existence of which can be established using perturbation theory, and, because of this, tuning the gauge coupling to zero reduces the lattice spacing to zero relative to any physical scale, such as the size of a hadron. Thus, dimensionless ratios of physical quantities become insensitive to the lattice spacing and equal to their continuum values in this limit. Of course, the volume of the lattice must be kept larger than any of the important physical scales as this limit is taken, which means that the number of lattice sites and the computational cost grow, actually very rapidly. There are many ways of formulating lattice QCD so that the correct continuum theory is recovered. It is sufficient to ensure that the lattice theory either retains QCD’s essential symmetries (e.g. gauge invariance), or breaks them in ways that vanish in the continuum limit (e.g. Lorentz invariance). Lattice QCD is now so well underpinned theoretically that it is widely accepted as the best way to define QCD.

Lattice QCD explains the confinement of quarks inside hadrons when the gauge coupling (and hence the lattice spacing) is large, because the potential energy of a static quark-antiquark pair grows linearly with their separation. It has not yet been established that this property remains true in the continuum limit. However, lattice QCD did not become a viable tool for computing the properties of hadrons until Creutz, Jacobs and Rebbi (1979) realised that the path integral in Euclidean space-time could be estimated by computer simulation using Monte Carlo methods. It has taken over 30 years of effort developing the theory, algorithms and computer technology to reach the point today where we can compute the values of many hadron masses and matrix elements for continuum QCD to a precision of a few percent and start to confront experimental measurements. For most practical purposes, QCD can now be solved from first principles, although the computations are enormously demanding and many are still too expensive. This will change as computer performance continues to increase exponentially for problems of this type. The lattice approach can be applied to other quantum field theories and there has been a surge of interest in applying it to possible models of electroweak symmetry breaking in anticipation of discoveries at the LHC. All that is needed is an understanding of how to realise the symmetries of the continuum theory correctly and a fixed point at which to define the continuum limit. However, neither is guaranteed to be easy for any particular theory.

The Origin of Mass

Asymptotic freedom of QCD enables us to use perturbation theory to determine how physical quantities, such as hadron masses, depend on the lattice spacing when this is small (because then the coupling is also small). All quantities with dimensions can be expressed as a computable number times the appropriate power of a fixed energy scale, Λ_{QCD} , which is related to the inverse of the lattice spacing (the “cut-off”) by a factor that becomes exponentially small at small coupling. If we imagine QCD to be embedded in a more complete theory, so that new physics enters when the lattice spacing reaches a small enough value, the energy scale of this new physics can be much larger than Λ_{QCD} and, consequently, the masses of hadrons. Thus, asymptotic freedom explains why hadrons can be “light” compared, say, to the Planck mass.

Computer simulation of lattice QCD may be used to compute the numbers that relate physical quantities to Λ_{QCD} , or, equivalently, dimensionless ratios of physical quantities. The first such calculation of the nucleon mass by Hamber and Parisi (1981) obtained 950 ± 100 MeV. This illustrates the challenge for the field – to decide whether QCD is correct requires reducing the uncertainties in such calculations to something comparable to the experimental uncertainty. Hamber and Parisi did not correctly include the effects of virtual quark loops (or “sea quarks”), but it was not until 1998 that CP-PACS announced at the annual Lattice Conference that this gives the wrong result for the nucleon mass and other light hadron masses (Aoki et al., 2000). Ten years later, the light hadron spectrum computed in 2+1 flavour QCD (i.e., including all the effects of u , d and s quarks, with u and d assumed to be degenerate in mass so that isospin is an exact symmetry) was shown to agree with experiment to within a few percent (Dürr et al., 2008). The inputs to this computation are the observed masses of the (isospin averaged) pion, kaon and Ξ baryon, used to fix the average u and d mass, the s mass and the scale – the quark masses in the simulation are varied until the computed ratios of the pion to Ξ baryon masses and the kaon to Ξ baryon masses match experiment. In this way, the quark masses are determined.

Since the masses of the u and d quarks turn out to be only a few MeV, roughly 99% of all the visible mass in the Universe is, therefore, explained as the binding energy of QCD. It remains for us to understand the origin of the masses of the quarks, leptons, electroweak gauge bosons and, presumably, the Higgs. Lattice QCD enables precision determination of the quark masses, which is an important first step towards understanding their origin. Today’s QCD simulations typically include u , d , s and c quarks in the isospin-symmetric limit for the sea quarks. Isospin breaking and QED effects are included for the valence quarks to account, at least approximately, for the mass difference of the neutron and proton. The current world averages for the light quark masses obtained this way are (Laiho et al., 2010)

$$m_u = 2.09 \pm 0.09 \text{ MeV}, \quad m_d = 4.73 \pm 0.11 \text{ MeV}, \quad m_s = 93.6 \pm 1.1 \text{ MeV}.$$

The result for the u quark rules out the possibility that it is massless and, consequently, that this could be an explanation for the “strong CP problem”. Evidently, lattice QCD has not only established that QCD is a good description of hadrons at low energies, but also that it can be used to determine precisely otherwise inaccessible parameters of the Standard Model.

The Search for Physics Beyond the Standard Model

In the absence of the discovery of new particles, the search for new physics is proceeding through tests of the Standard Model. Lattice QCD is starting to provide a tool of sufficient precision to confront predictions of the Standard Model with experiment and to seek discrepancies. The focus of

this search is flavour physics, because the existence of only three generations of quarks and leptons, inherent in the Standard Model, imposes a constraint on the parameters which specify the strengths of the mixings between different quark flavours. Like the quark masses, these parameters, or “CKM matrix elements”, are inputs to the Standard Model, presumably originating in some more fundamental underlying theory, and they must be inferred from experimental measurements. If there are only three generations, the 3×3 CKM mixing matrix must be unitary – a statement that the probabilities of all possible mixings of a given flavour must add up to one and a set of “unitarity triangle” constraints. It is possible that new physics violates these constraints and this can be observed if we can determine the mixing parameters precisely enough. Also, like the quark masses, since the quark mixings can only be observed in hadronic processes, QCD effects must be computed to extract the mixing parameters from experimental measurements. The strength of these tests of the Standard Model then depends on our ability to reduce the uncertainties of both the computations and the experiments. Until recently, the computational uncertainties dominated. As the precision of lattice QCD calculations of hadronic matrix elements steadily improves, this situation is changing.

Our most stringent test of CKM unitarity is for the mixing of the u quark with d , s and b quarks. The mixing with the b quark is so tiny that it can be ignored. The other two mixing parameters can be determined from kaon semileptonic decays (using the computed form factor at zero momentum transfer), and kaon and pion leptonic decays (using the computed ratio of the decay constants), where there are reliable lattice QCD computations of the hadronic decay matrix elements from both 2 flavour (degenerate u and d quarks only in the sea) and 2+1 flavour (u , d and s quarks) simulations. The former have larger systematic uncertainties, but both give values for the mixing parameters that satisfy the unitarity constraint (at the level of 4% and 2% respectively). Taking the ud mixing from the more precisely measured nuclear beta decay confirms CKM unitarity at the per mille level (Colangelo et al., 2011).

The progress achieved over the past 20 years in lattice QCD computations of hadronic weak matrix elements is nicely illustrated by B_K , the matrix element needed to extract the size of CP violation in the Standard Model from measurements of neutral kaon mixing (Lunghi & Soni 2011). A crucial feature of CKM mixing in the Standard Model is that CP violation is determined by a single parameter. Thus, the same value should be obtained from kaon and from B meson decays. The construction of the two B -Factories in the 1990s was motivated in large part by this test of the Standard Model. So the beautiful experimental measurements of B mixing to an accuracy of a few percent that were achieved could only impact the underlying theory if B_K could be computed to a similar precision. Early lattice QCD results in the 1990s using the quenched approximation (no sea quarks) were comparable to those using non-lattice methods, obtaining values for the (renormalisation group invariant) matrix element around 0.70 ± 0.10 , but with no control over the systematic error. In the last five years, simulations with 2+1 flavours have achieved remarkable consistency in the central value and a steady reduction in the uncertainty, so that the current world average is 0.74 ± 0.02 .

Using the most reliable lattice QCD results available today (specifically, excluding results for the cb and ub mixing parameters obtained from inclusive and exclusive semileptonic b decays, because they differ by around 2σ), the unitarity triangle, whose area is proportional to the size of CP violation, exposes a 3σ tension in the CKM matrix. If this is due to new physics, then it seems predominantly to affect B mixing (Laiho et al., 2010, Lunghi & Soni 2011).

The central role that lattice QCD is now playing in the search for new physics is due to the 30 years of effort understanding the theoretical formulation, improving the algorithms and speeding up computer performance finally paying off. So we now have full control over all sources of uncertainty for some

phenomenologically important matrix elements and consistent results for them from different lattice formulations providing an independent check. We can expect the range of computable matrix elements to grow and the uncertainties in the results to reduce as the methodology and computer performance continue to improve.

Thermodynamics and the Quark-Gluon Plasma

Lattice field theory provides a theoretical laboratory in which we can explore the properties of QCD with different choices for its quark content. This has been exploited in the historical development by starting with a model in which only valence quarks are present (the “quenched approximation”), which substantially reduces the computational cost. Subsequently, at growing cost and edging ever closer to the Standard Model, two degenerate quark flavours were included in the sea, then 2+1 flavours (the 2 referring to degenerate u and d quarks), until today most simulations include 2+1+1 flavours of sea quark with isospin breaking effects incorporated in the valence quarks. These simulations may be performed at zero or non-zero temperature, enabling us to map out the phase diagrams. Unfortunately, the Monte Carlo algorithm fails at non-zero baryon chemical potential, so this region of the phase diagram is not accessible (yet) to direct simulation.

The phase structure is sensitive to the sea-quark content, although we have had to learn this the hard way. The temperature of the transition from the confining to the quark-gluon plasma phase turns out to be close to m_s , so it is essential to include the s quark in the sea, requiring at least 2+1 flavour simulations. (In fact, there is not a sharp transition, but rather a smooth cross-over between the two phases.) This is one reason why QCD thermodynamics has proved to be a harder problem than the computation of the zero-temperature spectrum and matrix elements (another is that zero-temperature results are needed as input to set the scale and quark masses). Furthermore, most non-zero temperature studies have used the staggered-quark formulation, which has additional copies of the quark flavours in the sea, called “tastes”, that decouple only in the continuum limit. The effects of tastes at non-zero lattice spacing can be reduced by modifying the staggered-quark action. After some initial discrepancies, results for the transition temperature and other properties derivable from the equation of state, such as the speed of sound and the pressure, obtained with different formulations are now converging. A typical result for the transition temperature is $T_c = 154 \pm 9$ MeV (Bazavov et al., 2012).

The goal of lattice QCD thermodynamics is to obtain a precise determination of the equation of state of QCD over the temperature range of 150 – 700 MeV that is being explored by experiments at RHIC and the LHC. Along with the determination of the transition temperature and transport coefficients, this will enable us to parametrise hydrodynamical models describing the quark-gluon plasma. The inclusion of the c quark in simulations is likely to be necessary at high temperatures, and these can be expected to follow close behind the zero-temperature 2+1+1 flavour simulations currently underway.

Dynamical Electroweak Symmetry Breaking

While the idea that electroweak symmetry is broken by the condensation of techniquarks, which feel a new technicolor gauge interaction, simply replicates what already happens to a limited extent in QCD, extending this to give masses to the quarks runs into trouble – the scale of the technicolor theory, Λ_{TC} , is either too big to generate the heavy-quark masses, or too small that it generates flavour-changing neutral current (FCNC) interactions in contradiction with experiment. A popular solution is to seek a technicolor gauge theory whose dynamics is different from QCD, being governed by a beta function that has an infrared stable (i.e. “conformal”) fixed point at non-zero gauge coupling. A suitable choice

of techniquark content and masses should destabilise this fixed point so that, between two scales, the gauge coupling is trapped close to the fixed-point value and stops running, a property called “walking”, before eventually running down to zero as in QCD. This dynamics introduces two scales: a high scale which generates acceptably small FCNCs and a low scale that generates big enough quark masses.

Lattice field theory is the only first-principles method available to search for fixed points at non-zero coupling. The challenge is that the set of possible technicolor theories is huge and, for each gauge group, there are many choices for the techniquark content (a classification of theories based on an approximate beta function provides a guide, see Sanino 2009). Simulating each specific choice is computationally demanding even with the most powerful algorithms developed for QCD. So work has so far concentrated on the simplest gauge groups, SU(2) and SU(3), for which efficient simulation codes already exist, and has varied the fermion content looking for a zero of the beta function. Since staggered fermions provide efficient implementations of theories with multiples of four flavours in the fundamental representation, the most systematic studies have been carried out for 8, 12 and 16 fundamental flavours with an SU(3) gauge group. This has established that the 16-flavour theory has a conformal fixed point, the 8-flavour theory does not, while the 12-flavour theory remains controversial, with the balance in favour of a conformal fixed point (Hasenfratz, 2010 and 2012).

Thus, these simulations are providing some encouragement for “walking” technicolor to be a viable theory of dynamical electroweak symmetry breaking. Of course, there is not a shred of experimental evidence yet that Nature exploits this possibility. If we are to explain electroweak symmetry breaking through some underlying strong dynamics, computer simulation of lattice field theory is likely to be the only technique available to us, both to construct the theory and to extract predictions that can be used to confront experiment. The computational cost of doing this will far exceed that which has been required for QCD, because we will not have asymptotic freedom and perturbation theory to guide our approach to the continuum limit.

Computers for Lattice Field Theory

The progress achieved in lattice QCD is generally ascribed equally to advances in algorithms and in computer technology. While the former is hard to plan for in the future, technological advances are expected to continue for the next ten years at the exponential “Moore’s Law” rate that we have benefited from for the past 50 years. Throughout its history, lattice QCD, more than any other application area, has driven the development of the most powerful supercomputers. This is because the translational symmetry and local interactions of the lattice theory make the simulations very efficient to implement on parallel computers. Also the balance between computations and memory accesses in lattice QCD turns out to be a good design target for machines to support a wide range of scientific applications. Thus, we have seen computers designed and built specifically for lattice QCD, design elements from them incorporated into commercial machines, and lattice QCD codes used to optimise performance of and to stress-test commercial systems.

This concept of “co-design”, in which the computer architecture, its system software, the algorithm and application software are all developed together, has been adopted as the plan for the next big step in supercomputer performance from the current petascale to exascale (10^{18} operations per second). This is expected to be accomplished around 2018, by scaling up today’s machines with hundreds of thousands of computational units operating in parallel, to systems with hundreds of millions, even billions. Memory access rates will be unable to keep pace and energy requirements will have to be driven down dramatically to keep operating costs at an acceptable level. This will be a huge

engineering challenge and, even for lattice QCD, it will not be straightforward to exploit exascale systems efficiently. The key point, though, is that computer performance should not present a limitation on lattice field theory, at least for the first decade of the LHC.

Prospects for the LHC Era

After 30 years of sustained effort to develop the theoretical formulation, speed up algorithms and build faster computers, lattice QCD has reached the point where it is delivering high-precision, model-independent results for a growing range of phenomenologically important quantities, in which all sources of uncertainty are under control and can be systematically reduced further. In flavour physics tests of the Standard Model, a combination of efforts to drive down both theoretical and experimental uncertainties is putting the Standard Model under increased stress and has already exposed a 3σ tension in the B meson sector. Independent of the discovery of new particles at the LHC, this work will tighten the constraints on Standard Model processes and will very likely expose areas where new physics is necessary.

Lattice simulations of QCD thermodynamics are reaching a similar point of sophistication, where the lattice approximations are fully under control. This should permit reliable determinations of a wide range of thermodynamic and transport properties of the quark-gluon plasma phase that will guide our interpretation of heavy-ion experiments. A major theoretical challenge remains to find a way to simulate QCD at non-zero baryon density to explore the properties of cold dense nuclear matter.

Beyond QCD, lattice field theory offers the only known way to understand strong dynamics which is not controlled by a perturbatively accessible fixed point and yet may explain electroweak symmetry breaking. Computationally, this will require a major step up in our capabilities, because we will not have perturbation theory to provide a guide. Fortunately, there is no end in sight to the exponential growth of computer power. With the full discovery potential of the LHC also yet to be realised, the only limit to our understanding further how Nature works at the most fundamental level will be our own ingenuity.

References

- Aoki, S., Boyd, G., Burkhalter, R., Ejiri, S., Fukugita, M., Hashimoto, S., Iwasaki, Y., Kanaya, K., Kaneko, T., Kuramashi, Y., Nagai, K., Okawa, M., Shanahan, H.P., Ukawa, A., & Yoshié, T. (2000). Quenched Light Hadron Spectrum. *Physical Review Letters* 84, 238-241.
- Bazavov, A., Bhattacharya, T., Cheng, M., DeTar, C., Ding, H.-T., Gottlieb, S., Gupta, R., Hegde, P., Heller, U. M., Karsch, F., Laermann, E., Levkova, L., Mukherjee, S., Petreczky, P., Schmidt, C., Soltz, R. A., Soeldner, W., Sugar, R., Toussaint, D., Unger, W., & Vranas, P. (2012). The chiral and deconfinement aspects of the QCD transition. *Physical Review D* 85, 054503.
- Colangelo, G., Dürr, S., Jüttner, A., Lellouch, L., Leutwyler, H., Lubicz, V., Necco, S., Sachrajda, C.T., Simula, S., Vladikas, A., Wenger, U., & Wittig, H. (2011). Review of lattice results concerning low-energy particle physics. *The European Physical Journal C* 71, 1695.
- Creutz, M., Jacobs, L., & Rebbi, C. (1979). Experiments with a gauge-invariant Ising system. *Physical Review Letters* 42, 1390-1393.
- Dürr, S., Fodor, Z., Frison, J., Hoelbling, C., Hoffmann, R., Katz, S. D., Krieg, S., Kurth, T., Lellouch, L., Lippert, T., Szabo, K. K., & Vulvert, G. (2008). Ab Initio Determination of Light Hadron Masses. *Science* 322, 1224-1227.
- Hamber, H., & Parisi, G. (1981). Numerical estimates of hadronic masses in a pure SU(3) gauge theory. *Physical Review Letters* 47, 1792-1795.
- Hasenfratz, A. (2010). Conformal or walking? Monte Carlo renormalization group studies of SU(3) gauge models with fundamental fermions. *Physical Review D* 82, 014506.
- Hasenfratz, A., (2012). Infrared fixed point of the 12-fermion SU(3) gauge model based on 2-lattice MCRG matching. *Physical Review Letters* 108, 061601.
- Laiho, J., Van de Water, R. S., & Lunghi, E. (2010). Lattice QCD inputs to the CKM unitarity triangle analysis. *Physical Review D* 81, 034503 and <http://www.latticeaverages.org>.
- Lunghi, E., & Soni, A. (2011). Demise of CKM & its aftermath. arXiv:1104.2117v3 [hep-ph].
- Sannino, F. (2009). Conformal Dynamics for TeV Physics and Cosmology. *Acta Physica Polonica B* 40, 3533-3743.
- Wilson, K. G., (1974). Confinement of quarks. *Physical Review D* 10, 2445-2459.

THE LARGE HADRON COLLIDER OF CERN AND THE ROADMAP TOWARD HIGHER PERFORMANCE

■ LUCIO ROSSI

CERN, Technology Department

Abstract: The Large Hadron Collider is exploring the new frontier of particle physics. It is the largest and most ambitious scientific instrument ever built and 100 years after the Rutherford experiment it continues that tradition of “smashing atoms” to unveil the secret of the infinitely small. LHC makes use of all what we learnt in 40 years of hadron colliders, in particular of ISR and Sp-pbarS at CERN and Tevatron at Fermilab, and it is based on Superconductivity, discovered also 100 years ago. Designing, developing the technology, building and finally commissioning the LHC took more than twenty years. While LHC is now successfully running, we are already preparing the future for the next step. First, by increasing of a factor five the LHC luminosity in ten years from now, and then by increasing its energy by a factor two or more, on the horizon of the next twenty years. These LHC upgrades, in luminosity and energy, will be the super-exploitation of the CERN infrastructure and is the best investment that the HEP community can make in order to extend the boundary of our knowledge at an affordable cost.

1- Introduction: Centennial of Superconductivity and Accelerators

On April 8 of 1911, K. H. Onnes and co-workers first observed the disappearance of electrical resistivity, in a sample of highly purified mercury. Onnes achieved this result because he was a great instrument maker: the first ten year after he took the chair of experimental Physics in Leiden he did not produce a single paper, concentrating his energy and will in founding and developing a school for the education and training of young technicians, and in developing the instrument for one of the most exciting adventures of physics at the end of XIX century: the race toward absolute zero temperature. Onnes specialized in gas refrigeration and in using it to test a key theory, the electrical conduction in metal. He first liquefied Oxygen (90 K) in 1894, lost to Dewar the race for Hydrogen liquefaction (20 K) but then won the most difficult one when he first liquefied helium at 4.2 K in 1908. This allowed him to carry out new fundamental experiments on electrical conduction. In 1911 he not only observed the “resistance almost nul” (Kes, 2011) but – thanks to the unique skills of the team he formed with patient work over many years – he was able to repeat the experiment three times that same year. Eventually, after having collected enough statistics he was able to state that what was happening was not what he expected: resistance was not going to zero smoothly when temperature was approaching zero; rather it passes through a sharp transition into a new phase that he called later superconductivity.

Onnes talked openly of a possibility to realize ten tesla magnets, only to be deceived soon after when he discovered that superconductivity was destroyed by small field of less than 50 mT. It was only in the 1970s, when the availability of modern alloyed superconductors like Nb-Ti made type II multifilamentary wires possible, that the race toward high fields really started. From then on the

destiny of the accelerator was signed (Wilson, 1999): SuperConductivity (SC) became the choice of preference for accelerators, as illustrated in Figure 1.

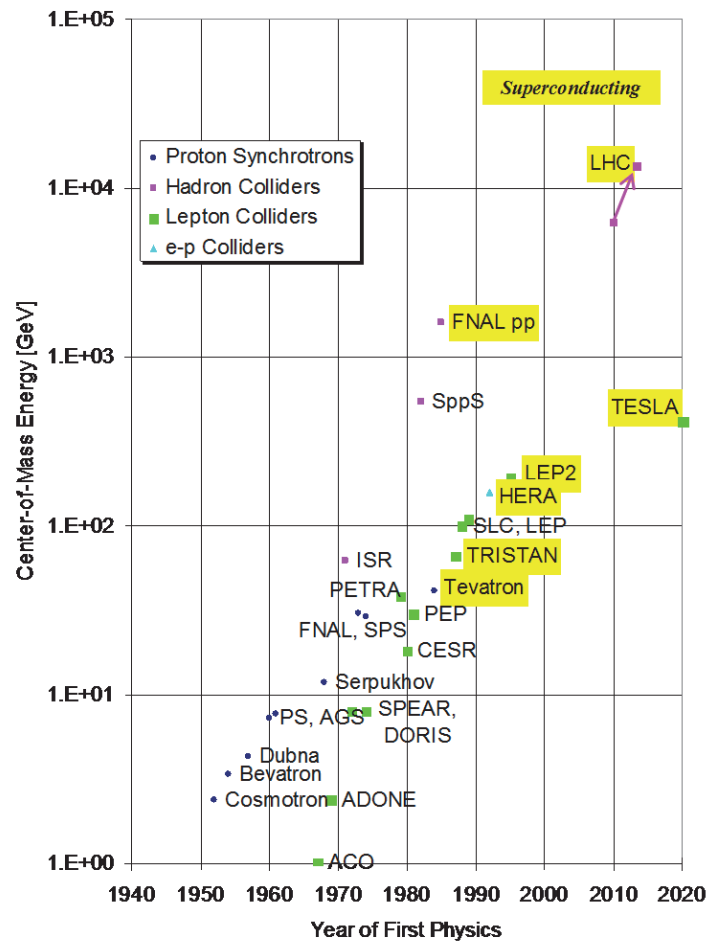


Figure 1. Evolution of accelerators with those making use of superconductivity highlighted in yellow

2- The advance of superconducting hadron accelerators and LHC early R&D

2.1 Early times and Tevatron

Hadron colliders have been at the forefront of Physics since the ISR in the 1970s. They can provide very intense beam and luminosity at the highest energy. When superconductivity was emerging in the seventies a project, called Isabelle and later CBa (Colliding Beam Accelerator) was developing SC magnets for a 2x200 TeV proton collider. Some delays and then the attempt to increase SC magnet field to 5 T troubled the project in the critical moment. Meanwhile in 1982 Rubbia et al. discovered the field particles W and Z at the CERN SPS, transformed for the purpose into a p-pbar collider. These factors contributed to the stop of Isabelle, favouring the start of the SSC project design. Meanwhile the construction of the Fermilab Tevatron, a machine to be installed in the tunnel of the Main Ring and meant to double its energy to 1 TeV/beam by means of 4.5 T superconducting magnets (Tollenstrup, 1979), was progressing with full steam. Much like the CERN p-pbar collider, the Tevatron was able to accommodate two counter-circulating beams of protons and antiprotons in

the same vacuum pipe, providing collisions at 2 TeV center-of-mass energy (Edwards, 1985). The Tevatron, inaugurated in 1983 at reduced energy, was made possible by the vision of Fermilab founder and director Robert R. Wilson, who stubbornly fought for it (eventually at the price of an early retirement as the condition to move on with the project), offering the first large application of superconductivity. This in turn kept Fermilab primacy of the energy frontier for more than 25 years.

2.2 HERA

The success of Tevatron, which was the first superconducting accelerator and the first very large superconducting system, paved the ground for a similar project in Europe, HERA, and for the “superproject”: SSC, the Superconducting SuperCollider in the USA. HERA, more or less the size of Tevatron, had the goal to collide a 0.8 TeV proton beam against a 30 GeV electron beam. The main contribution of HERA dipoles to the technology advancement was the use of a cold iron yoke (Wolff, 1988) while Tevatron magnets had a warm iron yoke. Tevatron made the choice of warm iron in order to minimize the time of warm-up and cool-down, and then the dead time for physics. However, following the good operation experience of Tevatron and HERA, all projects after 1985 were designed with cold iron, which make much easier force containment and alignment. HERA dipoles also employed aluminium collars, rather than stainless steel like the Tevatron dipole, to benefit from the larger thermal contraction of aluminium during cooling. HERA came into operation at 4.7 T in 1989, eventually reaching 5.5 T for 0.92 TeV proton beam energy about ten years later.

2.3 SSC

In the meantime a large R&D effort was going on in the USA for SSC. Based on 6.6 tesla magnets, SSC was constituted of two independent rings in a tunnel with a circumference of 87 km length, sited in Texas. For a decade, up to its cancellation by Congress on 21 October 1993, SSC was the cradle of main developments of SC technology for accelerators. The critical current density of Nb-Ti was raised to more than 3000 A/mm² at 5 T and 4.2 K, while the size of the Nb-Ti filaments was reduced to 5-6 μ m to limit magnetization effects; Nb-Ti ingots were produced with high homogeneity and clad by a 4-6% Nb sheath, to prevent formation of brittle intermetallic compounds and improve performance and yield. Superconducting cable technology and QA made great progress. Studies of the magnet field quality were pursued systematically as well as new insulation technologies. New magnet designs were worked out: Two-in-One design (to host the two rings in one magnet), superferric magnets (for low cost and longer accelerators), partitioning the coils into different electrical circuits; all these new ideas came during these times. However, the project overall made slow progress, given the resources and the enormous intellectual effort. The management also under-evaluated LHC progress: despite use of a circumference three times smaller than that of SSC (CERN was bound to use the ring excavated to host the LEP machine), LHC was promising to reach the same physics performance, thanks to higher field magnets – which could partially compensate for the smaller ring – and to higher luminosity (LHC Study Group, 1991). LHC also profited from the great advances made for the SSC and made some winning choices. For example, the Two-in-One design, proposed for SSC but never accepted by the management, was picked up by LHC and brought to perfection with the LHC Twin Dipole (Perin, 1991). In Figure 2 the cross sections of the dipole magnets for the principal hadron colliders are shown.



accelerator magnets normally work at 80%, or less, of the short-sample value. The results of the 1-m LHC models also made it clear that the cable's mechanical and electrical characteristics and the field quality of the magnet, both during ramp and at the flat top, were not far from the quality required for the LHC. The final step of the R&D toward LHC was to manufacture 10 m long magnets of the twin design to demonstrate that full-size, LHC dipoles of the final design were feasible.

In 1988 and 1989, in the wake of a long term effort on superconducting technology for accelerator launched by Prof. Zichichi at beginning of the '80s, the Italian INFN signed a collaboration with CERN for a special contribution to LHC R&D. INFN then launched the design and manufacture of LHC-type superconducting cables for long magnets (Acerbi et al., 1992) and in 1989 ordered two 10 m long twin dipoles from Ansaldo Componenti (Italy). INFN followed this job through LASA, a new lab devoted to applied superconductivity for accelerators, a further heritage of the superconductor development program of INFN President Zichichi. The development of the superconductors was pursued in LASA first by means of a National project (a Cyclotron built in Milan and later installed at INFN-LNS of Catania) and then through a strong participation to the HERA project (about 240 superconducting dipoles for the accelerator and the large thin superconducting solenoid of ZEUS detector). The LASA laboratory became one of the main collaborating institutes of CERN for the LHC project. Parallel to the INFN effort, the French CEA-Saclay Laboratory, DAPNIA department, took over the design and construction of the first two full-size superconducting quadrupoles for the LHC. The engagement of CEA-Saclay on the LHC quadrupoles continued throughout the duration of the project, as a special French contribution to LHC construction.

In 1993 the LHC project had to pass through a tough review devoted to the cryo-magnet system, led by Robert Aymar, who as CERN's director-general 10 years later would harvest the fruit of the review. With the review over and completion of the long magnet prototypes approaching, the credibility of the LHC project increased. In autumn 1993, the SSC came to a halt - certainly because of high and increasing cost (more than \$12 billion) and the low economic cycle in America, but also because the LHC now seemed a credible alternative to reach similar goals at a much lower cost (\$2 billion in CERN accounting). Rubbia, near the end of his mandate as director-general, led the project without rival. In a symbolic coincidence, the demise of the SSC occurred at the same time as leadership of the LHC project passed from Giorgio Brianti, who had led the project firmly from its birth through the years of uncertainty, to Lyn Evans, who was to be in charge until completion 15 years later. The end of the SSC and the green light for the LHC was marked by the delivery to CERN of the first INFN dipole magnet in December 1993, just in time to be shown to the Council. This was followed four months later by the second INFN magnet and then by the CERN magnets as well as by the two quadrupoles designed and built by CEA.

Returning to the first dipole, see Figure 3, it was tested in time for a very special April session of the Council in 1994. The magnet passed with flying colours, going above the operational field of 8.4 T at the first quench, beyond 9 T in two quenches, and a first quench above 9 T after a thermal cycle i.e. full memory. The excellent performance was actually misleading, giving the idea that the construction of LHC might be easy. In fact it took a long period of six years before another magnet as good as that one was again on the CERN test bench. However, the other 10 m long magnets performed reasonably well and with the two excellent CEA quadrupoles (3.5 m long), CERN was able to set up the first LHC magnet string, to test it thoroughly and finally receive the first official

approval of the project in December 1994, still with a missing magnet scheme to be amended at end of 1996 when USA and Japan special contributions were secured.

Many other formidable challenges were still to be resolved both on the technical side and on the managerial and financial side. The technical issues included the non-uniformity of quench results and the problem of retraining that plagued the second generation of LHC prototypes, the unresolved question of the inter-strand resistance, the change of aluminium for austenitic steel as the material for the collars and the lengthening of the magnets from 10 m to 15 m with the consequent curvature of the cold mass. Looking back at the decade 1985-1995 when the base for the LHC was established, it is clear that a big leap forward was accomplished during this period. The vision initiated by Robert Wilson for the Tevatron was brought to fruition, pushing the limit of Nb-Ti to its extreme on a very large scale. New superconducting cables, new superconducting magnet architectures and new cooling schemes were also put to the test, in the constant search for economic solutions that would be applicable later to large scale production.



Figure 3. First LHC dipole (collaboration CERN-INFN) on the test bench in April 1994.

3- Performance of LHC and ten year plan

From the early prototypes of 1995 to the end of hardware commissioning about 13 year passed, comprising long years of industrialization, construction and installation (Evans, 2007, Rossi, 2007, Evans and Bryant, 2008, Evans, 2009). LHC beam first circulated on 10th September 2008, only to be stopped nine days later by the very serious incident caused by a faulty magnet interconnection (Rossi, 2009). It took more than fourteen months to repair and recommissioning the accelerator. On 29th November 2009 beam was circulating again and quickly gained the record beam energy. From 30th March 2010 the machine is operating at 3.5 TeV/beam (half the design value) and at 50 ns bunch spacing.

The machine has since then performed remarkably well with a steady increase in luminosity at a pace that has been a rather good surprise (Lamont, 2011). The progress of luminosity so far is plotted in Fig. 4.

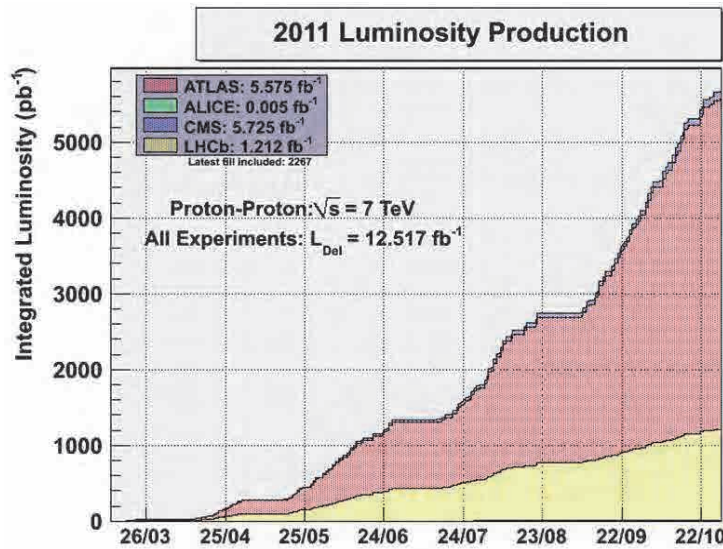


Figure 4. LHC integrated luminosity in 2011. For comparison in 2010 it was 50 pb^{-1} , i.e., 5 times less than the difference between ATLAS and CMS integrated luminosity in this graph.

The reasons for such a success are manifold and in general can be traced back to clever design, to careful construction and to unprecedented readiness in commissioning and operation. Some specific points are listed below:

- The magnetic machine is more stable and reproducible than expected. The field quality of the magnets is excellent and the aperture is considerably larger than anticipated.
- The head-on beam-beam limit is at least a factor 2 higher than anticipated. Actually a few runs at tune shift of $\Delta Q = 0.023$ have been performed with acceptable beam losses. The long-range beam-beam encounters, which are today limited by the 50 ns beam structure, well fits the simulations, giving hope that they can be controlled and limited for 25 ns spacing.
- For the 50 ns bunch spacing the emittance preservation in the injector chain and through LHC injection and acceleration is much better than anticipated. Furthermore, the single bunch population limit in the injector chain and namely in the SPS is higher than expected.
- With better than expected minimum beam lifetime, the present collimation system is capable to protect the beam up to nominal current and more: actually if the extrapolation of a recent experiment will be confirmed, the ultimate current (0.86A) can be fed into the ring without quenching the superconducting magnets.

The LHC long term plan, see Fig. 5, foresees a first Long Shutdown in 2013-14, LS1, mainly intended to consolidate the defective splices in between magnets. This long term plan ends with the project High Luminosity LHC (HL-LHC). A few equipment items requested for the HL-LHC project will be put in place in LS1, like installation of the Long Range beam-beam compensation wires and some civil

works in IP1 and IP5 and P7 related to SC links. A second Long Shutdown, LS2, which is today foreseen in 2018, will feature a number of equipment installations in the tunnel in view of the high luminosity, specifically addressing intensity limitations: 1) collimation in the cold arc coupled with novel technology 11 T twin dipoles; 2) installation of a new cryo-plant to decouple the SC magnet arc and IR from SCRF for sector 3-4, removing present low- β limitations on the left side of the CMS; 3) installation of LR b-b wires (and/or electron lenses) in all points; 4) SC links installation for removing some power converters from radiation sensible zones; 5) civil engineering work and infrastructure for the hardware to be installed in 2022; 6) installation of a crab cavity prototype to study its behaviour in LHC. These activities will be complemented by the interventions for upgrading the injectors: a) connection of Linac4 to the LHC chain; b) upgrade from 1.4 to 2 GeV of the PS Booster; c) removal of e-cloud limitations and 200 MHz RF upgrade in the SPS, etc. Finally, the third Long Shutdown LS3 in 2022-23 will be dedicated to the main hardware installation for the HL-LHC run.

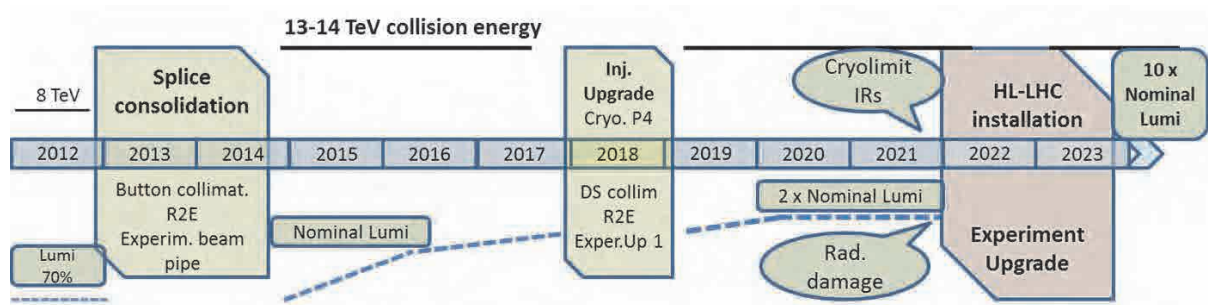


Figure 5. LHC plan for the next ten years, with the main interventions and increase of energy and luminosity indicated.

4- LHC luminosity upgrade

Based on the previous assumptions the integrated luminosity until LS3 is plotted in Fig. 6, where the region of radiation damage to triplet magnets is shown to be reached around 2021. In addition the time to half the statistical error on the physics data is also reported (halving time). Both main indicators for the timing of the upgrade, radiation damage and halving-time well above 10 years, call for the upgrade right after 2020, very consistent with the assumed timing of LS3.

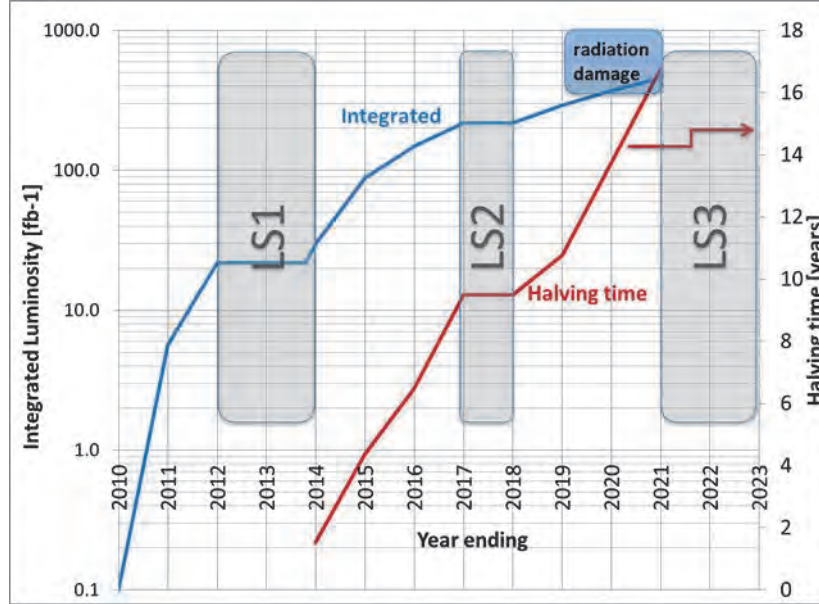


Figure 6. Evolution of LHC integrated luminosity in the next ten years. The time of running to half the statistical errors is also plotted vs. time.

The main goal of the HL-LHC has been set: to reach 3000 fb^{-1} of accumulated luminosity in 10-12 years after the upgrade while “limiting” the maximum peak luminosity to $5 \cdot 10^{34} \text{ cm}^{-2} \text{ s}^{-1}$ to limit the experimental pile-up (Rossi, 2011, IPAC). This implies automatically that the peak luminosity must be very near to the average luminosity in the run, i.e. the luminosity levelling is strictly necessary. Levelling means having a virtual luminosity at the beginning of the run (L_{peak}) much higher than the levelled luminosity (L_{lev}): however the instantaneous lumi is kept at the – lower – levelling value by “detuning” from optimal value one (or more) of the parameters controlling the lumi itself. This parameter is then slowly “retuned” toward its optimal value to compensate the protons lost in nuclear collisions (proton burning). Levelling has been already tested in 2011 in the LHCb experiment (IP8) at $L_{\text{lev}} = 3.2 \cdot 10^{32} \text{ cm}^{-2} \text{ s}^{-1}$ by varying the vertical beam separation.

Luminosity levelling is very attractive because it limits the pile-up in the experiment, reducing the technical difficulty and cost of the detector upgrade and limiting the power deposited in the magnetic elements of the IRs (Interaction Region) and of the DS (Dispersion Suppressor).

The classical formula for luminosity for the LHC conditions (short bunches, equal round beams) reads:

$$L = \gamma \frac{f_{\text{rev}} n_b N_b^2}{4\pi \varepsilon_n \beta^*} R \quad R = \frac{1}{\sqrt{1 + \left(\frac{\theta_c \sigma_s}{2\varepsilon_n \beta^*} \gamma\right)^2}}$$

γ being the relativistic factor, n_b the number of bunches, N_b the bunch population, ε_n the normalized transverse emittance, β^* the beta function at beam crossing, θ_c the full crossing angle and R the geometric reduction factor.

In Fig. 7 a few parameter sets for HL-LHC are reported with minimum separation for parasitic beam-beam encounters of 10σ (L is in unit of $L_0 = 10^{34} \text{ cm}^{-2} \text{ s}^{-1}$). The parameter set of column 2 should produce the ideal luminosity cycle and the integrated luminosity evolution plotted in Fig. 7, with an

efficiency of 60% (in LHC at present it is less than 40%). In bold are the “pushed” parameters and in red the ones that are considered very difficult or dubious. As mentioned before we use the new parameter space opened by $\Delta Q_{\text{beam-beam}}=0.02\div0.03$ (with full compensation of the long-range beam-beam tune shift) and by injected brightness twice the initial design (Bruning, 2011). Also we assume a beam current around 1.1 A (impacting on cryogenics, RF, collimation, beam losses, beam dump, machine protection, ...) and β^* as low as 15 cm thanks to the ATS scheme (Fartoukh, 2011) that produces β_{peak} of 20 km in the triplet and enhances the chromatic correction capability of the machine. We assume attaining the required gradient and aperture in the low- β quads (with Nb₃Sn technology) and to use crab cavities both to fully cancel the geometric reduction factor and as luminosity levelling tool.

Efficiency is defined as the ratio between the annual luminosity target of 250 fb⁻¹ over the potential luminosity that can be reached with an ideal cycle run time with no stop for 150 days; $t_{\text{run}} = t_{\text{lev}} + t_{\text{dec}} + t_{\text{turn}}$. The turnaround time after a beam dump is taken as 5 hours, t_{decay} is 3 h while t_{lev} depends on the total beam current

Parameter	Nom.	Target 25 ns	Target 50 ns	LIU 25 ns	LIU 50 ns
N_b [10 ¹¹]	1.15	2.0	3.3	1.7	2.5
n_b	2808	2808	1404	2808	1404
I [A]	0.56	1.02	0.84	0.86	0.64
θ_c [μrad]	300	475	445	480	430
β^* [m]	0.55	0.15	0.15	0.15	0.15
ϵ_n [μm]	3.75	2.5	2.0	2.5	2.0
ϵ_s [eV s]	2.5	2.5	2.5	2.5	2.5
IBS h [h]	111	25	17	25	10
IBS l [h]	65	21	16	21	13
Piwiński	0.68	2.5	2.5	2.56	2.56
F red.fact.	0.81	0.37	0.37	0.37	0.36
b-b/IP[10 ⁻³]	3.1	3.9	5	3	5.6
L_{peak}	1	7.4	8.4	5.3	7.2
Crabbing	no	yes	yes	yes	yes
$L_{\text{peak virtual}}$	1	20	22.7	14.3	19.5
Pileup $L_{\text{lev}}=5L_0$	19	141	257	137	274
Eff [†] 150 days	=	0.62	0.61	0.66	0.67

Figure 7. The parameter table of HL-LHC. The main target is the central one (target 25 ns spacing). In bold the main parameters that critically determine the upgraded performance.

5- LHC energy upgrade

The luminosity upgrade is a major step but it might not be the last one for the LHC tunnel. Indeed a study on a possible energy upgrade of the LHC, called High Energy LHC (HE-LHC) has been launched (Todesco and Zimmermann, 2011). The feasibility of such a machine critically depends upon achieving magnetic fields twice higher than the LHC. First studies have indicated that there is no show stopper for a HE-LHC. In particular the synchrotron power, passing from 0.17 W/m-beam in LHC to 2.8 W/m-beam in the HE-LHC, may be dealt with a beam screen operating around 60 K, a value still reasonable for vacuum. The maximum energy goal of the HE-LHC has been set to 33 TeV collision energy. The 16.5 TeV/beam can be reached by dipole field around 20 T, with a 2/3 filling factor as in the present LHC ring. HE-LHC magnets are the natural evolution of the one needed for HL-LHC, see Fig. 8, where the big leap forward in magnet technology needed for the upgrades is well depicted.

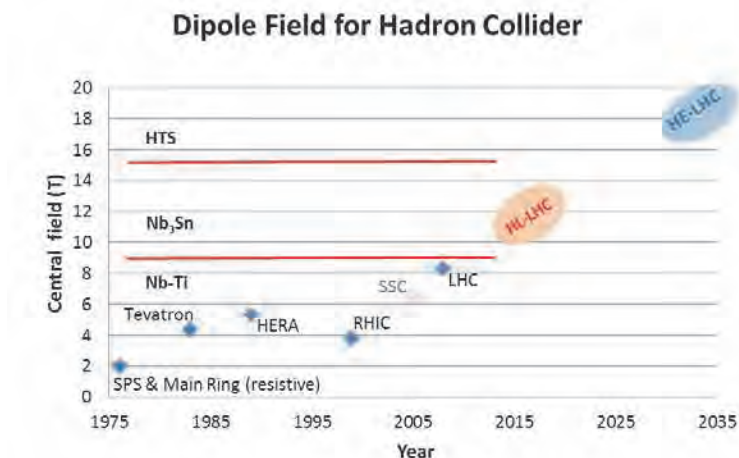


Figure 8. Evolution in time of the field of dipole magnets for hadron colliders, indicating the time scale and filed level for the LHC upgrades in Luminosity and Energy.

At levels beyond 15 tesla, the magnetic structure become complicated, given the stored energy and forces that are five time the present LHC level! A possible lay-out of the magnet cross section is shown in Fig. 9: the lay-out is based on rectangular coil blocks rather than classical $\cos\theta$ shape and needs to use all type of existing superconductors: Nb-Ti for the 0-8 T coils, Nb₃Sn for the 8-16 T coils and HTS for the 16-20 T coils. The cost of such a 20 T dipole is about three times the present LHC dipole. Indeed the magnetic system would be 80% of the cost of the entire machine, estimated at about 6,000 MCHF with a very crude approximation. The cost can be reduced considerably with a field of 15-16 T, rather than 20 T: in such a case Nb₃Sn technology will be sufficient without using expensive and still-far-from-being-developed HTS cables. However, in such a case the energy of the collider would be “limited” at 27 TeV in the centre of mass.

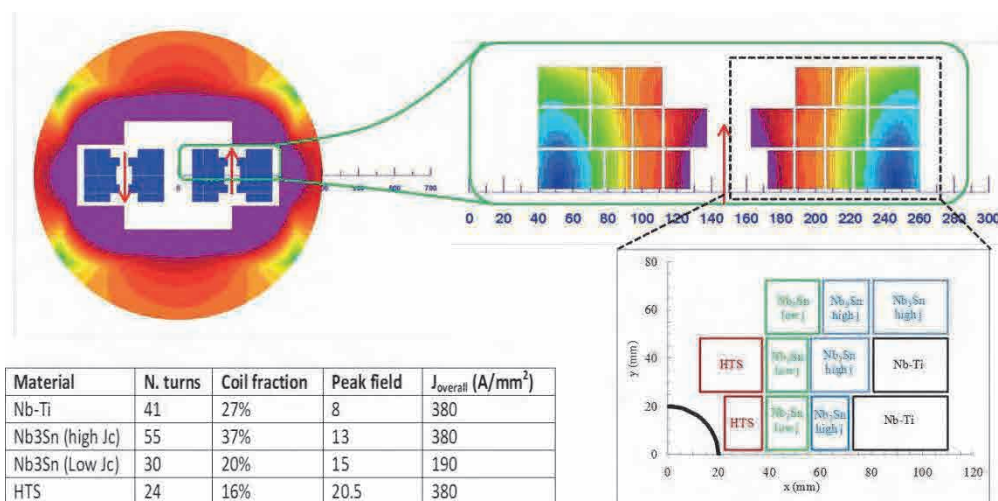


Figure 9. Cross section of a 20 T dipole magnet for the HE-LHC. Top left: full cross section (800 mm of diameter of the iron yoke); top right: expansion of one quadrant of the coils, showing the bloc structure. Bottom right: further expansion of the right half of the coil quadrant, with indicated the various SC material employed in

each single coil bloc. In the bottom left table the percentage of the different SC material is indicated. Arrows indicate magnetic field.

Other beam dynamics issues for HE-LHC appear not more difficult than LHC itself, thanks also to the excellent beam damping time of 2 hours (26 hours in the LHC). Also collimation seems not more difficult than the HL-LHC case since the beam power and power density will not increase. HE-LHC relies on injection energy > 1 TeV (0.45 TeV in LHC) to permit a small magnet aperture: 40 mm (56 mm in LHC), a critical issue to attaining 20 T. The 1 TeV injection calls for an upgrade of the present SPS, called SPS+. The main magnet needed for such machine would be very similar to the one already under development by the GSI-INFN collaboration for FAIR-SIS300 (Fabbriatore, 2011): maximum field of 4.5 T, 1T/s of field ramp rate. The magnet model, full cross section and 3 m of length, is already built and test is just under way. The advantage of SPS+ is the saving of a good fraction of the 70 MW of today's SPS consumption and the possibility of providing a 2 MW beam to LAGUNA experiment for neutrino search with a machine that is anyway needed for the LHC upgrade program.

For HE-LHC many issues need to be addressed more deeply: one is quadrupole strength and the best lattice optimization since quadrupole gradients cannot be doubled as "easily" as dipole field. In addition to the main magnets possible critical points are the beam injection and extraction. In particular the beam dump with beam rigidity more than double and the more or less the same space allocated for the kickers looks problematic, but not impossible.

HE-LHC is certainly a very difficult machine but it is also a "saving" machine with continuity, making re-use of all existing infrastructure of CERN, and is one of the main options for the future of CERN and High Energy Physics. In any case the main technology for the HE relies on the advance already on going for the HL-LHC, plus a specific development on HTS that is just starting. In about four years we believe that the energy reach of HE-LHC can be finally assessed, allowing determining its physics reach, the design and construction issues as well as its cost with a reasonable accuracy.

6- Conclusions

LHC is the pinnacle of more than thirty years of hadron collider development. Superconductivity, discovered just 100 year ago, has been the choice of preference for HEP accelerators since the Tevatron and possibly will also be the workhorse for the future. The roadmap for the future foresees a luminosity upgrade in ten years from now, to extend the physics reach of the present machine. Based on 12 tesla magnets, the luminosity upgrade is the ideal "preparatory phase" for a much more ambitious project, the LHC energy upgrade (Bottura et al, 2012). Meant to reach between 27÷33 TeV c.o.m. collision energy, the High Energy LHC will be the ultimate exploitation of the LHC tunnel. It requires an extensive R&D on SC magnets, which must reach 16 to 20 Tesla field in operation. R&D must be carried out in this decade in the shadow of the HL-LHC construction, in this way HE-LHC could be installed in around 2035, i.e., after the collection of 3000 fb^{-1} of integrated luminosity at LHC energy. Beyond HE-LHC energy, a new larger circumference tunnel would be necessary for attaining even higher energy, or new technology like plasma acceleration must be pursued.

7- References

- Acerbi, E., Ceresara, S., Garré, R., Rossi, L., Volpini, G. (1992), Italian Development of a Superconducting Cable for the Main Dipoles of the Large Hadron Collider, proceedings of the European Particle Accelerator Conference 1992 (EPAC92), <http://accelconf.web.cern.ch/AccelConf/>
- Bottura, L., de Rijk, G., Rossi, L., Todesco, E. (2012) "Advanced Accelerator Magnets for Upgrading the LHC", accepted for publication in *IEEE Trans. Appl. Supercond.* in 2012.
- Bruning, O. (2011), Do we really need the LHC luminosity upgrade?, Proceedings of the LHC Performance Workshop, Chamonix 2011, <https://espace.cern.ch/acc-tec-sector/chamonix.aspx>
- Edwards, H. T. (1985), The Tevatron energy doubler: a superconducting accelerator, *Annual Review of Nucl. Part. Sci.*, 35, pp. 605-660, 1985.
- Evans, L. (2007), LHC: Construction And Commissioning Status, proceedings of the Particle Accelerator Conference 2007 (PAC07), <http://accelconf.web.cern.ch/AccelConf/>
- Evans, L., Bryant, P. (2008), The CERN Large Hadron Collider: Accelerator And Experiments, 2008 JINST 3 S08001 (<http://iopscience.iop.org/1748-0221/3/08/S08001>)
- Evans, L., editor (2009), *Large Hadron Collider – A Marvel of Technology*, EPFL Press, 2009.
- Fabbricatore, P. et al., The Construction of the Model of the Curved Fast Ramped Superconducting Dipole for FAIR SIS300 Synchrotron, *IEEE Trans. Appl. Supercond.*, **21**, No. 3, June 2011, pp. 1863-1867.
- Fartoukh, S. (2011), An Achromatic Telescopic Squeezing (ATS) Scheme for the LHC Upgrade, proceedings of the Int. Particle Accelerator Conference 2011 (IPAC11), <http://accelconf.web.cern.ch/AccelConf/>
- LHC Study Group (1991), Design Study of the Large Hadron Collider (LHC), CERN 91-03, 2 May 1991
- Kes, P. (2011), Kamerlingh Onnes's Notebooks and the Discovery of Superconductivity, *100 Years of Superconductivity*, April 8, 2001, Copyright © 2011 Museum Boerhaave, Leiden (NL), p. 10.
- Lamont, M. (2011), The LHC from Commissioning to Operation, proceedings of the Int. Particle Accelerator Conference 2011 (IPAC11), <http://accelconf.web.cern.ch/AccelConf/>
- Perin, R. (1991) The Superconducting Magnet System for the LHC, *IEEE Trans. Appl. Supercond.*, **3**, 1991.
- Rossi, L. (2007), LHC and the Role of Superconductivity in one of the Largest Scientific Enterprises, *IEEE Trans. App. Sup.*, vol. 17, No.2, June 2007, pp. 1005-1014.
- Rossi, L. (2010), Superconductivity: its role, its success and its setback in the Large Hadron Collider (LHC) of CERN, *Supercond. Sci. Technol.* **23** (2010) 034001 (17pp)
- Rossi, L. (2011), LHC Upgrade Plans: Options and Strategy, proceedings of the Int. Particle Accelerator Conference 2011 (IPAC11), <http://accelconf.web.cern.ch/AccelConf/>

Rossi, L. (2011), Superconductivity and the LHC: the early days, *CERN Courier*, issue November 2011, p.21-27.

Todesco, E., Zimmermann, F., editors (2011), Proceedings of the workshop on “The High-Energy Large Hadron Collider”, Malta October 2010, CERN- 2011-03, 8 April 2011.

Tollestrup, A. V. (1979), “Superconducting magnets”, in R. A. Carrigan, F. R. Hudson and M. Monthé editors, *Physics of High Energy Accelerators, AIP Proceedings*, 87, pp. 699-804, 1979.

Wilson, M.N. (1999), Superconductivity and Accelerators: the Good Companions, *IEEE Trans. Appl. Supercond*, **9**, p.111-121

Wolff, S. (1988), Superconducting HERA magnets, *IEEE Trans. on Mag.*, 24(2), pp. 719-722, 1988.

LATEST RESULTS FROM MRPC TIME RESOLUTION

■ CRISPIN WILLIAMS

INFN Bologna

Abstract

The Multigap Resistive Plate Chamber (MRPC) is an important detector that was inspired with the R&D performed by the LAA project. The latest results from this detector will be presented. The NINO asic, used as the front-end amplifier/discriminator, will also be described.

1. Introduction

We have heard already about the LAA project set up at CERN in the 1980's by Professor Zichichi. In this paper, I will talk about one of the inventions that resulted from the LAA project, the 'Multigap Resistive Plate Chamber'. This device has revolutionised the time-of-flight (TOF) arrays used in particle physics throughout the world. As an example, the ALICE TOF array is an excellent candidate. This is a detector in form of a barrel of radius 3.7 m and 7 m long. It has 160,000 readout channels. Currently it is taking data and typically the system time resolution of the whole detector is ~ 80 ps. To achieve such a resolution, one needs a detector with excellent and stable timing characteristics and that is easy to calibrate, and also very good front-end electronics. To this end, we developed, within the LAA project, a special front-end asic, known as the 'NINO': this asic will also be briefly described in this paper.

The precise measurement of the time it takes a particle to travel a certain distance is, in reality, a measurement of its velocity. This measurement, together with the momentum, measured from the curvature of tracks inside the magnetic field, allows the mass of the particle to be calculated. This is a very important aspect in particle physics as it classifies

the particle: all known stable particles have different mass. Thus with a TOF array one can search, for example, for strangeness enhancement, an important signature of the formation of quark-gluon plasma, a new state of matter expected to be observed with the ALICE detector with heavy-ion collisions.

2. The Multigap Resistive Plate Chamber (MRPC)

The Multigap Resistive Plate Chamber (MRPC) was invented in 1996 [1]. Since its conception, it has had particularly stable operating characteristics. The key difference between the MRPC and the more traditional single-gap resistive plate chamber (RPC), is that the multigap consists of a series of gas gaps all read out with a single set of readout pads. These gaps are created by inserting extra plates of resistive material in-between the two outer resistive plates. These extra resistive plates are allowed to electrically float, however there is a strong feedback mechanism that keeps all the plates at the correct voltage.

The detector built for the ALICE TOF [2] used glass plates for the resistive material and fishing line (250 micron diameter) as spacers between these plates. A schematic of the cross section of the detector is shown in figure 1.

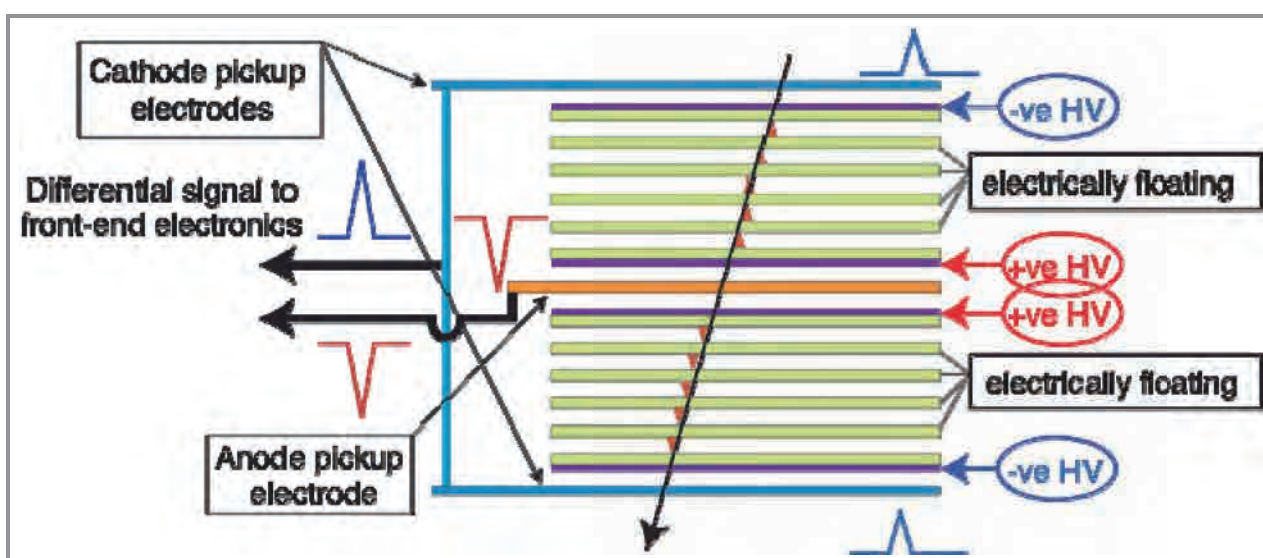


Figure 1: ALICE-TOF has 10 gas gaps (two stacks of 5 gas gaps). Each gap is 250 micron wide; it is built in the form of strips, each with an active area of $120 \times 7.2 \text{ cm}^2$ and readout by 96 pads.

Since these internal plates are electrically floating, it makes the detector particularly easy to build. One simply stacks up the resistive plates and separates them with a spacer, fishing line is commonly used. However there are other important benefits of this type of detector that used very narrow gas gap, such as space charge effects that limit the growth of the avalanche. This effect limits the transition to streamers, and thus there is a long efficiency plateau versus voltage that is completely streamer-free. In addition, the positive and negative ions created in the gas gap recombine [3] rather than drift to the resistive plates. This allows the MRPC to operate at higher particle fluxes than expected.

The performance of the ALICE TOF is well documented [4]. It should be also noted that the same voltage is applied to all the MRPC modules and all the thresholds are set to the same value.

The performance of the MRPC in the ALICE TOF is exceptional and now there are many experiments that have followed the lead of ALICE, such as STAR at RHIC [5] and FOPI at GSI [6]. All these arrays are operating with a time resolution below 100 ps. However the question remains concerning what time resolution can be achieved with this detector.

The system time resolution of 80 ps for the ALICE TOF is made up of many contributions. The most important ones concern the track length. The trajectory of the particle is extrapolated from the TPC (that has an outer radius of 2.5 m) to the surface of the TOF detector at 3.7 m. In addition the pads of the ALICE TOF are read out only on one side so there is a correction that has to be made according to the impact point. There is also the time resolution of the TDC and the jitter introduced by the front-end electronics and cables. The actual intrinsic time resolution of the ALICE TOF MRPC is 15 ps. Given this, there are those who dream of an array that is capable of obtaining an overall resolution of 10 ps. Can the MRPC be used for such an array?

An important improvement can be made by reading out both sides of the readout pad and obtain two times, t_{left} and t_{right} . The time difference $(t_{\text{left}} - t_{\text{right}})$ will give the position along the pad while the average time sum $(t_{\text{left}} + t_{\text{right}})/2$ will give the time that the particle passed through the MRPC, and this time is independent of the hit position along the readout pad. The time resolution of the MRPC can also be improved by making the gas gaps smaller and by having more of them. In figure 2 we show a schematic of a particular test setup. Two 24 gap MRPCs were placed in a gas box, one behind the other. Each MRPC is

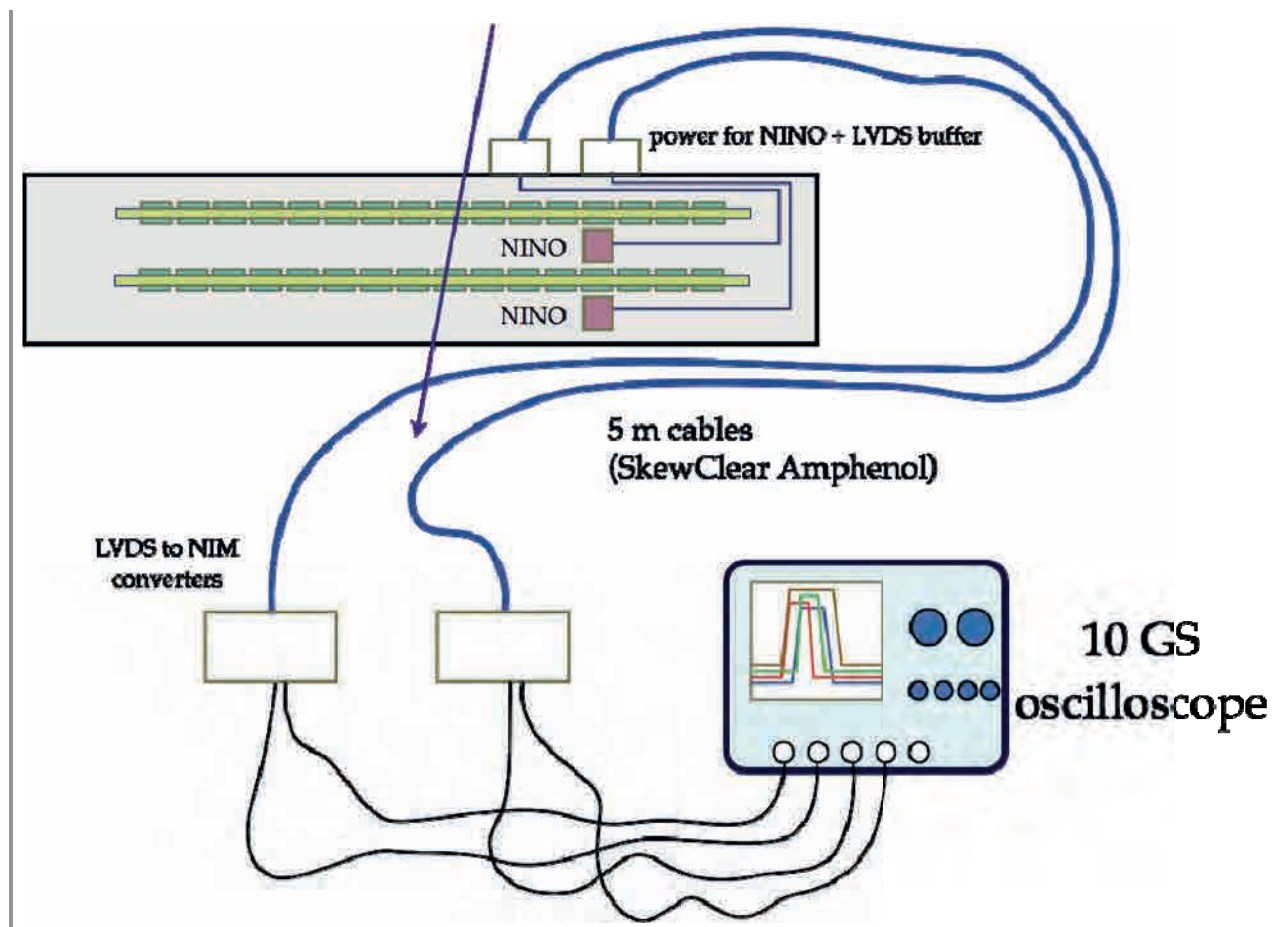


Figure 2: Two 24 gap MRPCs mounted one behind the other. The time of one MRPC was measured with respect to the other and the time resolution extracted.

arranged in 4 stacks of six gaps; the gap size is 160 micron. The front-end electronics (the NINO ASIC) was mounted on the chamber itself inside the gas volume. Since we do not have a TDC with suitable time resolution, a four channel digital oscilloscope was used to record the times. The complete setup is shown in figure 3.

The results of testing these chambers in a test beam at CERN (T10 of the East Hall) are shown in figure 4. A time resolution of 16 ps was obtained. We expect that the intrinsic time resolution of such an MRPC to be 8.5 ps and the contribution of the measuring system to be also 8.5 ps giving a total of 12 ps. Thus 16 ps, although excellent still has room for improvement. Details of these tests can be found in ref [7]

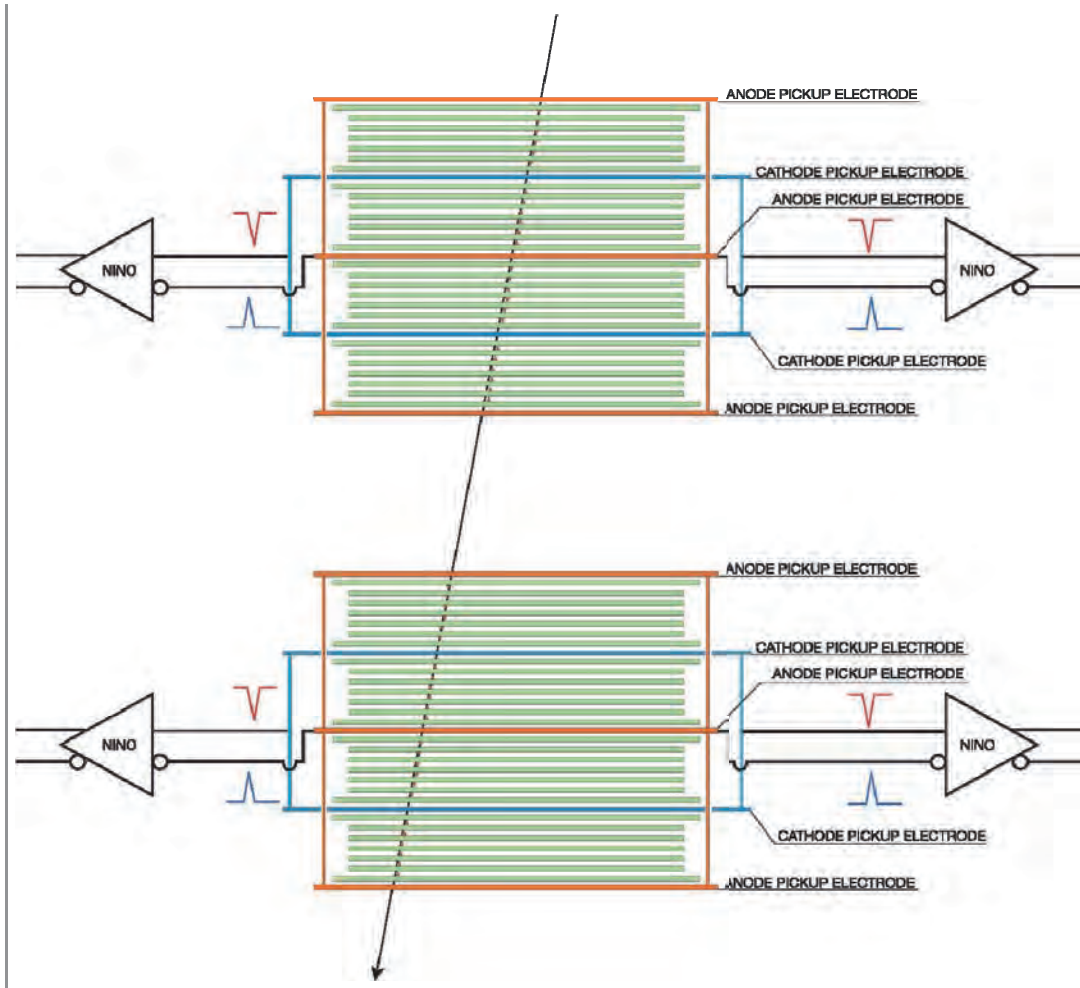


Figure 3: The two 24 gap MRPCs mounted one behind the other in a gas tight box. The front-end amplifier/discriminator (NINO asic) was mounted on the MRPC strip as close to the pickup pad as possible. To obtain the necessary time resolution, a digital oscilloscope was used to record the times of the signals.

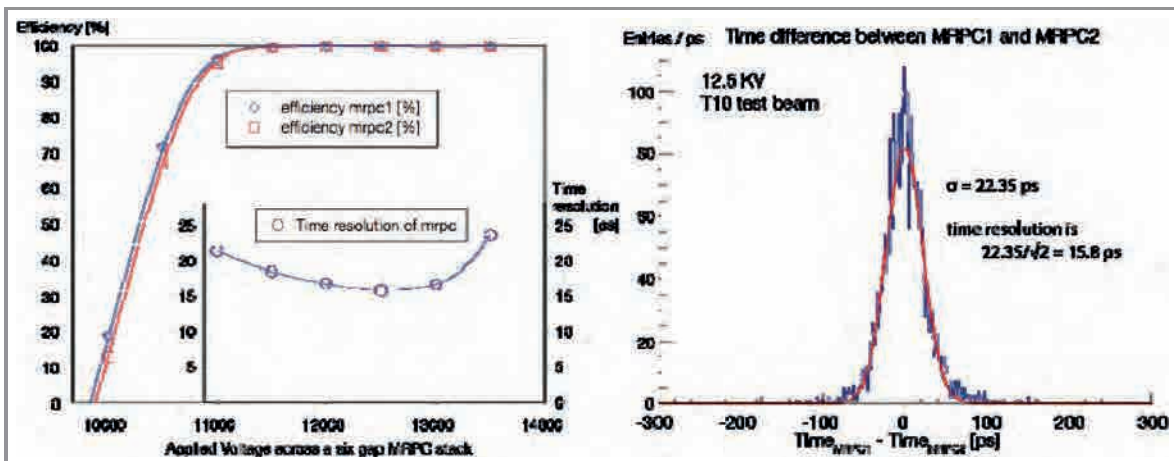


Figure 4: The time difference between MRPC1 and MRPC2 is shown by the histogram on the right hand side. The plot on the left hand side shows the efficiency and the time resolution as a function of applied voltage.

3. The NINO ASIC

A critical device for precise timing is the front-end electronics. The lowest noise front-end electronics is a single-ended amplifier followed by a discriminator. A differential front-end multiplies the electronic noise by $\sqrt{2}$. However, and especially for large devices, the intrinsic noise of the electronics is not the dominating contribution. Instead, the biggest contribution comes from the detector itself. Single-ended electronics measures everything with respect to ground; however all the other channels inject fast current pulses into the ground and this becomes dominant source of noise for large systems. Early on during the ALICE TOF R&D phase, we found that we could not get better time resolution than 150 ps when testing an MRPC built as single-ended device (anode readout pads and a common cathode plane). However this time resolution improves dramatically when a differential signal is derived from the MRPC; this can be easily seen with the result from the previous section. Thus a key ingredient for precise timing is a detector that produces a differential signal and front-end electronics designed to fully exploit it. The NINO asic [8], developed within the LAA project, is just such electronics.

The NINO asic was designed with the following criteria: (a) differential architecture throughout; (b) fast peaking time, (1 ns) to minimise jitter; (c) input charge encoded into the width of the output pulse (so that a charge measurement can be made with a TDC measuring the leading and trailing edges of the output pulse); (d) low power (45 mW/channel). This asic was realised in 0.25 micron CMOS. In figure 5 the first NINO prototype is shown bonded to a PCB.

The jitter of the NINO amplifier/discriminator is very low - we measured 2 ps on the test bench, but much of this measured jitter was contributed by the test set up. This asic has quickly becoming the 'asic of choice' in all experiments that require precise timing.

4. Conclusions

The LAA project was dedicated to advance R&D in detectors used for particle physics, and the Multigap RPC and the NINO asic are two examples where the frontiers have been pushed back.

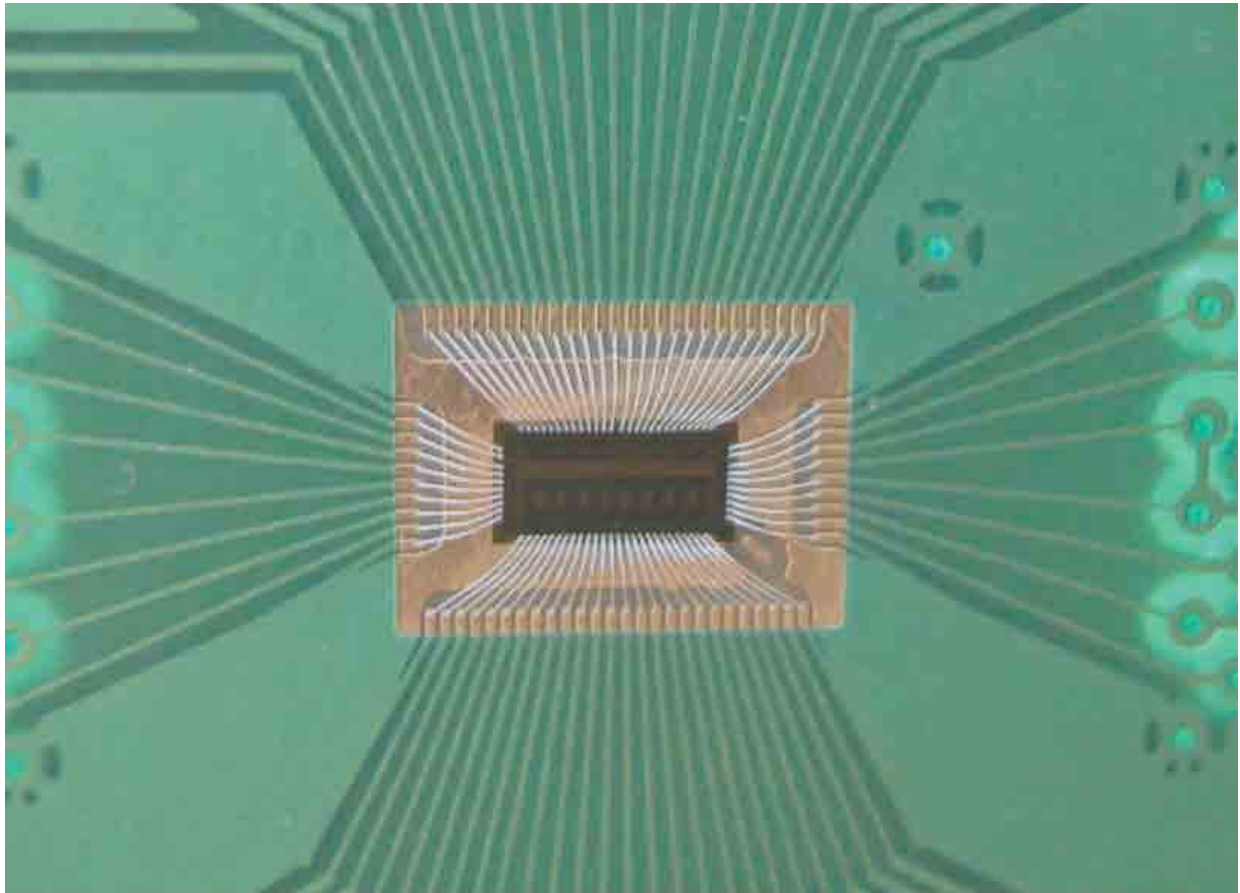


Figure 5: A photograph of the NINO prototype binded to PCB. Subsequently it was packaged in a plastic TAPP package and soldered onto the PCB used for the ALICE front end.

The MRPC has now generated a new interest in ‘time of flight’ arrays. It is now possible to build a highly segmented TOF that has exceptional timing. This is extremely relevant to heavy ion physics and has generated a wave of new TOF arrays in Europe and the United States.

References

1. E. Cerron Zeballos, I. Crotty, D. Hatzifotiadou, J. Lamas-Valverde, S. Neupane, M. C. S. Williams, A. Zichichi, “A new type of resistive plate chamber: the multigap RPC”, Nucl. Instr. Meth., vol. A374, pp. 132-135, 1996.
2. A.N. Akindinov et al., “Latest results on the performance of the multigap resistive plate chamber used for the ALICE TOF”, Nucl. Instr. Meth., vol. A533, pp 74-78, 2004.

3. K. Doroud, H. Afarideh, D. Hatzifotiadou, J. Rahighii, M.C.S. Williams, A. Zichichi, “Recombination: An important effect in multigap resistive plate chambers”, Nucl. Instr. Meth., vol. A610, pp 649–653, 2009.
4. A. Akindinov et al., “The MRPC-based ALICE Time-Of-Flight detector: Commissioning and first performance”, Nucl. Instr. Meth., vol. A661, pp S98-S101, 2012.
5. W.J. Llope for the STAR Collaboration, “Multigap RPCs in the STAR experiment at RHIC”, Nucl. Instr. Meth., vol. A661, pp S110-S113, 2012.
6. M. Kiš et al. “A Multi-strip Multi-gap RPC Barrel for Time-of-Flight Measurements”, Nucl. Instr. Meth., vol. A646, pp 27–34, 2011.
7. S. An, Y.K. Jo, J.S. Kim, M.M. Kim, D. Hatzifotiadou, M.C.S. Williams, A. Zichichi, R. Zuyeuski, “A 20 ps timing device—A Multigap Resistive Plate Chamber with 24 gas gaps”, Nucl. Instr. Meth., vol. A594, pp 39–43, 2008.
8. F. Anghinolfi, P. Jarron, A.N. Martemiyarov, E. Usenko, H. Wenninger, M.C.S. Williams, A. Zichichi, “NINO: an ultra-fast and low-power front-end amplifier/discriminator ASIC designed for the multigap resistive plate chamber”, Nucl. Instr. Meth., vol. A533, pp 183–187, 2004.

HIGHLIGHTS FROM CMS

■ TEJINDER S. VIRDEE

Imperial College, London, U.K.

ABSTRACT

The LHC accelerator has collided protons and lead ions at unprecedented high energies. Outstanding progress has seen the proton-proton interaction rate increase from about 100/s in March 2010 to about 300 million/s in November 2011. The CMS experiment is also performing very well, close to the desired and ambitious design performance parameters laid down some fifteen years ago. The emerging physics measurements are confronting, more and more precisely, the predictions of the Standard Model of particle physics, whilst looking for a broad range of potentially new physics.

Keywords: LHC, CMS experiment, experimental measurements of standard model processes, experimental searches for new physics.

1. INTRODUCTION

The LHC Project [1], the accelerator and its experiments, have required a 20 year-long and painstaking effort to get to this point. This has been accomplished by a global project that is a tribute to human ingenuity, collaboration and resolve.

The Standard Model (SM) of particle physics contains the unification of electromagnetism and weak interaction elucidated in the 1960's. The programme of physics of CMS, and ATLAS, comprises a broad range of physics including the clarification of electro-weak symmetry breaking, identification of the particles that make up the dark matter in the universe, and the search for new physics at the TeV energy scale. CMS also has specific capabilities in the study of b-physics and in study of heavy ion collisions using hard probes.

The paper will briefly outline some of the challenges faced in the last 20 years during the construction of the CMS experiment, its operation and performance, the first physics results from the experiment, and the outlook.

2. THE CMS COLLABORATION AND DETECTOR

CMS today comprises 3375 scientists and engineers of which 1740 are Ph.D. physicists, 845 Ph.D students, and 790 engineers from 170 institutions in 40 countries. The talents and the resources of all these participants have been needed over the last 20 years for the phases of design, prototyping, construction, installation, commissioning, data-taking and now distributed data analysis.

The central feature of the CMS apparatus [2] is a superconducting solenoid of 6 m internal diameter, providing a magnetic field of 3.8 T. Within the field volume is an all-silicon pixels (comprising ~ 65 million channels) and silicon strip tracker

(comprising $\sim 200 \text{ m}^2$ of detecting area), a scintillating crystals electromagnetic calorimeter (ECAL), and a brass-scintillator sampling hadron calorimeter (HCAL). Muons are detected in gas-ionization detectors embedded in the steel return yoke. In addition to the barrel and endcap detectors, CMS has extensive forward calorimetry. A transverse view of the CMS experiment during its installation in the underground cavern is shown in Fig. 1.

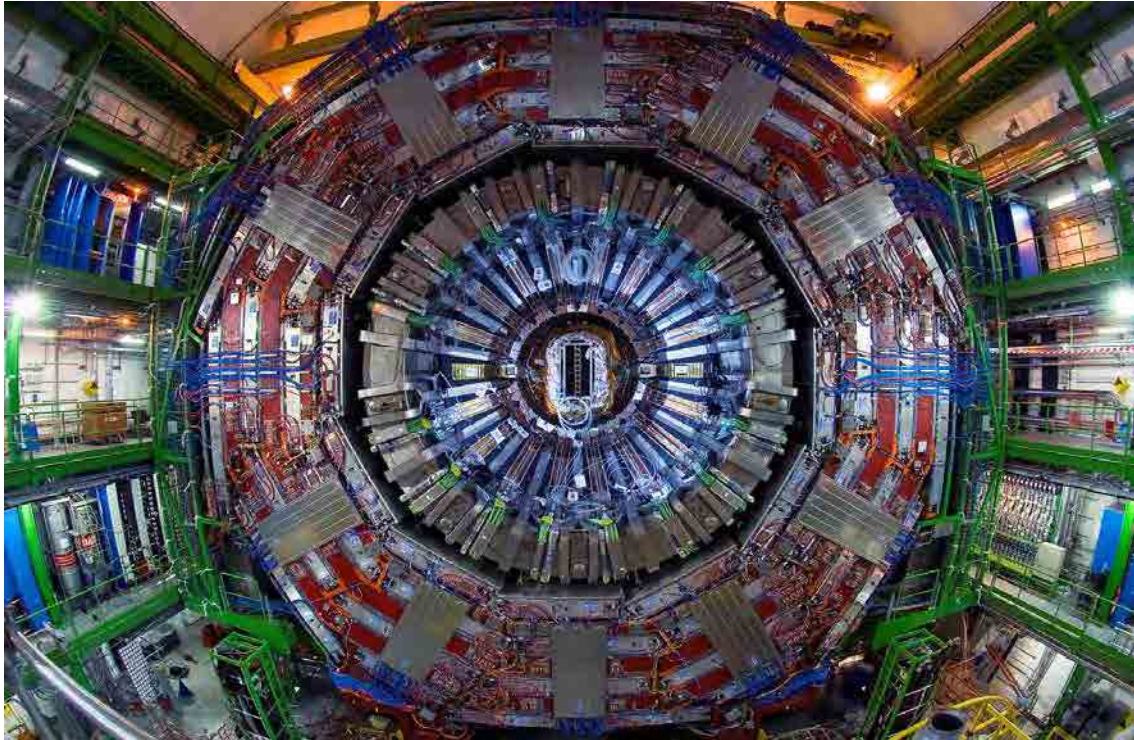


Fig. 1: A photograph of the transverse “cut” of CMS barrel showing the four principal layers namely, from inside out, the inner tracker, the electromagnetic calorimeter, the hadronic calorimeter, the superconducting solenoid, and the muon system sandwiching the field-return yoke.

The inner tracker measures charged particle trajectories in the pseudorapidity range $|\eta| < 2.5$ and provides an impact parameter resolution of $\sim 15 \text{ } \mu\text{m}$ and a transverse momentum (p_T) resolution of about 1% for charged particles with $p_T \sim 40 \text{ GeV}$. The electromagnetic calorimeter provides a coverage in pseudorapidity of $|\eta| < 3.0$. The ECAL has an energy resolution of better than 0.5% for unconverted photons with transverse energies (E_T) above 100 GeV.

The jets and missing transverse energy resolutions are substantially improved with respect to only calorimetric reconstruction by using a particle flow (PF) algorithm. PF aims at reconstructing all stable particles in the event, i.e. electrons, muons, photons and charged and neutral hadrons, from the combined information from all CMS sub-detectors, to optimize the determination of particle types, directions and energies. CMS is well suited for this due to its powerful Si tracker (the good tracker momentum resolution is used to improve the energy measurement of charged hadrons), its lead-tungstate ECAL with fine lateral granularity & small Moliere radius (the electromagnetic showers are very compact). It should be noted that the 4T magnetic field of CMS spreads out (of the jet defining cone) the energy carried by low-momentum charged particles and that its HCAL has a moderate

performance (with a pion energy resolution of $\Delta E \sim 100\%/\sqrt{E}(\text{GeV})$).

Muons are detected in the pseudorapidity window $|\eta| < 2.4$, with detection planes based on three gas-detector technologies: drift tubes, cathode strip chambers, and resistive plate chambers. A high- p_T muon originating from the interaction point produces track segments typically in three or four muon stations. Matching these segments to tracks measured in the inner tracker results in a p_T resolution between 1 and 2% for p_T values up to 100 GeV/c.

The first level of the CMS trigger system, composed of custom hardware processors, is designed to select the most interesting events in less than 4 μs , using information from the calorimeters and muon detectors. The High Level Trigger processor farm further decreases the event rate to a few hundred Hz before data storage.

During construction many challenges had to be faced. We list a few: the procurement of some 200 m^2 of silicon strip detectors, the development of deep-sub-micron (0.25 μm) radiation hard technology for the front-end electronics of the inner tracker and the ECAL, and the development and production, over ten years, of lead-tungstate scintillating crystals, the control of quality of all elements that were installed in the underground cavern, including their services (optical cables for signals, low and high voltage power cables, pipes for water and other cooling fluid etc.). It is difficult to do full justice to what it has taken to get to this point and the reader is referred to references [2] and [3] to get an idea.

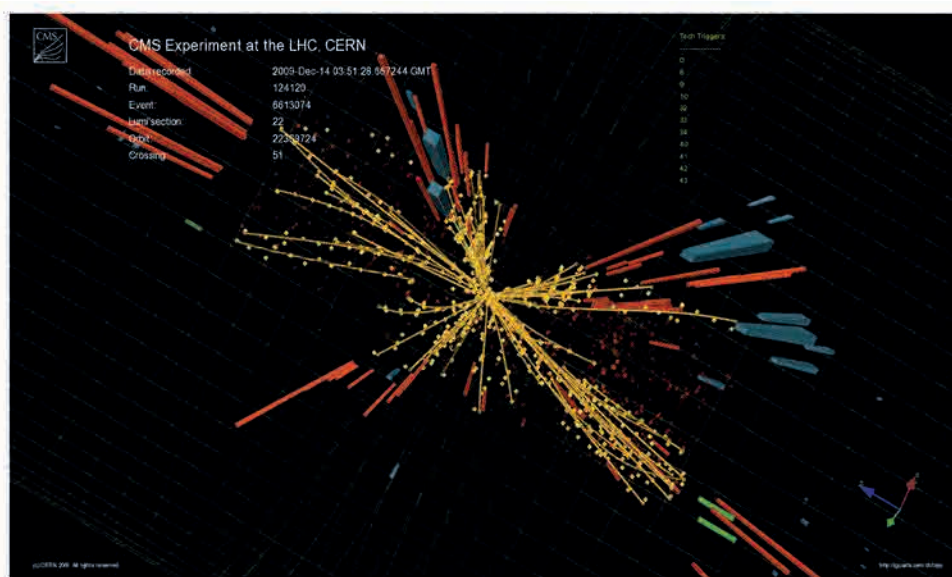


Fig. 2: A candidate multi-jet event from proton-proton collisions at the LHC.

3. THE RUNNING CONDITIONS AND THE PERFORMANCE OF CMS

The LHC accelerator and the CMS experiment are working very well. In the later stages of 2011 the bunch spacing was 50 ns and each bunch contained some 1.5×10^{11} protons/bunch. The peak luminosity achieved was $3.65 \times 10^{33} \text{cm}^{-2}\text{s}^{-1}$ and some 500 pb^{-1} were delivered in the most productive week. The LHC delivered 5.75fb^{-1} of

which CMS recorded 91% on mass storage. The conditions of event pileup, at $\langle 12 \rangle$ interactions per crossing, were not far short of design.

Most (close to 100% of the channels) of the detector components in CMS were fully functional. The experiment is very well described in software code. Monte-Carlo simulated events are usually generated with a matrix-element generator interfaced with PYTHIA. After generation the events are passed through the full-detector simulation with GEANT4 and analysed with the same code as used for analysis of beam-data. The whole chain of CMS software, from simulation to reconstruction and distributed analysis has performed marvellously well.

An event display (Fig. 2) of a proton-proton collision in CMS illustrating the inner tracking detector hits and the energy deposits in the electromagnetic calorimeter (red) and the hadron calorimeter (blue). The height of the red and blue towers is indicative of the energy deposited. The muon system is not displayed. The production of “jets” is evident from the collimated bunches of particles.

The thorough preparation of the hardware and software of the CMS experiment meant that very rapid progress could be made in the first months of data taking in 2010. The data taken were used to establish that the performance of the experiment was indeed close to design. An example is shown in Figure 3 where the distribution is plotted of effective masses of all di-muon pairs detected in CMS upon examination of some 3 trillion proton-proton interactions (we have now examined some 300 trillion interactions). The sharpness (due to good mass resolution) and clarity of the signal peaks (due to high signal/background) is evident for several known particles that decay to di-muons. It is remarkable that the CMS experiment, arguably one of the most technologically challenging scientific instruments ever built, achieved close-to-design performance after only a few months of data-taking.

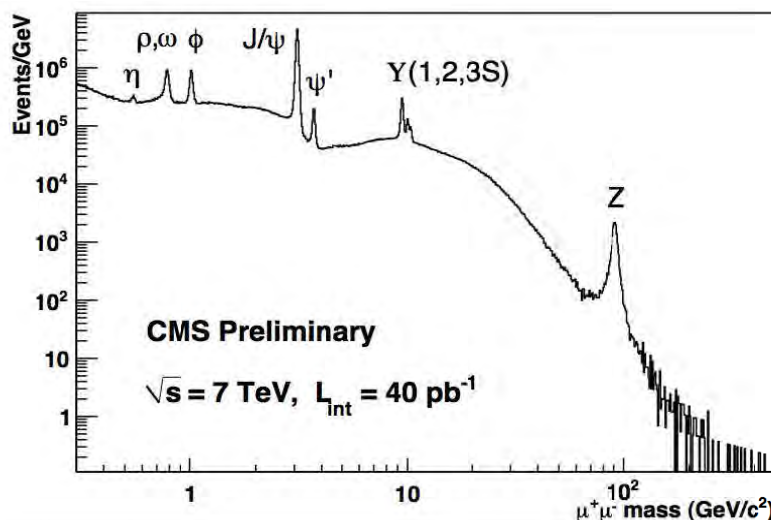


Fig. 3: The distribution of di-muon effective masses showing the various resonant states. The mass resolutions in the central region are; 28 MeV/c² (0.9%) for J/ψ, 69 MeV/c² (0.7%) for Y(1S), both dominated by instrumental resolution and $\Gamma = 2.5$ GeV/c² for the Z dominated by its natural width.

4. THE PHYSICS RESULTS

The Standard Model makes precise predictions for the production of known particles such as quarks and gluons, manifesting themselves as jets, prompt γ 's, J/ψ , Y , bottom and top quarks etc., W/Z boson and multi vector-boson (WW, WZ, ZZ) production, etc.. The CMS (and ATLAS) experiments must measure these processes and verify these precise predictions before being able to claim any discoveries. This is imperative as known processes can mimic signals of new physics and thus generate backgrounds, sometimes quite severe, to new physics. Already a very large number of measurements have been made, and published in around 100 papers by CMS. Here we shall only be able to discuss a few cases. These confirm the predictions of the Standard Model. In this sense we can consider the CMS to have been “physics commissioned”.

4.1 Measuring Standard Model Processes

4.1.1 Inclusive quarks/gluons production

In order to understand whether the known standard model physics is reproduced correctly one of the important processes to study, and check, is the production of quarks or gluons (jets). The energy of a jet is determined by adding all the energy in a cone of half-angle of $R=\sqrt{(\Delta\eta)^2+(\Delta\phi)^2}=0.5$ (one-half of a unit of solid angle). Fig. 4 shows the rate of production of jets as a function of transverse momentum, and various angular ranges with respect to the beam direction [4]. It can be seen that the agreement is excellent with the theoretical predictions over about ten orders of magnitude and in the different angular ranges.

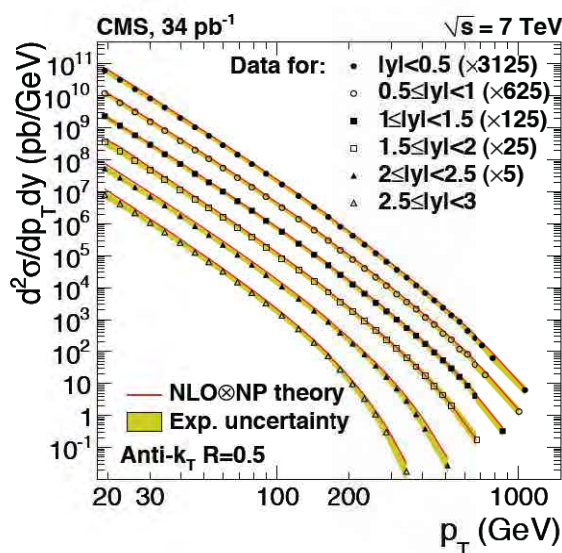


Fig. 4: The rate of production of jets as a function of transverse momentum and in various angular ranges.

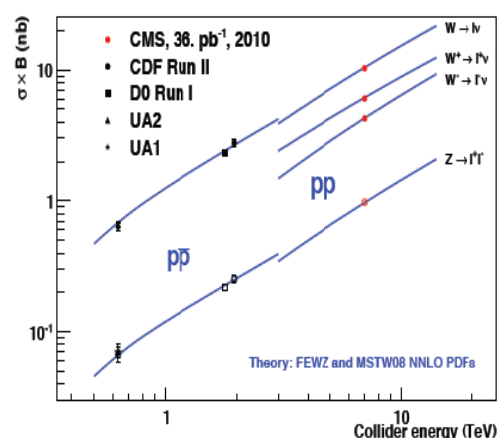


Fig. 5: Measurements of inclusive W and Z production cross sections times branching ratios as a function of center-of-mass energy for CMS and experiments at lower-energy colliders. The lines are the NNLO theory predictions.

4.1.2 Inclusive W and Z boson production

Another important process to understand well is the inclusive production of W and Z bosons as it presents substantial background to any new-physics that involves charged leptons and missing transverse energy such as the production of conjectured supersymmetric particles. This process also tests the efficiency and the accuracy of the reconstruction of charged leptons (electrons and muons) and missing transverse momentum (from neutrinos). As can be seen from Figure 5 the CMS measurements are already starting to test the theoretical predictions at the levels of the precision of these predictions (a few percent) [5].

4.1.3 Top quark production

Finally, we look at the production of top quarks. The top quark decay chain involves, charged leptons, neutrinos, b-quarks and light quarks. This is a particularly revealing measurement as it tests the efficiency and the accuracy of the reconstruction of all of the physics objects namely electrons, muons, missing E_T , b-quarks and light-quark jets. The top cross-section has been measured in many different decay-channels and is found to be consistent with the standard model predictions [6].

In summary, a wide range of measurements made by CMS [7] has shown that the SM predictions for known physics have been essentially spot on. This is no small measure due to the large amount of work carried out over the last decade or so by our theory colleagues along with the results from the other collider experiments at LEP, Tevatron, HERA, b-factories etc.

4.2 The Study of Quark-gluon Fluid

In 2010 the LHC has also collided lead ions at a centre-of-mass energy of 2.76 TeV per nucleon. CMS recorded collisions corresponding to an integrated luminosity of $10 \mu\text{b}^{-1}$. Previous experiments, at lower energies, have already indicated that quark-gluon fluid is being formed. This is very clearly the case at the LHC. At the LHC hard probes such as high- p_T jets, prompt photons, upilon production and W/Z bosons can be employed to study the properties of the fluid. For the creation of quark-gluon fluid the lead-lead ions must interact head-on. This latter aspect is determined by a quantity labeled centrality. Centrality is defined by the amount of transverse energy (E_T) measured in the forward calorimeters $|\eta| > 3.0$, and quantified by the percentile of events, in E_T . Central, head-on, events have a large amount of E_T in the forward region and hence a small value of centrality (e.g. 0-10%).

Fragmentation of quarks and gluons into jets is expected to be strongly modified as they traverse the quark-gluon medium created in the head-on (central) high-energy Pb-Pb collisions. We look for unbalanced two-jet events where one of the partons has suffered substantial modification whilst the other has not. Such situations arise when the parton-parton hard scattering takes place near the surface of the quark gluon fluid and one of the partons has to traverse much more fluid than the second one. This phenomenon is labeled “jet quenching”. Jets are reconstructed using the energy deposited in the CMS calorimeters and studied as a function of collision centrality. With increasingly central collisions (e.g. approaching very small percentile values), a striking imbalance in di-jet transverse momentum is observed, consistent with jet quenching [8]. The observed effect extends from the lower cutoff used in this study

(jet $p_T = 120$ GeV/c) up to the statistical limit of the available data sample (jet $p_T \approx 210$ GeV/c). Correlations of charged particle tracks with jets indicate that the momentum imbalance is accompanied by a softening of the fragmentation pattern of the second most energetic, away-side jet. The di-jet momentum balance is recovered when integrating low transverse momentum particles distributed over a wide angular range relative to the direction of the away-side jet. The results provide qualitative constraints on the nature of the jet modification in Pb-Pb collisions and quantitative input to models of the transport properties of the medium created in these collisions.

If the quark-gluon fluid is formed in heavy-ion collisions, it is expected to screen the confining potential of heavy quark-antiquark pairs, leading to the melting of charmonia (J/ψ , ψ' , ...) and bottomonia ($Y(1S)$, $Y(2S)$, $Y(3S)$, ...). The melting temperature depends on the binding energy of the quarkonium state. The ground states J/ψ , and $Y(1S)$, are expected to dissolve at significantly higher temperatures than the more loosely bound excited states. Quenched lattice QCD calculations predict that the $Y(nS)$ states melt at $1.2 T_c(3S)$, $1.6 T_c(2S)$, and above $4 T_c(1S)$, where T_c is the critical temperature at which the transition takes place to a quark-gluon fluid. CMS has observed suppression effects in the upsilon family [9]. More precisely the quantity measured is

$$\frac{[Y(2S+3S)/Y(1S)]_{PbPb}}{[Y(2S+3S)/Y(1S)]_{pp}} = 0.31^{+0.19}_{-0.15} \pm 0.03$$

It is significantly different from unity indicating that the production of the excited states $Y(2S)$ and $Y(3S)$ is being suppressed relative to that of $Y(1S)$.

4.3 The Search for New Physics

A very wide range of new physics has been searched [7]. Here we only can give a few examples.

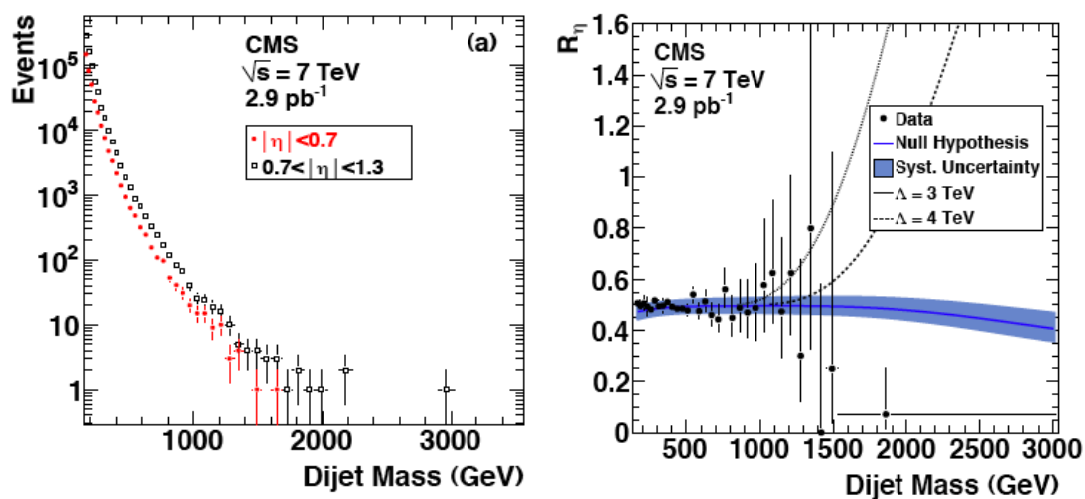


Fig. 6:(left) Event counts for di-jets in the two angular ranges examined, (right) the observed di-jet centrality ratio as function of m_{jj} compare with the null (QCD) hypothesis (solid line), including the total systematic uncertainty (band) and to hypotheses of quark contact interactions with $\Lambda=3$ TeV (dotted line) and 4 TeV (dashed line).

4.3.1 Search for Substructure

One of the first searches that is made at a new and higher energy accelerator is to look for sub-structure. In similarity with the experiment that Rutherford performed exactly 100 years ago we look for sub-structure in quarks by examining the production of quarks and gluons (jets) at large angles with respect to the beam-line. In QCD, the jet production rate peaks at small angles. Several new physics scenarios, including models of quark compositeness, produce a more isotropic angular distribution leading to enhanced jet production at large angles. The ratio, of the number of jet pairs produced in a more central region with that in an angular region closer to the beam-line, is compared with the predictions from QCD. No deviation is found from expectation (Fig. 6) and a limit is set on the size of the quarks is smaller than 5×10^{-18} cm.

4.3.2 Search for Supersymmetry

Even if the Higgs boson exists and is found (see Section 4.3.5), all is not completely well with the SM alone. The next question is “why is the mass of the Higgs boson so low”. If a new symmetry (supersymmetry) is the answer, then it must manifest itself at the 1 TeV energy scale. Supersymmetry, predicts a doubling of the known particle spectrum, each known particle would have a super-partner with its mass determined by the parameters of the model being considered. In models which conserve R-parity the lowest mass superpartner (LSP) is considered to be a prime candidate for dark matter. *R-parity* is defined as $P_R = (-1)^{S+3B+L}$, where S is the spin, B the baryon number and L the lepton number. The LSP is expected to escape detection leading to significant missing E_T in the final state. The rest of the cascade can result in an abundance of leptons, b -jets and/or τ -jets.

One example of such a search is to look for events with a large amount of hadronic transverse energy in events with multiple-jets and sizeable missing transverse energy. A quantity, α_T , is formed which quantifies the imbalance in the measured transverse energies of back-to-back “pseudo” jets. An excess of such events with respect to the predictions would indicate new physics. No such deviation from expectations is found and a limit on the mass of the squarks and gluinos is set at around $1 \text{ TeV}/c^2$ in the context of CMSSM [11]. Fig. 7 summarizes the current (August 2011) status of searches for supersymmetry in CMS using diverse signatures [7]. The searches are now starting to focus on well-motivated models where the squarks are at quite high masses ($\sim 10 \text{ TeV}/c^2$) with the gluinos around $1.5 \text{ TeV}/c^2$, the stops and sbottoms around $0.5 \text{ TeV}/c^2$.

4.3.3 The Search for Heavy Vector Bosons

Many models of new physics predict the existence of narrow resonances, at the TeV mass scale, that decay to a pair of charged leptons. These resonances are predicted in the context of Grand Unified Theories, theories with extra space dimensions, new strong interactions with a new charge such as “technicolour” in analogy with the “colour” charge of QCD, amongst others. A search has been made along the lines of W and Z production but at higher masses [12,13]. As can be seen from Fig. 7 no evidence has yet been found for such resonances and lower limits on their masses are set at around $2 \text{ TeV}/c^2$. In setting these limits the branching fraction to the leptonic decay modes has been assumed to be the one that is observed for the known W and Z

particles. This does not have to be the case, and if so the limits would then be correspondingly weaker.

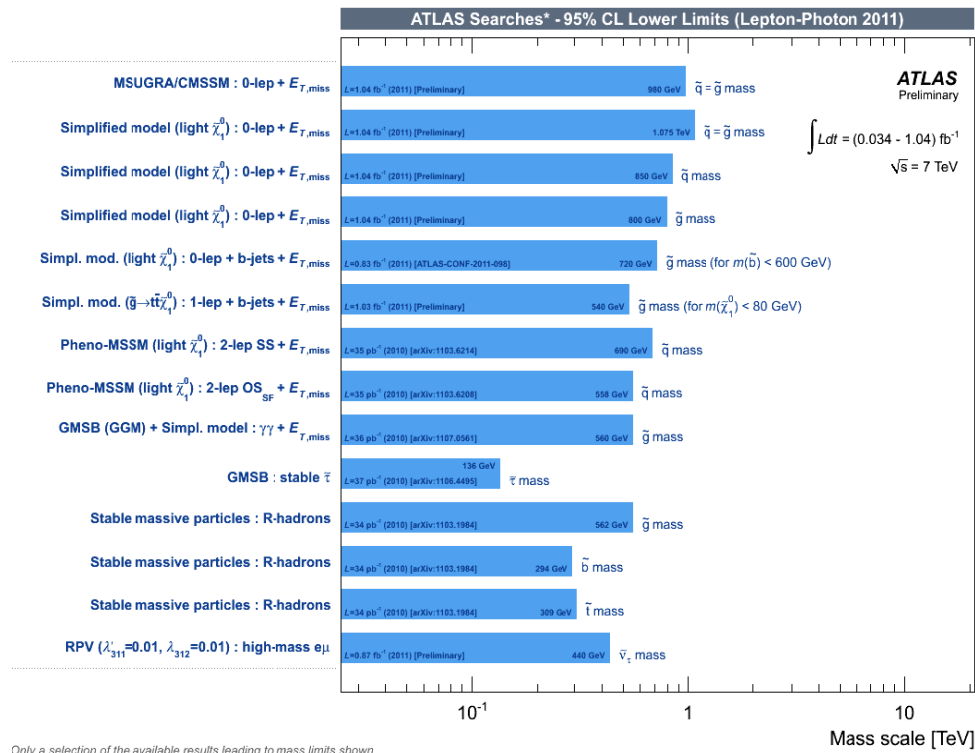


Fig. 7: The status of searches for supersymmetry in CMS using diverse signatures.

4.3.3 The Search for Heavy Vector Bosons

Many models of new physics predict the existence of narrow resonances, possibly at the TeV mass scale, that decay to a pair of charged leptons. These resonances are predicted in the context of Grand Unified Theories, theories with extra space dimensions, new strong interactions with a new charge such as “technicolour” in analogy with the “colour” charge of QCD, amongst others. A search has been made along the lines of W and Z production but at higher masses [12,13]. As can be seen from Figure 8 no evidence has yet been found for such resonances and lower limits on their masses is set at around 2 TeV/c². In setting these limits the branching fraction to the leptonic decay modes has been assumed to be the one that is observed for the known W and Z particles. This does not have to be the case, and if so the limits would then be correspondingly weaker.

4.3.4 Other Searches

Many other searches for new physics have been made in CMS [7]. These are summarized in Fig. 9.

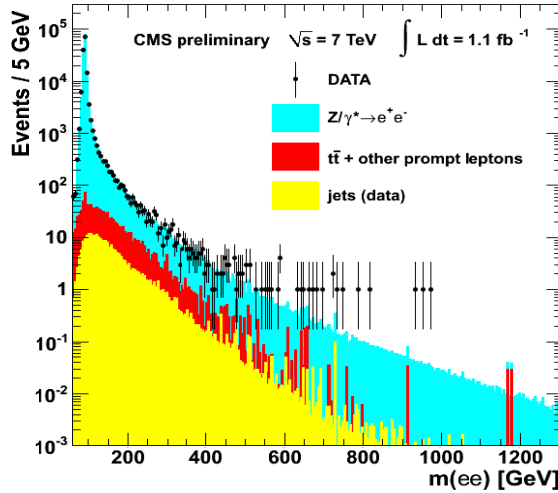


Fig. 8a: Invariant mass spectrum of e^+e^- events. The uncertainties on the data points (statistical only) represent 68% confidence intervals for the Poisson means. The filled histograms represent the expectations from SM processes as indicated in the legend.

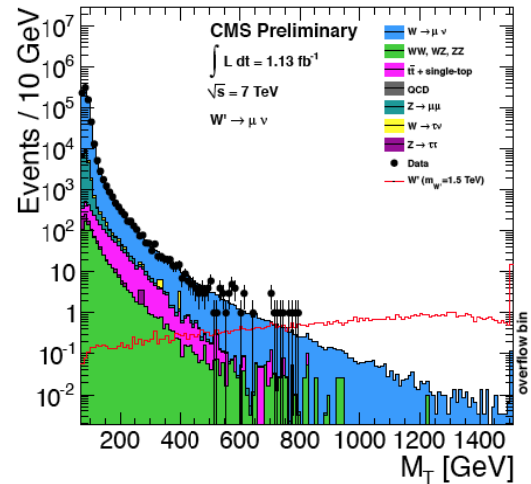


Fig. 8b: Transverse mass distribution for the muon channel. The uncertainties on the data points (statistical only) represent 68% confidence intervals for the Poisson means. The filled histograms represent the expectations from SM processes as indicated in the legend.



Fig. 9: The status of searches for new physics in CMS(not including Supersymmetry).

4.3.5 The Search for the Standard Model Higgs Boson

The detection of the SM Higgs boson was a particularly appropriate benchmark to test the performance of the experiment designs in the early 1990's. The Higgs boson is the only particle in the Standard Model that has not yet been seen by experiments. Its mass is not predicted by theory. Its production cross-section and natural width vary widely over the allowed mass range (114 GeV/ c^2 – 1TeV/ c^2). A search has to be made over

this wide mass range leading to diverse final states: two photons; two tau leptons; two W bosons; or two Z bosons. The W is observed through its decay to an electron plus a neutrino, or a muon plus a neutrino. The Z is observed through its decay to a pair of electrons, or a pair of muons, or a pair of jets of hadronic particles. Analysing all these channels ensures that the search is sensitive to observing the Higgs irrespective of its mass. Particularly challenging is the search in the low mass region, a region indicated by the precision electro-weak measurements, and proscribed by supersymmetry ($M_H \leq 135 \text{ GeV}/c^2$). CMS chose the lead tungstate crystals electromagnetic calorimeter partly to address the search in this region.

Analysis of the full 2011 data set is being pursued vigorously but the results presented here are the ones presented at the August 2011 International Symposium for Lepton-Photon Interactions at High Energies [14 and references therein]. The data from the two high mass-resolution channels is shown in Fig. 10. No excess is observed. Figure 11 summarizes the status of the search for the SM Higgs boson in CMS. So far we have not examined a sufficient number of such collisions to make any meaningful statement about the existence or not of the Standard Model Higgs boson in the mass range favoured by previous results (115 and 135 GeV/c^2). Nevertheless, current data disfavour, at a confidence level of 95%, the existence of a Higgs boson in the hatched ranges.

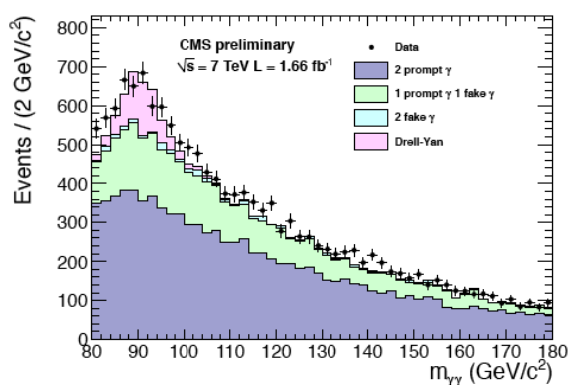


Fig. 10a: Diphoton mass distribution for data (points) and Monte Carlo simulation of SM processes which constitute the background to the search (histograms).

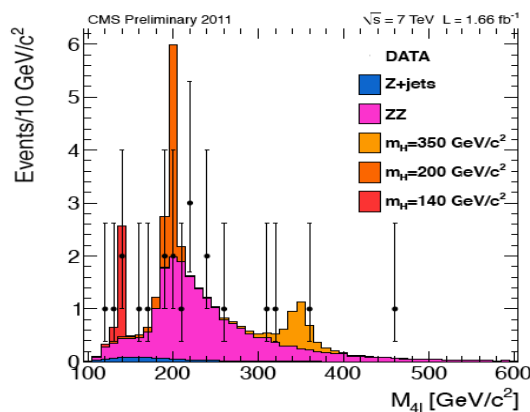


Fig. 10b: Distribution of four-lepton reconstructed mass for all 4l channels (ee, eμ, μμ). Points represent data, shaded histograms represent the signal and background expectations.

Figure 12 shows the best fit of the observed cross-section to the one predicted for the SM Higgs boson as a function of its mass. It can be concluded that in the mass range 114-135 GeV/c^2 a SM Higgs boson could still exist but, if found in this range the SM theory would still be incomplete; if found beyond 600 GeV it would become so strongly coupled needing some new physics; it could still be found in the range 135-500 GeV/c^2 but it would not have SM couplings – they would be weaker by some amount – and again some new type of physics would be needed. Even more interesting, especially from an experimentalist's point of view, would be if the Higgs boson were not to exist – this would really force us to rethink the ideas we have been pursuing over the last half a century!

It is anticipated that by the end of 2011 we shall have examined some 300 trillion proton-proton collisions and more significant results can be presented.

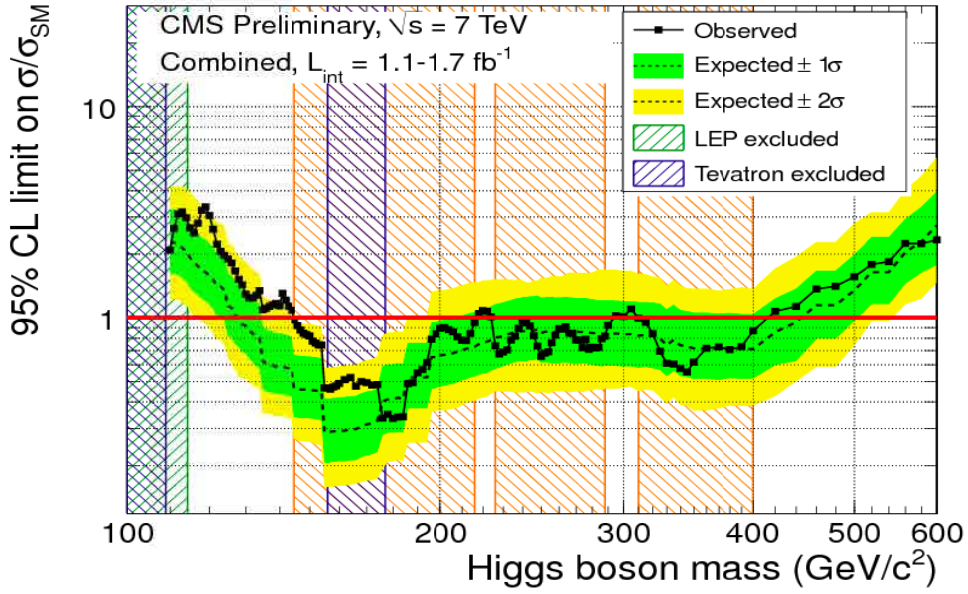


Fig. 11: The 95% CL upper limits on the signal strength parameter $\mu = \sigma/\sigma^{\text{SM}}$ for the SM Higgs boson hypothesis as a function of the Higgs boson mass. The dashed line indicates the median expected results for the background-only hypothesis while the green (dark) and yellow (light) bands indicate the ranges that are expected to contain 68% and 95% of all observed excursions from the median, respectively.

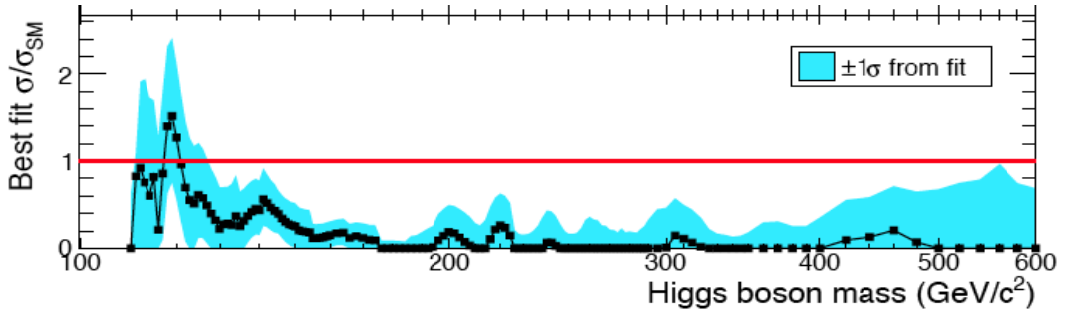


Fig. 12: The ratio of the best fit of the observed cross-section to the one predicted for the SM Higgs boson as a function of its mass

4.3.5 Physics Summary and Outlook

No sign of new physics has yet been found. However, these are early days and only a small fraction of the number of proton-proton collisions finally expected has been examined. By the end of 2012 we shall have increased, by a factor of 10, the sample used for the results presented here. This will not only allow a more precise confrontation with the predictions for known physics, but also the extension of the searches for new physics, and especially the making of a meaningful statement as to the existence or not of the Standard Model Higgs boson.

5. CONCLUSIONS

The LHC project (the accelerator and experiments) was conceived and designed to tackle fundamental questions in science: about the origin, the evolution and the composition of our universe. In particular, what is the origin of mass, what constitutes dark matter, do we live in more than 3 space dimensions, why is the universe composed of matter, and not anti-matter, and more.

CMS, the accelerator and the other LHC experiments, are unprecedented instruments in scale and complexity operating in an unprecedented & hostile environment. Driven by the science many technologies have been pushed to their limits in their construction.

After twenty years of design, R&D, prototyping, construction, assembly and commissioning CMS is recording high-energy collisions. It is operating well and has become a “physics-producing engine”. Much physics has already come out and it is exploring new territory but we are just at the beginning of this adventure and all the expectations are that what we shall find at the LHC will alter the way we view the universe at the fundamental level.

ACKNOWLEDGEMENTS

We would like to thank the Pontifical Academy of Sciences and Professor A. Zichichi for the invitation to this very interesting Symposium, and for the generous hospitality in the Vatican City. It was quite a privilege and honour to present first results from the CMS experiment in such august surroundings and to such an august audience.

REFERENCES

- [1] The Large Hadron Collider: a Marvel of Technology, ed. L. Evans, EPFL Press, 2009.
- [2] The CMS Collaboration, The CMS Experiment at the CERN Large Hadron Collider, JINST 3 (2008) S-8004.
- [3] T. Virdee, Physics World, Vol. 17 (2004) 35.
- [4] CMS Collaboration 2010, Search for Quark Compositeness with the Dijet Centrality Ratio in pp Collisions at $\sqrt{s} = 7$ TeV, *Phys. Rev. Lett.* 105 (2010) 262001
- [5] CMS Collaboration 2011, Measurements of Inclusive W and Z production cross Sections in pp Collisions at $\sqrt{s} = 7$ TeV with the CMS Experiment, *J. High Energy Phys.* 10 (2011) 132
- [6] CMS Collaboration, Combination of top quark pair production cross section measurements, available from reference [7]
- [7] All CMS public results are available on the site: <http://cms.web.cern.ch/org/cms-papers-and-results>
- [8] CMS Collaboration 2010, Observation and studies of jet quenching in Pb-Pb Collisions at $\sqrt{s_{NN}} = 2.76$ TeV, *Phys. Rev. C* 84 (2011) 024906

- [9] CMS Collaboration 2011, Indications of Suppression of Excited Υ States in Pb-Pb Collisions at $\sqrt{s_{NN}} = 2.76$ TeV, *Phys. Rev. Lett.* 107 (2011) 052302
- [10] CMS Collaboration 2010, Search for Quark Compositeness with the Dijet Centrality Ratio in pp Collisions at $\sqrt{s} = 7$ TeV, *Phys. Rev. Lett.* 105 (2010) 262001
- [11] CMS Collaboration, Search for Supersymmetry at the LHC in Events with Jets and Missing Transverse Energy, *Phys. Rev. Lett.* 107 (2011) 221804
- [12] CMS Collaboration, Search for Resonances in the Dilepton Mass Distribution in pp Collisions at $\sqrt{s} = 7$ TeV, available from reference [7]
- [13] CMS Collaboration, Search for W' in the leptonic channels in pp Collisions at $\sqrt{s} = 7$ TeV, CMS PAS EXO-11-024, available from reference [7]
- [14] CMS Collaboration, Combination of CMS Searches for a Standard Model Higgs boson, CMS PAS HIG-11-032, available from reference [7]

THE ALPHA MAGNETIC SPECTROMETER (AMS) EXPERIMENT

■ SAMUEL TING

Massachusetts Institute of Technology

Presented at the International Symposium on Subnuclear Physics: Past, Present and Future, November 1, 2011



Figure 1: *The AMS Detector was installed on the International Space Station (ISS) on May 19, 2011 to conduct a program of fundamental physics research. AMS will continue to collect data for the entire lifetime of the ISS.*

The Alpha Magnetic Spectrometer (AMS) is a particle physics detector designed and built to explore some of the most fundamental issues shared by physics, astrophysics and cosmology on the origin and structure of the universe. As an external payload onboard the International Space Station, AMS will study with unprecedented precision, to one part in ten billion, the composition of primary cosmic rays originating in stars and galaxies billions of light years beyond our Milky Way. AMS originated from discussions at the Erice Center. The scientific objectives discussed in Erice included searching for cosmic antimatter, studying the origin of dark matter, and exploring cosmic rays to the TEV region. The most exciting objective of AMS is to explore the unknown from the unique vantage point of space. AMS is the first precision magnetic particle physics detector in space. AMS involves an international collaborating composed of 16

countries, sponsored by the U.S. Department of Energy (DOE) and in close cooperation with the National Aeronautics and Space Administration (NASA).

The scientific importance of AMS is based on the early seminal work of A. Zichichi as exemplified in Figures 2a, 2b, 3, 4, 5 and 6.

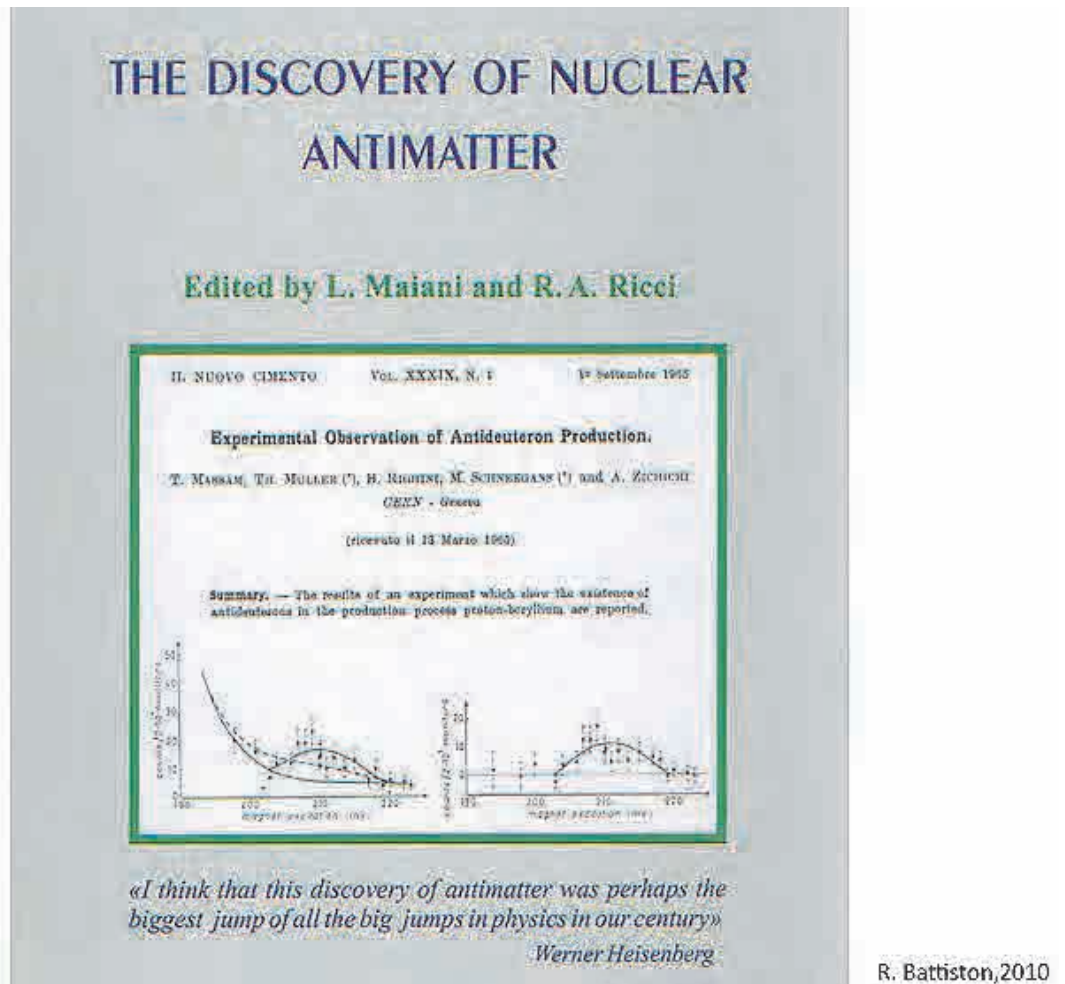
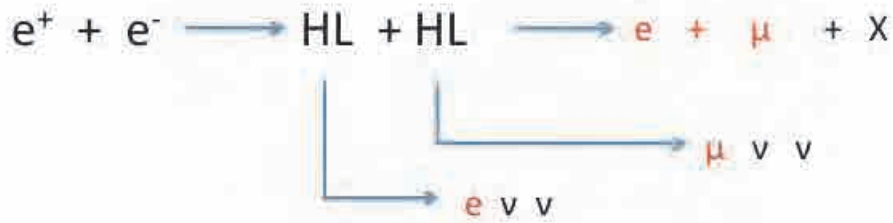


Figure 2a: *The Discovery of Nuclear Antimatter* based on seminal work by A. Zichichi on the *Experimental Observation of Antideuteron Production* (1965) published in *II Nuovo Cimento*.

Search for Heavy Leptons (HL) 1970-1972(ZICHICHI)



R. Battiston, 2010

Figure 4: Pioneering work by A. Zichichi on search for heavy leptons (1970-72).

Heavy Lepton search regions using the ADONE e+e- storage ring at Frascati

Limits on the Mass of Heavy Leptons, M. Bernardini, A. Zichichi *et al.*, Nuovo Cimento 17A, 383 (1973)

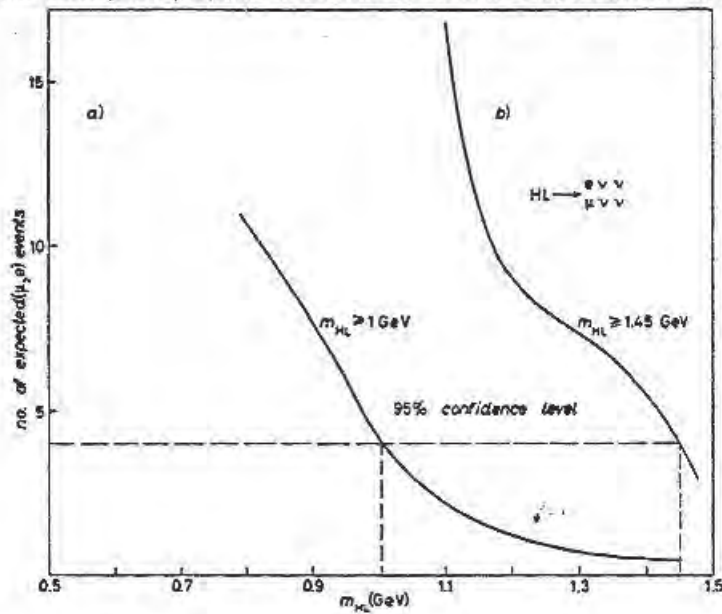


Fig. 2. - The expected number of (μ^+e^+) pairs vs. m_{HL} for two types of universal weak couplings of the heavy leptons. The dashed lines indicate the 95% confidence levels for m_{HL} . a) HL universally coupled with ordinary leptons and hadrons, b) HL universally coupled with ordinary leptons.

R. Battiston, 2010

Figure 5: Published results of heavy lepton search at ADONE by A. Zichichi.

How does the muon differ from the electron?

Experiments at SLAC on muon-proton deep inelastic scattering are part of the continuing search for differences between the muon and the electron.

Martin L. Perl

34 PHYSICS TODAY / JULY 1971

Fortunately these problems can be overcome in the newly developed electron-positron colliding-beam accelerators where charged leptons can be copiously produced through the process⁵

$$e^+ + e^- \rightarrow \mu^+ + \mu^-$$

Within five years, through this process, we shall know if the electron-muon family has additional members with masses in the several-GeV ranges.

5. V. Alles-Borelli, A. Zichichi et al., *Limits on the Electromagnetic Production of Heavy Leptons*, *Nuovo Cimento Letters* 4, 1156 (1970)

R. Battiston, 2010

Figure 6: Excerpt from *Physics Today* article dated July 1971.

Indeed, the study of leptons from pp collisions have resulted in the discoveries of the J particle, the Upsilon, the Z and W particles, and so forth.

The AMS Detector instrumentation is based on ground based accelerator physics technology but adapted to withstand the hostile environment of space, including forces of 3-12 g's at launch. For AMS, the instrumentation is required to operate flawlessly in zero gravity without the possibility of astronaut intervention for repair or maintenance.

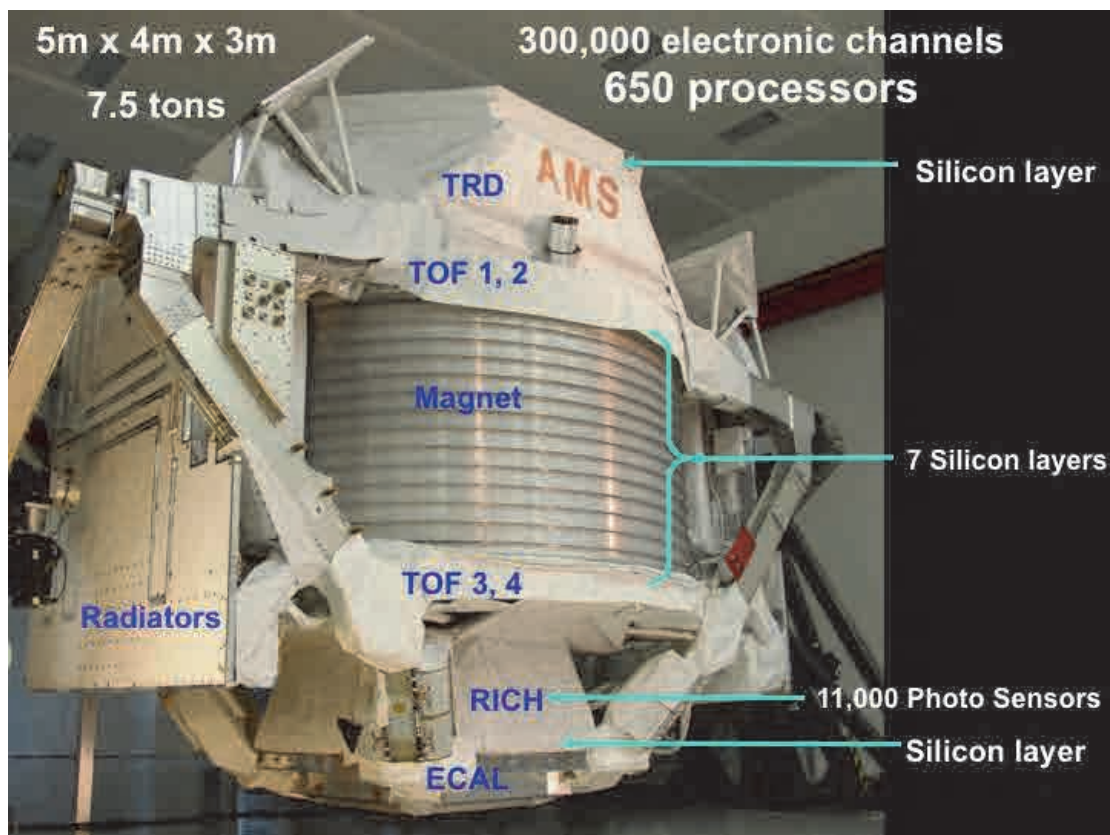


Figure 7: The 7.5 ton AMS Detector contains an array of sub-detectors, 650 processors and many complex systems to ensure its safe and successful performance in space.

As shown in Figure 7, AMS measures 5m x 4m x 3m and weighs 7.5 tons. It was built to fit within the Unique Support Structure (USS), constructed by NASA, which cradles the Detector within the shuttle cargo bay during its journey to the Space Station as well as to the attachment site on the Space Station external truss.

To ensure mission success, many modules were constructed for each sub-detector component, the magnet and the 60 microprocessors (Engineering modules (EM), qualification modules (QM), flight modules (FM) and flight spare modules (FS)), so that every system could be thoroughly tested and space qualified. Multiple redundancies have been built in every flight system, some as much as 400%. Associated with the detector instrumentation, are complex systems such as ultra fast electronics, thermal control, ground and flight software, alignment and positioning systems, interface and support structures, etc. These systems have also been developed specifically for AMS and have pushed existing technology to the limit.

Since particles are defined by their mass, charge and energy, the AMS Detector has been designed and built to contain a magnet and an array of the state of the art precision particle detectors. Together, this instrumentation defines and characterizes the charged particles that pass through AMS from the far reaches of space. The main subdetector components and their functions are illustrated in Figure 8.

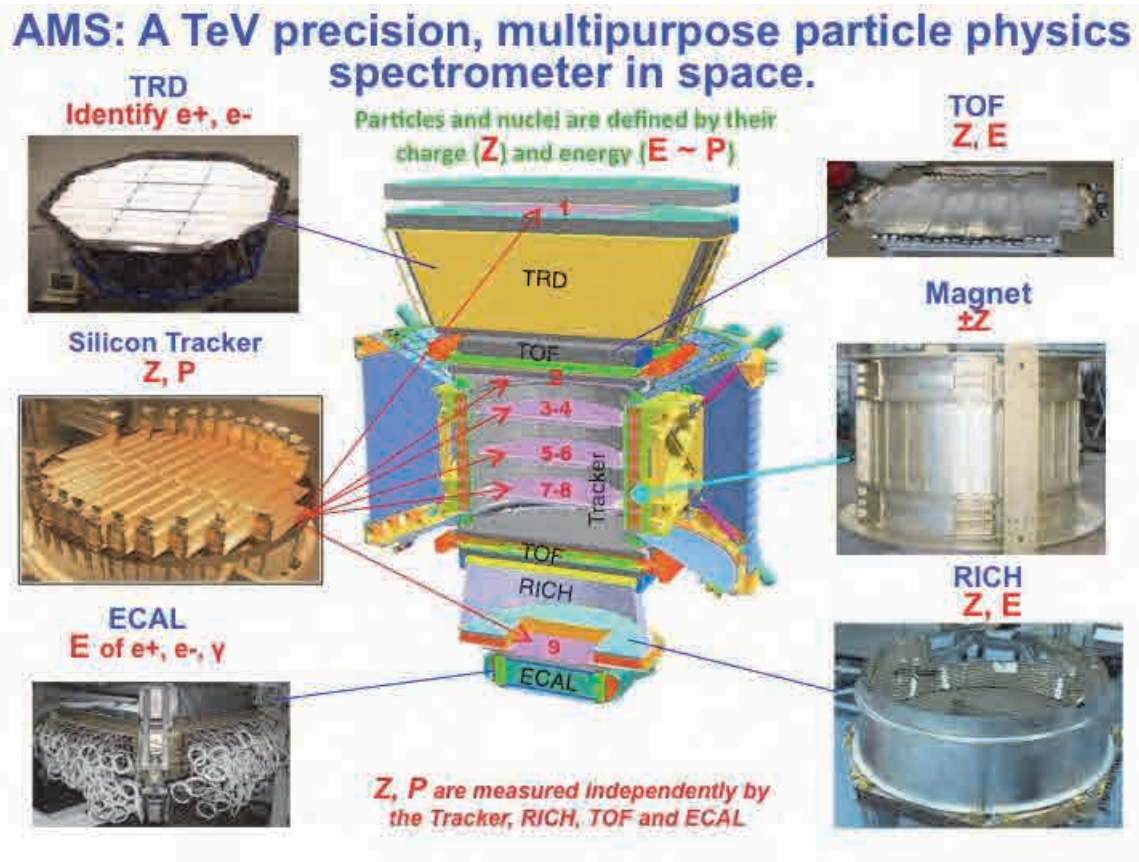


Figure 8: Cut-away view of the AMS Detector showing the arrangement of its precision detector components.

The centerpiece of the AMS Detector is the large volume permanent magnet that measures the sign of the charge and momentum of each particle traversing AMS. Particles and anti-particles will be identified according to their bending trajectories in the magnetic field.

The magnet was made of 4,000 blocks of Neo-dymium Iron Boron ($\text{Nd}_2\text{Fe}_{14}\text{B}$) with a field intensity of 1,400 Gauss. The magnet was flown successfully on the ten day AMS-01 mission (STS-91) in 1998. Thirteen years after this flight, the magnet was tested and the field map showed no change in the magnetic field with the experimental

accuracy of about 1%. Originally built in China, there were ten magnets fabricated for tests including one to test to destruction. The magnet was designed and built to eliminate the effect of torque on the Shuttle or ISS instruments and underwent intensive space qualification testing including vibration, centrifugal acceleration and static loading. The magnet was approved and certified for flight by the AMS NASA Lockheed Martin team.

The Magnet

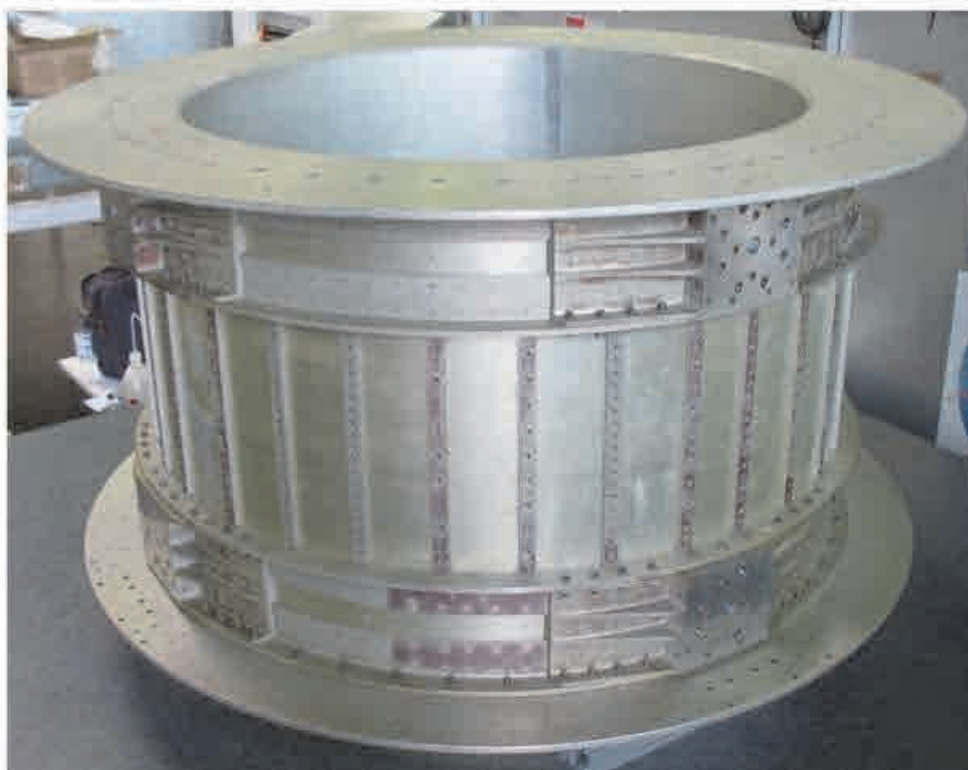


Figure 9: *The AMS Permanent Magnet was flown in the AMS-01 mission (STS-91) in 1998 and in the AMS-02 mission on the ISS in 2011.*

The extended lifetime of the International Space Station agreed by NASA and all the ISS international partners meant that the AMS Experiment would be active for more than the three years as originally planned with the use of a superconducting magnet. To remain operational for the full lifetime of the ISS, the AMS Collaboration installed the Permanent Magnet and optimized the geometry of the Detector by adding more silicon planes and rearranging the existing silicon planes thereby increasing the measurement arm. This technique recovered the full sensitivity (within 10% or less) for AMS on matter antimatter separation and tests showed that the momentum resolution is maintained.

As seen in Figure 8, the Transition Radiation Detector (TRD) is located on the upper portion of the AMS Detector. Its purpose is to identify and distinguish electrons and positrons from other cosmic rays. Since positrons can be mistaken for protons at high energies, the TRD suppresses the proton background which is important in the search for Dark Matter. Unlike the proton, the electrons and positrons emit transition radiation gamma rays while crossing the TRD radiator surfaces. These gamma rays are recorded when electrons and positrons pass through the 20 layers of 6mm diameter straw tubes alternating with 20 layers of polyethylene/polypropylene fleece radiator. The large number of surfaces increases the probability of the production of transition radiation gamma rays. As electrons and positrons pass through the TRD, the gamma rays start an ionizing cascade near a gold plated thin wire at high voltage. The abrupt current change induces a fast electric signal that can be read out at the end of the wire through a custom made Data Acquisition (DAQ) Microprocessor system. In this way, the identification of electrons and positrons is determined and protons are rejected. Of the 9,000 proportional mode straw tubes built, 5,248 were selected based on their leak rate. Samples were measured in a CAT scan at a hospital during night time hours to verify the centering accuracy of the signal wires to 100microns. The leak tight straw tubes are filled with an 80/20 ratio mixture of Xenon and CO₂ at 1 bar absolute pressure from a re-circulating gas system. The gas system is carefully regulated to eliminate contamination and ensure stable pressure. Gas supply and circulation is continuously monitored. The endurance of the consumables based on usage and leak rate has been studied and data has shown that the consumables are sufficient to maintain the operation of the TRD for 20 years in space.



Figure 10: *The octagonal mechanical structure of the Transition Radiation Detector was made of a light-weight carbon fiber and aluminum honeycomb sandwich material to support the 328 modules. Each module contains 16 straw tubes interleaved with the 20 layers of fleece radiators.*

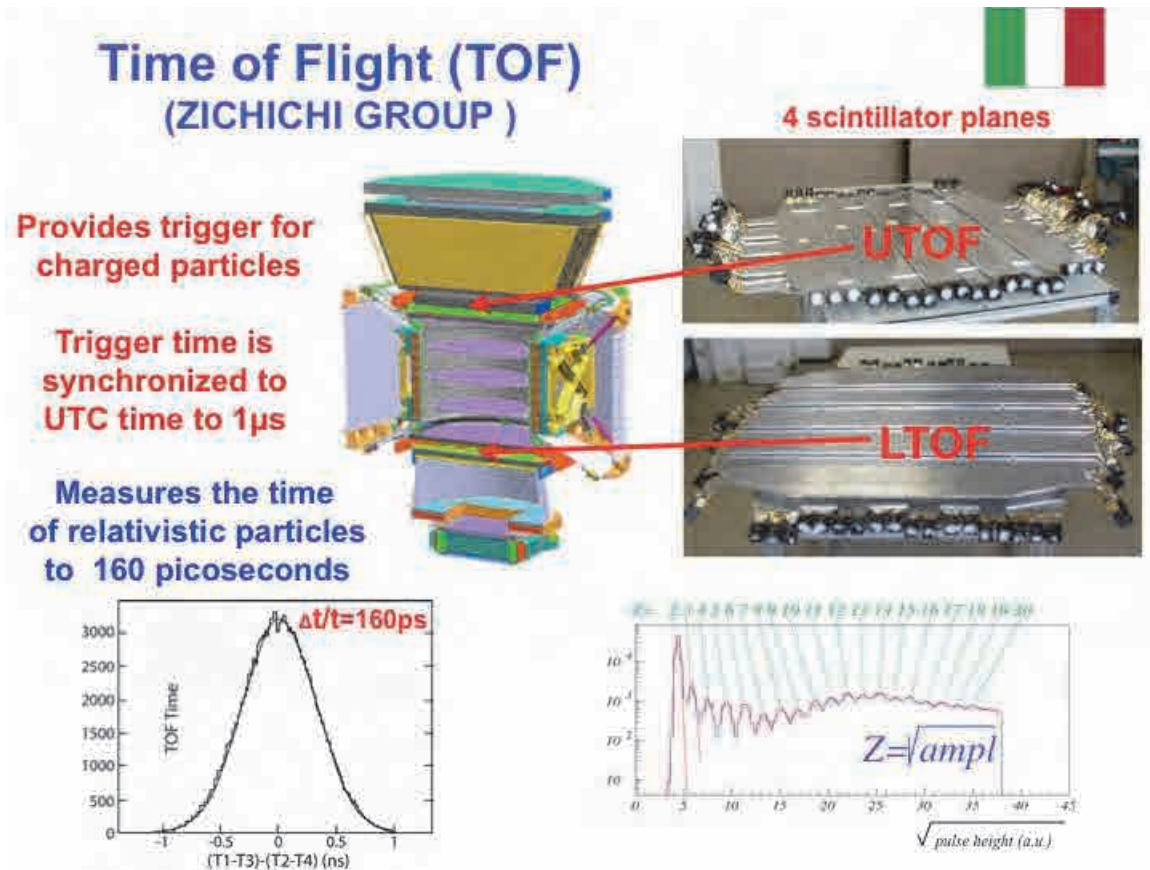


Figure 11: The Time of Flight system consists of four planes of scintillation counters containing paddles aligned along the x and y coordinates. Plexiglass light guides connect the scintillator assemblies to photomultipliers (PMTs). The light emitted by the charged particles interacting with the scintillating medium is collected by the light guides on the PMTs which convert the fluorescence light into a signal.

The upper and lower layers of the TOF detects the incoming signal of cosmic rays as well as measuring the mass, charge and energy of charged particles. The trigger time for the entrance and exit of the charged particles through the TOF is synchronized to the Universal Time Clock (UTC) to 1 microsecond. The upper and lower TOF measure the time of relativistic particles to 160 picoseconds as they travel at a velocity up to the speed of light.

When a particle enters the Upper and Lower TOF it triggers all the AMS subdetectors (Tracker, TRD and E-cal...) to collect data which is subsequently processed and stored. The level 1 trigger of the data acquisition system is initiated using information from the TOF (for charged particles), ACC (for veto information) and E-cal (for neutral particles). In addition, the TOF is capable of providing reliable information on the absolute charge of a particle that will definitively identify nuclei such as Helium, Carbon, Silicon and so forth.



Figure 12: *Professor A. Zichichi and physicists from INFN/Bologna at the AMS Clean Room at CERN during AMS Detector assembly.*

The array of Anti-Coincidence Counters (ACC) makes up the Veto system. The counters provide a signal that a cosmic ray has entered the detector side-ways. AMS is designed to analyze only particles that traverse the whole detector from the top to the bottom so the ACC counters reject the stray cosmic rays out of the two thousand particles per second, that traverse AMS. The veto system has been designed and tested to reach an efficiency of 0.99999.

The ACC consists of 16 paddles arranged on a cylindrical barrel surrounding the Tracker. The light coming from the scintillating paddles is collected in wavelength shifting fibers of 1 mm diameter embedded in grooves milled into the scintillation material. At both ends of the paddle, fibers are routed in 2 bunches of 37 fibers each to optical connectors located on the conical flanges of the magnet vacuum case (see Figure 13). From these connectors the light goes through clear fibers to 8 photomultiplier tubes (PMT) mounted on the rim of the vacuum case. The PMTs are oriented with axes parallel to the stray field in order to minimize the magnetic field effect.

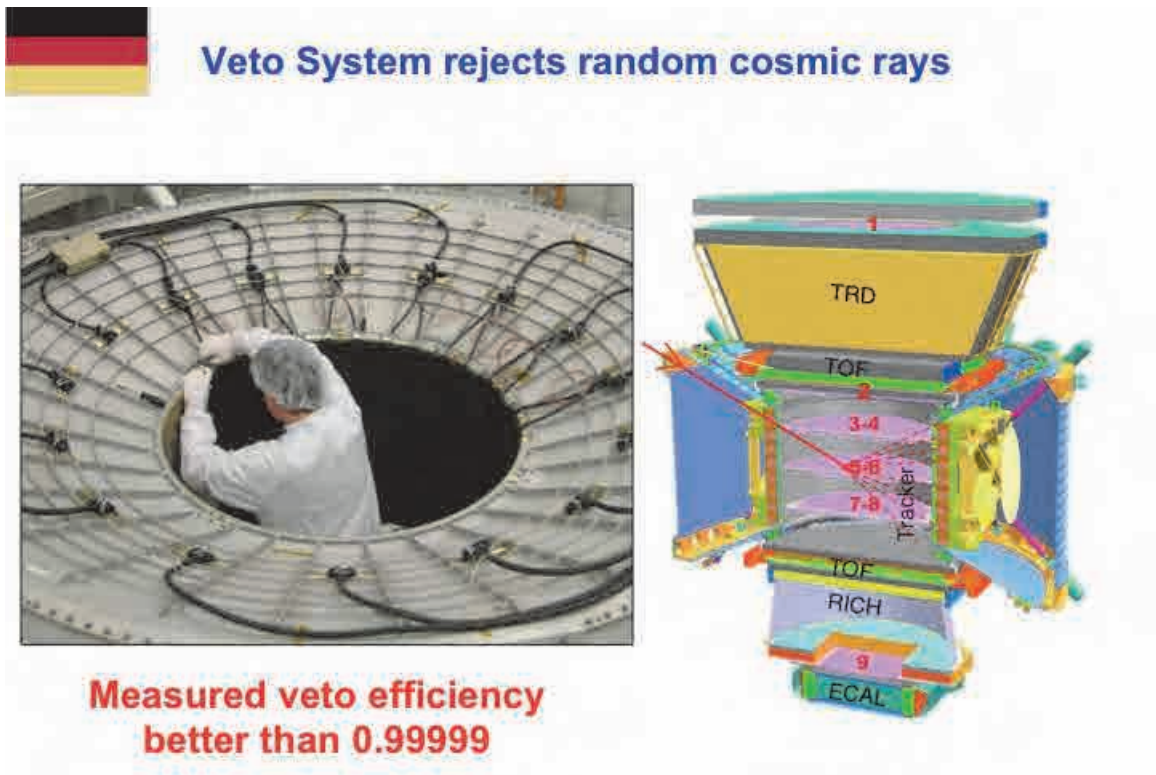


Figure 13: The installation of the Anti-Coincidence Counters (ACC) into AMS at CERN.



Figure 14: A view of the Silicon Tracker wafers and microbonds under a microscope. The Tracker provides a coordinate resolution of 10 microns.

The Silicon Tracker contains 200,000 channels. Nine layers of precision silicon measure the charge and momentum of the particles with unprecedented accuracy (a coordinate resolution of 10 microns).

The Tracker measures the curvature of the particles traversing the magnet. The curvature measurement allows the particle momentum (mass multiplied by velocity) to be determined. The pulse height in the Tracker measures the charge Z of the incoming nuclei or particle. Particle rigidity is the particle momentum divided by charge ($R=p/Z$). High energy particles are more rigid than low energy particles. Two particles with the same momentum could have different rigidities (i.e., the one with the higher charge is less rigid than the others). Since the Tracker measures the curvature, the corresponding rigidity can be immediately derived and if the charge Z is also measured then the particle momentum can be calculated.

The basic element of the Tracker is the double-sided micro strip sensor. There are 2,264 such sensors assembled in 192 readout units, called ladders. Each sensor consists of a substrate of high purity doped silicon 300 μm thick. The two sides of the substrate aluminum strips run in orthogonal directions. A position resolution of 10 μm is provided when a charged particle crosses the silicon substrate. The sum of the electric signals on the strips is proportional to the square of the absolute charge of the particle. The online processing of the Tracker data is performed by the dedicated Tracker Data Reduction boards. The readout electronics are characterized by a very low power consumption with low noise and large dynamic range.

There are 9 planes with 200,000 channels aligned to 3 microns

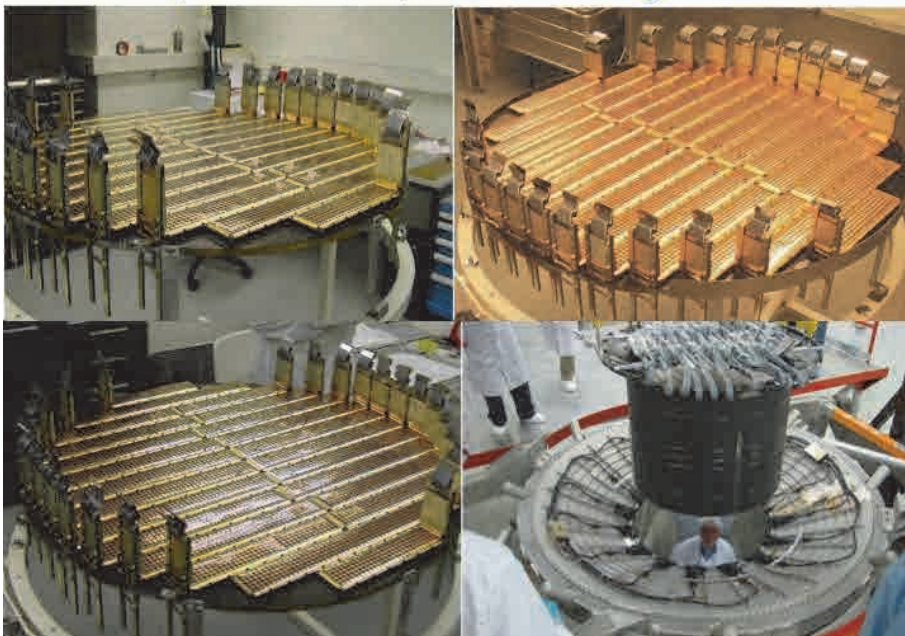


Figure 15: There are a total of nine Tracker planes. Seven Tracker planes are located within the magnet bore, one is mounted on top of the TRD and one is mounted below the RICH detector.

The Ring Image Cerenkov Counter (RICH) measures the charge and energy of passing particles by precisely determining their velocities with an accuracy of 0.1%. Both the charge and the velocity are calculated from the geometrical shapes, circles or rings, generated by the Cerenkov effect.

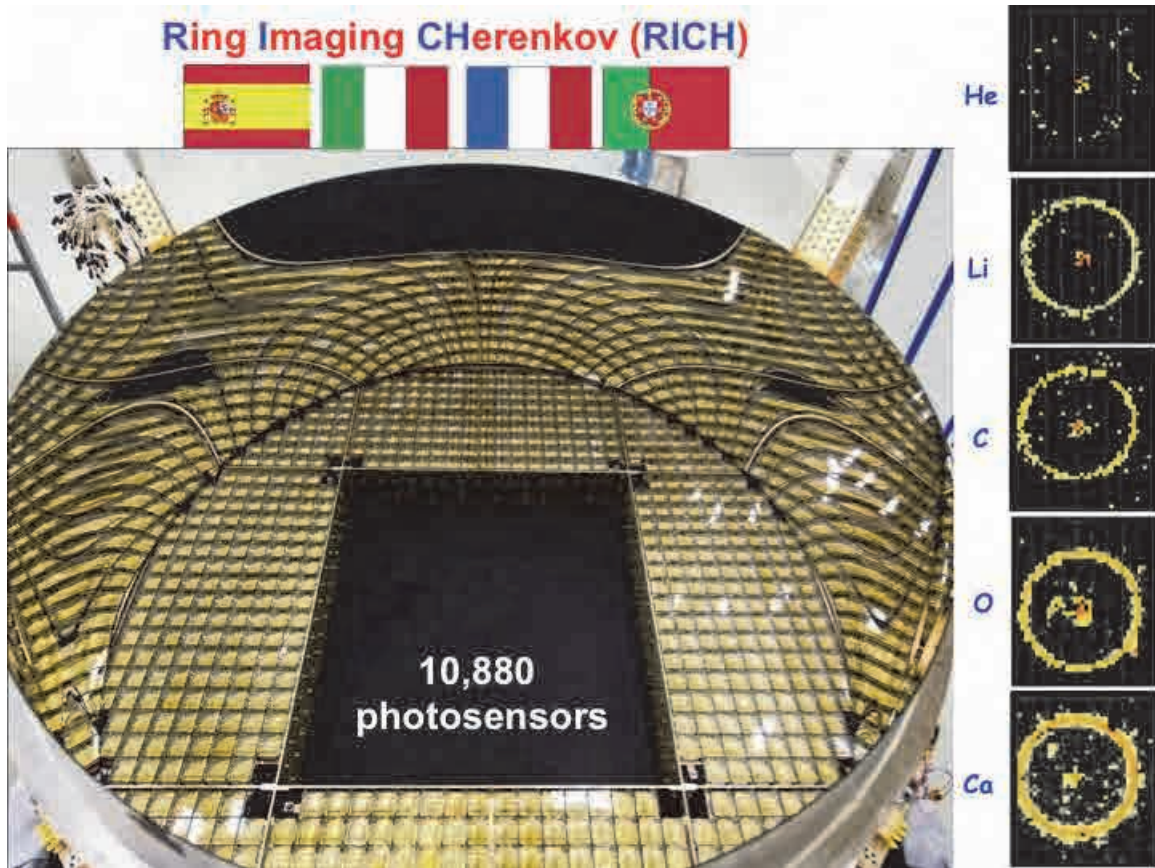


Figure 16: The RICH contains 10,880 photosensors to measure the velocity and charge of passing particles.

The RICH detector consists of a radiator plane, a conical mirror and a photon detection plane. The radiator produces the Cerenkov radiation with an array of 2,7 cm thick aerogel tiles and a refractive index between 1.03 surrounding a central region equipped with 5mm thick Sodium Fluoride (NaF) with a refractive index of 1.3. This combination optimizes the overall acceptance for different energy ranges since the Cerenkov photons radiated by the NaF in a large cone will fall within the detection area. The detector plane has an empty area in its center that matches the active area of the Ecal that is located immediately below the RICH. Around the exterior of the open space, 10,880 photosensors are arranged in a matrix to cover the circular surface at the bottom of the conical mirror. The radiator and the detection plane are enclosed in the column of the conical reflector multi-layer structure on a carbon fiber reinforced composite substrate.

The mirror amplifies the RICH acceptance reflecting high inclination photons and provides the necessary photon drift ring expansion.

Mass and nuclear charge are fundamental properties of particles and nuclei. Mass and charge are independently measured in AMS through the Tracker, Time of Flight and RICH. Velocity is measured by the RICH and Time of Flight. The RICH was designed to provide velocity measurements with a resolution of 0.1% for charged particles and $\sim 0.01\%$ for ions. Since energy is dependent on velocity $= \frac{1}{2}mv^2$, the RICH with its accurate velocity can be measured to an accuracy of 1/1000 and simultaneously nuclear charge can be identified up to Cu.

The Electromagnetic Calorimeter (E-cal) is a 3-dimensional instrument made of 1,200 lbs of lead sandwich and 50,000 optical fibers and measures the energy and direction of TeV light rays and electrons with high precision (see Figures 17 and 18).

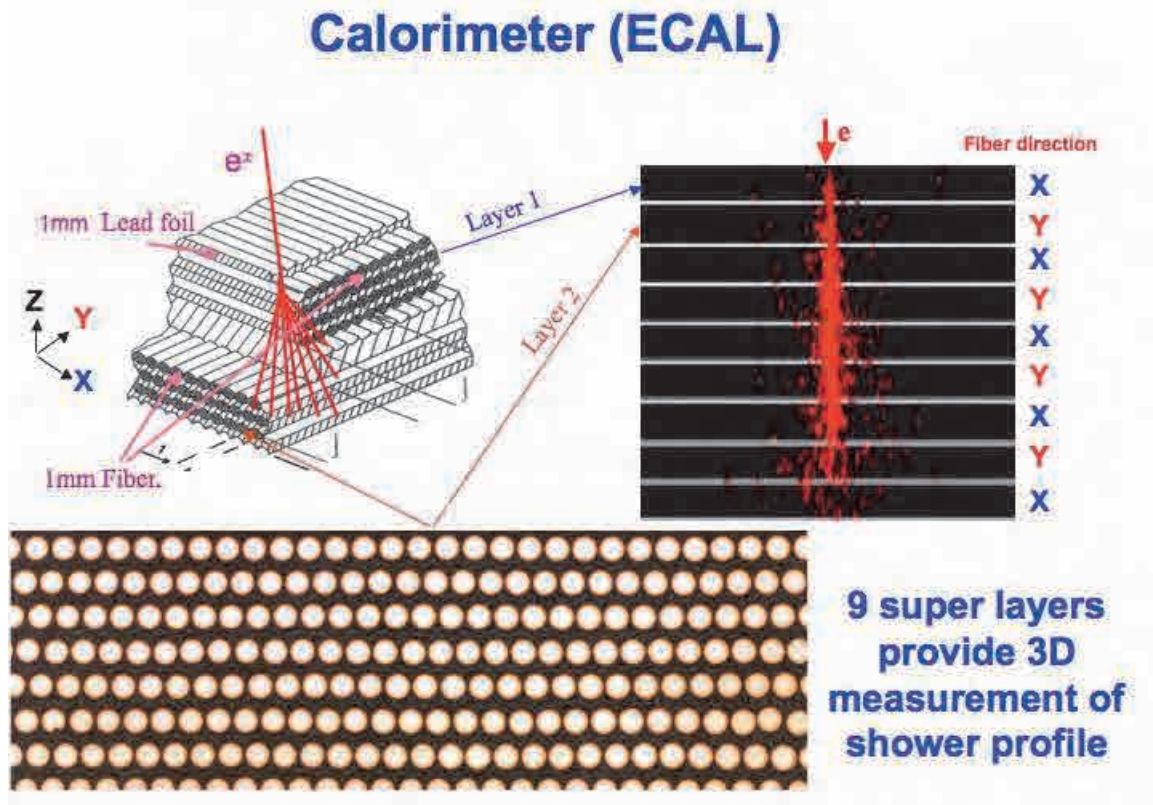
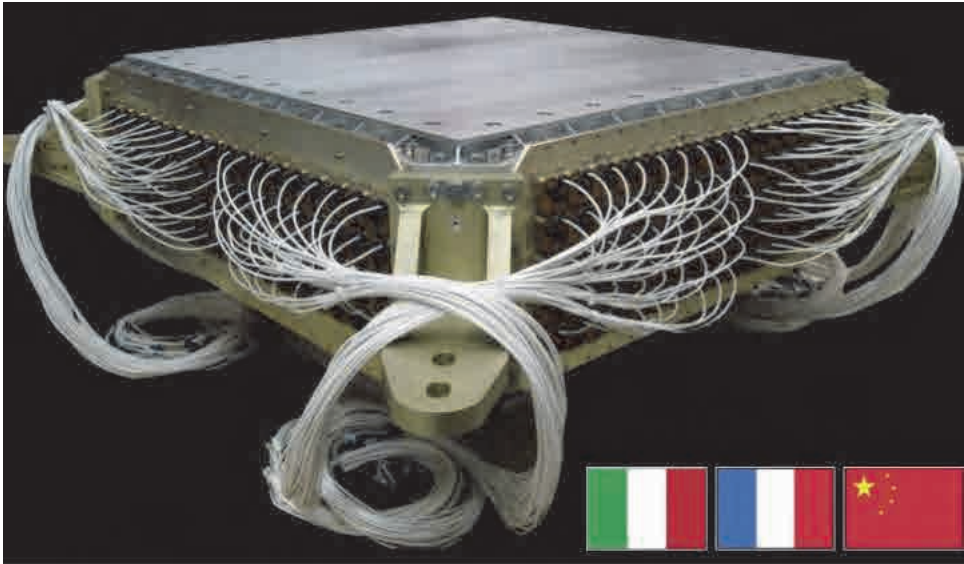


Figure 17: The principle and structure of the Electromagnetic Calorimeter.



50,000 fibers, $\phi=1\text{mm}$, distributed uniformly inside 1,200 lb of lead which provides a precision, 3-dimensional, $17X_0$ measurement of the directions and energies of light rays and electrons up to 1 TeV

Figure 18: Two Electromagnetic Calorimeters were built: one for space qualification tests and one for flight.

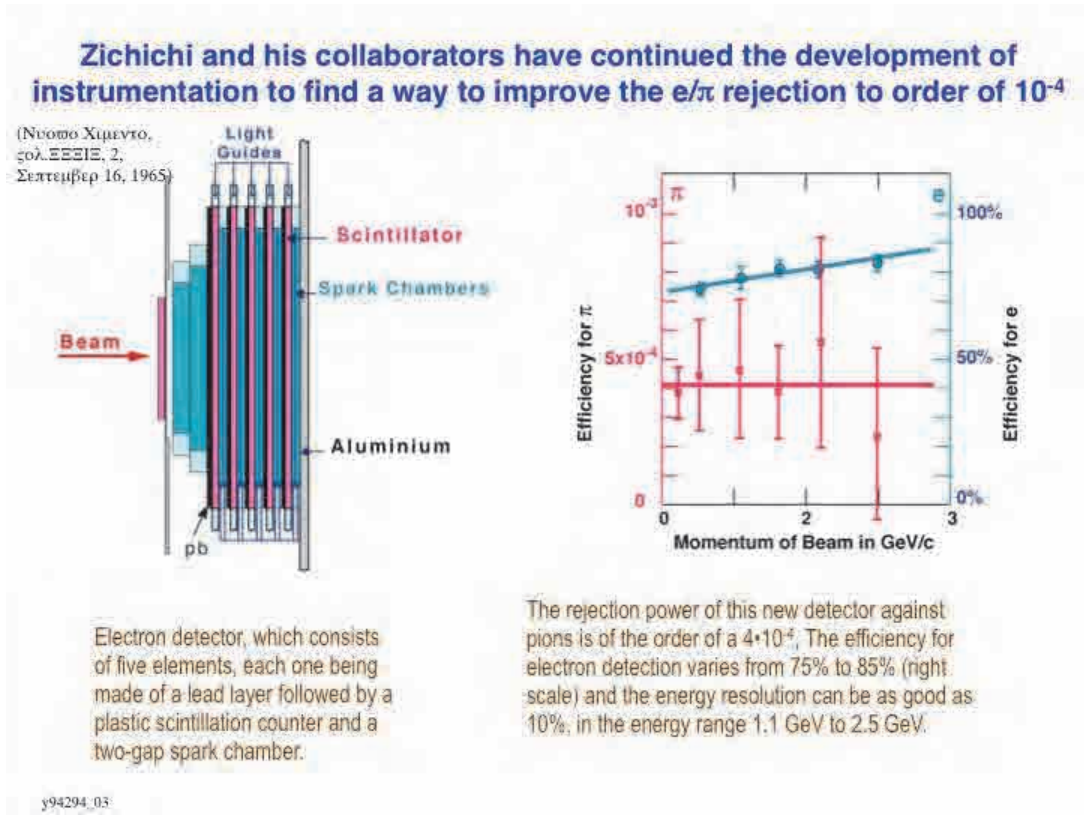


Figure 19: Successful instrumentation development using an electron detector has been carried out by A. Zichichi and his collaborators to significantly improve the rejection power against pions.

The E-cal consists of a pancake structure composed of 9 superlayers. Each superlayer is 18.5mm thick and is made of 11 grooved, 1 mm thick lead foils interleaved with layers of 1mm diameter scintillating fibers glued together. The detector imaging capability is obtained by arranging the superlayers with fibers alternating parallel to the x axis (5 layers) and y Axis (4 layers). Electrons, positrons and gamma rays interact in the dense material of the E-cal producing an electromagnetic shower of lower energy particles. From the shape of the shower it is possible to reconstruct the direction and energy of the incident particle. This is particularly important for the measurements of high energy photons. The shower ends either when secondary particles are absorbed or when they are able to escape from the material. In this way the E-cal distinguishes positrons and protons. Protons and heavy nuclei interact in a different way producing a different type of shower with a characteristic wider shape. The shower shape can also contribute to the reconstruction of the direction of the incident particle to a precision of a few degrees. Also, the E-cal is able to follow a 3-D shower profile at 18 different depths. Its precision will enable AMS to identify one positron from 10,000 protons. The E-cal thus works in concert with the TRD in its powerful rejection capability of protons and nuclei. The AMS E-cal follows the original development on preshower sampling technology invented by A. Zichichi as shown in Figure 19.

The ultra-precision of the AMS detector enables it to measure the particles with an accuracy of:

1) the coordinates to 10 microns; 2) the travel time to 160 ps; and 3) the velocity to an accuracy of 1 in 1000.

It will also simultaneously measure all cosmic ray atomic nuclei to an energy of a trillion electron volts (see Figure 20).

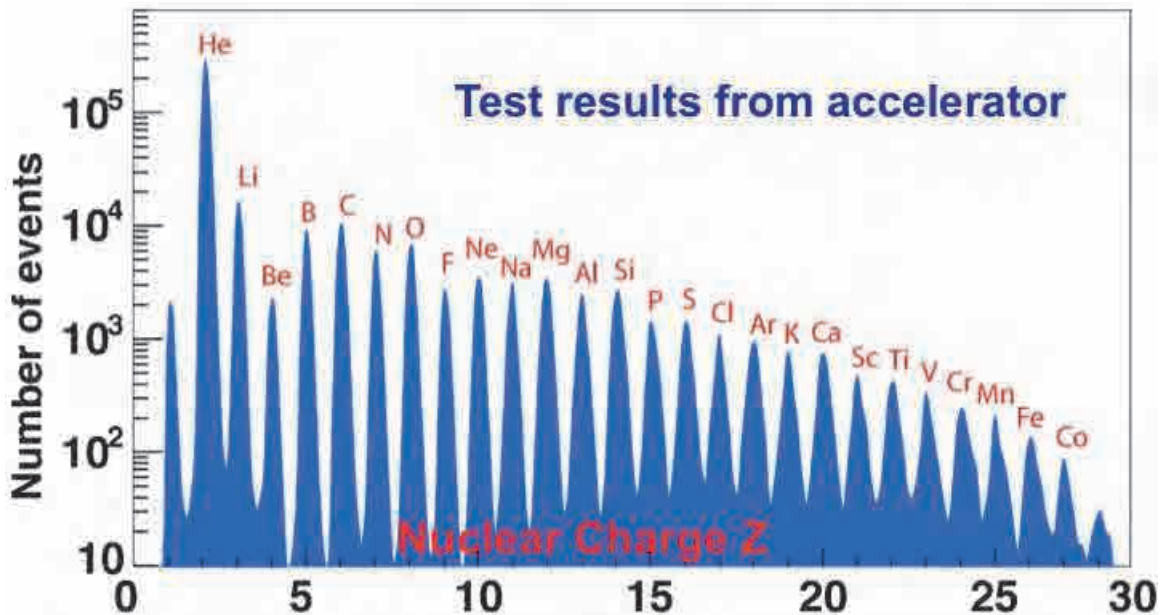


Figure 20: *With its ultraprecise detectors and resolution, AMS will measure cosmic ray spectra for nuclei, for energies from 100 MeV to 2 TeV, with 1% accuracy over the 11 year solar cycle.*

Figure 21 illustrates the scope of the AMS Collaboration.

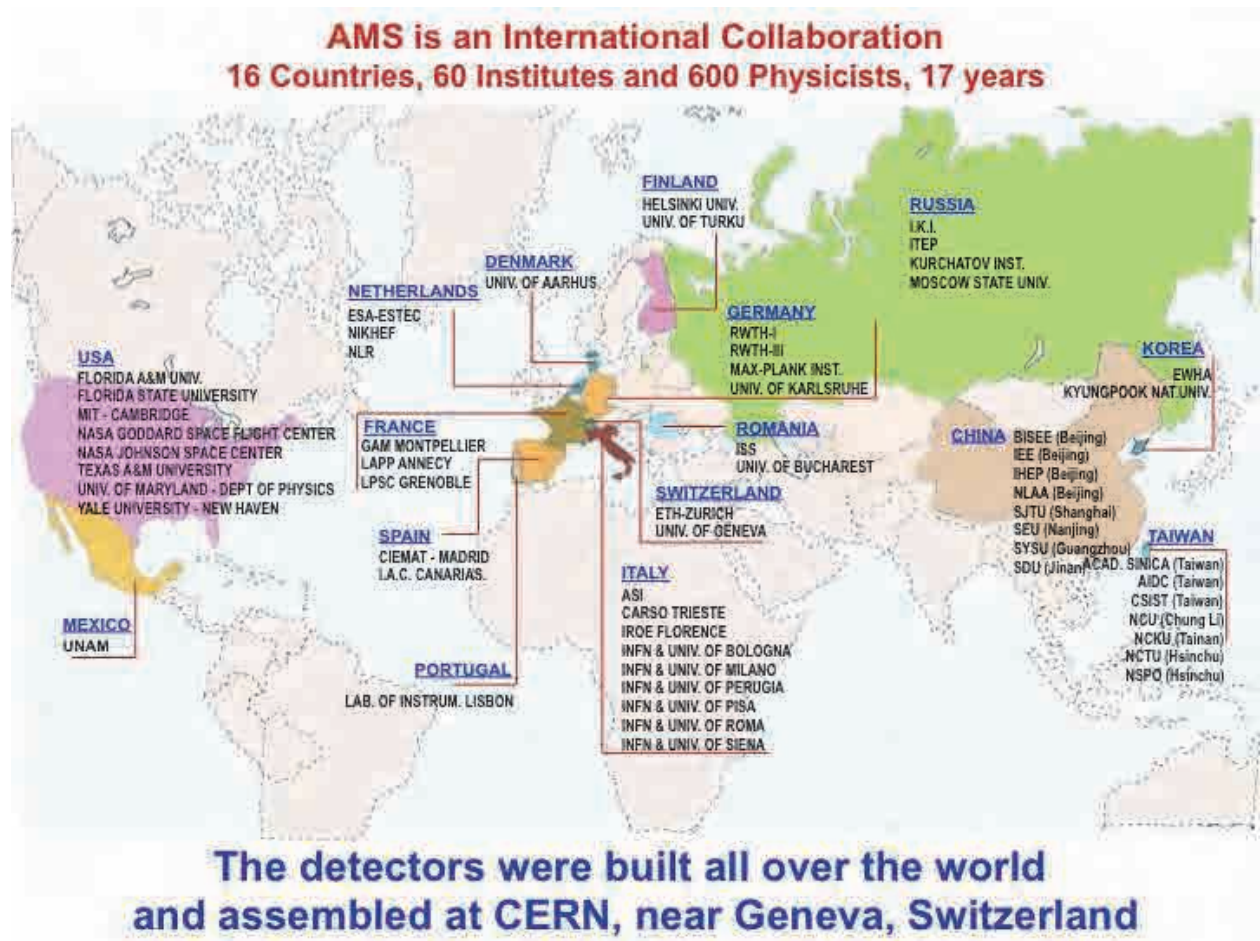


Figure 21: *The scope of the AMS international collaboration.*

After completion of detector assembly at CERN, AMS was moved to the European Space Agency Technology Center (ESTEC) in Noordwijk, the Netherlands for Thermal Vacuum Test and EMI/EMC tests in their unique facilities. The Large Space Simulator (LSS) at ESTEC is shown in Figure 22. The LSS measures 15 meters in height and 10 meters in diameter. Its powerful xenon lamps simulate the temperature of the sun and liquid nitrogen cooled walls simulate the opposite extreme of temperature in space.

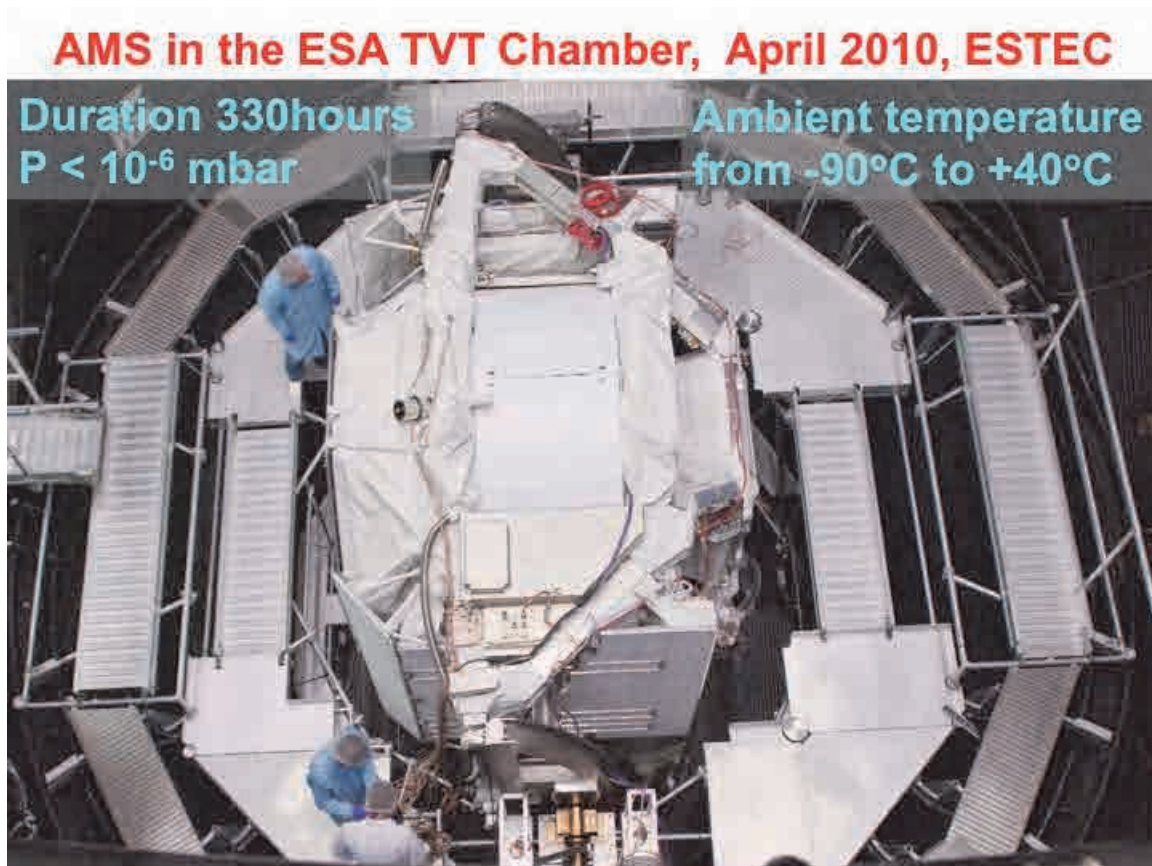


Figure 22: The completed AMS Detector underwent crucial thermal vacuum testing and EMC testing at the European Space Agency Technology Center (ESTEC) in Noordwijk, the Netherlands to test the performance of the Detector in space flight conditions.

In addition to Thermal Vacuum Testing, AMS underwent EMI and EMC testing in ESTEC's Maxwell Test Chamber. Results verified that AMS systems and the ISS and Shuttle systems do not generate any electromagnetic interference that might have an adverse affect on each other's performances.

Following the test procedures at ESTEC, AMS was moved back to CERN-Geneva to undergo test beam calibration. Figure 23 shows the AMS Detector in the CERN test beam and the results are shown in Figures 24 and 25.

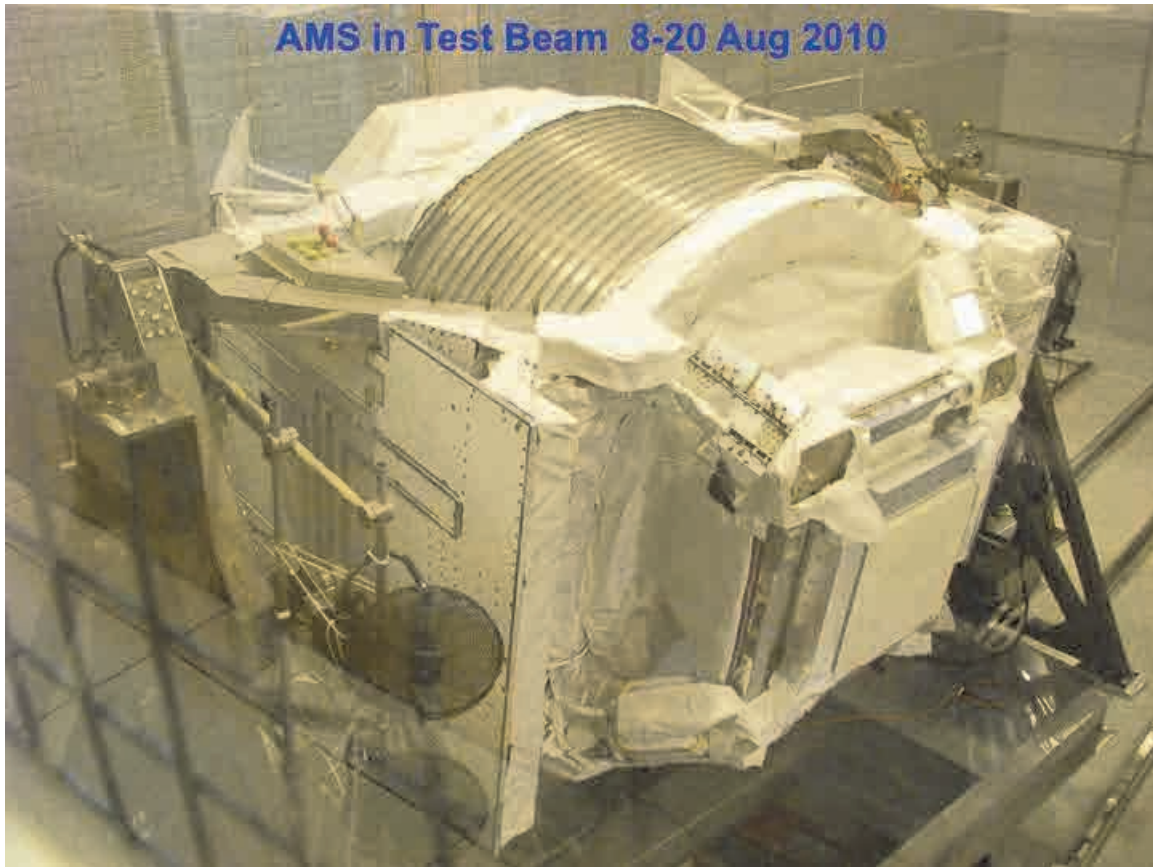


Figure 23: *CERN provided test beam time from its accelerator complex to calibrate AMS.*

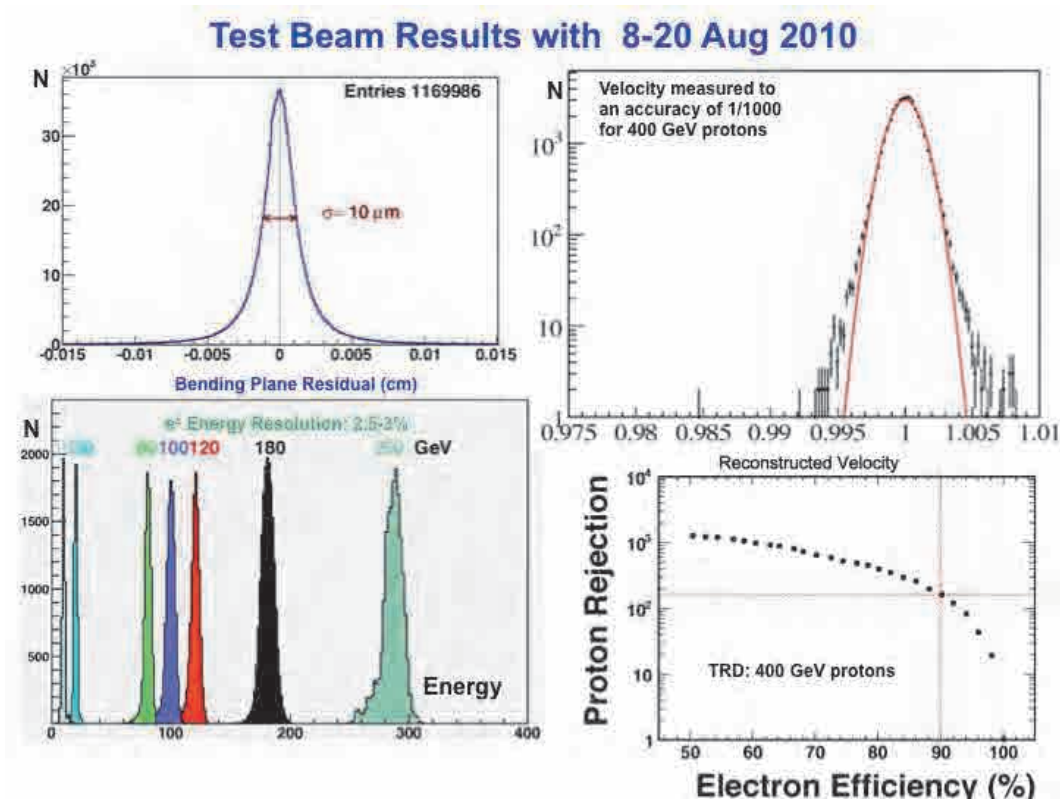


Figure 24: AMS test beam results from CERN accelerator beam (2010) prior to AMS departed to Kennedy Space Center.

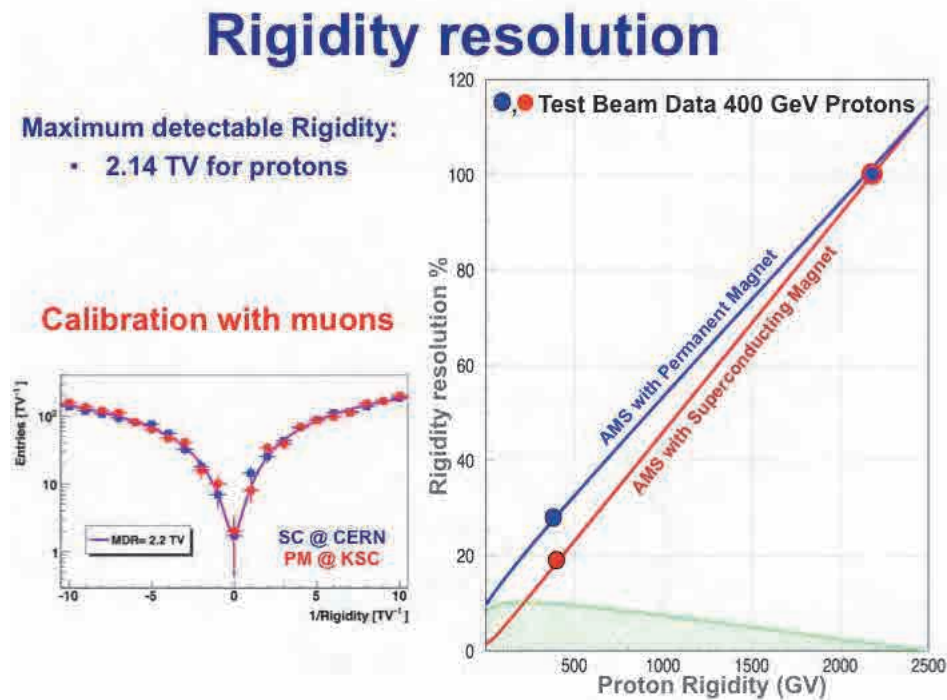


Figure 25: AMS test beam data showing measurements of 400 GeV proton rigidity resolution for the superconducting magnet and the permanent magnet.

AMS was delivered to the Kennedy Space Center from Geneva on August 26, 2010 in a special U.S. Air Force C5-M aircraft. Landing on the Shuttle Landing facility at Kennedy Space Center, AMS was immediately transported to the Space Station Processing Facility (SSPF) at KSC for preflight testing and processing.

Figure 26 through Figure 38 illustrate activities at Kennedy Space Center including the launch of STS-134, docking with the ISS and deployment of AMS on the ISS on 19 May 2011.

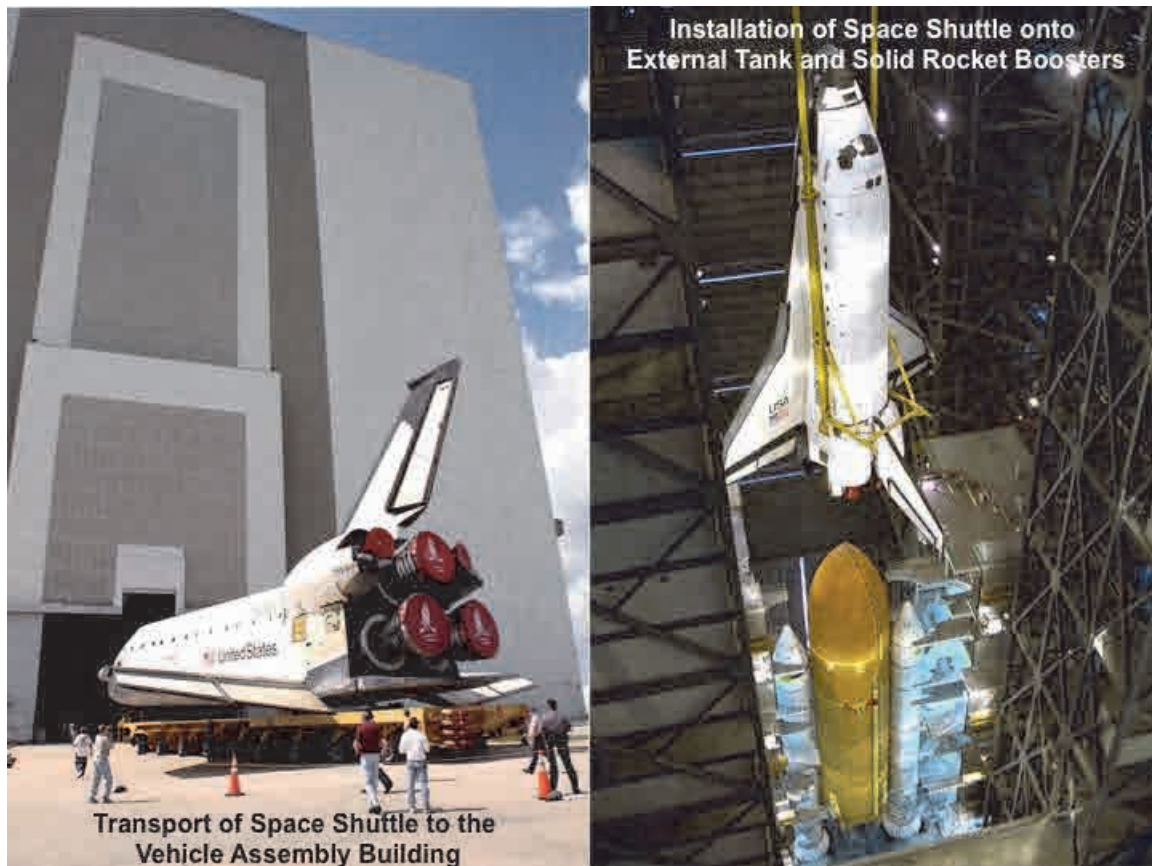


Figure 26: Orbiter *Endeavour* being prepared at Kennedy Space Center for its final launch to carry AMS to the ISS. Left: *Endeavour* entering the Vehicle Assembly Building (VAB). Right: *Endeavour* being mated with its large External Tank and two Solid Rocket Boosters (SRB) in the VAB.



Transfer of STS-134 to the launch pad

Figure 27: Orbiter *Endeavour* being rolled out to Launch Pad 39A at Kennedy Space Center (March 2011) to await launch.



Figure 28: A view of AMS installed in *Endeavour*'s cargo bay awaiting launch.

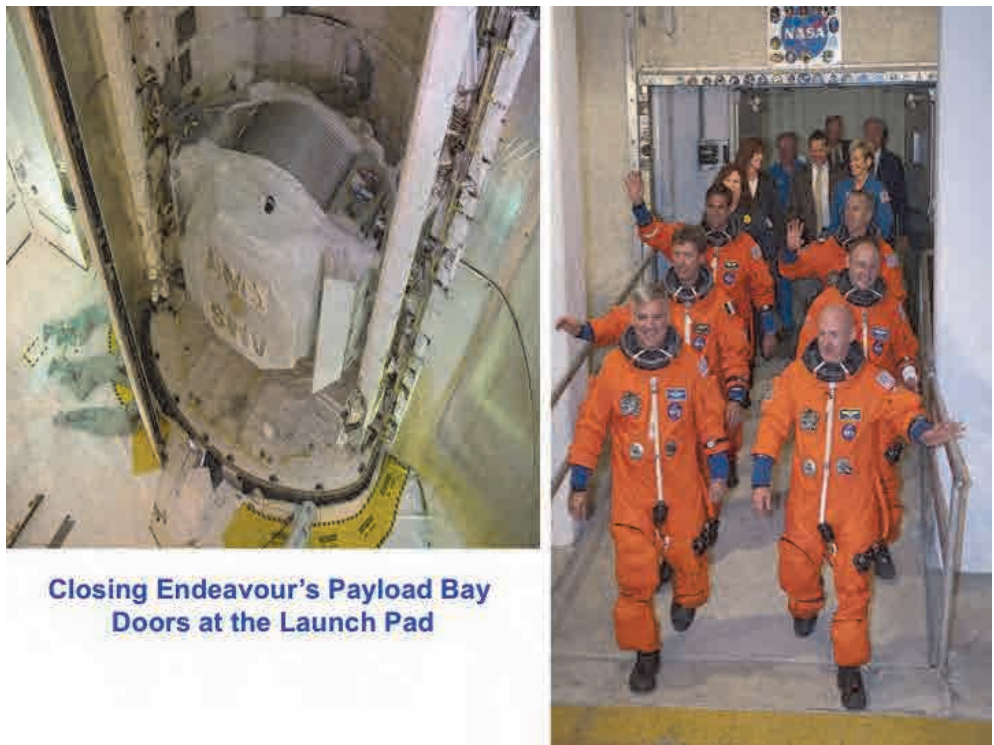


Figure 29: Left: Closing of *Endeavour's* payload bay doors prior to launch. Right: The crew of STS-134, under the command of Captain Mark Kelly (USN), proceed to the launch pad on May 16, 2011. Among the six member crew was Colonel Roberto Vittori, ESA and Italian Air Force, who is seen in the second row, left side.

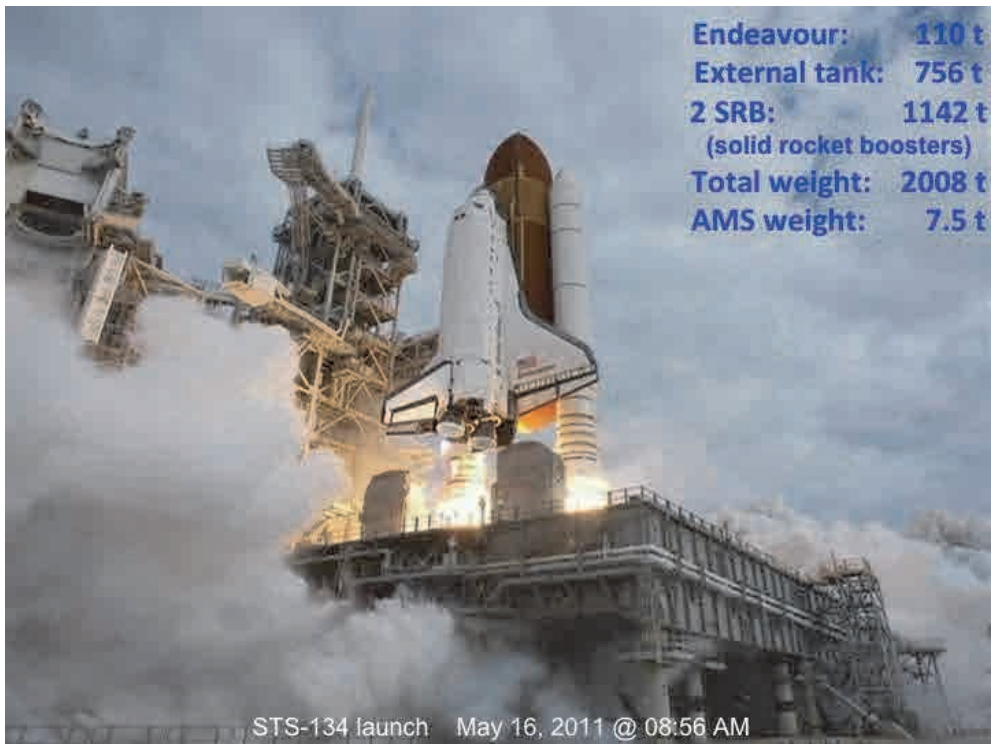


Figure 30: The final launch of *Endeavour* carrying AMS to the International Space Station took place on May 16, 2011 at 0856.



Figure 31: *Seconds after launch, **Endeavour** pierced the clouds over Kennedy Space Center en route to the ISS.*



Figure 32: *Separation of the Solid Rocket Boosters.*



Figure 33: *View of **Endeavour** (with cargo bay doors open) approaching the ISS.*

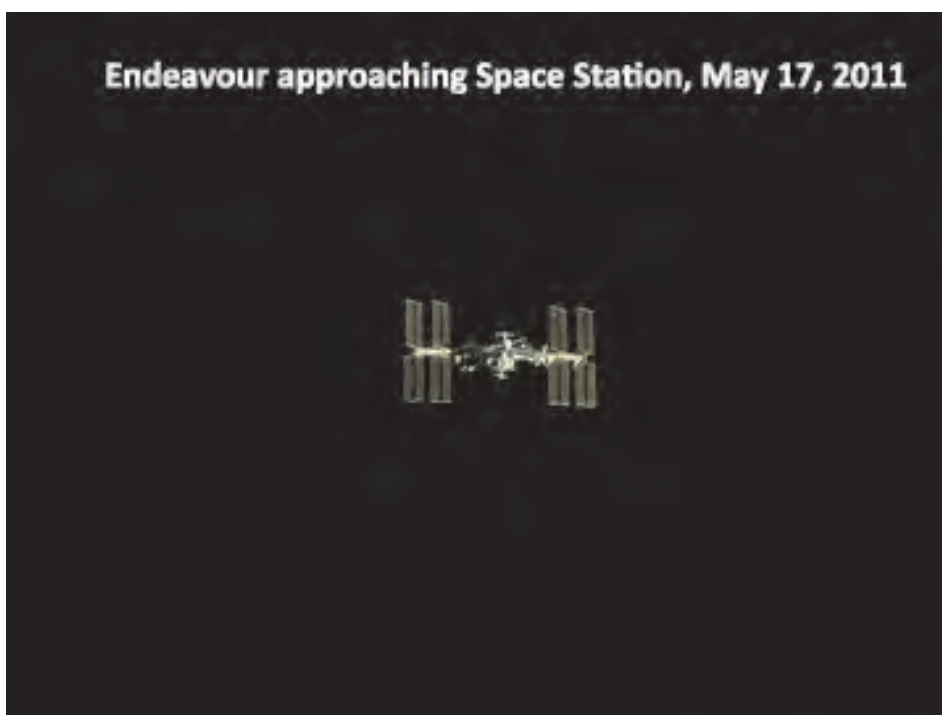




Figure 35: *View of the ISS through the flight deck windows of Endeavour during docking procedures*



Figure 36: *View of the ISS from Endeavour.*



Figure 37: After docking with the ISS, AMS was removed from *Endeavour's* cargo bay by the shuttle Remote Manipulator System and transferred to the ISS robotic arm that placed AMS on its permanent attachment site on an external truss of the ISS.



Figure 38: On May 19, 2011, AMS was deployed on the ISS. After three hours of checking all systems, AMS began to collect and transmit data to the AMS team on the ground.

After the launch, deployment and initial testing and commissioning of AMS on the ISS, the AMS team returned to CERN-Geneva. CERN had constructed a new building to house the main AMS Payload Operations Control Center (POCC) as seen in Figure 39. This facility was inaugurated on 19 June 2011. Since that time, AMS has been monitored and controlled by the AMS team working in close communication with NASA's ISS Control Center in Houston, Texas and Marshall Space Flight Center in Huntsville, Alabama.



Figure 39: *The interior of the main AMS Payload Operations Control Center (POCC) at CERN-Geneva. The main Science Operations Center (SOC) is also located at CERN-Geneva.*

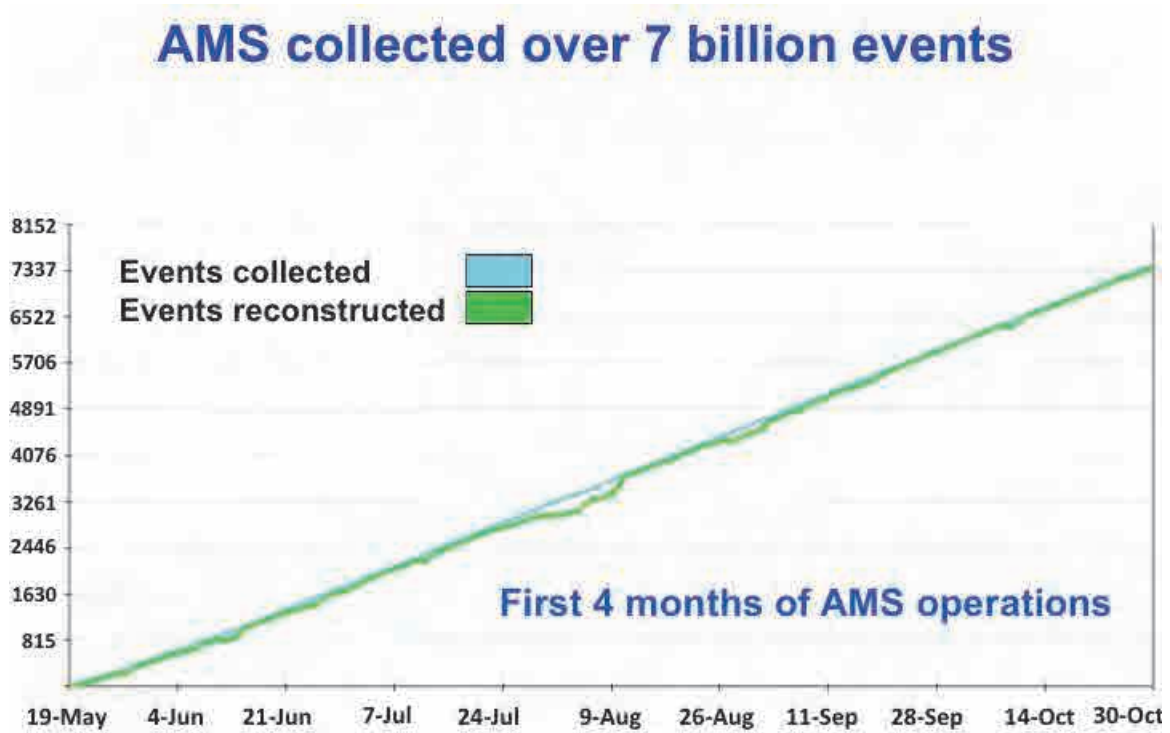


Figure 40: *In the first four months of operations on the ISS, AMS collected and reconstructed over 7 billion cosmic ray events*

In the first four months of operations, we have determined that the detectors function exactly as designed and have collected 7 billion events (see Figure 40). Therefore, every year, we will collect 1.5×10^{10} triggers and in 20 years we will collect 3×10^{11} triggers. This will provide unprecedented sensitivity to search for new physics. Figure 41 presents an example of the data from the first week.

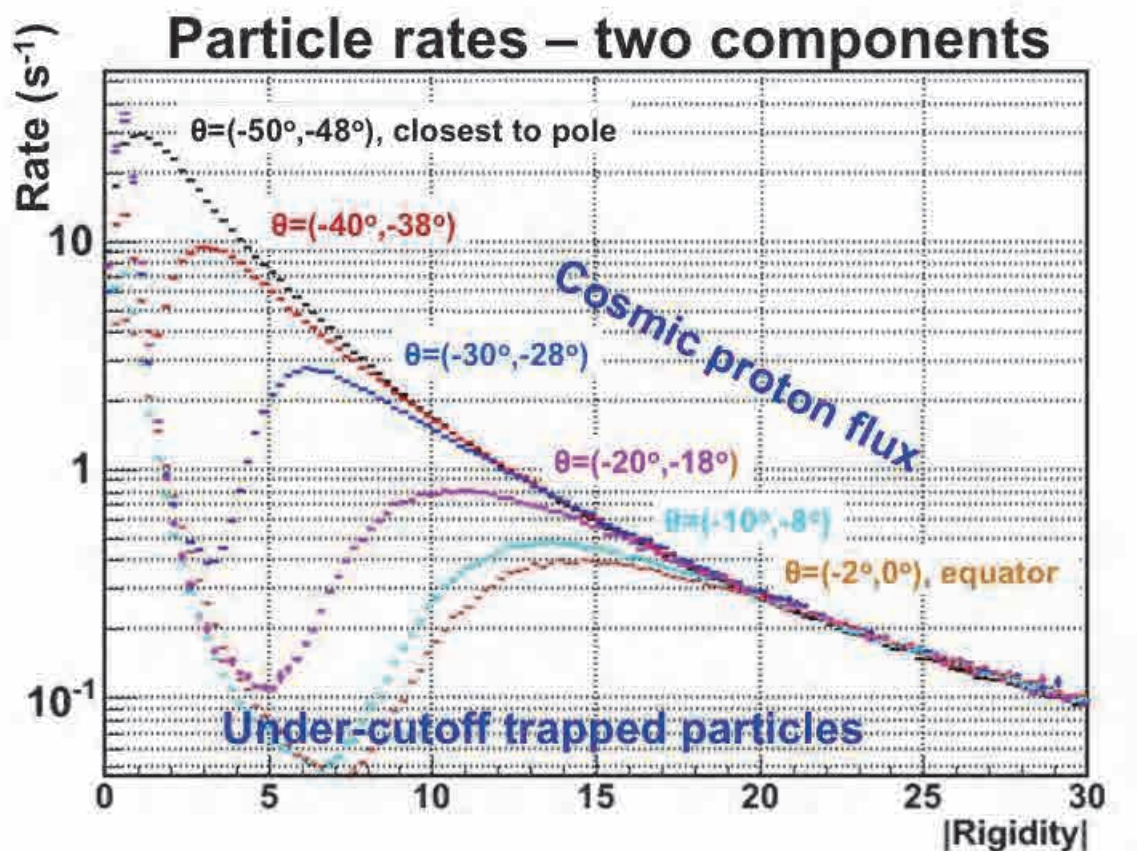


Figure 41: *Cosmic proton flux of particles collected by AMS.*

The physics objectives of AMS include the search for the origin of Dark Matter, the study of primary Cosmic Rays, the existence of Antimatter and to explore new phenomena, such as Strangelets.

Figures 42 though 51 present actual AMS data collected during the first three months of operation (19 May to 19 August 2011) as well as current theoretical models.

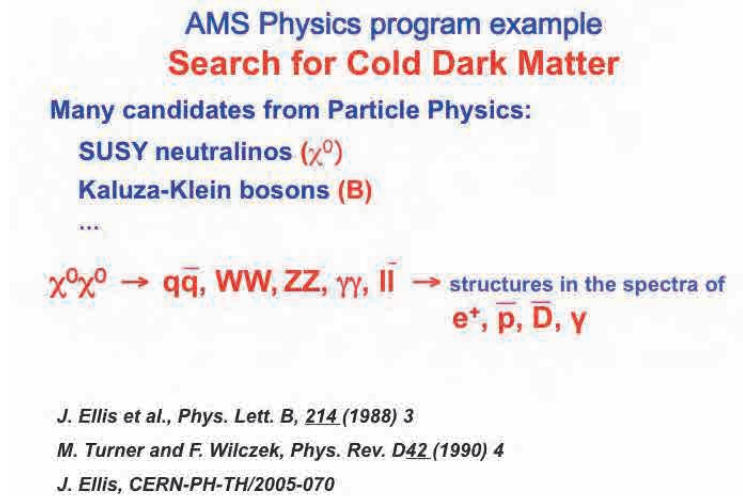


Figure 42: The search for the origin of Cold Dark Matter has several theoretical candidates such as SUSY neutralinos and Kaluza-Klein bosons, etc.

Indeed, the leading candidate for Dark Matter is the SUSY neutralino, as shown in Figure 43. AMS will be able to definitively identify the origin of Dark Matter through the excess in the spectra of e^+ in the collisions of X^0 , which is different from known cosmic ray collisions. Figure 44 shows AMS's ability to measure accurately the cosmic ray flux over the 11 year solar cycle from which the e^+ production from the collision of ordinary cosmic rays can be determined.

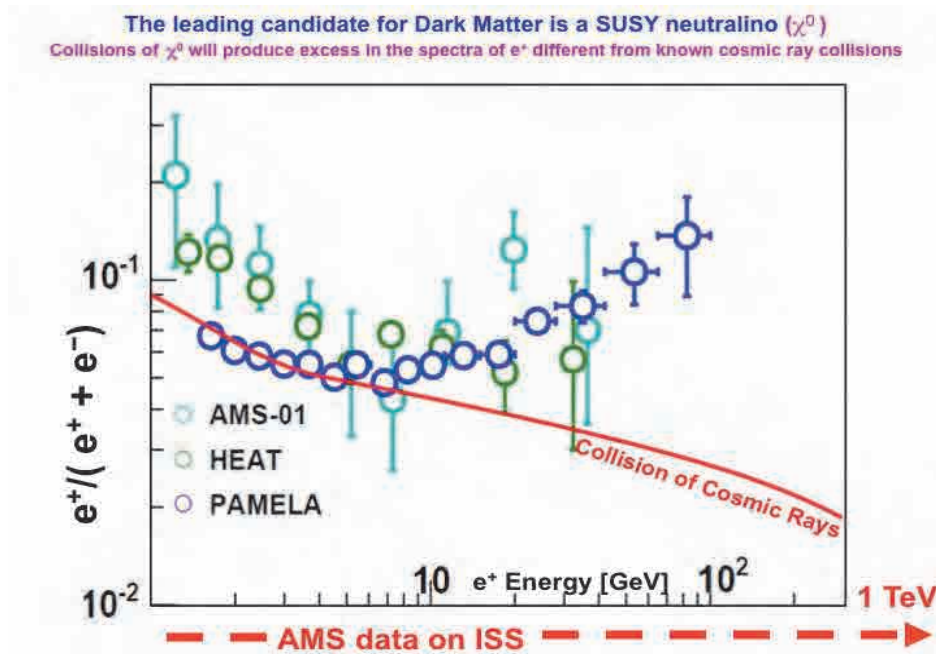


Figure 43: One of the leading theoretical candidates responsible for Dark Matter is the SUSY neutralino. AMS will be able to definitively identify the origin of Dark Matter through the excess in the spectra of e^+ in the collisions of X^0 , which is different from known cosmic ray collisions.

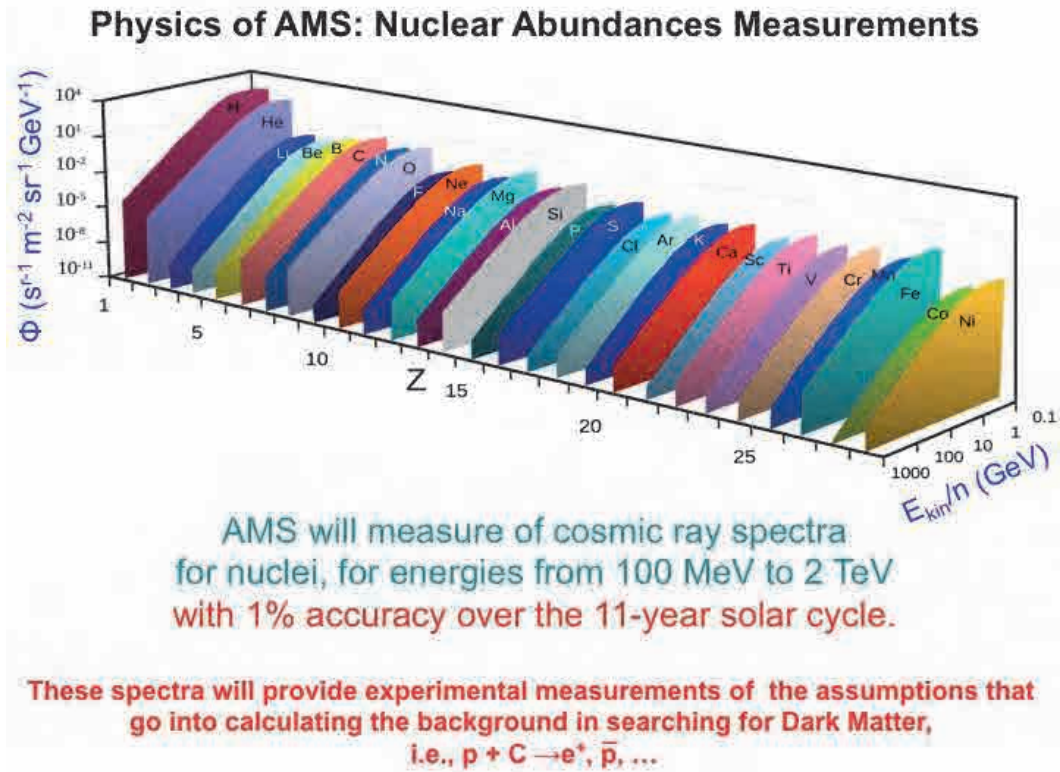


Figure 44: Data from AMS will be used to measure the cosmic ray spectra for nuclei for energies from 100 MeV to 2 TeV with unprecedented accuracy. This data will be applied to the calculation of background in the search for Dark Matter as noted above.

Figures 45 and 46 present Monte Carlo simulations of AMS data and current theoretical models. Figures 47 and 48 show 240 GeV electron events seen by AMS.

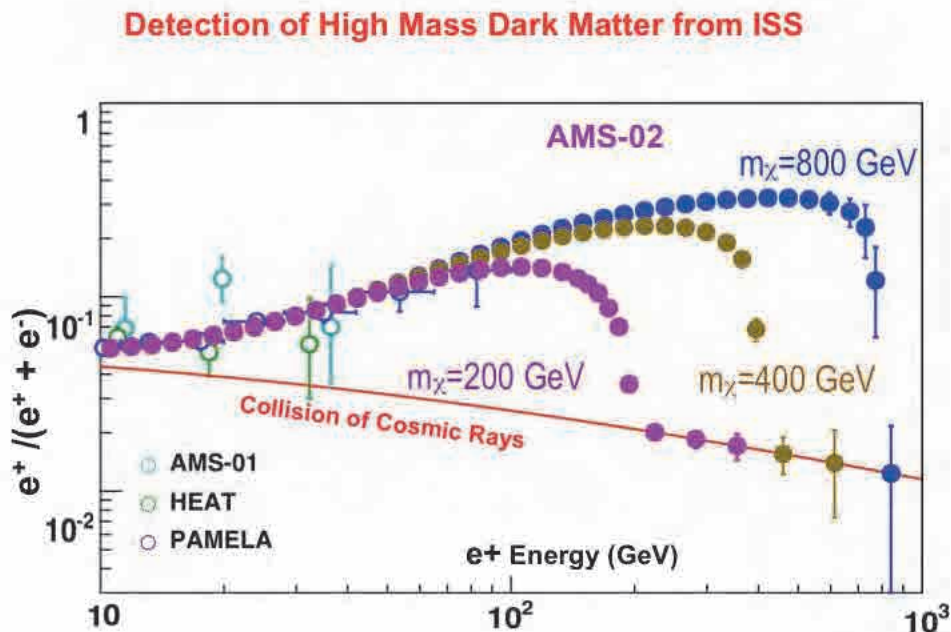


Figure 45: Comparison of Monte Carlo data for High Mass Dark Matter searches.

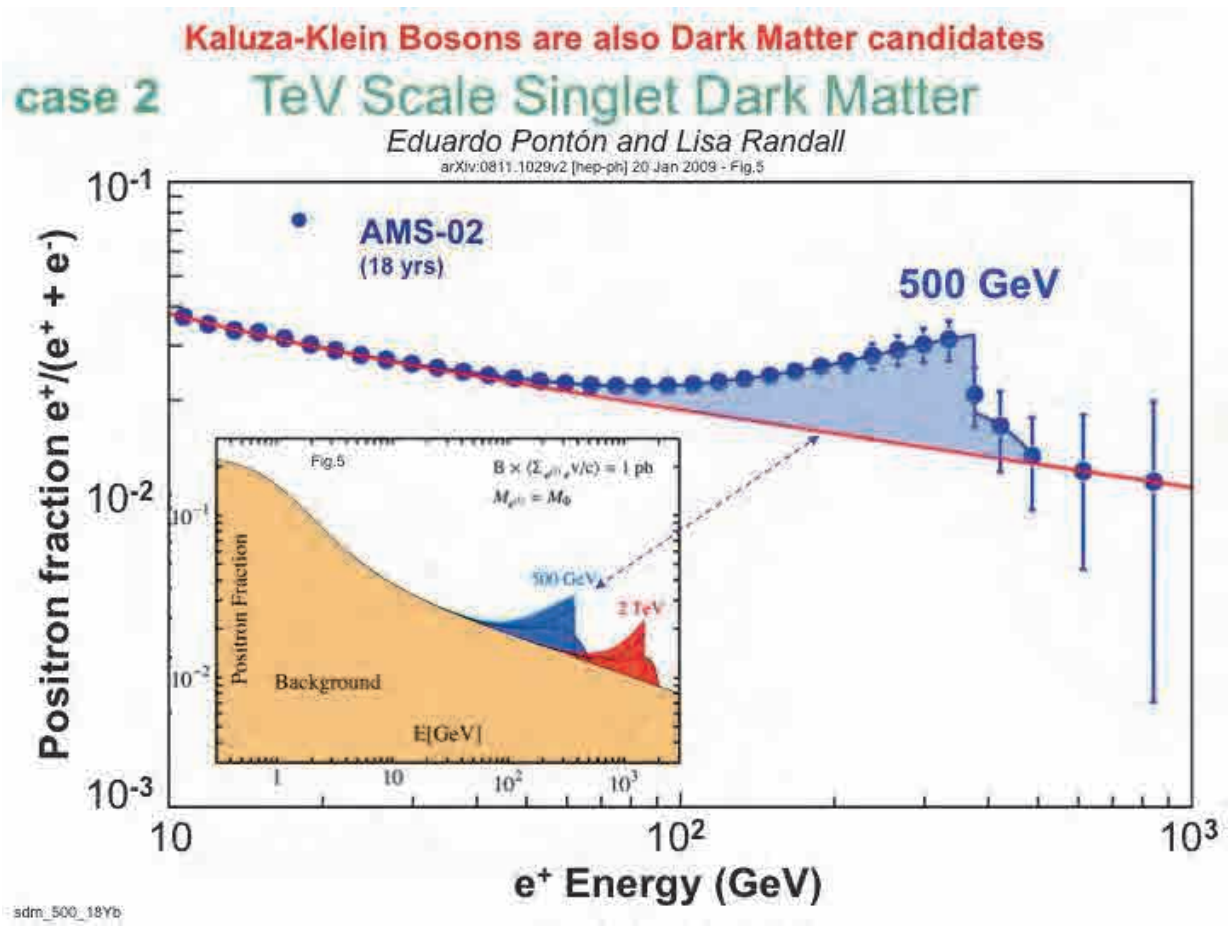


Figure 46: In addition to the SUSY Neutralinos, the Kaluza-Klein Bosons are also theoretical candidates responsible for Dark Matter.

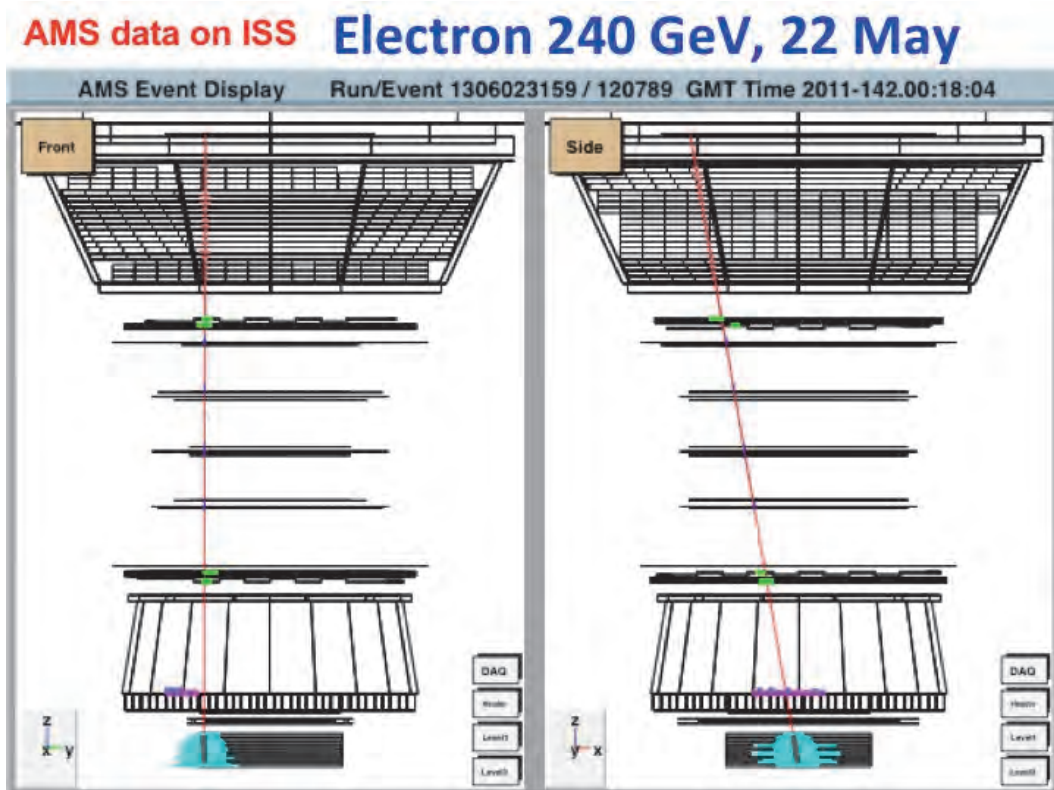


Figure 47: Actual event display from AMS on the ISS of a 240 GeV Electron.

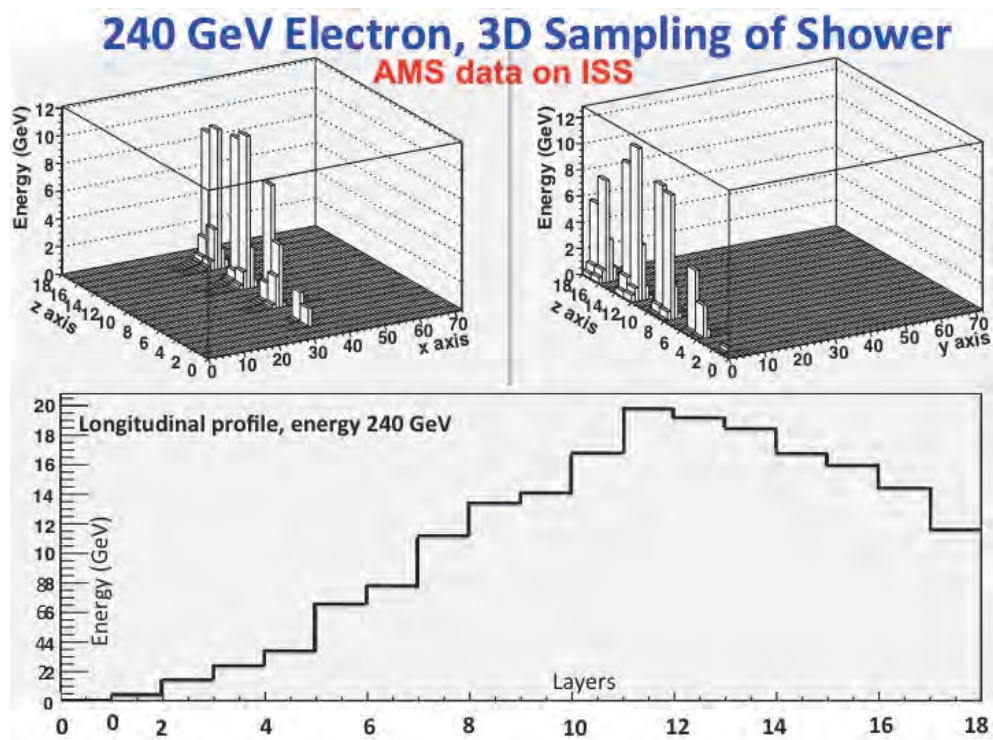


Figure 48: Actual data from AMS on the ISS of a 240 GeV Electron and 3D Sampling of Shower.

Another physics example of AMS is to search for Antimatter, the physics of which is illustrated in Figure 49.

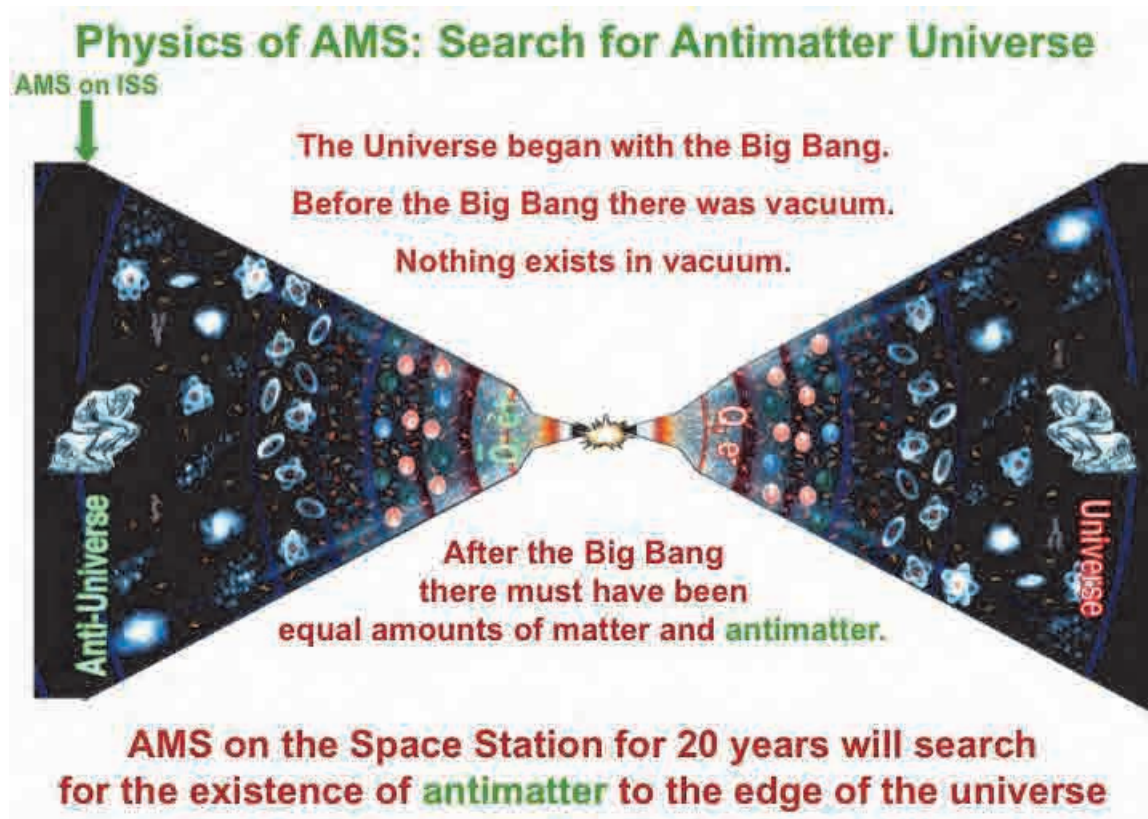


Figure 49: The search for the Antimatter Universe is based on the Big Bang Theory of the Universe which states that equal amounts of matter and antimatter must have existed at the time of the Big Bang.

AMS has often been referred to as the “Hubble Telescope for Charged Particles” since there has never before been a magnetic spectrometer in space for a long duration that could collect and study charged particles from primary sources in the far reaches of space before they enter the Earth’s atmosphere. Examples of current work on Antimatter are shown in Figure 50.

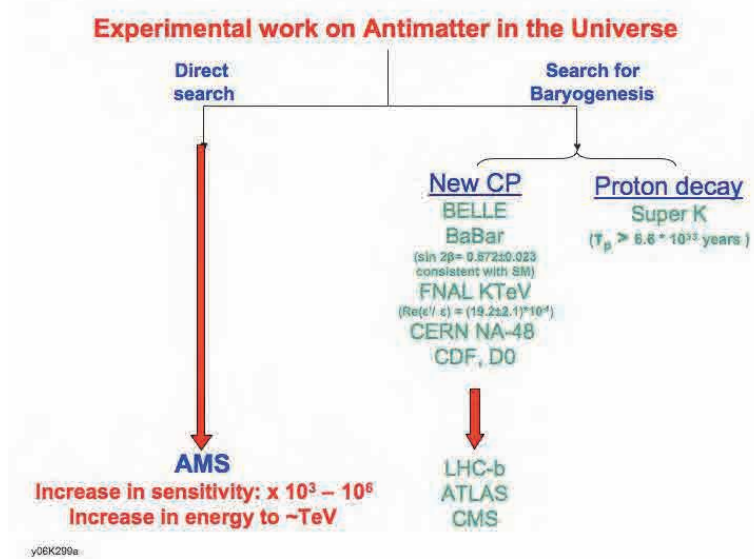


Figure 50: Current experimental work to search for Antimatter in the Universe is via the indirect search for Baryogenesis by new CP and Proton Decay, as represented by Belle, BaBar, FNAL, CERN the LHC experiments and by Super K. AMS is unique in that it is conducting a direct search for Antimatter.

Figure 51 shows an example of AMS’s ability to search for Antimatter and Figure 52 presents an example from the first three days of data measuring cosmic nuclei.

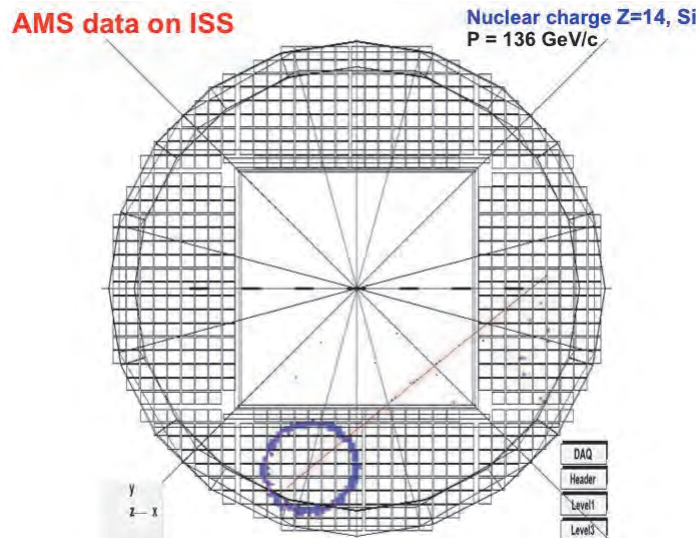


Figure 51: In order to ensure that an instrument can detect Antimatter, it must first detect Matter. This is illustrated above in the detection of Matter in the AMS RICH detector.

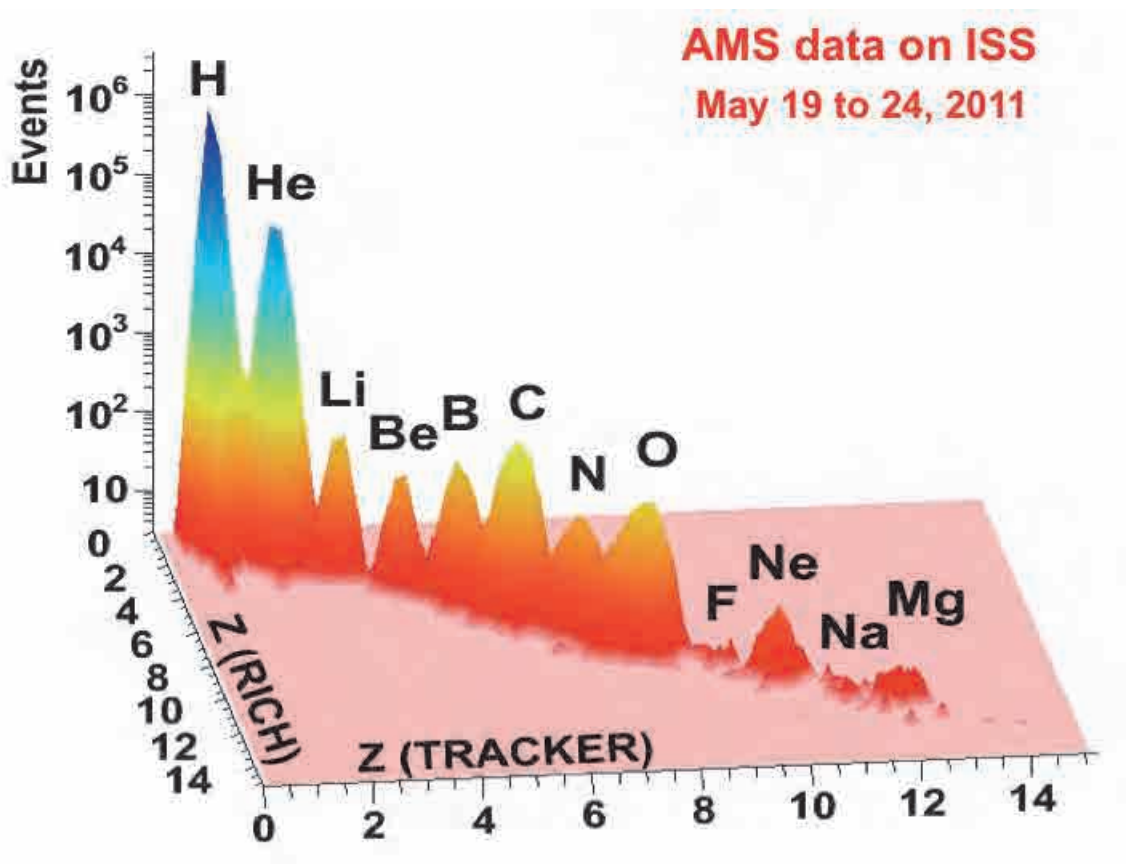


Figure 52: Data from the first week of AMS operations on the ISS. AMS will continue to collect nuclei to further expand the above spectra.

In conclusion, as illustrated in Figure 53, the cosmos is the ultimate laboratory, producing cosmic rays with energies far beyond what is possible to observe on Earth. AMS seeks to explore many of the fundamental questions in modern physics but the most important objective is to explore the unknown.

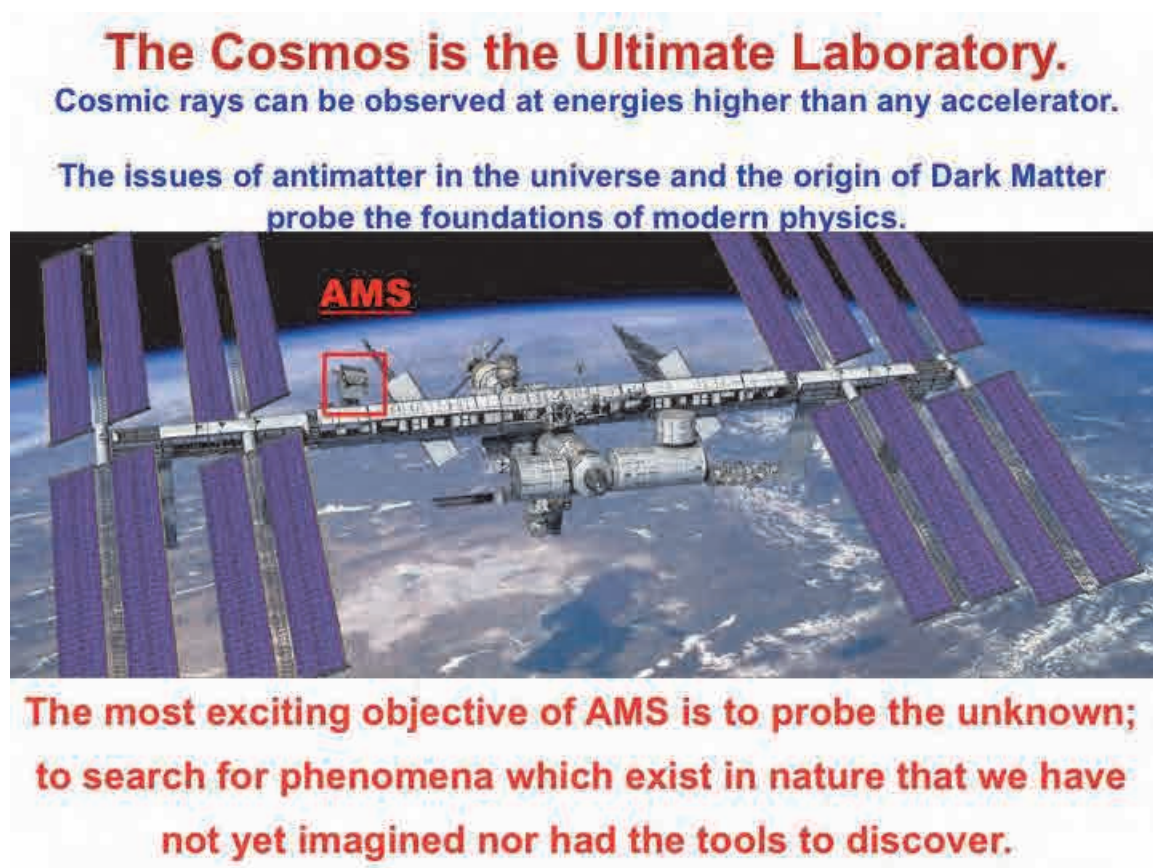


Figure 53: AMS on board the ISS will study the origin and structure of the cosmos which has the potential to make discoveries that will expand our reservoir of knowledge.

However, discoveries in physics cannot be predicted in advance because objectives are always based on existing knowledge or “expert’s opinions”. As shown in Figure 54, most of the advances in physics were not originally the purpose of the facility or the experiment when approved. Advancements in our understanding of Nature and the Universe can only be made through experimental discoveries.

Discoveries in Physics		
Facility	Original purpose, Expert Opinion	Discovery with Precision Instrument
P.S. CERN (1960's)	π N interactions	Neutral Currents \rightarrow Z, W
Brookhaven (1960's)	π N interactions	ν_e, ν_μ CP violation, J
FNAL (1970's)	Neutrino physics	b, t quarks
SLAC Spear (1970's)	ep, QED	Scaling, Ψ , τ
PETRA (1980's)	t quark	Gluon
Super Kamiokande (2000)	Proton decay	Neutrino oscillations
Hubble Space Telescope (1990's)	Galactic survey	Curvature of the universe, dark energy
AMS on ISS	Dark Matter, Antimatter Strangelets,...	?
Exploring a new territory with a precision instrument is the key to discovery.		

y96402nac.ppt

Figure 54: Discoveries in physics compared to original purpose over the past fifty years.

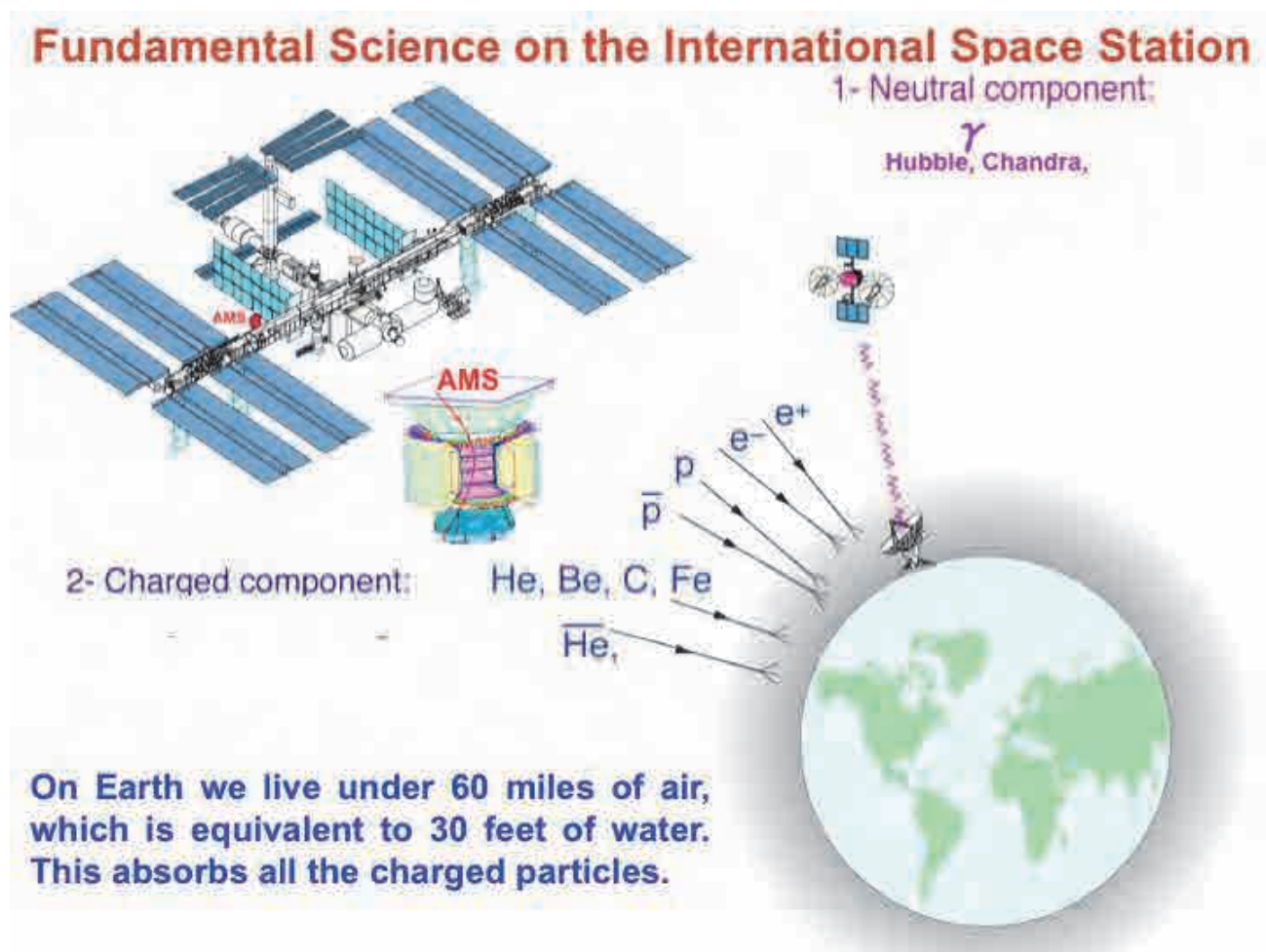


Figure 55: *The International Space Station provides a unique opportunity to support fundamental science above the Earth's atmosphere.*

As seen in Figure 55, fundamental physics on the International Space Station has the potential to yield important information impossible to attain on the ground or with short duration balloon experiments. AMS will thus explore a new domain in particle physics research.